This Page is Inserted by IFW Indexing and Scanning Operations and is not part of the Official Record

BEST AVAILABLE IMAGES

Defective images within this document are accurate representations of the original documents submitted by the applicant.

Defects in the images include but are not limited to the items checked:

- ☐ BLACK BORDERS
- ☐ IMAGE CUT OFF AT TOP, BOTTOM OR SIDES
- ☐ FADED TEXT OR DRAWING
- ☐ BLURRED OR ILLEGIBLE TEXT OR DRAWING
- ☐ SKEWED/SLANTED IMAGES
- ☐ COLOR OR BLACK AND WHITE PHOTOGRAPHS
- ☐ GRAY SCALE DOCUMENTS
- ☐ LINES OR MARKS ON ORIGINAL DOCUMENT
- ☐ REFERENCE(S) OR EXHIBIT(S) SUBMITTED ARE POOR QUALITY
- ☐ OTHER: _____

IMAGES ARE BEST AVAILABLE COPY.
As rescanning these documents will not correct the image problems checked, please do not report these problems to the IFW Image Problem Mailbox.

[Translator's Note: The first portion of page 509 is the concluding part of the preceding paper]

Pharmazie 46 (1991), No. 7, pages 509-512

The Berlin-Adlershof Analytical Center[1] and Arzneimittelwerk Dresden GmbH[2]

Crystal structures of the carbamazepine/ammonium chloride and carbamazepine/ammonium bromide adducts and their transformation into carbamazepine dihydrate

G. RECK[1] and W. THIEL[2]

The adducts carbamazepine ammonium chloride and carbamazepin ammonium bromide have isomorphous crystal structures. Drug molecules, ammonium, and chloride (bromide) ions are connected by 6 symmetry independent hydrogen bonds forming stable layers in the crystal. In water the adducts are transformed completely to carbamazepine dihydrate by a topotactic reaction.

1. Introduction

The anti-epileptic active substance 5H-dibenz[b,f]-azepine-5-carboxamide (carbamazepine, **1**) forms an adduct (**2**) with ammonium chloride during recrystallization in ethanol, whereby this adduct melts at more than 200 °C and thus possesses a significantly higher melting point than the pure active substance (189-193 °C). Its IR spectrum exhibits a distinct change in some bands [1].

Since ammonium chloride can be washed out with ease using water, weak interactions between the components were initially inferred. The crystallized material consists of colorless crystals that are linked together in a felt-like manner and are of varying thickness (predominantly thinner than 0.005 mm).

On the one hand, the existence of an adduct was to be demonstrated with the help of single crystal structural analysis and, on the other hand, the intramolecular and intermolecular interactions in the crystal were to be investigated in detail. In addition, it was to be shown by means of powder diffraction photographs that the adduct consists only of one crystalline modification. Analogous investigations as in the case of **2** were also carried out for the ammonium bromide adduct (**3**). The analyses showed that **2** and **3** have isomorphous crystal structures.

2. Investigations and results

2.1 Crystal data and structure determination

The following crystal data were ascertained for **2** and **3**.

2: $C_{15}H_{12}N_2O.NH_4Cl$; monoclinic $P2_1/n$; a = 10.869(4), b = 5.341(3), c = 25.153(11) Å, β = 100.90(3)°; Z = 4; D_c = 1.378 g/cm^3; MoK_α radiation; 1772 reflections in the range $1.5 < \theta < 22°$ of which 1301 were with $I(hkl) > 5\,\sigma(I)$. R value = 0.11 for 1301 reflections.

3: $C_{15}H_{12}N_2O.NH_4Br$; monoclinic $P2_1/n$; a = 11.051(3), b = 5.464(2), c = 24.928(9) Å, β = 100.81(4)°; Z = 4; D_c = 1.502 g/cm^3; MoK_α radiation; 2036 reflections in the range $1.5 < \theta < 23°$ of which 1524 reflections were with $I(hkl) > \sigma(I)$. R value = 0.053 for 1524 reflections.

The reflection intensities that are required for the structure analyses were measured using an ENRAF-NONIUS CAD-4 diffractometer. The structure analytical calculations were all carried out on a PDP 11/34 minicomputer using the SDP ENRAF-NONIUS program system.

The positions of all the non-hydrogen atoms of **2** could be ascertained using a RANTAN procedure in MULTAN-83[2]. The H atoms were, in part, localized in differential Fourier syntheses and, in the other cases, their positions were calculated in accordance with the geometrical conditions. The subsequent least squares refinement of the

atomic coordinates and anisotropic temperature factors converged with R = 0.11. This relatively high value can be attributed to bad crystal quality.

The aforementioned crystal data and the Weißenberg photographs showed that the crystal structures of **2** and **3** are isomorphous. The atomic positions of **2** could therefore be transferred to **3** and then they could be refined using least squares calculations. The refinement converged with R = 0.053. The resulting parameters for **2** and **3** are listed in Table 1.

Table 1 Atomic coordinates ($\cdot 10^4$) of **2** and **3** (standard deviations in parentheses)

Atom	**2** x/a	y/b	z/c	**3** x/a	y/b	z/c
Cl1, Br1	8583(2)	2004(6)	4349(1)	8584(1)	1907(2)	4294(1)
O18	11259(5)	−2862(10)	316(2)	11258(4)	−2916(10)	300(2)
N1A	13558(7)	−2071(20)	21(4)	13507(4)	−2002(10)	29(3)
N15	10866(6)	−558(10)	1003(3)	10848(5)	−598(10)	1003(2)
N17	9325(6)	−2851(20)	459(3)	9331(5)	−2916(10)	464(2)
C1	9214(9)	1756(20)	1289(4)	9195(7)	1680(20)	1305(3)
C2	8391(9)	2142(20)	1643(4)	8427(7)	2052(20)	1668(4)
C3	8468(10)	726(20)	2083(4)	8513(7)	582(20)	2117(4)
C4	9351(9)	−1222(20)	2194(4)	9392(8)	−1226(20)	2209(3)
C5	11135(9)	−3473(20)	1984(4)	11168(8)	−3485(20)	1979(3)
C6	12294(10)	−3553(20)	1851(4)	12283(7)	−3486(20)	1847(3)
C7	14173(9)	−1360(20)	1675(4)	14101(7)	−1247(20)	1672(3)
C8	14736(8)	570(20)	1434(4)	14626(7)	650(20)	1427(3)
C9	14039(8)	2116(20)	1080(4)	13916(7)	2198(20)	1074(4)
C10	12738(9)	1741(20)	949(4)	12666(7)	1826(20)	945(3)
C11	12171(8)	−99(20)	1176(4)	12142(6)	−101(10)	1174(3)
C12	12872(8)	1688(20)	1567(4)	12837(7)	−1619(20)	1560(3)
C13	10206(8)	−1552(20)	1843(4)	10205(7)	−1630(20)	1856(3)
C14	10098(7)	−135(20)	1384(3)	10071(6)	−135(10)	1394(3)
C16	10480(6)	−2171(20)	591(3)	10503(6)	−2203(10)	570(3)

A Guinier powder diffraction diagram (Table 2) was calculated with the atomic parameters of **2** that had been ascertained. The calculated d values and intensities agree very well with the measured d values and the visually estimated intensities of a Guinier film photograph of a larger sample quantity. It was shown in this way that the crystallized material does not contain additional crystalline forms.

Table 2 Powder diffraction diagrams of **2** and **4**

2 d(Å) calcd.	I calcd.	d(Å) exp.	I exp.	**4** d(Å) calcd.	I calcd.	Probe 1* d(Å) exp.	I exp.	Probe 2** d(Å) exp.	I exp.
12,35	29	12,32	30	14,34	6	14,34	9	14,33	16
10,55	100	10,50	100	9,88	88	9,90	66	9,86	22
7,21	2	7,19	1	7,17	74	7,19	89	7,19	91
6,18	26	6,17	35	5,80	14	5,80	28	5,80	11
5,99	21	5,99	20	4,77	14	4,79	27	4,79	21
5,33	5	5,33	5	4,71	4	4,72	17	4,72	17
5,22	34	5,24	40	4,67	20	4,67	29	4,66	9
4,90	28	4,91	25	4,53	100	4,53	100	4,53	100
4,85	2	—	—	4,27	20	4,28	44	4,27	56
4,78	6	4,78	5	4,06	6	4,07	17	4,06	3
4,62	9	4,62	10	3,90	10	3,91	20	3,90	6
4,48	69	4,48	60	3,80	10	3,80	19	3,80	6
4,34	10	4,33	15	3,67	24	3,67	61	3,67	67
4,30	13	4,30	15	3,64	38	3,65	61	3,65	31
4,19	21	4,19	20	3,58	14	3,59	44	3,59	44
4,11	22	—	—	3,45	12	3,46	28	3,46	17
4,04	8	4,04	10	3,43	6	3,43	3	—	—
3,98	7	3,99	10	3,38	6	3,38	25	3,37	24
3,94	5	3,94	5	3,24	4	3,25	9	3,25	7
3,80	3	—	—	3,21	2	3,21	4	—	—
3,77	34	3,78	40	3,11	26	3,11	55	3,11	61
3,70	18	3,71	15	3,06	6	3,06	10	—	—
3,64	25	3,64	30	3,04	14	3,04	41	3,04	39
3,59	11	3,59	10						
3,55	3	—	—						
3,48	3	3,48	2						
3,43	20	3,43	20						

*transformation of 1 into the dihydrate at 20 °C

*transformation of 1 into the dihydrate at 100 °C

[KEY TO TABLE 2]:

Probe 1* = Sample 1*

Probe 2** = Sample 2**

2.2 Molecular structures of **2** and **3**

Figure 1 shows a stereoscopic illustration of a **1** molecule of **2** and **3**, respectively. Because of the significantly higher accuracy, only the bond distances and bond angles of **3** are shown in Fig. 2. All the values agree well with the corresponding values for pure **1** [3, 4] and of **1** dihydrate (**4**) [5].

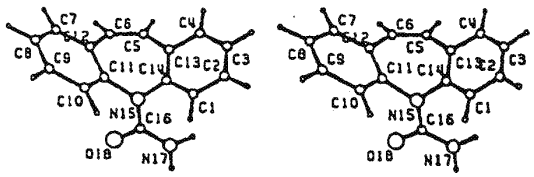


Fig. 1. Stereoscopic illustration of a carbamazepine molecule

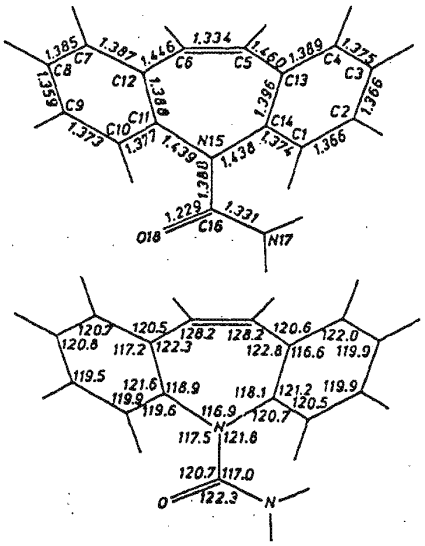


Fig. 2. Bond distances and bond angles of a carbamazepine molecule in **3** (mean standard deviations 0.008 Å and 0.5°, respectively)

The central azepine ring possesses a boat conformation with respect to the planes C11, C12, C13, C14. The planes C1, C2, C3, C4, C13, C14, C5, N15, and N15, C11, C10, C9, C8, C7, C12, C6 form a dihedral angle of 128° in **2** and **3**. The atoms O18, N17, C16 and N15 form a plane that, in comparison to the plane C16, N15, C14, C11, has been rotated by 6.5° and 6.8°, respectively, about the bond N15-C16. These values agree very well with the angle (6.0°) in solvate free **1** that had been ascertained by Himes [2].

2.3. Intermolecular interactions

As already mentioned above, **2** and **3** are isomorphous, i.e. the position of Cl^- in **2** is adopted by Br^- in **3**. All the other atomic positions are the same, with minor deviations, in the two structures.

Fig. 3 shows the arrangement of the carbamazepine molecules (some are not illustrated completely), the Cl(Br) ions and the NH_4 ions in the crystal. There are 6 symmetry independent hydrogen bridges in the crystal structure (Table 3). The components are linked to layers parallel to the x,y plane via these [hydrogen bridges] and symmetry equivalent bonds. In each case, two active substance molecules, which are connected between the carboxamide groups by means of two N-H...O bridges, form a centro-symmetric dimer. This arrangement was observed both in solvate free **1** [3, 4] and also in **4** [5].

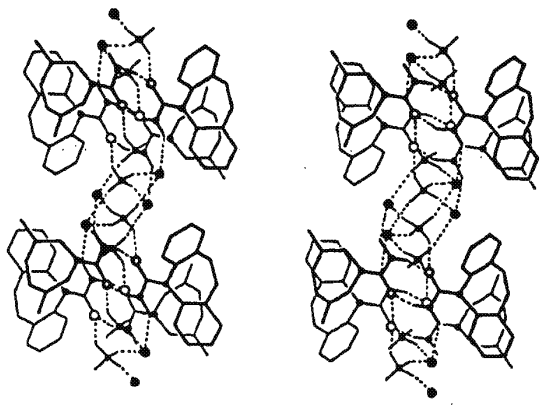


Fig. 3. Linking of the carbamazepine molecules, the NH^4 ions, and the Cl^- ions or Br^- ions in the crystal (stereoscopic illustration).

Table 3 Hydrogen bridges A-H...B in 2 and 3

Atom A	Atom B	2 d(A—B) (Å)		3 d(H—B)		symm. f. B
N17	O18	2,997	2,963	2,01	1,96	2 − x; −1 − y; −z
N1A	O18	2,770	2,741	1,83	1,86	x; y; z
N17	Cl1, Br1	3,287	3,387	2,46	2,59	1,5 − x; − 0,5 + y; 0,5 − z
Cl1, Br1	N1A	3,133	3,256	2,14	2,38	−0,5 + x; 0,5 − y; 0,5 + z
Cl1, Br1	N1A	3,193	3,342	2,21	2,39	−0,5 + x; −0,5 − y; 0,5 + z
Cl1, Br1	N1A	3,247	3,392	2,27	2,58	2,5 − x; 0,5 + y; 0,5 − z

[KEY TO TABLE 3]:

symm f. B = symm. for B [?]

Each Cl(Br) ion is a proton acceptor for four hydrogen bridges: one to the N atom of the carboxamide group, and three additional ones to the adjacent NH_4 ions. By contrast, each NH_4 ion is a proton donor for, likewise, four H bridging bonds: one to the C atom of the carboxamide group, and three to adjacent Cl^- ions. These bridges connect the dimers directly. The aforementioned layers of molecules are formed in the crystal as a result of this.

Fig. 4a shows a clearly arranged illustration of the hydrogen bridge system of **2** and **3**, whereby only those groups that are involved in the H bonds have been drawn. The layers are shown parallel to the plane of the drawing. The band-like arrangement of Cl(Br) ions and NH_4 ions is clearly seen in the middle of the diagram.

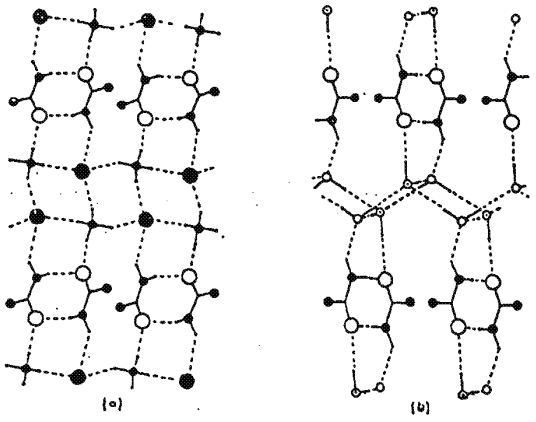


Fig 4. Illustration of the hydrogen bridges in **3** (a) and carbamazepine dihydrate (b). In order to provide a better overview, only the carboxamide groups of the active substance molecules are shown.

2.4. Transformation of carbamazepine/ammonium chloride into carbamazepine dihydrate

A close relationship exists between the crystal structures of **2** and **4**. Fig. 4b shows the hydrogen bridge system of the dihydrate. Layers of molecules are also formed in this structure in which dimers are linked via water molecules. There are two symmetry independent water molecules in the crystal, whereby each forms four hydrogen bridges. The kinship of the two structures becomes clear if the Cl^- is replaced by the first water molecule and the NH_4^+ is replaced by the second water molecule. Whereas chloride is exclusively the donor in **2**, each water molecule in the dihydrate functions as an acceptor and also as a donor. In terms of detail, somewhat different linkages arise as a result of this and these lead to a mutual displacement of the **1** chain in the dihydrate in comparison to **2**.

As mentioned above, ammonium chloride can be washed out of the crystallized material with great ease by means of water. The close structural kinship of the dihydrate and **2** provides an explanation of this. The water molecules form significantly stronger hydrogen bridges than chloride and ammonium, so that their replacement with water is understandable. In order to document this exchange experimentally, the single crystal that was used for the structural analysis was immersed in water for 3 hours. Schwenk photographs and Weißenberg photographs that were recorded thereafter showed that a single crystal of **4** had been produced from the single crystal of **2**. Topo-tactical reactions with substance exchange are very rare in organic chemistry. The transformation of **2** into **4** was also repeated with a larger quantity of crystal powder (several mg) and 5 mL of water at room temperature. A comparison of an experimental Guinier powder photograph to a calculated diagram showed the complete transition to the dihydrate. The same applies also to a second sample in which 5 g of **2** were stirred with 150 mL of distilled water along with an addition of 2 drops of a dish washing detergent over a period of 2 hours in a boiling water bath; crystallization then took place using a cold water bath over a period of 2 hours. This crystallized material also proved to be pure **4**.

Table 2 shows a comparison of both experimental diagrams to the theoretical diagram. The differences in the experimental intensities are attributable to texture phenomena and possibly to structure disorder phenomena in the dihydrate [5].

Literature

[Translator's Note:: The bibliographic references on page 512 read as shown in the original paper]

1 Wunderlich, H.; Zenker, L.; Stark, A.; Lohmann, D.; Usbeck, H.; Thiel, W.: Pharmazie 46, (1991)
2 Main, P.; Fiske, S. J.; Hull, S. E.; Lessinger, L.; Germain, G.; Declercq, I. P.; Woolfson, M.; MULTAN-82 – A System of Computer Programs for the Automatic Solution of Crystal Structures from X-ray Diffraction Data
3 Reboul, J. P.; Cristan, B.; Soyfer, J. C.: Acta Cryst. B37, 1844 (1981)
4 Himes, V. L.; Mighell, A. D.: de Camp, W. H.: ibid, B37, 2242 (1981)
5 Reck, G.; Dietz, G.: Cryst. Res. Technol. 21, 1463 (1986)

Received on July 25, 1990

Dr. G. Reck
Rudower Chaussee 5
O-1199 Berlin

[Translator's Note: The last portion of page 512 is the beginning part of the next paper]

UM00012316
NOVARTIS EXHIBIT 1017
Novartis v. Regents, IPR2023-01346
Page 1062 of 4460

5 ist aus wasserfreien Alkoholen (Methanol, Ethanol) in Gegenwart von 1 bis 5% Formamid unzerlegt umkristallisierbar. Bei Anwendung von wäßrigen Alkoholen erfolgt eine vollständige Zerlegung des Adduktes. Aus der warmen Mutterlauge kristallisiert reines 1 aus, das bei Raumtemperatur völlig klar in Chloroform löslich ist. Das Addukt ist im Unterschied dazu in Chloroform schwer löslich.
Formamid verdrängt offenbar auf Grund seiner stärkeren Affinität zu 1 Ammoniumchlorid. Bei Anwendung von Methyl- oder Dimethylformamid anstelle von Formamid ist dies nicht der Fall, vielmehr wird hierbei 2 isoliert.

3. Experimenteller Teil

Die IR-Spektren wurden mit einem Spektralphotometer Specord 75 IR (Carl Zeiss JENA) aufgenommen, die Schmb. wurden mit einem Heiztischgerät nach Boëtius sowie dem Thermosystem FP5 (Mettler) bestimmt, wobei Übereinstimmung erzielt wurde.

3.1. 5-Carbamoyl-5H-dibenz[b, f]azepin (1)-NH_4Cl-Addukt (2)

3.1.1. 47,2 g (0,2 mol) 1 werden unter Erwärmen in 500 ml 96%

C_2H_5OH gelöst. Dann wird eine filtrierte Lösung von 10,7 g (0,2 mol) NH_4Cl in 5 ml H_2O zugesetzt. Man erwärmt die Mischung 15 min zum Sieden, kühlt sie auf 15 °C und saugt den entstandenen Niederschlag nach 24 h ab. Dieser wird mit wenig C_2H_5OH gewaschen und bei 100 °C getrocknet. Nach Umkristallisation aus der 20fachen Menge C_2H_5OH erhält man Nadeln. Schmb. 195,5–199 °C.
$C_{15}H_{14}ClN_3O$ (289,8)

Ber.:	C	62,17	H	5,57	N	14,50	Cl	12,24
Gef.:	C	61,93	H	5,54	N	14,40	Cl	12,02
		62,21		5,63		14,43		12,17

3.1.2. 12,8 g (0,05 mol) 5-Chlorcarbonyl-5H-dibenz[b, f]azepin

werden in 45 ml Butylacetat verrührt. Man erwärmt auf 80 °C, tropft in die entstehende Lösung 15 ml einer 25% wäßrigen NH_3-Lösung und rührt 1 h bei 80 °C. Anschließend werden über einen Wasserabscheider ca. 10 ml H_2O abdestilliert. Der Ansatz wird dann auf 12 °C gekühlt, das Kristallisat über eine Filternutsche abgesaugt und zweimal mit je 10 ml Butylacetat gewaschen. Es wird bei 100 °C getrocknet und aus 90% wäßrigem i-C_3H_7OH umkristallisiert.

3.2. 1-NH_4Br-Addukt (3)

47,2 g (0,2 mol) 1 werden im siedenden Wasserbad in 200 ml Butylacetat gelöst. Man tropft eine Lösung von 20 g (0,224 mol) NH_4Br in 10 ml H_2O zu, erhitzt 0,5 h, kühlt die Mischung auf 15 °C und filtriert den ausgefallenen Niederschlag ab. Dieser wird mit Butylacetat gewaschen und bei 100 °C getrocknet. Durch Umkristallisation aus C_2H_5OH erhält man das 1:1-Addukt als farblose, verfilzte Nadeln.
Schmb. 119–201 °C.
$C_{15}H_{16}BrN_3O$ (334,2)

Ber.:	C	53,89	H	4,82	N	12,56	Br	23,93
Gef.:	C	52,69	H	4,84	N	12,50	Br	25,10
		52,46		4,86		12,50		25,11

3.3. 1-Formamid-Addukt (5)

23,6 g (0,1 mol) 1 werden bei Raumtemperatur in 100 ml $CHCl_3$ unter Rühren gelöst. In die klare Lösung werden unter Rühren 5,6 g (0,125 mol) NH_2-CHO zugegeben. Die Lösung beginnt sich einzutrüben und in wenigen min erfolgt die Kristallisation. Nach 2–3 h Kühlen im fließenden Wasserbad wird das Kristallisat abgesaugt und mit gekühltem $CHCl_3$, das 1% NH_2-CHO enthält, gewaschen. Der farblose Filterkuchen wird im Trockenschrank bei ca. 70 °C getrocknet. Man erhält 23 g (81,7%) 5. Schmb. 189–192 °C (bei 142–145 °C erfolgt eine deutliche Kristallumwandlung).
$C_{16}H_{13}N_2O_2$ (281,3)

Ber.:	C	68,31	H	5,37	N	14,94
Gef.:	C	68,55	H	5,36	N	15,10

3.4. Bestimmung der Löslichkeit von 1, 2 und 3

Substanzeinwaagen von ca. 20 mg und 25 ml dest. H_2O (A) bzw. 100 mg und 25 ml dest. H_2O (B) werden in je einem 100 ml-Schliff-Erlenmeyer gegeben. Die verschlossenen Kolben werden bei 25 °C 125 rotierenden Schüttelbewegungen je min ausgesetzt. Das Klarfiltrat einer Probenahme wird 1:10 mit dest. H_2O verdünnt und die UV-Absorption in einer 10 mm Küvette bei 286 nm gegen dest. H_2O gemessen. Für die analog auszuführende Eichmessung werden ca. 8 mg Einwaage 1 in 100 ml dest. H_2O durch leichtes Erwärmen und ggf. mit Ultraschall klar gelöst.

Literatur

1 Pöhlmann, H.; Gulde, Ch.; Jahn, R.; Pfeifer, S.: Pharmazie 30, 709 (1975)
2 Kaneniwa, N.; Yamaguchi, T.; Watari, N.; Otsuka, M.: Yakugaku Zasshi 104 2, 184 (1984)
3 Arzneimittelwerk Dresden: DD 133 053 (8. 9. 77., 29. 11. 78.)
4 Dünnbier, U.; Jugelt, W.: Pharmazie 46, 512 (1991)
5 Reck, G.; Thiel, W.: ibid. 46, 509 (1991)
6 Geigy, Ag.: DAS 1 136 707 (19. 2. 58, 20. 9. 62)
7 Arzneimittelwerk Dresden, DD 260 696 (25. 5. 87., 5. 10. 88.)

Eingegangen am 25. Juli 1990

Dr. H. Wunderlich
Wilhelm-Pieck-Str. 35,
Radebeul 1,
O-8122

T9052

Analytisches Zentrum Berlin-Adlershof[1] und Arzneimittelwerk Dresden GmbH[2]

Kristallstrukturen der Addukte Carbamazepin-Ammoniumchlorid und Carbamazepin-Ammoniumbromid sowie deren Umwandlung in Carbamazepin-Dihydrat

G. RECK[1] und W. THIEL[2]

Die Addukte Carbamazepin-Ammoniumchlorid und Carbamazepin-Ammoniumbromid haben isomorphe Kristallstrukturen. In ihnen gibt es stabile Schichten, in denen die Wirkstoffmoleküle, Ammonium- und Chloridbzw. Bromidionen über 6 symmetrieunabhängige Wasserstoffbrücken miteinander verknüpft sind. In Wasser werden die Addukte durch eine topotaktische Reaktion vollständig in Carbamazepin-Dihydrat umgewandelt.

Crystal structures of the adducts carbamazepine-ammonium chloride and carbamazepine-ammonium bromide and their transformation in carbamazepine dihydrate

The adducts carbamazepine ammonium chloride and carbamazepin ammonium bromide have isomorphous crystal structures. Drug molecules, ammonium, and chloride (bromide) ions are connected by 6 symmetry independent hydrogen bonds forming stable layers in the crystal. In water the adducts are transformed completely to carbamazepine dihydrate by a topotactic reaction.

1. Einleitung

Der antiepileptische Wirkstoff 5H-Dibenz[b, f]-azepin-5-carboxamid (Carbamazepin, 1) bildet mit Ammoniumchlorid beim Umkristallisieren in Ethanol ein Addukt (2), das über 200 °C schmilzt und damit eine wesentlich höhere Schmelztemperatur als der reine Wirkstoff (189–193 °C) besitzt. Das IR-Spektrum zeigt eine deutliche Veränderung einiger Banden [1].

UM00012317
NOVARTIS EXHIBIT 1017
Novartis v. Regents, IPR2023-01346
Page 1063 of 4460

Da Ammoniumchlorid leicht mit Wasser ausgewaschen werden kann, wurde anfangs auf schwache Wechselwirkungen zwischen den Komponenten geschlossen. Das Kristallisat besteht aus filzartig verknüpften farblosen Kristallen sehr unterschiedlicher Dicke (überwiegend dünner als 0,005 mm).

Mit Hilfe der Einkristallstrukturanalyse sollte einerseits die Existenz eines Addukts nachgewiesen und andererseits die intra- und intermolekularen Wechselwirkungen im Kristall detailliert untersucht werden. Durch Pulverbeugungsaufnahmen sollte darüber hinaus gezeigt werden, daß das Addukt nur aus einer kristallinen Modifikation besteht. Analoge Untersuchungen wie bei 2 wurden auch für das Ammoniumbromid-Addukt (3) durchgeführt. Die Analysen zeigten, daß 2 und 3 isomorphe Kristallstrukturen haben.

2. Untersuchungen und Ergebnisse

2.1. Kristalldaten und Strukturbestimmung

Folgende Kristalldaten wurden von 2 und 3 ermittelt.

2: $C_{15}H_{12}N_2O$. NH_4Cl; monoklin $P2_1/n$; $a = 10{,}869(4)$, $b = 5{,}341(3)$, $c = 25{,}153(11)$ Å, $\beta = 100{,}90(3)°$; $Z = 4$; $D_c = 1{,}378$ g/cm³; MoK_α-Strahlung; 1772 Reflexe im Bereich $1{,}5 < \theta < 22°$, davon 1301 mit $I(hkl) > 0{,}5\sigma(I)$. R-Wert = 0,11 für 1301 Reflexe.

3: $C_{15}H_{12}N_2O$. NH_4Br; monoklin $P2_1/n$; $a = 11{,}051(3)$, $b = 5{,}464(2)$, $c = 24{,}928(9)$ Å, $\beta = 100{,}81(4)$; $Z = 4$; $D_c = 1{,}502$ g/cm³; MoK_α-Strahlung; 2036 Reflexe im Bereich $1{,}5 < \theta < 23°$; davon 1524 Reflexe mit $I(hkl) > \sigma(I)$. R-Wert = 0,053 für 1524 Reflexe.

Die für die Strukturanalysen erforderlichen Reflexintensitäten wurden auf einem ENRAF-NONIUS CAD-4-Diffraktometer gemessen. Alle strukturanalytischen Rechnungen wurden auf einem PDP 11/34-Minicomputer mit dem SDP ENRAF-NONIUS-Programmsystem durchgeführt.

Die Positionen aller Nichtwasserstoffatome von 2 konnten mit einer RANTAN-Prozedur in MULTAN-82[2] ermittelt werden. Die H-Atome wurden teilweise in Differenzfouriersynthesen lokalisiert; zum anderen Teil wurden ihre Positionen entsprechend den geometrischen Bedingungen berechnet. Die folgende least-squares Verfeinerung der Atomkoordinaten und anisotropen Temperaturfaktoren konvergierte mit R = 0,11. Dieser relativ hohe Wert ist auf die schlechte Kristallqualität zurückzuführen.

Die oben aufgeführten Kristalldaten sowie Weißenbergaufnahmen zeigten, daß die Kristallstrukturen von 2 und 3 isomorph sind. Die Atompositionen von 2 konnten deshalb auf 3 übertragen und anschließend mit least-squares-Rechnungen verfeinert werden. Die Verfeinerung konvergierte mit R = 0,053. Die resultierenden Parameter für 2 und 3 sind in Tabelle 1 aufgeführt.

Mit den ermittelten Atomparametern von 2 wurde ein Guinier-Pulverbeugungsdiagramm (Tabelle 2) berechnet. Die berechneten d-Werte und Intensitäten stimmen sehr gut mit den gemessenen d-Werten und visuell geschätzten Intensitäten einer Guinier-Filmaufnahme einer größeren Probenmenge überein. Damit wurde gezeigt, daß das Kristallisat keine weiteren kristallinen Formen enthält.

Tabelle 2 Pulverbeugungsdiagramme von 2 und 4

2 d(Å) calcd.	2 I calcd.	d(Å) exp.	I exp.	4 d(Å) calcd.	4 I calcd.	Probe 1* d(Å) exp.	Probe 1* I exp.	Probe 2** d(Å) exp.	Probe 2** I exp.
12,35	29	12,32	30	14,34	6	14,34	9	14,33	16
10,55	100	10,50	100	9,88	88	9,90	66	9,86	22
7,21	2	7,19	1	7,17	74	7,19	89	7,19	91
6,18	26	6,17	35	5,80	14	5,80	28	5,80	11
5,99	21	5,99	20	4,77	14	4,79	27	4,79	21
5,33	5	5,33	5	4,71	4	4,72	17	4,72	17
5,22	34	5,24	40	4,67	20	4,67	29	4,66	9
4,90	28	4,91	25	4,53	100	4,53	100	4,53	100
4,85	2	–	–	4,27	20	4,28	44	4,27	56
4,78	6	4,78	5	4,06	6	4,07	17	4,06	3
4,62	9	4,62	10	3,90	10	3,91	20	3,90	6
4,48	69	4,48	60	3,80	10	3,80	19	3,80	6
4,34	10	4,33	15	3,67	24	3,67	61	3,67	67
4,30	13	4,30	15	3,64	38	3,65	61	3,65	31
4,19	21	4,19	20	3,58	14	3,59	44	3,59	44
4,11	22	–	–	3,45	12	3,46	28	3,46	17
4,04	8	4,04	10	3,43	6	3,43	3	–	–
3,98	7	3,99	10	3,38	6	3,38	25	3,37	24
3,94	5	3,94	5	3,24	4	3,25	9	3,25	7
3,80	3	–	–	3,21	2	3,21	4	–	–
3,77	34	3,78	40	3,11	26	3,11	55	3,11	61
3,70	18	3,71	15	3,06	6	3,06	10	–	–
3,64	25	3,64	30	3,04	14	3,04	41	3,04	39
3,59	11	3,59	10						
3,55	3	–	–						
3,48	3	3,48	2						
3,43	20	3,43	20						

* Umwandlung von 1 in Dihydrat bei 20 °C
** Umwandlung von 1 in Dihydrat bei 100 °C

Tabelle 1 Atomkoordinaten ($\cdot 10^4$) von 2 und 3 (Standardabweichungen in Klammern)

Atom	2 x/a	2 y/b	2 z/c	3 x/a	3 y/b	3 z/c
Cl1, Br1	8583(2)	2004(6)	4349(1)	8584(1)	1907(2)	4294(1)
O18	11259(5)	−2862(10)	316(2)	11258(4)	−2916(10)	300(2)
N1A	13558(7)	−2071(20)	21(4)	13507(4)	−2002(10)	29(3)
N15	10866(6)	−558(10)	1003(3)	10848(5)	−598(10)	1003(2)
N17	9325(6)	−2851(20)	459(3)	9331(5)	−2916(10)	464(2)
C1	9214(9)	1756(20)	1289(4)	9195(7)	1680(20)	1305(3)
C2	8391(9)	2142(20)	1643(4)	8427(7)	2052(20)	1668(4)
C3	8468(10)	726(20)	2083(4)	8513(7)	582(20)	2117(4)
C4	9351(9)	−1222(20)	2194(4)	9392(8)	−1226(20)	2209(3)
C5	11135(9)	−3473(20)	1984(4)	11168(8)	−3485(20)	1979(3)
C6	12294(10)	−3553(20)	1851(4)	12283(7)	−3486(20)	1847(3)
C7	14173(9)	−1360(20)	1675(4)	14101(7)	−1247(20)	1672(3)
C8	14736(8)	570(20)	1434(4)	14626(7)	650(20)	1427(3)
C9	14039(8)	2116(20)	1080(4)	13916(7)	2198(20)	1074(4)
C10	12738(9)	1741(20)	949(4)	12666(7)	1826(20)	945(3)
C11	12171(8)	−99(20)	1176(4)	12142(6)	−101(10)	1174(3)
C12	12872(8)	1688(20)	1567(4)	12837(7)	−1619(20)	1560(3)
C13	10206(8)	−1552(20)	1843(4)	10205(7)	−1630(20)	1856(3)
C14	10098(7)	−135(20)	1384(3)	10071(6)	−135(10)	1394(3)
C16	10480(6)	−2171(20)	591(3)	10503(6)	−2203(10)	570(3)

UM00012318
NOVARTIS EXHIBIT 1017
Novartis v. Regents, IPR2023-01346
Page 1064 of 4460

2.2. Molekülstrukturen von 2 und 3

Abbildung 1 zeigt eine Stereodarstellung eines 1-Moleküls von 2 bzw. von 3. Wegen der wesentlich höheren Genauigkeit sind in Abb. 2 nur die Bindungsabstände und -winkel von 3 aufgeführt. Alle Werte stimmen gut mit entsprechenden Werten des reinen 1 [3, 4] und des 1-Dihydrats (4) [5] überein.

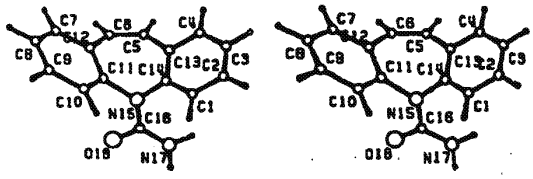


Abb. 1. Stereodarstellung eines Carbamazepinmoleküls

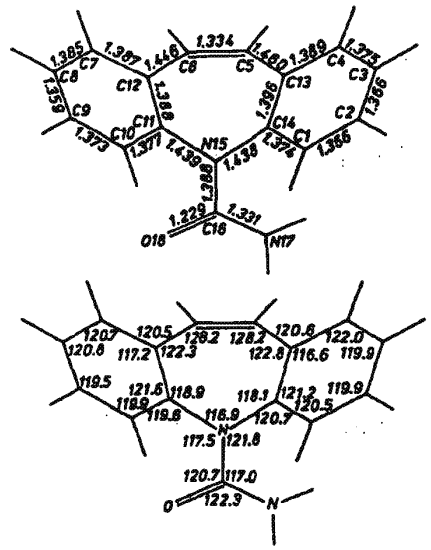


Abb. 2. Bindungsabstände und -winkel eines Carbamazepinmoleküls in 3 (mittlere Standardabweichungen 0,008 Å bzw. 0,5°)

Der zentrale Azepinring besitzt eine Boot-Konformation bezüglich der Ebene C11, C12, C13, C14. Die Ebenen C1, C2, C3, C4, C13, C14, C5, N15 und N15, C11, C10, C9, C8, C7, C12, C6 bilden in 2 und in 3 einen Dihedralwinkel von 128°. Die Atome O18, N17, C16 und N15 bilden eine Ebene, die im Vergleich zur Ebene C16, N15, C14, C11 um die Bindung N15-C16 um 6,5° bzw. 6,8° verdreht ist. Diese Werte stimmen sehr gut mit dem von Himes [2] ermittelten Winkel (6,0°) im solvatfreien 1 überein.

2.3. Intermolekulare Wechselwirkungen

Wie bereits oben erwähnt, sind 2 und 3 isomorph, d. h. die Position von Cl^- in 2 wird in 3 von Br^- eingenommen. Alle anderen Atompositionen sind mit geringen Abweichungen in beiden Strukturen gleich.
Abb. 3 zeigt die Anordnung der Carbamazepinmoleküle (einige nicht vollständig dargestellt), Cl(Br)- und NH_4-Ionen im Kristall. In der Kristallstruktur gibt es 6 symmetrieunabhängige Wasserstoffbrücken (Tabelle 3). Durch diese und die symmetrieäquivalenten Bindungen werden die Komponenten zu Schichten parallel zur x,y-Ebene verknüpft. Jeweils zwei Wirkstoffmoleküle bilden, verbunden über zwei N–H ... O-Brücken zwischen den Carboxamidgruppen, ein zentrosymmetrisches Dimer. Diese Anordnung wurde sowohl im solvatfreien 1 [3, 4] als auch im 4 [5] beobachtet.

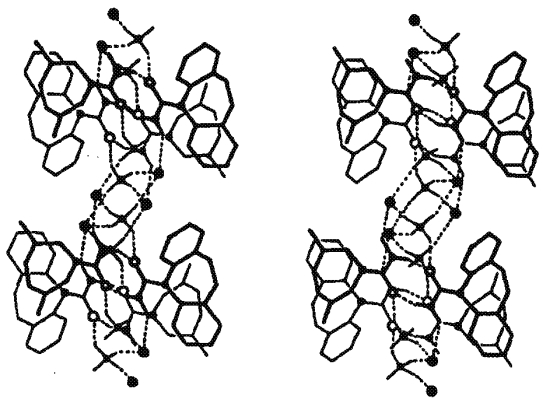


Abb. 3. Verknüpfung der Carbamazepinmoleküle, NH_4- und Cl- bzw. Br-Ionen im Kristall (Stereodarstellung)

Tabelle 3 Wasserstoffbrücken A–H ... B in 2 und 3

Atom A	Atom B	2 d(A–B) (Å)		3 d(H–B)		symm. f. B
N17	O18	2,997	2,963	2,01	1,96	2 – x; –1 – y; –z
N1A	O18	2,770	2,741	1,83	1,86	x; y; z
N17	Cl1, Br1	3,287	3,387	2,46	2,59	1,5 – x; – 0,5 + y; 0,5 – z
Cl1, Br1	N1A	3,133	3,256	2,14	2,38	–0,5 + x; 0,5 – y; 0,5 + z
Cl1, Br1	N1A	3,193	3,342	2,21	2,39	–0,5 + x; –0,5 – y; 0,5 + z
Cl1, Br1	N1A	3,247	3,392	2,27	2,58	2,5 – x; 0,5 + y; 0,5 – z

Jedes Cl(Br)-Ion ist Protonenakzeptor für vier Wasserstoffbrükken, eine zum N-Atom der Carboxamidgruppe, drei weitere zu benachbarten NH_4-Ionen. Dagegen ist jedes NH_4-Ion Protonendonator für ebenfalls vier H-Brückenbindungen, eine zum C-Atom der Carboxamidgruppe, drei zu benachbarten Cl-Ionen. Diese Brücken verbinden mittelbar die Dimere. Dadurch entstehen die bereits oben erwähnten Molekülschichten im Kristall.
Abb. 4a zeigt eine übersichtliche Darstellung des Wasserstoffbrückensystems von 2 bzw. 3, indem nur die Gruppen gezeichnet wurden, die an den H-Bindungen beteiligt sind. Die Schichten sind parallel zur Zeichenebene dargestellt. In der Mitte der Abbildung erkennt man deutlich die bandartige Anordnung von Cl(Br)- und NH_4-Ionen.

2.4. Transformation von Carbamazepin-Ammoniumchlorid in Carbamazepin-Dihydrat

Zwischen den Kristallstrukturen von 2 und 4 gibt es eine enge Beziehung. Abb. 4b zeigt das Wasserstoffbrückensystem des Dihydrats. Auch in dieser Struktur wurden Molekülschichten gebildet, in denen Dimere über die Wassermoleküle verknüpft sind. Im Kristall gibt es zwei symmetrieunabhängige Wassermoleküle, von denen jedes vier Wasserstoffbrücken bildet. Die Verwandtschaft beider Strukturen wird deutlich, wenn man Cl^-

UM00012319
NOVARTIS EXHIBIT 1017
Novartis v. Regents, IPR2023-01346
Page 1065 of 4460

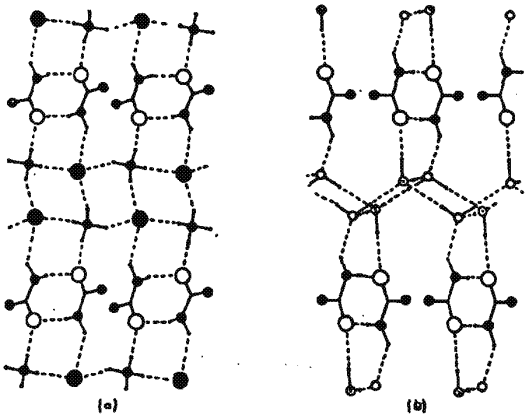


Abb. 4. Darstellung der Wasserstoffbrücken in 3 (a) und Carbamazepin Dihydrat (b). Der besseren Übersicht wegen sind von den Wirkstoffmolekülen nur die Carboxamidgruppen dargestellt.

durch das erste und NH_4^+ durch das zweite Wassermolekül ersetzt. Während in 2 aber Chlorid ausschließlich Donator ist, fungiert jedes Wassermolekül im Dihydrat sowohl als Akzeptor als auch als Donator. Im Detail ergeben sich dadurch etwas andere Verknüpfungen, die zu einer gegenseitigen Verschiebung der 1-Ketten im Dihydrat im Vergleich zu 2 führen.

Wie oben erwähnt, läßt sich Ammoniumchlorid mit Wasser sehr leicht aus dem Kristallisat auswaschen. Die enge strukturelle Verwandtschaft von Dihydrat und 2 gibt hierfür eine Erklärung. Die Wassermoleküle bilden wesentlich stärkere Wasserstoffbrücken als Chlorid und Ammonium, so daß deren Ersatz durch Wasser verständlich ist. Um diesen Austausch experimentell zu beweisen, wurde der Einkristall, der für die Strukturanalyse verwendet wurde, 3 h in Wasser getaucht. Danach angefertigte Schwenk- und Weißenbergaufnahmen zeigten, daß aus dem 2-Einkristall ein 4-Einkristall entstanden war. Topotaktische Reaktionen mit Stoffaustausch sind in der organischen Chemie sehr selten. Die Umwandlung von 2 in 4 wurde auch mit einer größeren Kristallpulvermenge (einige mg) und 5 ml Wasser bei Raumtemperatur wiederholt. Der Vergleich einer experimentellen Guinier-Pulveraufnahme mit einem berechneten Diagramm, zeigte einen vollständigen Übergang zum Dihydrat. Das gleiche gilt auch für eine zweite Probe, bei der 5 g 2 mit 150 ml dest. Wasser unter Zusatz von 2 Tropfen eines Geschirrspülmittels 2 h im siedenen Wasserbad gerührt und anschließend im kalten Wasserbad 2 h auskristallisiert wurde. Auch dieses Kristallisat erwies sich als reines 4.

In Tabelle 2 werden beide experimentellen Diagramme mit dem theoretischen verglichen. Unterschiede in den experimentellen Intensitäten sind auf Texturerscheinungen und evtl. auf die Fehlordnungserscheinungen im Dihydrat [5] zurückzuführen.

Literatur

1 Wunderlich, H.; Zenker, L.; Stark, A.; Lohmann, D.; Usbeck, H.; Thiel, W.: Pharmazie 46, (1991)
2 Main, P.; Fiske, S. J.; Hull, S. E.; Lessinger, L.; Germain, G.; Declercq, J. P.; Woolfson, M.; MULTAN-82 – A System of Computer Programs for the Automatic Solution of Crystal Structures from X-ray Diffraction Data
3 Reboul, J. P.; Cristau, B.; Soyfer, J. C.: Acta Cryst. B37, 1844 (1981)
4 Himes, V. L.; Mighell, A. D.; de Camp, W. H.: ibid. B37, 2242 (1981)
5 Reck, G.; Dietz, G.: Cryst. Res. Technol. 21, 1463 (1986)

Eingegangen am 25. Juli 1990

Dr. G. Reck
Rudower Chaussee 5
O-1199 Berlin

Fachbereich Chemie – Institut für Organische Chemie – Humboldt-Universität zu Berlin

Elektrochemische Reduktion von 5H-Dibenz[b,f]azepin-Derivaten

6. Mitteilung[1]: Kathodisches Verhalten von Carbamazepin-Ammoniumhalogenid-Addukten

U. DÜNNBIER und W. JUGELT

In Fortführung von Untersuchungen zum elektrochemischen Verhalten des Antiepileptikums Carbamazepin (1,5-Carbamoyl-5H-dibenz[b,f]azepin, Finlepsin®, Tegretol®) wird die kathodische Reduktion von Carbamazepin-Ammoniumchlorid- bzw. -Ammoniumbromid-Additionsverbindungen 2a, 2b beschrieben. Beobachtet wird die indirekte Hydrierung der C,C-Doppelbindung der 1-Komponente von 2 zu 10,11-Dihydrocarbamazepin durch bei der Reduktion der Ammoniumionen an der Quecksilber-Kathode gebildetes Ammoniumamalgam. Diese Reaktion ist auf andere 5H-Dibenz[b,f]azepin-Derivate und phenylsubstituierte Ethene übertragbar. Neben der mechanistischen Klärung dieser indirekten Reduktion wird ihre Anwendung auf die quantitative Analyse von 1-Ammoniumhalogenid-Gemischen gezeigt, die für die Kontrolle des Herstellungsprozesses, die analytische Charakterisierung und Reinheitsprüfung von 2 eingesetzt werden kann.

Electrochemical reduction of 5H-dibenz[b,f]azepine derivatives Part 5: Cathodic behaviour of carbamazepine-ammonium halide addition compounds

In connection with the electrochemical behaviour of the drug carbamazepine (1,5-carbamoyl-5H-dibenz[b,f]azepine, Finlepsin®, Tegretol®) an information on the cathodic reduction of 1-ammonium chloride and 1-ammonium bromide addition compound 2a, 2b, respectively, is given. The electrochemical conversion of the 1 component of 2 into 10,11-dihydrocarbamazepine is the result of indirect hydrogenation of the C,C-double bond by ammonium amalgam, produced at the mercury cathode. The indirect hydrogenation was also observed for other 5H-dibenz[b,f]azepine derivatives and for phenyl substituted ethylenes. On the basis of electroanalytical and electropreparative results the mechanism of the indirect cathodic hydrogenation by ammonium amalgam is discussed. This reaction can be used for analyt-

UM00012320

NOVARTIS EXHIBIT 1017
Novartis v. Regents, IPR2023-01346
Page 1066 of 4460

This Page is Inserted by IFW Indexing and Scanning Operations and is not part of the Official Record

BEST AVAILABLE IMAGES

Defective images within this document are accurate representations of the original documents submitted by the applicant.

Defects in the images include but are not limited to the items checked:

- ☐ BLACK BORDERS
- ☐ IMAGE CUT OFF AT TOP, BOTTOM OR SIDES
- ☐ FADED TEXT OR DRAWING
- ☐ BLURRED OR ILLEGIBLE TEXT OR DRAWING
- ☐ SKEWED/SLANTED IMAGES
- ☐ COLOR OR BLACK AND WHITE PHOTOGRAPHS
- ☐ GRAY SCALE DOCUMENTS
- ☐ LINES OR MARKS ON ORIGINAL DOCUMENT
- ☐ REFERENCE(S) OR EXHIBIT(S) SUBMITTED ARE POOR QUALITY
- ☐ OTHER: _____

IMAGES ARE BEST AVAILABLE COPY.
As rescanning these documents will not correct the image problems checked, please do not report these problems to the IFW Image Problem Mailbox.

[Translator's Note: The first portion of page 633 is the concluding part of the preceding paper]

"*Solubilization of aminophenazone*"

Arch. Pharm. (Weinheim) *315*, 633-641 (1982)

On the solubilization of aminophenazone by thiourea

Helmut Wiedenfeld[*)**)], Armin Kirfel[***)] and Gabriel Koop[***)]

[**)] Pharmaceutical Institute of the University, An der Immenburg 4, D-5300 Bonn-Endenich
[***)] Mineralogical Institute of the University, Poppelsdorfer Schloss, D-5300 Bonn-Poppelsdorf

Received on August 14, 1982

The nature of the complex formed from aminophenazone and thiourea was determined by X-ray analysis.

[printer's code number]

© Verlag Chemie GmbH, Weinheim 1982

Thiourea is a commonly used solubilizer for many medicinal drugs even though this substance has been under suspicion for a long time in regard to its possible carcinogenicity[1,2,3]. In the case of solubilization by thiourea, the nature and stability of the compounds that are produced are of importance in order to be able to evaluate any possible change in activity.

It is therefore of interest to be familiar with the physical properties and the chemical structure of the complexes with thiourea.

The assembly and structure of such a compound will be elucidated using the example of the solubilization of aminophenazone by thiourea.

It is known that thiourea and aminophenazone form a complex that is capable of being crystallized. This complex exhibits distinctly changed properties relative to the starting compounds: thus, in addition to its changed dissolution characteristics in water, its melting point of 140 °C is also markedly different from that of thiourea, namely 177 °C, and from that of aminophenazone, namely 108 °C.

Rohdewald was able to determine the stoichiometric composition of this complex, namely 3 parts of thiourea to 1 part of aminophenazone, by means of elemental analysis[4]. As a consequence of interpreting the IR spectra, he came to the conclusion that there are indications that point to the presence of an inclusion compound. The change in the N-H valence vibration, the N-H deformation vibration, the C=O valence vibration and the C-N deformation vibration appears to substantiate this view. However, an interesting aspect in this connection is that the complex is capable of being crystallized, with an identical composition and with an identical structure, from water and also from acetone, methanol or ethanol. This fact contradicts the theory of a simple inclusion compound.

Schlenk and *Lenné* investigated various thiourea complexes and found that thiourea participates in the formation of channel inclusion compounds with many organic compounds[5,6]. In this connection, the size of the included molecule is limited by the channel length. The authors demonstrated this via the formation of thiourea complexes with various types of hydrocarbons.

In the present case, however, doubts seemed to arise in regard to a channel inclusion compound because of the size and spatial structure of the aminophenazone. Rotation crystal photographs, which ought to elucidate the structure of the complex in a definitive manner, did not meet with success since no conclusions could be drawn in regard to the optical axes of the unit cell[4]. Since an unambiguous elucidation of the complex was still unavailable at this point in time, a more modern approach to this problem was put into effect.

Results and discussion

The material for the present investigations was recrystallized from water. Clear, octahedral crystal plates were obtained.

^{13}C-NMR spectroscopy was intended to generate initial indications regarding the nature of the complex. Special attention was paid in this connection to the chemical shifts of the carbons in the C=O group of the aminophenazone and in the C=S group of the thiourea; this was because these carbons would be

affected, in terms of their chemical shift, by the presence of chemical bonds or hydrogen bridges in the event of complex formation. However, it was found that no change in the expected signal positions arose relative to the starting compound; only a paramagnetic shift took place in the aromatic region. Table 1 gives a comparison of the ^{13}C-NMR data. The assignment took place via the interpretation of the coupled and noise-decoupled spectra.

Table 1: *^{13}C-NMR data for aminophenazone and complex*

δ = ppm of pyramidone	Carbon	δ = ppm of complex	δ = ppm of pyramidone	Carbon	δ = ppm of complex
10.00	7	10.48	125.52	14	129.86
36.48	6	34.86	128.89	13 / 15	130.89
43.57	9 / 10	44.57	135.52	11	134.03
122.57	4	119.89	150.96	3	149.31
122.71	12 / 16	127.57	162.84	5	163.39
-			-	17 / 18 / 19	183.26

This result points to a compound that is not held together by chemical bonds but, rather, that has been produced on the basis of a special spatial arrangement, whereby the high stability of the complex compound appears to be worthy of note. An important aspect is also the fact that hydrogen bridges could not be inferred from the spectroscopic data.

A simple indication of the structure of the complex is given by the fact that the crystals can be cleaved only with great difficulty, or not at all, perpendicularly to the crystal surface, whereas, by contrast, this takes place successfully and without effort in the direction of the surface. This permits one to infer a layer-like structure and not a channel-like structure.

In order to obtain final elucidation of the structure, an x-ray structural analysis was carried out on a naturally grown crystal.

Since optical orientation of the crystal was not possible, a preliminary x-ray examination was dispensed with and the measurements were all undertaken using a four circle diffractometer. The crystal system was established by means of crystal diffractometry as triclinic with the angles $\alpha = 69.55°$, $\beta = 83.55°$ and $\gamma = 75.33°$; the lattice constants were a = 9.378 Å, b = 11.724 Å and c = 11.880 Å. The space group is P1 = $\sqrt{C^1_i}$.

This triclinic type of crystal and its space group might also have been the reason for our failures in the rotation crystal photographs[4]. Following structure refinement and an evaluation of the analysis, it was found that the thiourea molecules are mutually connected in a network-like manner by means of N-H-S bridges of differing strength and that the molecules form layers that are oriented one above the other. The aminophenazone molecules, which are connected to the thioureas by N-H-O bridges, are located

between these layers. The ratio of 3:1 for thiourea and aminophenazone, which had already been ascertained, arises in this way.

Fig. 1 illustrates the cross-linking arrangement. The relative heights are appended in parentheses in order to provide a three-dimensional illustration. The free numbers indicate the numbering of the heavy atoms. The bond lengths of the H-S bridges differ. The individual values are listed in Table 2.

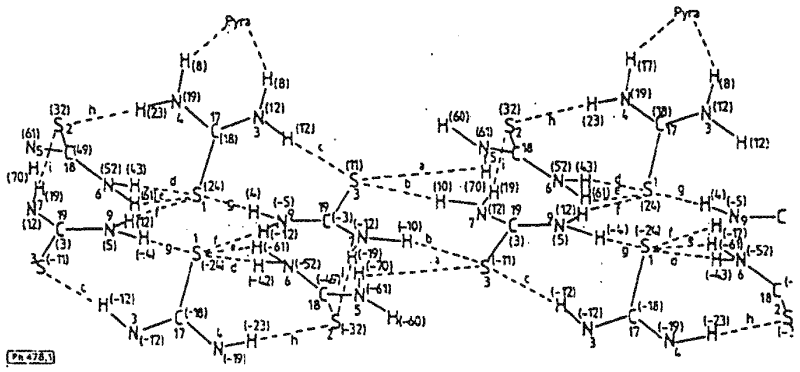


Fig. 1: Cross-linking of the complex

Table 2: *Bond lengths of the sulfur-hydrogen bridges* (Å)

a	2.55	f	2.62
b	2.40	g	2.40
c	2.41	h	2.46
d	2.51	i	2.48
e	2.71		

Fig. 2 illustrates the bond lengths and Fig. 3 illustrates the angles in the aminophenazone.

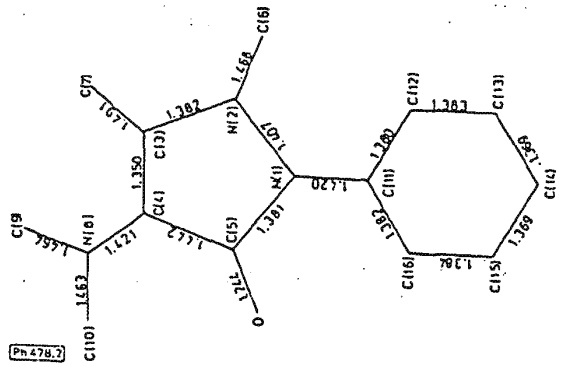


Fig. 2: Bond lengths in the aminophenazone (Å)

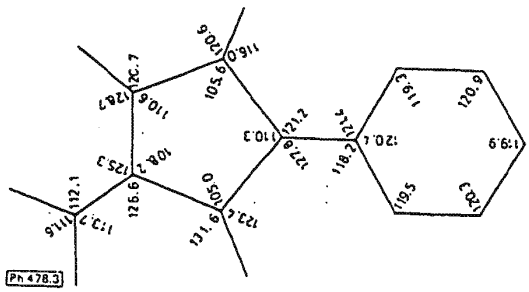


Fig 3: Angles in the aminophenazone (°)

Fig. 4 shows the same for the three thioureas. The N-H-O bridges from the thiourea to the carbonyl group of the aminophenazone are also of differing length: the length amounts to 2.43 Å for the N3-H and 1.96 Å for the N4-H.

A noteworthy feature is that, despite the presence of these hydrogen bridges, which exhibit normal lengths, the C=O and the C=S bond lengths also lie in the normal range; the latter could already be expected in accordance with the result of ^{13}C-NMR spectroscopy. Widening of the carbonyl bond in question can otherwise usually be expected in the case of hydrogen bridges.

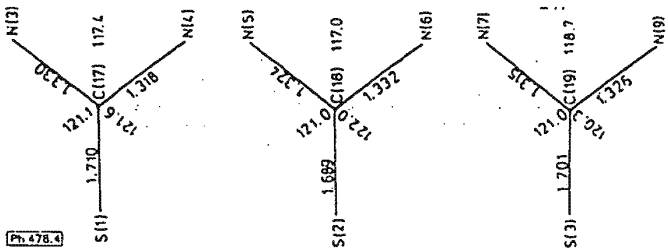


Fig. 4: Lengths (Å) and angles (°) in the three thioureas

A three dimensional network is linked via these hydrogen bridges, which differ in nature, with the aminophenazone molecules in the cavities. This arrangement progresses to the crystal surface in a step-wise manner.

11 hydrogen bridges are to be found in each asymmetrical unit, whereby these hydrogen bridges bring about the change in physical and chemical properties and lead to a stable complex compound with the structure that has been described.

The absolute configuration and arrangement of three thioureas and one aminophenazone in the unit cell can be seen in Fig. 5 in the ORTEP illustration[7].

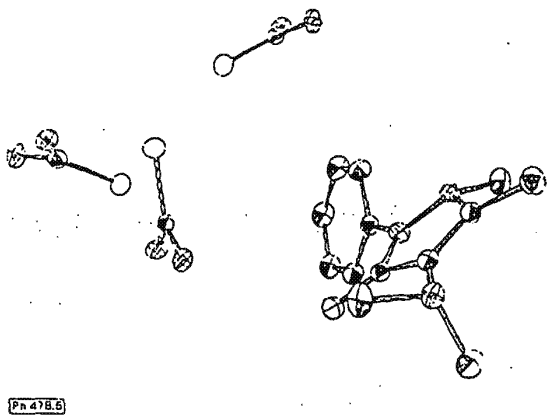


Fig. 5: ORTEP illustration of the complex

Table 3: *Atomic coordinates* (10^4)

Atom	x/a (δ)	y/b (δ)	z/c (δ)
C3	-3963(2)	2610(2)	11944(2)
C4	-3277(2)	3335(2)	12204(2)
C5	-2437(2)	3923(2)	11132(2)
C6	-4857(3)	2709(3)	10022(2)
C7	-4959(3)	1835(2)	12742(2)
C9	-4286(2)	4680(2)	13350(2)
C10	-1819(3)	3382(3)	13762(2)
C11	-2248(2)	3770(2)	9059(2)
C12	-1815(2)	2833(2)	8557(2)
C13	-1361(3)	3136(2)	7362(2)
C14	-1293(3)	4337(3)	6690(2)
C15	-1683(3)	5257(2)	7201(2)
C16	-2181(2)	4985(2)	8386(2)
C17	1790(2)	2286(2)	9629(2)
C18	4927(2)	1717(2)	6540(2)
C19	-304(2)	42(2)	2975(2)
O	-1558(2)	4609(1)	10950(1)
S1	2408(1)	722(0)	9854(0)
S2	3211(1)	2482(0)	6047(1)
S3	1058(1)	614(1)	3264(0)
N1	-2805(2)	3526(1)	10260(1)
N2	-3673(2)	2642(1)	10768(1)
N3	1226(2)	2696(2)	10534(2)
N4	1876(2)	3133(2)	8562(2)
N5	6088(2)	1791(2)	5795(2)
N6	5180(2)	1025(2)	7688(2)
N7	-1230(2)	-414(2)	3831(2)

NOVARTIS EXHIBIT 1017
Novartis v. Regents, IPR2023-01346
Page 1073 of 4460

Table 3: Continuation

Atom	x/a (δ)	y/b (δ)	z/c (δ)
N8	−3273(2)	3508(2)	13334(1)
N9	−460(2)	60(2)	1873(2)
H1N6	608(2)	59(2)	793(2)
H2N6	436(3)	91(2)	821(2)
H1N7	−104(3)	−50(2)	468(2)
H2N7	−191(3)	−81(2)	372(2)
H1N9	−113(2)	−23(2)	171(2)
H2N9	39(3)	26(3)	123(3)
H1C6	−538(3)	204(2)	1048(2)
H2C6	−454(2)	269(2)	928(2)
H3C6	−559(3)	355(2)	990(2)
H1C7	−464(3)	103(3)	1278(2)
H2C7	−505(3)	189(2)	1348(2)
H3C7	−606	204	1245
H1C9	−431(3)	471(2)	1420(2)
H2C9	−395(3)	550(2)	1284(2)
H3C9	−526(3)	468(2)	1318(2)
H1C10	−116(3)	259(3)	1382(2)
H2C10	−192(2)	341(2)	1456(2)
H3C10	−122(3)	403(2)	1329(2)
HC12	−185(2)	199(2)	902(2)
HC13	−103(2)	247(2)	701(2)
HC14	−95(2)	455(2)	583(2)
HC15	−156(2)	608(2)	675(2)
H1N3	81(2)	349(2)	−961(2)
H2N3	117(2)	210(2)	−873(2)
H1N4	170(2)	395(2)	853(2)
H2N4	226(2)	288(2)	792(2)
H1N5	690(3)	136(2)	603(2)
H2N5	601(3)	229(2)	490(3)

Measured data, structure elucidation and refinement

The complex compound was prepared in accordance with the procedure that has been described by *Rohdewald*, and then it was recrystallized from water[4]. The solvent for the ^{13}C-NMR spectroscopy was d_6-DMSO; internal standard: TMS. The spectrum was measured using a Bruker WH 90 at 22.63 MHz.

In order to carry out the x-ray structural analysis, the intensities of 4356 reflections from an approximately 0.25 x 0.3 mm sample were measured in the ω mode of an automatic Syntex $P2_1$ four circle diffractometer; graphite monochromator MoK_α (λ = 0.7107 Å).

Elucidation of the structure took place using the MULTAN 78[8] computer program. Refinement of the structure was achieved via anisotropic temperature factors for the heavy atoms[9]. The positions of the hydrogens was established via differential analysis of the densities. The temperature factor for a hydrogen, which is difficult to determine, was fixed at B = 3.0 Å.

A weighting arrangement was used on the basis of W = 2.88 for /F/ > 20.0 and W = 0.144 x F^2 for /F/ ≥ 20.0.

The R and R_w values that were ultimately observed were R = 0.045 and 0.033 (omitting unobserved), and R_w = 0.027 and 0.026 (o.u. [omitting unobserved]).

Table 4: *Temperature factors* (10^3)

Atom	U_{11}	U_{22}	U_{33}	U_{12}	U_{13}	U_{23}
C3	42(1)	42(1)	45(1)	−15(1)	2(1)	−14(1)
C4	39(1)	42(1)	39(1)	−13(1)	2(1)	−15(1)
C5	38(1)	38(1)	43(1)	−11(1)	0(1)	18(1)
C6	54(1)	85(1)	58(1)	−31(1)	−4(1)	−31(1)
C7	67(2)	69(2)	63(1)	−9(1)	11(1)	−22(1)
C9	64(2)	74(2)	66(2)	−16(1)	8(1)	40(1)
C10	58(2)	98(2)	50(1)	−28(2)	−4(1)	28(1)
C11	37(1)	49(1)	40(1)	−13(1)	−1(1)	18(1)
C12	58(1)	50(1)	51(1)	−11(1)	−4(1)	−22(1)
C13	68(2)	72(2)	53(1)	−9(1)	2(1)	−37(1)
C14	67(2)	90(2)	41(1)	−24(1)	3(1)	−23(1)
C15	64(2)	65(2)	49(1)	−14(1)	0(1)	−9(1)
C16	52(1)	49(1)	49(1)	−14(1)	−1(1)	−19(1)
C17	35(1)	45(1)	45(1)	−15(1)	−5(1)	−16(1)
C18	59(1)	47(1)	46(1)	−21(1)	−3(1)	−17(1)
C19	51(1)	49(1)	49(1)	−9(1)	−5(1)	−17(1)
O	57(1)	52(1)	48(1)	−31(1)	8(1)	−24(1)
S1	57(0)	39(0)	40(0)	−12(0)	−1(0)	−12(0)
S2	58(0)	63(0)	47(0)	−15(0)	−7(0)	14(0)
S3	61(0)	75(0)	43(0)	−30(0)	−1(0)	−20(0)
N1	48(1)	46(1)	40(1)	−22(1)	4(1)	−20(1)
N2	44(1)	47(1)	49(1)	−23(1)	−1(1)	−18(1)
N3	61(1)	45(1)	48(1)	−14(1)	4(1)	−19(1)
N4	65(1)	41(1)	43(1)	−15(1)	−2(1)	−11(1)
N5	55(1)	90(2)	55(1)	−17(1)	4(1)	−8(1)
N6	57(1)	58(1)	44(1)	−12(1)	−4(1)	−10(1)
N7	68(1)	97(2)	55(1)	−46(1)	6(1)	−26(1)
N8	47(1)	55(1)	41(1)	−20(1)	3(1)	21(1)
N9	66(1)	77(1)	52(1)	−28(1)	−6(1)	−29(1)

Table 4: Continuation

HC12	1.2(4)	H2N3	1.9(5)
HC13	3.2(5)	H1N4	3.6(6)
HC14	3.2(5)	H2N4	3.3(6)
HC15	4.1(6)	H1N5	3.4(6)
H1C6	4.1(6)	H2N5	6.3(8)
H2C6	3.4(6)	H1N6	1.6(5)
H3C6	5.2(7)	H2N6	3.4(6)
H1C9	4.8(6)	H1N7	5.1(7)
H2C9	4.8(7)	H2N7	4.1(6)
H3C9	3.2(5)	H1N9	2.7(6)
H1C10	5.8(8)	H2N9	7.5(8)
H2C10	3.7(6)	H1C7	6.5(8)
H3C10	5.0(7)	H2C7	4.8(8)
H1N3	2.8(6)	H3C7	3.0

UM00012329
NOVARTIS EXHIBIT 1017
Novartis v. Regents, IPR2023-01346
Page 1075 of 4460

Literature

[Translated references]:

1 H. Sucker, P. Fuchs and P. Speiser, Pharmazeutische Technologie ["Pharmaceutical Technology"], page 238, Georg Thieme Verlag, Stuttgart 1978.

2 R. Voigt, Lehrbuch der Pharmazeutischen Technologie ["Textbook of Pharmaceutical Technology"], page 487, Verlag Chemie, Weinheim - New York 1979.

3 A.N. Martin, J. Swarbrick and A. Camarata, Physikalische Pharmazie ["Physical Pharmacy"], page 322, Wissenschaftliche Verlagsgesellschaft, Stuttgart 1975.

4 P. Rohdewald, Unpublished Results.

References

1 H. Sucker, P. Fuchs und P. Speiser, Pharmazeutische Technologie, S. 238, Georg Thieme Verlag, Stuttgart 1978.
2 R. Voigt, Lehrbuch der Pharmazeutischen Technologie, S. 487, Verlag Chemie, Weinheim – New York 1979.
3 A.N. Martin, J. Swarbrick und A. Camarata, Physikalische Pharmazie, S. 322, Wissenschaftliche Verlagsgesellschaft, Stuttgart 1975.
4 P. Rohdewald, Unveröffentlichte Ergebnisse.
5 W. Schlenk, Experientia *6*, 292 (1950).
W. Schlenk, Justus Liebigs Ann. Chem. *573*, 142 (1952).
6 H.U. Lenné, Z. Kristallogr. Kristallgeom. Kristallphys. Kristallchem. *118*, 439 (1963).
H.U. Lenné, ebenda *118*, 454 (1963).
H.U. Lenné, ebenda *118*, 468 (1963).
7 C. K. Johnson, Oak-Ridge Nat. Lab. Report, ORNL-3794, 1965.
8 G. Germain, P. Main and M. M. Woolfson, Acta Crystallogr. *A27*, 368 (1971).
9 W. H. Zachariasen, Acta Crystallogr. *16*, 1139 (1963).

[Translator: the last portion of page 641 is the beginning part of the next paper]

T9051

Nach Abziehen des Lösungsmittels i.Vak. violettfarbene, luftempfindliche, mikrokristalline Substanz. – Ausb. 28 mg (23 %). – Schmp. 216–220 ° (Zers.). – $C_{27}H_{20}OS_4$ Ber. 488.0411, Gef. 488.0404 (ms). – IR (KBr): 3000, 2920, 2860 (CH); 1580, 1585 (C=C); 1490, 1460 (C=C); 1300, 1260, 1030 (S=O); 890, 870, 850, 800, 745 cm^{-1} (C–H, C–C). – UV/VIS (CH_2Cl_2): λ_{max} (lgε) = 264 (4.36, Sch); 525 nm (4.34). – UV/VIS (CH_3CN): λ_{max} (lgε) = 228 (4.69, Sch); 241 (4.63, Sch); 281 (4.33, Sch); 512 nm (4.31). – ^{1}H-NMR (90 MHz, CD_2Cl_2): δ (ppm) = 1.55 (s, 2H, CH_2); 2.32 (s, 3H, CH_3-b); 2.41 (s, 3H, CH_3-a); 6.09–6.59; 6.94–7.87 (2m, 12H, olefinische u. arom. H). –

Literatur

1 5. Mitt.: R. Neidlein und H. Zeiner, Chem. Ber. *115*, 1409 (1982).
2 Nach Vorträgen von R. Neidlein 1981 an den Departments of Chemistry der Universitäten in Düsseldorf, Haifa, Graz, Jerusalem, Tel-Aviv, Wien, anläßlich der wissenschaftlichen Hauptversammlung der Österreichischen Pharmazeutischen Gesellschaft, beim „2nd European Symposium on Organic Chemistry, Stresa/Italien", „8th International Congress of Heterocyclic Chemistry, Graz", „4th International Symposium on the Chemistry of Novel Aromatic Compounds, Jerusalem" (ISNA IV).
3 Dissertation *H. Zeiner*, Heidelberg 1981.
4 R. Neidlein und H. Zeiner, Angew. Chem. *93*, 1117 (1981); Angew. Chem., Int. Ed. Engl. *20*, 1032 (1981).
5 R. Neidlein und H. Zeiner, Heterocycles *16*, 641 (1981).
6 R. Neidlein und H. Zeiner, Angew. Chem. *92*, 199 (1980); Angew. Chem., Int.Ed.Engl. *19*, 204 (1980).
7 R. Neidlein und H. Zeiner, Arch. Pharm. (Weinheim) *313*, 970, (1980).
8 G. Cimino, S. DeStefano, L. Minale und E. Trivellone, Experientia *34*, 1425 (1978).

[Ph 477]

Arch. Pharm. (Weinheim) *315*, 633–641 (1982)

Zur Frage der Lösungsvermittlung von Aminophenazon durch Thioharnstoff

Helmut Wiedenfeld*)**), Armin Kirfel***) und Gabriele Koop***)

**) Pharmazeutisches Institut der Universität, An der Immenburg 4, D-5300 Bonn-Endenich,
***) Mineralogisches Institut der Universität, Poppelsdorfer Schloß, D-5300 Bonn-Poppelsdorf
Eingegangen am 14. August 1981

Durch Röntgenstrukturanalyse wird die Komplexverbindung zwischen Aminophenazon und Thioharnstoff aufgeklärt.

On the Solubilisation of Aminophenazone by Thiourea

The nature of the complex formed from aminophenazone and thiourea was determined by X-ray analysis.

0365-6233/82/0707-0633 $ 02.50/0

© Verlag Chemie GmbH, Weinheim 1982

UM00012331
NOVARTIS EXHIBIT 1017
Novartis v. Regents, IPR2023-01346
Page 1077 of 4460

Thioharnstoff ist ein für viele Arzneistoffe gebräuchlicher Lösungsvermitler, obgleich diese Substanz bereits längere Zeit unter dem Verdacht einer möglichen Kanzerogenität steht[1,2,3]. Bei der Lösungsvermittlung des Thioharnstoffes ist von Bedeutung, welcher Art und wie stabil die entstandenen Verbindungen sind, um eine evtl. Wirkveränderung beurteilen zu können.

Es ist daher von Interesse, die physikalischen Eigenschaften und den chemischen Aufbau der Komplexe mit Thioharnstoff zu kennen.

Am Beispiel der Lösungsvermittlung des Aminophenazons durch Thioharnstoff wird der Aufbau und die Struktur einer solchen Verbindung geklärt.

Bekannt ist, daß Thioharnstoff und Aminophenazon einen kristallisierbaren Komplex bilden. Dieser Komplex weist deutlich veränderte Eigenschaften gegenüber den Ausgangsverbindungen auf: So ist neben dem veränderten Lösungsverhalten in Wasser auch sein Schmelzpunkt von 140° stark unterschieden von denen des Thioharnstoffes: 177° – und des Aminophenazons: 108°.

Die stöchiometrische Zusammensetzung dieses Komplexes konnte *Rohdewald* durch Elementaranalyse als 3 T. Thioharnstoff und 1 T. Aminophenazon bestimmen[4]. Durch Interpretation der IR-Spektren kommt er zu dem Ergebnis, daß Hinweise auf das Vorliegen einer Einschlußverbindung deuten. Die Veränderung der N-H-Valenzschwingung, N-H-Deformationsschwingung, der C=O-Valenzschwingung und der C-N-Deformationsschwingung scheint diese Auffassung zu erhärten. Interessant in diesem Zusammenhang ist jedoch, daß der Komplex in identischer Zusammensetzung und in identischem Aufbau sowohl aus Wasser, als auch aus Aceton, Methanol oder Ethanol kristallisierbar ist. Diese Tatsache spricht gegen die Theorie einer einfachen Einschlußverbindung.

Schlenk und *Lenné* untersuchten verschiedene Thioharnstoffkomplexe und fanden, daß Thioharnstoff mit vielen organischen Verbindungen Kanal-Einschlußverbindungen eingeht[5,6]. Dabei wird die Größe des eingeschlossenen Moleküls durch die Kanallänge begrenzt. Die Autoren zeigten dies durch Bildung von Thioharnstoffkomplexen mit verschiedenartigen Kohlenwasserstoffen.

Im vorliegenden Fall schienen jedoch Zweifel an einer Kanal-Einschlußverbindung durch die Größe und den räumlichen Aufbau des Aminophenazons angebracht. Drehkristallaufnahmen, die die Struktur des Komplexes endgültig klären sollten, führten nicht zum Erfolg, da keine Rückschlüsse auf die optischen Achsen der Elementarzelle gezogen werden konnten[4]. Da bislang noch keine eindeutige Klärung des Komplexes vorlag, war eine neuerliche Bearbeitung dieses Problems angebracht.

Ergebnisse und Diskussion

Das Material für die vorliegenden Untersuchungen wurde aus Wasser umkristallisiert. Es wurden klare, oktaedrische Kristallplatten erhalten.

Erste Hinweise auf die Natur des Komplexes sollte die ^{13}C-NMR-Spektroskopie liefern. Hierbei wurde besondere Aufmerksamkeit den chemischen Verschiebungen der Kohlenstoffe der C=O-Gruppe des Aminophenazons und der C=S-Gruppe des Thioharnstoffes gewidmet, da diese Kohlenstoffe bei Komplexbildung durch Vorliegen von chemischen Bindungen oder Wasserstoffbrücken in ihrer chemischen Verschiebung beeinflußt

UM00012332
NOVARTIS EXHIBIT 1017
Novartis v. Regents, IPR2023-01346
Page 1078 of 4460

würden. Es zeigte sich jedoch, daß keine Veränderung der erwarteten Signallagen gegenüber der Ausgangsverbindung auftrat; lediglich im Aromatenbereich fand eine paramagnetische Verschiebung statt. Die Gegenüberstellung der ^{13}C-NMR-Daten gibt Tab. 1 wieder. Die Zuordnung erfolgte durch Interpretation von gekoppelten und rauschentkoppelten Spektren.

Tab. 1: *^{13}C-NMR-Daten von Aminophenazon und Komplex*

δ = ppm Pyramidon	Kohlenstoff	δ = ppm Komplex	δ = ppm Pyramidon	Kohlenstoff	δ = ppm Komplex
10,00	7	10,48	125,52	14	129,86
36,48	6	34,86	128,89	13 / 15	130,89
43,57	9 / 10	44,57	135,52	11	134,03
122,57	4	119,89	150,96	3	149,31
122,71	12 / 16	127,57	162,84	5	163,39
–			–	17 / 18 / 19	183,26

Dieses Ergebnis deutete auf eine Verbindung hin, die nicht durch chemische Bindungen zusammengehalten wird, sondern aufgrund einer speziellen räumlichen Anordnung entstanden ist, wobei jedoch die große Stabilität der Komplexverbindung bemerkenswert erscheint. Wichtig ist auch, daß aus den spektroskopischen Daten nicht auf Wasserstoffbrücken geschlossen werden konnte.

Einen einfachen Hinweis auf den Aufbau des Komplexes gibt die Tatsache, daß die Kristalle senkrecht zur Kristalloberfläche nicht oder nur sehr schwer zu spalten sind, wogegen dies mühelos in Richtung der Oberfläche gelingt. Dies läßt auf einen schichtähnlichen und nicht kanalartigen Aufbau schließen.

Um eine endgültige Klärung der Struktur zu erhalten, wird eine Röntgenstrukturanalyse an einem natürlich gewachsenen Kristall durchgeführt.

Da eine optische Orientierung des Kristalles nicht möglich war, wurde auf eine röntgenologische Voruntersuchung verzichtet und alle Messungen auf einem Vier-Kreis-Diffraktometer vorgenommen. Durch Kristalldiffraktometrie konnte die Kristallart als triklin mit den Winkeln $\alpha = 69{,}55°$, $\beta = 83{,}55°$ und $\gamma = 75{,}33°$ und den Gitterkonstanten $a = 9{,}378$ Å, $b = 11{,}724$ Å und $c = 11{,}880$ Å festgelegt werden. Die Raumgruppe ist $P1 = \sqrt{C_1^1}$.

Diese trikline Kristallart mit ihrer Raumgruppe dürfte auch der Grund für das Mißlingen der Drehkristallaufnahmen gewesen sein[4]. Nach Strukturverfeinerung und Auswertung der Analyse zeigt sich, daß die Thioharnstoffmoleküle untereinander netzartig durch verschieden starke N-H-S-Brücken verbunden sind und übereinanderliegende Schichten bilden. Zwischen diesen Schichten befinden sich die Aminophenazonmoleküle, die durch N-H-O-Brücken an Thioharnstoffe gebunden sind. Dabei tritt das bereits ermittelte Verhältnis von 3:1 für Thioharnstoff und Aminophenazon auf.

Abb. 1 gibt die Vernetzung wieder. Um die dreidimensionale Wiedergabe zu gewährleisten, sind in den Klammern die relativen Höhen beigefügt. Die freien Zahlen geben die Numerierung der schweren Atome an. Die Bindungslängen der H-S-Brücken sind unterschiedlich. Die einzelnen Werte sind in Tab. 2 aufgeführt.

UM00012333
NOVARTIS EXHIBIT 1017
Novartis v. Regents, IPR2023-01346
Page 1079 of 4460

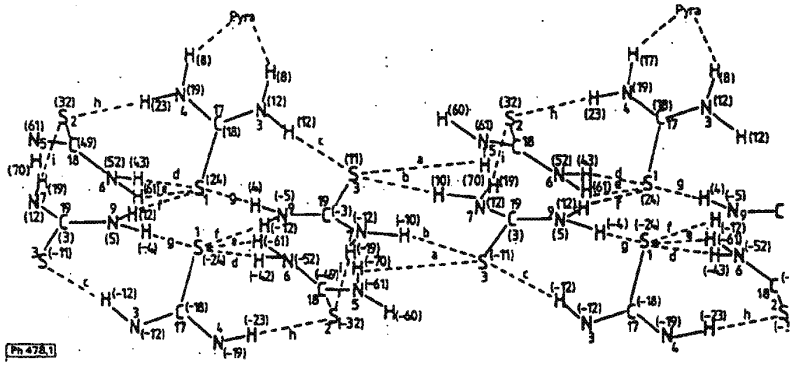


Abb. 1: Vernetzung des Komplexes

Tab. 2: *Bindungslängen der Schwefel-Wasserstoffbrücken* (Å)

a	2,55	f	2,62
b	2,40	g	2,40
c	2,41	h	2,46
d	2,51	i	2,48
e	2,71		

In Abb. 2 sind die Bindungslängen und in Abb. 3 die Winkel im Aminophenazon wiedergegeben.

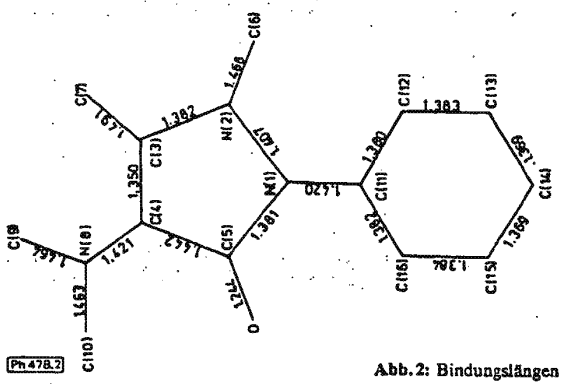


Abb. 2: Bindungslängen im Aminophenazon (Å)

UM00012334
NOVARTIS EXHIBIT 1017
Novartis v. Regents, IPR2023-01346
Page 1080 of 4460

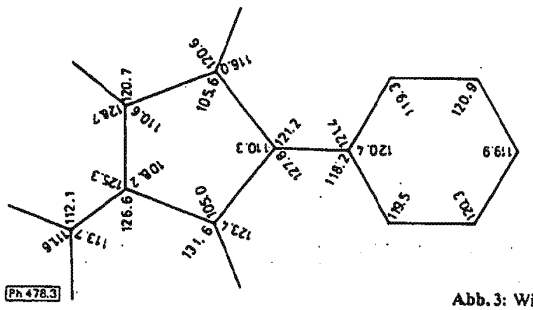


Abb. 3: Winkel im Aminophenazon (°)

Abb. 4 zeigt das gleiche für die drei Thioharnstoffe. Die N-H-O-Brücken vom Thioharnstoff zur Carbonylgruppe des Aminophenazons sind ebenfalls unterschiedlich lang: Vom N3-H beträgt die Länge 2,43 Å und vom N4-H 1,96 Å

Bemerkenswert ist, daß trotz des Vorhandenseins dieser Wasserstoffbrücken, die Normallänge aufweisen, ebenfalls die C=O und C=S-Bindungslänge im Normalbereich liegen; letzteres war bereits nach dem Ergebnis der ^{13}C-NMR-Spektroskopie zu erwarten. Bei Wasserstoffbrücken kann sonst üblicherweise mit der Aufweitung der betroffenen Carbonylbindung gerechnet werden.

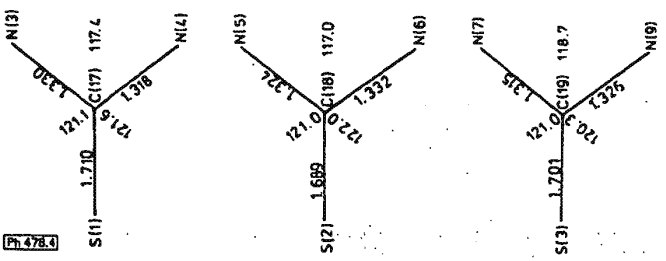


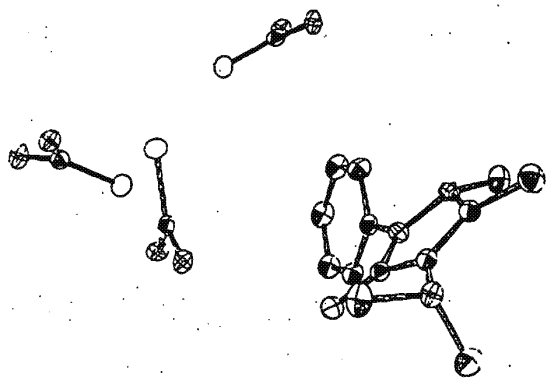
Abb. 4: Längen (Å) und Winkel (°) in den drei Thioharnstoffen

Durch diese verschiedenartigen Wasserstoffbrücken ist ein dreidimensionales Netzwerk verknüpft mit den Aminophenazonmolekülen in den Hohlräumen. Diese Anordnung verläuft schichtenweise zur Kristalloberfläche.

In jeder asymmetrischen Einheit befinden sich 11 Wasserstoffbrücken, die die Änderung der physikalischen und chemischen Eigenschaften bewirken und zu einer stabilen Komplexverbindung des beschriebenen Aufbaus führen.

Die absolute Konfiguration und die Anordnung von drei Thioharnstoffen und einem Aminophenazon in der Elementarzelle ist in Abb. 5 in der ORTEP-Wiedergabe zu sehen[7].

UM00012335
NOVARTIS EXHIBIT 1017
Novartis v. Regents, IPR2023-01346
Page 1081 of 4460



Ph478.6

Abb. 5: ORTEP-Wiedergabe des Komplexes

Tab. 3: *Atomkoordinaten* (10^4)

Atom	x/a (δ)	y/b (δ)	z/c (δ)
C3	−3963(2)	2610(2)	11944(2)
C4	−3277(2)	3335(2)	12204(2)
C5	−2437(2)	3923(2)	11132(2)
C6	−4857(3)	2709(3)	10022(2)
C7	−4959(3)	1835(2)	12742(2)
C9	−4286(2)	4680(2)	13350(2)
C10	−1819(3)	3382(3)	13762(2)
C11	−2248(2)	3770(2)	9059(2)
C12	−1815(2)	2833(2)	8557(2)
C13	−1361(3)	3136(2)	7362(2)
C14	−1293(3)	4337(3)	6690(2)
C15	−1683(3)	5257(2)	7201(2)
C16	−2181(2)	4985(2)	8386(2)
C17	1790(2)	2286(2)	9629(2)
C18	4927(2)	1717(2)	6540(2)
C19	−304(2)	42(2)	2975(2)
O	−1558(2)	4609(1)	10950(1)
S1	2408(1)	722(0)	9854(0)
S2	3211(1)	2482(0)	6047(1)
S3	1058(1)	614(1)	3264(0)
N1	−2805(2)	3526(1)	10260(1)
N2	−3673(2)	2642(1)	10768(1)
N3	1226(2)	2696(2)	10534(2)
N4	1876(2)	3133(2)	8562(2)
N5	6088(2)	1791(2)	5795(2)
N6	5180(2)	1025(2)	7688(2)
N7	−1230(2)	−414(2)	3831(2)

UM00012336
NOVARTIS EXHIBIT 1017
Novartis v. Regents, IPR2023-01346
Page 1082 of 4460

Tab. 3 Forts.

Atom	x/a (δ)	y/b (δ)	z/c (δ)
N8	−3273(2)	3508(2)	13334(1)
N9	−460(2)	60(2)	1873(2)
H1N6	608(2)	59(2)	793(2)
H2N6	436(3)	91(2)	821(2)
H1N7	−104(3)	−50(2)	468(2)
H2N7	−191(3)	−81(2)	372(2)
H1N9	−113(2)	−23(2)	171(2)
H2N9	39(3)	26(3)	123(3)
H1C6	−538(3)	204(2)	1048(2)
H2C6	−454(2)	269(2)	928(2)
H3C6	−559(3)	355(2)	990(2)
H1C7	−464(3)	103(3)	1278(2)
H2C7	−505(3)	189(2)	1348(2)
H3C7	−606	204	1245
H1C9	−431(3)	471(2)	1420(2)
H2C9	−395(3)	550(2)	1284(2)
H3C9	−526(3)	468(2)	1318(2)
H1C10	−116(3)	259(3)	1382(2)
H2C10	−192(2)	341(2)	1456(2)
H3C10	−122(3)	403(2)	1329(2)
HC12	−185(2)	199(2)	902(2)
HC13	−103(2)	247(2)	701(2)
HC14	−95(2)	455(2)	583(2)
HC15	−156(2)	608(2)	675(2)
H1N3	81(2)	349(2)	−961(2)
H2N3	117(2)	210(2)	−873(2)
H1N4	170(2)	395(2)	853(2)
H2N4	226(2)	288(2)	792(2)
H1N5	690(3)	136(2)	603(2)
H2N5	601(3)	229(2)	490(3)

Meßdaten, Strukturaufklärung und Verfeinerung

Die Komplexverbindung wurde nach dem von *Rohdewald* beschriebenen Verfahren hergestellt und aus Wasser umkristallisiert[4]. Lösungsmittel für die ^{13}C-NMR-Spektroskopie war d_6-DMSO; int. Stand. TMS. Das Spektrum wurde auf einem Bruker WH 90 bei 22,63 MHz vermessen.

Für die Röntgenstrukturanalyse wurden die Intensitäten von 4356 Reflexen einer ca. 0,25 × 0,3 mm Probe in der ω-Art eines automatischen Syntex $P2_1$ Vier-Kreis-Diffraktometers gemessen; Graphit Monochromat MoK_α ($\lambda = 0{,}7107$ Å).

Die Strukturaufklärung erfolgte durch das Computerprogramm MULTAN 78[8]. Die Strukturverfeinerung wurde durch anisotrope Temperaturfaktoren für die schweren Atome erreicht[9]. Die Positionen der Wasserstoffe wurde durch die Differenzanalyse der Dichten festgelegt. Ein Temperaturfaktor für ein schwer zu ermittelndes Wasserstoff wurde bei B = 3,0 Å fixiert.

Ein Wichtungsschema wurde angewendet bezogen auf $W = 2{,}88$ für $|F| > 20{,}0$ und $W = 0{,}144 \times F^2$ für $|F| \geq 20{,}0$.

Die letztlich beobachteten R- und R_w-Werte lagen bei R = 0,045 und 0,033 (omitting unobserved) und R_w = 0,027 und 0,026 (o.u.).

UM00012337

NOVARTIS EXHIBIT 1017
Novartis v. Regents, IPR2023-01346
Page 1083 of 4460

Tab. 4: *Temperaturfaktoren* (10^3)

Atom	U_{11}	U_{22}	U_{33}	U_{12}	U_{13}	U_{23}
C3	42(1)	42(1)	45(1)	−15(1)	2(1)	−14(1)
C4	39(1)	42(1)	39(1)	−13(1)	2(1)	−15(1)
C5	38(1)	38(1)	43(1)	−11(1)	0(1)	18(1)
C6	54(1)	85(1)	58(1)	−31(1)	−4(1)	−31(1)
C7	67(2)	69(2)	63(1)	−9(1)	11(1)	−22(1)
C9	64(2)	74(2)	66(2)	−16(1)	8(1)	40(1)
C10	58(2)	98(2)	50(1)	−28(2)	−4(1)	28(1)
C11	37(1)	49(1)	40(1)	−13(1)	−1(1)	18(1)
C12	58(1)	50(1)	51(1)	−11(1)	−4(1)	−22(1)
C13	68(2)	72(2)	53(1)	−9(1)	2(1)	−37(1)
C14	67(2)	90(2)	41(1)	−24(1)	3(1)	−23(1)
C15	64(2)	65(2)	49(1)	−14(1)	0(1)	−9(1)
C16	52(1)	49(1)	49(1)	−14(1)	−1(1)	−19(1)
C17	35(1)	45(1)	45(1)	−15(1)	−5(1)	−16(1)
C18	59(1)	47(1)	46(1)	−21(1)	−3(1)	−17(1)
C19	51(1)	49(1)	49(1)	−9(1)	−5(1)	−17(1)
O	57(1)	52(1)	48(1)	−31(1)	8(1)	−24(1)
S1	57(0)	39(0)	40(0)	−12(0)	−1(0)	−12(0)
S2	58(0)	63(0)	47(0)	−15(0)	−7(0)	14(0)
S3	61(0)	75(0)	43(0)	−30(0)	−1(0)	−20(0)
N1	48(1)	46(1)	40(1)	−22(1)	4(1)	−20(1)
N2	44(1)	47(1)	49(1)	−23(1)	−1(1)	−18(1)
N3	61(1)	45(1)	48(1)	−14(1)	4(1)	−19(1)
N4	65(1)	41(1)	43(1)	−15(1)	−2(1)	−11(1)
N5	55(1)	90(2)	55(1)	−17(1)	4(1)	−8(1)
N6	57(1)	58(1)	44(1)	−12(1)	−4(1)	−10(1)
N7	68(1)	97(2)	55(1)	−46(1)	6(1)	−26(1)
N8	47(1)	55(1)	41(1)	−20(1)	3(1)	21(1)
N9	66(1)	77(1)	52(1)	−28(1)	−6(1)	−29(1)

Tab. 4: Forts.

HC12	1.2(4)	H2N3	1.9(5)
HC13	3.2(5)	H1N4	3.6(6)
HC14	3.2(5)	H2N4	3.3(6)
HC15	4.1(6)	H1N5	3.4(6)
H1C6	4.1(6)	H2N5	6.3(8)
H2C6	3.4(6)	H1N6	1.6(5)
H3C6	5.2(7)	H2N6	3.4(6)
H1C9	4.8(6)	H1N7	5.1(7)
H2C9	4.8(7)	H2N7	4.1(6)
H3C9	3.2(5)	H1N9	2.7(6)
H1C10	5.8(8)	H2N9	7.5(8)
H2C10	3.7(6)	H1C7	6.5(8)
H3C10	5.0(7)	H2C7	4.8(8)
H1N3	2.8(6)	H3C7	3.0

UM00012338
NOVARTIS EXHIBIT 1017
Novartis v. Regents, IPR2023-01346
Page 1084 of 4460

Literatur

1 H. Sucker, P. Fuchs und P. Speiser, Pharmazeutische Technologie, S. 238, Georg Thieme Verlag, Stuttgart 1978.
2 R. Voigt, Lehrbuch der Pharmazeutischen Technologie, S. 487, Verlag Chemie, Weinheim – New York 1979.
3 A.N. Martin, J. Swarbrick und A. Camarata, Physikalische Pharmazie, S. 322, Wissenschaftliche Verlagsgesellschaft, Stuttgart 1975.
4 P. Rohdewald, Unveröffentlichte Ergebnisse.
5 W. Schlenk, Experientia *6*, 292 (1950).
W. Schlenk, Justus Liebigs Ann. Chem. *573*, 142 (1952).
6 H.U. Lenné, Z. Kristallogr. Kristallgeom. Kristallphys. Kristallchem. *118*, 439 (1963).
H.U. Lenné, ebenda *118*, 454 (1963).
H.U. Lenné, ebenda *118*, 468 (1963).
7 C. K. Johnson, Oak-Ridge Nat. Lab. Report, ORNL-3794, 1965.
8 G. Germain, P. Main and M. M. Woolfson, Acta Crystallogr. *A27*, 368 (1971).
9 W. H. Zachariasen, Acta Crystallogr. *16*, 1139 (1963).

[Ph 478]

Arch. Pharm. (Weinheim) *315*, 641–645 (1982)

H_2-Antihistaminika, 8. Mitt.[1]

Synthese potentieller H_2-Antihistaminika der Ethylendiamin-Reihe

Jürgen Herke** und Walter Schunack*

Fachbereich Pharmazie der Johannes Gutenberg-Universität, Saarstraße 21, 6500 Mainz 1
Eingegangen am 21. August 1981

Als potentielle H_2-Antihistaminika wurden die Ethylendiaminderivate **8**, **9** und **13** dargestellt und auf ihre H_2-antihistaminische Wirksamkeit untersucht.

H_2-Antihistaminics, VIII: Synthesis of Potential H_2-Antihistaminics with Ethylenediamine Structure

As potential H_2-antihistaminics, the ethylenediamine derivatives **8**, **9** and **13** were prepared and tested for their H_2-antihistaminic activity.

Die H_2-Antihistaminika Metiamid[2,3] und Cimetidin[4,5] besitzen u.a. eine Thioethergruppe als charakteristisches Strukturelement. Wie wir früher zeigen konnten, führt der Austausch des Schwefels durch Sauerstoff bzw. durch eine Sulfoxid- oder Sulfon-Gruppe zu einem relativ starken Wirkungsverlust[6,7]. Im Rahmen dieser Arbeit interessierte die Beeinflussung der pharmakologischen Wirkung bei Austausch des Schwefels durch eine substituierte Aminogruppe. Die zur präparativen Darstellung von **8** und **9** benötigte

0365-6233/82/0707-0641 $ 02.50/0
© Verlag Chemie GmbH, Weinheim 1982

UM00012339
NOVARTIS EXHIBIT 1017
Novartis v. Regents, IPR2023-01346
Page 1085 of 4460

This Page is Inserted by IFW Indexing and Scanning Operations and is not part of the Official Record

BEST AVAILABLE IMAGES

Defective images within this document are accurate representations of the original documents submitted by the applicant.

Defects in the images include but are not limited to the items checked:

- ☐ BLACK BORDERS
- ☐ IMAGE CUT OFF AT TOP, BOTTOM OR SIDES
- ☐ FADED TEXT OR DRAWING
- ☐ BLURRED OR ILLEGIBLE TEXT OR DRAWING
- ☐ SKEWED/SLANTED IMAGES
- ☐ COLOR OR BLACK AND WHITE PHOTOGRAPHS
- ☐ GRAY SCALE DOCUMENTS
- ☐ LINES OR MARKS ON ORIGINAL DOCUMENT
- ☐ REFERENCE(S) OR EXHIBIT(S) SUBMITTED ARE POOR QUALITY
- ☐ OTHER: _____

IMAGES ARE BEST AVAILABLE COPY.
As rescanning these documents will not correct the image problems checked, please do not report these problems to the IFW Image Problem Mailbox.

Noncovalent Assembly of Functional Groups on Calix[4]arene Molecular Boxes

Peter Timmerman, Remko H. Vreekamp, Ron Hulst, Willem Verboom, David N. Reinhoudt,* Kari Rissanen, Konstantin A. Udachin, and John Ripmeester

Abstract: Calix[4]arenes diametrically substituted at the upper rim with two melamine units spontaneously form well-defined box-like assemblies in the presence of two equivalents of 5,5-diethylbarbituric acid. These assemblies, consisting of nine different components, are held together by 36 hydrogen bonds and are stable in apolar solvents at concentrations of up to 10^{-4} M. This paper reports the first X-ray crystal structure, and the MALDI TOF mass spectra together with the complete ^{1}H NMR spectroscopic characterization of these hydrogen-bonded assemblies. The crystal structure clearly shows that the assemblies are stereogenic, as a result of the antiparallel orientation of the two rosette motifs. Furthermore, the synthesis of twelve new 1,3-bis(melamine)calix[4]arenes carrying different numbers and types of functionalities at the upper rim is described. Detailed ^{1}H NMR spectroscopic studies on the assembly behavior of these functionalized calix[4]arenes shows that 1) polar substituents (e.g. nitro, cyano) hardly affect the stability of the hydrogen-bonded assembly; 2) hydrogen bond donating or accepting groups, like amino and acetamido, can disturb assembly of the boxes under certain conditions by destabilizing the calix[4]arene pinched cone conformation as a result of intramolecular hydrogen bond formation; and 3) sterically bulky groups (e.g. *t*Bu) can significantly inhibit the formation of the hydrogen-bonded assembly, but this effect very much depends on the exact positions of the groups.

Keywords
calixarenes · hydrogen bonds · molecular boxes · noncovalent assembly · supramolecular chemistry

Introduction

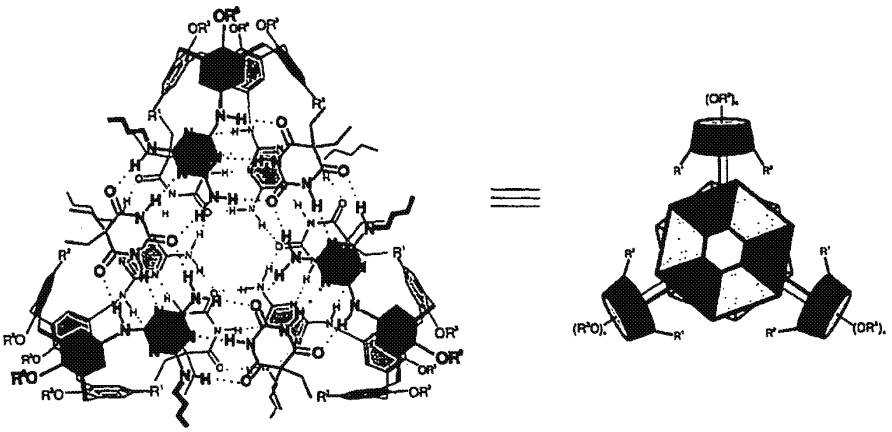
The unique ability of enzymes,[1] monoclonal antibodies,[2] and T-cell receptors[3] to recognize their targets with exquisite selectivity arises from the cooperative action of a unique set of functional groups in a specific three-dimensional arrangement. Utilizing the highly specific way proteins fold into well-defined three-dimensional structures, nature can generate a large variety of functional group arrays simply by varying the amino acid sequence in the peptide chain. Supramolecular chemists are trying to achieve the same goal in a different way, namely, by anchoring functional groups to synthetic platforms, such as cyclodextrins,[4] calix[4]arenes,[5] resorcinarenes,[6] or a combination thereof,[7] using the stepwise, irreversible formation of covalent bonds. However, for functional group arrays of increasing complexity this approach has severe limitations, such as the time required for syntheses and the yields obtained. As a result, reversible noncovalent assembly is increasingly being considered as a valuable alternative to classical covalent synthesis, because it allows self-correction.[8] Very recently, Kang and Rebek described a unique type of catalysis inside a self-assembled dimeric capsule.[9] Other examples include the noncovalent assembly of dendrimers,[10, 11] tetrahedral cavities,[12] and molecular boxes[13] or squares.[14]

In a previous communication we reported the hydrogen bond directed assembly of calix[4]arene molecular box $(\mathbf{1a})_3 \cdot (\mathbf{DEB})_6$ (Scheme 1; **DEB**: 5,5-diethylbarbituric acid),[15] a process that involves the cooperative formation of 36 hydrogen bonds in a rosette motif, which was first described by Whitesides[16] and Lehn.[17] In this assembly six functionalizable sites (R^1 and R^2, see Figure 1) are situated at the periphery of a box-like cavity. In view of our objective to generate functional group diversity in or around noncovalently assembled cavities, we undertook a study of how the nature of the functionality at positions R^1 and R^2 affects the stability of such calix[4]arene box-like assemblies. In this paper we present the first X-ray crystal structure and MALDI TOF mass spectrum of a hydrogen-bonded assembly of this type, and describe ten new molecular boxes carrying different numbers and types of functional groups at the periphery. Furthermore, we show that formation of intramolecular hydrogen bonds in the calix[4]arene units can disturb assembly of the boxes under certain conditions by destabilization of the pinched cone conformation.

[*] Prof. dr. ir. D. N. Reinhoudt, Dr. P. Timmerman, Dr. ir. R. H. Vreekamp, Dr. W. Verboom
Laboratory of Supramolecular Chemistry and Technology
University of Twente, P. O. Box 217, 7500 AE Enschede (The Netherlands)
Fax: Int. code +(53)489-4645
e-mail: smct@ct.utwente.nl
Dr. R. Hulst
Laboratory of Chemical Analysis, University of Twente
Prof. dr. K. Rissanen
Laboratory of Organic Chemistry, University of Jyväskylä
P. O. Box 35, FIN-40351 Jyväskylä (Finland)
Dr. K. A. Udachin, Prof. dr. J. Ripmeester
Steacie Institute for Molecular Science, National Research Council, Ottawa, K1A0R6 (Canada)

 © WILEY-VCH Verlag GmbH, D-69451 Weinheim, 1997 0947-6539/97/0311-1823 $ 17.50+.50/0

UM00012341
NOVARTIS EXHIBIT 1017
Novartis v. Regents, IPR2023-01346
Page 1087 of 4460



$(X)_3 \cdot (DEB)_6$

$X = 1\text{-}12$

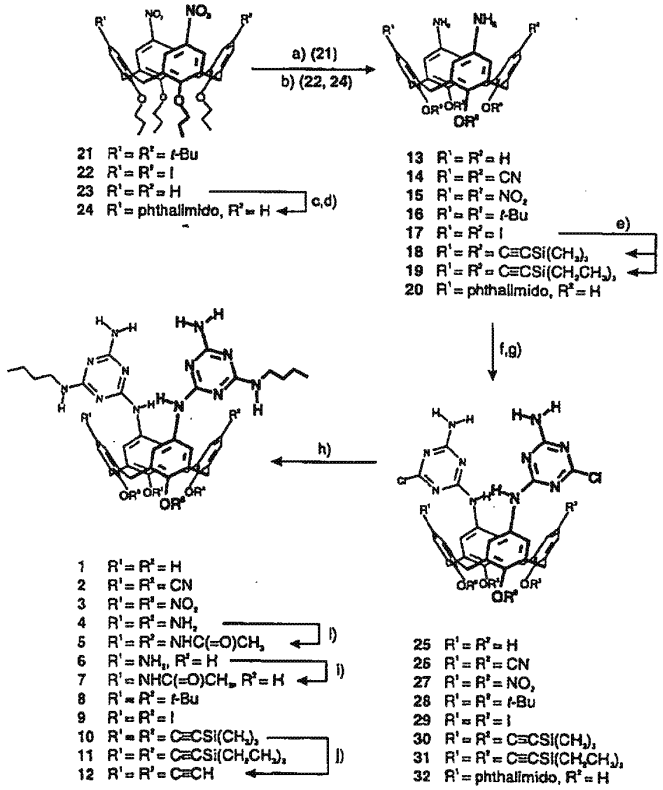
Figure 1. Schematic representation of the noncovalently assembled calix[4]arene molecular boxes $(X)_3 \cdot (DEB)_6$ ($X = 1-12$).

Results and Discussion

In order to investigate the structure–stability relationship of noncovalently assembled calix[4]arene molecular boxes, we synthesized bis(melamine)calix[4]arenes **1–12** carrying a variety of different functionalities at positions R^1 and R^2 (Scheme 1). Using a combination of ^1H NMR spectroscopy, MALDI TOF mass spectrometry, and single crystal X-ray diffraction, we then tested their ability to self-organize into box-like assemblies in the presence of two equivalents of 5,5-diethylbarbituric acid (**DEB**).

Synthesis of Bis(melamine)calix[4]arenes: Bis(melamine)calix[4]arenes **1–12** were prepared starting from the corresponding calix[4]arene diamines **13–20**, some of which (**13–15**) had been synthesized previously.[18,19] Diaminocalix[4]arenes **16** and **17** were prepared from the corresponding 1,3-dinitrocalix[4]arenes **21**[20] and **22**,[19] either by reduction with hydrazine/Raney Ni in MeOH[21] (**16**) or with $SnCl_2$ in EtOH[22] (**17**); both methods gave quantitative yields. The trimethyl- and triethylsilylacetylene functions in **18** and **19** were introduced by means of a Heck-type coupling of 1,3-diiodocalix[4]arene **17** with either trimethylsilylacetylene (yield not determined owing to extensive decomposition during column chromatography) or triethylsilylacetylene (50% yield) in the presence of 5–10 mol% $Pd(PPh_3)_2Cl_2$ and CuI in NEt_3.[23] Monophthalimidocalix[4]arene **24** was prepared in 50% yield by treatment of 1,3-dinitrocalix[4]arene **21**[24] with one equivalent of $AgCF_3COO/I_2$ followed by a Cu^I-catalyzed reaction with phthalimide in refluxing collidine.[25] Finally, reduction of **24** with $SnCl_2$ in EtOH[22] gave diamine **20** in 93% yield.

The melamine units were introduced in **1–12** by slightly modifying the procedure reported by Whitesides.[26] 1,3-Diaminocalix[4]arenes **13–20** were treated with cyanuric chloride and then NH_3 to afford the bis(chloro-



Scheme 1. For compounds 1, 13, and 25: a, $R^3 = C_{12}H_{25}$; b, $R^3 = C_7H_7$. For compounds 2–12, 14–20, and 26–32: $R^3 = C_7H_7$. Reaction conditions: a) excess hydrazine/Raney Ni in refluxing MeOH, 2 h (>95%); b) $SnCl_2$ (10 equiv), EtOH, reflux, 15 h, acidic workup (>95%); c) $AgCF_3COO$ (1.0 equiv), I_2 (1.0 equiv), $CHCl_3$, reflux, 30 min.; d) phthalimide (1.5 equiv), Cu_2O (0.75 equiv), collidine, reflux, 16 h (overall 50%); e) trimethyl- (18) or triethyl- (19) silylacetylene (3.0 equiv), $Pd(PPh_3)_2Cl_2$ (10 mol%), CuI (10 mol%), NEt_3, 40–45 °C, 15 h; f) cyanuric chloride (2.5–3.0 equiv), diisopropylethylamine (5–6 equiv), THF, 0 °C, 2 h; g) excess gaseous NH_3, THF, 0 °C, 3 h; h) $nBuNH_2$ (36 equiv), DIPEA (12 equiv), THF, reflux, 5–19 h; i) acetyl chloride (excess), 1 M K_2CO_3, EtOAc/THF, RT, 1 h; j) 1 N NaOH, THF/MeOH (1:1), RT, 1 h.

© WILEY-VCH Verlag GmbH, D-69451 Weinheim, 1997
0947-6539/97/0311-1824 $ 17.50+.50/0 *Chem. Eur. J.* 1997, 3, No. 11

UM00012342
NOVARTIS EXHIBIT 1017
Novartis v. Regents, IPR2023-01346
Page 1088 of 4460

triazine)calix[4]arenes **25**–**32** as stable intermediates, the majority of which have very limited solubility in most organic solvents. Compounds **25**–**31** were converted into the corresponding dimelamines **1**–**3** and **8**–**11** in overall yields of between 49 and 100%, by reaction with excess *n*-butylamine in refluxing THF. During the reaction of bis(chlorotriazine) **32** with *n*-butylamine the phthalimide group was partially removed and therefore the product was treated additionally with excess hydrazine in refluxing EtOH to give directly the monoamino dimelamine **6** in 54% yield. Reduction of the nitro groups in **3** with hydrazine/Raney Ni in MeOH[21] gave diamino dimelamine **4** in quantitative yield. Of all the dimelamines synthesized, compound **4** was by far the least soluble; this might be related to the cavity becoming significantly more rigid because of the formation of intramolecular hydrogen bonds (vide infra). Acylation of the amino groups in **4** and **6** with excess acetyl chloride under Schotten–Baumann conditions gave the corresponding dimelamines **5** and **7** in 83 and 65% yield, respectively. The trimethylsilyl groups in **10** were removed with 1 N NaOH to give diacetylene **12** in quantitative yield, as was unambiguously confirmed by the appearance of the acetylene resonance at $\delta = 2.95$ in the ^{1}H NMR spectrum.

Noncovalent Synthesis of Calix[4]arene Molecular Boxes: Titration of dimelamine **1a** with **DEB** in [D_1]chloroform shows several characteristic features (Figure 2). Already at very low concentrations of **DEB** two signals become evident at very low field. These resonances, which remain at $\delta = 14.10$ and 13.32 regardless of the **1a**:**DEB** ratio, are assigned to the hydrogen-bonded NH protons of **DEB** in the complex. These protons are observed at different chemical shifts as a result of the unsymmetrical substitution of the melamine units, which gives the two protons a chemically different environment in the complex. When the amount of **DEB** is increased, the signal corresponding to the NH_2 protons of free **1a** decreases in intensity, but remains at the same position. At the same time, two signals are observed at around $\delta = 6.9$ (c) and 6.7 (d) corresponding to the two NH_2 protons. Two additional signals appear at $\delta = 8.37$ (e) and 7.43 (f), which correspond to the two secondary amine protons of **1a** in the hydrogen-bonded complex. The aromatic protons of the melamine-substituted aromatic rings of calix[4]arene **1a** give rise to signals at $\delta = 7.15$ (g) and 6.03 (h). In free **1a** these protons are observed as broad signals at $\delta = 6.65$–6.05. The resonance at $\delta = 6.03$ is in accordance with a pinched cone structure in which the two melamines approach each other.[27] The fact that the other aromatic proton (g) is observed at significantly lower field is the result of formation of an intramolecular hydrogen bond with a triazene ring nitrogen (N–H distance in crystal structure (vide infra) is 2.23 Å).

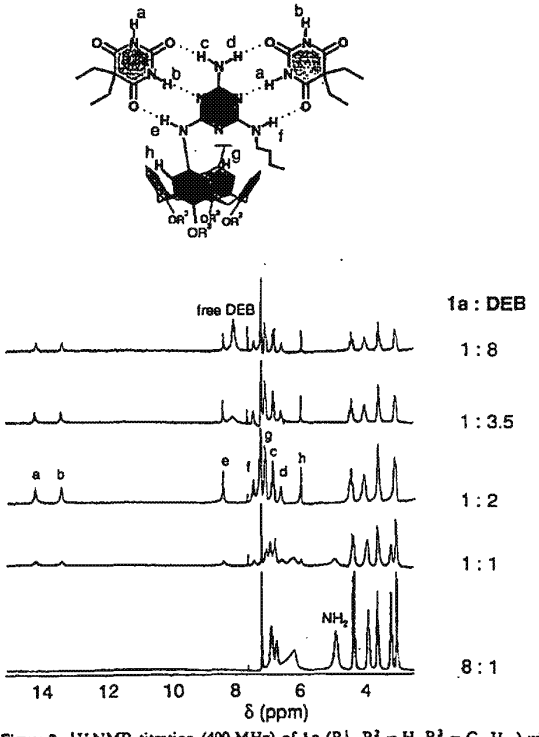


Figure 2. ^{1}H NMR titration (400 MHz) of **1a** (R^1, R^2 = H, R^3 = $C_{11}H_{23}$) with **DEB** in [D_1]chloroform at 25 °C. Separate 10 mM solutions of **1a** and **DEB** were mixed in various ratios.

At a ratio of **1a**:**DEB** of 1:2 the spectrum is sharp; this indicates the absence of free **1a**. The 1:2 ratio is consistent with the box-like assembly that is represented in Figure 1. When more than two equivalents of **DEB** are added, the signal for the NH protons of free **DEB** is observed alongside the two signals for the hydrogen-bonded **DEB**. This indicates that exchange between hydrogen-bonded and free **DEB** is slow on the NMR timescale. The self-assembled calix[4]arene boxes $(\mathbf{1})_3\cdot(\mathbf{DEB})_6$ are stable in apolar solvents like chloroform and toluene. For instance, in [D_1]chloroform $(\mathbf{1b})_3\cdot(\mathbf{DEB})_6$ is the only assembly (>97%) observed in the spectrum over a concentration range of at least 10^{-1}–10^{-4} M (lower limit for ^{1}H NMR spectroscopy). However, their stability progressively decreases when significant amounts (10–20%) of highly polar solvents (like DMSO and methanol) are added.

In order to investigate to what extent functional groups can alter the assembly of the calix[4]arene molecular boxes, we tested the ability of calix[4]arene dimelamines **2**–**12** to self-organize into box-like assemblies in the presence of two equivalents of 5,5-diethylbarbituric acid (**DEB**). The nature of the substituents at positions R^1 and R^2 significantly influences the assembly of the boxes. The results are summarized in Table 1. Diagnostic for the formation of the box-like assemblies is the appearance of the barbituric acid NH signals around $\delta = 14.1$ and 13.3 ([D_1]chloroform) or $\delta = 14.6$ and 13.8 ([D_8]toluene) in the ^{1}H NMR spectra.[15, 26] The introduction of polar substituents at positions R^1 and R^2, such as nitro or cyano, does not influence the stability of the cyclic hydrogen-bonded assembly to any significant extent. Compounds **2** (R^1, R^2 = CN) and **3** (R^1, R^2 = NO_2) readily assemble in [D_1]chloroform solution in the presence of **DEB**, and their ^{1}H NMR spectra are virtually identical to that of $(\mathbf{1b})_3\cdot(\mathbf{DEB})_6$ (R^1, R^2 = H), except for the signals of the aromatic protons *ortho* to R^1 and R^2. The titration of **2** with **DEB** clearly proved the 3:6 stoichiometry of the box-like assembly formed.

Recrystallization of the assembly $(\mathbf{3})_3\cdot(\mathbf{DEB})_6$ from toluene gave large single crystals suitable for X-ray diffraction studies. The crystal structure (see Figure 3) provides the first crystallo-

 © WILEY-VCH Verlag GmbH, D-69451 Weinheim, 1997 0947-6539/97/0311-1825 $ 17.50+.50/0

UM00012343
NOVARTIS EXHIBIT 1017
Novartis v. Regents, IPR2023-01346
Page 1089 of 4460

Table 1. Characteristic ^{1}H NMR resonances for the hydrogen-bonded assemblies obtained by mixing dimelamines 2–12 with 2 equiv of DEB (overall ±5 mM solutions).

	δ in [D$_1$]chloroform			δ in [D$_8$]toluene		
	Imide NH resonance I	Imide NH resonance II	ArNH resonance	Imide NH resonance I	Imide NH resonance II	ArNH resonance
2	14.0 (s)	13.2 (s)	8.4 (s)	– [a]	– [a]	– [a]
3	13.9 (s)	13.2 (s)	8.4 (s)	14.3 (s)	13.6 (s)	8.8 (s)
4	14.6–14.1 (brm) [b]		9.6–9.4 (brm) [b]	14.6 (s)	13.9 (s)	8.9 (s)
5	14.5–14.0 (brm) [c]		9.6–9.4 (brm)[c]	– [d]	– [d]	– [d]
6	14.2 (brs)	13.5–13.3 (brm)	8.4 (s)	14.8–14.6 (m)	14.1–13.9 (m)	9.0–8.9 (m)
7	14.1 (brs)	13.5–13.2 (brm)	8.4 (s)	14.6 (brs)	13.9–13.7 (m)	8.9–8.7 (m)
8	– [e]	– [e]	9.2–9.4 (brm)	– [a]	– [a]	– [a]
9	14.1 (brs)	13.4 (brs)	8.4 (s)	– [a]	– [a]	– [a]
10	14.1 (brs)	13.4 (brs)	8.35 (s)	– [a]	– [a]	– [a]
11	14.1 (brs)	13.4 (brs)	8.3 (s)	– [a]	– [a]	– [a]
12	14.0 (brs)	13.3 (brs)	8.35 (s)	– [a]	– [a]	– [a]

[a] Not measured. [b] Spectrum recorded at −30 °C. [c] Spectrum recorded at 0 °C. [d] No resonances observed at room temperature owing to very low solubility. [e] No resonances observed at room temperature.

graphic evidence for the formation of this type of molecular box.[28] The structure confirms that the calix[4]arene units are fixed in a pinched cone conformation,[27] which is the only conformation that allows simultaneous participation of the calix[4]arene units in both rosette motifs. The two rosettes tightly stack on top of each other with an interatomic separation of 3.5 Å at the edges and 3.2 Å at the center of the box, which leaves little space for guest molecules. Interestingly, the structure reveals that the two rosette motifs are oriented in an antiparallel fashion[29] (see also Figure 1), which means that the assembly is stereogenic. The enantiomers are expected to have a lifetime of the order of seconds, considering the fact that their racemization requires the simultaneous breakage of at least nine cooperative hydrogen bonds.[30]

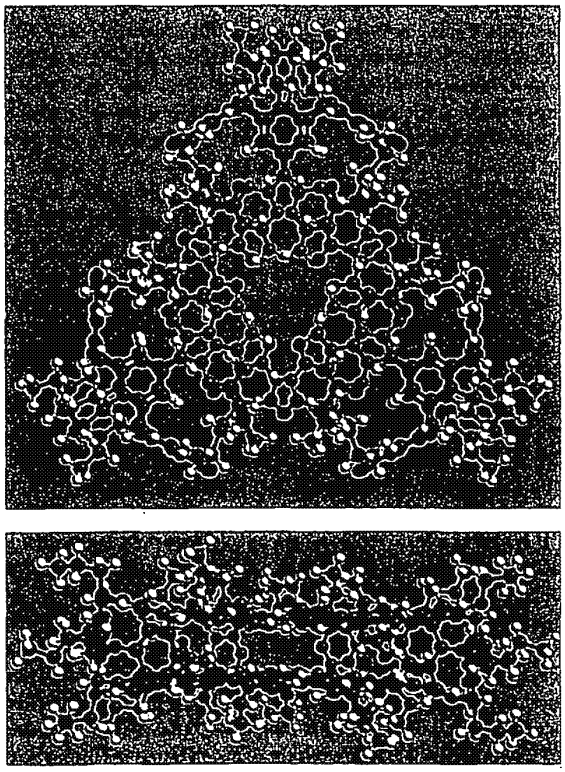


Figure 3. Top (top) and side (bottom) view (some atoms are omitted for clarity) of the X-ray crystal structure of calix[4]arene box-like assembly $(3)_3\cdot(DEB)_6\cdot(toluene)_{12}$ (R^1, R^2 = NO_2) obtained by crystallization from toluene (solvent molecules are not shown). Nitrogen atoms are represented in blue, oxygen atoms in red, carbon atoms in black, and hydrogen atoms in white.

The crystals of $(3)_3\cdot(DEB)_6$ belong to the highly symmetric space group $R\bar{3}c$. The box is of trigonal shape (triangle); its sides are approximately 3.2 nm long, and its thickness lies between about 0.7 (center) and 1.3 (periphery) nm. The O–N and the N–N distances in the hydrogen-bonded network forming the rosettes lie between 2.85 and 3.03 Å; the range of values arises because the rosettes in the crystal lattice are slightly unsymmetrical. The crystal packing of the flat boxes is quite remarkable. The boxes are separated by 1.7–1.8 nm, and thus form large cavities accommodating up to 20 toluene sites (Figure 4). Some toluene molecules occupy a single site, while others are disordered over 2–3 locations. Significant disordering of the hydrocarbon chains in the rosette is observed: the propyl chains at the calix[4]arene skeleton are disordered over four sites with the site occupancy varying from 0.1 to 0.4; the *n*-butyl chains connected to the NH groups are disordered over five locations with the site occupancy varying from 0.1 to 0.3.

Evidence for the fact that the solid state structure of $(3)_3\cdot(DEB)_6$ resembles the structure in solution comes from a strong NOE enhancement observed between the NCH_2 protons in 3 and one of the ethyl CH_2 groups of DEB. The interatomic distance of these protons within a single rosette is too large (ca. 6.4 Å) to cause the observed NOE connectivity. Therefore, it must arise from a proximity effect between the two rosette motifs, and this puts a limit on the possible orientations that they can adopt relative to one another. In the antiparallel orientation observed in the crystal structure, the two protons are 2.8 Å apart, which is in perfect agreement with the strong NOE observed. The presence of this NOE connectivity provides strong evidence for the fact that the structure in solution closely resembles the solid state structure determined by X-ray crystallography.

Additional evidence for the self-assembly of the boxes was obtained by using MALDI TOF spectroscopy.[31] In the presence of 1.5–2.0 equiv of $Ag^{(I)}CF_3COO$ the assembly $(2)_3\cdot(DEB)_6$ gives rise to an intense signal at an *m*/z of 4220

© WILEY-VCH Verlag GmbH, D-69451 Weinheim, 1997
0947-6539/97/0311-1826 $ 17.50+.50/0 Chem. Eur. J. 1997, 3, No. 11

UM00012344
NOVARTIS EXHIBIT 1017
Novartis v. Regents, IPR2023-01346
Page 1090 of 4460

(calcd for $^{13}C_2{}^{12}C_{214}H_{282}N_{54}O_{30}\cdot{}^{107}Ag^{(I)}$ complex: 4219) in the mass spectrum (see Figure 5).[32] Signals corresponding to partially formed aggregates or higher oligomers were not observed in the spectrum. In the absence of $Ag^{(I)}CF_3COO$, none of the assemblies 1–3 showed any significant signal in the MALDI-TOF spectrum. Apparently, a Ag^+ ion is coordinated to one of the cyano groups in 2, giving the assembly an overall positive charge. The applicability of this method for the mass spectrometric detection of other hydrogen-bonded assemblies is currently being investigated.

Surprisingly, the stability of assembly $(4)_3\cdot(\mathbf{DEB})_6$ (R^1, $R^2 = NH_2$) is highly solvent dependent. The ^1H NMR spectrum in [D_8]toluene is very well-defined (see Figure 6) and shows two singlets at $\delta = 14.55$ and 13.85 for the magnetically inequivalent barbituric acid NH protons. In [D_1]chloroform, however, the spectrum is very broad and does not show any resonance in the region between $\delta = 13$ and 15 at room temperature; this indicates a preference for nonspecific oligo- or polymer formation in this solvent.[33] The decreased stability of $(4)_3\cdot(\mathbf{DEB})_6$ in the more polar solvent [D_1]chloroform is most probably related to the hydrogen bond donating ability of the two NH_2 groups.

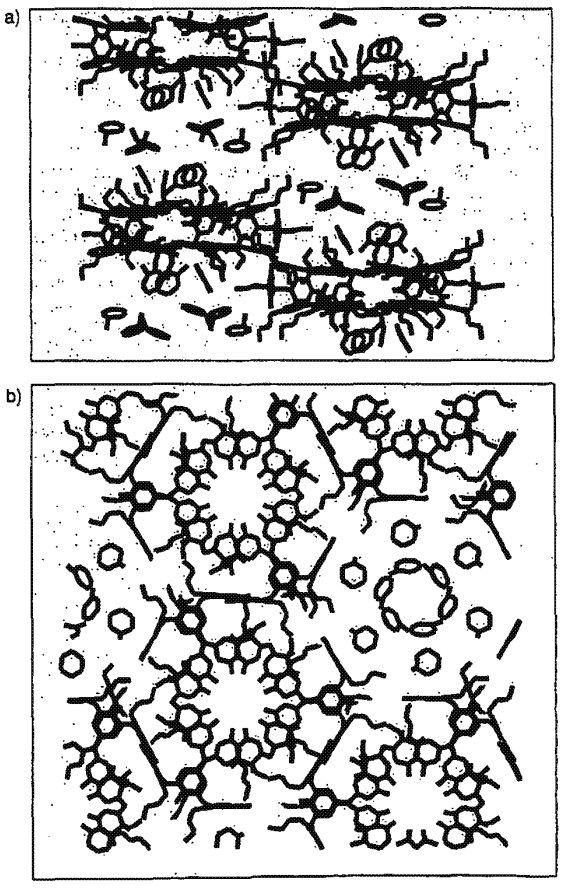


Figure 4. Different views a) and b) of the crystal packing of $(3)_3\cdot(\mathbf{DEB})_6\cdot(\text{toluene})_{12}$ (R^1, $R^2 = NO_2$) showing the positioning of the solvent molecules (disorder as well as 50% of the solvent molecules in view b) are excluded for clarity).

Molecular modeling studies with monomer 4 suggest that an intramolecular hydrogen bond is formed between the $ArNH_2$ groups and the melamine NH protons, which forces the calixarene to adopt a perfect cone conformation. In the pinched cone conformation observed in the box-like assembly (vide supra) these hydrogen bonds, which lead to an overall decrease in stability of the hydrogen-bonded assembly relative to the monomers, cannot be formed. Supporting evidence for the importance of intramolecular hydrogen bond formation was obtained from the assembly of 6 ($R^1 = NH_2$, $R^2 = H$), which possesses only one of the two $ArNH_2$ groups in 4. The overall decrease in stability of the hydrogen-bonded assembly $(6)_3\cdot(\mathbf{DEB})_6$ is only half of that in $(4)_3\cdot(\mathbf{DEB})_6$. Both in [$D_8$]toluene and in [$D_1$]chloroform compound 6 forms a stable box-like assembly (see Figure 6c). Apparently, the presence of the additional intramolecular hydrogen bond in calix[4]arene 4 is responsible for the fact that assembly into the box-like aggregate is not observed in the more polar solvent [D_1]chloroform.

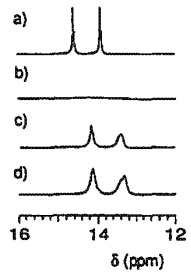


Figure 6. ^1H NMR spectra (400 MHz, RT) of calix[4]arene box-like assemblies: a) $(4)_3\cdot(\mathbf{DEB})_6$ (R^1, $R^2 = NH_2$) in [D_8]toluene (5 mM), b) $(4)_3\cdot(\mathbf{DEB})_6$ (R^1, $R^2 = NH_2$) in [D_1]-chloroform (5 mM), c) $(6)_3\cdot(\mathbf{DEB})_6$ ($R^1 = NH_2$, $R^2 = H$) in [D_1]chloroform (5 mM), d) $(7)_3\cdot(\mathbf{DEB})_6$ [$R^1 = NHC(O)CH_3$, $R^2 = H$] in [D_1]-chloroform (5 mM).

Compound 5 [R^1, $R^2 = NHC(O)CH_3$] does not form the box-like assembly in either [D_1]chloroform or [D_8]toluene. Both ^1H NMR spectra exhibit broad resonances indicating nonspecific aggregation. Removal of one of the acetamido substituents of 5 fully restores the ability of the system to form the box-like assembly. Compound 7 [$R^1 = NHC(O)CH_3$, $R^2 = H$] gives a well-defined ^1H NMR spectrum both in [D_1]chloroform and [D_8]toluene, which is fully in agreement with the formation of the corresponding box-like assembly. Again, the formation of intramolecular hydrogen bonds, namely, between the amide carbonyl and the melamine NH proton, seems to be primarily responsible for preventing the assembly of 5. Molecular mechanics calculations predict a somewhat stronger intramolecular hydrogen bond for acetamido-substituted calix[4]arene 5 [R^1, $R^2 = NHC(O)CH_3$] than for 4 (R^1, $R^2 = NH_2$);[34] this most probably explains the different assembly behavior of these two compounds in [D_8]toluene.

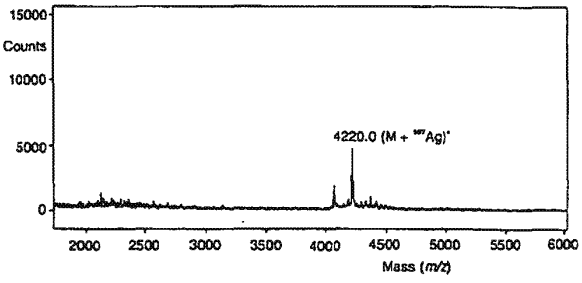


Figure 5. MALDI TOF mass spectrum of calix[4]arene box-like assembly $(2)_3\cdot(\mathbf{DEB})_6$ (R^1, $R^2 = CN$) in the presence of 2 equiv of $Ag^{(I)}CF_3COO$. Dihydroxybenzoic acid (DHB) was used as a matrix.

 © WILEY-VCH Verlag GmbH, D-69451 Weinheim, 1997 0947-6539/97/0311-1827 $ 17.50+.50/0

UM00012345
NOVARTIS EXHIBIT 1017
Novartis v. Regents, IPR2023-01346
Page 1091 of 4460

Introduction of the bulky iodo substituents at positions R^1 and R^2 in **9** significantly broadens the imide resonances at $\delta = 13.3$ and 14.1; this reflects the reduced stability of the assembly as a result of unfavorable steric interactions. Increasing the steric bulkiness of the substituents further, completely inhibits the assembly into the box-like aggregates. Thus, the ^{1}H NMR spectrum of **8** [R^1, R^2 = *t*Bu] in the presence of two equivalents of **DEB** is extremely broad and poorly defined, and does not show the imide signals at $\delta = 13.3$ and 14.1. In sharp contrast to this, the dimelamines **10** [R^1, $R^2 = C{\equiv}CSi(CH_3)_3$] and **11** [$R^1$, $R^2 = C{\equiv}CSi(CH_2CH_3)_3$], in which the bulky trialkylsilyl substituents are separated from the aromatic rings by an acetylene spacer, do form rosette structures, as judged from the appearance of the somewhat broadened resonances at $\delta = 13.3$ and 14.1. The corresponding free acetylenes give much sharper imide resonances; this proves that the trimethylsilyl substituents also destabilize the assemblies to some extent. The strikingly different behavior of compounds **9** [R^1, $R^2 = C(CH_3)_3$], and **10** [R^1,$R^2 = C{\equiv}CSi(CH_3)_3$] nicely demonstrates that the exact position of the bulky substituents does have a profound effect on the stability of the box-like assemblies.

Conclusions

In this paper we have presented the complete characterization of noncovalently assembled calix[4]arene molecular boxes by ^{1}H NMR spectroscopy, single crystal X-ray diffraction, and MALDI TOF mass spectrometry. The assemblies, which are highly stable in apolar solvents, are stereogenic as a result of an antiparallel orientation of the two rosette motifs. Comparing the stability of the various molecular boxes carrying different types of functionalities at the periphery, we have shown that:

1) Polar substituents, like nitro and cyano groups, hardly influence the stability of the hydrogen-bonded assembly.
2) The exact position of steric bulky groups strongly influences the stability of the corresponding box-like aggregates.
3) intramolecular hydrogen-bond formation can destabilize the pinched cone conformation of the calix[4]arene units and thus prevent assembly of the corresponding box-like aggregates.

We believe that additional conformational constraints at the calixarene skeleton will be required in order to observe the noncovalent assembly of calix[4]arene molecular boxes in the presence of multiple hydrogen bond donating and/or accepting groups.

Experimental Section

General: All experiments were carried out in an argon atmosphere. THF was distilled from Na/benzophenone ketyl, and hexane (referring to petroleum ether fraction with b.p. 60–80 °C), CH_2Cl_2 and EtOAc from K_2CO_3. All chemicals were of reagent grade and used without further purification. NMR spectra were recorded on a Bruker AC250 (^{1}H NMR 250 MHz) or a Varian Unity 400 (^{1}H NMR 400 MHz) spectrometer in [D]chloroform at room temperature, unless stated otherwise. Residual solvent protons were used as internal standard, and chemical shifts are given relative to tetramethylsilane (TMS). FAB and EI spectra were measured on a Finnigan MAT90 spectrometer with *m*-nitrobenzyl alcohol (NBA) as a matrix. MALDI-TOF mass spectra were recorded on a PerSpective Biosystems Voyager-DE-RP spectrometer. A 337 nm UV nitrogen laser producing 3 ns pulses was used in the linear and reflectron modes. Melting points were determined with a Reichert melting point apparatus and are uncorrected. Flash chromatography was performed on silica gel (SiO_2, E. Merck, 0.040–0.063 mm, 230–240 mesh). The presence of solvents in the analytical samples was confirmed by ^{1}H NMR spectroscopy. The synthesis of compounds **13a**,[18] **13b–15**,[19] **21**,[20] **23**,[24] and **22**[19] have been described elsewhere.

5,17-Dinitro-11-phthalimido-25,26,27,28-tetrapropoxycalix[4]arene (24): A solution of 1,3-dinitrocalix[4]arene **23** (1.0 g, 1.5 mmol) in $CHCl_3$ (25 mL) was added to a suspension of $AgCF_3COO$ (0.32 g, 1.5 mmol) in refluxing $CHCl_3$ (25 mL), and the cloudy solution was refluxed for 15 min. Then I_2 (0.37 g, 1.5 mmol) was added in portions until the deep purple color was permanent. During the addition, AgI precipitated from the solution as a yellow solid. The reaction mixture was refluxed for another 15 min, filtered over Celite, and evaporated to dryness. The residue was taken up in EtOAc (50 mL), washed with a 10% $Na_2S_2O_3$ solution (10 mL), H_2O (3 × 10 mL), and brine (10 mL), and dried over Na_2SO_4. The solvent was removed under vacuum, and the crude material refluxed in collidine (25 mL) for 24 h in the presence of phthalimide (0.33 g, 2.2 mmol) and Cu_2O (0.16 g, 1.0 mmol). The reaction mixture was cooled to RT and diluted with CH_2Cl_2 (50 mL). It was then washed with 5% H_2SO_4 (2 × 25 mL), 2N NaOH (10 mL), H_2O (2 × 25 mL), and brine (25 mL), and dried over Na_2SO_4. Evaporation of the solvent gave a black solid material, which was purified by column chromatography (SiO_2, CH_2Cl_2) to give monophthalimide **24** in 50% yield as a yellow solid. M.p. 148–150 °C (CH_2Cl_2/MeOH). ^{1}H NMR: $\delta = 8.0–7.7$ (m, 4H, ArH), 7.7–7.6 (m, 4H, *o*-NO_2ArH), 6.78 (s, 2H, *o*-phthalimidoArH), 6.7–6.4 (m, 3H, ArH), 4.52, 4.49 (2d, 4H, ^2J(H,H) = 13.6 Hz, $ArCH_2Ar$), 4.1–3.9 (m, 4H, OCH_2), 3.86, 3.83 (2t, 4H, ^3J(H,H) = 8.0 and 7.7 Hz, OCH_2), 3.31, 3.28 (2d, 4H, ^2J(H,H) = 13.6 Hz, $ArCH_2Ar$), 2.1–1.8 (m, 8H, OCH_2CH_2), 1.1–0.9 [m, 12H, $O(CH_2)_2CH_3$]. MS (FAB): m/z = 828.2 (100) ($[M+H]^+$, calcd 828.3). $C_{48}H_{49}N_3O_{10}$: calcd C 69.63, N 5.08, H 5.97; found: C 69.54, N 4.99, H 5.98.

5,17-Diamino-11,23-bis(1,1-dimethylethyl)-25,26,27,28-tetrapropoxycalix[4]arene (16): A solution of 1,3-dinitro **21** (0.50 g, 0.63 mmol), hydrazine monohydrate (0.50 mL), and a catalytic amount of Raney Ni in MeOH (25 mL) was refluxed for 2 h. After filtering the hot solution over Celite, the solvent was removed under reduced pressure. The residue was dissolved in CH_2Cl_2 (50 mL), washed with H_2O (2 × 25 mL) and brine (25 mL), and dried over Na_2SO_4. Evaporation of the solvent gave 1,3-diamine **16** as an orange-brown solid in quantitative yield. ^{1}H NMR: $\delta = 6.98$ (s, 4H, *o*-*t*BuArH), 5.39 (s, 4H, *o*-NH_2ArH), 4.32, 2.95 (ABq, 8H, ^2J(H,H) = 13.3 Hz, $ArCH_2Ar$), 3.9–3.8 (m, 4H, OCH_2), 3.54 (t, 4H, ^3J(H,H) = 6.6 Hz, OCH_2), 1.9–1.7 (m, 8H, OCH_2CH_2), 1.30 [s, 18H, $C(CH_3)_3$], 1.01, 0.77 [2t, 12H, ^3J(H,H) = 7.4 Hz, $O(CH_2)_2CH_3$]. ^{13}C NMR: $\delta = 155.8$, 149.3, 144.1, 140.1, 136.1, 134.1, 125.6, 115.8, 34.1, 31.8, 31.4, 23.5, 22.9, 10.9, 9.8. MS (FAB): m/z = 735.9 (100) ($[M+H^+]$, calcd 735.5). $C_{48}H_{66}N_2O_4 \cdot 0.5\ H_2O$: calcd C 77.48, N 3.77, H 9.08; found: C 77.42, N 3.56, H 8.92.

5,17-Diamino-11,23-diiodo-25,26,27,28-tetrapropoxycalix[4]arene (17): A suspension of 1,3-dinitro **22** (1.16 g, 1.24 mmol) and $SnCl_2 \cdot 2H_2O$ (2.8 g, 12 mmol) in EtOH (50 mL) was refluxed for 15 h, and the hot solution was then poured onto ice. CH_2Cl_2 (100 mL) was added, and the solution stirred at RT for 1 h. This was followed by the addition of 1N NaOH (100 mL) and stirring for another 30 min at RT. The organic layer was washed with H_2O (2 × 25 mL) and brine (25 mL), and dried over Na_2SO_4. Evaporation of the solvent gave pure 1,3-diamine **17** in quantitative yield as a white solid. M.p. > 280 °C (CH_2Cl_2). ^{1}H NMR: $\delta = 7.16$ (s, 4H, *o*-IArH), 5.81 (s, 4H, *o*-NH_2ArH), 4.30, 2.97 (ABq, 8H, ^2J(H,H) = 13.3 Hz, $ArCH_2Ar$), 3.9–3.8 (m, 4H, OCH_2), 3.67 (t, 4H, ^3J(H,H) = 7.2 Hz, OCH_2), 3.1 (brs, 4H, NH_2), 2.0–1.7 (m, 8H, OCH_2CH_2), 0.99, 0.90 [2t, 12H, ^3J(H,H) = 7.5 and 7.4 Hz, $O(CH_2)_2CH_3$]. ^{13}C NMR: $\delta = 157.4$, 149.2, 141.0, 138.6, 137.0, 134.1, 115.7, 85.5, 30.8, 23.3, 23.1, 10.6, 10.1. MS (FAB): m/z = 874.3 (100) (M^+, calcd 874.2). $C_{48}H_{66}N_2O_4$: calcd C 54.93, N 3.20, H 5.53; found: C 55.04, N 3.52, H 5.57.

5,17-Diamino-11,23-[(trimethylsilyl)ethynyl]-25,26,27,28-tetrapropoxycalix[4]arene (18): $Pd(PPh_3)_2Cl_2$ (10 mg, 10 mol%), CuI (2 mg, 10 mol%), and trimethylsilylacetylene (50 µL, 0.34 mmol) were added to a thoroughly degassed suspension of 1,3-diamine **17** (0.10 g, 0.11 mmol) in NEt_3 (20 mL).

© WILEY-VCH Verlag GmbH, D-69451 Weinheim, 1997
0947-6539/97/0311-1828 $ 17.50+.50/0 *Chem. Eur. J.* 1997, *3*, No. 11

UM00012346
NOVARTIS EXHIBIT 1017
Novartis v. Regents, IPR2023-01346
Page 1092 of 4460

The reaction mixture was heated at 40 °C for 16 h. The solvent was removed, and the residue dissolved in CH_2Cl_2 (50 mL), washed with H_2O (2 × 25 mL) and brine (25 mL), and dried over Na_2SO_4. Evaporation of the solvent gave crude 1,3-diamine **18**, which was used as such in further reaction. ^{1}H NMR: δ = 7.16 (s, 4H, *o*-TMSC≡CArH), 5.41 (s, 4H, *o*-NH_2ArH), 4.20, 2.90 (ABq, 8H, ^2J(H,H) = 13.3 Hz, $ArCH_2Ar$), 3.9–3.8 (m, 4H, OCH_2), 3.45 (t, 4H, ^3J(H,H) = 7.2 Hz, OCH_2), 2.6 (brs, 4H, NH_2), 1.9–1.6 (m, 8H, OCH_2CH_2), 0.94, 0.71 [2t, 12H, ^3J(H,H) = 7.4 Hz, $O(CH_2)_2CH_3$], 0.16 [s, 18H, $Si(CH_3)_3$]. MS (70 eV, EI) *m/z* 814.3 (100) (M^+, calcd for $C_{50}H_{66}N_2O_4Si_2$ 814.5).

5,17-Diamino-11,23-bis[(triethylsilyl)ethynyl]-25,26,27,28-tetrapropoxycalix[4]arene (19): $Pd(PPh_3)_2Cl_2$ (50 mg, 20 mol%), CuI (5 mg, 10 mol%), and triethylsilylacetylene (0.19 mL, 1.0 mmol) were added to a thoroughly degassed suspension of 1,3-diamine **17** (0.30 g, 0.34 mmol) in NEt_3 (30 mL). The reaction mixture was heated at 45 °C for 15 h. The solvent was removed, and the residue dissolved in CH_2Cl_2 (50 mL), washed with H_2O (2 × 25 mL) and brine (25 mL), and dried over Na_2SO_4. Evaporation of the solvent gave crude 1,3-diamine, which was purified by column chromatography (SiO_2, 5% MeOH/CH_2Cl_2) to give pure diamine **19** as a foam in 50% yield. ^{1}H NMR: δ = 7.25 (s, 4H, *o*-TESC≡CArH), 5.54 (brs, 4H, *o*-NHArH), 4.33, 3.03 (ABq, 8H, ^2J(H,H) = 13.3 Hz, $ArCH_2Ar$), 4.1–3.9 (m, 4H, OCH_2), 3.57 (t, 4H, ^3J(H,H) = 6.6 Hz, OCH_2), 2.9 (brs, 4H, NH_2), 2.0–1.7 (m, 8H, OCH_2CH_2), 1.2–1.0 [m, 24H, $O(CH_2)_2CH_3$ + $Si(CH_2CH_3)_3$], 0.84 [t, 6H, ^3J(H,H) = 7.4 Hz, $O(CH_2)_2CH_3$], 0.71 [q, 12H, ^3J(H,H) = 7.8 Hz, $Si(CH_2CH_3)_3$]. ^{13}C NMR: δ = 159.0, 137.2, 132.7, 116.0, 107.4, 89.7, 76.6, 31.0, 23.5, 22.9, 10.9, 9.8, 7.6, 4.6. MS (FAB): *m/z* = 899.6 (100) ($[M+H]^+$, calcd for $C_{56}H_{78}N_2O_4Si_2$: 899.6).

5,17-Diamino-11-phthalimido-25,26,27,28-tetrapropoxycalix[4]arene (20): A solution of 1,3-dinitro **24** (0.50 g, 0.60 mmol) and $SnCl_2 \cdot 2H_2O$ (1.4 g, 6.0 mmol) in EtOH (50 mL) was refluxed for 13.5 h. The hot solution was then poured onto ice. CH_2Cl_2 (100 mL) was added, and the solution stirred at RT for 1 h. This was followed by the addition of 1 N NaOH (100 mL) and stirring for another 30 min at RT. The organic layer was washed with H_2O (2 × 25 mL) and brine (25 mL), and dried over Na_2SO_4. Evaporation of the solvent gave pure 1,3-diamine **20** in 93% yield as a yellow foam. ^{1}H NMR: δ = 8.0–7.7 (m, 4H, ArH), 6.98 (s, 2H, *o*-phthalimidoArH), 6.87 (d, 2H, ^3J(H,H) = 7.4 Hz, ArH), 6.73 (t, 1H, ^3J(H,H) = 7.4 Hz, ArH), 5.83, 5.76 (2d, 4H, ^4J(H,H) = 2.7 Hz, *o*-NH_2ArH), 4.43, 4.40 (2d, 4H, ^2J(H,H) = 13.3 Hz, $ArCH_2Ar$), 4.0–3.8 (m, 4H, OCH_2), 3.69 (t, 4H, ^3J(H,H) = 7.1 Hz, OCH_2), 3.09, 3.05 (2d, 4H, ^2J(H,H) = 13.3 Hz, $ArCH_2Ar$), 3.0 (brs, 4H, NH_2), 2.1–1.8 (m, 8H, OCH_2CH_2), 1.04 [t, 6H, ^3J(H,H) = 7.4 Hz, $O(CH_2)_2CH_3$], 1.0–0.9 [m, 6H, $O(CH_2)_2CH_3$]. ^{13}C NMR: δ = 167.6, 157.5, 157.2, 149.3, 140.9, 136.7, 136.1, 134.8, 134.2, 134.0, 132.0, 128.6, 126.4, 125.0, 123.5, 121.8, 115.8, 115.6, 76.7, 76.6, 31.1, 23.4, 23.1 (2×), 10.7, 10.1, 10.0. MS (FAB): *m/z* = 767.5 (100) (M^+, calcd for $C_{48}H_{53}N_3O_6$: 767.4).

General Procedure for the Preparation of Bis(chlorotriazine)calix[4]arenes 25a–32: A solution of the 1,3-diaminocalix[4]arene in THF was added dropwise to an ice-cooled solution of cyanuric chloride (2.5–3.0 equiv) and diisopropylethylamine (DIPEA, 5–6 equiv) in THF. The solution was stirred at 0 °C for 2 h. Then gaseous NH_3 was gently bubbled through the solution for another 3 h, while keeping the temperature at 0 °C. The reaction mixture was subsequently diluted with CH_2Cl_2 (50 mL), washed with H_2O (25 mL) and brine (25 mL), and dried over Na_2SO_4. Evaporation of the solvent gave crude bis(chlorotriazine), which was used without further purification.

5,17-*N,N'*-Bis[4-amino-6-chloro-1,3,5-triazin-2-yl]diamino-25,26,27,28-tetrakis(dodecyloxy)calix[4]arene (25a) was prepared from diamine **13a** (1.47 g, 1.30 mmol), cyanuric chloride (0.72 g, 3.9 mmol), and DIPEA (1.35 mL, 7.82 mmol) in THF (30 mL). The yellowish bis(chlorotriazine) **25a** was obtained in 63% yield after trituration with *n*-butanol and *n*-hexane and used without further purification. ^{1}H NMR ([D_6]DMSO) δ = 9.73 (brs, 2H, ArNH), 7.15–6.65 (brm, 6H, ArH), 6.27 (s, 4H, *o*-NHArH), 4.40, 3.19 (ABq, 8H, ^2J(H,H) = 12 Hz, $ArCH_2Ar$), 4.1–3.85 (brm, 4H, OCH_2), 3.75–3.35 (brm, 4H, OCH_2), 2.0–1.65 (brm, 8H, CH_2), 1.40–1.05 (m, 72H, CH_2), 0.81 (t, 12H, ^3J(H,H) = 6.2 Hz, CH_3). MS (FAB): *m/z* = 1384.5 (100) ($[M+H]^+$, calcd for $C_{82}H_{114}{}^{35}Cl_2N_{10}O_4$: 1384.0).

5,17-*N,N'*-Bis[4-amino-6-chloro-1,3,5-triazin-2-yl]diamino-25,26,27,28-tetrapropoxycalix[4]arene (25b) was prepared from diamine **13b** (0.50 g, 0.80 mmol), cyanuric chloride (0.45 g, 2.4 mmol), and DIPEA (0.84 mL, 4.8 mmol) in THF (50 mL). Instead of the normal workup, H_2O (100 mL) was added to the reaction mixture, and the resulting suspension stirred for 15 min at RT. The white solid was filtered off and washed successively with H_2O, *n*-butanol, and *n*-hexane. After the solid had been dried under high vacuum, bis(chlorotriazine) **25b** was obtained in 93% yield and used without further purification. ^{1}H NMR ([D_6]DMSO) δ = 9.65 (brs, 2H, ArNH), 7.6–7.3 (m, 6H, ArH), 6.27 (s, 4H, *o*-NHArH), 4.34, 3.12 (ABq, 8H, ^2J(H,H) = 12.9 Hz, $ArCH_2Ar$), 4.0–3.8 (m, 4H, OCH_2), 3.64 (t, 4H, ^3J(H,H) = 6.5 Hz, OCH_2), 2.0–1.8 (m, 8H, OCH_2CH_2), 1.07, 0.90 [2t, 12H, ^3J(H,H) = 7.4 Hz, $O(CH_2)_2CH_3$]. MS (FAB): *m/z* = 878.1 (100) (M^+, calcd for $C_{46}H_{52}{}^{35}Cl_2N_{10}O_4$: 878.4).

5,17-*N,N'*-Bis[4-amino-6-chloro-1,3,5-triazin-2-yl]diamino-11,23-dicyano-25,26,27,28-tetrapropoxycalix[4]arene (26) was prepared from diamine **14** (0.90 g, 1.3 mmol), cyanuric chloride (0.74 g, 4.0 mmol), and DIPEA (1.4 mL, 8.0 mmol) in THF (50 mL). Bis(chlorotriazine) **26** was obtained in 61% yield after trituration with EtOH and used without further purification. ^{1}H NMR: δ = 7.45 (s, 4H, *o*-CNArH), 6.4 (brs, 4H, *o*-NHArH), 4.45, 3.22 (ABq, 8H, ^2J(H,H) = 13.3 Hz, $ArCH_2Ar$), 4.2–4.0 (m, 4H, OCH_2), 3.8–3.5 (m, 4H, OCH_2), 2.0–1.7 (m, 8H, OCH_2CH_2), 1.06, 0.90 [2t, 12H, ^3J(H,H) = 7.4 Hz, $O(CH_2)_2CH_3$]. MS (FAB): *m/z* = 929.5 (100) ($[M+H^+]$, calcd for $C_{48}H_{50}{}^{35}Cl_2N_{12}O_4$: 929.3).

5,17-*N,N'*-Bis[4-amino-6-chloro-1,3,5-triazin-2-yl]diamino-11,23-dinitro-25,26,27,28-tetrapropoxycalix[4]arene (27) was prepared from diamine **15** (0.40 g, 0.56 mmol), cyanuric chloride (0.32 g, 1.7 mmol), and DIPEA (0.60 mL, 3.4 mmol) in THF (25 mL). Bis(chlorotriazine) **27** was obtained in 86% yield after recrystallization from DMSO/CH_2Cl_2. ^{1}H NMR ([D_6]DMSO) δ = 9.9 (brs, 2H, ArNH), 7.8–7.4 (m, 8H, *o*-NO_2ArH + NH_2), 6.89 (s, 4H, *o*-NHArH), 4.35, 3.30 (ABq, 8H, ^2J(H,H) = 13.6 Hz, $ArCH_2Ar$), 4.3–4.1 (m, 4H, OCH_2), 3.92, 3.74 (2t, 8H, ^3J(H,H) = 6.3 Hz, OCH_2), 1.9–1.8 (m, 8H, OCH_2CH_2), 1.09, 0.86 [2t, 12H, ^3J(H,H) = 7.4 Hz, $O(CH_2)_2CH_3$]. MS (FAB): *m/z* = 969.5 (100) ($[M+H^+]$, calcd for $C_{46}H_{50}{}^{35}Cl_2N_{12}O_8$: 969.4).

5,17-*N,N'*-Bis[4-amino-6-chloro-1,3,5-triazin-2-yl]diamino-11,23-bis(1,1-dimethylethyl)-25,26,27,28-tetrapropoxycalix[4]arene (28) was prepared from cyanuric chloride (0.38 g, 2.0 mmol), DIPEA (0.71 mL, 4.0 mmol), and diamine **16** (0.50 g, 0.68 mmol) in THF (25 mL). Crude **28** was obtained as an orange solid in quantitative yield and used without further purification. ^{1}H NMR: δ = 7.04 (s, 4H, *o*-*t*BuArH), 6.1–5.8 (m, 6H, *o*-NHArH + NH_2), 4.38, 3.06 (ABq, 8H, ^2J(H,H) = 13.5 Hz, $ArCH_2Ar$), 4.0–3.9 (m, 4H, OCH_2), 3.58 (t, 4H, ^3J(H,H) = 6.5 Hz, OCH_2), 2.0–1.7 (m, 8H, OCH_2CH_2), 1.30 [s, 18H, $C(CH_3)_3$], 1.02 [t, 6H, ^3J(H,H) = 7.4 Hz, $N(CH_2)_3CH_3$], 1.03, 0.79 [2t, 12H, ^3J(H,H) = 7.4 Hz, $O(CH_2)_2CH_3$]. MS (FAB): *m/z* = 991.5 (100) ($[M+H^+]$, calcd for $C_{54}H_{68}{}^{35}Cl_2N_{10}O_4$: 991.5).

5,17-*N,N'*-Bis[4-amino-6-chloro-1,3,5-triazin-2-yl]diamino-11,23-diiodo-25,26,27,28-tetrapropoxycalix[4]arene (29) was prepared from 1,3-diamine **17** (0.88 g, 1.0 mmol), cyanuric chloride (0.56 g, 3.0 mmol), and DIPEA (1.0 mL, 6.0 mmol) in THF (50 mL). Crude bis(chlorotriazine) **29** was obtained as a white solid in quantitative yield and used without further purification. ^{1}H NMR: δ = 8.3 (brs, 1H, NH), 7.43 (s, 4H, *o*-IArH), 6.3 (brs, 4H, *o*-NHArH), 5.3 (brs, 1H, NH), 4.31, 3.01 (ABq, 8H, ^2J(H,H) = 13.4 Hz, $ArCH_2Ar$), 4.0–3.9 (m, 4H, OCH_2), 3.54 (t, 4H, ^3J(H,H) = 6.6 Hz, OCH_2), 2.0–1.7 [m, 8H, OCH_2CH_2], 1.01, 0.81 [2t, 12H, ^3J(H,H) = 7.4 Hz, $O(CH_2)_2CH_3$]. MS (FAB): *m/z* = 1131.2 (100) ($[M+H^+]$, calcd for $C_{46}H_{50}{}^{35}Cl_2I_2N_{10}O_4$: 1131.1).

5,17-*N,N'*-Bis[4-amino-6-chloro-1,3,5-triazin-2-yl]diamino-11,23-bis(trimethylsilylethynyl)-25,26,27,28-tetrapropoxycalix[4]arene (30) was prepared from crude diamine **18** (125 mg, 0.114 mmol), cyanuric chloride (63 mg, 0.34 mmol), and DIPEA (0.12 mL, 0.69 mmol) in THF (15 mL). Crude **30** was obtained quantitatively and used without further purification. ^{1}H NMR: δ = 7.32 (s, 4H, *o*-TMSC≡CArH), 6.3 (brs, 4H, *o*-NHArH), 5.3 (brs, 2H, NH_2), 4.39, 3.11 (ABq, 8H, ^2J(H,H) = 13.3 Hz, $ArCH_2Ar$), 4.1–3.9 (m, 4H, OCH_2), 3.63 (t, 4H, ^3J(H,H) = 6.6 Hz, OCH_2), 2.0–1.7 (m, 8H, OCH_2CH_2), 1.10, 0.89 [2t, 12H, ^3J(H,H) = 7.3 Hz, $O(CH_2)_2CH_3$], 0.20 [s, 18H, $Si(CH_3)_3$]. MS (FAB): *m/z* = 1073.1 (100) ($[M+H^+]$, calcd for $C_{56}H_{68}{}^{35}Cl^{37}ClN_{10}O_4Si_2$: 1073.4).

UM00012347
NOVARTIS EXHIBIT 1017
Novartis v. Regents, IPR2023-01346
Page 1093 of 4460

5,17-*N,N'*-Bis[4-amino-6-chloro-1,3,5-triazin-2-yl]diamino-11,23-bis(triethylsilylethynyl)-25,26,27,28-tetrapropoxycalix[4]arene (31) was prepared from cyanuric chloride (55 mg, 0.30 mmol), DIPEA (0.11 mL, 0.60 mmol), and diamine 19 (90 mg, 0.10 mmol) in THF (15 mL). Crude 31 was obtained as an off-white solid in quantitative yield and used without further purification. ^{1}H NMR: δ = 7.32 (s, 4H, *o*-TESC≡CArH), 6.3 (brs, 4H, *o*-NHArH), 5.3 (brs, 2H, NH_2), 4.39, 3.11 (AB q, 8H, ^2J(H,H) = 13.3 Hz, $ArCH_2Ar$), 4.1–3.9 (m, 4H, OCH_2), 3.63 (t, 4H, ^3J(H,H) = 6.6 Hz, OCH_2), 2.0–1.7 (m, 8H, OCH_2CH_2), 1.2–1.0 [m, 24H, $O(CH_2)_2CH_3$ + $Si(CH_2CH_3)_3$], 0.87 [t, 6H, ^3J(H,H) = 7.3 Hz, $O(CH_2)_2CH_3$], 0.69 [q, 12H, ^3J(H,H) = 7.8 Hz, $Si(CH_2CH_3)_3$]. MS (FAB): *m/z* = 1155.6 (100) ([*M*+H$^+$], calcd for $C_{62}H_{80}{}^{35}Cl_2N_{10}O_4Si_2$: 1155.5).

5,17-*N,N'*-Bis[4-amino-6-chloro-1,3,5-triazin-2-yl]diamino-11-phthalimido-25,26,27,28-tetrapropoxycalix[4]arene (32) was prepared from diamine 21 (0.43 g, 0.56 mmol), cyanuric chloride (0.26 g, 1.4 mmol), and DIPEA (0.49 g, 2.8 mmol) in THF (25 mL). Crude 32 was obtained in 70% yield and used without further purification. ^{1}H NMR ([D$_4$]methanol/[D$_1$]chloroform 1:9): δ = 7.6–7.4 (m, 4H, ArH), 6.95 (d, 2H, ^3J(H,H) = 7.4 Hz, ArH), 6.85–6.75 (m, 1H, ArH), 6.2 (brs, 2H, *o*-NHArH), 4.39 (d, 4H, ^2J(H,H) = 13.4 Hz, $ArCH_2Ar$), 4.0–3.8 (m, 4H, OCH_2), 3.64 (t, 4H, ^3J(H,H) = 6.9 Hz, OCH_2), 3.2–3.0 (m, 4H, $ArCH_2Ar$), 2.0–1.7 (m, 8H, OCH_2CH_2), 1.01 [t, 6H, ^3J(H,H) = 7.3 Hz, $O(CH_2)_2CH_3$], 0.9–0.8 [m, 6H, $O(CH_2)_2CH_3$]. MS (FAB): *m/z* = 1063.4 (40) ([*M*+H^{37}Cl+H]$^+$), 1042.3 (100) ([*M*+NH$_4$]$^+$), 1024.4 (50) ([*M*+H]$^+$, calcd for $C_{54}H_{55}{}^{35}Cl_2N_{11}O_6$ 1024.4].

General Procedure for the Preparation of Bis(melamine)calix[4]arenes 1–3, 6, and 8–11: A solution of the bis(chlorotriazine), *n*-butylamine (36 equiv), and DIPEA (12 equiv) in THF (25–50 mL) was refluxed for 5.5–19 h. The mixture was then evaporated to dryness. The residue was dissolved in CH_2Cl_2 (50 mL), washed with H_2O (3 × 25 mL) and brine (25 mL), and dried over Na_2SO_4. Evaporation of the solvent gave the crude calix[4]arene dimelamine as a white solid, which was further purified when necessary.

5,17-*N,N'*-Bis[4-amino-6-(butylamino)-1,3,5-triazin-2-yl]diamino-25,26,27,28-tetrakis(dodecyloxy)calix[4]arene (1a) was prepared from bis(chlorotriazine) 13a (1.0 g, 0.72 mmol), *n*-butylamine (2.5 mL, 25 mmol), and DIPEA (1.5 mL, 8.7 mmol) in THF (250 mL). Crude dimelamine 1a was triturated with acetone and recrystallized from EtOAc and CH_2Cl_2 to give pure dimelamine 1a in 74% yield. ^{1}H NMR: δ = 7.05–6.7 (brm, 6H, ArH), 6.65–6.05 (brm, 6H, *o*-NHArH + NH), 5.25–4.7 (brm, 6H, NH), 4.42, 3.11 (AB q, 8H, ^2J(H,H) = 13.3 Hz, $ArCH_2Ar$), 4.1–3.9 (brm, 4H, OCH_2), 3.8–3.6 (m, 4H, OCH_2), 3.4–3.2 (m, 4H, NCH_2), 2.0–1.75 (m, 8H, OCH_2CH_2), 1.6–1.15 (m, 72H, CH_2), 1.0–0.8 (m, 12H, CH_3). MS (FAB): *m/z* = 1458.4 (100) ([*M*+H$^+$], calcd 1458.1). $C_{90}H_{144}N_{12}O_4$: calcd C 74.14, N 11.53, H 9.95; found: C 74.29, N 11.60, H 10.26.

5,17-*N,N'*-Bis[4-amino-6-(butylamino)-1,3,5-triazin-2-yl]diamino-25,26,27,28-tetrapropoxycalix[4]arene (1b) was prepared from bis(chlorotriazine) 13b (0.50 g, 0.57 mmol), *n*-butylamine (2.0 mL, 21 mmol), and DIPEA (1.2 mL, 6.8 mmol) in THF (50 mL). Crude dimelamine 1b was absorbed on silica gel by addition of silica gel (5% of dry weight used for column) to a solution in THF (10–15 mL) followed by careful removal of the solvent and drying under high vacuum. Subsequent purification by column chromatography (SiO_2, 10% MeOH/CH_2Cl_2) and recrystallization from EtOAc gave dimelamine 1b as a light orange solid in 74% yield. M.p. 175–180 °C. ^{1}H NMR: δ = 7.0–6.7 (brm, 6H, ArH), 6.6–6.2 (brm, 4H, *o*-NHArH + NH), 5.0–4.8 (brm, 6H, NH), 4.43, 3.11 (AB q, 8H, ^2J(H,H) = 13.3 Hz, $ArCH_2Ar$), 4.1–3.9 (m, 4H, OCH_2), 3.69 (t, 4H, ^3J(H,H) = 6.7 Hz, OCH_2), 3.31 (q, 4H, ^3J(H,H) = 6.5 Hz, NCH_2), 2.0–1.7 (m, 8H, OCH_2CH_2), 1.6–1.3 (m, 8H, $NCH_2CH_2CH_2$), 1.06 [t, 6H, ^3J(H,H) = 7.4 Hz, $O(CH_2)_2CH_3$], 1.0–0.8 [m, 12H, $N(CH_2)_3CH_3$ + $O(CH_2)_2CH_3$]. MS (FAB): *m/z* = 954.0 (100) ([*M*+H$^+$], calcd 953.6). $C_{54}H_{72}N_{12}O_4$·0.5EtOAc: calcd C 67.43, N 16.86, H 7.68; found: C 67.31, N 16.98, H 7.52.

5,17-*N,N'*-Bis[4-amino-6-(butylamino)-1,3,5-triazin-2-yl]diamino-11,23-dicyano-25,26,27,28-tetrapropoxycalix[4]arene (2) was prepared from bis(chlorotriazine) 26 (0.76 g, 0.82 mmol), *n*-butylamine (2.9 mL, 29 mmol), and DIPEA (1.7 mL, 9.8 mmol) in THF (50 mL). Crude dimelamine 2 was absorbed on silica gel by addition of silica gel (5% of dry weight used for column) to a solution in THF (10–15 mL) followed by careful removal of the solvent and drying under high vacuum. Subsequent purification by column chromatography (SiO_2, 10% MeOH/CH_2Cl_2) and recrystallization from CH_2Cl_2/MeOH gave bismelamine 2 as a light brown solid in 49% yield (based on diamine 14). M.p. 231–233 °C. ^{1}H NMR: δ = 7.2–7.0 (brm, 4H, *o*-CNArH), 6.7–6.2 (brm, 6H, *o*-NHArH + ArNH), 5.0–4.7 (brm, 6H, NH), 4.35, 3.09 (AB q, 8H, ^2J(H,H) = 13.6 Hz, $ArCH_2Ar$), 4.0–3.8 (m, 4H, OCH_2), 3.75–3.55 (m, 4H, OCH_2), 3.28 (q, 4H, ^3J(H,H) = 6.6 Hz, NCH_2), 2.0–1.7 (m, 8H, OCH_2CH_2), 1.6–1.2 (m, 8H, $NCH_2CH_2CH_2$), 1.0–0.8 [m, 18H, $O(CH_2)_2CH_3$ + $N(CH_2)_3CH_3$]. MS (FAB): *m/z* = 1003.4 (100) ([*M*+H$^+$], calcd 1003.6). $C_{56}H_{70}N_{14}O_4$·0.5 MeOH: calcd C 66.60, N 19.25, H 7.12; found: C 66.18, N 19.52, H 7.08.

5,17-*N,N'*-Bis[4-amino-6-(butylamino)-1,3,5-triazin-2-yl]diamino-11,23-dinitro-25,26,27,28-tetrapropoxycalix[4]arene (3) was prepared from bis(chlorotriazine) 27 (4.6 g, 4.8 mmol), *n*-butylamine (17.0 mL, 171 mmol), and DIPEA (10.0 mL, 57.0 mmol) in THF (100 mL). The residue was recrystallized from CH_2Cl_2/EtOH to give pure dimelamine 3 as a yellow solid in 81% yield. M.p. 185–190 °C. ^{1}H NMR: δ = 7.7 (brs, 4H, *o*-NO_2ArH), 6.7–6.2 (m, 4H, *o*-NHArH + ArNH), 5.2–4.7 (m, 6H, NH), 4.39, 3.17 (AB q, 8H, ^2J(H,H) = 13.6 Hz, $ArCH_2Ar$), 4.1–3.9 (m, 4H, OCH_2), 3.8–3.6 (m, 4H, OCH_2), 3.3–3.1 (m, 4H, NCH_2), 2.0–1.6 (m, 8H, OCH_2CH_2), 1.6–1.2 (m, 8H, $NCH_2CH_2CH_2$), 1.1–0.8 [m, 18H, $O(CH_2)_2CH_3$ + $N(CH_2)_3CH_3$]. MS (FAB): *m/z* = 1044.3 (100) ([*M*+2H$^+$], calcd 1044.6). $C_{54}H_{70}N_{14}O_8$·EtOH: calcd C 61.74, N 18.00, H 7.03; found: C 61.67, N 18.23, H 7.12.

5,17-Diamino-11,23-*N,N'*-bis[4-amino-6-(butylamino)-1,3,5-triazin-2-yl]-diamino-25,26,27,28-tetrapropoxycalix[4]arene (4): Excess hydrazine monohydrate (1.0 mL) and a catalytic amount of Raney Ni were added to a suspension of 1,3-dinitro 3 (0.50 g, 0.48 mmol) in THF/MeOH (100 mL, 1:1 *v/v*). The mixture was refluxed for 2 h. Then the suspension was filtered immediately over Celite and evaporated to dryness to give pure diamine 4 as a white solid in quantitative yield. M.p. 175–180 °C (MeOH). ^{1}H NMR: δ = 6.6–6.2 (m, 10H, ArH + NH), 5.1–4.8 (m, 6H, NH), 4.35, 2.97 (AB q, 8H, ^2J(H,H) = 13.0 Hz, $ArCH_2Ar$), 3.9–3.6 (m, 8H, OCH_2), 3.34 (q, 4H, ^3J(H,H) = 6.5 Hz, NCH_2), 2.0–1.3 [m, 16H, OCH_2CH_2 + $NCH_2CH_2CH_2$], 1.04 [t, 6H, ^3J(H,H) = 7.2 Hz, $O(CH_2)_2CH_3$], 1.0–0.8 [m, 12H, $N(CH_2)_3CH_3$ + $O(CH_2)_2CH_3$]. MS (FAB): *m/z* = 983.9 (100) ([*M*+H$^+$], calcd 983.6). $C_{54}H_{74}N_{14}O_4$·2H_2O: calcd C 63.62, N 19.24, H, 7.71; found: C 63.76, N 19.00, H, 7.52.

5,17-Bis(acetamido)-11,23-*N,N'*-bis[4-amino-6-(butylamino)-1,3,5-triazin-2-yl]diamino-25,26,27,28-tetrapropoxycalix[4]arene (5): K_2CO_3 (1 M) was added to a turbid solution of 1,3-diamine 4 (100 mg, 0.102 mmol) in THF/EtOAc (40 mL, 1:1 *v/v*), which rapidly clarified. Excess acetyl chloride (0.3 mL) was then added, and the two-phase solution was vigorously stirred for 1 h, after which TLC analysis showed the complete disappearance of starting material. The reaction mixture was washed with H_2O (3 × 25 mL) and brine (25 mL) and dried over Na_2SO_4. Removal of the solvent and recrystallization from $CHCl_3$/hexane gave pure 5 as an off-white solid in 83% yield. M.p. 258–260 °C. ^{1}H NMR ([D$_4$]methanol/[D$_1$]chloroform 1:9) δ = 7.0 (brs, 4H, ArH), 6.4 (brs, 4H, ArH), 4.32, 3.03 (AB q, 8H, ^2J(H,H) = 13.2 Hz, $ArCH_2Ar$), 4.0–3.8 (m, 4H, OCH_2), 3.56 (t, 4H, ^3J(H,H) = 6.6 Hz, OCH_2), 3.4–3.2 (m, 4H, NCH_2), 2.0–1.7 (m, 8H, OCH_2CH_2), 1.84 [s, 6H, $C(O)CH_3$], 1.6–1.2 (m, 8H, $NCH_2CH_2CH_2$), 1.00 [t, 6H, ^3J(H,H) = 7.3 Hz, $O(CH_2)_2CH_3$], 1.0–0.7 [m, 12H, $N(CH_2)_3CH_3$ + $O(CH_2)_2CH_3$]. MS (FAB): *m/z* = 1068.1 (100) ([*M*+H]$^+$, calcd 1067.6). $C_{58}H_{78}N_{14}O_6$·0.25$CHCl_3$·0.5*n*-hexane: calcd C 64.52, N 17.20, H 7.54; found: C 64.58, N 17.48, H 7.53.

11-Amino-5,17-*N,N'*-bis[4-amino-6-(butylamino)-1,3,5-triazin-2-yl]diamino-25,26,27,28-tetrapropoxycalix[4]arene (6) was prepared from monophthalimide 32 (0.20 g, 0.20 mmol), *n*-butylamine (0.7 g, 7.0 mmol), and DIPEA (0.49 g, 2.8 mmol) in THF (25 mL). The crude material was refluxed for 2 h in EtOH/THF (30 mL, 5:1) in the presence of excess hydrazine (0.20 mL). After evaporation of the solvents, the residue was dissolved in CH_2Cl_2 (50 mL), washed with 1 N NaOH (2 × 25 mL), H_2O (2 × 25 mL), and brine (25 mL), and dried over Na_2SO_4. Removal of the solvent gave crude dimelamine 6, which was recrystallized from CH_2Cl_2/hexane to give pure 6 in 54% yield. M.p. 150–155 °C (slow phase transition). ^{1}H NMR: δ = 7.0–6.1 (m, 9H, ArH), 4.9 (brs, 6H, NH), 4.41, 4.35 (2d, 4H, ^2J(H,H) = 13.5 and 13.2 Hz, $ArCH_2Ar$), 4.0–3.6 (m, 8H, OCH_2), 3.5–3.2 (m, 6H, NCH_2 + NH_2), 3.09, 2.96 (2d, 4H, ^2J(H,H) = 13.4 and 13.3 Hz, $ArCH_2Ar$),

© WILEY-VCH Verlag GmbH, D-69451 Weinheim, 1997
0947-6539/97/0311-1830 $ 17.50+.50/0 Chem. Eur. J. 1997, 3, No. 11

UM00012348
NOVARTIS EXHIBIT 1017
Novartis v. Regents, IPR2023-01346
Page 1094 of 4460

2.0–1.8 (m, 8H, OCH_2CH_2), 1.6–1.3 (m, 8H, $NCH_2CH_2CH_2$), 1.04 [t, 6H, $^3J(H,H) = 7.4$ Hz, $O(CH_2)_2CH_3$], 1.0–0.8 [m, 12H, $O(CH_2)_2CH_3 + N(CH_2)_3CH_3$]. MS (FAB): $m/z = 968.8$ (100) ($[M+H]^+$, calcd 968.6). $C_{54}H_{73}N_{13}O_4 \cdot 0.6CH_2Cl_2 \cdot 0.25n$-hexane: calcd C 64.74, N 17.50, H 7.52; found: C 64.61, N 17.54, H 7.48.

11-Acetamido-5,17-*N,N'*-bis[4-amino-6-(butylamino)-1,3,5-triazin-2-yl]diamino-25,26,27,28-tetrapropoxycalix[4]arene (7): The reaction was carried out according to the procedure described for compound **5**, by using monoamine **6** (50 mg, 52 μmol) and excess acetyl chloride (0.10 mL) in a mixture of EtOAc/1 M K_2CO_3 (20 mL, 1:1), to give monoamide **7** in 65% yield after recrystallization from CH_2Cl_2/hexane. M.p. 150–155 °C (slow phase transition). ^{1}H NMR: $\delta = 7.0$–6.1 (m, 9H, ArH), 5.1 (brs, 6H, NH), 4.41, 4.38 (2d, 4H, $^2J(H,H) = 13.1$ and 13.2 Hz, $ArCH_2Ar$), 4.0–3.6 (m, 8H, OCH_2), 3.5–3.2 (m, 4H, NCH_2), 3.09, 3.07 (2d, 4H, $^2J(H,H) = 13.3$ and 12.9 Hz, $ArCH_2Ar$), 2.06 [s, 3H, $C(O)CH_3$], 2.0–1.7 (m, 8H, OCH_2CH_2), 1.6–1.2 (m, 8H, $NCH_2CH_2CH_2$), 1.01 [t, 6H, $^3J(H,H) = 7.3$ Hz, $O(CH_2)_2CH_3$], 0.92 [t, 12H, $^3J(H,H) = 7.1$ Hz, $O(CH_2)_2CH_3 + N(CH_2)_3CH_3$]. MS (FAB): $m/z = 1011.0$ (100) ($[M+H]^+$, calcd 1010.6). $C_{56}H_{75}N_{13}O_5 \cdot 0.5CH_2Cl_2 \cdot 0.5n$-hexane: calcd C 65.21, N 16.62, H 7.30; found: C 65.22, N 16.64, H 7.47.

5,17-*N,N'*-Bis[4-amino-6-(butylamino)-1,3,5-triazin-2-yl]diamino-11,23-bis(1,1-dimethylethyl)-25,26,27,28-tetrapropoxycalix[4]arene (8) was prepared from crude bis(chlorotriazine) **28** (0.57 g, 0.57 mmol), *n*-butylamine (2.0 mL, 21 mmol), and DIPEA (1.2 mL, 6.9 mmol). Calix[4]arene dimelamine **8** was obtained as an orange oil in 97% overall yield (based on diamine **16**). ^{1}H NMR: $\delta = 6.97$ (s, 4H, *o*-*t*BuArH), 6.2–5.8 (m, 4H, *o*-NHArH), 5.5–4.8 (m, 6H, NH), 4.34, 3.03 (ABq, 8H, $^2J(H,H) = 13.3$ Hz, $ArCH_2Ar$), 4.0–3.8 (m, 4H, OCH_2), 3.57 (t, 4H, $^3J(H,H) = 6.6$ Hz, OCH_2), 3.19 (q, 4H, $^3J(H,H) = 6.5$ Hz, NCH_2), 2.0–1.7 (m, 8H, OCH_2CH_2), 1.5–1.2 (m, 8H, $NCH_2CH_2CH_2$), 1.25 [s, 18H, $C(CH_3)_3$], 1.02, 0.78 [2t, 12H, $^3J(H,H) = 7.4$ Hz, $O(CH_2)_2CH_3$], 0.84 [t, 6H, $^3J(H,H) = 7.2$ Hz, $N(CH_2)_3CH_3$]. HRMS (FAB): $m/z = 1065.7$ (100) ($[M+H^+]$, calcd for $C_{62}H_{88}N_{12}O_4$: 1065.7).

5,17-*N,N'*-Bis[4-amino-6-(butylamino)-1,3,5-triazin-2-yl]diamino-11,23-diiodo-25,26,27,28-tetrapropoxycalix[4]arene (9) was prepared from crude bis(chlorotriazine) **29** (1.3 g, 1.0 mmol), *n*-butylamine (4.0 mL, 40 mmol), and DIPEA (2.3 mL, 13 mmol). Crude calix[4]arene dimelamine was mixed with 2 equiv of DEB and subsequently purified by flash column chromatography (SiO_2, $MeOH/CH_2Cl_2$ 10:90). The product containing fractions were washed with 1 N NaOH (3 × 25 mL), H_2O (3 × 25 mL), and brine (25 mL), and dried over Na_2SO_4. Evaporation of the solvent in vacuo gave pure dimelamine **9** as a yellow solid in a 75% overall yield (based on 1,3-diamine **17**). M.p. 185–187 °C (CH_2Cl_2). ^{1}H NMR: $\delta = 7.35$ (s, 4H, *o*-IArH), 6.6–6.1 (m, 6H, *o*-NH_2ArH + NH), 4.9 (brs, 6H, NH), 4.35, 3.05 (ABq, 8H, $^2J(H,H) = 13.3$ Hz, $ArCH_2Ar$), 4.0–3.9 (m, 4H, OCH_2), 3.64 (t, 4H, $^3J(H,H) = 6.9$ Hz, OCH_2), 3.34 (q, 4H, $^3J(H,H) = 6.5$ Hz, NCH_2), 2.0–1.8 (m, 8H, OCH_2CH_2), 1.7–1.3 (m, 8H, $NCH_2CH_2CH_2$), 1.1–0.8 [m, 18H, $O(CH_2)_2CH_3 + N(CH_2)_3CH_3$]. MS (FAB): $m/z = 1205.6$ (100) ($[M+H^+]$, calcd 1205.4). $C_{54}H_{70}I_2N_{12}O_4$: calcd C 53.82, N 13.95, H 5.86; found: C 53.95, N 13.93, H 6.00.

5,17-*N,N'*-Bis[4-amino-6-(butylamino)-1,3,5-triazin-2-yl]diamino-11,23-bis[(trimethylsilyl)ethynyl]-25,26,27,28-tetrapropoxycalix[4]arene (10) was prepared using crude bis(chlorotriazine) **30** (110 mg, 0.114 mmol), *n*-butylamine (0.41 mL, 4.1 mmol), and DIPEA (0.24 mL, 1.4 mmol) in THF (20 mL). The crude material was purified by flash column chromatography (SiO_2, 5% $MeOH/CH_2Cl_2$) to give pure dimelamine **10** as a colorless sticky solid in 46% overall yield (based on 1,3-diamine **18**). ^{1}H NMR: $\delta = 7.19$ (s, 4H, *o*-TMSC≡CArH), 6.3–6.0 (m, 6H, *o*-NHArH + NH), 5.3–4.7 (brm, 6H, NH), 4.30, 3.01 (ABq, 8H, $^2J(H,H) = 13.4$ Hz, $ArCH_2Ar$), 4.0–3.9 (m, 4H, OCH_2), 3.55 (t, 4H, $^3J(H,H) = 6.7$ Hz, OCH_2), 3.25 (q, 4H, $^3J(H,H) = 6.5$ Hz, NCH_2), 1.9–1.7 (m, 8H, OCH_2CH_2), 1.5–1.2 (m, 8H, $NCH_2CH_2CH_2$), 1.01 [t, 6H, $^3J(H,H) = 7.4$ Hz, $O(CH_2)_2CH_3$], 0.9–0.7 [m, 12H, $O(CH_2)_2CH_3 + N(CH_2)_3CH_3$], 0.21 [s, 18H, $Si(CH_3)_3$]. MS (FAB): $m/z = 1145.7$ (100) ($[M+H^+]$, calcd 1145.7). $C_{64}H_{88}N_{12}O_4Si_2 \cdot 1.5H_2O$: calcd C 65.55, N 14.33, H 7.82; found: C 65.62, N 14.39, H 7.63.

5,17-*N,N'*-Bis[4-amino-6-(butylamino)-1,3,5-triazin-2-yl]diamino-11,23-bis[(triethylsilyl)ethynyl]-25,26,27,28-tetrapropoxycalix[4]arene (11) was prepared from crude bis(chlorotriazine) **31** (90 mg, 0.10 mmol), *n*-butylamine (0.36 mL, 3.6 mmol), and DIPEA (0.21 mL, 1.2 mmol) in THF (15 mL). Pure dimelamine **11** was obtained as a colorless foam in quantitative yield. ^{1}H NMR: $\delta = 7.19$ (s, 4H, *o*-TESC≡CArH), 6.3–6.1 (m, 6H, *o*-NHArH + NH), 4.9 (brs, 4H, NH_2), 4.7 (brs, 2H, NH), 4.30, 3.02 (ABq, 8H, $^2J(H,H) = 13.4$ Hz, $ArCH_2Ar$), 4.0–3.9 (m, 4H, OCH_2), 3.55 (t, 4H, $^3J(H,H) = 6.6$ Hz, OCH_2), 3.24 (q, 4H, $^3J(H,H) = 6.5$ Hz, NCH_2), 1.9–1.7 (m, 8H, OCH_2CH_2), 1.5–1.2 (m, 8H, $NCH_2CH_2CH_2$), 1.1–1.0 [m, 24H, $O(CH_2)_2CH_3 + Si(CH_2CH_3)_3$], 0.86 [t, 6H, $^3J(H,H) = 7.1$ Hz, $N(CH_2)_3CH_3$], 0.79 [t, 6H, $^3J(H,H) = 7.5$ Hz, $O(CH_2)_2CH_3$], 0.63 [q, 12H, $^3J(H,H) = 7.8$ Hz, $Si(CH_2CH_3)_3$]. MS (FAB): $m/z = 1229.9$ (100) ($[M+H^+]$, calcd 1229.8). $C_{70}H_{100}N_{12}O_4Si_2 \cdot H_2O$: calcd C 67.37, N 13.47, H 8.24; found: C 67.28, N 13.47, H 8.41.

5,17-*N,N'*-Bis[4-amino-6-(butylamino)-1,3,5-triazin-2-yl]diamino-11,23-diethynyl-25,26,27,28-tetrapropoxycalix[4]arene (12): To a solution of calix[4]arene dimelamine **11** (33 mg, 29 μmol) in THF/MeOH (10 mL, 1:1 *v/v*) was added 1 N NaOH (1–2 mL), and the mixture was stirred at RT for 1 h. After removal of the solvent, the residue was taken up in CH_2Cl_2 (25 mL), washed with H_2O (3 × 10 mL) and brine (10 mL), and dried over Na_2SO_4. Evaporation of the solvent gave diacetylene **13** as a colorless solid in quantitative yield. M.p. 165–180 °C (slow phase transition). ^{1}H NMR: $\delta = 7.16$ (s, 4H, *o*-HC≡CArH), 6.5–6.1 (brm, 6H, NH/ArH), 5.2–4.8 (brm, 6H, NH), 4.32, 3.02 (ABq, 8H, $^2J(H,H) = 13.5$ Hz, $ArCH_2Ar$), 4.0–3.9 (m, 4H, OCH_2), 3.57 (t, 4H, $^3J(H,H) = 6.7$ Hz, OCH_2), 3.24 (q, 4H, $^3J(H,H) = 6.5$ Hz, NCH_2), 2.95 (s, 2H, ArC≡CH), 2.0–1.7 (m, 8H, OCH_2CH_2), 1.6–1.2 (m, 8H, $NCH_2CH_2CH_2$), 1.0 [t, 6H, $^3J(H,H) = 7.4$ Hz, $O(CH_2)_2CH_3$], 0.9–0.7 [m, 12H, $O(CH_2)_2CH_3 + N(CH_2)_3CH_3$]. MS (FAB): $m/z = 1002.1$ (100) ($[M+H^+]$, calcd 1001.6). $C_{58}H_{72}N_{12}O_4 \cdot 0.5H_2O$: calcd C 68.95, N 16.64, H 7.28; found: C 68.65, N 16.62, H 7.27.

Rosette Formations: Calix[4]arene dimelamine **2**–**12** (10 mg) were each mixed with 2 equiv of DEB and suspended in $[D_1]$chloroform or $[D_8]$toluene. The resulting mixtures were stirred until all solid material had dissolved. In cases where the material did not dissolve, addition of 10% methanol was usually sufficient to rapidly dissolve the solid material. The resulting solution was then evaporated to dryness, and the residue redissolved in $[D_1]$chloroform or $[D_8]$toluene to give clear solutions of the corresponding hydrogen-bonded assemblies.

MALDI-TOF Mass Spectra: The samples were prepared by stirring a solution of 10 mg of $(2)_3 \cdot (DEB)_6$ and ±1.0 mg (1.0 equiv) of $Ag^{(I)}CF_3COO$ in 1.0 mL of $CHCl_3$ until all solid material had dissolved. 10 μL of this solution was then mixed with 20 μL of a solution containing 3 mg L^{-1} of 2,5-dihydroxybenzoic acid in nitromethane. 1 μL of the resulting solution was finally loaded on the gold sample plate and submitted for the MALDI-TOF measurement.

Single Crystal X-Ray Diffraction: Crystal data and structure refinement for $(3)_3 \cdot (DEB)_6 \cdot (toluene)_{20}$ ($C_{350}H_{442}N_{54}O_{42}$); crystal size = 0.60 × 0.60 × 0.50 mm, $M_r = 6077.58$, rhombohedral crystal system, space group $R\bar{3}c$, $a = 38.7950(4)$, $c = 42.0004(9)$ Å, $\gamma = 120°$, $V = 54743.9(14)$ Å^3, $Z = 6$, $\rho_{calcd} = 1.106$ Mgm^{-3}. The diffraction data were collected with $Mo_{K\alpha}$ radiation ($\lambda = 0.71073$ Å, $2\theta_{max} \leq 40°$, ω scan mode, absorption coefficient = 0.066 mm^{-1}) and a graphite monochromator on a Siemens SMART diffractometer equipped with a CCD detector. Reflections collected 90185, independent reflections 5693 ($R_{int} = 0.0478$). The structure was solved by direct methods using the SHELXTL suite of programs.[35] All non-hydrogen atoms on the host were refined anisotropically; those of the guest (solvent) molecules were refined isotropically by full-matrix least-squares on F^2; hydrogen atoms were placed in calculated positions and allowed to ride on the parent atoms. No corrections were made for polarization or absorption. Data/restraints/parameters 5151/93/611, goodness-of-fit on $F^2 = 1.090$, final R indices [$I > 2.5\sigma(I)$]: $R_1 = 0.1236$, $wR_2 = 0.3359$, R indices (all data) $R_1 = 0.1641$, $wR_2 = 0.4331$, extinction coefficient 0.00051(11), largest diff. peak and hole 0.515 and −0.352 Å^{-3}.

The crystals are very sensitive to the absence of the solvent and are destroyed by exposure to air within several seconds. Selection of crystals to be introduced into the capillary was carried under the solvent. After the crystal was placed inside the capillary, a small amount of solvent was added and the capillary sealed.

UM00012349
NOVARTIS EXHIBIT 1017
Novartis v. Regents, IPR2023-01346
Page 1095 of 4460

Experiments were carried out on the same crystal at two temperatures; −150 °C and +20 °C. At a temperature of approximately −60 °C, the reflection widths broadened by several orders of magnitude, indicating a change in the crystal. Therefore the experimental errors at −150 °C were much more significant. However, the low-temperature experiment made it possible to observe the toluene molecules and these coordinates were used as the starting points for the refinement of their locations for the experiment at +20 °C.

Crystallographic data (excluding structure factors) for the structure reported in this paper have been deposited with the Cambridge Crystallographic Data Centre as supplementary publication no. CCDC-100 561. Copies of the data can be obtained free of charge on application to The Director, CCDC, 12 Union Road, Cambridge CB21EZ, UK (Fax: Int. code +(1223)336-033; e-mail: deposit@ccdc.cam.ac.uk).

Acknowledgements: We thank NATO for the Research Visit Grant to Dr. Udachin. We are grateful to Prof. N. Nibbering and R. Fokkens (Institute of Mass Spectrometry, University of Amsterdam) for the MALDI-TOF measurements.

Received: June 17, 1997 [F730]

[1] A. Fersht, *Enzyme Structure and Mechanism*, 2nd ed., Freeman and Company, New York, 1985.
[2] J. H. Arevalo, M. J. Taussig, I. A. Wilson, *Nature* 1993, *365*, 859–863.
[3] K. C. Garcia, M. Degano, R. L. Stanfield, A. Brunmark, M. R. Jackson, P. A. Peterson, L. Teyton, I. A. Wilson, *Science* 1996, *274*, 209–219.
[4] R. Breslow, *Acc. Chem. Res.* 1995, *28*, 146–153.
[5] J. Oriol Magrans, A. R. Ortiz, A. Molins, P. H. P. Lebouille, J. Sánchez-Quesada, P. Prados, M. Pons, F. Gago, J. de Mendoza, *Angew. Chem.* 1996, *108*, 1816–1819; *Angew. Chem. Int. Ed. Engl.* 1996, *35*, 1712–1715.
[6] a) Y. Aoyama, *Advances in Supramolecular Chemistry*; (Ed.: G. W. Gokel), JAI, Greenwich, 1992; b) Y. Aoyama, Y. Tanaka, H. Toi, H. Ogoshi, *J. Am. Chem. Soc.* 1988, *110*, 634–635; c) Y. Aoyama, Y. Tanaka, H. S. Sugahara, *ibid.* 1989, *111*, 5397–5404; d) For a recent review on resorcinarenes, see: P. Timmerman, W. Verboom, D. N. Reinhoudt, *Tetrahedron* 1996, *52*, 2663–2704.
[7] a) P. Timmerman, K. G. A. Nierop, E. A. Brinks, W. Verboom, F. C. J. M. van Veggel, W. P. van Hoorn, D. N. Reinhoudt, *Chem. Eur. J.* 1996, *1*, 132–143; b) I. Higler, P. Timmerman, W. Verboom, D. N. Reinhoudt, *J. Org. Chem.* 1996, *61*, 5920–5931; c) A. M. A. van Wageningen, P. Timmerman, J. P. M. van Duynhoven, W. Verboom, F. C. J. M. van Veggel, D. N. Reinhoudt, *Chem. Eur. J.* 1997, *3*, 639–654; d) E. Van Dienst, B. H. M. Snellink, I. Von Piekartz, M. H. B. Grote Gansey, F. Venema, M. C. Feiters, R. J. M. Nolte, J. F. J. Engbersen, D. N. Reinhoudt, *J. Org. Chem.* 1995, *60*, 6537–6545.
[8] For reviews on this topic, see: a) D. Philp, J. F. Stoddart, *Angew. Chem.* 1996, *108*, 1242–1286; *Angew. Chem. Int. Ed. Engl.* 1996, *35*, 1154–1194; b) D. S. Lawrence, T. Jiang, M. Levett, *Chem. Rev.* 1995, *95*, 2229–2260; c) J. S. Lindsey, *New J. Chem.* 1991, *15*, 153–180.
[9] J. Kang, J. Rebek, Jr., *Nature* 1997, *385*, 50–52.
[10] S. C. Zimmerman, F. Zeng, D. E. C. Reichert, S. V. Kolotuchin, *Science* 1996, *271*, 1095–1098.
[11] a) W. T. S. Huck, F. C. J. M. van Veggel, D. N. Reinhoudt, *Angew. Chem.* 1996, *108*, 1304–1306; *Angew. Chem. Int. Ed. Engl.* 1996, *35*, 1213–1215; b) W. T. S. Huck, F. C. J. M. van Veggel, B. L. Kropman, D. H. A. Blank, E. G. Keim, M. M. A. Smithers, D. N. Reinhoudt, *J. Am. Chem. Soc.* 1995, *117*, 8293–8294.
[12] M. Fujita, D. Oguro, M. Miyazawa, H. Oka, K. Yamaguchi, K. Ogura, *Nature* 1995, *378*, 469–471.
[13] a) M. Fujita, S. Nagao, K. Ogura, *J. Am. Chem. Soc.* 1995, *117*, 1649–1650; b) M. Fujita, K. Ogura, *Bull. Chem. Soc. Jpn.* 1995, *69*, 1471–1482 and references therein.
[14] a) M. Fujita, J. Yazaki, K. Ogura, *J. Am. Chem. Soc.* 1990, *112*, 5645–5647; b) P. J. Stang, V. V. Zhdankin, *ibid.* 1993, *115*, 9808–9809.
[15] R. H. Vreekamp, M. Hubert, J. P. M. van Duynhoven, W. Verboom, D. N. Reinhoudt, *Angew. Chem.* 1996, *108*, 1306–1309; *Angew. Chem. Int. Ed. Engl.* 1996, *35*, 1215–1218.
[16] M. Mammen, E. E. Simanek, G. M. Whitesides, *J. Am. Chem. Soc.* 1996, *118*, 12614–12623. For a general overview of this work, see: G. M. Whitesides, E. E. Simanek, J. P. Mathias, C. T. Seto, D. N. Chin, M. Mammen, D. M. Gordon, *Acc. Chem. Res.* 1995, *28*, 37–44 and references therein.
[17] A. Marsh, M. Silvestri, J.-M. Lehn, *Chem. Commun.* 1996, 1527–1528 and references therein.
[18] R. H. Vreekamp, W. Verboom, D. N. Reinhoudt, *Recl. Trav. Chim. Pays-Bas* 1996, *115*, 363–370.
[19] P. Timmerman, H. Boerrigter, W. Verboom, D. N. Reinhoudt, *Recl. Trav. Chim. Pays-Bas* 1995, *114*, 103–111.
[20] W. Verboom, A. Durie, R. J. M. Egberink, Z. Asfari, D. N. Reinhoudt, *J. Org. Chem.* 1992, *57*, 1313–1316.
[21] J.-D. van Loon, J. F. Heida, W. Verboom, D. N. Reinhoudt, *Recl. Trav. Chim. Pays-Bas* 1992, *111*, 353–359.
[22] D. M. Rudkevich, W. Verboom, D. N. Reinhoudt, *J. Org. Chem.* 1994, *59*, 3683–3686.
[23] S. Takahashi, Y. Kuroyama, K. Sonogashira, N. Hagihara, *Synthesis* 1980, 627–630.
[24] E. Kelderman, L. Derhaeg, G. J. T. Heesink, W. Verboom, J. F. J. Engbersen, N. F. van Hulst, A. Persoons, D. N. Reinhoudt, *Angew. Chem.* 1992, *104*, 1107–1109; *Angew. Chem. Int. Ed. Engl.* 1992, *31*, 1075–1077.
[25] P. Timmerman, W. Verboom, D. N. Reinhoudt, A. Arduini, S. Grandi, A. R. Sicuri, A. Pochini, R. Ungaro, *Synthesis* 1994, 185–189.
[26] J. P. Mathias, E. E. Simanek, G. M. Whitesides, *J. Am. Chem. Soc.* 1994, *116*, 4326–4340.
[27] "Pinched" means that two opposite aromatic rings become parallel, while the other two twist outward and "flatten" the calixarene.
[28] Two X-ray crystal structures from single rosette assemblies have been reported so far: a) J. P. Mathias, E. E. Simanek, J. A. Zerkowski, C. T. Seto, G. M. Whitesides, *J. Am. Chem. Soc.* 1994, *116*, 4316–4325; b) M. Mascal, N. M. Hecht, R. Warmuth, M. H. Moore, J. P. Turkenburg, *Angew. Chem.* 1996, *108*, 2348–2350; *Angew. Chem. Int. Ed. Engl.* 1996, *35*, 2204–2206.
[29] The question of which of the two possible conformers ("staggered or eclipsed") is formed is extensively discussed in ref. [22].
[30] The energetically most favorable pathway for racemization involves dissociation of one of the two rosettes, which subsequently reforms on the other side of the remaining rosette in an antiparallel orientation.
[31] Mass spectrometric evidence for noncovalent rosette assemblies has so far only been obtained with ESMS: a) K. C. Russell, E. Leize, A. Van Dorsselaer, J.-M. Lehn, *Angew. Chem.* 1995, *107*, 244–248; *Angew. Chem. Int. Ed. Engl.* 1995, *34*, 209–213; b) X. Cheng, Q. Gao, R. D. Smith, E. E. Simanek, M. Mammen, G. M. Whitesides, *J. Org. Chem.* 1996, *61*, 2204–2206.
[32] Addition of more than 2.0 equiv of $AgCF_3COO$ led to complete destruction of the box-like assembly.
[33] Recently, Rebek et al. reported a very similar solvent dependency for hydrogen-bonded assemblies: R. Meissner, X. Garcias, S. Mecozzi, J. Rebek, Jr., *J. Am. Chem. Soc.* 1997, *119*, 77–85.
[34] The minimized gas-phase structure of 4 shows a 2.3 Å hydrogen bond between the *p*-amino group and the melamine NH protons. The minimized gas-phase structure of 5 gives a much shorter hydrogen bond of 1.9 Å between the amide carbonyl group and the melamine NH protons.
[35] G. M. Sheldrick, *Acta Crystallogr.* 1990, *A46*, 467–473.

© WILEY-VCH Verlag GmbH, D-69451 Weinheim, 1997
0947-6539/97/0311-1832 $ 17.50+.50/0

UM00012350
NOVARTIS EXHIBIT 1017
Novartis v. Regents, IPR2023-01346
Page 1096 of 4460

COMMUNICATION

ChemComm www.rsc.org/chemcomm

Mechanochemistry and co-crystal formation: effect of solvent on reaction kinetics†

Ning Shan,[a] Fumio Toda[b] and William Jones*[a]

[a] *Department of Chemistry, University of Cambridge, Lensfield Road, Cambridge, UK CB2 1EW. E-mail: wj10@cam.ac.uk; Fax: 44 1223 336362; Tel: 44 1223 336468*

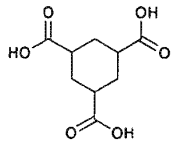
[b] *Department of Chemistry, Faculty of Science, Okayama University of Science, Okayama, 700-0005, Japan*

Received (in Cambridge, UK) 26th July 2002, Accepted 6th September 2002
First published as an Advance Article on the web 18th September 2002

We demonstrate that significant improvements in kinetics of co-crystal formation by grinding can be achieved by the addition of minor amounts of appropriate solvent.

The synthesis of crystalline supramolecular structures mediated by hydrogen bonds is of considerable importance.[1–4] In the case of co-crystals, these are generally formed by dissolution and re-crystallisation from a suitable solvent, although sublimation and growth from the melt are also used. The use of grinding a solid mixture has also been described. Solid-state grinding, *i.e.* the use of mechanical forces to create new molecular and supramolecular assemblies—mechanochemistry—can be regarded as an attractive and eco-friendly alternative route, avoiding the use of large amounts of solvent.[5–10] The utilisation of solid-state grinding, however, is limited. In certain instances, it is known that even though co-crystals are readily formed from solution, co-crystals are difficult to form even after extensive grinding.[11] Here, we report a significant increase in kinetics by the appropriate use of very small quantities of solvent.

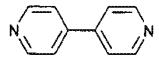
Several co-crystals of cyclohexane-1,3*cis*,5*cis*-tricarboxylic acid (**CTA**, $C_6H_9(COOH)_3$), the symmetry analogue of benzene-1,3,5-tricarboxylic acid ($C_6H_3(COOH)_3$, trimesic acid) which has been extensively employed as a building block in supramolecular chemistry,[12,13] have been synthesized using the solution-based method and their structures have been determined.[14]



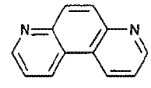
CTA



HTMA



Bipy



fPh

When a mixture of **CTA** and hexamethyltetramine (**HMTA**) are ground together in a ball mill for 20 min,[15] a distinct change in the powder X-ray diffraction pattern takes place.[16] Fig. 1 shows the powder XRD patterns of pure **CTA**, pure **HMTA** as well as the 1:1 mixture after 20 min grinding. Reflections associated with the reactants decrease in intensity while new reflections appear. The simulated powder pattern of **CTA·HMTA** (generated on the basis of its determined single crystal XRD structure[17]) and the pattern obtained show excellent agreement. The structures generated by grinding and from solution are, therefore, identical.

† Electronic supplementary information (ESI) available for PXRD profiles showing the grinding results for **CTA** + **Bipy** with and without solvent as well as **CTA** + **2fPh** with different solvents. See http://www.rsc.org/suppdata/cc/b2/b207369m/

DOI: 10.1039/b207369m

Co-crystallisation by simple grinding is, however, not always successful. The co-crystal structure of **CTA** and 4,4′-bipyridine (**Bipy**) has been determined by single-crystal X-ray diffraction analysis with co-crystals grown from MeOH solution.[18] When an equimolar mixture of **CTA** and **Bipy** is ground for 1 h, however, only partial reaction occurs. Reflections in the PXRD pattern of the ground sample associated with the original components are still clearly present. When the reaction of **CTA** and **Bipy** is repeated, however, but now with the addition of approximately 0.05 ml of MeOH,[19,20] co-crystallisation is found to be significantly accelerated such that complete conversion (as monitored by PXRD) is achieved in 20 min.†

For co-crystals of **CTA** and 4,7-phenanthroline (**fPh**), few reflections corresponding to the simulated **CTA·2fPh** PXRD pattern appear even after a considerable length of time grinding **CTA** with **fPh** (molar ratio of 1:2), despite the fact that the **CTA·2fPh** co-crystals can be readily obtained from MeOH solution. Fig. 2 shows the PXRD patterns of **CTA·2fPh** prepared by grinding with small amount of MeOH. After 5 min, reflections in the powder pattern associated with **CTA·2fPh** appear while the peaks matching the original reactants still remain but with diminished intensities. The observed PXRD pattern after 10 min is found to be very similar to the simulated PXRD pattern (Fig. 2(g)), and the reflections associated with **CTA** and **fPh** absent.

In order to rationalize how small amounts of solvent may influence the co-crystal formation, several different kinds of solvents have been tested. Water, in which **CTA** is very soluble but **fPh** only partially, is found to accelerate the reaction. Similarly, co-crystals were also formed by grinding using ethyl acetate in which **fPh** is soluble but not **CTA**. Acetonitrile, in which both **CTA** and **fPh** are only partly soluble, also accelerates the reaction. An important distinction, however, arises with cyclohexane—a liquid in which neither **CTA** nor

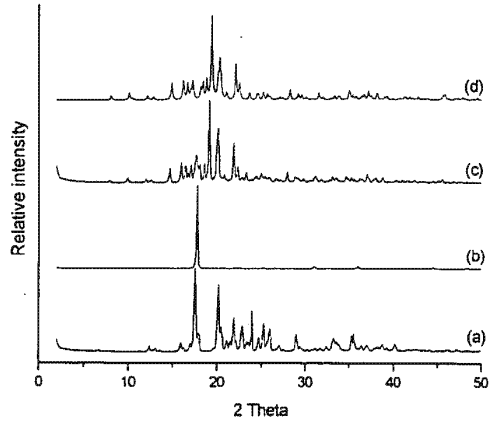


Fig. 1 Powder X-ray diffraction pattern of (a) **CTA**, (b) **HMTA**, (c) ground mixture of **CTA** + **HMTA** (20 min), (d) simulated pattern from single-crystal structure of **CTA·HMTA**.

 This journal is © The Royal Society of Chemistry 2002

UM00012351
NOVARTIS EXHIBIT 1017
Novartis v. Regents, IPR2023-01346
Page 1097 of 4460

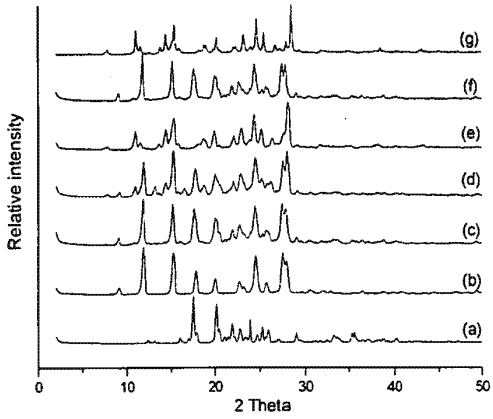


Fig. 2 Powder X-ray diffraction pattern of (a) **CTA**, (b) **fPh**, (c) ground dry mixture of **CTA** + 2**fPh** (1 h), (d) ground mixture of **CTA** + 2**fPh** with MeOH (5 min), (e) ground mixture of **CTA** + 2**fPh** with MeOH (10 min), (f) ground mixture of **CTA** + 2**fPh** with cyclohexane (1.5 h), (g) simulated pattern from single-crystal structure of **CTA.2fPh**.

fPh are soluble. In this case no kinetic enhancement is observed and no reaction occurs even after 1.5 hour grinding (Fig. 2(f)).

This paper reports the important observation that the addition of relatively minor amounts of a solvent can significantly enhance the rate of co-crystal formation. Whilst clearly of benefit to the organic solid-state chemists, it is likely to be of interest to all areas of chemistry where mechanochemistry methods are envisaged. The observed enhancement in kinetics might be rationalised by the additional degrees of orientational and conformational freedom open to molecules at the various interfaces as well as the enhancement of opportunities for molecular collisions. In addition, tiny co-crystal seeds may be envisaged to form within the solvent during the grinding process so that the rate of co-crystallisation can be increased. The choice of solvent used in grinding, therefore, should be one that is necessarily able to dissolve at least part of the original components. On the other hand, solid-state grinding involving small amount of solvents, might also be utilised to pre-test whether co-crystals can be synthesized from solutions. For instance, the co-crystal of **CTA** and phenazine, whose structure has not been reported in the Cambridge Structural Database[21] to date, cannot be synthesized from solution in our study. Interestingly, it cannot be obtained by grinding in the presence of various kinds of solvent either. Given the potential for tailoring solid-state properties *via* co-crystal formation, the use of small amounts of solvent allied with sample mechanical treatment may provide an important synthetic route in organic solid-state chemistry.

We are grateful for a DWEF Cambridge Scholarship and ORS Award (N. S.).

Notes and references

1 W. Jones, *Organic Molecular Solids: Properties and Applications*, CRC Press, New York, 1997, p. 181.
2 J. L. Atwood, J. E. D. Davies, D. D. MacNicol and F. Vogtle, *Comprehensive Supramolecular Chemistry*, Pergamon, Oxford, 1996, Vol. 9.
3 A. D. Bond and W. Jones, in *Supramolecular Organization and Materials Design*, ed. W. Jones and C. N. R. Rao, Cambridge University Press, Cambridge, 2002, p. 391.
4 G. R. Desiraju, *Crystal Engineering: The Design of Organic Solids*, Elsevier, New York, 1989.
5 M. C. Etter and G. M. Frankenbach, *Chem. Mater.*, 1989, **1**, 10.
6 F. Toda and H. Miyamoto, *Chem. Lett.*, 1995, 861.
7 F. Toda, *Acc. Chem. Res.*, 1995, **28**, 480.
8 V. R. Pedireddi, W. Jones, A. P. Chorlton and R. Docherty, *Chem. Commun.*, 1996, 987.
9 J. Schmeyers, F. Toda, J. Boy and G. Kaupp, *J. Chem. Soc., Perkin Trans. 2*, 1998, 989.
10 K. Tanaka and F. Toda, *Chem. Rev.*, 2000, **100**, 1025.
11 E. Batchelor, PhD thesis, University of Cambridge, 2000, 189.
12 C. V. K. Sharma and M. J. Zaworotko, *Chem. Commun.*, 1996, 2655.
13 S. V. Kolotuchin, P. A. Thiessen, E. E. Fenlon, S. R. Wilson, C. J. Loweth and S. C. Zimmerman, *Chem. Eur. J.*, 1999, **5**, 2537.
14 N. Shan, A. D. Bond and W. Jones, submitted for publication.
15 Samples used for PXRD analysis were prepared using a Retsch MM 200 Mixer Mill, with oscillation frequency of 15 Hz. The mixtures used in grinding are *ca.* 200 mg in weight.
16 The PXRD pattern was recorded at room temperature using a Philips PW3710 diffractometer with Cu Kα radiation (λ = 1.5418 Å). Patterns were obtained using a 2-theta range of 2.00 to 50.00 degrees in increments of 0.02 degrees with a count time of 1.00 second per step.
17 Cerius,[2] Accelrys Ltd., Cambridge, UK.
18 N. Shan, A. D. Bond and W. Jones, *Cryst. Eng.*, 2002, **5**, 9.
19 All solvents introduced into the grinding system are *ca.* 0.05ml (2 drops from a pipette) in scale. The solvents have been evaporated at room temperature before the PXRD analysis.
20 **Bipy** and **fPh** are very soluble in alcohol (V. R. Lide, *Handbook of Chemistry and Physics*, CRC Press, Boca Raton, New York, 1997). In our test, **CTA** is found to be soluble in MeOH. The solubility of chemicals in different solvents is considered at room temperature.
21 CCDC, The Cambridge Structural Database, ConQuest 1.4, Cambridge, UK, 2002.

UM00012352
NOVARTIS EXHIBIT 1017
Novartis v. Regents, IPR2023-01346
Page 1098 of 4460

Journal of Inclusion Phenomena and Molecular Recognition in Chemistry 20: 277–290, 1995.

© 1995 *Kluwer Academic Publishers. Printed in the Netherlands.*

X-Ray Structure and Thermal Analysis of a 1 : 1 Complex between (*S*)-Naproxen and Heptakis(2,3,6-tri-*O*-methyl)-β-cyclodextrin

MINO R. CAIRA,* VIVIENNE J. GRIFFITH and LUIGI R. NASSIMBENI
Department of Chemistry, University of Cape Town, Rondebosch, 7700, South Africa.

and

BOSCH VAN OUDTSHOORN
South African Druggists, Scientific and Medical Affairs, P.O. Box 787028, Sandton, 2146, South Africa.

(Received: 2 November 1994; in final form: 24 January 1995)

Abstract. An inclusion complex between TRIMEB and (*S*)-naproxen has been crystallised and characterised by physicochemical methods including X-ray analysis. The complex crystallises in the orthorhombic crystal system, space group $P2_12_12_1$, with $a = 15.179(4)$, $b = 21.407(5)$, $c = 27.67(1)$ Å and $Z = 4$. The structure was solved using published coordinates for the skeleton atoms of TRIMEB in an isomorphous complex. Refinement by full-matrix least-squares analysis yielded $R = 0.0571$ for 6573 unique observed reflections. Hydrophobic forces are responsible for the inclusion of the drug, which has its methoxy group buried in the cavity of the host and its propionic acid moiety protruding from the O(2), O(3) side of the TRIMEB molecule. Both host and guest undergo conformational changes on complexation relative to their conformations observed in the TRIMEB monohydrate and naproxen crystal structures respectively. Complex units pack in a screw-channel mode in a head-to-tail fashion with their axes almost parallel to the *b*-axis.

Key words: Permethylated β-cyclodextrin, (*S*)-naproxen, inclusion complex, X-ray crystal structure.

1. Introduction

The cyclodextrins and their derivatives are finding increasing application in the pharmaceutical industry as carrier molecules for many drugs, as complexation can result in improved physical characteristics such as increased aqueous solubility [1]. The interaction between the non-steroidal anti-inflammatory drug, naproxen ((*S*)-6-methoxy-α-methyl-2-naphthaleneacetic acid), and β-cyclodextrin has been investigated in solution and in the solid state [2–7]. Molecular modelling and NMR studies have generated proposals on the mode of inclusion of the drug by β-cyclodextrin [2, 5–7] and stability constants for the complex have been estimated by phase solubility, NMR, fluorescence, circular dichroism and U.V. techniques [2, 5–7]. The ^{13}C-NMR study by Bettinetti *et al.* [2] also includes the

* Author for correspondence.

UM00012353
NOVARTIS EXHIBIT 1017
Novartis v. Regents, IPR2023-01346
Page 1099 of 4460

calculation of stability constants in solution of naproxen complexes with some β-cyclodextrin derivatives, amongst which is a partially methylated β-cyclodextrin. However, there are no data available on the interaction between naproxen and permethylated β-cyclodextrin ((2,3,6-tri-*O*-methyl)-β-cyclodextrin, or TRIMEB). Permethylation of β-cyclodextrin renders it many times more soluble and, as such, potentially more useful in the pharmaceutical industry [8]. We report here the preparation, thermal analysis and crystal structure of a naproxen–TRIMEB complex.

2. Experimental

2.1. MATERIALS

TRIMEB (Cyclolab, Hungary) and (*S*)-naproxen (Syntex, U.S.A.) were used as received.

2.2. THERMOGRAVIMETRIC ANALYSIS AND DIFFERENTIAL SCANNING CALORIMETRY

Thermogravimetric (TGA) and differential scanning calorimetric (DSC) traces were recorded on a Perkin–Elmer PC7-Series Thermal Analysis System in the range 30–180 °C at a scanning rate of 5 °C/min under N_2 gas-purge. Sample masses were 7–8 mg. Samples were placed in vented pans.

2.3. PREPARATION OF THE NAPROXEN–TRIMEB COMPLEX

Crystals of the complex, which are colourless and prismatic, were grown at approximately 50 °C from an aqueous solution prepared by mixing equimolar amounts of (*S*)-naproxen and TRIMEB in distilled water at room temperature and then filtering off the undissolved naproxen.

2.4. CRYSTAL STRUCTURE SOLUTION

In order to optimise diffraction data quality, reflection intensities were measured from a crystal of dimensions 0.50 × 0.50 × 0.50 mm cooled to −15 °C (258 K) on an Enraf–Nonius CAD-4 diffractometer using graphite-monochromated MoKα radiation ($\lambda = 0.71069$ Å). Accurate cell dimensions were obtained by least-squares analysis of the setting angles of 24 reflections in the range $16 \leq \theta \leq 17°$. Intensity data were collected by the ω-scan technique. To ensure accurate measurement of weak reflections, a pre-scan acceptance parameter of zero was chosen to force their final intensity scans up to a maximum time of 100 s per reflection. Data were collected to $(\sin\theta/\lambda)_{max} = 0.595$ Å^{-1}. Three standard reflections (2 13 15; 2 16 8; 10 3 13), which were monitored every hour, showed a 4% decrease in intensity during data collection. Orientation control was performed every 150 reflections. Data were corrected for Lp effects. Crystal data collection and refinement details

UM00012354
NOVARTIS EXHIBIT 1017
Novartis v. Regents, IPR2023-01346
Page 1100 of 4460

are listed in Table I. The structure was solved using published coordinates for the non-hydrogen cyclodextrin atoms (excluding the O(6), C(7), C(8) and C(9) atoms of each methylglucose residue – see Figure 2 for numbering scheme) of the isomorphous *p*-iodophenol–TRIMEB tetrahydrate complex [9]. A difference Fourier synthesis after refinement by full-matrix least-squares techniques (minimisation of $[\sum(w(F_0^2 - F_c^2)^2)/\sum(w(F_0^2)^2]^{1/2}$) [10] revealed all the non-hydrogen atoms of the guest and many of the remaining non-hydrogen atoms of the host. Once all non-hydrogen atoms had been located from subsequent difference Fourier syntheses, all the cyclodextrin hydrogen atoms linked to carbon atoms were inserted at idealised positions with C—H = 1.00 Å. All the methyl hydrogen atoms were assigned a common variable isotropic temperature factor and the remaining hydrogen atoms of each methylglucose moiety were assigned common variable isotropic temperature factors. All non-hydrogen atoms were assigned anisotropic temperature factors, except for C(7G3), which was disordered, and C(l), C(5), C(9) and C(10) of the naproxen molecule, which, in addition, were refined subject to the following distance constraints, on account of abnormally long bond distances for C(1)—C(9) and C(5)—C(10): C(1)—C(2), C(1)—C(9), C(5)—C(6) and C(5)—C(10) with C—C = 1.42 Å, σ = 0.005 Å. The hydrogen atoms attached to the carbon atoms of the guest were also inserted at idealised positions with C—H = 1.00 Å and assigned a common isotropic temperature factor. The carboxyl hydrogen atom of the guest was located in a difference Fourier synthesis and allowed to refine subject to a distance constraint (O—H = 1.00 Å, σ = 0.05 Å). Final fractional coordinates for non-hydrogen atoms are given in Table II.

3. Results and Discussion

3.1. THERMOGRAVIMETRIC ANALYSIS AND DIFFERENTIAL SCANNING CALORIMETRY

TGA and DSC traces are given in Figure 1. TGA of the complex showed a loss of 0.4 weight percent from 30 to 150 °C. This is negligible and probably represents surface water. There was no evidence for any water molecules in the structure solution and crystals of the complex showed no signs of cracking in this temperature range on a hot-stage microscope. It was therefore concluded that the complex contains no water molecules of crystallisation. The DSC trace confirmed this as it was featureless except for an endotherm corresponding to fusion of the complex at 165.7 °C (onset melting temperature).

3.2. CRYSTAL STRUCTURE SOLUTION

Numbering schemes for the host and guest are given in Figure 2, which shows the host and guest molecules separately. Figure 3 shows a stereodiagram of the (*S*)-naproxen–TRIMEB complex. The naproxen molecule is inserted in the host cavity, with the propionic acid moiety protruding from the O(2), O(3) face. The mode of

UM00012355
NOVARTIS EXHIBIT 1017
Novartis v. Regents, IPR2023-01346
Page 1101 of 4460

TABLE I. Crystal data, experimental and refinement parameters for the title compound.

Molecular formula	$C_{63}H_{112}O_{35}\cdot C_{14}H_{14}O_3$
M_r/g mol^{-1}	1659.8
Crystal system	Orthorhombic
Space Group	$P2_12_12_1$
Z	4
a (Å)	15.179(4)
b (Å)	21.407(5)
c (Å	27.67(1)
V (Å^3)	8991(5)
D_x	1.226 g cm^{-3}
Crystal dimensions (mm)	0.5 × 0.5 × 0.5
Range scanned θ (°)	$1 \leq \theta \leq 25$
Index range	h: 0,18; k: 0,25; l: 0,32
Scan width (°)	0.8 + 0.35 tan θ
Aperture width (mm)	1.12 + 1.05 tan θ
No. of reflections collected	8655
No. of unique reflections	8613
No. of reflections with $I > 2\sigma(I)$	6573
No. of L.S. parameters	1050
$R1$ ($I > 2\sigma(I)$)	0.0571
$wR2$ (F^2)	0.1456
w	$[\sigma^2(F_0)^2 + (0.0859 \times P)^2 + (1.79 \times P)]^{-1}$ $P = (\max(F_0^2, 0 + F_c^2)/3$
S	1.120
Shift/e.s.d. max., average	0.362, 0.006
$(\Delta\rho)_{max}$ final (e Å^{-3})	0.56
$(\Delta\rho)_{min}$ final (e Å^{-3})	−0.27

inclusion will be discussed in more detail once the conformation of the host has been described. All seven methylglucose moieties of the TRIMEB molecule are in the $^4C_1$ chair conformation. Average bond lengths and angles for the host are within the standard deviations of those reported for other TRIMEB complexes [9, 12]. Atom C(7G3) is disordered over three sites with site occupancies of 0.56, 0.22 and 0.22. As is normally the case for TRIMEB, the O(2)—C(7) bonds are directed away from the cavity and the O(3)—C(8) bonds are directed towards the cavity [9, 11–14]. The C(6)—O(6) bonds of residues G1, G3, G5, and G6 are directed away from the cavity in the (−)-*gauche* conformation [15], while those of G2, G4 and G7 point towards the cavity in the (+)-*gauche* conformation. The O(6)—C(9) bonds of all glucose residues are *trans* to the corresponding C(5)—C(6) bonds except in G6, where the relationship is *gauche*. Table III lists values for the O(4)···O(4′)···O(4″) angles of the O(4) heptagon, radii of the O(4) heptagon, O(4)···O(4′) distances,

UM00012356
NOVARTIS EXHIBIT 1017
Novartis v. Regents, IPR2023-01346
Page 1102 of 4460

TABLE II. Final fractional atomic coordinates ($\times 10^4$) and equivalent isotropic displacement parameters ($Å^2 \times 10^3$) for the naproxen–TRIMEB complex.

$$U_{eq} = (1/3) \sum_i \sum_j U_{ij} a_i^* a_j^* a_i \cdot a_j$$

	x	y	z	U_{eq}/U_{iso}^*
C(1G1)	8639(3)	4589(2)	4730(2)	41(1)
C(2G1)	7926(3)	4129(2)	4883(2)	42(1)
C(3G1)	7392(3)	3910(2)	4447(2)	40(1)
C(4G1)	7014(3)	4495(2)	4210(2)	41(1)
C(5G1)	7758(3)	4930(2)	4063(2)	45(1)
C(6G1)	7449(4)	5522(2)	3830(2)	55(1)
C(7G1)	8543(4)	3703(3)	5595(2)	63(2)
C(8G1)	6683(4)	2936(3)	4350(3)	75(2)
C(9G1)	6413(6)	6332(3)	3897(3)	90(2)
O(2G1)	8277(2)	3590(2)	5113(1)	50(1)
O(3G1)	6718(2)	3507(2)	4602(1)	49(1)
O(4G1)	6497(2)	4310(2)	3802(1)	46(1)
O(5G1)	8250(2)	5104(1)	4488(1)	45(1)
O(6G1)	6787(3)	5800(2)	4118(1)	65(1)
C(1G2)	11859(3)	4139(2)	4046(2)	46(1)
C(2G2)	11565(3)	3720(2)	4468(2)	47(1)
C(3G2)	10566(3)	3716(2)	4504(2)	42(1)
C(4G2)	10166(3)	4360(2)	4507(2)	43(1)
C(5G2)	10558(3)	4774(2)	4109(2)	45(1)
C(6G2)	10313(4)	5447(2)	4164(2)	62(1)
C(7G2)	12721(4)	2985(4)	4536(3)	101(3)
C(8G2)	9928(4)	2798(2)	4869(2)	61(1)
C(9G2)	10344(8)	6406(3)	3761(4)	132(4)
O(2G2)	11823(2)	3093(2)	4421(1)	63(1)
O(3G2)	10311(2)	3402(2)	4941(1)	49(1)
O(4G2)	9244(2)	4278(2)	4426(1)	42(1)
O(5G2)	11506(2)	4742(2)	4129(1)	51(1)
O(6G2)	10517(3)	5770(2)	3734(2)	86(1)
C(1G3)	12446(3)	3881(2)	2176(2)	47(1)
C(2G3)	12445(4)	3270(2)	2451(2)	52(1)
C(3G3)	11927(4)	3293(2)	2916(2)	51(1)
C(4G3)	12174(3)	3863(2)	3213(2)	44(1)
C(5G3)	12090(3)	4441(2)	2896(2)	45(1)
C(6G3)	12316(3)	5058(2)	3125(2)	52(1)
C(7G3)[a]	12736(15)	2269(9)	2151(7)	120(6)*
C(73A)[b]	11511(21)	2504(15)	2076(11)	70(7)*
C(73B)[b]	12292(19)	2177(12)	2185(9)	51(6)*
C(8G3)	11382(6)	2412(3)	3354(3)	100(3)
C(9G3)	13409(6)	5602(3)	3528(3)	97(2)

UM00012357
NOVARTIS EXHIBIT 1017
Novartis v. Regents, IPR2023-01346
Page 1103 of 4460

TABLE II. Continued.

$U_{eq} = (1/3)\sum_i \sum_j U_{ij} a_i^* a_j^* a_i \cdot a_j$

	x	y	z	U_{eq}/U_{iso}^*
O(2G3)	12147(4)	2784(2)	2143(2)	83(1)
O(3G3)	12114(3)	2734(2)	3171(2)	70(1)
O(4G3)	11556(2)	3883(2)	3611(1)	46(1)
O(5G3)	12666(2)	4373(2)	2486(1)	47(1)
O(6G3)	13166(2)	5023(2)	3335(2)	66(1)
C(1G4)	10507(3)	4571(3)	694(2)	51(1)
C(2G4)	11356(3)	4194(3)	629(2)	54(1)
C(3G4)	11621(3)	3882(3)	1103(2)	48(1)
C(4G4)	11599(3)	4326(2)	1529(2)	46(1)
C(5G4)	10780(3)	4737(2)	1537(2)	45(1)
C(6G4)	10898(4)	5279(2)	1885(2)	55(1)
C(7G4)	11266(7)	3915(5)	−199(2)	119(3)
C(8G4)	12619(5)	3027(3)	932(3)	85(2)
C(9G4)	10188(6)	6099(3)	2277(3)	88(2)
O(2G4)	11284(3)	3719(2)	279(1)	72(1)
O(3G4)	12506(2)	3659(2)	1073(1)	57(1)
O(4G4)	11602(2)	3972(2)	1970(1)	46(1)
O(5G4)	10642(2)	5012(2)	1068(1)	50(1)
O(6G4)	10102(3)	5596(2)	1949(1)	70(1)
C(1G5)	7095(3)	4077(2)	582(2)	43(1)
C(2G5)	7682(3)	3709(2)	240(2)	46(1)
C(3G5)	8598(3)	3632(2)	425(2)	46(1)
C(4G5)	8973(3)	4267(2)	570(2)	41(1)
C(5G5)	8344(3)	4614(2)	904(2)	43(1)
C(6G5)	8624(3)	5270(2)	1028(2)	50(1)
C(7G5)	6571(4)	3108(3)	−147(3)	89(2)
C(8G5)	9431(6)	2766(3)	147(4)	108(3)
C(9G5)	9147(5)	6203(3)	697(2)	76(2)
O(2G5)	7330(3)	3105(2)	149(1)	64(1)
O(3G5)	9149(2)	3380(2)	62(1)	64(1)
O(4G5)	9803(2)	4160(2)	801(1)	46(1)
O(5G5)	7492(2)	4660(1)	677(1)	43(1)
O(6G5)	8859(2)	5586(2)	603(1)	52(1)
C(1G6)	4987(3)	3627(2)	2040(2)	47(1)
C(2G6)	5313(4)	3014(2)	1820(2)	53(1)
C(3G6)	6160(4)	3105(2)	1545(2)	49(1)
C(4G6)	6093(3)	3640(2)	1180(2)	46(1)
C(5G6)	5713(3)	4223(2)	1418(2)	44(1)
C(6G6)	5508(4)	4756(2)	1079(2)	54(1)

UM00012358
NOVARTIS EXHIBIT 1017
Novartis v. Regents, IPR2023-01346
Page 1104 of 4460

TABLE II. Continued.

$U_{eq} = (1/3)\sum_i \sum_j U_{ij} a_i^* a_j^* a_i \cdot a_j$

	x	y	z	U_{eq}/U_{iso}^*
C(7G6)	5099(7)	1973(3)	2090(3)	110(3)
C(8G6)	7263(5)	2354(3)	1317(4)	105(3)
C(9G6)	4171(4)	4480(4)	690(2)	85(2)
O(2G6)	5414(3)	2572(2)	2190(1)	68(1)
O(3G6)	6364(3)	2532(2)	1301(2)	69(1)
O(4G6)	6974(2)	3741(2)	1015(1)	49(1)
O(5G6)	4906(2)	4077(2)	1669(1)	49(1)
O(6G6)	5083(2)	4587(2)	643(1)	64(1)
C(1G7)	5679(3)	4617(2)	3742(2)	49(1)
C(2G7)	4940(3)	4140(2)	3678(2)	51(1)
C(3G7)	5108(3)	3746(2)	3227(2)	46(1)
C(4G7)	5211(3)	4172(2)	2791(2)	47(1)
C(5G7)	5856(4)	4703(2)	2884(2)	52(1)
C(6G7)	5811(5)	5198(3)	2506(2)	64(2)
C(7G7)	4609(4)	4033(4)	4515(2)	79(2)
C(8G7)	4485(4)	2727(3)	3322(2)	68(2)
C(9G7)	6695(9)	5907(5)	2086(4)	149(5)
O(2G7)	4854(2)	3729(2)	4078(1)	60(1)
O(3G7)	4382(2)	3345(2)	3134(1)	54(1)
O(4G7)	5576(2)	3817(2)	2397(1)	45(1)
O(5G7)	5683(2)	5013(2)	3335(1)	51(1)
O(6G7)	6626(4)	5506(3)	2471(2)	128(2)
C(1)	7191(5)	2085(3)	3160(2)	84(2)*
C(2)	7441(4)	1610(3)	3475(2)	74(2)
C(3)	8235(5)	1686(4)	3732(3)	95(2)
C(4)	8770(6)	2194(4)	3688(3)	98(2)
C(5)	9057(5)	3213(3)	3331(3)	99(2)*
C(6)	8774(5)	3693(3)	3017(3)	81(2)
C(7)	8000(5)	3605(4)	2781(3)	88(2)
C(8)	7496(6)	3090(4)	2816(3)	100(2)
C(9)	7738(4)	2628(3)	3109(2)	70(2)*
C(10)	8503(4)	2670(3)	3372(2)	68(2)*
C(11)	6876(4)	1044(3)	3558(2)	60(1)
C(12)	6524(5)	716(4)	3114(3)	81(2)
C(13)	6139(4)	1240(3)	3897(2)	64(2)
O(14)	5401(3)	1354(3)	3765(2)	93(2)
O(15)	6385(3)	1272(3)	4342(2)	85(1)
O(16)	9278(5)	4230(3)	2989(3)	129(2)
C(17)	8939(12)	4725(6)	2712(6)	181(6)

[a] Site occupancy 0.56.
[b] Site occupancy 0.22.

UM00012359
NOVARTIS EXHIBIT 1017
Novartis v. Regents, IPR2023-01346
Page 1105 of 4460

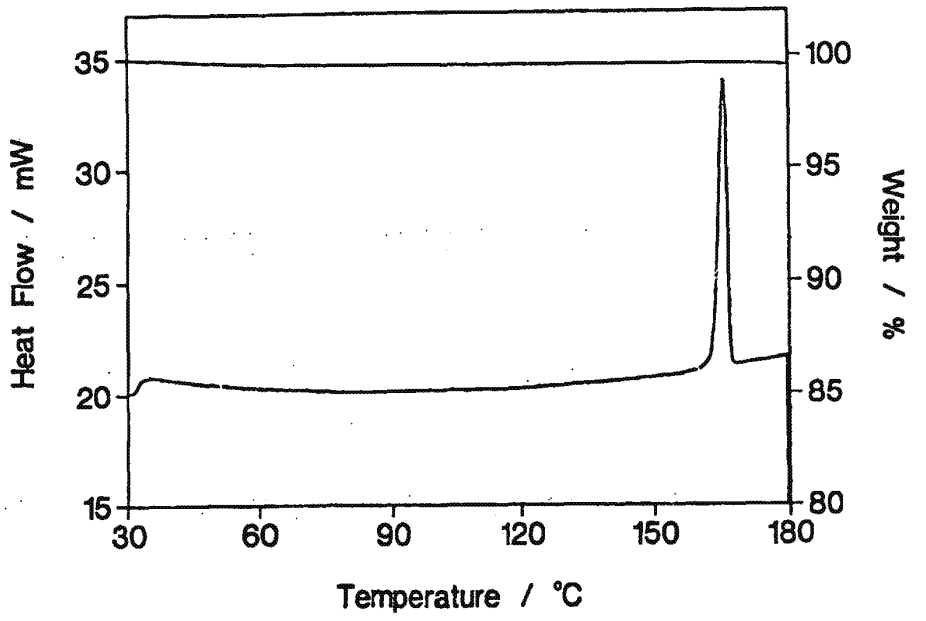


Fig. 1. TGA and DSC traces for the title compound.

tilt angles and deviations of the O(4) atoms from their least-squares plane. The values calculated for these parameters are comparable with those found for other TRIMEB complexes [9, 11–14] and, as usual, two glucose moieties have negative tilt angles (in this case G3 and G6), while all the others have positive tilt angles [11]. The TRIMEB molecule is cup-shaped with the C(6)—O(6)—C(9) groups of G1, G2, G4, G5 and G7 almost closing off the O(6) side of the TRIMEB cavity.

The distorted conformation of the TRIMEB molecule relative to the conformation observed for the parent β-cyclodextrin molecule is stabilised by numerous intramolecular C—H···O interactions, a common interaction found in carbohydrate crystal structures [16]. We have found that in the crystal strucure of TRIMEB monohydrate [17] the conformation of TRIMEB is stabilised by four intramolecular C($6G_n$)—H···O($5G_{n-1}$) hydrogen bonds. Furthermore, we have noted that in the known crystal structures of TRIMEB complexes, five of the relevant C(6)···O(5) distances are in the range 3.0–3.4 Å [17]. These hydrogen bonds are also present in the naproxen–TRIMEB crystal structure. In addition, there are two C—H···O interactions stabilising the negative tilt angles of G3 and G6, namely C(1G3)—H···O(3G4) and C(1G5)—H···O(6G6). Table IV lists C—H···O hydrogen bonding parameters.

Figure 3 is a stereoview of the title complex. The naproxen molecule is held in the TRIMEB cavity by hydrophobic forces and is inserted from the O(2), O(3) side of the cyclodextrin molecule with the methoxy group buried in the cavity near the

UM00012360
NOVARTIS EXHIBIT 1017
Novartis v. Regents, IPR2023-01346
Page 1106 of 4460

TABLE III. Geometrical data for TRIMEB.

i. Glycosidic oxygen angle (°) and radius (Å) of the O(4) heptagon (measured from the centre of gravity of seven O(4) atoms to each O(4) atom).

O(4G7)···O(4G1)···O(4G2)	130.4	G1	4.86
O(4G1)···O(4G2)···O(4G3)	124.2	G2	5.21
O(4G2)···O(4G3)···O(4G4)	122.2	G3	5.14
O(4G3)···O(4G4)···O(4G5)	139.0	G4	4.64
O(4G4)···O(4G5)···O(4G6)	120.1	G5	5.17
O(4G5)···O(4G6)···O(4G7)	125.5	G6	5.12
O(4G6)···O(4G7)···O(4G1)	130.2	G7	4.86
Average	127.4	Average	5.00

ii. O(4)···O(4′) distance (Å)

O(4G1)···O(4G2)	4.513	O(4G5)···O(4G6)	4.425
O(4G2)···O(4G3)	4.256	O(4G6)···O(4G7)	4.377
O(4G3)···O(4G4)	4.543	O(4G7)···O(4G1)	4.265
O(4G4)···O(4G5)	4.251	Average	4.376

iii. Tilt angle (°) and deviation (Å) of each O(4) atom from the least-squares plane through the seven O(4) atoms.

Residue	Tilt-angle	O(4) atom	Deviation
G1	27.0	O(4G1)	0.430(3)
G2	20.8	O(4G2)	0.225(2)
G3	−9.4	O(4G3)	−0.504(3)
G4	44.3	O(4G4)	−0.037(3)
G5	34.3	O(4G5)	0.581(3)
G6	−14.4	O(4G6)	−0.317(3)
G7	34.4	O(4G7)	−0.377(3)

TABLE IV. Intramolecular C—H···O hydrogen bonds.

		Distance (Å)			Angle (°)
C H	O	C···O	C—H	H···O	C—H···O
C(6G1)—H(261)	O(5G7)	3.201(7)	0.97	2.54	125.5
C(6G2)—H(162)	O(5G1)	3.341(7)	0.97	2.44	155.1
C(6G3)—H(263)	O(5G2)	3.114(6)	0.97	2.35	134.9
C(6G5)—H(265)	O(5G4)	3.112(6)	0.97	2.42	128.5
C(6G6)—H(266)	O(5G5)	3.216(6)	0.97	2.45	136.2
C(1G3)—H(1G3)	O(3G4)	3.090(6)	0.98	2.44	123.5
C(1G5)—H(1G5)	O(6G6)	3.247(6)	0.98	2.45	138.1

UM00012361
NOVARTIS EXHIBIT 1017
Novartis v. Regents, IPR2023-01346
Page 1107 of 4460

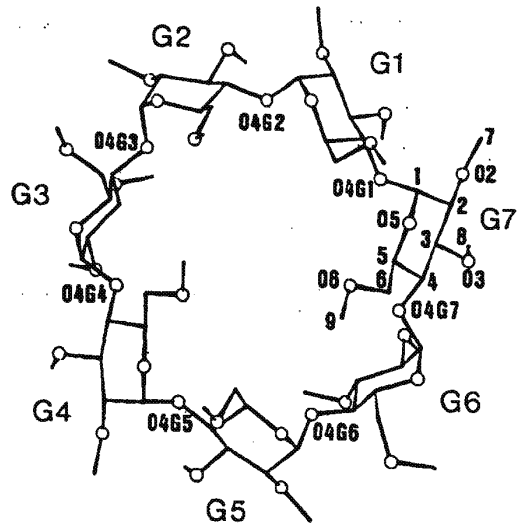


Fig. 2a. Numbering scheme for the host. C atoms are labelled with numerals only.

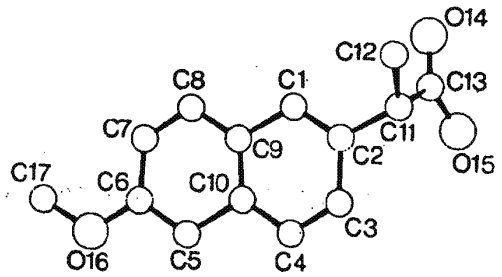


Fig. 2b. Numbering scheme for the guest.

O(6) side and the propionic acid group protruding from the O(2), O(3) side. Bond lengths and bond angles for the naproxen molecule are listed in Table V. The way in which the naproxen molecule is included by TRIMEB in the solid state is similar

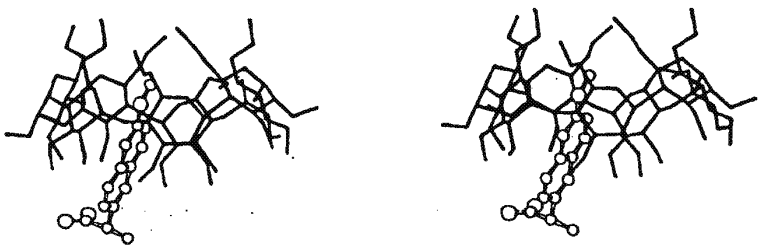


Fig. 3. Stereodiagram of the title compound.

UM00012362
NOVARTIS EXHIBIT 1017
Novartis v. Regents, IPR2023-01346
Page 1108 of 4460

TABLE V. Bond lengths (Å) and angles (°) for naproxen.

C(1)—C(2)	1.392(5)	C(2)—C(1)—C(9)	119.7(6)
C(1)—C(9)	1.435(5)	C(1)—C(2)—C(3)	117.7(7)
C(2)—C(3)	1.41(1)	C(1)—C(2)—C(11)	122.0(6)
C(2)—C(11)	1.502(9)	C(3)—C(2)—C(11)	120.3(6)
C(3)—C(4)	1.36(1)	C(4)—C(3)—C(2)	123.8(8)
C(4)—C(10)	1.40(1)	C(3)—C(4)—C(10)	117.6(7)
C(5)—C(6)	1.412(5)	C(6)—C(5)—C(10)	117.3(6)
C(5)—C(10)	1.440(5)	C(7)—C(6)—C(5)	117.2(7)
C(6)—C(7)	1.36 (1)	C(7)—C(6)—O(16)	124.6(7)
C(6)—O(16)	1.383(8)	C(5)—C(6)—O(16)	118.1(7)
C(7)—C(8)	1.34(1)	C(8)—C(7)—C(6)	124.8(8)
C(8)—C(9)	1.33(1)	C(9)—C(8)—C(7)	119.8(8)
C(9)—C(10)	1.374(9)	C(8)—C(9)—C(10)	120.4(6)
C(11)—C(12)	1.513(9)	C(8)—C(9)—C(1)	120.2(6)
C(11)—C(13)	1.519(8)	C(10)—C(9)—C(1)	119.4(6)
C(13)—O(14)	1.204(7)	C(9)—C(10)—C(4)	121.8(6)
C(13)—O(15)	1.286(7)	C(9)—C(10)—C(5)	120.4(6)
O(16)—C(17)	1.40(2)	C(4)—C(10)—C(5)	117.8(6)
		C(12)—C(11)—C(2)	116.8(5)
		C(12)—C(11)—C(13)	111.7(5)
		C(2)—C(11)—C(13)	107.0(5)
		O(14)—C(13)—O(15)	123.3 (6)
		O(14)—C(13)—C(11)	123.7(6)
		O(15)—C(13)—C(11)	113.0(6)
		C(17)—O(16)—C(6)	117.1(9)

to the modes of inclusion of naproxen by β-cyclodextrin proposed by Bettinetti *et al.* [2], Otero-Espinar *et al.* [5] and Ganza-Gonzalez *et al.* [7] on the basis of their NMR and/or molecular modelling studies. The guest is not as fully included in the TRIMEB molecule on account of the host's cup-like shape as opposed to the toroidal shape of β-cyclodextrin. However, the mode of inclusion proposed by Wang and Warner [6] for naproxen and β-cyclodextrin, where the methoxy group is near the secondary hydroxyl side and the carboxyl group near the primary hydroxyl side, cannot be ruled out by the results of the present study as it has been noted by Harata that for some guests an 'upside-down relationship is found between cyclodextrin complexes and methyl-cyclodextrin complexes' [11].

As we reported earlier [17], the uncomplexed TRIMEB molecule has a somewhat collapsed structure, partially attributed to its attempt to minimise the hydrophobic cavity size in the absence of a hydrophobic guest, thereby facilitating more efficient packing and simultaneously avoiding accommodation of water molecules in a relatively hydrophobic environment. On complexation with the (*S*)-naproxen molecule, the ellipticity of the TRIMEB molecule is significantly reduced. We not-

UM00012363
NOVARTIS EXHIBIT 1017
Novartis v. Regents, IPR2023-01346
Page 1109 of 4460

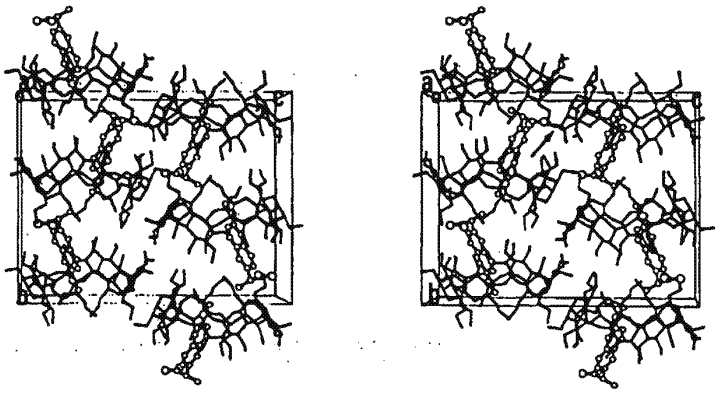


Fig. 4. Stereo packing diagram of the title compound viewed down the a-axis. The O—H···O hydrogen bond is indicated by the dashed line.

ed that one of the seven methylglucose residues in uncomplexed TRIMEB adopts the unusual $^1C_4$ conformation [17] in the crystal while the title complex and other TRIMEB complexes contain only residues of $^4C_1$ conformation. Since the most stable conformation of uncomplexed TRIMEB in solution may not coincide with that observed in the crystal, inclusion of guests by TRIMEB is not necessarily accompanied by the $^1C_4$ to $^4C_1$ conformational change. We intend to use molecular mechanics and NMR techniques to investigate the dynamics of complexation in solution.

The conformation of the methoxy group in naproxen with respect to the naphthalene ring is defined by the torsion angle $\tau 1$ C(5)—C(6)—O(16)—C(17) and that of the propionic acid substituent by $\tau 2$ C(1)—C(2)—C(11)—C(12), $\tau 3$ C(1)—C(2)—C(11)—C(13) and $\tau 4$ C(2)—C(11)—C(13)—O(15). The values for these torsion angles are −173.9(9), 48.1(8), −77.9(7), and −78.4(7)°, respectively. The values for the corresponding torsion angles in the crystal structure of naproxen have been calculated for the (*S*)-isomer using the published coordinates [18] and are −2, −129, 112 and −90° (e.s.d.s ≤ 1°) respectively. The methoxy group, while still coplanar with the naphthalene ring has C(17) *anti*-periplanar to C(5) as opposed to a *syn*-periplanar relationship in the naproxen crystal structure. The former conformation is favoured for inclusion as it reduces the width of the naproxen molecule. The propionic acid substituent itself is in much the same conformation as that in the naproxen crystal structure, but, like the methoxy group, is rotated by approximately 180° with respect to the naphthalene ring (i.e. around C(2)—C(11)). The dihedral angle between the least-squares planes of the two rings of the naphthalene moiety is only 1.4(5)° compared with a value of 5.2(2)° in the naproxen crystal structure [18].

Calculation of the propionic acid group torsion angles in (*S*)-flurbiprofen using published coordinates for the crystal structures of flurbiprofen [19] and the (*S*)-

UM00012364
NOVARTIS EXHIBIT 1017
Novartis v. Regents, IPR2023-01346
Page 1110 of 4460

flurbiprofen–TRIMEB complex [12] reveal similar conformations for the propionic acid substituent as in the (*S*)-naproxen–TRIMEB complex. The values for the torsion angles corresponding to $\tau 2$, $\tau 3$ and $\tau 4$ are 52, -70 and $-102°$ respectively (e.s.d.s $\leq 1°$) in uncomplexed (*S*)-flurbiprofen and 39, -87 and $-88°$ respectively (e.s.d.s $\leq 1.6°$) in the (*S*)-flurbiprofen–TRIMEB complex. This means that this residue of the (*S*)-flurbiprofen molecule undergoes little change in conformation on complexation with TRIMEB, in contrast to what is reported here for the complexation of naproxen by TRIMEB.

An intermolecular hydrogen bond between the carboxyl group of naproxen and a methoxy oxygen atom of a symmetry-related TRIMEB molecule, namely O(15)—H···O(3G2)^{I} (I = $x-1/2, -y+1/2, -z+1$ with O···O 2.661(6), H···O 1.80(8) Å and O—H···O 141(12)°), stabilises the packing arrangement of the complex. This interaction is also present in the (*S*)-flurbiprofen–TRIMEB crystal structure [12] as may have been expected, given the similar way in which this guest molecule interacts with the host compound. Figure 4 shows a stereo packing diagram for the naproxen–TRIMEB complex. Complex units pack in screw-channel mode in a head-to-tail fashion with their axes almost parallel to the *b*-axis. This is a common type of packing arrangement for TRIMEB complexes and has been observed in all the TRIMEB complex structures published to date [11–14], with the exception of the *m*-iodophenol–TRIMEB complex [13].

Acknowledgements

Financial assistance from the Foundation for Research Development (Pretoria), the University of Cape Town and South African Druggists is gratefully acknowledged.

References

1. J. Szejtli: *Topics in Inclusion Science — Cyclodextrin Technology*, Ch. 3, Dordrecht, The Netherlands, Kluwer Academic Publishers (1988).
2. G. Bettinetti, F. Melani, P. Mura, R. Monnanni, and F. Giordano: *J. Pharm. Sci.* **80**, 1162 (1991).
3. G. Bettinetti, A. Gazzaniga, P. Mura, F. Giordano, and M. Setti: *Drug Dev. Ind. Pharm.* **18**, 39 (1992).
4. N. Celebi and N. Erden: *Int. J. Pharm.* **78**, 183 (1992).
5. F.J. Otero-Espinar, S. Anguiano-Igea, N. Garcia-Gonzalez, J.L. Vila-Jato, and J. Blanco-Mendez: *Int. J. Pharm.* **79**, 149 (1992).
6. J. Wang and I. M. Warner: *Microchemical J.* **48**, 229 (1993).
7. A. Ganza-Gonzalez, J.L. Vila-Jato, S. Anguiano-Igea, F.J. Otero-Espinar, and J. Blanco-Mendez: *Int. J. Pharm.* **106**, 179 (1994).
8. J. Szejtli: *J. Incl. Phenom.* **14**, 25 (1992).
9. K. Harata, K. Uekama, M. Otagiri, and F. Hirayama: *Bull. Chem. Soc. Jpn.* **56**, 1732 (1983).
10. G.M. Sheldrick: *J. Appl. Crystallogr.* in preparation (1993).
11. K. Harata, K. Uekama, M. Otagiri, and F. Hirayama: *J. Incl. Phenom.* **1**, 279 (1984).
12. K. Harata, K. Uekama, T. Imai, F. Hirayama, and M. Otagiri: *J. Incl. Phenom.* **6**, 443 (1988).
13. K. Harata, F. Hirayama, H. Arima, K. Uekama, and T. Miyaji: *J. Chem. Soc. Perkin Trans.* **2**, 1159 (1992).
14. D. Mentzafos, I. Mavridis, and H. Schenk: *Carbohydr. Res.* **253**, 39 (1994).

UM00012365
NOVARTIS EXHIBIT 1017
Novartis v. Regents, IPR2023-01346
Page 1111 of 4460

15. W. Saenger: *Inclusion Compounds*, Vol. 2, Ch. 8, London, Academic Press, edited by J. L. Atwood, J.E.D. Davies and D.D. MacNicol (1984).
16. T. Steiner and W. Saenger: *J. Am. Chem. Soc.* **114**, 10146 (1992).
17. M.R. Caira, V.J. Griffith, L.R. Nassimbeni, and B. van Oudtshoorn: *J. Chem. Soc. Perkin. Trans. 2*, 2071 (1994).
18. K. Ravikumar, S.S. Rajan, V. Pattabhi, and E.J. Gabe: *Acta Crystallogr.* **C41**, 280 (1985).
19. J.L. Flippen and R.D. Gilardi: *Acta Crystallogr.* **B31**, 926 (1975).

UM00012366
NOVARTIS EXHIBIT 1017
Novartis v. Regents, IPR2023-01346
Page 1112 of 4460

One-Dimensional Zigzag Chain Structures with Intermolecular C–H···π and C–H···O Interactions Consisted of Phthalic Acid and Pyridine Derivatives

Masaaki Tomura* and Yoshiro Yamashita†

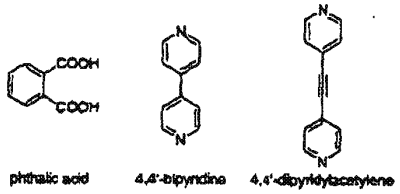
Institute for Molecular Science, Myodaiji, Okazaki 444-8585

†*Department of Electronic Chemistry, Interdisciplinary Graduate School of Science and Engineering, Tokyo Institute of Technology, 4259 Nagatsuta, Midori-ku, Yokohama 226-8502*

(Received February 16, 2001; CL-010137)

Crystal structures of co-crystals of phthalic acid with 4,4'-bipyridine or 4,4'-dipyridylacetylene contain one-dimensional zigzag chains connected by intermolecular O–H···N hydrogen bonds and edge-to-face packing of phthalic acid and pyridine rings stabilized by intermolecular C–H···π and C–H···O interactions.

Compounds containing a one-dimensional zigzag chain structure have attracted much attention for developing molecular based magnets[1-3] and non-linear optical materials.[4] Such a zigzag chain structure can be achieved by the reaction of a metal complex having two vacant or two substitutable coordination sites with a bridging ligand.[5] Bis(hexafluoroacetylacetonato)manganese(II) $Mn(hfac)_2$ and a bipyridine type ligand have been widely used for this purpose.[6] Zigzag chain structures composed of only organic molecules are also of interest from the viewpoint of crystal engineering as well as development of organic molecular materials. Such structures seem to be formed from phthalic acid and dipyridyl compounds because carboxyl moieties and nitrogen atoms of pyridyl groups form intermolecular hydrogen bondings with linear and robust structures,[7,8] and the angle of the direction of the two carboxyl groups of phthalic acid is 60°. On the other hand, edge-to-face packing with T-shaped geometry is important in crystal engineering.[9] Close packing of zigzag chains may produce such a T-shaped geometry of the two components by intermolecular C–H···π interactions.[10] From these viewpoints we have now carried out co-crystallization of phthalic acid with 4,4'-bipyridine or 4,4'-dipyridylacetylene[11] and have succeeded in constructing the expected crystal structures.



phthalic acid 4,4'-bipyridine 4,4'-dipyridylacetylene

The 1:1 co-crystals (**1**) and (**2**) were prepared from an acetone solution of phthalic acid with 4,4'-bipyridine and 4,4'-dipyridylacetylene, respectively. Single crystals suitable for X-ray crystallographic analysis[12] were grown at room temperature by slow evaporation. Both co-crystals form in the monoclinic crystal system with space group *C2/c*. The crystal structures of **1**[13] and **2**[14] consist of an infinite one-dimensional zigzag chain structure along the [1 0 −1] and the [2 0 1] directions, respectively (Figure 1). The zigzag chains are connected by strong intermolecular O–H···N hydrogen bonds (N···O distance 2.64 Å; N···H distance 1.42 Å for both **1** and **2**). The two pyridine rings of 4,4'-bipyridine and 4,4'-dipyridylacetylene lie in a plane, and the angles between the least-squares planes of the pyridine rings and the benzene ring of phthalic acid are 89.4° and 61.9° for **1** and **2**, respectively. The angles between the zigzag chains (angles between the planes of the pyridine rings within the zigzag chains) are close to 60° (54.7° for **1**, 56.1° for **2**).

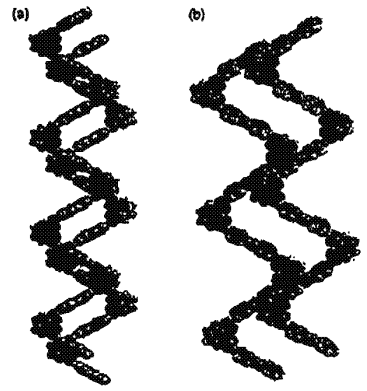


Figure 1. (a) Two one-dimensional zigzag chain structures in co-crystal **1** along the [1 0 1] direction, viewed along the [1 0 1] direction. (b) Two one-dimensional zigzag chain structures in co-crystal **2** along the [-1 0 1] direction, viewed along the [-1 0 1] direction.

Figure 2 shows the zigzag chain structures in the co-crystals **1** and **2** along a direction different from those in Figure 1. In both of **1** and **2**, edge-to-face packing with C–H···π intermolecular interactions between phthalic acid and pyridine rings was observed, and the zigzag chains form two-dimensional undulated sheet-like structures. The C–H···π distances (distances between the least-squares planes of the pyridine rings and the 3- and 4-position carbon and hydrogen atoms in phthalic acid) are 3.69, 3.64, 2.75, 2.84 Å for **1** and 3.45, 3.40, 2.70, 2.77 Å for **2**, respectively. The strong herringbone interactions with characteristic T-shaped geometry are similar to those found in crystals of benzene[15] and 2-aminophenol.[16] The unique structural patterns with the edge-to-face packing observed here are stabilized by various types of intermolecular hydrogen bonding interactions such as O–H···N, C–H···π and C–H···O. Thus, short C–H···O intermolecular interactions between the carbonyl oxygen atoms of phthalic acid and the aromatic hydrogen atoms at the 4-position carbon of the next phthalic acid exist in the crystals of **1** and **2** [2.54 Å (H···O), 3.42 Å (C···O) and 144.4° for **1**; 2.74 Å (H···O), 3.53 Å (C···O) and 139.5° for **2**]. These kinds of weak C–H···O interactions are also known to play an important role in determining the crystal packing in organic solids.[17] In the C–H···O interactions,

Copyright © 2001 The Chemical Society of Japan

UM00012367
NOVARTIS EXHIBIT 1017
Novartis v. Regents, IPR2023-01346
Page 1113 of 4460

05/23/2006 14:02 PRI LIBRARY → 917818637208

typical values for H···O and C···O distances are 2.4–3.0 Å[17a] and 3.3–3.8 Å,[17b] respectively. The interchain distances between the planes of the pyridine derivatives in Figure 2 are 3.6 Å for 1 and 3.7 Å for 2. Strong resemblance between the crystal structures of 1 and 2 suggests robustness and reproducing ability of the supramolecular synthon[18] formed with phthalic acid and pyridine rings. In this case a zigzag chain structure seems to be "programmed" to form in a crystal.

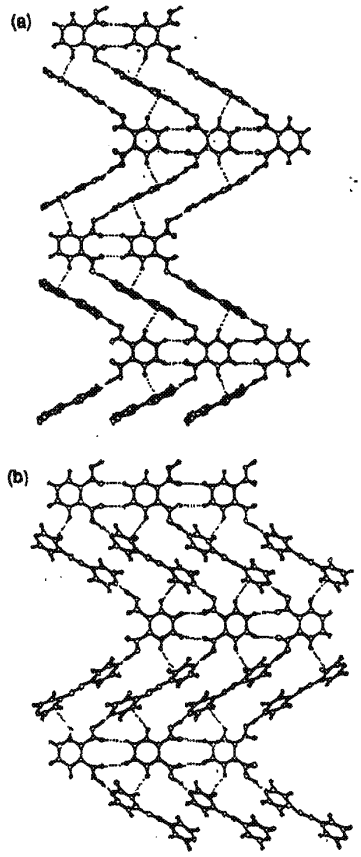


Figure 2. (a) Packing of the zigzag chain structures in co-crystal 1 along the b axis, viewed along the [1 0 1] direction. (b) Packing of the zigzag chain structures in co-crystal 2 along the b axis, viewed along the [-1 0 1] direction. Dotted lines show the intermolecular O–H···N hydrogen bonds, C–H···π and C–H···O interactions.

In conclusion the supramolecular synthons genetated by combination of simple compounds such as phthalic acid and bipyridine type derivatives were successfully used in the design of one-dimensional zigzag chain structures and could realize unique preserved crystal structures. Close packing of the zigzag chains produces edge-to-face packing with intermolecular C–H···π and C–H···O interactions. Studies on the construction of new one-dimensional zigzag chain structures containing functional molecules are now in progress.

This work was supported by a Grant-in-Aid for Scientific Research on Priority Areas from the Ministry of Education, Culture, Sports, Science and Technology, Japan.

References and Notes

1 a) A. Caneschi, D. Gatteschi, and R. Sessoli, *Acc. Chem. Res.*, 22, 392 (1989). b) C. T. Chen and K. S. Suslick, *Coord. Chem. Rev.*, 128, 293 (1993).

2 a) S. Karasawa, M. Tanaka, N. Koga, and H. Iwamura, *Chem. Commun.*, 1997, 1359. b) S. Karasawa, Y. Sano, T. Akita, N. Koga, T. Itoh, H. Iwamura, P. Rabu, and M. Drillon, *J. Am. Chem. Soc.*, 120, 10080 (1998).

3 a) A. Caneschi, D. Gatteschi, J. P. Renard, P. Rey, and R. Sessoli, *Inorg. Chem.*, 28, 3314 (1989). b) M. S. Haddad, D. N. Hendrickson, J. P. Cannady, R. S. Drago, and D. S. Bieksza, *J. Am. Chem. Soc.*, 101, 898 (1979). c) A. Escuer, R. Vincente, and X. Solans, *J. Chem. Soc., Dalton Trans.*, 1997, 531.

4 W. Chiang, D. M. Ho, D. V. Engen, and M. E. Thompson, *Inorg. Chem.*, 32, 2886 (1993).

5 O. R. Evans and W. Lin, *Cryst. Growth Des.*, 1, 9 (2001).

6 a) G. Mago, M. Hinago, H. Miyasaka, N. Matsumoto, and H. Okawa, *Inorg. Chem. Acta*, 245, 145 (1997). b) H.-Y. Shen, D.-Z. Liao, Z.-H. Jiang, S.-P. Yan, B.-W. Sun, G.-L. Wang, X.-K. Yao, and H.-G. Wang, *Polyhedron*, 17, 1953 (1998). c) K. Inoue and H. Iwamura, *J. Am. Chem. Soc.*, 116, 3173 (1994).

7 a) V. R. Pedireddi, W. Jones, A. P. Chorlton, and R. Docherty, *Chem. Commun.*, 1996, 997. b) E. Batchelor, J. Klinowski, and W. Jones, *J. Mater. Chem.*, 10, 839 (2000).

8 a) M. B. Zaman, M. Tomura, and Y. Yamashita, *Chem. Commun.*, 1999, 999. b) M. B. Zaman, M. Tomura, and Y. Yamashita, *Org. Lett.*, 2, 273 (2000). c) M. Tomura and Y. Yamashita, *CrystEngComm*, 2000, 16.

9 a) D. E. J. Williams, *J. Chem. Phys.*, 45, 3770 (1965). b) S. K. Burley and G. A. Petsko, *Science*, 229, 23 (1985). c) S. K. Burley and G. A. Petsko, *J. Am. Chem. Soc.*, 108, 7995 (1986). d) A. Gavezzotti and G. R. Desiraju, *Acta Crystallogr., Sect. B*, 44, 427 (1988).

10 a) M. Nishio, Y. Umezawa, M. Hirota, and Y. Takeuchi, *Tetrahedron*, 51, 8665 (1995). b) Y. Umezawa, S. Tsuboyama, K. Honda, J. Uzawa, and M. Nishio, *Bull. Chem. Soc. Jpn.*, 71, 1207 (1997).

11 M. Tanner and A. Ludi, *Chimica*, 34, 23 (1980).

12 Reflection data for 1 and 2 were collected on a Rigaku R-AXIS IV imaging plate area detector with Mo Kα radiation (λ = 0.71070 Å) at 296(2) K. The structures were solved by direct methods and refined by full-matrix least-squares on F^2 with SHELX-97.[19] All non-hydrogen atoms were refined anisotropically. Hydrogen atoms were localized in the Fourier map and refined isotropically.

13 Crystal data for 1: $C_{18}H_{14}N_2O_4$, M_r = 322.31, monoclinic, space group $C2/c$, a = 15.761(2), b = 7.821(2), c = 13.396(3) Å, β = 98.060(9)°, V = 1634.9(5) Å^3, Z = 4, D_c = 1.309 g cm^{-3}, $F(000)$ = 672, μ = 0.094 mm^{-1}, crystal dimensions 0.30 × 0.25 × 0.05 mm, 3304 reflections collected, 1212 independent (R_{int} = 0.0734), R_1 = 0.0570, wR_2 = 0.1505 for $I > 2\sigma(I)$, R_1 = 0.0902, wR_2 = 0.1881, S = 0.803 for all data. CCDC 152982.

14 Crystal data for 2: $C_{20}H_{14}N_2O_4$, M_r = 346.33, monoclinic, space group $C2/c$, a = 11.936(6), b = 7.947(3), c = 20.077(6) Å, β = 107.76(3)°, V = 1814(1) Å^3, Z = 4, D_c = 1.268 g cm^{-3}, $F(000)$ = 720, μ = 0.090 mm^{-1}, crystal dimensions 0.20 × 0.20 × 0.10 mm, 2705 reflections collected, 1177 independent (R_{int} = 0.0850), R_1 = 0.0850, wR_2 = 0.1894 for $I > 2\sigma(I)$, R_1 = 0.1514, wR_2 = 0.2393, S = 1.117 for all data. CCDC 152983.

15 E. G. Cox, D. W. J. Cruickshank, and J. A. S. Smith, *Proc. Roy. Soc. London*, 247, 1 (1958).

16 F. H. Allen, V. J. Hoy, J. A. K. Howard, V. R. Thalladi, G. R. Desiraju, C. C. Wilson, and G. J. McIntyre, *J. Am. Chem. Soc.*, 119, 3477 (1997).

17 a) R. Taylor and O. J. Kennard, *J. Am. Chem. Soc.*, 104, 5063 (1982). b) G. R. Desiraju, *Acc. Chem. Res.*, 24, 290 (1991). c) T. Suzuki, H. Fujii, T. Miyashi, and Y. Yamashita, *J. Org. Chem.*, 57, 6745 (1992).

18 G. R. Desiraju, *Angew. Chem., Int. Ed. Engl.*, 34, 2311 (1995).

19 SHELX-97: Program for the Structure Solution and Refinement of Crystal Structures. G. M. Sheldrick, University of Göttingen, Germany (1997).

UM00012368
NOVARTIS EXHIBIT 1017
Novartis v. Regents, IPR2023-01346
Page 1114 of 4460

Top Curr Chem (2005) 254: 41–70
DOI 10.1007/b100995
© Springer-Verlag Berlin Heidelberg 2005

Crystal Engineering of Organic Cocrystals by the Solid-State Grinding Approach

Andrew V. Trask · William Jones (✉)

University of Cambridge, Department of Chemistry, Lensfield Road, Cambridge CB2 1EW, UK
wj10@cam.ac.uk

1 Introduction 42

2 A Historical Perspective 43

3 Cocrystals Produced Exclusively by the Grinding Approach 53

4 A Recent Enhancement to the Grinding Approach 59

5 Structure Determination from Powder XRD Data 64

6 Concluding Remarks 68

References 69

Abstract Crystal engineering of organic cocrystals is gaining interest across a variety of disciplines. The solid-state grinding approach to preparing cocrystals is an alternative to the traditional method of solution crystallisation, and possesses several distinct advantages. This review first demonstrates that the approach of solid-state cocrystal preparation is well established in the literature by providing a brief historical account of its applications. Several cases are then examined in which certain cocrystal materials can be prepared only by solid-state grinding methodologies. These examples underscore the importance of this approach in the search for new cocrystal materials. This is particularly advantageous when searching for new cocrystal stoichiometries. The focus then turns to a recent modification of the solid-state grinding process, in which small quantities of solvent are introduced either to increase solid-state cocrystallisation kinetics or to provide polymorph control – the latter having particular significance in the pharmaceutical field. Finally, a significant analytical advancement with direct implications for the field of solid-state cocrystal preparation is considered by examining recent examples of crystal structure determination from powder X-ray diffraction data.

Keywords Solid-state grinding · Cocrystal formation · Crystal engineering · Pharmaceutical materials · Polymorphism

Abbreviations
XRD X-ray diffraction

UM00012369
NOVARTIS EXHIBIT 1017
Novartis v. Regents, IPR2023-01346

1 Introduction

One flourishing area in the field of crystal engineering is based upon the formation of crystalline molecular complexes, or cocrystals. Cocrystals may be defined as materials which contain two or more discrete molecular entities in the crystal lattice. Crystal engineering, when applied to cocrystal systems, generally involves the design and study of new materials in order to widen the knowledge base of successful engineering strategies, and the application of that knowledge to provide cocrystals with specific properties for a multitude of applications. Crystal engineering is actively applied within a variety of scientific disciplines as diverse as materials science, nanotechnology and the pharmaceutical industry [1].

In designing a cocrystal, it is necessary to evaluate the potential intermolecular interactions that a given molecule may exhibit. Due to their robust and directional nature, hydrogen bonds are a valuable tool in cocrystal synthesis. Hydrogen bonds of varying strengths may be employed, including the traditional OH···O and OH···N strong hydrogen bonds and the weaker CH···π or CH···Cl variety. Other intermolecular associations which may be employed in cocrystal design include halogen–halogen, nitro–nitro and π···π interactions, among others [2–4].

Cocrystals are often prepared by a traditional solution crystallisation approach such as solvent evaporation, cooling, or anti-solvent addition. There are a number of reasons for the popularity of the solution-based approach. Solution crystallisation can yield large, well-formed single crystals, from which one may easily evaluate crystal habit and surface features. Analysis of the diffraction pattern of a single crystal is typically the best means of obtaining an absolute crystal structure determination. Further, solution crystallisation is an established and effective purification step.

There are, however, several accompanying drawbacks to the solution-based approach to cocrystal formation. The solubility of the starting components is one obstacle, as a suitable solvent for all ingoing materials must be identified before cocrystallisation may occur. Unexpected solvate formation may also pose a problem. The solvent employed in the cocrystallisation may possess the ability to interfere with the desired cocrystal intermolecular interactions, and thus may become incorporated into the crystal lattice. In this way, solvate formation hampers rational cocrystal design. In the case of polymorphic cocrystal systems, it could be the case that solution crystallisation leads to an undesired kinetically controlled metastable polymorph. An additional drawback to cocrystallisation from solution is the typically large volume of solvent necessary to prepare the cocrystals. As cocrystals emerge as products in industrial applications, avoidable waste streams will be increasingly scrutinised as environmentally and fiscally imprudent.

An alternative to the solution-based approach exists in the approach of solid-state grinding. The act of solid-state grinding to induce chemical change,

UM00012370
NOVARTIS EXHIBIT 1017
Novartis v. Regents, IPR2023-01346
Page 1116 of 4460

known as mechanochemistry, has relevance to a variety of fields [5], and has several attractive aspects with regard to forming organic cocrystals. The relative solubility of ingoing components in a particular solvent is not a concern when solid-state grinding is employed, thereby increasing the utility of this technique over the solution approach by greatly easing the burden of experiment design. Solvent-free solid-state cocrystallisation also eliminates the possibility of forming undesired solvates. There is some evidence to indicate that, at least in single-component systems, solid-state grinding leads to the high-melting thermodynamically stable polymorph [6]. Further, the absence of solvent makes this an inherently 'green' approach to forming cocrystals by eliminating large volumes of solvent waste; the minimization of excess crystallisation solvent could help achieve corporate green chemistry targets [7]. Finally, while it is not yet fully understood, there are instances in which certain structures or stoichiometries of cocrystals may only be obtained via the solid state.

Solid-state cocrystallisation also possesses drawbacks. While the field of crystal engineering develops, the primary point of interest upon forming a cocrystal material is often the elucidation of its crystal structure. Single crystal X-ray diffraction (XRD), which requires a crystal of sufficient size, is incompatible with solid-state grinding, which is a particle size reduction technique. Thus, a cocrystal prepared only by solid-state grinding will require alternative, less common means of revealing structural features of interest, such as the hydrogen bond motif that may be present. Other disadvantages to solid-state grinding include the lack of purification that solution crystallisation may provide, and the increase in crystalline disorder which accompanies some materials upon energetic grinding. A grinding-induced change in a compound's degree of crystallinity may lead to changes in its physicochemical properties [8, 9].

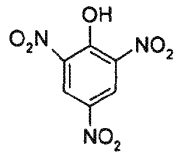
2
A Historical Perspective

Despite its simplicity, the solid-state grinding approach remains less familiar than cocrystal formation from solution. There is, however, ample precedence of the solid-state approach in the literature. Over a century ago, researchers in the field of charge-transfer complexes reported cocrystal formation by grinding [10]. In a paper describing halogen derivatives of quinhydrone, Ling and Baker reported the formation of a tetrachloroquinhydrone by grinding together equal weights of metadichloroquinone and metadichloroquinol, followed by purification from light petroleum.

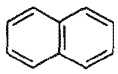
To date, very little research has been directed at understanding the mechanism of organic cocrystal formation by solid-state grinding. Work by Rastogi and co-workers in the 1960s, which was aimed at improving the understanding of the solid-state kinetics of several systems containing picric acid 1, appeared to suggest that a vapour diffusion mechanism might operate in some of the

UM00012371
NOVARTIS EXHIBIT 1017
Novartis v. Regents, IPR2023-01346
Page 1117 of 4460

systems they studied. One interesting example described solid-state complex formation between **1** and naphthalene **2** in the absence of grinding [11].



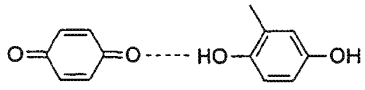
1



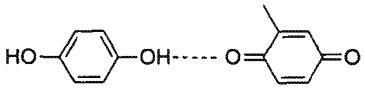
2

The two starting components were packed into a glass capillary from opposite ends until they met in the centre. A coloured reaction product was observed visually after 7 to 10 min at the reactant interface. As time progressed, the product interface was observed to advance in the direction of the picric acid reactant. Further study of this reaction supported a vapour diffusion mechanism, bolstered in part by the observation that complexation proceeds even if a small gap of space exists between the two reactants [12]. The nature of the complex was investigated in additional work, whereby it was proposed that a donor/acceptor π-complex was produced [13]. A crystal structure confirming this deduction was later published [14].

Quinhydrone charge-transfer complexes were the subject of study by Paul, Curtin and co-workers in the 1980s [15–18]. Unsymmetrically substituted quinhydrones, which are very labile in solution with respect to redox self-isomerisation, form asymmetric charge-transfer complexes upon solid-state grinding. For example, 1,4-benzoquinone and 2-methylhydroquinone form the charge-transfer complex **3** upon solid-state grinding with a mortar and pestle.



3



4

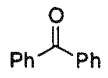
The product of solid-state grinding exhibits no evidence of complex **4**, which would be expected to result following solution-mediated redox isomerisation of the starting components. Solid-state grinding preparation of quinhydrone complexes was later pursued by Guarrera et al. [19].

Several examples of solid-state formation of cocrystals without charge-transfer interaction were reported by Toda and co-workers in 1987 [20]. Various or-

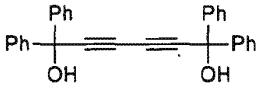
UM00012372
NOVARTIS EXHIBIT 1017
Novartis v. Regents, IPR2023-01346
Page 1118 of 4460

ganic reagents were combined in a test tube and agitated with a mechanical test tube shaker for specific lengths of time. A total of seven resulting cocrystal products were formed in this manner.

The amount of time necessary to effect complete cocrystallisation, as judged by IR and melting point, varied significantly. A cocrystallisation between 5 and 6 was deemed complete after only 12 min of solid-state agitation, while the

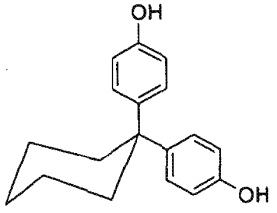


5

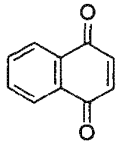


6

complexation of 7 and 8 required 48 h of agitation. Interestingly, while many of the complexes could be formed both by solid-state agitation and by solution methods, the cocrystal containing 7 and 8 could not be obtained by solvent crystallisation; this was also the cocrystallisation that required the longest solid-state agitation time.



7



8

Beginning in the late 1980s with work directed at understanding the preferences of hydrogen bonds, Etter and co-workers consistently attempted to prepare cocrystals by both solution evaporation and solid-state grinding techniques [21–29]. The sustained effort of the Etter group towards consistently reporting results from both solution and grinding cocrystallisation attempts provided confirmation that the grinding approach was a viable means of generating a variety of hydrogen-bonded cocrystal materials.

In order to illustrate the value of hydrogen bonding in designing acentric organic solids for non-linear optical materials, Etter and Frankenbach studied the 1:1 cocrystal of 4-aminobenzoic acid and 3,5-dinitrobenzoic acid [21]. The carboxylic acid heterodimer hydrogen-bonding pattern (Fig. 1) was confirmed by XRD analysis on a single crystal obtained by evaporation of an equimolar solution in methanol. The same cocrystal material, as determined by powder XRD, was produced by grinding the solid components together for 5 min (grinding was performed in a dental amalgamator).

A cocrystallisation study of the hydrogen bond preferences of 2-aminopyrimidine 9 by Etter and Adsmond provided further evidence of the utility

UM00012373
NOVARTIS EXHIBIT 1017
Novartis v. Regents, IPR2023-01346
Page 1119 of 4460

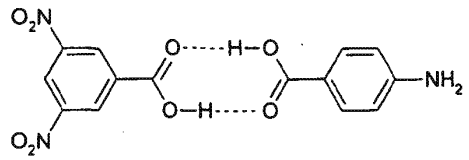
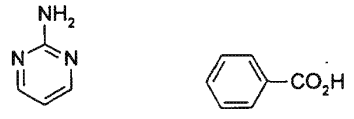


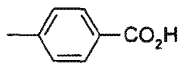
Fig. 1 Carboxylic acid heterodimer formed by solution and solid-state grinding cocrystallisation approaches [21]

of solid-state grinding, especially with regard to stoichiometry selection [23]. A total of 11 cocrystals were reported with different mono- and dicarboxylic acids. Interestingly, both 1:2 and 1:1 cocrystal stoichiometries were observed in cocrystals of 9 with 10, 11 and 12. For both solution and solid-state grind-

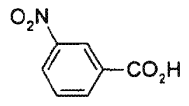


9

10



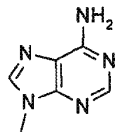
11



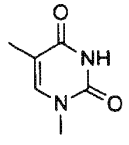
12

ing approaches, it was found that the resulting cocrystal stoichiometry could be dictated by the stoichiometry of the ingoing components. Different crystallisation behaviour was observed in one instance with two stoichiometries of a cocrystal with succinic acid; this case is described in the following section.

A further example of interest reported by Etter and co-workers involved the base pair consisting of the pyrimidine 1-methylthymine T and the purine 9-methyladenine A [28]. These are derivatives of the base pairs found in the



A



T

DNA structure. The hydrogen-bonding interaction of the AT base pair was previously described from XRD analysis by Hoogsteen on a single crystal grown from aqueous solution (Fig. 2a) [30]. Etter et al. reported that grinding A and

UM00012374
NOVARTIS EXHIBIT 1017
Novartis v. Regents, IPR2023-01346
Page 1120 of 4460

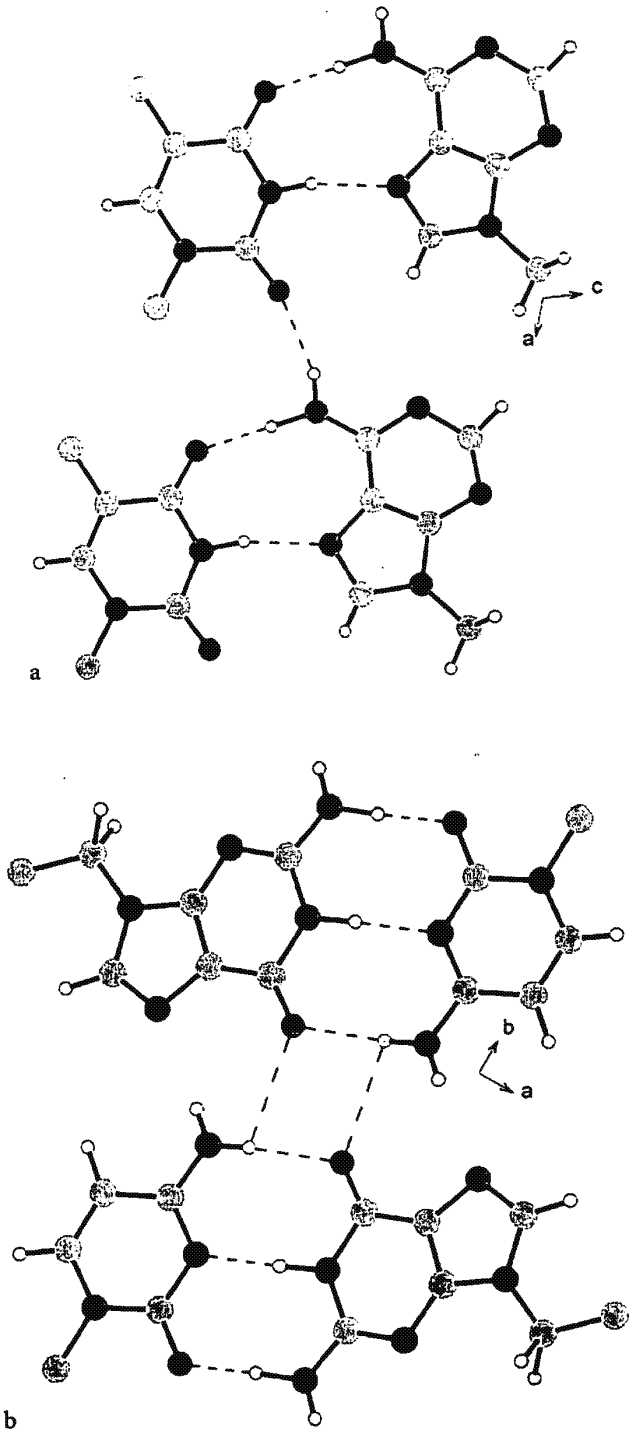
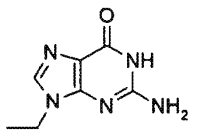


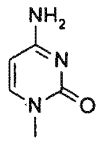
Fig. 2 a AT crystal packing [30] and b CG crystal packing [31] (some methyl hydrogens are absent from both reported crystal structures)

UM00012375
NOVARTIS EXHIBIT 1017
Novartis v. Regents, IPR2023-01346
Page 1121 of 4460

T together in the solid state for 20 min produced a material which had the same powder XRD pattern as that calculated from the known crystal structure AT. By comparison, however, an interesting distinction exists with an analogous base pair involving 9-ethylguanine G and 1-methylcytosine C, which had also



G



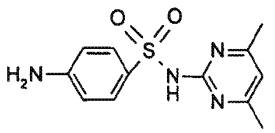
C

been grown from solution and characterised by single crystal XRD (Fig. 2b) [31]. While AT formed after grinding for only 20 min, CG showed no cocrystallisation after intermittent grinding and heating for up to 7 days. This is surprising, particularly in light of the increased number of hydrogen bonds that are possible in the CG base pair as compared to the AT pair. This illustration underscores a lack of full understanding of the factors which influence successful solid-state grinding.

Resulting from their efforts at using the grinding approach with a variety of cocrystal systems, Etter and co-workers related two factors which appeared to be important determinants of cocrystal formation by solid-state grinding. Etter et al. state that "at least one of the components should have some volatility at the temperature of the grinding experiments, and the product dimers should have a stronger intermolecular hydrogen bond than any of the hydrogen bonds in the structures of the two starting materials" [25]. The comment regarding volatility, which calls to mind the findings of Rastogi et al. [12], is experimentally supported by the observation of Etter et al. that the yield of a solid-state cocrystallisation may be improved by heating the product following grinding [25]. The heating was always at least 50 °C below the melting temperature of either starting component, and no melting or fusing of the particles was observed. While this topic appears not to have been further explored, it is interesting to consider the possibility that 'activation' of a cocrystallisation mixture may also be accomplished by other methods, such as the input of ultrasound [32] or microwave energy.

Cocrystallisation has gained recent interest in application to pharmaceuticals [33–35]. The ability to tailor the physiochemical properties of a drug substance via complexation is highly desirable for bioavailability, stability and processing considerations. In 1995, Caira and co-workers demonstrated the pharmaceutical application of cocrystallisation via solid-state grinding by systematically studying a range of different pharmaceutical cocrystals [36]. Cocrystals of the sulfa drug sulfadimidine 13 (also known as sulfamethazine) with various carboxylic acids were prepared from solution, and crystal structures were obtained [37, 38]. It was then demonstrated that six of the cocrystals

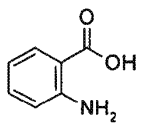
UM00012376
NOVARTIS EXHIBIT 1017
Novartis v. Regents, IPR2023-01346
Page 1122 of 4460



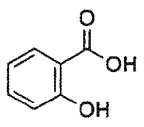
13

could be prepared by grinding with mortar and pestle or with a ball mill. The cocrystals formed by grinding exhibited identical powder XRD patterns to those grown from solution.

A remarkable preference was demonstrated for one particular cocrystal, the sulfadimidine:anthranilic acid (13:14) cocrystal. In a grinding competition experiment, a sulfadimidine:salicylic acid (13:15) cocrystal, for which the crystal structure had been previously determined [39], was ground in the presence of anthranilic acid 14. The result was a displacement of salicylic acid 15 by



14



15

anthranilic acid 14 as the cocrystal partner of sulfadimidine 13. Because of the common hydrogen-bonding pattern in both cocrystals (Fig. 3), the authors base their explanation for the preference on the intermolecular bonding of the ingoing homomeric acid crystals. Salicylic acid 15 is observed to pack with familiar carboxylic acid dimers, while the particular polymorph of anthranilic acid 14 employed in the experiment consists of an unusual helical packing of un-ionised and zwitterionic molecules. The preferential formation of the sulfadimidine:anthranilic acid (13:14) cocrystal is attributed to an increased reactivity of the pure anthranilic acid material due to its presumably less stable hydrogen-bonding pattern.

This elegant demonstration of the displacement of one cocrystallisation partner with another via solid-state grinding may indicate the possibility of a more general application. A new route may exist to obtaining novel cocrystals whereby one first produces an intermediate cocrystal, or precursor, containing a cocrystallising agent which may then be displaced by a second cocrystallising agent en route to the desired product. While this has not yet been widely demonstrated with organic cocrystals, a similar methodology has been demonstrated in the field of layered inorganic solids. In order to generate an isopolymetalate pillared clay, a precursor is first prepared in which a large organic anion is inserted between brucite layers. The precursor is then subjected to polymetalate exchange to allow the even larger heptamolybdate or decavanadate anion to intercalate within the solid [40–42].

UM00012377
NOVARTIS EXHIBIT 1017
Novartis v. Regents, IPR2023-01346
Page 1123 of 4460

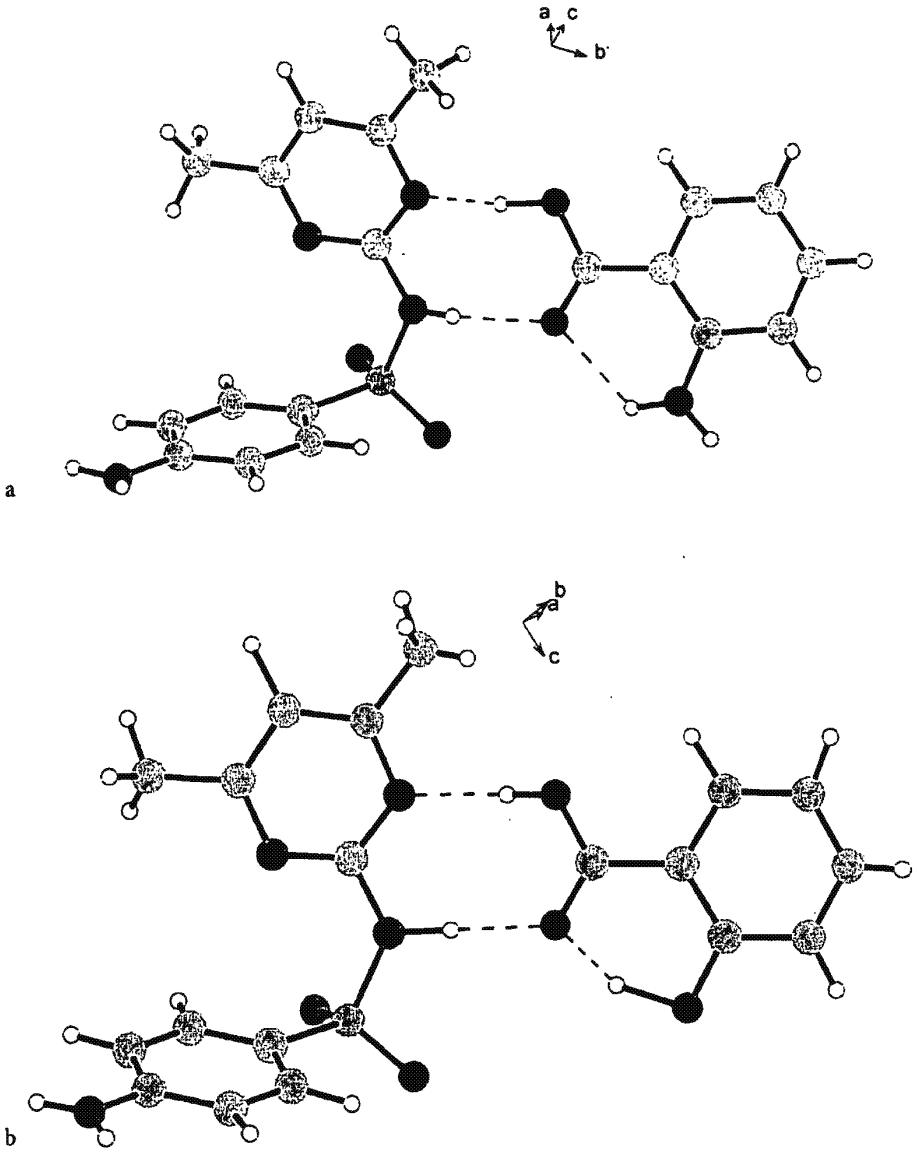
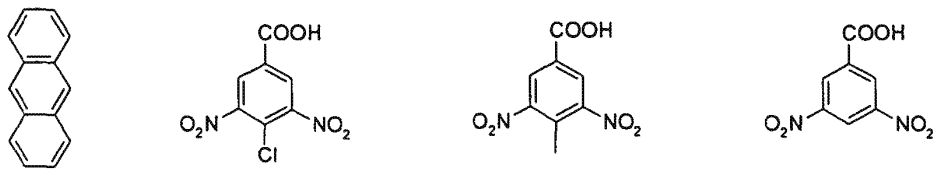


Fig. 3 Hydrogen bonding motif of a sulfadimidine:anthranilic acid (13:14) [37] and b sulfadimidine:salicylic acid (13:15) [39]

As mentioned above, Caira et al. implicated the stability of an ingoing cocrystallisation component as a factor in the preferential formation of a sulfadimidine cocrystal [36]. A year later, in a detailed structural analysis of three anthracene **16** cocrystals, Pedireddi et al. concluded that the ability of potential constituents to satisfy a network of hydrogen bonds dictated solid-state cocrystal formation [43]. Cocrystallisations of anthracene **16** with 4-chloro-3,5-dinitrobenzoic acid **17**, 3,5-dinitro-4-methylbenzoic acid **18** and 3,5-dinitrobenzoic

UM00012378
NOVARTIS EXHIBIT 1017
Novartis v. Regents, IPR2023-01346
Page 1124 of 4460



16 17 18 19

acid **19** were attempted by solution precipitation and by solid-state grinding. Solid-state grinding led to cocrystallisation of **17**:**16** and **18**:**16** but not **19**:**16**. Solution precipitation also yielded **17**:**16** and **18**:**16**. A cocrystal of **16** and **19** resulted from solution precipitation from benzene only.

Crystal structures of the three cocrystal materials were solved by single crystal XRD. The inability of a **19**:**16** cocrystal to form by solid-state grinding was revealed by the fact that a benzene molecule was incorporated into the cocrystal structure formed from solution. Hydrogen bonding of the **17**:**16** and **18**:**16** cocrystals is nearly identical (Fig. 4a,b). In each, a planar hexagonal hydrogen-bonded ring composed of **17** or **18** surrounds the anthracene **16**. In order to maintain favourable contacts around the ring, the following three

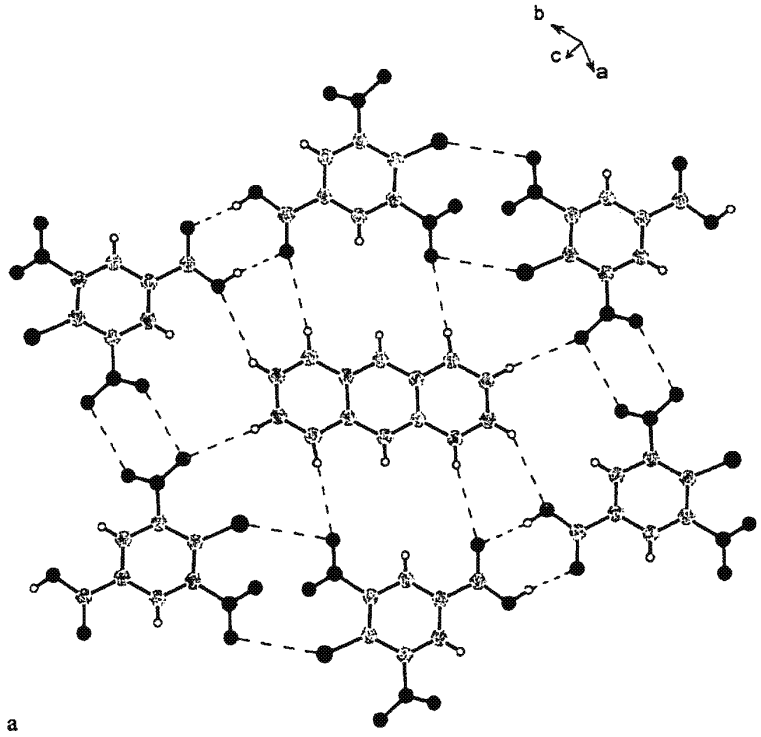


Fig. 4 Crystal packing diagrams of a **17**:**16** and b **18**:**16**, both with 2:1 stoichiometry, and c **19**:**16**:benzene with 2:1:1 stoichiometry (*dashed lines* represent hydrogen bonds and close contacts) [43]

UM00012379
NOVARTIS EXHIBIT 1017
Novartis v. Regents, IPR2023-01346
Page 1125 of 4460

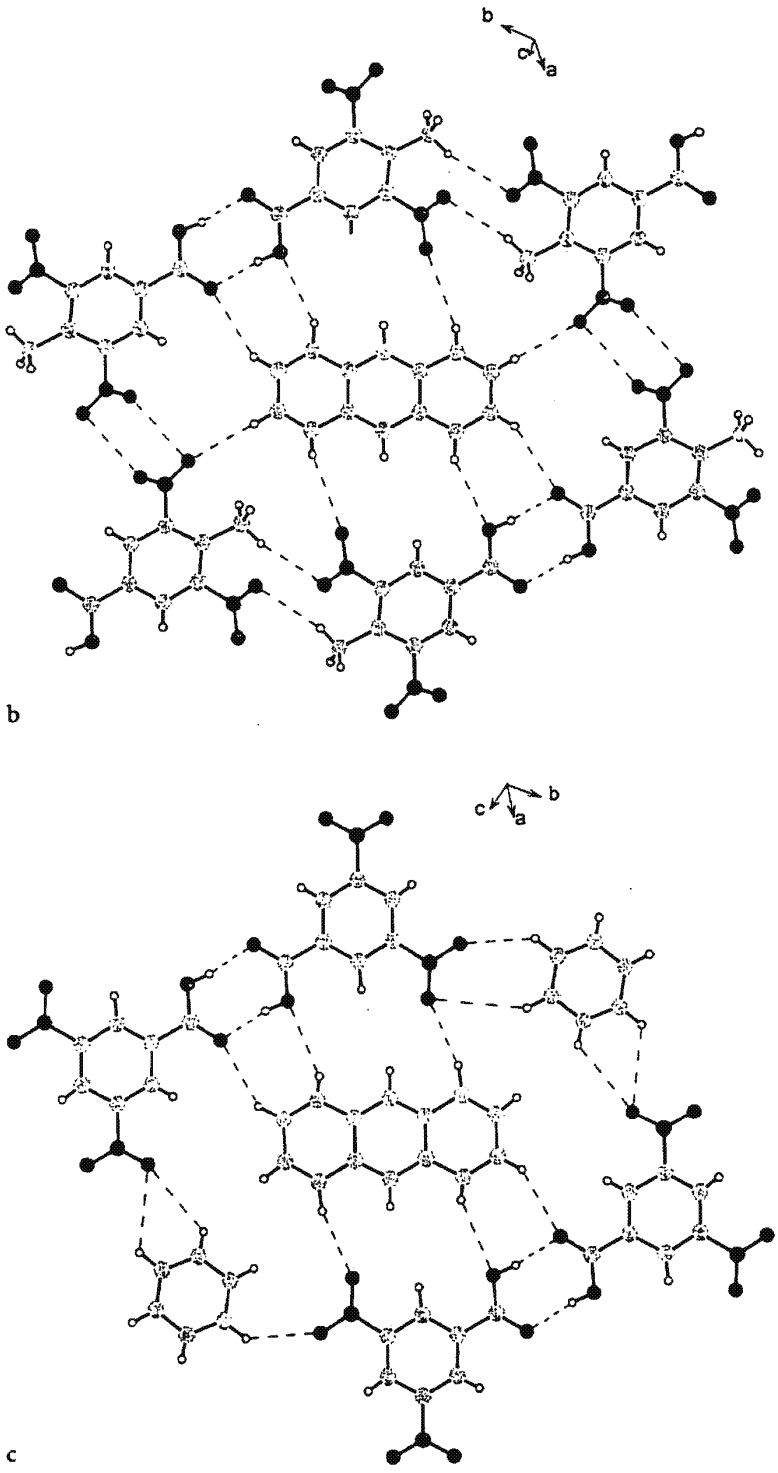


Fig. 4 (continued)

UM00012380
NOVARTIS EXHIBIT 1017
Novartis v. Regents, IPR2023-01346
Page 1126 of 4460

interactions are necessary for the cocrystal involving **18**: carboxylic acid dimer, O···O close contact of nitro groups, and C–H···O hydrogen bonding between the methyl and a nitro. In the case of **17**, a Cl···O interaction replaces one of the C–H···O hydrogen bonds.

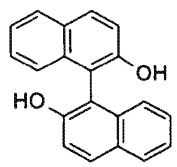
Lacking a *meta* constituent, it is clear that **19** alone cannot satisfy an analogous ring of continuous intermolecular interactions around anthracene. Hence, no cocrystallisation occurred by solid-state grinding, and the incorporation of a benzene solvent molecule upon solution evaporation was necessary to permit cocrystallisation (Fig. 4c). The authors thus attributed the lack of cocrystal formation by solid-state grinding to an inability of reactants to satisfy the desired intermolecular interactions, rather than the relative stability of reactants.

A selection from early reports on the solid-state grinding cocrystallisation approach has been offered here. The quantity and scope of solid-state grinding cocrystallisation examples continues to grow today. Interest is also turning towards varied constituent types, such as organometallic cocrystals [44–46]. Additionally, the use of grinding as a means of inducing chemical reactivity has been demonstrated by Toda and others to be of tremendous utility [47–49]. It is anticipated that as interest grows with respect to cocrystals and green chemistry practices alike, so too will the field of cocrystal formation by solid-state grinding continue to develop.

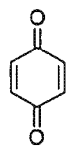
3
Cocrystals Produced Exclusively by the Grinding Approach

One great attraction of preparing cocrystals by solid-state grinding is that, in certain cases, cocrystals unobtainable by other methods may be prepared. The number of reported instances of these cases is small, but may grow as the field of solid-state cocrystal preparation widens. From the standpoint of novel materials design, these cases are of great interest in that they may lead to understanding, prediction and exploitation of this phenomenon.

An illustrative example was provided by the work of Kuroda and co-workers [50]. They reported that different methods of preparation resulted in distinct cocrystal products in their work with racemic bis-β-napthol (BN) **20** and benzoquinone (BQ) **21**. Upon solid-state grinding with a mortar and pestle, a 1:1.5 BN:BQ cocrystal resulted, termed form I. In contrast, from a solution of ether and hexane, a cocrystal containing **20** and **21** in a 1:1 BN:BQ ratio resulted,



20



21

UM00012381
NOVARTIS EXHIBIT 1017
Novartis v. Regents, IPR2023-01346
Page 1127 of 4460

termed form II. Further, cooling a mixture of the two components from the melt resulted in a third cocrystal, form III.

Several of the experimental details were varied in order to elucidate a possible mechanism for the variation in products derived from the different techniques. The starting ratio of components was varied without successfully producing form II by grinding, showing that the formation of form I occurred independently of the starting ratio. Additional experiments were performed to demonstrate that the grinding procedure was not affected by light, oxygen, or static charge. It was also illustrated that either mixing without grinding or exposure of solid **20** to **21** vapour did not induce cocrystallisation. Coupled with the observation that a third cocrystal form was obtained from the melt of these materials, the experiments seem to highlight the importance of solid–solid interaction and grinding-induced crystal cleavage during the cocrystallisation process.

It was fortunate that in one case of solution crystallisation, a few crystals of the grinding product, form I, were found as a minor component, which allowed for structure determination of both form I and form II by single crystal XRD. A crystal structure of the material from the melt is not available. The asymmetric unit of form I contains one **20** and two **21** molecules, one of which rests on a centre of symmetry. The expected O–H···O hydrogen bond between the hydroxyl of **20** and the carbonyl of **21** is observed, although one of the four total carbonyls does not participate in any hydrogen bonding. This results in a discrete hydrogen bond chain consisting of five alternating participants (see Fig. 5). In the structure of form II, which contains three each of **20** and **21** in the asymmetric unit, all hydrogen-bonding donors and acceptors are satisfied. This provides an infinite chain of hydrogen bond connectivity, as viewed in Fig. 6. π-Stacking interactions seem to play a role in both structures, as the BQ rings are always stacked between BN rings.

Whether the difference in hydrogen bonding between the cocrystal structures has a role in their crystallisation preferences is not clear. The authors suggested that crystal shearing together with molecular diffusion may have a role in the preference for form I formation by grinding. A structural confirmation of the shearing hypothesis, however, is not readily apparent from the crystal structures. In viewing the packing of a unit cell of both cocrystals, a cleavage plane may be envisaged in each structure. In viewing form I along the *c* axis, one may identify planes parallel to the *a* axis across which no hydrogen bonding occurs (Fig. 7). Similarly, when viewed from an appropriate angle, the unit cell of form II shows what may be interpreted as non-polar cleavage planes (Fig. 8). From this analysis, it is possible that both crystals may possess the capability for shearing. Thus, an examination of unit cell packing alone is not sufficient to explain the crystallisation behaviour of these cocrystals. As the authors suggested, further investigation into the solid-state cocrystallisation mechanism will provide a foundation for exciting future work.

The example illustrated above is unusual, in that the crystal structures of the cocrystals from both solution and grinding have been determined and hence

UM00012382
NOVARTIS EXHIBIT 1017
Novartis v. Regents, IPR2023-01346
Page 1128 of 4460

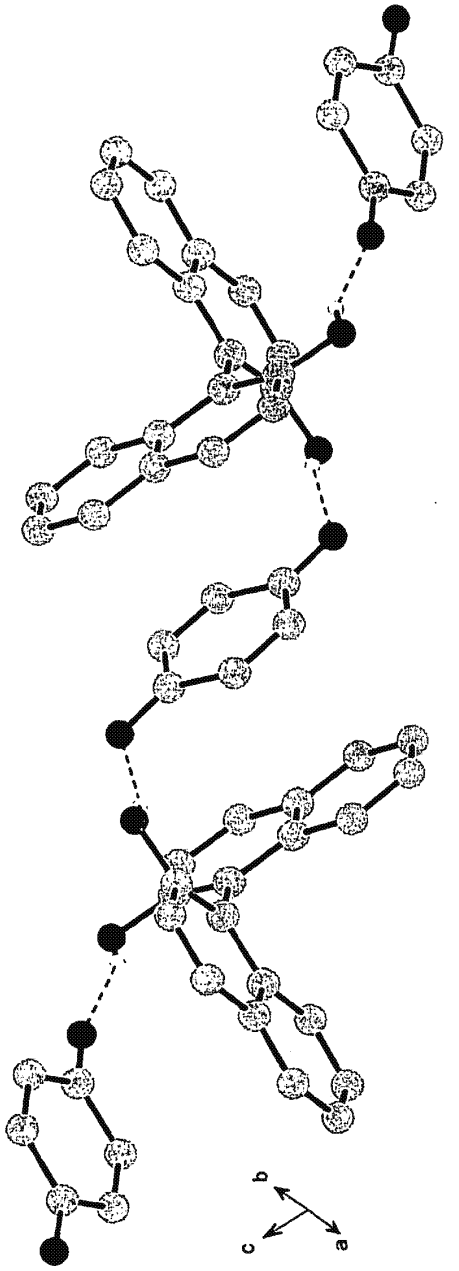


Fig. 5 Form I cocrystal of 20:21 showing discrete hydrogen-bonded unit (non-hydroxyl hydrogens removed for clarity) [50]

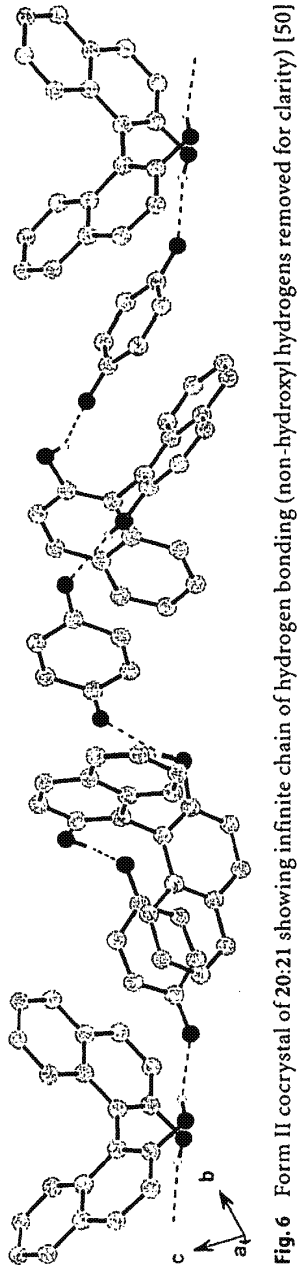


Fig. 6 Form II cocrystal of 20:21 showing infinite chain of hydrogen bonding (non-hydroxyl hydrogens removed for clarity) [50]

NOVARTIS EXHIBIT 1017
Novartis v. Regents, IPR2023-01346
Page 1129 of 4460

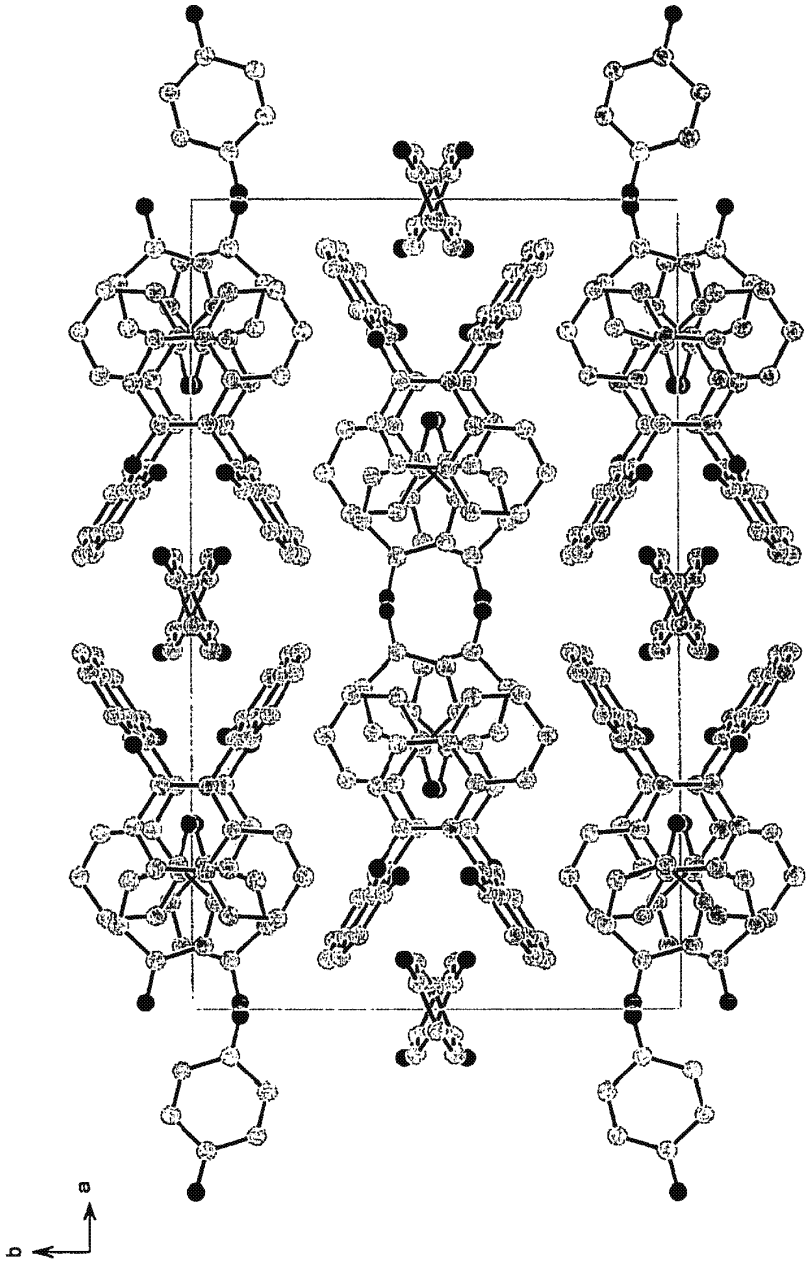


Fig. 7 Form I unit cell packing of cocrystal **20**:**21** – possible cleavage planes are projected horizontally [50]

NOVARTIS EXHIBIT 1017
Novartis v. Regents, IPR2023-01346
Page 1130 of 4460

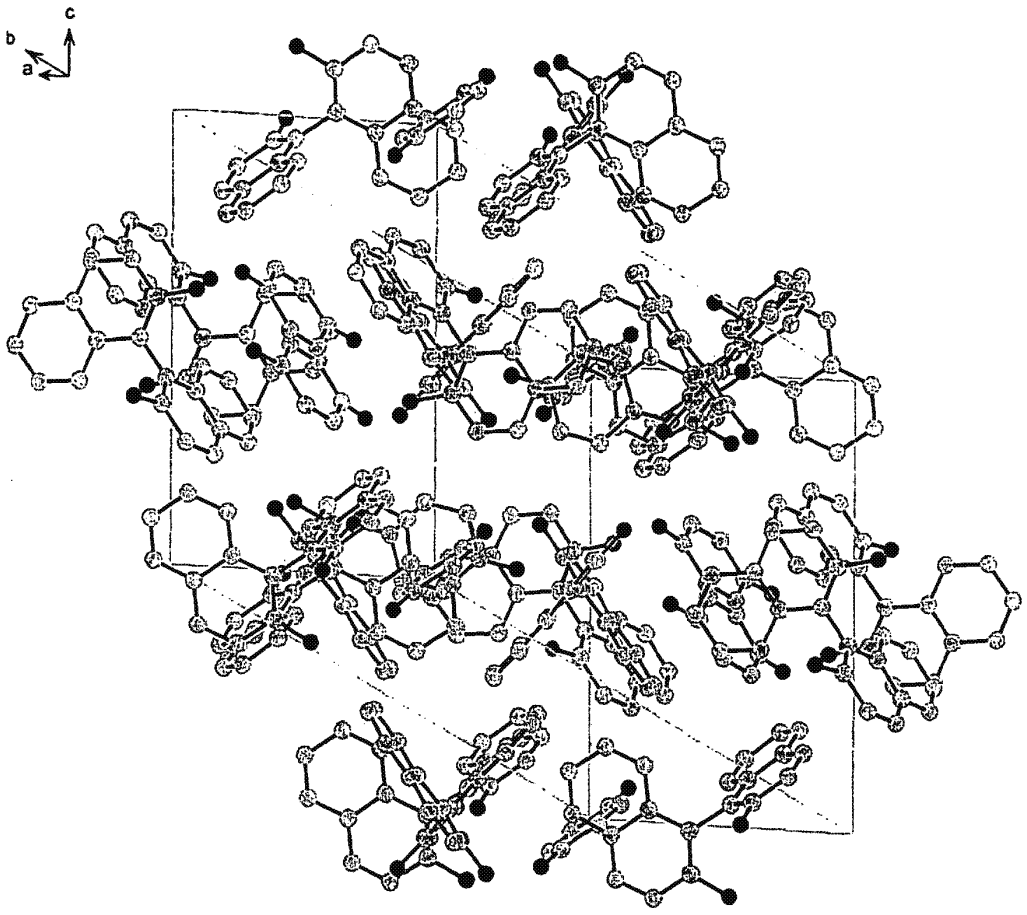
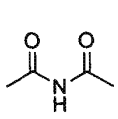


Fig. 8 Form II unit cell packing of cocrystal **20**:**21**, showing potential cleavage planes projected horizontally [50]

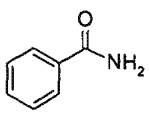
may be studied. Typically this is not the case, particularly for materials produced only by grinding. Etter and co-workers frequently prepared cocrystals by multiple methods, including grinding, solution evaporation and crystallisation from the melt. Often the same cocrystal was obtained by all techniques. However, there were certain instances in which grinding afforded a unique cocrystal product.

Etter and Reutzel conducted a series of experiments designed to understand the hydrogen bonding preferences of acyclic imides [27]. They identified two cocrystals containing the compound diacetamide **22**, which could only be prepared by the solid-state grinding approach. The first is a 1:1 cocrystal of **22** and benzamide **23**. A crystal structure was not determined; however, infrared spectroscopy, solid-state NMR and melting range characterization data were reported. The second material obtainable only by solid-state grinding is a 1:1 cocrystal containing diacetamide **22** and 3,4-dinitrobenzoic acid **24**. A crystal structure is also unavailable for this compound. The authors offer the expla-

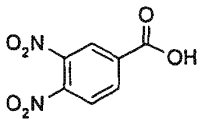
UM00012385
NOVARTIS EXHIBIT 1017
Novartis v. Regents, IPR2023-01346
Page 1131 of 4460



22



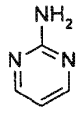
23



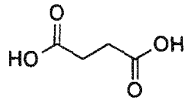
24

nation of disparate solubilities for why these two compounds could not be formed from solution.

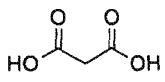
In contrast, solubility was not an issue in a second case of a product obtained only from grinding. In work with Adsmond on cocrystals of 2-aminopyrimidine 25, Etter found that by grinding the base 25 with succinic acid 26, two cocrystal



25



26



27

stoichiometries were obtained, 1:1 and 2:1 base:acid [23]. The outcome depended upon the ingoing starting material ratio. Solution crystallisation, conversely, yielded only the 1:1 product. The crystal structure of the product obtained only by grinding is not known, so a structure-based rationalisation of this observation is difficult. It may be possible that a certain preference for the 1:1 stoichiometry exists in solution, which is not as dominant during solid-state grinding.

Interestingly, in the same work [23] Etter and Adsmond reported two polymorphs of a 1:1 cocrystal containing 25 and malonic acid 27. Both crystallised from solution, but only one was obtainable from solid-state grinding. Contrary to the examples mentioned above, this instance suggests that solution crystallisation may at times offer more product diversity than grinding.

Hollingsworth et al. demonstrated the utility of the grinding approach in preparing a cocrystal material not initially accessible from solution [51, 52]. The researchers aimed to prepare a series of cocrystals with α,ω-dinitriles of the formula $NC(CH_2)_nCN$ with urea, with varying aliphatic chain lengths (n). Success was achieved in growing from solution a number cocrystals of different chain lengths; however, the n=3 (glutaronitrile) derivative could not be prepared from solution. Solid-state grinding of the two components, on the other hand, allowed for cocrystal formation with greater than 98% yield. When growth from solution was re-attempted, with the introduction of cocrystal seeds from the grinding experiment, the solution growth was successful and a single crystal of this compound was grown, thereby enabling crystal structure determination. This case establishes that the initial use of solid-state grinding for the preparation of cocrystal seeds may allow subsequent solution growth of novel cocrystal materials. The method was also demonstrated to apply to organometallic cocrystal systems [53, 54].

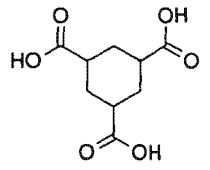
UM00012386
NOVARTIS EXHIBIT 1017
Novartis v. Regents, IPR2023-01346
Page 1132 of 4460

At the moment, the aforementioned examples serve as curious exceptions to the general trend that most cocrystals can be produced by both the grinding and solution approaches. However, as research continues in this field, it is hoped that an improved understanding will develop regarding the different mechanisms of these cocrystallisation approaches. With a better understanding in hand, novel solid-state materials for various uses may eventually arise as a consequence.

4
A Recent Enhancement to the Grinding Approach

The technique of solid-state grinding by mortar and pestle to induce cocrystal formation has been known for at least a century [10], and unlike many scientific techniques, this basic approach has seen little advancement since that time. Notwithstanding the development of more sophisticated mechanical grinders, grinding solids together with a mortar and pestle is still performed today exactly as it was then. Recent reports, however, have introduced a new variable into the process. The addition of a small amount of a particular solvent to the grinding process has been termed 'solvent-drop grinding', and has been shown to influence the cocrystallisation process in two specific ways: reaction kinetics and polymorph control.

Shan et al. first illustrated this solid-state enhancement technique in the context of cocrystals of the compound cyclohexane-1,3*cis*,5*cis*-tricarboxylic acid (CTA) **28** [55]. CTA readily formed phase-pure cocrystal material with hexamethylenetetramine (HMTA) **29** upon grinding for 20 min (as judged from powder XRD data).



28



29

The same was not true of a cocrystal of CTA **28** with 4,4′-bipyridine (Bipy) **30**. The structure of a cocrystal containing these two components was determined by single crystal XRD, using crystals grown from methanol [56]. When the ingoing powders were ground together without solvent, only partial formation of this cocrystal occurred after 1 h of grinding. The kinetics of the cocrystallisation, however, could be accelerated by introducing approximately 0.05 ml of methanol (i.e. two drops from a pipette) to the two powders before grinding commenced. In this case of the CTA:Bipy (**28**:**30**) cocrystal, the kinetics were increased so that the pure cocrystal was obtained in 20 min.

UM00012387
NOVARTIS EXHIBIT 1017
Novartis v. Regents, IPR2023-01346
Page 1133 of 4460

A second illustration of such reaction acceleration was reported using CTA **28** and 4,7-phenanthroline (fPh) **31**[55]. A 1:2 CTA:fPh (**28:30**) cocrystal, known



30 **31**

to precipitate readily from a methanol solution, was observed by powder XRD only as a minor component after grinding for a considerable period of time. The addition of two drops of methanol, water, ethyl acetate, or acetonitrile were all shown to accelerate this cocrystal formation. At least one of the components was soluble in each of these solvents. To demonstrate that solubility was a factor in this phenomenon, the researchers noted that the addition of cyclohexane, in which neither material was soluble, did not noticeably improve the reaction rate.

Solvent-drop grinding was next applied as an eco-friendly modification to a previously described preparation of a crystalline organic inclusion compound. Initial work had demonstrated solution-mediated supramolecular organisation and solid-state topochemically controlled reactivity in a system involving 1,2-bis(4-pyridyl)ethylene (bpe) **32** and 1,2,4,5-benzenetetracarboxylic acid (bta) **33** [57]. A single crystal of a 2:1 bpe:bta **32:33** cocrystal was



32 **33**

obtained from a dimethyl sulfoxide (DMSO) solution of the starting components, and its structure was determined (Fig. 9). UV-irradiation of this cocrystal induced [2+2] photodimerisation between adjacent bpe molecules in the

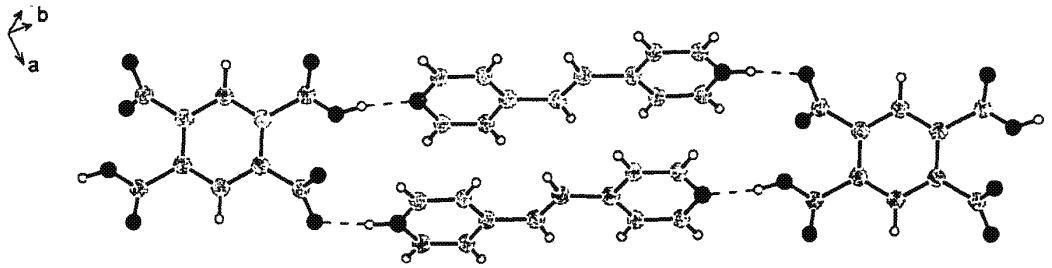
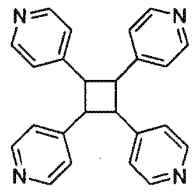


Fig. 9 Crystal packing of bpe:bta (**32:33**) cocrystal material, showing topochemical alignment of bpe molecules prior to UV radiation-induced solid-state dimerisation [57]

UM00012388
NOVARTIS EXHIBIT 1017
Novartis v. Regents, IPR2023-01346
Page 1134 of 4460

solid state to produce *rctt*-tetrakis(4-pyridyl)cyclobutane (tpcb) **34**. Following a DMSO recrystallisation of the irradiated product, single crystals of a novel



34

cocrystalline inclusion compound were isolated and were shown to contain 1:1 tpcb:bta **34**:**33** with disordered DMSO and water molecules in the supramolecular channels (Fig. 10).

A 'green' modification to this process, utilising the approach of solvent-drop grinding, was then demonstrated [58]. It was found that the initial cocrystal material (Fig. 9) containing bpe **32** and bta **33** could not be prepared by grinding the starting components for 2 h. However, the addition of several drops of the solvent methanol permitted complete cocrystallisation in 20 min, as determined by a comparison of the powder XRD pattern of the ground material to the pattern simulated from the known cocrystal structure. The cocrystal was irradiated as before to induce solid-state dimerisation. The irradiated mater-

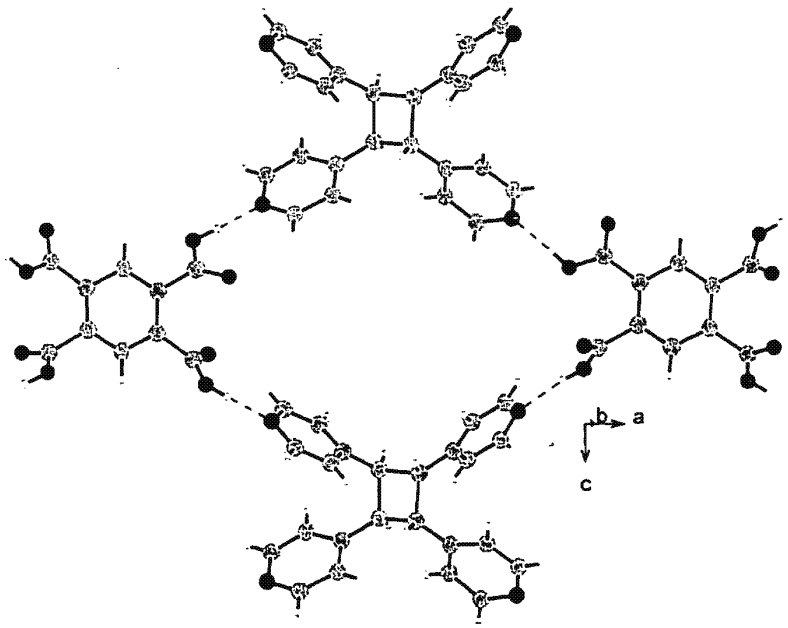
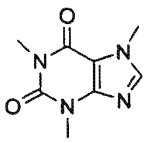


Fig. 10 Crystal packing of tpcb:bta (**34**:**33**) cocrystal material; disordered water and DMSO molecules have been omitted from supramolecular cavity [57]

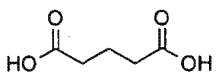
UM00012389
NOVARTIS EXHIBIT 1017
Novartis v. Regents, IPR2023-01346
Page 1135 of 4460

ial was then subjected to 20 min of solvent-drop grinding with DMSO to produce the desired organic inclusion compound as before (Fig. 10). This was an efficient demonstration of the value of solvent-drop grinding in providing 'greener' routes to novel supramolecular materials.

The utility of the solvent-drop grinding approach was recently extended by Trask et al. with a cocrystal system containing the model pharmaceutical



35



36

compound caffeine **35** and glutaric acid (GA) **36** [59]. Evaporation of a solution containing both components produced single crystals of two habits. Rod-like crystals were solved as monoclinic form I; block-like crystals were solved as triclinic form II. Both exhibited 1:1 stoichiometry; with identical chemical composition, the two cocrystals were designated polymorphs.

The hydrogen bonding scheme is identical in both crystals as seen in Fig. 11 and Fig. 12. The molecules pack so as to provide what may be aptly described as a hydrogen-bonded comb, with a GA **36** backbone and caffeine **35** teeth. In fact, the major difference between the two polymorphs on the secondary level of supramolecular architecture resides in the torsion of the GA **36** aliphatic chain.

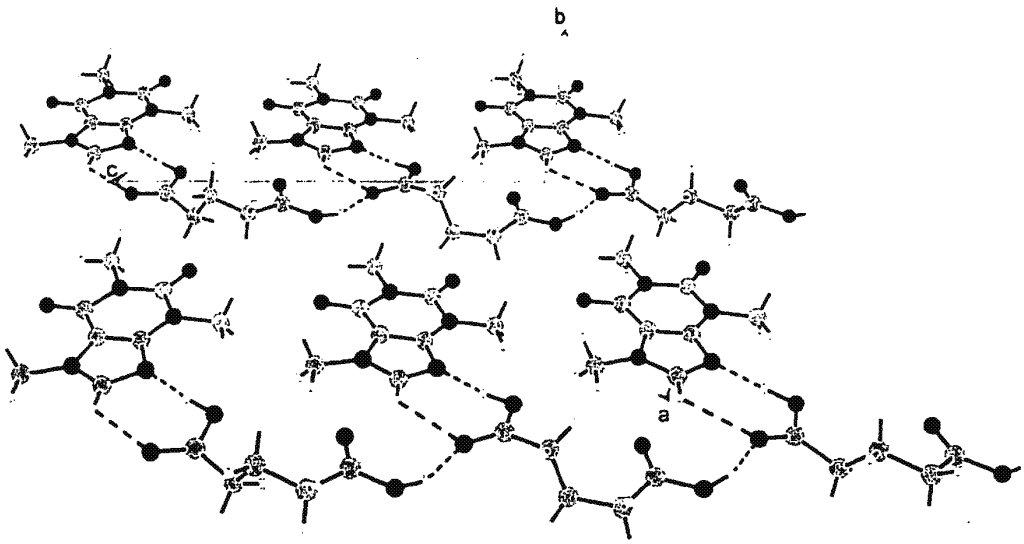


Fig. 11 Caffeine:glutaric acid (35:36) form I crystal packing, showing two hydrogen-bonded combs [59]

UM00012390
NOVARTIS EXHIBIT 1017
Novartis v. Regents, IPR2023-01346
Page 1136 of 4460

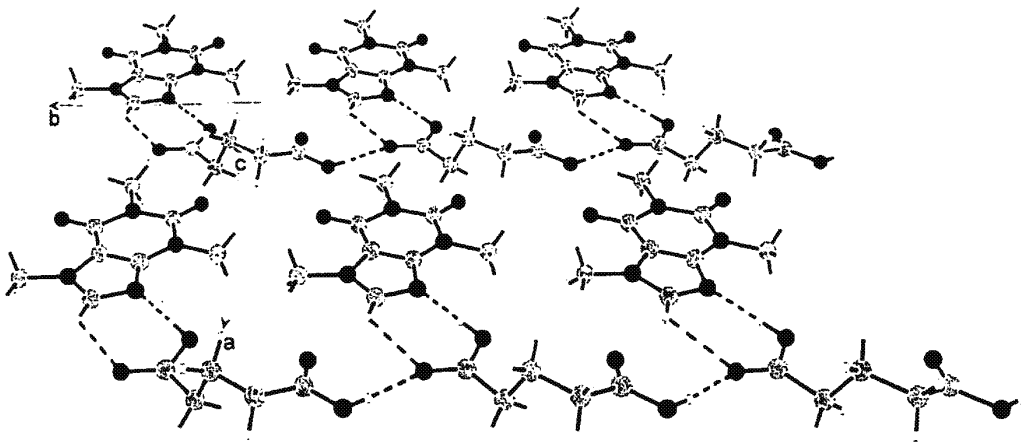


Fig. 12 Caffeine:glutaric acid (35:36) form II crystal packing, showing two hydrogen-bonded combs [59]

Given the identical hydrogen bonding arrangement, it may not be surprising that these two polymorphs precipitated concomitantly. Unexpectedly, however, it was found that application of the solvent-drop grinding approach allowed preparation of each crystal form essentially pure from the other. Grinding equimolar starting components in the absence of solvent produced form I. Similarly, grinding in the presence of a solvent in which neither component was soluble, including cyclohexane, hexane and heptane, also provided form I. Grinding with several drops of a more polar solvent, on the other hand, produced predominantly form II. Such solvents included chloroform, dichloromethane, acetonitrile and water.

A clear explanation for this observation was not offered. However, as a consequence of the space group symmetry, the crystals differ in their tertiary level of supramolecular architecture (see Fig. 13 and Fig. 14). The authors note that this difference affords a potential non-polar cleavage plane in form I but not in form II. As it is form I that preferentially formed in the presence of non-polar solvents, it is possible that this may play a role in the phenomenon.

The examples of this section summarise the recent application of the solvent-drop grinding approach to solid-state cocrystal preparation. The approach has been shown in certain instances to provide for either acceleration of cocrystallisation kinetics or selection of a particular polymorph via solid-state grinding. The approach is attractive, as it appears to incorporate some of the beneficial aspects of solvent participation while maintaining an essentially green, eco-friendly process.

UM00012391
NOVARTIS EXHIBIT 1017
Novartis v. Regents, IPR2023-01346
Page 1137 of 4460

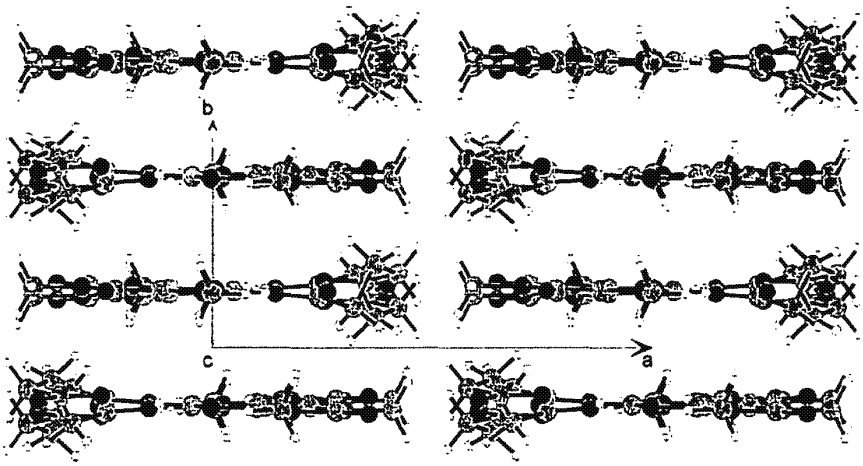


Fig. 13 Form I crystal packing of caffeine:glutaric acid (35:36), as viewed down the length of the hydrogen-bonded combs, showing potential non-polar cleavage plane, projected vertically [59]

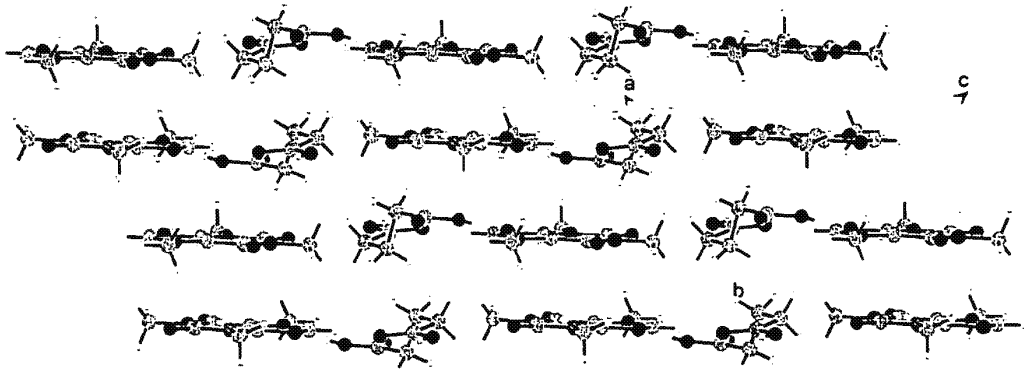


Fig. 14 Form II crystal packing of caffeine:glutaric acid (35:36), as viewed down the length of the hydrogen-bonded combs, showing lack of analogous cleavage plane [59]

5 Structure Determination from Powder XRD Data

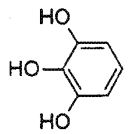
The solid-state grinding approach to cocrystal formation is simple, easily performed and environmentally friendly. So why is it not the clear favourite for obtaining cocrystal material? The answer may in part pertain to the fact that grinding results in microcrystalline powders, which are unsuitable for single crystal XRD. In other words, the most common means of obtaining a crystal structure is incompatible with solid-state cocrystal preparation. Thus, in order to ascertain the intermolecular interactions and packing features of a particular cocrystal via single crystal XRD, the researcher must grow a suitably sized

UM00012392
NOVARTIS EXHIBIT 1017
Novartis v. Regents, IPR2023-01346
Page 1138 of 4460

crystal of the same structure and stoichiometry from solution. A simulated powder XRD pattern from the solved crystal structure can then be compared to other powdered materials which may have been produced by solid-state grinding.

However, recent advancements in the field of crystal structure determination from powder XRD data may soon change this bias [60]. For some time, researchers have been developing the technique for solving homomeric crystal structures of materials with an increasingly large number of degrees of freedom [61]. Commonly these freedoms exist as molecular torsions or independent molecules in the asymmetric unit. The direct-space approach has seen much recent success in solving structures from powder data. This approach is an iterative process consisting of (1) generating a trial crystal structure independently of the experimental powder diffraction pattern, (2) simulating the powder diffraction pattern of the generated structure, and (3) comparing the simulated pattern to the experimental pattern. The crystal structure corresponding to the best agreement between the two patterns is found by a particular global optimisation strategy such as Monte Carlo, simulated annealing, or genetic algorithm. When the agreement is within an acceptable standard, the crystal structure has been solved.

In 2000 Tremayne and Glidewell claimed the first instance of a structure determination of a cocrystal material by the direct-space approach [62]. Their work involved a 1:1 cocrystal of 1,2,3-trihydroxybenzene **37** and hexamethyl-



37

enetetramine (HMTA) **29**, which was crystallised from solution but could not be grown as sufficiently sized single crystals. The experimental powder XRD pattern was collected using a monochromated laboratory instrument. The pattern was indexed to a monoclinic cell; its volume was consistent with one molecule each of **37** and **29** in the asymmetric unit. Both molecules **37** and **29** are rigid, so no torsional variables were necessary. However, within the asymmetric unit, each molecule must be described by three positional coordinates (x,y,z) and three rotational coordinates (θ,φ,ψ). This system, therefore, possessed a total of 12 degrees of freedom.

The crystal structure obtained from structure solution and subsequent refinement shows a rational pattern of hydrogen bonding, with each hydroxyl group of **37** participating in an OH···N intermolecular hydrogen bond to a tertiary amine of **29** to form a ribbon parallel to the a axis (Fig. 15). Such interactions are consistent with structures obtained from single crystal XRD data on other hydroxyl compounds complexed with HMTA [63].

UM00012393
NOVARTIS EXHIBIT 1017
Novartis v. Regents, IPR2023-01346
Page 1139 of 4460

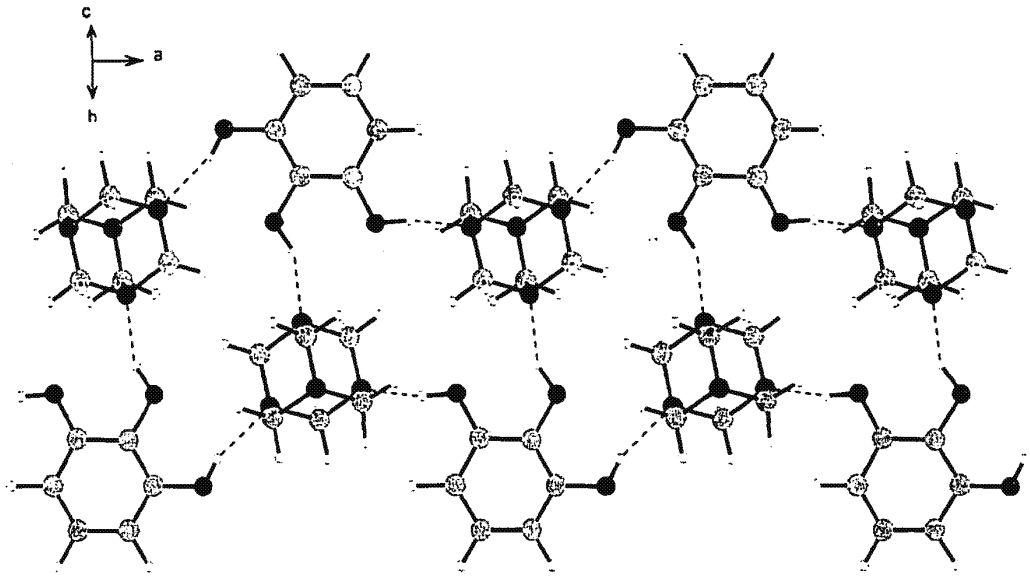


Fig. 15 Hydrogen-bonded ribbons of **37**:**29**; the crystal structure was solved from powder XRD data [62]

The structure solution of the cocrystal of **37** and **29** from powder XRD illustrates the current utility of this approach in the field of crystal engineering. While the material above was prepared from solution crystallisation, it is clear that this approach directly impacts cocrystals prepared by solid-state grinding.

Recently, Harris, Kuroda and co-workers claimed the first example of a direct structure determination of a cocrystal prepared by solid-state grinding [64]. The cocrystal involved was an extension of a system described earlier [50], consisting of the three components benzoquinone (BQ) **21**, bis-β-naphthol (BN) **20** and anthracene (AN) **16**. The authors noted that this system was yet another example in which solution and grinding approaches yielded different cocrystal products, as judged by their powder XRD patterns. This example highlights the significance of powder XRD structure determination, as the likelihood of obtaining sizable single crystals of this compound appears small.

The stoichiometry of the ground cocrystal material was confirmed by NMR and elemental analysis to be 1:1:0.5 (**21**:**20**:**16**). Interestingly, however, it was reported that a slight excess of BQ **21** was necessary to generate phase-pure material, in order to compensate for partial sublimation during the 60 min of manual mortar and pestle grinding.

Both BQ **21** and AN **16** are rigid structures, but BN **20** contains a molecular torsion about the two napthol rings. The unit cell volume and the *C*2/*c* space group assignment indicated that AN **16** spanned a symmetry element, therefore requiring the evaluation of only one half of that molecule. The crystal structure was confirmed by the resulting agreement between the experimental and simulated powder XRD pattern following Rietveld refinement (Fig. 16).

UM00012394
NOVARTIS EXHIBIT 1017
Novartis v. Regents, IPR2023-01346
Page 1140 of 4460

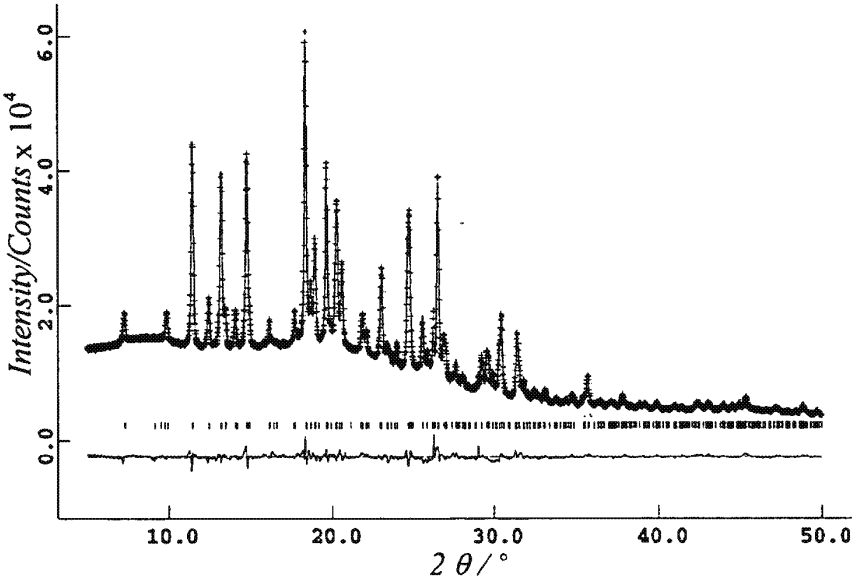


Fig. 16 Experimental (+ *marks*), calculated (*solid line*) and difference (*lower line*) powder X-ray diffraction profiles for the three-component material after final Rietveld refinement, as reported by the authors [64]. (Reprinted with permission from Cheung et al. (2003) J Am Chem Soc 125:14658. Copyright 2003 American Chemical Society)

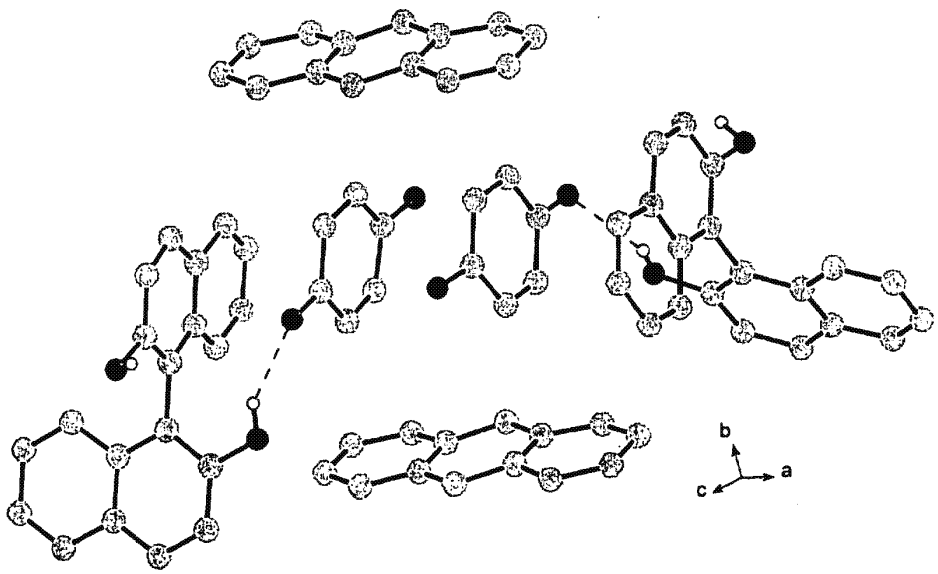


Fig. 17 The intermolecular interactions of the BN:BQ:AN (21:20:16) cocrystal, as solved from powder XRD data (non-hydroxyl hydrogens removed for clarity) [64]

UM00012395
NOVARTIS EXHIBIT 1017
Novartis v. Regents, IPR2023-01346
Page 1141 of 4460

The structure determination allows for an examination of the intermolecular interactions of the three-component cocrystal (Fig. 17). Hydrogen bonding is observed between the carbonyls of BQ **21** and the hydroxyls of BN **20**. A four-component π-stacking motif is apparent among two molecules each of BQ **21** and BN **20**. Finally, edge-to-face interactions are observed with two molecules each of BQ **21** and AN **16**.

Such a detailed understanding of the structural features of these two cocrystals would not have been possible without the advent of the developing technique of powder XRD crystal structure determination. Further progress in this exciting area of research will undoubtedly continue to benefit the advancement of solid-state cocrystal preparation.

6 Concluding Remarks

Crystal engineering is a prospering scientific field, comprised of practitioners with a variety of interests. The field at present remains to some extent in an information-gathering phase. Researchers are producing an abundance of novel cocrystal structures, cataloguing intermolecular interactions, and revealing crystallisation preferences. With evolving computational methodology and clever mining of the Cambridge Structural Database, the ultimate goal of reliable crystal structure prediction will someday be realised. Until then, novel cocrystal structures will be discovered through a process which combines design and chance: while the design of cocrystals using discrete intermolecular interactions, such as hydrogen bonding, is increasingly common, the entire three-dimensional architecture of the cocrystal structure, which often results from weaker, non-directional forces, is quite often left to chance. Because of this present inability to understand and control all contributing forces of the crystallisation process, researchers in search of novel cocrystal materials must increase the diversity of experimental conditions to plumb all chances for success.

A variety of cocrystallisation approaches, including solid-state grinding, will provide the most gainful outcome to a series of cocrystallisation experiments. The solid-state approach is certainly well precedented, but until more research is conducted its mechanism will remain far from well understood. It is simplistic in its application, and its environmental benefits, particularly on a large scale, could provide tremendous cost savings and hazard reduction. In what may someday provide a reliable source of novel materials, the solid-state grinding approach has been demonstrated to produce materials which will not form by traditional solution crystallisation. Enhancement by the solvent-drop method is known to provide increased cocrystallisation kinetics or polymorph control in certain instances. Finally, the arrival of structure determination from powder XRD data is beginning to overcome what may have comprised the most significant deficiency of the grinding approach: an inability to conclusively analyse the intermolecular interactions within the cocrystal produced. As

UM00012396
NOVARTIS EXHIBIT 1017
Novartis v. Regents, IPR2023-01346
Page 1142 of 4460

researchers further demonstrate the utility of solid-state grinding and more thoroughly examine its mechanism in cocrystal formation, its role in the field of crystal engineering will certainly grow.

Acknowledgements The authors gratefully acknowledge funding from the Pfizer Institute for Pharmaceutical Materials Science at the University of Cambridge. AVT additionally wishes to thank the Sidney Sussex North American Foundation for funding.

References

1. Braga D (2003) Chem Commun 2751
2. Desiraju GR (1989) Crystal engineering: the design of organic solids. Elsevier, Amsterdam
3. Jones W (1997) In: Jones W (ed) Organic molecular solids: properties and applications. CRC, New York, p 149
4. Bond AD, Jones W (2002) In: Jones W, Rao CNR (eds) Supramolecular organization and materials design. Cambridge University Press, Cambridge, p 391
5. Fernandez-Bertran JF (1999) Pure Appl Chem 71:581
6. Chan HK, Doelker E (1985) Drug Dev Ind Pharm 11:315
7. Anastas PT, Warner JC (1998) Green chemistry: theory and practice. Oxford University Press, Oxford, UK
8. Otsuka M, Kaneniwa N (1983) Chem Pharm Bull 31:4489
9. Otsuka M, Kaneniwa N (1984) Chem Pharm Bull 32:1071
10. Ling AR, Baker JL (1893) J Chem Soc 63:1314
11. Rastogi RP, Bassi PS, Chadha SL (1962) J Phys Chem 66:2707
12. Rastogi RP, Bassi PS, Chadha SL (1963) J Phys Chem 67:2569
13. Rastogi RP, Singh NB (1966) J Phys Chem 70:3315
14. Banerjee A, Brown CJ (1985) Acta Crystallogr C 41:82
15. Patil AO, Curtin DY, Paul IC (1984) J Am Chem Soc 106:4010
16. Patil AO, Curtin DY, Paul IC (1984) J Am Chem Soc 106:348
17. Scheffer JR, Wong YF, Patil AO, Curtin DY, Paul IC (1985) J Am Chem Soc 107:4898
18. Patil AO, Pennington WT, Desiraju GR, Curtin DY, Paul IC (1986) Mol Cryst Liq Cryst 134:279
19. Guarrera D, Taylor LD, Warner JC (1994) Chem Mater 6:1293
20. Toda F, Tanaka K, Sekikawa A (1987) J Chem Soc Chem Commun 279
21. Etter MC, Frankenbach GM (1989) Chem Mater 1:10
22. Etter MC, Frankenbach GM, Bernstein J (1989) Tetrahedron Lett 30:3617
23. Etter MC, Adsmond DA (1990) Chem Commun 8:589
24. Etter MC, Urbanczyklipkowska Z, Ziaebrahimi M, Panunto TW (1990) J Am Chem Soc 112:8415
25. Etter MC, Frankenbach GM, Adsmond DA (1990) Mol Cryst Liq Cryst 187:25
26. Etter MC (1991) J Phys Chem 95:4601
27. Etter MC, Reutzel SM (1991) J Am Chem Soc 113:2586
28. Etter MC, Reutzel SM, Choo CG (1993) J Am Chem Soc 115:4411
29. Huang KS, Britton D, Etter MC, Byrn SR (1997) J Mater Chem 7:713
30. Hoogsteen K (1963) Acta Crystallogr 16:907
31. O'Brien EJ (1967) Acta Crystallogr 23:92
32. Ueno S, Ristic RI, Higaki K, Sato K (2003) J Phys Chem B 107:4927
33. Remenar JF, Morissette SL, Peterson ML, Moulton B, MacPhee JM, Guzman HR, Almarsson O (2003) J Am Chem Soc 125:8456

UM00012397
NOVARTIS EXHIBIT 1017
Novartis v. Regents, IPR2023-01346
Page 1143 of 4460

34. Fleischman SG, Kuduva SS, McMahon JA, Moulton B, Walsh RDB, Rodriguez-Hornedo N, Zaworotko MJ (2003) Cryst Growth Des 3:909
35. Bailey Walsh RD, Bradner MW, Fleischman S, Morales LA, Moulton B, Rodriguez-Hornedo N, Zaworotko MJ (2003) Chem Commun 186..
36. Caira MR, Nassimbeni LR, Wildervanck AF (1995) J Chem Soc Perkin Trans 2:2213
37. Caira MR (1991) J Crystallogr Spectrosc Res 21:641
38. Caira MR (1992) J Crystallogr Spectrosc Res 22:193
39. Patel U, Haridas M, Singh TP (1988) Acta Crystallogr C 44:1264
40. Drezdzon MA (1988) Inorg Chem 27:4628
41. Jones W, Chibwe M (1990) In: Mitchell IV (ed) Pillared layered solids. Elsevier, Amsterdam, p 67
42. Newman SP, Jones W (2002) In: Jones W, Rao CNR (eds) Supramolecular organization and materials design. Cambridge University Press, Cambridge, p 295
43. Pedireddi VR, Jones W, Chorlton AP, Docherty R (1996) Chem Commun 987
44. Nichols PJ, Raston CL, Steed JW (2001) Chem Commun 1062
45. Braga D, Maini L, Polito M, Mirolo L, Grepioni F (2002) Chem Commun 2960
46. Braga D, Maini L, Polito M, Mirolo L, Grepioni F (2003) Chem-Eur J 9:4362
47. Toda F (1994) J Syn Org Chem Jpn 52:923
48. Toda F (1995) Acc Chem Res 28:480
49. Tanaka K, Toda F (2000) Chem Rev 100:1025
50. Kuroda R, Imai Y, Tajima N (2002) Chem Commun 2848
51. Hollingsworth MD, Santarsiero BD, Oumar-Mahamat H, Nichols CJ (1991) Chem Mater 3:23
52. Hollingsworth MD, Brown ME, Santarsiero BD, Huffman JC, Goss CR (1994) Chem Mater 6:1227
53. Braga D, Maini L, Polito M, Mirolo L, Grepioni F (2002) Chem Commun 2960
54. Braga D, Maini L, Polito M, Mirolo L, Grepioni F (2003) Chem-Eur J 9:4362
55. Shan N, Toda F, Jones W (2002) Chem Commun 2372
56. Shan N, Bond AD, Jones W (2002) Cryst Eng 5:9
57. Shan N, Jones W (2003) Tetrahedron Lett 44:3687
58. Shan N, Jones W (2003) Green Chem 5:728
59. Trask AV, Motherwell WDS, Jones W (2004) Chem Commun 890
60. Harris KDM, Johnston RL, Cheung EY, Turner GW, Habershon S, Albesa-Jove D, Tedesco E, Kariuki BM (2002) Crystengcomm 356
61. Harris KDM, Tremayne M, Kariuki BM (2001) Angew Chem Int Ed 40:1626
62. Tremayne M, Glidewell C (2000) Chem Commun 2425
63. Coupar PI, Glidewell C, Ferguson G (1997) Acta Crystallogr B 53:521
64. Cheung EY, Kitchin SJ, Harris KDM, Imai Y, Tajima N, Kuroda R (2003) J Am Chem Soc 125:14658

UM00012398
NOVARTIS EXHIBIT 1017
Novartis v. Regents, IPR2023-01346
Page 1144 of 4460

CRYSTAL GROWTH & DESIGN
2005
VOL. 5, NO. 3
1013–1021

Pharmaceutical Cocrystallization: Engineering a Remedy for Caffeine Hydration

Andrew V. Trask,[†] W. D. Samuel Motherwell,[‡] and William Jones*[,†]

Pfizer Institute for Pharmaceutical Materials Science, Department of Chemistry, University of Cambridge, Lensfield Road, Cambridge, United Kingdom CB2 1EW, and Cambridge Crystallographic Data Centre, 12 Union Road, Cambridge, UK CB2 1EZ

Received October 12, 2004; Revised Manuscript Received December 7, 2004

ABSTRACT: A systematic crystal engineering study was performed on the model pharmaceutical compound caffeine to prepare a cocrystal that, unlike caffeine, is physically stable at all relative humidities (RH). Six cocrystal materials containing caffeine with one of several dicarboxylic acids are described herein. Methods of cocrystallization included solution growth, neat solid-state grinding, and grinding with solvent-drop addition. Crystal structures are reported for a total of five cocrystals containing caffeine (with oxalic acid, malonic acid, maleic acid, and glutaric acid), including two recently reported polymorphic caffeine cocrystals. In each of these structures, a predicted intermolecular hydrogen-bonding motif is observed. The stability with respect to RH is evaluated for the six cocrystal materials. The cocrystal with oxalic acid exhibits complete stability to humidity over a period of several weeks. Other cocrystals demonstrate lesser degrees of stability with respect to humidity.

Introduction

The field of crystal engineering enables the design of crystalline molecular complexes, or cocrystals, using robust, reliable supramolecular synthons.[1–4] The extension of the field to pharmaceuticals has been previously demonstrated with several drug substances.[5,6] Cocrystallization of pharmaceutically active molecules represents a viable means of enhancing the physical properties of a drug substance, particularly when the options for forming ionic complexes are limited and the inherent instability of the amorphous material is undesired. In recent literature, pharmaceutical cocrystals have been demonstrated to alter the physical properties of melting point[7,8] and solubility.[9] In a related example, the solid-state chemistry of a pharmaceutical cocrystal containing two active pharmaceutical ingredients was investigated with regard to its anhydrous and hydrate crystal forms.[10]

The stability of a solid drug substance in the presence of atmospheric moisture is of concern to the pharmaceutical industry as it has practical implications for processing, formulation, packaging, and storage.[11,12] It is sometimes the case that an anhydrous crystal form is stable below a certain critical relative humidity (RH), but at higher RH it will convert to a crystalline hydrate.[13] In these cases, solid form selection is often employed to search for a polymorph or salt form that exhibits greater stability at high RH values.

Caffeine (1,3,7-trimethyl-2,6-purinedione) is a model pharmaceutical compound that is known to exhibit instability with respect to humidity, with the formation of a crystalline nonstoichiometric hydrate.[14] Caffeine is a central nervous system stimulant and a smooth muscle relaxant, and is commonly employed as a formulation additive to analgesic remedies. Its solid-state properties have been widely investigated; it is known to exist as two anhydrous crystal forms (α, β) and one crystalline nonstoichiometric hydrate.[15] The stable anhydrous β-caffeine crystal form converts to the metastable α-caffeine at high temperature.[16] Neither anhydrous crystal structure has been fully determined according to the most recent version of the Cambridge Structural Database (CSD).[17,18]

The nonstoichiometric crystalline hydrate of caffeine has been reported to contain 0.8 moles of water per mole of caffeine.[14] This unusual ratio appears to result from a channel inclusion of water in the hydrate crystal structure, which has been previously determined (CSD reference code CAFINE01).[19] Crystalline powder of anhydrous α- or β-caffeine converts to caffeine hydrate at high RH; conversely, caffeine hydrate loses its water of hydration at low RH and reverts to β-caffeine.[20] The dehydration of caffeine hydrate has been studied in detail,[19,21,22] with one study in particular finding that the critical humidity necessary for conversion, the dehydration boundary, occurs at 61% RH, although the dehydration rate varies with particle size.[14] Significantly less research has been done on the hydration process, i.e., crystalline hydrate formation, from anhydrous caffeine to caffeine hydrate.[20]

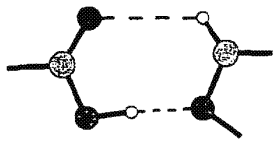
Given the hydration behavior of caffeine, the development of this model drug substance into a marketed form would potentially require the synthesis of a crystalline salt form to improve upon its physical properties. A search of the CSD reveals only one pharmaceutically acceptable salt form of caffeine, a hydrochloride dihydrate.[23] It appears, however, that a stable, anhydrous, pharmaceutically acceptable[24] form of caffeine is not yet known. The fact that the structure of only one pharmaceutically acceptable caffeine salt has been reported may result from the limited salt-forming capability of caffeine. The weakly basic imidazole nitrogen of caffeine results in a pK_a of 3.6.[25] As salt formation requires a significant acid–base pK_a difference (ca. 3.75 for a series of pyridine/benzoic acid complexes[26]), the potential salt-

* To whom correspondence should be addressed. E-mail: wj10@cam.ac.uk. Fax: (44) 1223 762829. Tel: (44) 1223 336468.
† University of Cambridge.
‡ Cambridge Crystallographic Data Centre.

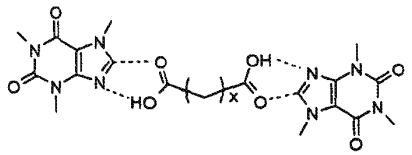
10.1021/cg0496540 CCC: $30.25 © 2005 American Chemical Society
Published on Web 02/03/2005

UM00012399
NOVARTIS EXHIBIT 1017
Novartis v. Regents, IPR2023-01346

Scheme 1. Heteromeric Synthon Showing Strong O−H···N and Weaker C−H···O Hydrogen Bond Interactions



Scheme 2. Expected Intramolecular Interactions of 2:1 Caffeine/Dicarboxylic Acid Cocrystals



forming acids for caffeine are limited to only strong acids.

By the same token, given its weak basicity, caffeine may be particularly suited for cocrystallization in its neutral form. A search of the CSD reveals 12 neutral organic cocrystals of caffeine. Several of these are pharmaceutically acceptable cocrystals, including 1:1 complexes of caffeine with the antibiotic sulfa drugs sulfacetamide[27] and sulfaproxyline[28] (CSD reference codes SACCAF and VIGVOW), and a cocrystal of caffeine with the sedative barbital[29] (CAFBAR20). Two other cocrystals, while not pharmaceutically acceptable, illustrate a hydrogen-bonded interaction between the imidazole nitrogen of caffeine with an un-ionized aromatic carboxylic acid (CAFSAL and DIJVUN). However, despite the existence of a number of caffeine cocrystals, a systematic crystal engineering study of pharmaceutical cocrystals of caffeine has not been described.

The aim of this study, therefore, was to rationally design and prepare a series of pharmaceutically acceptable caffeine cocrystals and to evaluate the stability of the cocrystals with respect to atmospheric humidity. Dicarboxylic acids were selected as cocrystal formers. The desired supramolecular interaction was the $R_2^2(7)$ acid−base heterodimer synthon (Scheme 1), so as to permit strong O−H···N and weaker C−H···O hydrogen bonding.[30] The CSD illustrates the precedence of this heteromeric synthon: a search of all organic compounds for heteromeric interactions involving the Scheme 1 synthon yields 131 crystal structures.[31] In the context of the current crystal engineering experiment, it was expected that the combination of caffeine with dicarboxylic acids would induce the formation of trimeric caffeine−acid−caffeine hydrogen-bonded units (Scheme 2). This arrangement would necessitate a resultant 2:1 caffeine/acid cocrystal stoichiometry.

The following caffeine cocrystals were prepared in this study: **A** caffeine/oxalic acid (2:1); **B** caffeine/malonic acid (2:1); **C** caffeine/maleic acid (2:1); **D** caffeine/maleic acid (1:1), **E** caffeine/glutaric acid (1:1) form I; and **F** caffeine/glutaric acid (1:1) form II. The chemical structures of the successful cocrystallizing agents are presented in Scheme 3. Crystal structures are reported here for the first time for **A**, **B**, and **D**. They are compared to the recently reported structures of **E** and **F**.[32] All of the crystal structures exhibit the expected Scheme 1 supramolecular synthon. Stoichiometry of 2:1 caffeine/acid is observed for **A**, **B**, and **C**, and the crystal structures of **A** and **B** confirm the hydrogen-bonded trimers described in Scheme 2. A stoichiometry of 1:1 caffeine/acid was observed for **D**, **E**, and **F**. In these instances, one of the carboxyl groups participates in the Scheme 1 synthon with caffeine, while the other carboxyl group associates in an alternative hydrogen-bonding arrangement. The pharmaceutical acceptability of each of these cocrystallizing agents has been confirmed by their precedence as pharmaceutical salt formers,[24] with the exception of glutaric acid.

Cocrystal preparation was attempted by the methods of solution precipitation and solid-state grinding. While less common than solution methods, cocrystal preparation in the solid state is well established and offers several advantages, such as a more environmentally friendly synthesis and an experimental design free from solubility considerations.[33−36] It was recently reported that solvent-drop grinding, i.e., grinding with the addition of a small amount of appropriate solvent, allowed for polymorphic control of the cocrystallization of caffeine with glutaric acid.[32] In this work, solvent-drop grinding was employed to obtain bulk powder of **D**, which could not otherwise be prepared as essentially phase-pure.

Experimental Procedures

Materials. All chemicals were obtained from the Sigma-Aldrich Company, Ltd. (Gillingham, UK) and were used as received.

(a) Caffeine. Anhydrous β-caffeine was used as received from the Sigma-Aldrich Company. PXRD analysis of this material agreed with that of previously analyzed β-caffeine.[19]

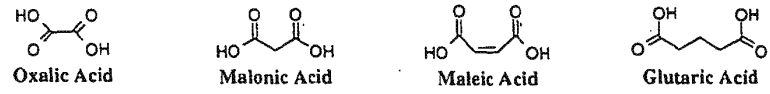
(b) Cocrystal A (2:1 Caffeine/Oxalic Acid). This material was prepared by both solution precipitation and by solid-state grinding. From solution, caffeine (4.85 g; 25.0 mmol) and maleic acid (1.12 g; 0.5 eq) were dissolved in 7:2 (v:v) chloroform/methanol (90 mL) by heating to reflux. The solution was concentrated in vacuo until precipitation commenced. Crystals were isolated by filtration. Cocrystals were also prepared by grinding β-caffeine (0.38 g; 2.0 mmol) and oxalic acid (0.89 g; 0.5 eq) for 60 min. A single crystal for XRD analysis was obtained by slow evaporation of a chloroform/methanol solution of dissolved cocrystal material.

(c) Cocrystal B (2:1 Caffeine/Malonic Acid). This material was prepared by solution and grinding techniques. Caffeine (1.43 g; 7.4 mmol) and malonic acid (0.38 g; 0.5 eq) were dissolved in 30:1 (v:v) chloroform/methanol (30 mL) and heated to reflux. The solution was then seeded (with single crystals as obtained below) and stirred at ambient temperature while permitting evaporation until precipitation commenced. This cocrystal material was also obtained by grinding caffeine (0.30 g; 1.5 mmol) and malonic acid (0.81 g; 0.5 eq) for 30 min. Single crystals were obtained by dissolving this material in chloroform/methanol and evaporating slowly at ambient conditions.

(d) Cocrystal C (2:1 Caffeine/Maleic Acid). Cocrystal material with minor β-caffeine content could be prepared by dissolving caffeine (2.42 g; 12.5 mmol) and maleic acid (0.73 g; 0.5 eq) in 8:1 (v:v) chloroform/methanol (17 mL) with heating to reflux, followed by seeding, and then prompt addition of *n*-hexane to effect sudden crystallization. Initial seeds of essentially phase-pure **C** material were obtained in small quantities by the removal of a small (ca. 1 mL) aliquot from a solution of caffeine (2.70 g; 13.9 mmol) and maleic acid (0.82 g; 0.5 eq) in 15:1 chloroform/methanol (32 mL), and the addition of cyclohexane (ca. 1 mL) to the aliquot to effect crystallization, followed by filtration. As an alternative to the solution-based approach, cocrystal powder of **C** with substan-

UM00012400
NOVARTIS EXHIBIT 1017
Novartis v. Regents, IPR2023-01346
Page 1146 of 4460

Scheme 3. Molecules That Successfully Formed Cocrystals with Caffeine



tial β-caffeine content was obtained by grinding caffeine (0.41 g; 2.1 mmol) and maleic acid (0.12 g; 0.5 eq) for 60 min. The 2:1 caffeine/maleic acid stoichiometry was confirmed by ^{1}H NMR analysis of crystals filtered from solution. While the crystal structure of **C** was not successfully determined, X-ray diffraction from a single crystal at 180(2) K provided unit cell dimensions of a, b, c = 13.1356(5), 6.8750(3), 26.1807(12); α, β, γ = 90, 97.739(3), 90; volume = 2342.77(17) Å^3. This unit cell volume agrees with the existence of eight caffeine molecules and four maleic acid molecules per unit cell.[37] The experimental PXRD pattern was indexed to similar unit cell parameters.

(e) Cocrystal D (1:1 Caffeine/Maleic Acid). **C** material, obtained by grinding, was dissolved in dichloromethane, and the solution was permitted to evaporate slowly to yield a single crystal of 1:1 stoichiometry, **D**. This is the only instance of solution precipitation of the **D** material. This cocrystal material could be prepared in bulk powder form by grinding caffeine (0.40 g; 2.1 mmol) and maleic acid (0.24 g; 1 eq) with the addition of methanol (5 drops from a pipet; ca. 0.06 mL) for 90 min.

(f) Cocrystals E and F (1:1 Caffeine/Glutaric Acid Forms I and II, respectively). Essentially pure form I was prepared by grinding caffeine (0.53 g; 2.7 mmol) and glutaric acid (0.63 g; 1 eq) with cyclohexane (5 drops from a pipet; ca. 0.06 mL) for 90 min. Essentially pure form II was prepared by grinding caffeine (0.51 g; 2.6 mmol) and glutaric acid (0.35 g; 1 eq) with chloroform (5 drops from a pipet; ca. 0.04 mL) for 90 min. Single crystals of form I (rods) and form II (blocks) were obtained concomitantly by slow evaporation of a chloroform solution of the starting components, in which there was a slight excess of caffeine.[32]

General Methods. RH conditions were achieved at ambient temperature (ca. 20 °C) within sealed glass desiccator jars containing P_2O_5 for the 0% RH condition and the appropriate saturated aqueous salt solutions for other RH values (K_2CO_3 for 43%; NaCl for 75%; and K_2SO_4 for 98%).[38] RH conditions were monitored with humidity-indicator cards (Sigma-Aldrich Company).

To compare the stability of anhydrous caffeine to the various cocrystals produced, cocrystals **A** through **F** were evaluated along with anhydrous caffeine for physical stability at the conditions of 0, 43, 75, and 98% RH for time periods of 1 day, 3 days, 1 week, and 7 weeks. Cocrystal materials formed from solution (**A**, **B** and **C**) were ground gently with a mortar and pestle to homogenize the particle size to ca. 10−50 μm, as observed by optical microscopy, before the experiment commenced. The cocrystal materials necessarily formed by solid-state grinding (**D**, **E** and **F**) were obtained as microcrystalline powders and were used as isolated. Open glass vials containing 40−60 mg of powdered cocrystal material were stored in the RH chambers at ambient temperature. A vial was removed for each cocrystal material at each time point. Upon removal from the chamber, the samples were promptly evaluated for any form change by PXRD.

Powder X-ray diffraction (PXRD) data was collected on a Philips X'Pert Pro diffractometer, using Ni-filtered CuKα radiation (λ = 1.5418 Å) at 40 kV and 40 mA with a X'Celerator RTMS detector. Each sample was analyzed between 4 and 40 °2θ with a step size of ca. 0.02 °2θ and a total scan time of 3 min 5 s. Experimental PXRD patterns were compared to PXRD patterns simulated from available crystal structures to confirm the composition of those materials.[39]

Fourier transform infrared (FT-IR) spectra were collected in the mid-IR region on crystalline powders with a ThermoNicolet Nexus spectrometer equipped with a Smart Golden Gate Attenuated Total Reflection accessory.

Solid-state grinding was performed with a Retsch MM200 Mixer mill, equipped with stainless steel 10-mL grinding jars and two 7-mm stainless steel grinding balls per jar. All grinding was performed at a rate of 30 Hz. The temperature of the grinding jars following grinding experiments did not exceed ca. 30 °C.

Single-crystal X-ray diffraction data was collected at 180(2) K with a Nonius Kappa CCD diffractometer using MoKα radiation (λ = 0.71073) and equipped with an Oxford Cryosystems cryostream. Data reduction and cell refinement were performed with the programs *DENZO* (University of Texas, Southwestern Medical Center at Dallas, HKL Denzo and Scalepack, USA, 1997) and *COLLECT* (Nonius, B. V. Delft, The Netherlands, 1998). Multiscan absorption corrections were applied with the program *SORTAV*.[40] Structures were solved by direct methods using *SHELXS-97* (University of Göttingen, Germany, 1997) and refined on F^2 against all data using *SHELXL-97* (University of Göttingen, Germany, 1997). All non-hydrogen atoms were refined with anisotropic displacement parameters. The OH hydrogen atoms were located in difference Fourier maps and refined isotropically. All other hydrogen atoms were placed geometrically and were allowed to ride during subsequent refinement. Experimental details of the structure determinations of **A**−**F** are given in Table 1.

Results and Discussion

Cocrystal Structure Analysis. In examining the caffeine/acid materials, the matter of locating the acidic proton was of significance, as it differentiated between salts (ionic complexes) and cocrystals (neutral complexes). For each of the crystal structures obtained, acidic protons were located on the acid in the X-ray difference maps, which confirmed in each case that salt formation (ionization) had not occurred. Typical O−H bond distances were observed in all instances.[41] It is also noted that ambient temperature FT-IR spectra of each powder sample exhibited a broad peak ranging from ca. 2200 to 2800 cm^{-1}, interpreted as the O−H stretching modes of un-ionized, strongly hydrogen-bonded carboxylic acids.[26] The lack of a band associated with a symmetric carboxylate stretch, which typically would be observed from ca. 1300 to 1420 cm^{-1}, is further indication of the nonionic character of these complexes.

A stoichiometry of 2:1 caffeine/acid is observed for **A** and **B** from the solved crystal structures, and for **C** from ^{1}H NMR. The expected heteromeric synthon (Scheme 1) is observed in the crystal structures of **A** and **B**. Further, the trimeric caffeine−acid−caffeine motif (Scheme 2) is also demonstrated in both structures. However, the varied geometries of oxalic and malonic acids necessitate differences in crystal packing.

Cocrystal **A**, which crystallizes in the $P2_1/c$ space group, has the highest calculated density (1.542 g cm^{-3}) of all the solved cocrystal structures. The planarity of the oxalic acid molecule allows a flat trimeric motif to stack along the a axis (Figure 1a). If the trimeric units are considered to be "dumbbell-shaped," whereby the acid is the "handle" and the bulky caffeines are the "weights," then it can be noted that these units best fill space on (h, 0, 0) by placing the end of one weight

UM00012401
NOVARTIS EXHIBIT 1017
Novartis v. Regents, IPR2023-01346
Page 1147 of 4460

Table 1. Crystallographic Data for Caffeine Cocrystals

	A 2:1 caffeine/ oxalic acid	B 2:1 caffeine/ malonic acid	D 1:1 caffeine/ maleic acid	E[32] 1:1 caffeine/ glutaric acid form I	F[32] 1:1 caffeine/ glutaric acid form II
experimental formula	$2(C_8H_{10}N_4O_2)\cdot C_2H_2O_4$	$2(C_8H_{10}N_4O_2)\cdot C_3H_4O_4$	$C_8H_{10}N_4O_2\cdot C_4H_4O_4$	$C_8H_{10}N_4O_2\cdot C_5H_8O_4$	$C_8H_{10}N_4O_2\cdot C_5H_8O_4$
formula weight	478.44	492.46	310.27	326.31	326.31
crystal system	monoclinic	orthorhombic	monoclinic	monoclinic	triclinic
space group	$P2_1/c$	$Fdd2$	$P2_1/n$	$P2_1/c$	$P\bar{1}$
a (Å)	4.41430(10)	30.3992(12)	6.8565(2)	13.0129(5)	8.3212(8)
b (Å)	14.7701(5)	31.2845(16)	12.5051(4)	6.6017(2)	8.6667(8)
c (Å)	15.9119(6)	4.6739(2)	15.8362(5)	17.1427(8)	11.3636(12)
α (deg)	90	90	90	90	68.955(4)
β (deg)	96.4850(10)	90	93.6100(10)	97.8360(10)	78.559(4)
γ (deg)	90	90	90	90	74.236(4)
V (Å^3)	1030.81(6)	4445.0(3)	1355.12(7)	1458.93(10)	731.43(12)
Z	2	8	4	4	2
θ range (deg)	3.78–27.46	3.74–27.45	3.56–27.48	1.58–27.5	3.69–27.47
data/restraints/parameters	2354/0/161	1413/1/168	3093/2/208	3343/2/217	3094/0/217
ρ_{calc} (g cm^{-3})	1.541	1.472	1.521	1.486	1.482
T (K)	180(2)	180(2)	180(2)	180(2)	180(2)
R1	0.0462	0.0425	0.0437	0.0645	0.0581
wR2	0.1162	0.0855	0.0962	0.1870	0.1592

adjacent to a neighboring handle. An angling of the stacks with respect to one another appears necessary to achieve a close-packed arrangement (Figure 1b).

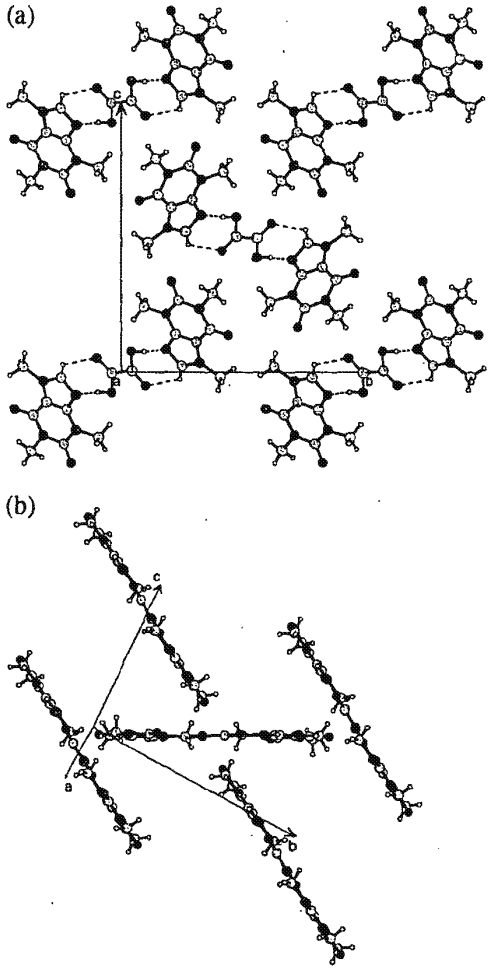


Figure 1. Crystal packing of **A**, showing (a) stacks of planar trimeric units along the a axis, and (b) an angling of the trimeric units with respect to one another.

Cocrystal **B** crystallizes in the orthorhombic $Fdd2$ space group, with a calculated crystal density of 1.472 g cm^{-3}. Like **A**, this cocrystal also possesses stacks of trimeric intermolecular hydrogen-bonded units, whereby the weights and handles interdigitate as before (Figure 2a). However, the central sp^3 carbon of malonic acid imposes a V-shaped geometry to the trimeric unit, so that the motif may be better described as a kinked dumbbell. As a result, packing is significantly different from **A** (Figure 2b). The stacks of V-shaped trimeric units fill space by a 90° rotation of each successive stack to allow interdigitation.

The 1:1 caffeine/acid stoichiometry was observed for **D**, **E**, and **F**. In each of these cocrystals, the Scheme 1 heteromeric synthon was observed with only one of the

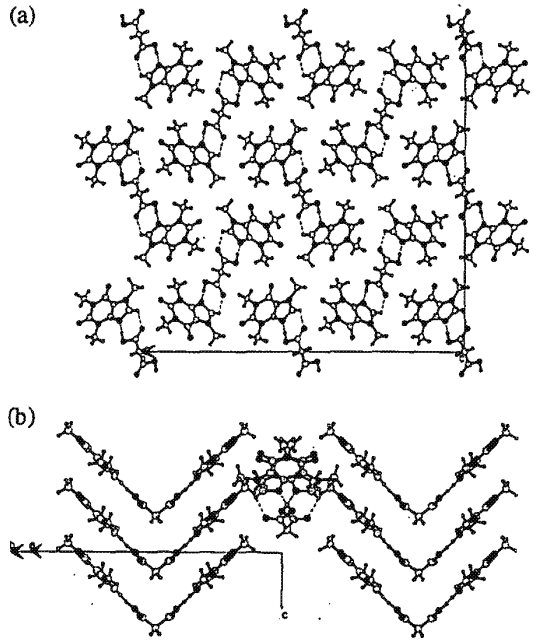


Figure 2. 2:1 Caffeine/malonic acid crystal packing, showing (a) stacks of trimeric units as viewed down the c axis, and (b) V-shaped geometry of the interdigitated trimeric units.

UM00012402
NOVARTIS EXHIBIT 1017
Novartis v. Regents, IPR2023-01346
Page 1148 of 4460

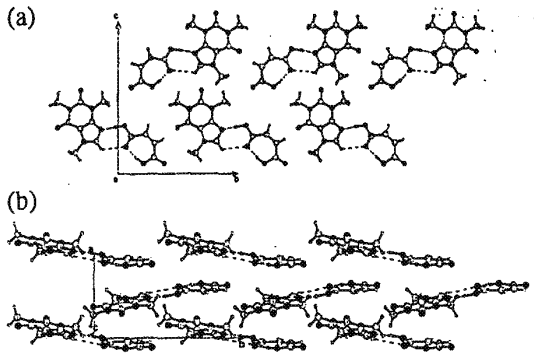


Figure 3. Cocrystal **D** showing (a) sheets of dimeric hydrogen-bonded units and (b) angled vertical stacks of dimeric units.

two carboxyl groups of each dicarboxylic acid. The other carboxyl group formed a hydrogen bond to another carboxyl group. This implies that in these cocrystals the hydrogen bond acceptor ability of the caffeine imidazole nitrogen did not successfully compete with that of a carboxyl group in dictating the hydrogen-bonding preference of the second carboxyl of each acid.

It is important to note that the caffeine/maleic acid cocrystal exists in both 2:1 and 1:1 stoichiometries (**C** and **D**); however, the crystal structure of **C** was not determined. It is perhaps not surprising to find a 1:1 stoichiometry involving maleic acid. A cis orientation of the carboxyl groups about the double bond predisposes maleic acid to form intramolecular $S_1^1(7)$ hydrogen-bonded rings, as evidenced in its reported crystal structure (CSD Refcode MALIAC11)[42] and in a recently determined polymorph.[43] The crystal structure of **D** indeed validates this intramolecular hydrogen-bond preference. The structure packs in the space group $P2_1/n$ with a relatively high calculated density of 1.521 g cm^{-3}. Dimeric caffeine–acid units are formed by the expected Scheme 1 hydrogen-bonded interaction. These units form two-dimensional sheets in the *bc* plane by translation and 2_1-screw axis symmetry (Figure 3a). The units are propagated in the *a* axis direction via the *n* glide plane (Figure 3b)

The two caffeine/glutaric acid polymorphs **E** and **F** exhibit a similar hydrogen-bonded interaction to that of **D**, in that the Scheme 1 interaction occurs with one of the two carboxyl groups (Figure 4). The 1:1 stoichiometry may have resulted from the very weak acidity of the second carboxyl group of glutaric acid: the potential acid–base interaction between caffeine and glutaric acid was sufficiently weak that a hydrogen bond to another carboxylic oxygen was more favorable than a bond to the caffeine imidazole nitrogen. The two different structures of caffeine/glutaric acid are in fact conformational polymorphs,[44] differing in the torsion of the glutaric acid aliphatic chain (Figure 5).

Cocrystal Preparation by Grinding. It was generally possible to prepare most cocrystals by the dual methods of solution growth and solid-state grinding, but the exceptions are of interest. Polymorphs **E** and **F** precipitated concomitantly from solution in our experiments. As described previously,[32] solvent-drop grinding enabled the preparation of essentially pure samples of both of these polymorphs. For this study, the solvent-drop grinding approach was performed with cyclohexane and chloroform to prepare **E** and **F**, respectively.

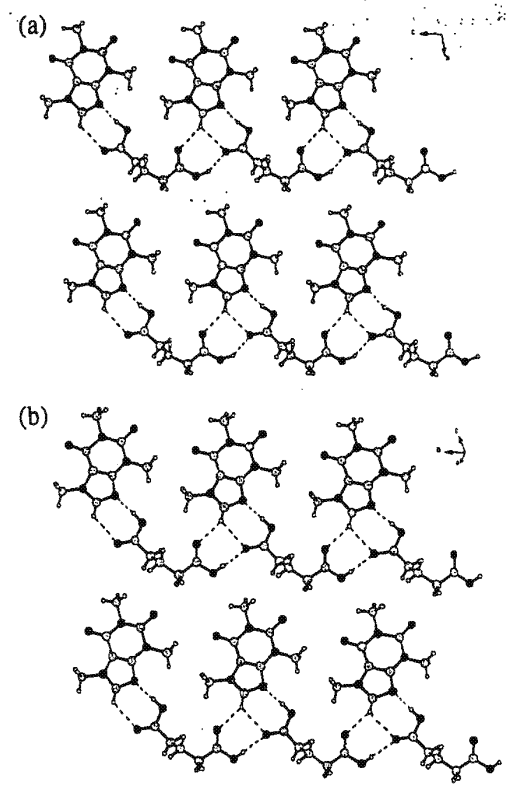


Figure 4. Sheets of caffeine:glutaric acid ribbons showing identical packing in projection of the two conformational polymorphs: (a) **E** (b) **F**.

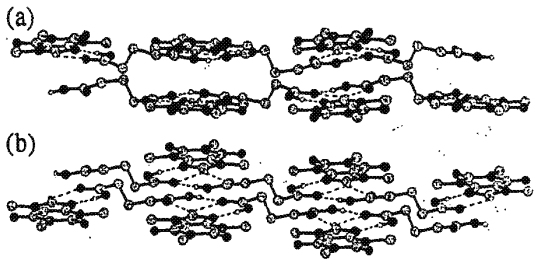
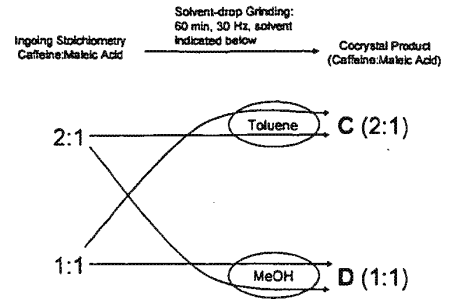


Figure 5. Stacked ribbons of caffeine:glutaric acid cocrystal polymorphs illustrating conformational differences in glutaric acid torsions: (a) **E** (b) **F**.

The stoichiometric competition between the two caffeine:maleic acid cocrystals **C** and **D** also resulted in interesting crystallization behavior. Aside from the one instance in which a single crystal was obtained of **D**, solution growth never yielded the 1:1 stoichiometry in this system. Neat grinding of caffeine and maleic acid in a 2:1 ratio produced mostly **C** with residual unreacted material apparent by PXRD. Neat grinding of a 1:1 ratio of caffeine and maleic acid produced a mixture of **C** and **D** cocrystals. Thus, a bulk quantity of essentially pure **D** could not be prepared by traditional solution or dry grinding methods.

UM00012403
NOVARTIS EXHIBIT 1017
Novartis v. Regents, IPR2023-01346
Page 1149 of 4460

Scheme 4. Summary of Caffeine/Maleic Acid Stoichiometry Control via Solvent-Drop Grinding



The solvent-drop grinding method was investigated as a potential means of obtaining pure **D**. Upon addition of several drops of methanol to the 1:1 ingoing mixture, the resulting product from grinding was predominantly **D**, with a slight component of unreacted starting materials and no **C** material observable by PXRD. It is noted that methanol addition provides a significant preference for **D** formation: grinding of an ingoing 2:1 caffeine/maleic acid ratio with methanol addition produces **D** with excess caffeine without any evidence of **C**, the 2:1 product, by PXRD.

Just as methanol favors **D** upon grinding, toluene appears to favor **C**. Solvent-drop grinding of ingoing 1:1 material with toluene provides **C** with excess maleic acid and some unreacted residual caffeine as a minor component. Additionally, solvent-drop grinding of ingoing 2:1 material with toluene provides **C** with some unreacted material, mimicking the results of neat (solvent-free) grinding. These results are summarized diagrammatically in Scheme 4, and PXRD data are presented in Figure 6. While the mechanism underlying this phenomenon has not yet been fully explained, it was employed to generate nearly phase-pure **D** material for use in the RH stability study.

It should be noted that not all the dicarboxylic acids that were attempted successfully formed cocrystals with caffeine. When screened for cocrystallization by the grinding method, the following three pharmaceutically acceptable dicarboxylic acids were determined to be unsuccessful cocrystallizing agents with caffeine: fumaric acid, L-tartaric acid, and adipic acid. Further, a cocrystal involving caffeine and succinic acid was isolated from solution, but due to significant physical instability resulting from weakly bound solvent of crystallization, it was not included in this study.

Relative Humidity Challenges. The RH stability results of caffeine and of each cocrystal are described in turn below and are summarized diagrammatically in Table 2. Analysis of powders by PXRD provided an effective means of analyzing the different cocrystals (Figure 7). Generally, it is noted that cocrystal hydrates were not formed from any of these cocrystals. Rather, the materials that possessed instability with respect to RH demonstrated dissociation of the cocrystal into its crystalline starting components, as observed by PXRD. The exception to this was one case of polymorph conversion seen from **E** to **F**. Dissociation at high RH (75 and 98%) was apparent from the emergence of crystalline caffeine hydrate peaks by PXRD; dissociation

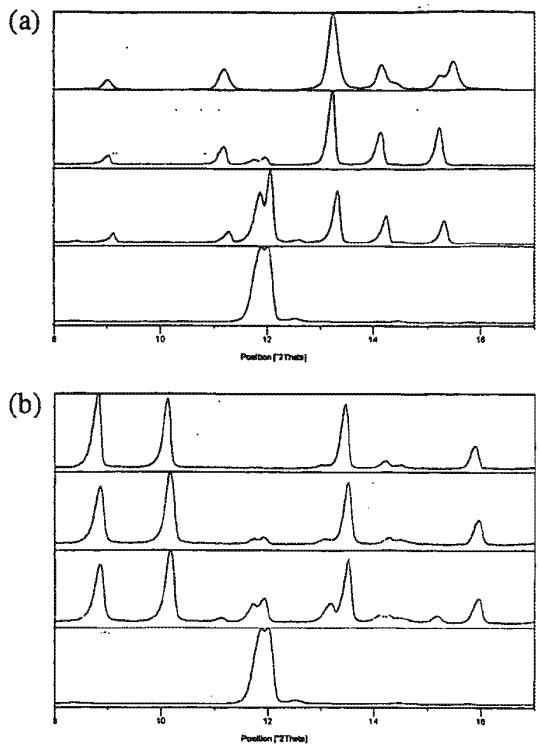


Figure 6. PXRD patterns of results from caffine:maleic acid solvent-drop grinding: (a) from top to bottom: simulated pattern of **D**; result from grinding an ingoing 1:1 mixture with methanol; result from grinding an ingoing 2:1 mixture with methanol; anhydrous β-caffeine; and (b) from top to bottom: pattern of **C** from solution precipitation; result from grinding an ingoing 1:1 mixture with toluene; result from grinding an ingoing 2:1 mixture with toluene; anhydrous β-caffeine. Patterns plotted in units of relative intensity

at low RH (0 and 43%) was observed by the growth of crystalline anhydrous caffeine peaks. Acid peaks were less evident in the dissociated product.

(a) Anhydrous β-Caffeine. Crystalline anhydrous caffeine was stored in humidity chambers alongside the cocrystal materials. At 98% RH, caffeine showed partial conversion to the hydrate after 1 day and full conversion after 3 days and beyond. Interestingly, no hydration was apparent at 75% RH or below at seven weeks. The difference between this observed hydration behavior of anhydrous caffeine and the reported dehydration boundary of caffeine hydrate (61% RH)[14] may reflect the physical differences between the solid-state processes of hydration and dehydration. It is also possible that a hydration/dehydration hysteresis, as has been observed elsewhere,[45,46] may have had a kinetic influence on the transition.

(b) Cocrystal A. This material was found to be stable at all relative humidities across all time points. This cocrystal clearly demonstrates enhanced stability over anhydrous caffeine. Its stability was additionally demonstrated by slurrying the cocrystal material in water for 2 days at ambient temperature without any observed physical form change.

UM00012404
NOVARTIS EXHIBIT 1017
Novartis v. Regents, IPR2023-01346
Page 1150 of 4460

Table 2. Stability of Cocrystals with Respect to RH

Material	Condition (% RH)	Observed Relative Humidity Stability*			
		1 day	3 days	1 week	7 weeks
Caffeine	0	✓	✓	✓	✓
	43	✓	✓	✓	✓
	75	✓	✓	✓	✓
	98	x	x	x	x
A	0	✓	✓	✓	✓
	43	✓	✓	✓	✓
	75	✓	✓	✓	✓
	98	✓	✓	✓	✓
B	0	✓	✓	✓	✓
	43	✓	✓	✓	✓
	75	✓	✓	✓	✓
	98	✓	✓	✓	x
C	0	✓	✓	✓	✓
	43	✓	✓	✓	✓
	75	✓	✓	✓	✓
	98	x	x	x	x
D	0	✓	✓	✓	✓
	43	✓	✓	✓	✓
	75	✓	✓	✓	✓
	98	x	x	x	x
E	0	✓	✓	✓	✓
	43	✓	x	x	x
	75	x	x	x	x
	98	x	x	x	x
F	0	✓	✓	✓	✓
	43	✓	✓	✓	✓
	75	✓	✓	✓	✓
	98	✓	✓	x	x

*Note: The symbol ✓ indicates that the crystalline material was stable at that condition and time point. The symbol x indicates that the crystalline material exhibited physical instability at that time point: caffeine converted to caffeine hydrate; cocrystals B, C, D and F dissociated into molecular components; and cocrystal E was observed in some instances to convert to polymorph F before dissociating. See text for details.

(c) Cocrystal B. This material was stable at 75% RH and below for the duration of the study. At 98% RH, however, **B** showed evidence of partial dissociation at 1 week, as seen by growth of peaks associated with crystalline caffeine hydrate. At 7 weeks, this material had deliquesced to a liquid.

(d) Cocrystal C. This material was stable at 75% RH and below for the duration of the study. Similar to the malonic acid cocrystal material, this cocrystal also demonstrated instability at 98% RH. At just 1 day at this RH condition, crystalline caffeine hydrate was observed by PXRD.

(e) Cocrystal D. The 1:1 cocrystal stoichiometry of **D** exhibited identical RH stability to the 2:1 material of **C**. It was stable at 75% RH and below for 7 weeks, and exhibited complete dissociation at 1 day at 98% RH.

(f) Cocrystal E. This cocrystal material demonstrated a tendency for conversion to **F**, the form II polymorph of the caffeine/glutaric acid system. The only storage condition at which **E** showed stability across all time points was 0% RH. Cocrystal **E** showed partial conversion to **F** at 1 day at 43% RH and full conversion to **F** at 43% RH, 3 days. At 75% RH **E** converted to **F** after 1 day. Cocrystal **E** at 98% RH converted by 1 day to **F** with some evidence of minor dissociation to caffeine hydrate. At one week, the 98% RH sample was predominantly caffeine hydrate by PXRD, and by 7 weeks the material had deliquesced. The stability of this material following polymorph conversion to **F** agreed with the RH stability observations of **F**, below.

(g) Cocrystal F. Of the two 1:1 caffeine/glutaric acid polymorphs that were analyzed, **F** was found to be more stable with regard to humidity. Cocrystal **F** remained unchanged at 75% RH and below for 7 weeks. At 98% RH, it showed a minor caffeine hydrate component at 1 day. This conversion was nearly complete by 1 week, and the material had deliquesced by 7 weeks.

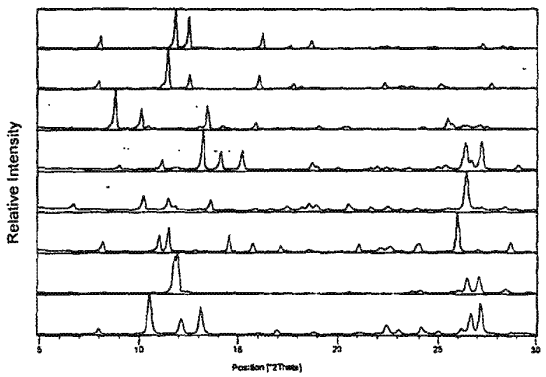


Figure 7. PXRD patterns of caffeine cocrystals, from top to bottom: simulated pattern of **A**; simulated pattern of **B**; experimental pattern of **C**; simulated pattern of **D**; simulated pattern of **E**; simulated pattern of **F**; experimental pattern of anhydrous caffeine; simulated pattern of caffeine hydrate.

In considering the RH stability of the caffeine cocrystals, it is clear that **A** was most stable, while **E** was least stable. Intermediate in stability were **C** and **D**, which had dissociated at 98% RH by 1 day, and **B** and **F**, which persisted at 98% RH for 7 and 3 days, respectively. An ordering of the stability of these intermediate cocrystals was not performed because the kinetic differences in stability at 98% RH may have been influenced by minor phase impurity or by variation in sample particle size, neither of which was rigorously controlled in this study. The overall cocrystal RH stability trend may thus be summarized as **A** > **B** ≈ **C** ≈ **D** ≈ **F** > **E**. It is noted that the strongest acid employed, oxalic acid, produced the most stable caffeine cocrystal (**A**), while the weakest acid of the group, glutaric acid, produced the least stable cocrystal (**E**). However, from the fact that cocrystal **F**, a polymorph of **E**, demonstrated intermediate stability, it is clear that acid pK_a is not the only factor dictating cocrystal stability.

In the current study, it has been possible to design a series of caffeine cocrystals, which could then be evaluated for their RH stability. A remarkable variation in RH stability was observed across the series. It was found in this study that no cocrystal hydrates were produced by exposure of the caffeine cocrystals to high humidity. This lack of cocrystal hydrate formation could potentially be characteristic of cocrystals in general. One driving force for the formation of cocrystals is presumably the introduction of additional stabilization by hydrogen bonding, which may mean that fewer unsatisfied hydrogen bond donors or acceptors exist in cocrystals. As such, cocrystals may exhibit a reduced tendency for hydration. In the case of caffeine, the introduction of a carboxylic acid as a hydrogen bond donor for the basic imidazole nitrogen seems to prevent the incorporation of lattice water into the cocrystal.

UM00012405
NOVARTIS EXHIBIT 1017
Novartis v. Regents, IPR2023-01346
Page 1151 of 4460

Conclusion

A series of cocrystals of the model pharmaceutical compound caffeine with dicarboxylic acids has been described. Cocrystals were formed in 2:1 and 1:1 caffeine/acid stoichiometries by the methods of solution precipitation and solid-state grinding. In some cases, solid-state grinding with the addition of a minor quantity of solvent afforded bulk cocrystal material that could not be produced by precipitation from solution.

The RH stability profile of these cocrystals differed from pure crystalline caffeine, in that no cocrystal hydrates have been found; rather, the cocrystals that were unstable with respect to RH generally exhibited dissociation into crystalline starting components. One humidity-induced cocrystal polymorphic transition was also observed. One cocrystal was stable at all relative humidities and for all time points, and thereby clearly demonstrated superior stability to anhydrous caffeine. Several other cocrystals demonstrated approximate stability to that of caffeine, whereby they were unstable at high RH but stable at lower RH.

The goal of pharmaceutical cocrystallization is to engineer pharmaceutical cocrystals with specific improved properties. While strategies for the design of pharmaceutical cocrystals appear to be growing increasingly rational and successful, the subject of property control has been largely latent. At least in the context of pharmaceuticals, crystal structure engineering is evidenced, while crystal property engineering has yet to fully emerge. It was the aim of this study to design a series of pharmaceutical cocrystals and measure the resultant change of a targeted physical property. Present work is focused on understanding the observed trend of RH stability of this series, with an aim toward predicting such properties in the future.

Acknowledgment. The authors wish to thank Dr. J. E. Davies for single crystal XRD data collection and structure solution, and Dr. N. Feeder, Dr. P. Marshall, Dr. A. Gillon, and Dr. M. Ticehurst for helpful discussions. Funding acknowledgments are due to the Pfizer Institute for Pharmaceutical Materials Science. A.V.T. additionally thanks the Sidney Sussex North American Foundation for financial support.

Supporting Information Available: X-ray crystallographic information files (CIF) are available for cocrystals **A**, **B**, **C**, **E** and **F**. The list of refcodes resulting from the CSD search for the Scheme 1 synthon is available in Excel file format. This material is available free of charge via the Internet at http://pubs.acs.org.

References

(1) Desiraju, G. R. *Crystal Engineering: The Design of Organic Solids*; Elsevier: Amsterdam, 1989; Vol. 54.
(2) Jones, W. In *Organic Molecular Solids: Properties and Applications*; Jones, W., Ed.; CRC Press: New York, 1997; pp 149–199.
(3) Bond, A. D.; Jones, W. In *Supramolecular Organisation and Materials Design*; Jones, W., Rao, C. N. R., Eds.; Cambridge University Press: Cambridge, 2002, p 391.
(4) Lehn, J. M. *Supramolecular Chemistry: Concepts and Perspectives*; VCH: Weinheim, Germany, 1995.
(5) Caira, M. R.; Nassimbeni, L. R.; Wildervanck, A. F. *J. Chem. Soc.-Perkin Trans. 2* **1995**, 2213–2216.
(6) Oswald, I. D. H.; Allan, D. R.; McGregor, P. A.; Motherwell, W. D. S.; Parsons, S.; Pulham, C. R. *Acta Crystallogr.* **2002**, *B58*, 1057–1066.
(7) Bailey Walsh, R. D.; Bradner, M. W.; Fleischman, S.; Morales, L. A.; Moulton, B.; Rodríguez-Hornedo, N.; Zaworotko, M. J. *Chem. Commun.* **2003**, 186–187.
(8) Fleischman, S. G.; Kuduva, S. S.; McMahon, J. A.; Moulton, B.; Walsh, R. D. B.; Rodríguez-Hornedo, N.; Zaworotko, M. J. *Cryst. Growth Des.* **2003**, *3*, 909–919.
(9) Remenar, J. F.; Morissette, S. L.; Peterson, M. L.; Moulton, B.; MacPhee, J. M.; Guzman, H. R.; Almarsson, Ö. *J Am. Chem. Soc.* **2003**, *125*, 8456–8457.
(10) Bettinetti, G.; Caira, M. R.; Callegari, A.; Merli, M.; Sorrenti, M.; Tadini, C. *J. Pharm. Sci.* **2000**, *89*, 478–489.
(11) Khankari, R. K.; Grant, D. J. W. *Thermochim. Acta* **1995**, *248*, 61–79.
(12) Byrn, S. R.; Pfeiffer, R. R.; Stowell, J. G. *Solid-State Chemistry of Drugs*; 2nd ed.; SSCI, Inc.: West Lafayette, Indiana, 1999.
(13) Ticehurst, M. D.; Storey, R. A.; Watt, C. *Int. J. Pharm.* **2002**, *247*, 1–10.
(14) Griesser, U. J.; Burger, A. *Int. J. Pharm.* **1995**, *120*, 83–93.
(15) Bothe, H.; Cammenga, H. K. *Thermochim. Acta* **1980**, *40*, 29–39.
(16) Lehto, V.-P.; Laine, E. *Thermochim. Acta* **1998**, *317*, 47–58.
(17) Cambridge Structural Database, version 5.25, November 2003.
(18) Allen, F. H. *Acta Crystallogr.* **2002**, *B58*, 380–388.
(19) Edwards, H. G. M.; Lawson, E.; de Matas, M.; Shields, L.; York, P. *J. Chem. Soc., Perkin Trans. 2* **1997**, 1985–1990.
(20) Pirttimäki, J.; Laine, E. *Eur. J. Pharm. Sci.* **1994**, *1*, 203–208.
(21) de Matas, M.; Edwards, H. G. M.; Lawson, E. E.; Shields, L.; York, P. *J. Mol. Struct.* **1998**, *440*, 97–104.
(22) Byrn, S. R.; Lin, C.-T. *J. Am. Chem. Soc.* **1976**, *98*, 4004–4005.
(23) Mercer, A.; Trotter, J. *Acta Crystallogr.* **1978**, *B34*, 450–453.
(24) Stahl, P. H.; Wermuth, C. G. In *Handbook of Pharmaceutical Salts*; Stahl, P. H., Wermuth, C. G., Eds.; Verlay Helvetica Chimica Acta & Wiley-VCH: Zurich, 2002; pp 265–327.
(25) *The Merck Index*; 13th ed.; Merck & Co.: Whitehouse Station, NJ, 2001.
(26) Johnson, S. L.; Rumon, K. A. *J. Phys. Chem.* **1965**, *69*, 74–86.
(27) Leger, J. M.; Alberola, S.; Carpy, A. *Acta Crystallogr.* **1977**, *B33*, 1455–1459.
(28) Ghosh, M.; Basak, A. K.; Mazumdar, S. K.; Sheldrick, B. *Acta Crystallogr.* **1991**, *C47*, 577–580.
(29) Craven, B. M.; Gartland, G. L. *Acta Crystallogr.* **1974**, *B30*, 1191–1195.
(30) Desiraju, G. R.; Steiner, T. *The Weak Hydrogen Bond: Applications to Structural Chemistry and Biology*; Clarendon Press: New York, 1999; Vol. 9.
(31) O···H and N···H contact distances are defined as less than the sum of the van der Waals radii O 1.52, N 1.55, and H 1.20 Angstroms; C–N bond type defined as "any". A list of the refcodes obtained from the CSD search is provided as Supporting Information.
(32) Trask, A. V.; Motherwell, W. D. S.; Jones, W. *Chem. Commun.* **2004**, 890–891.
(33) Toda, F.; Tanaka, K.; Sekikawa, A. *J. Chem. Soc.-Chem. Commun.* **1987**, 279–280.
(34) Etter, M. C.; Frankenbach, G. M. *Chem. Mater.* **1989**, *1*, 10–12.
(35) Pedireddi, V. R.; Jones, W.; Chorlton, A. P.; Docherty, R. *Chem. Commun.* **1996**, 987–988.
(36) Trask, A. V.; Jones, W. In *Organic Solid State Reactions*; Toda, F., Ed.; Springer Press: Berlin, 2005.
(37) Hofmann, D. W. M. *Acta Crystallogr.* **2002**, *B57*, 489–493.
(38) Greenspan, L. *J. Res. Natl. Bur. Stand.* **1977**, *81A*, 89–96.
(39) PXRD patterns simulated using the software X'Pert Plus, version 1.0, Philips Analytical B. V., 1999.
(40) Blessing, R. H. *Acta Crystallogr.* **1995**, *A51*, 33–38
(41) O–H bond distances for the carboxylic acid that bonds to the caffeine in each cocrystal structure are as follows, in angstroms: A – 0.97(2); B – 1.04(3); D – 1.06(2); E – 0.99(2); F – 0.92(3).

UM00012406
NOVARTIS EXHIBIT 1017
Novartis v. Regents, IPR2023-01346
Page 1152 of 4460

(42) James, M. N. G.; Williams, G. J. B. *Acta Crystallogr.* **1974**, *B30*, 1249–1257.
(43) Trask, A. V.; Motherwell, W. D. S.; Jones, W., manuscript in preparation.
(44) Bernstein, J.; Hagler, A. T. *J. Am. Chem. Soc.* **1978**, *100*, 673–681.
(45) Beckmann, W.; Winter, G. In *14th International Symposium on Industrial Crystallization*; Institution of Chemical Engineers: Cambridge, UK, 1999.
(46) Giron, D.; Grant, D. J. W. In *Handbook of Pharmaceutical Salts: Properties, Selection and Use*; Stahl, P. H., Wermuth, C. G., Eds.; Verlag Helvetica Chimica Acta: Zurich, 2002; pp 58–62

CG0496540

UM00012407
NOVARTIS EXHIBIT 1017
Novartis v. Regents, IPR2023-01346
Page 1153 of 4460

This Page is Inserted by IFW Indexing and Scanning Operations and is not part of the Official Record

BEST AVAILABLE IMAGES

Defective images within this document are accurate representations of the original documents submitted by the applicant.

Defects in the images include but are not limited to the items checked:

- ☐ BLACK BORDERS
- ☐ IMAGE CUT OFF AT TOP, BOTTOM OR SIDES
- ☐ FADED TEXT OR DRAWING
- ☐ BLURRED OR ILLEGIBLE TEXT OR DRAWING
- ☐ SKEWED/SLANTED IMAGES
- ☐ COLOR OR BLACK AND WHITE PHOTOGRAPHS
- ☐ GRAY SCALE DOCUMENTS
- ☐ LINES OR MARKS ON ORIGINAL DOCUMENT
- ☐ REFERENCE(S) OR EXHIBIT(S) SUBMITTED ARE POOR QUALITY
- ☐ OTHER: _____

IMAGES ARE BEST AVAILABLE COPY.

As rescanning these documents will not correct the image problems checked, please do not report these problems to the IFW Image Problem Mailbox.

COMMUNICATION

ChemComm www.rsc.org/chemcomm

Solvent-drop grinding: green polymorph control of cocrystallisation†

Andrew V. Trask,[a] W. D. Samuel Motherwell[b] and William Jones*[a]

[a] *Pfizer Institute for Pharmaceutical Materials Science, Department of Chemistry, University of Cambridge, Lensfield Road, Cambridge, UK CB2 1EW. E-mail: wj10@cam.ac.uk; Fax: 44 1223 336362; Tel: 44 1223 334468*

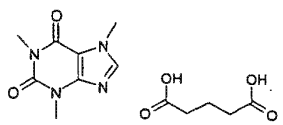
[b] *Cambridge Crystallographic Data Centre, 12 Union Road, Cambridge, UK CB2 1EZ*

Received (in Cambridge, UK) 21st January 2004, Accepted 20th February 2004
First published as an Advance Article on the web 5th March 2004

By grinding with a minimal addition of a solvent of appropriate polarity, control over the polymorphic outcome of a novel cocrystallisation involving the model pharmaceutical compound caffeine may be achieved.

The technique of cocrystallisation continues to gain significance for its application to the design of new supramolecular structures with desired functional properties.[1–3] Most recently, in the field of pharmaceuticals, cocrystallisation has been shown to be an effective means of altering a drug's physical properties, such as solubility and melting point.[4,5] However, one notable obstacle in the path of rational cocrystal design is the phenomenon of polymorphism. Different crystal forms of a given chemical entity will possess different physical properties;[6] thus, in the field of crystal engineering, polymorph control amounts to the control of physical properties. Polymorphic cocrystals are not uncommon, and at least 20 systems have been reported to date.[7] Herein we demonstrate a novel, eco-friendly means of controlling the outcome of a previously unreported polymorphic cocrystallisation of the model pharmaceutical compound **caffeine**.

The system under study specifically consists of two polymorphs of an unionised molecular cocrystal containing **caffeine** and glutaric acid (**GA**). Slow evaporation at ambient temperature of a chloroform solution containing both **caffeine** and **GA** produced crystals of two morphologies: rods and blocks.[8] Single crystal X-ray diffraction analysis identified the rods as monoclinic (form I) and the blocks as triclinic (form II).‡ Both polymorphs possess 1 : 1 **caffeine** : **GA** stoichiometry and exhibit identical secondary architecture, such that a two-dimensional sheet results from an array of hydrogen bond-containing ribbons. A conformational difference between the two crystal forms exists in the torsion of the methylene carbons of **GA** (Fig. 1).[9]



Caffeine **GA**

Given the calculated densities of 1.486 and 1.482 Mg m^{-3} for forms I and II, respectively, it may be assumed that the energies of these two polymorphic cocrystals are quite similar based upon the density rule.[10] That they precipitated concomitantly from solution is another indication of their comparable energies. Control of this polymorphic system was desired so that pure samples of each form could be obtained for subsequent study of physical properties.

Precipitation from solution is the most common route to obtaining cocrystals. An alternative approach is that of solid-state grinding, in which two solids are ground together with a mortar and pestle or in a mixer mill to induce cocrystal formation. In addition to its 'green' nature, in that it avoids excessive use of crystallisation solvent, solid-state grinding also offers a means of obtaining nearly quantitative yields with a common particle size. The technique of cocrystal formation by solid-state grinding has been established for some time.[11,12] A significant enhancement to solid-state grinding was recently illustrated, whereby the cocrystallisation kinetics may be considerably enhanced by the addition of a few drops of solvent.[13] We now observe that this 'solvent-drop grinding' methodology can provide a successful means of controlling the polymorphic outcome of a cocrystallisation.

Equimolar quantities of anhydrous **caffeine** and **GA** were combined in a stainless steel grinding jar with two grinding balls, and the material was ground together either with or without the addition of a few drops of solvent.[14] The resulting material was then characterized by PXRD,[15] having allowed any small amount of solvent present to evaporate. When **caffeine** and **GA** are ground together in the absence of solvent, cocrystal form I predominantly results. Similarly, the addition of four drops from a pipette of a non-polar solvent, such as n-hexane, cyclohexane, or heptane also produces form I. Conversely, upon addition of four drops of a more polar solvent, including chloroform, dichloromethane, acetonitrile, and water, the grinding experiment results in predominantly form II.[16]

Fig. 2 shows the powder XRD patterns calculated for both polymorphs[17] in addition to powder XRD results from solvent-drop grinding with cyclohexane and chloroform. It is apparent that the experiment involving cyclohexane produced predominantly form I, while the solvent-drop grinding with chloroform produced form II. A small peak at 11.9° 2θ corresponds to the most intense peak of the anhydrous **caffeine** starting material, indicating that the cocrystallisation with cyclohexane has not proceeded entirely to completion within the 60 min grinding time.

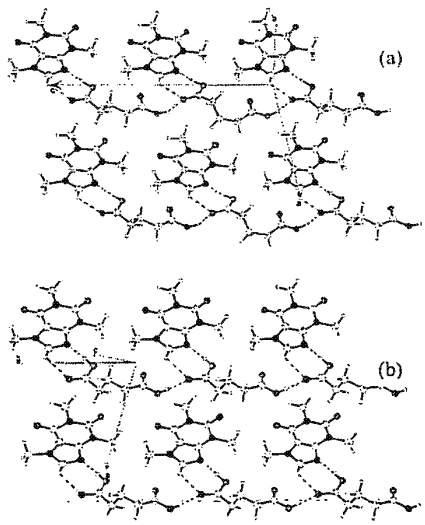


Fig. 1 Crystal packing diagrams of (a) **caffeine–GA** form I and (b) **caffeine–GA** form II, each showing a planar sheet composed of two hydrogen-bonded ribbons.

† Electronic supplementary information (ESI) available: additional powder XRD patterns. See http://www.rsc.org/suppdata/cc/b4/b400978a/

DOI: 10.1039/b400978a

This journal is © The Royal Society of Chemistry 2004

UM00012409
NOVARTIS EXHIBIT 1017
Novartis v. Regents, IPR2023-01346
Page 1155 of 4460

A detailed look at crystal packing reveals a difference which may be important in rationalising the observation that solvent polarity together with solid-state grinding offers a means of controlling polymorphism. While the two cocrystals possess a common secondary level of architecture, their tertiary level of architecture differs (Fig. 3). Orienting form I along the *c* axis provides a perspective down the length of the hydrogen-bonded ribbons. It can be seen that the sheets of form I stack along the *b* axis; one ribbon exactly overlays the next. This leads to what may be interpreted in form I as a non-polar cleavage plane (200) between the stacks of ribbons along the *b* axis. With only methyl and methylene groups exposed, it is possible that non-polar solvents would preferentially stabilise this exposed plane upon grinding-induced cleavage. In contrast, viewing form II from an analogous perspective reveals that sheets stack in a staggered fashion, so that the non-polar cleavage plane is not observed.

We have demonstrated that solvent-drop grinding represents a novel means of obtaining a particular cocrystal polymorph in a green chemistry fashion. Ongoing investigations include further rationalising this observation and exploring the possibility that this technique may have more general applications to other polymorphic systems, including single component systems.

The authors gratefully acknowledge funding from the Pfizer Institute for Pharmaceutical Materials Science. Thanks are due to Dr J. E. D. Davies for crystal data collection and structure solution, and to Dr Neil Feeder and Dr Pete Marshall for helpful discussions.

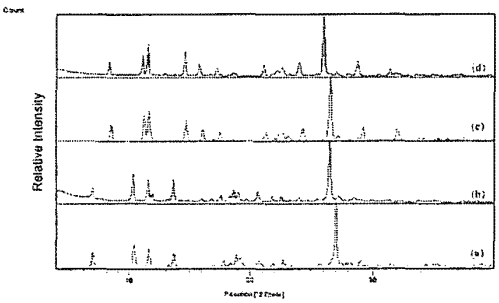


Fig. 2 Powder X-ray diffraction pattern of (a) simulated pattern from single-crystal structure of form I, (b) result of solvent-drop grinding of **caffeine** and **GA** with cyclohexane, (c) simulated pattern from single-crystal structure of form II, (d) result of solvent-drop grinding of **caffeine** and **GA** with chloroform (see ref. 15).

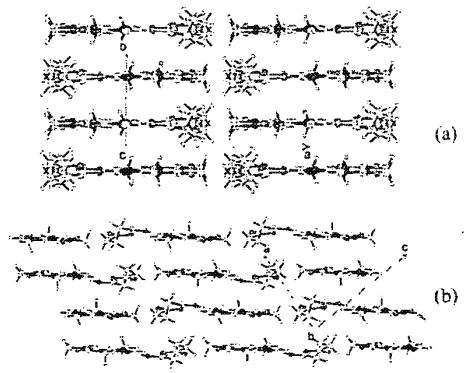


Fig. 3 Crystal packing diagrams of (a) **caffeine–GA** form I and (b) **caffeine–GA** form II, oriented perpendicular to the ribbon long axis, so as to reveal potential vertical cleavage planes.

Notes and references

‡ *Crystal data* for **caffeine–GA** form I: $C_{13}H_{18}N_4O_6$, M = 326.31, monoclinic, space group $P2_1/c$; a = 13.1029(5), b = 6.6017(2), c = 17.1427(8) Å, β = 97.8360(10)°, U = 1458.93(10) Å^3, T = 180(2) K, Z = 4, μ(Mo-Kα) = 0.119 mm^{-1}, D_c = 1.486 Mg m^{-3}, λ = 0.71073 Å, F(000) = 688, $2\theta_{max}$ = 27.52°. 8983 reflections measured, 3343 unique (R_{int} = 0.0418). Final residuals for 217 parameters were R_1 = 0.0645, wR_2 = 0.1870 for $I > 2\sigma(I)$, and R_1 = 0.1061, wR_2 = 0.2271 for all 3343 data. *Crystal data* for **caffeine–GA** form II: $C_{13}H_{18}N_4O_6$, M = 326.31, triclinic, space group $P\bar{1}$; a = 8.3212(8), b = 8.6667(8), c = 11.3636(12) Å, α = 68.955(4), β = 78.559(4), γ = 74.236(4)°, U = 731.43(12) Å^3, T = 180(2) K, Z = 2, μ(Mo-Kα) = 0.119 mm^{-1}, D_c = 1.482 Mg m^{-3}, λ = 0.71073 Å, F(000) = 344, $2\theta_{max}$ = 27.47°. 5689 reflections measured, 3094 unique (R_{int} = 0.0442). Final residuals for 217 parameters were R_1 = 0.0572, wR_2 = 0.1569 for $I > 2\sigma(I)$, and R_1 = 0.0815, wR_2 = 0.1771 for all 3094 data. In both crystal structures the carboxylic acid protons were located crystallographically and their positions were refined, confirming that proton transfer had not occurred. CCDC 229592 and 229593. See http://www.rsc.org/suppdata/cc/b4/b400978a/ for crystallographic files in CIF or other electronic format.

1 W. Jones, in *Organic Molecular Solids: Properties and Applications*, ed. W. Jones, CRC Press, New York, 1997, p. 177.
2 A. D. Bond and W. Jones, in *Supramolecular Organisation and Materials Design*, ed. W. Jones and C. N. R. Rao, Cambridge University Press, Cambridge, 2002, p. 391.
3 J. L. Atwood, J. E. D. Davies, D. D. MacNicol and F. Vogtle, *Comprehensive Supramolecular Chemistry*, Pergamon, Oxford, 1996, vol. 9.
4 J. F. Remenar, S. L. Morissette, M. L. Peterson, B. Moulton, J. M. MacPhee, H. R. Guzmán and Ö. Almarsson, *J. Am. Chem. Soc.*, 2003, **125**, 8456.
5 R. D. Bailey Walsh, M. W. Bradner, S. Fleischman, L. A. Morales, B. Moulton, N. Rodriguez-Hornedo and M. J. Zaworotko, *Chem. Commun.*, 2003, 186.
6 S. R. Byrn, R. R. Pfeiffer and J. G. Stowell, *Solid-State Chemistry of Drugs*, 2nd edn., SSCI, Inc., West Lafayette, Indiana, 1999, p. 143.
7 Cambridge Structural Database version 5.24 (November 2002). Conquest cocrystal search terms: ≥2 residues; text search 'polymorph'; must not have charged species or water; exclude text 'solvate' and 'clathrate'; search all organics with R < 0.1 and 3D coordinates determined. For further information concerning the CSD see F. H. Allen, *Acta Crystallogr., Sect. B*, 2002, **58**, 380.
8 The single crystals described here were obtained from a solution containing the components in an approximate ratio of 1.3 : 1 **caffeine** : **GA**.
9 J. Bernstein and A. T. Hagler, *J. Am. Chem. Soc.*, 1978, **100**, 673.
10 A. Burger and R. Ramberger, *Mikrochim. Acta*, 1979, **2**, 259.
11 M. C. Etter and G. M. Frankenbach, *Chem. Mater.*, 1989, **1**, 10.
12 V. R. Pedireddi, W. Jones, A. P. Chorlton and R. Docherty, *Chem. Commun.*, 1996, 987.
13 N. Shan, F. Toda and W. Jones, *Chem. Commun.*, 2002, 2372.
14 Experiments consisted of *ca.* 750 mg total material, ground for one hour at 30 revolutions per second with a Retsch Mixer Mill. Ratio of moles of added organic solvent per mole of total cocrystal material varied between 0.2 and 0.6, so that the solvent only slightly moistened the crystalline powder. This contrasts with conventional solution cocrystallisations, where the mole ratio of solvent to solid is commonly in the hundreds.
15 Powder XRD data were collected with a Philips X'Pert diffractometer with Cu Kα radiation and an X'Celerator detector.
16 In preliminary solution cocrystallisation work, equimolar solutions of the two components in chloroform and in dichloromethane produced crystalline powder of mixed polymorph content. Conversely, a solution cocrystallisation from acetonitrile provided predominantly form II, while cocrystallisation from water produced crystalline caffeine hydrate. Solution cocrystallisation from non-polar solvents was not possible due to poor solubility.
17 Calculated powder XRD patterns were generated from single crystal XRD data using X'Pert Plus, Philips Analytical B.V. The calculated PXRD patterns exhibit a peak shift which is particularly noticeable toward high 2θ values. A form II crystal was recollected near ambient temperature to confirm that this shift results only from crystal lattice contraction at the low temperature used for the single crystal data collection.

UM00012410
NOVARTIS EXHIBIT 1017
Novartis v. Regents, IPR2023-01346
Page 1156 of 4460

This journal is © The Royal Society of Chemistry 2004

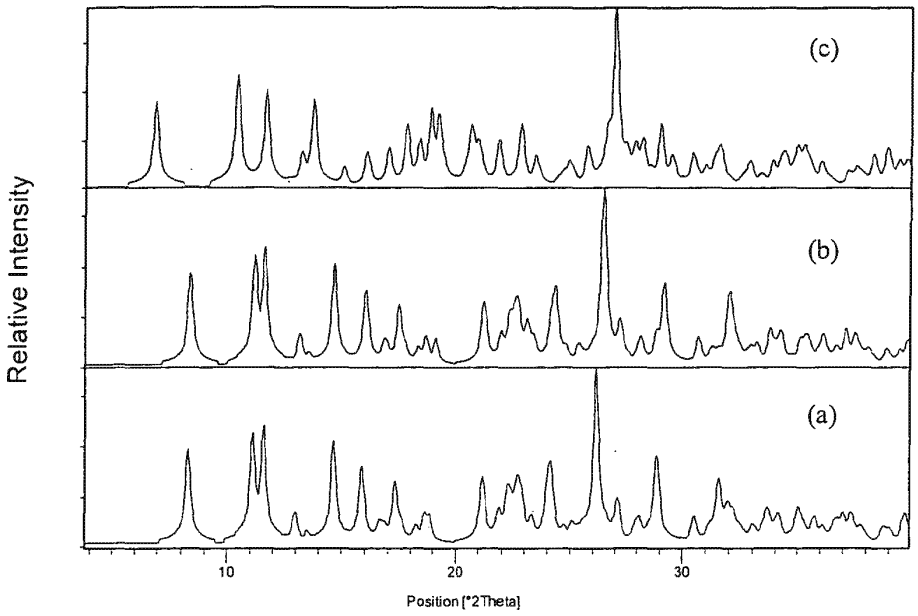


Fig. ESI 1 Simulated powder X-Ray diffraction patterns from single-crystal structures of (a) form II collected at 280K, (b) form II collected at 180K, (c) form I collected at 180K.

This journal is © The Royal Society of Chemistry 2004

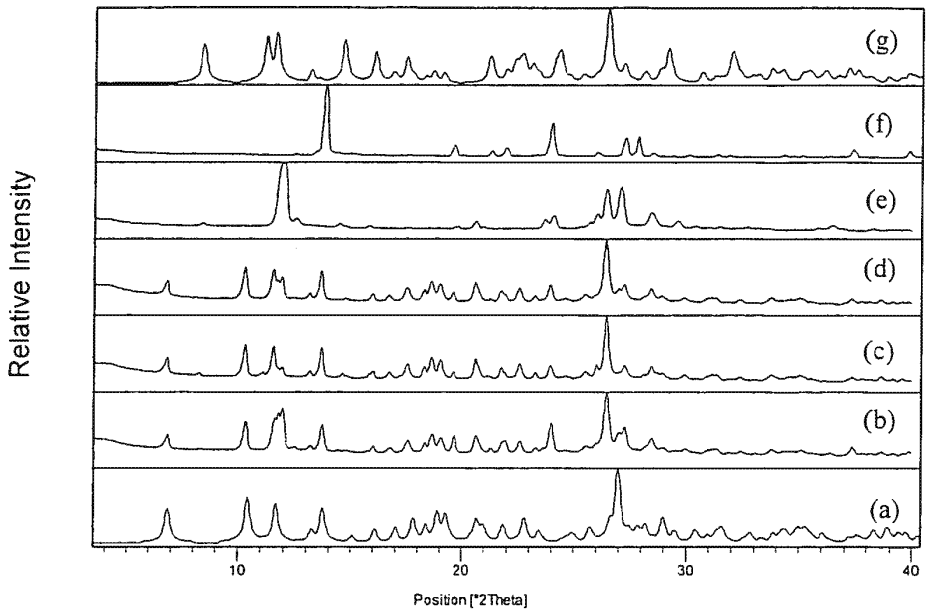


Fig. ESI 2 Powder X-Ray diffraction patterns of (a) form I simulated from single-crystal data collected at 180K, (b) results of dry grinding of 1:1 **caffeine**:**GA** for 60 min, (c) results of hexane solvent-drop grinding of 1:1 **caffeine**:**GA** for 60 min, (d) results of heptane solvent-drop grinding of 1:1 **caffeine**:**GA** for 60 min, (e) **caffeine** starting material, (f) **GA** starting material, (g) form II simulated from single-crystal data collected at 180K.

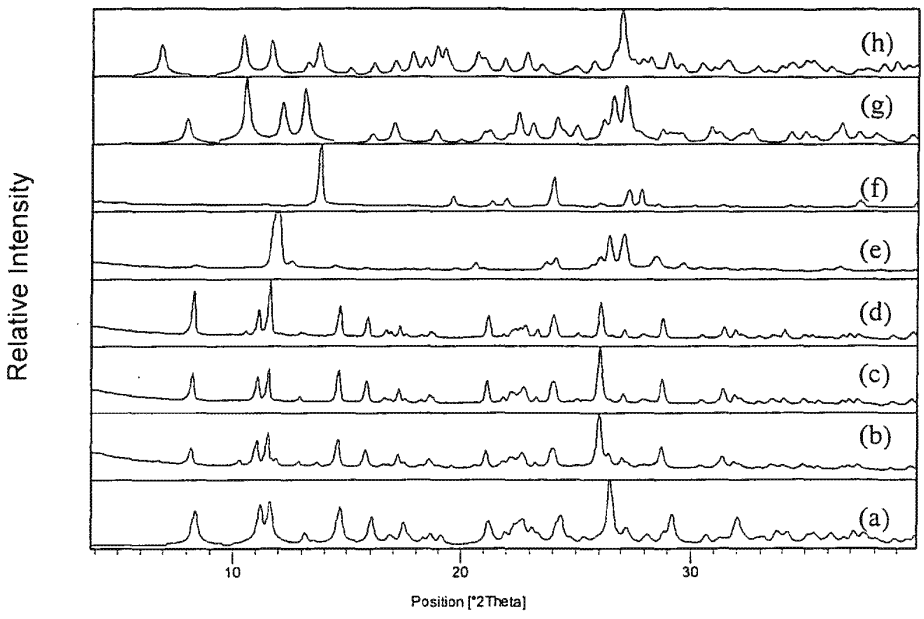


Fig. ESI 3 Powder X-Ray diffraction patterns of (a) form II simulated from single-crystal data collected at 180K, (b) results of dichloromethane solvent-drop grinding of 1:1 **caffeine**:**GA** for 60 min, (c) results of acetonitrile solvent-drop grinding of 1:1 **caffeine**:**GA** for 60 min, (d) results of water solvent-drop grinding of 1:1 **caffeine**:**GA** for 60 min, (e) **caffeine** starting material, (f) **GA** starting material, (g) caffeine hydrate simulated from single-crystal data deposited in the Cambridge Structural Database (reference code CAFINE01; see reference 7) (h) form I simulated from single-crystal data collected at 180K.

COMPOSITES FOR NONLINEAR OPTICS: CRYSTAL GROWTH AND POLYMORPHISM.

L. Trowbridge, C.B. Aakeröy, G.S. Bahra, P.A. Chaloner*, and K.R. Seddon

*School of Chemistry and Molecular Sciences, University of Sussex, Falmer, Brighton, UK

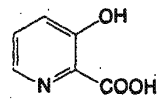
INTRODUCTION

The production of composite materials for applications in optoelectronic devices is now a well established technique. The combination of a crystalline guest with a transparent polymer, with desirable mechanical properties, offers numerous advantages over the use of single crystals.

Nonlinear optical effects are highly structure dependent. For a material to exhibit second harmonic generation (SHG) it must have an acentric crystal structure. Polymorphism can be defined as the ability of a substance to crystallise into more than one structure. The factors which effect the formation of polymorph over another are primarily temperature, pressure and the chemistry of its environment. Hall *et al* [1] noted that different polymorphs of N-(2-acetamido-4-nitrophenyl)pyrrolidine could be obtained by changing the speed of crystallization where as different polymorphs of 2-(4-methoxyphenyl)-5-(4-nitrophenyl)pyrazolidin-5-ene occurred on changing solvent.

The work of Miyata *et al* [2] on composites of 4-nitroaniline (4-NA) with poly(oxyethylene) and poly(ε-caprolactone) demonstrated that it was possible to produce a new polymorph of 4-NA by inducing crystal growth within a polymer matrix.

The powder SHG activity of 3-hydroxy-2-pyridinecarboxylic acid (1, 3hpca) has been recently measured and shown to be on a level comparable to urea [3]. Its high melting point, 220 °C, and propensity to form rectangular crystals make it a useful candidate for incorporation into composite films. Thus guest/host composites of **1** and a variety of water soluble polymers have been synthesised using the temperature gradient solution technique (TGST) [4]. However, 3hpca was found to exhibit polymorphism. One acentric polymorph (**1A**) is obtained cleanly from an aqueous solution of **1** in the presence of 30 wt% of poly(acrylamide). The other polymorph is centric (**1B**) and is obtained by recrystallization from methanol [3]. Therefore, a method of assessing the structural purity of the composite films was required.



(1)

RESULTS and DISCUSSION

Structural assessment of the composites was achieved by comparing the experimental x-ray powder diffraction pattern with the theoretical simulated patterns, calculated from the single crystal data of the two polymorphs. X-ray powder diffraction (XPD) was used to identify the structure of **1** after each stage of every experiment.

Quantitative analysis by x-ray powder diffraction is based on the fact that the intensity of the diffraction pattern of a particular phase in a mixture is dependant on the concentration of that phase in the mixture [5].

Recrystallization of **1** from an aqueous solution resulted in a mixture of the two polymorphs 70% of which was **1A**, as determined by XPD, *Figure 1*.

The incorporation of **1** into an aligned composite film with the host poly(acrylamide), (PAA), resulted in the recrystallization of the guest exclusively into the **1B** polymorph, *Figure 2*.

The result was the same for seven out of eight of the films prepared in which the poly(acrylamide) was replaced by different hosts. Only when the host was poly(vinylpyrrolidone), Mw. 44 000, was a mixture obtained in which the dominant form was still **1B**, however, approximately 30% of the total was in the active form. Unfortunately the degree of alignment was not very high.

EXPERIMENTAL

1 was recrystallized from aqueous solution and the resultant crystals were filtered, dried and ground to a uniform powder prior to analysis by XPD.

Aligned composite films were prepared using the TGST at 70 °C from a solution of 70 wt% of **1** and 30 wt% of poly(acrylamide), Mw 4-5 000 000. Additional films were prepared with solutions in which the PAA was replaced by poly(vinylpyrrolidone) and poly(ethylene oxide), in a range of molecular weights from 44 000 to 5 000 000, all other factors were held constant. A special sample holder was manufactured to facilitate the XPD of the composites on the glass substrates.

SUMMARY

X-ray powder diffraction has been used to assess the structural purity of composites produced by the TGST method. This methodology is not limited to composites produced by this technique alone but it is a valid method of assessing structural composition in all types of composites as long as single crystal data is available.

ACKNOWLEDGEMENTS

We gratefully acknowledge the financial support of the DRA (Fort Halstead).

REFERENCES

1. S.R. Hall *et al., J. Cryst. Growth*, 1986, 79, 745-751.
2. T. Watanabe, K. Yoshinaga, D. Fichou, & S. Miyata, *J. Chem. Soc., Chem. Commun.*, 1988, 250-251; *Jap. J. Appl. Phys.*, 1988, 27, 9, L1724-1725.
3. P.A. Chaloner, P. Hitchcock, K.R. Seddon, & L. Trowbridge, unpublished results.
4. C.B. Aakeröy, N. Azoz, M. Kadim, K.R. Seddon, & L. Trowbridge, *Adv. Mater.* 1993, Vol. 5, No. 5, 364-367.
5. B.D. Cullity, *Elements of X-ray Diffraction*, chapter 14, Addison Wesley, 1978.

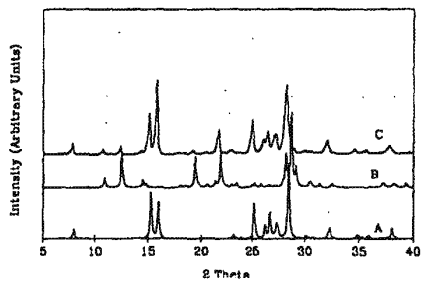


Figure 1: X-ray powder diffraction patterns of A) acentric 3hpca, B) centric 3hpca, C) 3hpca recryst. from water.

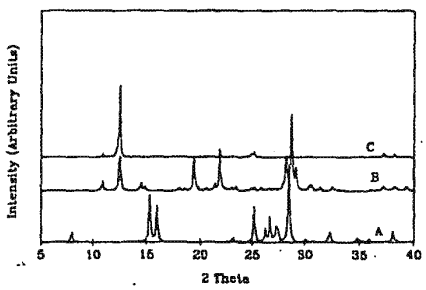


Figure 2: X-ray powder diffraction patterns of A) acentric 3hpca, B) centric 3hpca, C) Film of 3hpca with PAA.

UM00012414
NOVARTIS EXHIBIT 1017
Novartis v. Regents, IPR2023-01346
Page 1160 of 4460

Acta Cryst. (1980). B36, 2794–2796

Structure of 5,5-Diphenylhydantoin–1-(4-Bromophenyl)-4-dimethylamino-2,3-dimethyl-3-pyrazolin-5-one (1:1)

BY TOYOZO UNO AND NOBUYUKI SHIMIZU*

Faculty of Pharmaceutical Sciences, Kyoto University, Kyoto 606, Japan

(*Received* 26 *March* 1980; *accepted* 18 *June* 1980)

Abstract. $C_{15}H_{12}N_2O_2.C_{13}H_{16}BrN_3O$, M_r = 562·5, triclinic, $P\bar{1}$, a = 12·997 (8), b = 9·902 (5), c = 12·796 (9) Å, α = 113·21 (9), β = 118·18 (7), γ = 83·37 (19)°, U = 1329·0 Å^3, D_x = 1·405, D_m (n-heptane/CCl_4) = 1·408 Mg m^{-3}, Z = 2, μ = 1·74 mm^{-1}, $F(000)$ = 580, Mo $K\alpha$ radiation, λ = 0·71069 Å. The final R index was 0·033 for 2485 reflections. In the crystal, molecules of the title compound are held together by hydrogen bonds (NH···O) and weak charge-transfer interactions (O—Br), in the a-axis direction.

* Present address: Pharmaceutical Institute, School of Medicine, Keio University, Shinjuku-ku, Tokyo 160, Japan.

Introduction. 5,5-Diphenylhydantoin (DPH) is used as an antiepileptic drug. This analysis was undertaken to obtain information concerning the interactions between DPH and 1-(4-bromophenyl)-4-dimethylamino-2,3-dimethyl-3-pyrazolin-5-one (BDDP). Single crystals (colorless plates) of the title compound were obtained by slow evaporation of an equimolar mixture of DPH and BDDP dissolved in acetone. Lattice parameters

Table 1. *Positional parameters and isotropic thermal parameters with e.s.d.'s in parentheses*

	x	y	z	B_{iso}(Å^2)
DPH				
C(1)	0·4999 (4)	0·7976 (4)	0·7086 (4)	3·50
O(1)	0·5843 (2)	0·8431 (3)	0·8132 (3)	4·97
N(1)	0·4893 (3)	0·6721 (3)	0·6063 (3)	3·30
C(2)	0·3848 (3)	0·6572 (4)	0·4954 (4)	3·10
O(2)	0·3577 (2)	0·5567 (3)	0·3903 (2)	3·40
N(2)	0·3244 (2)	0·7709 (3)	0·5265 (2)	3·14
C(3)	0·3830 (3)	0·8684 (4)	0·6629 (3)	2·95
C(4)	0·3149 (3)	0·8610 (4)	0·7315 (3)	3·31
C(5)	0·1945 (4)	0·8625 (4)	0·6728 (3)	3·59
C(6)	0·1319 (3)	0·8695 (4)	0·7378 (4)	4·19
C(7)	0·1888 (4)	0·8709 (4)	0·8600 (4)	4·36
C(8)	0·3059 (4)	0·8670 (5)	0·9168 (4)	5·07
C(9)	0·3709 (3)	0·8624 (5)	0·8546 (4)	4·53
C(10)	0·4064 (3)	1·0272 (4)	0·6826 (3)	3·40
C(11)	0·4148 (3)	1·0563 (4)	0·5898 (4)	4·21
C(12)	0·4403 (4)	1·1991 (5)	0·6099 (5)	5·49
C(13)	0·4577 (4)	1·3137 (5)	0·7227 (5)	5·62
C(14)	0·4503 (4)	1·2868 (4)	0·8149 (4)	5·48
C(15)	0·4241 (3)	1·1441 (4)	0·7966 (3)	4·45
H(1)	0·543 (3)	0·607 (3)	0·609 (3)	3·30
H(2)	0·257 (3)	0·791 (3)	0·468 (3)	3·14
H(5)	0·153 (3)	0·850 (3)	0·579 (3)	3·59
H(6)	0·041 (3)	0·864 (4)	0·689 (3)	4·19
H(7)	0·142 (3)	0·876 (4)	0·904 (3)	4·36
H(8)	0·347 (3)	0·868 (4)	0·998 (3)	5·07
H(9)	0·459 (3)	0·860 (4)	0·896 (3)	4·53
H(11)	0·394 (3)	0·979 (4)	0·506 (3)	4·21
H(12)	0·435 (3)	1·216 (4)	0·540 (3)	5·49
H(13)	0·480 (3)	1·417 (4)	0·743 (3)	5·62
H(14)	0·458 (3)	1·369 (4)	0·898 (3)	5·48
H(15)	0·414 (3)	1·126 (4)	0·858 (3)	4·45

	x	y	z	B_{iso}(Å^2)
BDDP				
Br	−0·19832 (5)	0·59219 (5)	0·54575 (4)	5·14
C(16)	−0·1597 (3)	0·6339 (4)	0·4357 (3)	3·58
C(17)	−0·1565 (4)	0·5199 (4)	0·3329 (4)	4·62
C(18)	−0·1251 (4)	0·5486 (4)	0·2537 (4)	4·31
C(19)	−0·0987 (3)	0·6932 (4)	0·2798 (3)	3·29
C(20)	−0·1051 (3)	0·8071 (4)	0·3809 (3)	3·24
C(21)	−0·1360 (3)	0·7786 (4)	0·4600 (3)	3·71
N(3)	−0·0645 (3)	0·7282 (3)	0·2019 (3)	3·16
N(4)	−0·1236 (3)	0·6558 (3)	0·0672 (3)	3·39
C(22)	−0·2507 (4)	0·6666 (5)	0·0078 (4)	4·98
C(23)	−0·0570 (3)	0·6985 (4)	0·0247 (3)	3·01
C(24)	−0·0996 (4)	0·6518 (4)	−0·1168 (3)	4·43
C(25)	0·0421 (3)	0·7781 (4)	0·1250 (3)	3·08
N(5)	0·1327 (3)	0·8315 (3)	0·1154 (3)	3·81
C(26)	0·2385 (4)	0·7579 (5)	0·1567 (5)	6·55
C(27)	0·1545 (4)	0·9898 (5)	0·1767 (5)	6·04
C(28)	0·0411 (3)	0·7960 (4)	0·2422 (4)	3·10
O(3)	0·1160 (2)	0·8547 (2)	0·3570 (2)	3·40
H(17)	−0·173 (3)	0·417 (4)	0·313 (3)	4·62
H(18)	−0·130 (3)	0·462 (4)	0·168 (3)	4·31
H(20)	−0·090 (3)	0·913 (3)	0·396 (3)	3·24
H(21)	−0·144 (3)	0·859 (4)	0·535 (3)	3·71
H(221)	−0·267 (3)	0·770 (4)	0·019 (3)	4·98
H(222)	−0·281 (3)	0·606 (4)	−0·084 (4)	4·98
H(223)	−0·284 (3)	0·627 (4)	0·038 (3)	4·98
H(241)	−0·039 (3)	0·681 (4)	−0·127 (3)	4·43
H(242)	−0·117 (3)	0·549 (4)	−0·161 (3)	4·43
H(243)	−0·168 (3)	0·708 (4)	−0·147 (3)	4·43
H(261)	0·220 (4)	0·657 (5)	0·108 (4)	6·55
H(262)	0·296 (4)	0·789 (4)	0·143 (4)	6·55
H(263)	0·277 (4)	0·781 (4)	0·246 (4)	6·55
H(271)	0·210 (4)	1·020 (4)	0·158 (4)	6·04
H(272)	0·082 (4)	1·034 (4)	0·150 (4)	6·04
H(273)	0·185 (4)	1·030 (4)	0·267 (4)	6·04

0567-7408/80/112794-03$01.00 © 1980 International Union of Crystallography

UM00012415
NOVARTIS EXHIBIT 1017
Novartis v. Regents, IPR2023-01346
Page 1161 of 4460

were obtained by a least-squares method from the setting angles of 18 reflections. Three-dimensional intensity data with $(\sin\theta)/\lambda \leq 0{\cdot}6497$ Å^{-1} were collected on a Rigaku four-circle diffractometer using Zr-filtered Mo $K\alpha$ radiation from a crystal with dimensions 0·4 × 0·4 × 0·5 mm. A total of 2485 independent reflections were considered as observed $|I > 3{\cdot}0\sigma(I)|$ and used in this analysis. The data were corrected for Lorentz and polarization effects but not for absorption. The structure was solved by the standard heavy-atom method. Because there were too many variable parameters (418), including anisotropic temperature factors for the nonhydrogen atoms, the structure was refined by full-matrix least-squares calculations with parameters grouped into three blocks to yield $R = 0{\cdot}033$. Isotropic temperature factors of 28 H atoms were fixed to be equal to the isotropic temperature factors of their parent atoms (3·14–6·55 Å^2). Anomalous dispersion for Br was taken into account in the structure factor calculation. The atomic scattering factors were taken from *International Tables for X-ray Crystallography* (1962). Positional parameters are shown in Table 1.*

* Lists of structure factors and anisotropic thermal parameters have been deposited with the British Library Lending Division as Supplementary Publication No. SUP 35429 (5 pp.). Copies may be obtained through The Executive Secretary, International Union of Crystallography, 5 Abbey Square, Chester CH1 2HU, England.

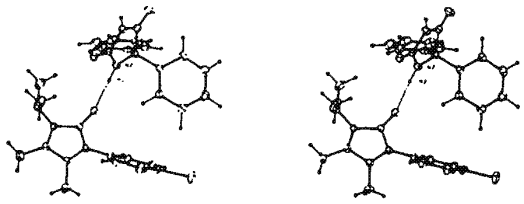


Fig. 1. Stereoscopic drawing of the title compound.

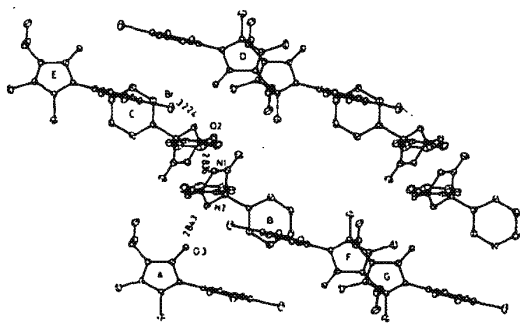


Fig. 2. Packing diagram of the title compound. Hydrogen bonding (– – –); charge transfer (——). The axial directions are a ↘, c→ and b^* out of the page.

Table 2. *Bond distances* (Å) *and bond angles* (°)

Estimated standard deviations are given in parentheses.

5,5-Diphenylhydantoin

C(1) O(1)	1·204 (5)	C(5) C(6)	1·393 (8)
C(1) N(1)	1·365 (5)	C(6)–C(7)	1·373 (7)
C(1) C(3)	1·543 (6)	C(7) C(8)	1·345 (7)
N(1) C(2)	1·393 (5)	C(8) C(9)	1·395 (9)
C(2) O(2)	1·225 (5)	C(10)–C(11)	1·380 (8)
C(2) N(2)	1·334 (5)	C(10)–C(15)	1·391 (5)
N(2) C(3)	1·464 (4)	C(11) C(12)	1·384 (7)
C(3)–C(4)	1·536 (7)	C(12)–C(13)	1·372 (7)
C(3) C(10)	1·534 (6)	C(13)–C(14)	1·354 (10)
C(4)–C(5)	1·381 (6)	C(14) C(15)	1·394 (6)
C(4) C(9)	1·383 (6)		

O(1) C(1)–N(1)	126·4 (4)	C(3) C(4)–C(9)	122·0 (3)
O(1) C(1) C(3)	127·3 (4)	C(5) C(4) C(9)	118·3 (4)
N(1) C(1) C(3)	106·3 (3)	C(4)–C(5)–C(6)	120·5 (4)
C(1) N(1) C(2)	112·3 (4)	C(5) C(6) C(7)	120·4 (4)
N(1)–C(2) O(2)	124·3 (4)	C(6) C(7) C(8)	119·3 (6)
N(1) C(2) N(2)	107·3 (3)	C(7) C(8) C(9)	121·5 (5)
O(2) C(2) N(2)	128·3 (3)	C(4) C(9)–C(8)	120·0 (3)
C(2)–N(2) C(3)	113·3 (3)	C(3) C(10) C(11)	120·7 (3)
C(1) C(3)–N(2)	100·3 (3)	C(3)–C(10)–C(15)	120·5 (4)
C(1) C(3) C(4)	111·0 (4)	C(11)–C(10)–C(15)	118·7 (4)
C(1) C(3) C(10)	109·7 (4)	C(10)–C(11) C(12)	120·6 (4)
N(2) C(3) C(4)	111·2 (3)	C(11) C(12)–C(13)	120·3 (6)
N(2) C(3) C(10)	112·0 (4)	C(12) C(13)–C(14)	119·8 (5)
C(4) C(3) C(10)	112·0 (3)	C(13) C(14)–C(15)	121·0 (4)
C(3) C(4) C(5)	119·5 (4)	C(10) C(15)–C(14)	119·7 (5)

1-(4-Bromophenyl)-4-dimethylamino-2,3-dimethyl-3-pyrazolin-5-one

Br C(16)	1·892 (5)	N(4)–C(22)	1·468 (6)
C(16) C(17)	1·370 (6)	N(4)–C(23)	1·391 (7)
C(16) C(21)	1·380 (6)	C(23) C(24)	1·500 (5)
C(17) C(18)	1·385 (9)	C(23)–C(25)	1·343 (5)
C(18) C(19)	1·381 (6)	C(25) N(5)	1·419 (7)
C(19) C(20)	1·372 (5)	C(25)–C(28)	1·445 (7)
C(19) N(3)	1·427 (7)	N(5) C(26)	1·445 (6)
C(20) C(21)	1·379 (7)	N(5)–C(27)	1·441 (5)
N(3) N(4)	1·406 (5)	C(28) O(3)	1·245 (4)
N(3) C(28)	1·368 (6)		

Br C(16) C(17)	119·4 (4)	N(3)–N(4)–C(23)	104·8 (3)
Br C(16) C(21)	119·4 (3)	C(22) N(4) C(23)	119·5 (4)
C(17)–C(16) C(21)	121·2 (5)	N(4)–C(23) C(24)	119·8 (3)
C(16) C(17)–C(18)	119·9 (4)	N(4) C(23)–C(25)	110·5 (4)
C(17) C(18)–C(19)	118·8 (4)	C(24)–C(23)–C(25)	129·7 (5)
C(18) C(19) C(20)	120·9 (5)	C(23)–C(25)–N(5)	125·0 (4)
C(18)–C(19) N(3)	120·9 (4)	C(23)–C(25) C(28)	108·4 (4)
C(20) C(19)–N(3)	118·2 (4)	N(5) C(25) C(28)	126·5 (3)
C(19)–C(20) C(21)	120·3 (4)	C(25)–N(5)–C(26)	112·8 (4)
C(16)–C(21) C(20)	118·7 (3)	C(25) N(5)–C(27)	112·7 (4)
C(19)–N(3)–N(4)	120·4 (3)	C(26) N(5)–C(27)	112·4 (4)
C(19) N(3)–C(28)	126·0 (3)	N(3) C(28)–C(25)	104·6 (3)
N(4) N(3) C(28)	111·1 (4)	N(3)–C(28) O(3)	124·1 (5)
N(3) N(4) C(22)	114·8 (4)	C(25) C(28) O(3)	131·2 (4)

Discussion. Table 2 lists bond distances and angles. Table 3 contains the best planes and deviations of the atoms from them. Bond lengths and angles in DPH are reasonable in comparison with our previous results for diamminediaquabis(5,5-diphenylhydantoinato)-nickel(II) (Shimizu & Uno, 1980*a*) and diamminebis(5,5-diphenylhydantoinato)copper(II) (Shimizu & Uno, 1980*b*), and with those for DPH (Camerman & Camerman, 1971). O(1) atoms deviate from plane (1) by 0·123 (3) Å. Dihedral angles between planes (1) and (2), between planes (1) and (3) and

UM00012416
NOVARTIS EXHIBIT 1017
Novartis v. Regents, IPR2023-01346
Page 1162 of 4460

Table 3. *Least-squares planes and deviations* (Å) *of atoms from them*

The planes are expressed by $lx + my + nz = d$ in Å.

5,5-Diphenylhydantoin

Plane (1): $-0{\cdot}6010x - 0{\cdot}7631y + 0{\cdot}2376z = 3{\cdot}9311$
C(1) −0·034 (5), N(1) 0·024 (4), C(2) 0·000 (4), N(2) −0·022 (3), C(3) 0·032 (4), O(1)* −0·123 (3), O(2)* −0·011 (3), H(1)* 0·064 (36), H(2)* −0·137 (36)

Plane (2): $0{\cdot}0752x - 0{\cdot}9236y - 0{\cdot}3758z = 1{\cdot}3938$
C(4) −0·006 (4), C(5) 0·010 (4), C(6) −0·006 (4), C(7) −0·001 (4), C(8) 0·005 (5), C(9) −0·001 (5), C(3)* −0·126 (4)

Plane (3): $-0{\cdot}8908x + 0{\cdot}2080y - 0{\cdot}4041z = -4{\cdot}7317$
C(10) −0·000 (4), C(11) −0·001 (4), C(12) 0·000 (5), C(13) 0·002 (5), C(14) −0·003 (5), C(15) 0·002 (4), C(3)* −0·058 (4)

1-(4-Bromophenyl)-4-dimethylamino-2,3-dimethyl-3-pyrazolin-5-one

Plane (4): $0{\cdot}5217x - 0{\cdot}8530y + 0{\cdot}0115z = 2{\cdot}2982$
N(3) −0·041 (4), N(4) 0·039 (4), C(23) −0·024 (4), C(25) 0·000 (4), C(28) 0·025 (4), C(19)* 0·190 (4), C(22)* −0·838 (5), C(24)* −0·082 (5), N(5)* 0·028 (4), O(3)* 0·117 (3)

Plane (5): $-0{\cdot}7772x + 0{\cdot}2242y - 0{\cdot}5880z = -0{\cdot}5460$
C(16) −0·013 (4), C(17) 0·008 (5), C(18) 0·003 (5), C(19) −0·010 (4), C(20) 0·005 (4), C(21) 0·006 (4), Br* −0·058 (1), N(3)* −0·032 (4)

* Atoms not included in the plane calculations.

Table 4. *Intermolecular hydrogen bonds and the charge-transfer interaction*

Donors			Acceptors			Parameters	
N(2)–H(2)	*B*	(i)	O(3)	*A*	(i)	N(2)–H(2)	0·91 (3) Å
						N(2)···O(3)	2·843 (5)
						H(2)···O(3)	1·938 (31)
						N(2)–H(2)···O(3)	173·9 (24)°
N(1)–H(1)	*C*	(ii)	O(2)	*B*	(i)	N(1)–H(1)	0·89 (3) Å
						N(1)···O(2)	2·836 (7)
						H(1)···O(2)	1·952 (32)
						N(1)–H(1)···O(2)	171·2 (37)°
O(2)	*C*	(ii)	Br	*E*	(iii)	Br–C(16)	1·892 (5) Å
						O(2)···Br	3·224 (5)
						O(2)···Br C(16)	154·6 (1)°

Symmetry code: (i) x, y, z; (ii) $1-x, 1-y, 1-z$; (iii) $1-x, y, z$.
B and *C*: 5,5-diphenylhydantoin.
A and *E*: 1-(4-bromophenyl)-4-dimethylamino-2,3-dimethyl-3-pyrazolin-5-one.

between planes (2) and (3), are 55·2, 73·7 and 96·2° respectively. In BDDP bond distances and angles are similar to those found in BDDP itself (Shimizu & Uno, 1980*c*). The notable contact in Fig. 1 is the hydrogen bond between N(2)–H of hydantoin and O=C(28) of 3-pyrazoline. The pyrazoline–phenyl angle in the BDDP part is 52·9° and our result for BDDP itself is 36·6°. This difference in rotation about C–N is mainly brought about by the adjacent plane (2) of DPH. The dihedral angle between planes (2) and (5) is 92·6°; H(6)···H(21), 2·268 Å, is shorter than the sum of the van der Waals radii (Pauling, 1960). Fig. 2 is the packing diagram. Table 4 gives the hydrogen-bond and charge-transfer parameters. DPH molecules form dimers (*B*–*C*) *via* hydrogen bonds N(1)–H···O(2). In the *a*-axis direction, *A*–*B*–*C*–*D* chains as a unit are linked by weak O(2)–Br (*C*–*E* and *B*–*F*) charge-transfer interactions (Gaultier, Hauw & Schvoerer, 1971). O(1) atoms do not participate in any hydrogen bonds. No short contacts exist between *F* and *G*.

We thank Professor Masao Kakudo, Osaka University, for collecting the diffraction data. The calculations and the drawing of the figures were carried out using the programs *UNICS* (Ashida, 1973) and *ORTEP* (Johnson, 1965) at the Data Processing Center, Kyoto University.

References

ASHIDA, T. (1973). *The Universal Crystallographic Computing System – Osaka*. The Computation Center, Osaka Univ.

CAMERMAN, A. & CAMERMAN, N. (1971). *Acta Cryst.* B27, 2205–2211.

GAULTIER, J., HAUW, C. & SCHVOERER, M. (1971). *Acta Cryst.* B27, 2199–2204.

International Tables for X-ray Crystallography (1962). Vol. III. Birmingham: Kynoch Press.

JOHNSON, C. K. (1965). *ORTEP*. Report ORNL-3794. Oak Ridge National Laboratory, Tennessee.

PAULING, L. (1960). *The Nature of the Chemical Bond*, 3rd ed., p. 260. Ithaca: Cornell Univ. Press.

SHIMIZU, N. & UNO, T. (1980*a*). *Cryst. Struct. Commun.* 9, 223–226.

SHIMIZU, N. & UNO, T. (1980*b*). *Cryst. Struct. Commun.* 9, 389–392.

SHIMIZU, N. & UNO, T. (1980*c*). *Cryst. Struct. Commun.* 9, 435–438.

UM00012417
NOVARTIS EXHIBIT 1017
Novartis v. Regents, IPR2023-01346
Page 1163 of 4460

J. Enzyme Inhibition, 1991, Vol. 5, pp. 119–132
Reprints available directly from the publisher
Photocopying permitted by license only

© 1991 Harwood Academic Publishers GmbH
Printed in the United Kingdom

STRUCTURE-ACTIVITY STUDIES OF NON-STEROIDAL AROMATASE INHIBITORS: THE CRYSTAL AND MOLECULAR STRUCTURES OF CGS 16949A AND CGS 18320B

PATRICK VAN ROEY†, KEITH A. BULLION and YOSHIO OSAWA
Medical Foundation of Buffalo, 73 High Street, Buffalo, NY 14203, USA

LESLIE J. BROWNE and ROBERT M. BOWMAN
CIBA-GEIGY Pharmaceuticals Division, Summit, NJ 07901, USA

and

DIETMAR G. BRAUN
CIBA GEIGY Ltd., CH-4002 Basel, Switzerland

(Received 23 April 1990)

The crystal and molecular structures of 4-(5,6,7,8-tetrahydroimidazo[1,5-a]pyridin-5-yl)benzonitrile hydrochloride (CGS 16949A) and bis(p-cyanophenyl)imidazo-1-yl methane hemisuccinate (CGS 18320B) have been determined as part of structure-activity relationship studies of non-steroidal aromatase inhibitors. CGS 18320B crystallizes with two inhibitor molecules in the asymmetric unit that are similar in conformation. The cyanophenyl groups and the imidazole moieties in the CGS 18320B molecules display a propellor-like arrangement. The orientation of the imidazole ring in CGS 16949A, which is constrained by the piperidine ring, differs by about 80° from the orientations in both CGS 18320B molecules. The conformations of both compounds are consistent with the proposed model (Banting *et al.* (1988) *J. Enz. Inhibit.*, **2**, 216) for inhibitor binding by positioning of the cyanophenyl group in the steroid A-ring binding site and interaction of the imidazole nitrogen with the iron of the haem.

KEY WORDS: Aromatase inhibitors, Crystal structure, CGS 16949A, CGS 18320B.

INTRODUCTION

Hormone deprivation by surgical or pharmacological means has been used in the treatment of a variety of hormone-dependent cancers.[1–3] Aromatase, a complex of a cytochrome P450 and a NADPH-cytochrome P450 reductase, has been shown to be an attractive target for chemotherapeutic treatment. Aromatase catalyzes the terminal androgen 19-desmolase step in the conversion of androgen to estrogen.[4] Specific inhibitors of aromatase have shown promising results.[5–7] Schematic diagrams of the non-steroidal inhibitors discussed in this paper are shown in Figure 1. 4-(5,6,7,8-Tetrahydroimidazo[1,5-a]pyridin-5-yl)benzonitrile (CGS 16949A) and bis(p-cyanophenyl)imidazo-1-yl methane hemisuccinate (CGS 18320B) are among the most

†Correspondence.

UM00012418
NOVARTIS EXHIBIT 1017
Novartis v. Regents, IPR2023-01346
Page 1164 of 4460

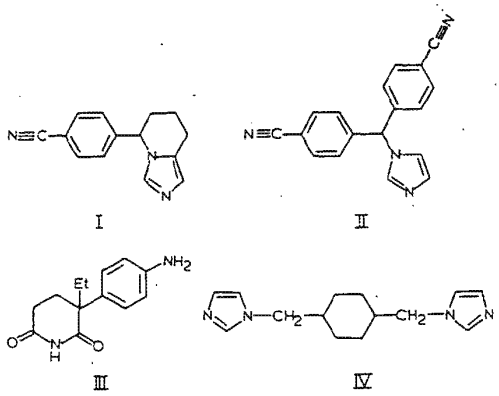


FIGURE 1 Schematic diagrams showing the structures of: (I) CGS 16949A; (II) CGS 18320B; (III) aminoglutethimide; and, (IV) CGS 14796C.

potent non-steroidal aromatase inhibitors in *in vitro* experiments.[8,9] Both are more than 100-fold more active than the clinically used non-steroidal inhibitor, aminoglutethimide. CGS 18320B exhibits a two-fold lower K_i than CGS 16949A towards androstenedione aromatization by human placental microsomal aromatase.[9]

The nature of the mechanism of action of non-steroidal aromatase inhibitors is not clearly understood. Many inhibitors lack any structural or chemical similarity with the steroid substrates and related inhibitors (for a recent review, see Cole and Robinson.[10]) Banting *et al.*[11] have proposed that the non-steroidal aromatase inhibitors, including aminoglutethimide and CGS 16949A, act by interaction with the haem iron of aromatase and that they bind in the active site in the same location as the A-ring of the steroidal substrates. This hypothesis forms the basis for recent structure-activity studies.[12]

In this paper we report the crystal structures of CGS 16949A and CGS 18320B as part of on-going studies aimed at determing structure-activity relationships of non-steroidal aromatase inhibitors. CGS 16949A contains an imidazole ring in a constrained conformation and a cyanophenyl moiety. Two cyanophenyl substituents and an unconstrained imidazole group are present in CGS 18320B. The goal of this analysis is to determine similarities in the overall molecular conformations and the location of the functional groups in particular and thus determine how the compounds may bind to the active site of the enzyme.

MATERIALS AND METHODS

Crystals of CGS 16969A and CGS 18320B were obtained by slow evaporation of aqueous methanol solutions at 37°C. X-ray diffraction intensities were measured on a Siemens (formely Nicolet) P3 diffractometer, using Nb-filtered Mo$K\alpha$ radiation (λ = 0.710 69 Å). The intensities of six reference reflections were monitored throughout the data collection but did not change significantly. Lorentz and polarization corrections were applied, but absorption corrections were not considered necessary.

UM00012419
NOVARTIS EXHIBIT 1017
Novartis v. Regents, IPR2023-01346
Page 1165 of 4460

The data with $F > 3\sigma(F)$ were considered observed and used in the refinement. The sructures were determined by direct methods, using the program MULTAN,[13] and refined by full-matrix least-squares. Coordinates for the hydrogen atoms were determined from difference maps and included in the refinement after the anisotropic refinement of the non-hydrogen atoms had converged. Programs used include Blessing's data reduction package,[14] locally modified versions of the refinement program contained in the Enraf-Nonius SDP package,[15] the plotting program ORTEP-II[16] and the least-squares molecular fitting program FITMOL.[17].

CGS 16949A

$C_{14}H_{13}N_3$. HCl, M_r = 258.73, orthorhombic, Fdd2, a = 15.982(2), b = 25.777(3), c = 13.156(2)Å, V = 5421.7(7)Å^3, Z = 16, D_x = 1.27 Mgm^{-3}, μ = 2.649 mm^{-1}, $F(000)$ = 2160. The sample was recrystallized from an aqueous methanol solution. The crystal was shaped as a triangular plate and had approximate dimensions of 0.30 × 0.40 × 0.60 mm. In total, 2640 intensity data with $4 < 2\theta < 55°$, $-2 < h < 20$, $-2 < k < 31$, $0 < l < 16$, were measured. Of the 1634 unique data, 1456 had $F > \sigma(F)$ and were considered observed. $\sigma(F)$ calculated according to Stout & Jensen:[18] $\sigma^2(F) = (k/4Lp1)[\sigma^2(I) + (0.01I)^2]$. The maximum value of the shift/e.s.d. during the last cycle of refinement was 0.03. Final R values are R = 0.036 and R_w = 0.041 for the observed data, and R_{all} = 0.042 for all 1634 data. The final value of the standard deviation of an observation of unit weight was s = 1.874. The final difference map has maximum and minimum densities of 0.057 and −0.056 eA^{-3}.

CGS 18320B

$C_{18}H_{12}N_4$. 1/2[CH_2–COOH]$_2$, M_r = 343.37, triclinic, $P1$, a = 9.753(1), b = 10.982(1), c = 17.443(2)Å, α = 100.51(1), β = 93.15(1), γ = 99.32(1)°, V = 1808.1(4)Å^3, Z = 4, D_x = 1.26 Mgm^{-3}, λ(Mo$K\alpha$) = 0.71069Å, μ = 7.90 mm^{71}, $F(000)$ = 716. The sample was recrystallized from an aqueous methanol solution. The crystal used had approximate dimensions of 0.10 × 0.40 × 0.60 mm. In total, 8160 total data with $4 < 2\theta < 52°$, $0 < h < 13$, $-14 < k < 14$, $-22 < l < 22$ were measured. Of the 6817 unique data, 4864 had $F > 3\sigma(F)$ and were considered observed ($\sigma^2(F) = (k/4Lp1)[\sigma^2(I) + (0.01I)^2]$. The maximum value of shifts/e.s.d. during the last cycle of refinement was 0.02. Final R values are R = 0.064, wR = 0.057 for 4864 observed data and R_{all} = 0.091 for all 6817 data; s = 2.204. The final difference map has maximum and minimum densities of 0.339 and −0.380 eA^{-3} respectively.

RESULTS

Atomic coordinates and isotropic thermal parameters for both compounds are listed in Table I.† Selected torsion angles that are important in describing the conformations are listed in Table II. Figure 2 shows the observed molecular conformations of both compounds and the numbering scheme used in the text and tables. Table III lists the geometries of the least-squares planes of the conjugated systems in both compounds.

†Tables of coordinates and thermal parameters have been deposited with the Cambridge Crystallographic Database. Tables of anisotropic thermal parameters, bond lengths and angles and observed and calculated structure factors are available from the authors (PVR) upon request.

NOVARTIS EXHIBIT 1017
Novartis v. Regents, IPR2023-01346
Page 1166 of 4460

TABLE I

Atomic coordinates ($\times 10^4$, $\times 10^5$ for Cl) and isotropic thermal parameters ($\times 10^2$) for CGS 16949A and CGS 18320B. The e.s.d.'s are given in parentheses. B_{eq} shown is the equivalent isotropic thermal parameter calculated from the refined anisotropic thermal parameters by means of the equation: $B_{eq} = 4/3\Sigma_i\Sigma_j B_{ij} a_i a_j$.

	x	*y*	*z*	B_{eq}
CGS 16949A				
N(1)	3324(2)	1663(1)	557	494(6)
C(2)	2628(2)	1400(1)	578(3)	446(7)
N(3)	2807(1)	900(1)	621(3)	390(5)
C(4)	3662(2)	846(1)	616(3)	465(7)
C(5)	3977(2)	1328(1)	586(3)	516(8)
C(6)	4064(2)	326(2)	643(4)	624(11)
C(7)	3464(3)	−92(1)	323(5)	691(12)
C(8)	2632(2)	−34(1)	875(4)	565(10)
C(9)	2196(2)	465(1)	555(3)	441(7)
C(10)	1421(2)	586(1)	1151(3)	431(7)
C(11)	1437(2)	683(1)	2185(3)	517(8)
C(12)	710(2)	781(2)	2710(4)	556(9)
C(13)	−47(2)	782(1)	2207(3)	459(7)
C(14)	−75(2)	682(1)	1177(3)	537(9)
C(15)	655(2)	582(1)	659(3)	519(8)
C(16)	−820(2)	881(1)	2741(3)	569(9)
N(17)	−1434(2)	958(2)	3138(3)	778(11)
CL(18)	10827(5)	22319(3)	9527(22)	584(2)
CGS 18320B				
C(2A)	6113(4)	1378(3)	3734(2)	837(14)
C(3A)	5250(3)	2156(3)	3433(2)	587(10)
C(4A)	5307(3)	2326(3)	2676(2)	614(11)
C(5A)	4542(3)	3143(3)	2400(2)	523(9)
C(6A)	3715(2)	3776(2)	2885(1)	419(7)
C(7A)	3646(3)	3574(3)	3641(2)	524(9)
C(8A)	4422(3)	2776(3)	3918(2)	594(10)
C(9A)	2963(3)	4743(2)	2593(2)	422(8)
C(10A)	1645(3)	4887(2)	2995(1)	423(8)
C(11A)	1594(3)	5862(3)	3598(2)	604(10)
C(12A)	402(3)	5915(3)	3989(2)	667(11)
C(13A)	−749(3)	4994(3)	3768(2)	518(9)
C(14A)	−723(3)	4025(3)	3150(2)	561(10)
C(15A)	469(3)	3987(3)	2766(2)	514(9)
(C16A)	−1986(3)	5051(3)	4180(2)	644(11)
C(19A)	4899(3)	6512(3)	3295(2)	518(9)
C(20A)	5461(3)	7625(3)	3137(2)	508(9)
C(22A)	3990(3)	6737(3)	2176(2)	439(8)
N(1A)	6813(4)	794(3)	3996(3)	1167(16)
N(17A)	−2938(3)	5108(3)	4524(2)	879(12)
N(18A)	3935(2)	5935(2)	2676(1)	415(6)
N(21A)	4896(2)	7772(2)	2435(1)	479(7)
C(1C)	4663(3)	4328(3)	−162(2)	470(8)
C(2C)	3376(3)	3903(3)	213(1)	432(8)
O(3C)	2846(2)	2714(2)	−30(1)	670(7)
O(4C)	2822(2)	4578(2)	663(1)	716(7)
C(2B)	2171(3)	5716(3)	8705(2)	537(9)
C(3B)	1351(3)	4475(2)	8547(1)	430(8)
C(4B)	173(3)	4200(3)	8934(2)	494(9)
C(5B)	−591(3)	3007(3)	8779(1)	470(8)
C(6B)	−217(2)	2072(2)	8229(1)	406(7)

CGS 18320B
C(7B)
C(8B)
C(9B)
C(10B)
C(11B)
C(12B)
C(13B)
C(14B)
C(15B)
C(16B)
C(19B)
C(20B)
C(22B)
N(1B)
N(17B)
N(18B)
N(21B)
C(1D)
C(2D)
O(3D)
O(4D)

FIGURE 2 M
18320B, molecul

UM00012421
NOVARTIS EXHIBIT 1017
Novartis v. Regents, IPR2023-01346
Page 1167 of 4460

TABLE I
Continued

	x	y	z	B_{eq}
CGS 18320B				
C(7B)	952(3)	2362(3)	7842(2)	512(9)
C(8B)	1739(3)	3552(3)	8002(2)	509(9)
C(9B)	−1126(3)	780(2)	8047(1)	446(8)
C(10B)	−1218(3)	169(2)	7192(1)	423(7)
C(11B)	−418(3)	−710(3)	6908(2)	531(9)
C(12B)	−496(3)	−1207(3)	6126(2)	536(9)
C(13B)	−1386(3)	−824(2)	5604(1)	441(8)
C(14B)	−2195(3)	51(3)	5880(2)	540(9)
C(15B)	−2112(3)	535(3)	6669(2)	533(9)
C(16B)	−1443(3)	−1349(3)	4785(2)	525(9)
C(19B)	608(3)	−195(3)	8813(2)	466(9)
C(20B)	440(3)	−1137(3)	9213(2)	526(9)
C(22B)	−1588(3)	−915(3)	8827(2)	504(9)
N(1B)	2833(3)	6694(3)	8823(2)	756(10)
N(17B)	−1467(3)	−1790(3)	4142(2)	706(9)
N(18B)	−701(2)	−43(2)	8564(1)	441(6)
N(21B)	−948(3)	−1591(2)	9223(1)	538(7)
C(1D)	5504(3)	10038(3)	348(2)	507(9)
C(2D)	4946(3)	9306(2)	939(2)	448(8)
O(3D)	5832(2)	9381(2)	1545(1)	599(6)
O(4D)	3785(2)	8691(2)	873(1)	685(7)

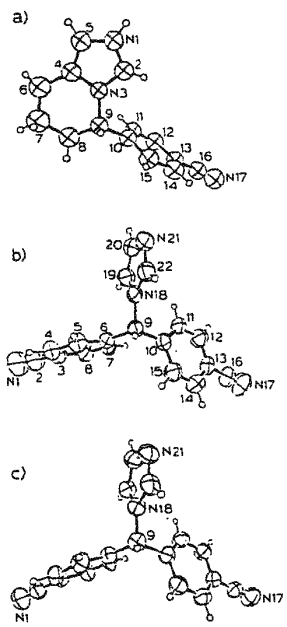


FIGURE 2 Molecular conformations of (a) CGS 16949A; (b) CGS 18320B, molecule A; and (c) CGS 18320B, molecule B showing the numbering scheme used in the text.

6949A and
(parameter
$\Sigma_i \Sigma_j B_{ij} a_i a_j$.

B_{eq}
494(6)
446(7)
390(5)
465(7)
516(8)
624(11)
691(12)
565(10)
441(7)
431(7)
517(8)
556(9)
459(7)
537(9)
519(8)
569(9)
778(11)
584(2)
837(14)
587(10)
614(11)
523(9)
419(7)
524(9)
594(10)
422(8)
423(8)
604(10)
667(11)
518(9)
561(10)
514(9)
644(11)
518(9)
508(9)
439(8)
1167(16)
879(12)
415(6)
479(7)
470(8)
432(8)
670(7)
716(7)
537(9)
430(8)
494(9)
470(8)
406(7)

NOVARTIS EXHIBIT 1017
Novartis v. Regents, IPR2023-01346
Page 1168 of 4460

TABLE II
Selected torsion angles (°) for CGS 16949A and CGS 18320B.

CGS 16949A									
N3	C2	N1	C5	0.2(4)	C10	C9	N3	C2	−41.2(4)
N1	C2	N3	C4	−0.8(4)	C10	C9	N3	C4	147.1(3)
N1	C2	N3	C9	−173.6(3)	N3	C9	C10	C11	−59.8(4)
C5	C4	N3	C2	1.1(4)	N3	C9	C10	C15	122.6(3)
C5	C4	N3	C9	174.0(3)	C8	C9	C10	C11	63.3(4)
C6	C4	N3	C2	−179.1(3)	C8	C9	C10	C15	−114.4(4)
C6	C4	N3	C9	−6.2(5)	N3	C4	C5	N1	−1.0(4)
C6	C4	C5	N1	179.2(4)	N3	C4	C6	C7	19.3(5)
C5	C4	C6	C7	−160.9(4)	C4	C5	N1	C2	0.5(4)
C4	C6	C7	C8	−48.0(5)	C6	C7	C8	C9	65.7(4)
C7	C8	C9	N3	−48.9(4)	C7	C8	C9	C10	−173.1(3)
C8	C9	N3	C2	−167.4(3)	C8	C9	N3	C4	21.0(4)
CGS 18320B									
C10A	C9A	N18A	C19A	83.0(3)	C10B	C9B	N18B	C19B	86.3(3)
C10A	C9A	N18A	C22A	−91.8(3)	C10B	C9B	N18B	C22B	−86.7(3)
C5A	C6A	C9A	C10A	153.0(2)	C5B	C6B	C9B	C10B	143.3(2)
C5A	C6A	C9A	N18A	−81.5(3)	C5B	C6B	C9B	N18B	−89.3(3)
C7A	C6A	C9A	C10A	−30.7(3)	C7B	C6B	C9B	C10B	−34.5(3)
C7A	C6A	C9A	N18A	94.8(3)	C7B	C6B	C9B	N18B	92.9(3)
C20A	C19A	N18A	C9A	−174.9(2)	C20B	C19B	N18B	C9B	−174.2(3)
C6A	C9A	C10A	C11A	100.3(3)	C6B	C9B	C10B	C11B	98.6(3)
C6A	C9A	C10A	C15A	−77.5(3)	C6B	C9B	C10B	C15B	−79.4(3)
N18A	C9A	C10A	C11A	−23.4(4)	N18B	C9B	C10B	C11B	−28.5(3)
N21A	C22A	N18A	C9A	175.1(2)	N21B	C22B	N18B	C9B	174.7(2)
N18A	C9A	C10A	C15A	158.9(2)	N18B	C9B	C10B	C15B	153.4(2)
C6A	C9A	N18A	C19A	−42.2(3)	C6B	C9B	N18B	C19B	−41.7(4)
C6A	C9A	N18A	C22A	142.9(2)	C6B	C9B	N18B	C22B	145.4(3)

CGS 16949A

N1 of the inhibitor molecule is protonated and forms a salt bridge with the chloride anion (N1–HN1 ... Cl18 : N ... Cl, 3.048(3) Å; N–H, 0.87(4) Å; H ... Cl, 2.22(4) Å, N–H ... Cl, 160(3)°). The only other significant intermolecular contact is a moderately close contact between C4 and N17 (3.226 Å).

The bond lengths and angles of the imidazole ring indicate only limited contribution of resonance forms in which N1–C5 (1.354(4) Å), N3–C2 (1.323(3) Å) and N3–C4 (1.375(3) Å) have double bond characteristics. The N1–C2 bond (1.302(4) Å) is much shorter than the N1–C5 bond and the C4–C5 bond (1.341(5) Å) is only slightly longer than a standard double bond. But the ring is planar. Atoms C9 and C6 are on the same side of the plane. The angle between the least-squares planes of the imidazole ring and the p-cyanophenyl group is 100.0°. The absolute configuration this compound has not been determind. The configuration used is that also used by Banting *et al.*[11] for their modeling studies.

CGS 18320B

The asymmetric unit contains two CGS 18320B molecules and two half succinic acid molecules. The two half succinic acid molecules are independent and located on

UM00012423
NOVARTIS EXHIBIT 1017
Novartis v. Regents, IPR2023-01346
Page 1169 of 4460

TABLE III

Least-squares planes geometry, deviations from the planes and interplanar angles of the conjugated systems in CGS 16949A (I) and CGS 18320B (II).

CGS 16949A (I).

Plane 1: Cyanophenyl moiety.
Atoms: C9, C10, C11, C12, C13, C14, C15, C16, N17
r.m.s. deviation: 0.008 Å
C8 −1.284 N3 1.160

Plane 2: Imidazole Ring
Atoms: C2, C4, C5, C6, C9, N1, N3
r.m.s. deviation: 0.027 Å
C8 0.343 C10 0.778

Plane 3: C9 substituents
Atoms: C8, C10, N3
C9 −0.457 N1 0.339 N17 1.399
Angle Plane 1-Plane 2: 100.0°
Angle Plane 1-Plane 3: 93.1°
Angle Plane 2-Plane 3: 17.3°

CGS 18320B Molecule A.

Plane 1: Cyanophenyl moiety.
Atoms: C2, C3, C4, C5, C6, C7, C8, C9, N1
r.m.s. deviation: 0.062 Å
C10 −0.509 N18 1.532

Plane 2: Cyanphenyl moiety.
Atoms: C9, C10, C11, C12, C13, C14, C15, C16, N17
r.m.s. deviation: 0.037 Å
C6 1.498 N18 −0.392

Plane 3: imidazole moiety.
Atoms: C9, C19, C20, C22, N18, N21
r.m.s. deviation: 0.024 Å
C6 0.863 C10 −1.449

Plane 4: C9 substituents
Atoms: C6, C10, N18
C9 −0.453 N1 1.859 N17 1.749 N21 0.022
Angle Plane 1-Plane 2: 93.2°
Angle Plane 1-Plane 3: 83.7°
Angle Plane 2-Plane 3: 75.2°
Angle Plane 1-Plane 4: 60.2°
Angle Plane 2-Plane 4: 54.3°
Angle Plane 3-Plane 4: 112.0°

CGS 18230B Molecule B.

Plane 1: Cyanophenyl moiety.
Atoms: C2, C3, C4, C5, C6, C7, C8, C9, N1
r.m.s. deviation: 0.013 Å
C10 −0.864 N18 1.322

Plane 2: Cyanophenyl moiety.
Atoms: C9, C10, C11, C12, C13, C14, C15, C16, N17
r.m.s. deviation: 0.017 Å
C6 1.433 N18 −0.569

Plane 3: imidazole moiety.
Atoms: C9, C19, C20, C22, N18, N21
r.m.s. deviation: 0.025 Å
C6 0.803 C10 −1.466

Plane 4: C9 substituents
Atoms: C6, C10, N18
C9, −0.428 N1 1.361 N17 1.541 N21 −0.064
Angle Plane 1-Plane 2: 92.5°
Angle Plane 1-Plane 3: 74.5°
Angle Plane 2-Plane 3: 79.6°
Angle Plane 1-Plane 4: 63.0°
Angle Plane 2-Plane 4: 56.2°
Angle Plane 3-Plane 4: 114.1°

distinct inversion centers (1/2, 1/2, 0 and 1/2, 0, 0). The bond lengths of C1 to the symmetry related atoms are C1C–C1C($1-x$, $1-y$, $-z$) 1.511(4) Å and C1D–C1D($1-x$, $2-y$, $-z$) 1.503(4) Å. Succinic acid molecules B and D form strong hydrogen bonds with CGS 18320B molecules C and A, respectively, with the following goemetries: O3D–HO3D...N21A:O...N, 2.640(3) Å; O–H, 1.10(3) Å; H...N, 1.55(3) Å; O–H...N, 178(2)° and O3C–HO3C...N21B:O...N, 2.662(3) Å; O–H, 1.06(4) Å; H...N, 1.66(4) Å; O–H...N, 155(3)°.

The two CGS 18320B molecules have nearly identical geometries and conformations. Again, both imidazole rings show limited resonance structure but are very planar. The only conjugated system that differs significantly from planarity is the first p-cyanophenyl group of molecule A. The phenyl ring appears to be bowed,

UM00012424
NOVARTIS EXHIBIT 1017
Novartis v. Regents, IPR2023-01346
Page 1170 of 4460

TABLE IV

Results of least-squares fitting of the molecular structures of CGS-16949 (I) and CGS-189320B, molecule A (IIA) and molecule B (IIB).

A. Fit of the Central atoms:

I: C9, C8, C10, N3
II: C9, C6, C10, N18

Molecules	Distances of fitted atoms (Å)				Other distances		
	Average	*Maximum*		*RMS*	*Atom*	*Atom*	*Distance*
IIA-IIB	0.017	0.023	C9	0.018	C8A	C8B	0.159
					C12A	C12B	0.044
					C20A	C20B	0.139
					N1A	N1B	0.867
					N17A	N17B	0.302
					N21A	N21B	0.164
IIA-I	0.016	0.022	C9	0.017	C5A	C7	0.799
					C12A	C12	0.570
					C13A	C13	0.244
					C20A	C5	0.870
					N17A	N17	0.542
					N21A	N1	0.425
IIB-I	0.21	0.031	C9	0.022	C5B	C7	1.002
					C12B	C12	0.595
					C13B	C13	0.132
					C20B	C5	0.857
					N17B	N17	0.241
					N21B	N1	0.450

B. Fit of the imidazole ring atoms:

I: C9, C4, C5, C2, N3, N1
II: C9, C19, C20, C22, N18, N21

Molecules	Distances of fitted atoms (Å)				Other distances		
	Average	*Average*		*RMS*	*Atom*	*Atom*	*Distance*
IIA-IIB	0.012	0.0187	C9	0.0127	C3A	C3B	0.568
					C8A	C8B	0.369
					C12A	C12B	0.269
					C13A	C13B	0.448
					N1A	N1B	1.190
					N17A	N17B	0.760
IIA-I	0.054	0.087	N18	0.0576	C5A	C7	2.594
					C6A	C8	1.251
					C10A	C10	1.373
					C12A	C12	3.723
					C13A	C13	3.965
IIB-I	0.058	0.099	N18	0.0627	C5B	C7	2.685
					C6B	C8	1.209
					C10B	C10	1.267
					C12B	C12	2.993
					C13B	C13	3.610
					N17B	N17	5.906

with C9 and N1 0.10 and 0.12 Å above the least-square plane. The second p-cyanophenyl group of molecule A is also somewhat distorted but the imidazole ring and all three groups of molecule B are very planar. N1 of molecule A also has a high thermal parameter, indicative of static or dynamic disorder in its position. No obvious

NOVARTIS EXHIBIT 1017
Novartis v. Regents, IPR2023-01346
Page 1171 of 4460

TABLE IV
Continued

C. Fit of the phenyl ring atoms:
I: C9, C10, C11, C12, C13, C14, C15, C16, C17
II: C9, C10, C11, C12, C13, C14, C15, C16, C17

Molecules	Distance of fitted atoms (Å)				Other distances		
	Average	*Maximum*		*RMS*	*Atom*	*Atom*	*Distance*
IIA-I	0.041	0.075	N17	0.0456	C5A	C7	1.659
					C6A	C8	0.884
					C20A	C5	2.534
					N18A	N3	0.956
					N21A	N1	2.090
IIB-I	0.037	0.081	N17	0.0417	C5B	C7	1.754
					C6B	C8	0.816
					C20B	C5	2.169
					N18B	N3	0.791
					N21B	N1	1.656

causes, such as intermolecular contacts, for the distortions in molecule A are observed. The main conformational features are to be found in the orientation of the two phenyl rings and the imidazole ring about the central atom C9. The presence of three bulky substitutents on C9 forces the molecule in a propeller-like conformation. The three bond angles between C6, C10 and N18 differ by small but significant amounts. The largest difference in the torsion angles about the bonds that link the rings to the central atom is 10°. The phenyl rings are nearly perpendicular in both molecules. The angles of the last squares planes of the imidazole ring with the phenyl rings are significantly different, but in the opposite direction in the two molecules.

Table IV summarizes the analysis of the least-squares fitting of the two molecules of CGS 18320B as well as those with the structure of CGS 16949A. Figure 3 shows the corresponding illustrations. Three different superpositions are shown. The two CGS 18320B molecules are very similar in conformation, indicating that this conformation is highly preferred. The small differences in the torsion angles do not affect the overall geometry. The largest difference in the geometry is in the positions of N1 as can best be seen at the bottom of Figure 3c. This is caused by small differences in the angles about C9 and the non-planarity of the one p-aminophenyl ring in molecule A described in the previous paragraph. This distortion is most likely not significant.

DISCUSSION

The most important differences between the conformations of CGS 16949A and CGS 18320B are in the orientations of the imidazole rings and the phenyl rings. Looking down the H9–C9 bond all three planar substituents in CGS 18320B make an angle of about 60° with the plane of the atoms C6, C10 and N18. This conformation is caused by steric interactions of the bulky substituents. In CGS 16949A, the phenyl ring is at a 93° angle with the corresponding plane (C8, C10, N3) but the plane of the imidazole ring is nearly parallel (15°) because of the constraint caused by the pyridine ringe on the orientation of the imidazole ring. Table IV summarizes the least-squares

UM00012426
NOVARTIS EXHIBIT 1017
Novartis v. Regents, IPR2023-01346
Page 1172 of 4460

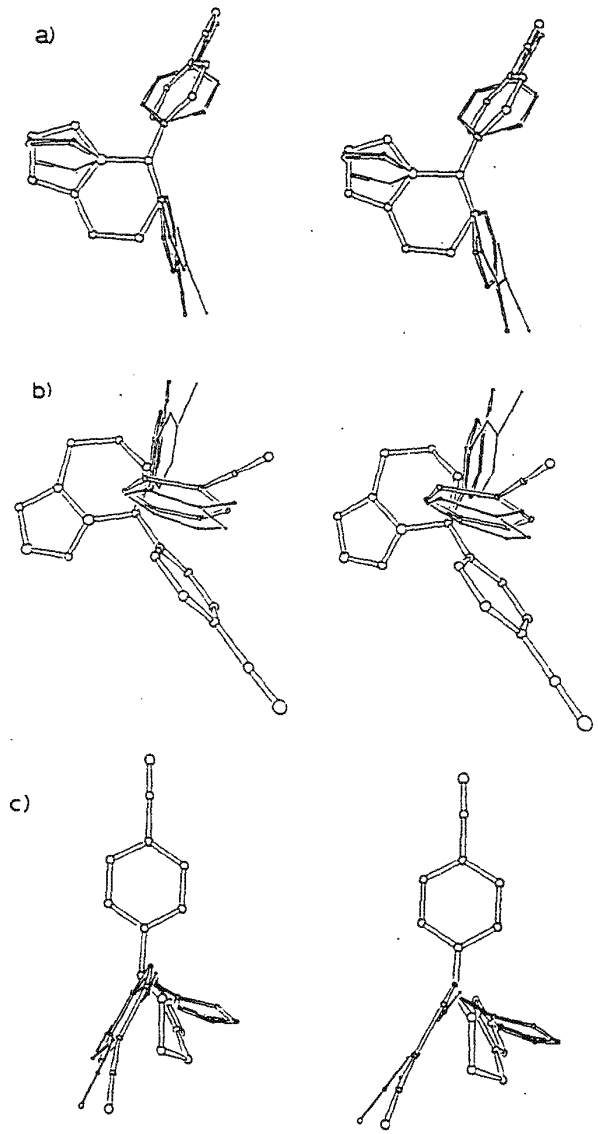


FIGURE 3 Stereodiagrams showing the overlap of CGS 16949A (largest bond radii) and CGS 18320B (molecule A, intermediate bond radii; and molecule B, smallest bond radii) after least-squares fitting of: (a) the four central atoms, (b) the imidazole rings, and (c) the cyanophenyl group. Note the similarity in the conformations of the two molecules of CGS 18320B, except for the slight change in the position of N1 and the significant differences in the orientation of the imidazole ring between the two compounds but with only small differences in the relative positions of the nitrogen atoms.

UM00012427
NOVARTIS EXHIBIT 1017
Novartis v. Regents, IPR2023-01346
Page 1173 of 4460

fitting of related structural parts of CGS 16949A and CGS 18320B with the accompanying illustrations shown in Figure 3. The overlap of functional groups appears to work best when the central four atoms are superimposed. Overlapping the phenyl groups or the imidazole moieties results in large distances between the positions of the other functional groups. This suggests, if the two compounds are to bind to the same binding site, that the imidazole conformation in the restrained molecule is a suitable conformation and that the more flexable compounds would have to adopt a similar conformation or, alternatively, that the location of the cyano and imidazole nitrogens are important but not the orientation of the phenyl or imidazole rings. If the imidazole ring of CGS 18320B would need to be rotated independently of the cyanophenyl rings, this would most likely result in a significantly higher energy conformation than the observed in the crystal structure. The observed two-fold higher inhibition by CGS 18320B would suggest that this higher energy conformation can be achieved upon binding to the enzyme or that the enzyme can accomodate a wider range of molecular geometries or conformations. The inhibition by CGS 14796C, aminoglutethimide and its analogues, the crystal structures of which have been reported elsewhere[20,21,12] and which differ even more significantly in structure, may provide additional evidence for this accommodation.

CGS 16949A and CGS 18320B are both active aromatase inhibitors that differ greatly in chemical structure when compared to other non-steroidal inhibitors such as aminogluetethimide. Both have the imidazole ring and the *p*-cyanophenyl group as functional groups. For the structure-activity studies we need to compare the two compounds in terms of the overall shape and size and distances between corresponding functional groups, specifically the cyano and imidazole nitrogen atoms, which according to the model of Banting *et al.*[11] form the anchor points for interaction with the binding site for the A-ring of the steroid and the interaction with the iron of the haem group. This analysis can provide information regarding the shape and properties of the binding site or active site of the target enzyme. If the two nitrogen atoms are the crucial functional groups for the effective binding and activity of the inhibitors their relative positions as well as the overall shape and geometry of the hydrophobic core are important. Both compounds have V-shaped hydrophobic cores with the nitrogen atoms at the extreme ends of essentially perpendicular axes. One of these would be oriented towards the haem iron and the other towards the protein component that interacts with the O3 of the steroid molecule. The additional cyanophenyl group of CGS 18320B may well fit within the remaining space for the steroid. Figure 3 shows that the relative positions of the nitrogen atoms do not differ greatly but that the orientation of the imidazole rings are different. For CGS 16949A the distance between the nitrogen atoms N1 and N17 is 8.525 Å. CGS 18320B has two cyano nitrogens. One, N17 is a similar distance from the imidazole nitrogen N21 : 8.931 Å in molecule A and 8.811 Å in molecule B. The distance of the other cyano nitrogen N1 to N21 is similar in molecule A, 9.004 Å, but significantly larger in molecule B, 9.409 Å.

Another non-steroidal aromatase inhibitor CGS 14796C has two imidazole rings at opposite ends of the molecule. The distance between the two free nitrogen atoms in the crystal structure of this compound[20] is 10.77 Å. However, the conformation observed in the crystal structure is highly extended. We have demonstrated by searching distance maps, using SYBYL[22] software, that this molecule can adopt several conformations in which the distances between the two nitrogen atoms are between 8.25 Å and 9.0 Å, without prohibitive steric interactions. One such confor-

GS 18320B
:s fitting of.
imilarity in
sition of N1
ıds but with

UM00012420
NOVARTIS EXHIBIT 1017
Novartis v. Regents, IPR2023-01346
Page 1174 of 4460

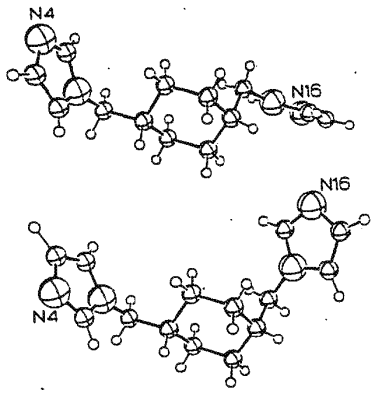


FIGURE 4 Conformation of CGS 14796C: top, extended conformation observed in the crystal structure; bottom, conformation obtained by rotating about the exocyclic bonds. This conformation has a distance of 8.95 Å between the two nitrogen atoms and does not have any prohibitive steric interactions.

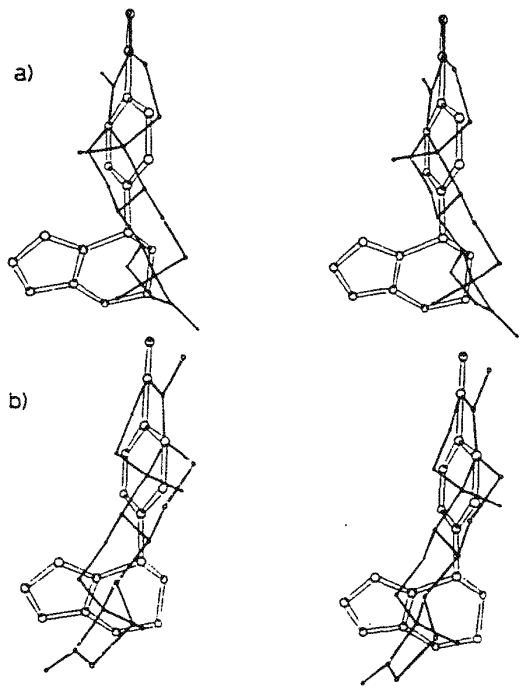


FIGURE 5 Stereodiagrams showing the superposition of CGS 16949A (largest bond radii) on the steroidal inhibitor 4-hydroxy-4-androstene-3,17-dione produced by the least squares fitting. (a) atoms N17, C16, C12 of CGS 16949A on the atoms O3, C3, C5 of the steroid, and (b) N17, C16 and C14 of CGS 16949A on O3, C3, O5 of the steroid. Fit (a) corresponds to the model of Banting *et al.*[11] where the imidazole ring is above the β-face of the steroid. Fit (b) has the imidazole ring above the α-face.

UM00012429
NOVARTIS EXHIBIT 1017
Novartis v. Regents, IPR2023-01346
Page 1175 of 4460

mation is shown in Figure 4. In this conformation the molecule can also be interpreted as having a V-shaped core with the free nitrogen atoms on nearly perpendicular axes. This would suggest that binding to the enzyme involving contacts with the two nitrogen atoms in a similar fashion as for CGS 16949A and CGS 18320B could be possible. Additional studies of the molecular conformations and activity of these and related compounds but especially structural data about the active site of the enzyme are required to further evaulate this hypothesis.

CGS 16949A and CGS 18320B and the other non-steroidal aromatase inhibitors do not resemble the natural substrates or steroidal inhibitors, yet are thought to function by binding in the same active site. The molecular modeling studies of Banting *et al.*[11] included the superposition of the inhibitors with the steroidal inhibitor 4-androstene-3,17-dione. Included was an overlap of CGS 16949A with the steroid based on the superposition of the cyano group of CGS 16949A on the O3 keto group of the steroid. The imidazole ring of CGS 16949A, which is supposed to interact with the haem group in the active site, was found to be placed perpendicular to the steroid and above the B-ring of the steroid. Similar superposition, using the experimentally determined structures of 4-hydroxy-4-androstene-3,17-dione[19] and CGS 16949A, is shown in Figure 5. Although similar to the modeled structure, the experimentally determined structure of CGS 16949A appears to be somewhat longer, placing the imidazole ring perpendicular to the plane of the steroid but above the D-ring rather than above the C-ring as shown by Banting *et al.*[11] This result and the similarities in the overall shape of CGS 19639A and CGS 18320B and especially the consistent distance between the two functional nitrogen atoms appears to support the proposed mechanism of action of the non-steroidal aromatase inhibitors.

Acknowledgements

This research was supported in part by the Ciba-Geigy Corporation and by research grants HD-049445 and RR-05716 from the National Institutes of Health, DHHS.

References

1. Shaw, M.A., Nicholls, P.J. and Smith, H.J. (1988) *J. Ster. Biochem.*, **31**, 137.
2. Brodie, A.M.H. (1985) *Biochem. Pharmacol.*, **34**, 3213.
3. Santner, S.J., Rosen, H., Osawa, Y. and Santen, R.J. (1984) *J. Ster. Biochem.*, **20**, 1239.
4. Osawa, Y., Higashiyama, T., Fronckowiak, M., Yoshida, N. and Yarborough, C. (1987) *J. Ster. Biochem.*, **278**, 781.
5. Goss, P.E., Powles, T.J., Dowsett, M., Hutchinson, G., Brodie, A.M.H., Gazet, J.-C. and Coombes, R.C. (1986) *Cancer Res.*, **46**, 4823.
6. Dowsett, M., Goss, P.E., Powles, T.J., Hutchinson, G., Brodie, A.M.H., Jeffcoate, S.L. and Coombes, R.C. (1987) *Cancer Res.*, **47**, 1957.
7. Santen, R.J., Santner, S., Davis, B., Veldhus, J., Samojlik, E. and Ruby, E. (1978) *J. Clin. Endocrinol. Metab.*, **47**, 1257.
8. Steele, R.E., Mellor, L.B., Sawyer, W.K. and Browne, L.J. (1987) *Steroids*, **50**, 147.
9. Bullion, K.A., Osawa, Y. and Braun, D.G. (1990) *Endocrin. Res.*, **16**, 255.
10. Cole, P.A. and Robinson, C.H. (1990) *J. Med. Chem.*, **33**, 2933.
11. Banting, L., Smith, H.J., James, M., Jones, G., Nazareth, W., Nicholls, P.J., Hewlins, M.J.E. and Rowlands, M.G. (1988) *J. Enz. Inhib.*, **2**, 215.
12. Laughton, C.A., McKenna, R., Neidle, S., Jarman, M., McCague, R. and Rowlands, M.G. (1990) *J. Med. Chem.*, **33**, 2673.
13. Germain, G., Main, P. and Woolfson, M.M. (1971) *Acta Cryst.*, **A27**, 368.
14. Blessing, R.H. (1987) *Crystallogr. Rev.*, **1**, 3.
15. Enraf-Nonius (1979) *Structure Determination Package*. The Netherlands; Delft Enraf-Nonius.

UM00012430
NOVARTIS EXHIBIT 1017
Novartis v. Regents, IPR2023-01346
Page 1176 of 4460

16. Johnson, C.K. (1976) ORTEP-II, Report ORNL-5138. Oak Ridge National Laboratory, Tennessee, USA.
17. Smith, G.D. Personal Communication.
18. Stout, G.H. and Jensen, L.H. (1968) *X-ray Structure Determination*, pp. 457. New York: Macmillan.
19. Griffin, J.F., Strong, P.D., Duax, W.L., Brodie, A.M.H. and Brodie, H.J. (1980) *Acta Cryst.*, **B36**, 201.
20. Van Roey, P., Bullion, K.A., Osawa, Y., Bowman, R.M. and Braun, D.G. (1991) *Acta Cryst.*, in press.
21. Van Roey, P., Bullion, K.A., Osawa, Y. and Braun, D.G. (1991) *Acta Cryst.*, in press.
22. SYBYL, a Molecular Modeling Program. St. Louis, Missouri: TRIPOS Associates, Inc.

UM00012431
NOVARTIS EXHIBIT 1017
Novartis v. Regents, IPR2023-01346
Page 1177 of 4460

This Page is Inserted by IFW Indexing and Scanning Operations and is not part of the Official Record

BEST AVAILABLE IMAGES

Defective images within this document are accurate representations of the original documents submitted by the applicant.

Defects in the images include but are not limited to the items checked:

- ☐ BLACK BORDERS
- ☐ IMAGE CUT OFF AT TOP, BOTTOM OR SIDES
- ☐ FADED TEXT OR DRAWING
- ☐ BLURRED OR ILLEGIBLE TEXT OR DRAWING
- ☐ SKEWED/SLANTED IMAGES
- ☐ COLOR OR BLACK AND WHITE PHOTOGRAPHS
- ☐ GRAY SCALE DOCUMENTS
- ☐ LINES OR MARKS ON ORIGINAL DOCUMENT
- ☐ REFERENCE(S) OR EXHIBIT(S) SUBMITTED ARE POOR QUALITY
- ☐ OTHER: _____

IMAGES ARE BEST AVAILABLE COPY.
As rescanning these documents will not correct the image problems checked, please do not report these problems to the IFW Image Problem Mailbox.

Acta Cryst. (1991). C47, 1015–1018

Structure of *cis*-1-{[4-(1-Imidazolylmethyl)cyclohexyl]methyl}imidazole–Succinic Acid Complex

BY PATRICK VAN ROEY,* KEITH A. BULLION AND YOSHIO OSAWA

Medical Foundation of Buffalo, Inc., 73 High Street, Buffalo, NY 14203, USA

ROBERT M. BOWMAN

CIBA–GEIGY Pharmaceuticals Division, Summit, NJ 07901, USA

AND DIETMAR G. BRAUN

CIBA–GEIGY Limited, CH-4002 Basel, Switzerland

(*Received* 10 *April* 1990; *accepted* 19 *August* 1990)

Abstract. CGS 14796C, $C_{14}H_{20}N_4.C_4H_6O_4$, M_r = 362·43, monoclinic, $C2/c$, a = 28·148 (4), b = 9·722 (1), c = 19·200 (2) Å, β = 133·06 (1)°, V = 3838·88 Å^3, Z = 8, D_x = 1·26 Mg m^{-3}, λ(Cu $K\alpha$) = 1·5418 Å, μ = 0·702 mm^{-1}, $F(000)$ = 1552, T = 294 K, R = 0·075 for all 3285 reflections. The structure is composed of linear chains of alternating CGS 14796C and succinic acid molecules. The CGS 14796C molecule is in an extended conformation.

Introduction. *cis*-1-{[4-(1-Imidazolylmethyl)cyclohexyl]methyl}imidazole–succinic acid [CGS 14796C, (I)] is an active non-steroidal aromatase inhibitor (Schiavo, Green, Triana, Spaet & Zaidi, 1988; Bullion, Osawa & Braun, 1990). Compound (I) is structurally unrelated to the natural substrates of the enzyme or to the clinically used inhibitor aminoglutethimide (II) (Santen, Santner, Davis, Veldhuis, Samojlik & Ruby, 1978; Shaw, Nicholls & Smith, 1988). However, (I) has the imidazole group in common with other potent aromatase inhibitors, CGS 16949A (III) and CGS 18320B (IV) (Steele, Meller, Sawyer & Brown, 1987), as shown in Fig. 1. The crystal structures of these compounds are being determined as part of on-going structure–activity studies of non-steriodal aromatase inhibitors (Van Roey, Bullion, Osawa, Browne, Bowman & Braun, 1990; Van Roey, Bullion, Osawa, Bowman & Braun, 1991).

Experimental. The sample was provided by the Ciba–Geigy Corporation. Crystals were obtained by slow evaporation over a period of about 6 weeks of a 3 ml methanol solution containing approximately 20 mg of compound. The sample was kept in a glass vial, sealed with a plastic cap and placed in a walk-in hot room at 310 (1) K. Very slow evaporation at high temperature yields excellent quality crystals for all compounds in this series and many other compounds. However, the benefits or effects of crystallization at the elevated temperature over room temperature have not been further evaluated. The crystal used for data collection had approximate dimensions 0·30 × 0·35 × 0·35 mm. Oscillation and Weissenberg photographs were used to determine the crystal system and preliminary cell dimensions. Systematic absences (hkl, $h+k \neq 2n$; $h0l$, $h,l \neq 2n$) are consistent with the space groups $C2/c$ or Cc. A body-centred orthorhombic cell was also consistent with the orientation angles but not with the diffraction pattern observed on the photographs. Equivalent reflections (hkl and $\bar{h}kl$) of the orthorhombic cell had different intensities. The highest symmetry monoclinic space group was selected for the first structure determination attempt and proved to be correct. Enraf–Nonius CAD-4 diffractometer, Cu $K\alpha$ radiation (λ = 1·5418 Å), Ni filter, $\theta/2\theta$ scan method. Unit-cell dimensions and orientation matrix

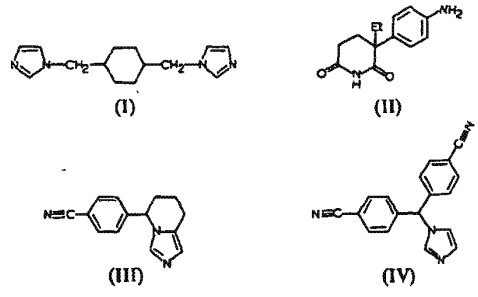


Fig. 1. Schematic diagrams of the structures of the non-steroidal aromatase inhibitors: (I), CGS 14796C, the title compound; (II), aminoglutethimide; (III), CGS 16949A; and (IV), CGS 18320B.

* Author to whom correspondence should be addressed.

0108-2701/91/051015-04$03.00

© 1991 International Union of Crystallography

UM00012433
NOVARTIS EXHIBIT 1017
Novartis v. Regents, IPR2023-01346
Page 1179 of 4460

were determined from 25 reflections with $41{\cdot}66 < 2\theta < 58{\cdot}76°$. 5373 total data with $3{\cdot}0 < 2\theta < 154{\cdot}0°$, $-35 < h < 35$, $0 < k < 12$, $-1 < l < 24$. Intensities of six standard reflections ($\bar{3}19$, $\bar{1}1,1,2$, 912, 533, $\bar{1}3,3,9$, 261) were monitored every 3 h but did not decline significantly. Orientation checks were made after every 400th intensity measurement. Lorentz and polarization corrections were applied but an absorption correction was not considered necessary. Of the 3992 unique data ($R_{int} = 0{\cdot}025$), 3290 had $F > 3\sigma(F)$. $\sigma(F)$ was calculated according to Stout & Jensen (1968): $\sigma^2(F) = (k/4\mathrm{Lp}I)[\sigma^2(I) + (0{\cdot}01I)^2]$. The structure was determined by direct methods using the program *MULTAN* (Germain, Main & Woolfson, 1971) and refined by full-matrix least squares, minimizing $\sum[w(F_o - F_c)^2]$ where $w = 1/\sigma^2(F)$ for the data with $F > 3\sigma(F)$. Coordinates for all H atoms, except the one bonded to O(25), were determined from difference maps and refined with the non-H atoms after the anisotropic refinement had converged. The maximum value of the shift/e.s.d. during the last cycle of refinement was 0·04. Two reflections were considered mismeasurements on the basis of a δR plot (Abrahams & Keve, 1971) and not included in the refinement during the last cycles. Final R values are $R = 0{\cdot}067$, $wR = 0{\cdot}078$ for the 3285 data included in the refinement (335 parameters) and $R_{all} = 0{\cdot}075$ for all 3992 data; $S = 3{\cdot}091$. The R values are somewhat higher than expected because of the higher thermal motion or disorder of the succinic acid molecule and because of high correlations caused by the large β angle. 45 correlation coefficients were greater than 0·75. O(26) has the highest thermal parameter and the two largest positive (0·520 and 0·379 e Å^{-3}) and the most negative ($-0{\cdot}664$ e Å^{-3}) peaks in the final difference map are within 1·5 Å from it. The remaining maximum and minimum densities of the map are 0·301 and $-0{\cdot}303$ e Å^{-3}. Atomic scattering factors and dispersion corrections were taken from *International Tables for X-ray Crystallography* (1974, Vol. IV, pp. 71–147). Other programs used include Blessing's (1987) data reduction package, locally modified refinement and structure analysis programs based on programs in the Enraf–Nonius *SDP* package (1979), and the plotting program *ORTEP*II (Johnson, 1976).

Discussion. Atomic coordinates and equivalent isotropic thermal parameters are listed in Table 1.* Fig. 2 shows the molecular conformation of (I) and the numbering scheme used. Selected bond lengths, bond angles and torsion angles are listed in Table 2. The structure is described as the complex of (I) with succinic acid, rather than the ion pair because H(19) is closer to O(19) than to N(16). The hydrogen bonds between the molecules are very strong. The hydrogen bond geometry is as follows: O(19)—H(19)···N(16) (x, y, z): O···N 2·610 (5), O—H 1·28 (7), H···N 1·35 (7) Å, O—H···N 167 (3)°; and O(25)···N(4)(x, y, $-1 + z$): O···N 2·648 (4) Å. The long O(19)—H(19) bond length may be a result of the strength of the hydrogen bond. The H atom of the other bond, O(25)···N(4), could not be located. A complex of neutral molecules was also observed in the structure of (IV) which was also determined as the complex with succinic acid (Van Roey, Bullion, Osawa, Browne, Bowman & Braun, 1990).

Table 1. *Atomic coordinates* ($\times 10^4$ *for non-*H *atoms;* $\times 10^3$ *for* H *atoms*) *and equivalent isotropic thermal parameters* (Å$^2 \times 10$) *for the succinic acid complex of* (I); *e.s.d.'s are given in parentheses*

$B_{eq} = (1/3)\sum_i\sum_j B_{ij} a_i^* a_j^* \mathbf{a}_i.\mathbf{a}_j$.

	x	y	z	B_{eq}
C(2)	7487 (2)	2190 (3)	3426 (2)	56 (2)
C(3)	7804 (2)	2308 (4)	4359 (3)	67 (2)
C(5)	8273 (1)	3683 (4)	4125 (2)	60 (2)
C(6)	7675 (2)	3250 (3)	2429 (2)	56 (2)
C(7)	7851 (1)	1978 (3)	2188 (2)	45 (1)
C(8)	7742 (1)	2228 (4)	1305 (2)	55 (1)
C(9)	7894 (1)	960 (3)	1022 (2)	56 (1)
C(10)	8569 (1)	395 (3)	1831 (2)	47 (1)
C(11)	8693 (2)	223 (3)	2733 (2)	56 (2)
C(12)	8549 (1)	1521 (3)	3010 (2)	48 (1)
C(13)	9098 (1)	1269 (3)	2024 (2)	48 (1)
C(15)	9141 (1)	2033 (3)	813 (2)	53 (1)
C(17)	9329 (2)	129 (4)	487 (2)	61 (2)
C(18)	9267 (1)	−170 (3)	1106 (2)	53 (2)
N(1)	7795 (1)	3077 (2)	3293 (1)	49 (1)
N(4)	8297 (1)	3255 (3)	4792 (2)	67 (1)
N(14)	9145 (1)	1056 (2)	1315 (1)	43 (1)
N(16)	9248 (1)	1508 (3)	302 (2)	60 (1)
C(20)	9471 (1)	3515 (3)	−954 (2)	50 (1)
C(22)	9888 (2)	4073 (4)	−1116 (2)	65 (2)
C(23)	9527 (2)	4902 (3)	−2014 (2)	56 (2)
C(24)	9173 (1)	4055 (3)	−2889 (2)	57 (2)
O(19)	9759 (1)	2544 (2)	−315 (1)	71 (1)
O(21)	8945 (1)	3972 (2)	−1330 (1)	66 (1)
O(25)	8898 (1)	4749 (3)	−3650 (2)	85 (2)
O(26)	9144 (3)	2841 (3)	−2905 (2)	115 (3)
H(2)	717 (1)	180 (3)	302 (2)	54 (7)
H(3)	769 (1)	185 (3)	468 (2)	80 (8)
H(5)	855 (1)	437 (3)	417 (2)	76 (8)
H(6a)	794 (2)	400 (4)	258 (2)	94 (10)
H(6b)	718 (2)	348 (3)	187 (2)	85 (8)
H(7)	751 (1)	121 (2)	198 (2)	51 (5)
H(8a)	729 (2)	253 (3)	74 (2)	95 (9)
H(8b)	802 (1)	299 (3)	146 (2)	61 (7)
H(9a)	755 (2)	27 (3)	79 (2)	87 (9)
H(9b)	779 (1)	118 (3)	39 (2)	68 (7)
H(10)	858 (1)	−45 (2)	165 (2)	45 (5)
H(11a)	843 (1)	−59 (3)	262 (2)	80 (8)
H(11b)	908 (2)	−5 (3)	326 (2)	80 (9)
H(12a)	886 (1)	231 (3)	323 (2)	52 (6)
H(12b)	861 (1)	130 (2)	356 (2)	41 (5)
H(13a)	898 (1)	231 (3)	196 (2)	51 (5)
H(13b)	949 (1)	108 (3)	260 (2)	59 (6)
H(15)	902 (1)	299 (3)	79 (2)	69 (7)
H(17)	941 (2)	−44 (3)	20 (2)	77 (8)
H(18)	927 (2)	−99 (3)	139 (2)	83 (9)
H(O19)	944 (2)	210 (4)	−10 (3)	131 (12)
H(22a)	1008 (2)	334 (3)	−114 (2)	78 (9)
H(22b)	1024 (2)	489 (5)	−47 (3)	139 (14)
H(23a)	919 (2)	558 (4)	−210 (3)	107 (11)
H(23b)	983 (1)	559 (3)	−196 (2)	71 (7)

* Lists of structure factors, anisotropic thermal parameters, full bond lengths and angles, and torsion angles have been deposited with the British Library Document Supply Centre as Supplementary Publication No. SUP 53492 (36 pp.). Copies may be obtained through The Technical Editor, International Union of Crystallography, 5 Abbey Square, Chester CH1 2HU, England.

LIM00012434
NOVARTIS EXHIBIT 1017
Novartis v. Regents, IPR2023-01346
Page 1180 of 4460

Table 2. *Selected bond lengths* (Å), *bond angles* (°) *and torsion angles* (°) *for the succinic acid complex of* (I)

C(2)—N(1)	1·336 (6)	C(2)—C(3)	1·354 (6)
C(3)—N(4)	1·373 (5)	C(5)—N(1)	1·331 (3)
C(5)—N(4)	1·304 (6)	C(13)—N(14)	1·467 (5)
C(6)—N(1)	1·459 (6)	C(15)—N(14)	1·348 (5)
C(15)—N(16)	1·310 (6)	C(17)—N(16)	1·366 (4)
C(17)—C(18)	1·344 (7)	C(18)—N(14)	1·375 (4)
C(20)—O(19)	1·301 (3)	C(23)—C(24)	1·486 (4)
C(20)—O(21)	1·205 (4)	C(24)—O(25)	1·282 (4)
C(20)—C(22)	1·506 (7)	C(24)—O(26)	1·182 (4)
C(22)—C(23)	1·504 (5)		
N(1)—C(2)—C(3)	105·3 (3)	C(13)—N(14)—C(18)	126·3 (2)
N(1)—C(5)—N(4)	111·7 (2)	N(14)—C(15)—N(16)	111·6 (2)
C(2)—C(3)—N(4)	109·8 (3)	N(16)—C(17)—C(18)	110·0 (3)
C(2)—N(1)—C(6)	127·0 (2)	C(15)—N(16)—C(17)	105·7 (2)
C(3)—N(4)—C(5)	105·4 (3)	C(13)—N(14)—C(15)	127·0 (2)
C(2)—N(1)—C(5)	107·8 (2)	C(15)—N(14)—C(18)	106·4 (2)
C(5)—N(1)—C(6)	125·0 (2)	N(14)—C(18)—C(17)	106·3 (2)
O(19)—C(20)—O(21)	123·4 (2)	O(19)—C(20)—C(22)	112·7 (2)
C(23)—C(24)—O(25)	114·4 (3)	O(21)—C(20)—C(22)	123·8 (2)
C(23)—C(24)—O(26)	124·3 (3)	O(25)—C(24)—O(26)	121·2 (3)
C(7)—C(6)—N(1)—C(5)	108·1 (4)	C(11)—C(10)—C(13)—N(14)	158·9 (3)
C(7)—C(6)—N(1)—C(2)	−65·4 (4)	C(9)—C(10)—C(13)—N(14)	−76·2 (3)
N(1)—C(6)—C(7)—C(8)	−177·9 (3)	C(10)—C(13)—N(14)—C(15)	128·4 (3)
N(1)—C(6)—C(7)—C(12)	−54·8 (4)	C(10)—C(13)—N(14)—C(18)	−58·8 (4)
O(19)—C(20)—C(22)—C(23)	164·1 (3)	C(22)—C(23)—C(24)—O(25)	−175·7 (3)
O(21)—C(20)—C(22)—C(23)	−20·2 (5)	C(22)—C(23)—C(24)—O(26)	3·3 (6)
C(20)—C(22)—C(23)—C(24)	−79·5 (4)		

Both imidazole rings are very planar with r.m.s deviations from planarity of 0·025 and 0·026 Å for the rings containing N(1) and N(14), respectively. The cyclohexyl ring has a nearly perfect chair conformation with no torsion angle differing by more than 4·8° from the average value of 54·4 (7)°. One of the imidazolylmethyl substituents, C(6), is equatorial and the other, C(13), is axial. The links between the cyclohexyl ring and the imidazolylmethyl substituents are in extended conformations, especially at the side of the equatorial substitution. The C(6)—N(1) bond is *trans* to the endocyclic C(7)—C(8) bond, while the N(14)—C(13) bond deviates by about 20° from coplanarity with C(10)—C(11). The angle between the planes of the imidazole rings is 120·1 (7)°.

The C(23)—C(24), C(24)—O(25) and C(24)—O(26) bond lengths appear significantly shortened, owing to the high thermal motion of that part of the succinic acid molecule. The angle between the two planar carboxyl groups is 92·2 (9)°.

Fig. 3 shows the crystal packing. The structure is composed of helical chains along the *c* axis of alternating molecules of (I) and succinic acid connected by strong hydrogen bonds as described earlier. No other intermolecular contacts shorter than 3·45 Å are observed.

Banting *et al.* (1988) proposed that imidazole-containing non-steroidal aromatase inhibitors bind in the active site in the place of the *A* ring of the steroid and that this would position the imidazole ring in a plane perpendicular to the steroid location and allow for interaction of the imidazole nitrogen with the haem group in the active site of the enzyme. It is conceivable that compound (I) could bind in the place of the steroid molecule but the observed conformation is not consistent with the required imidazole orientation.

The analysis of the structures of the more rigid compounds (III) and (IV) (Van Roey, Bullion, Osawa, Browne, Bowman & Braun, 1990) showed that both compounds have N atoms at the extreme ends of the molecules that are between 8·5 and 9·0 Å apart. This arrangement may be important for the interaction of the inhibitors with the enzyme. The distance between the two free imidazole N atoms in (I) is 10·77 (1) Å. However, distance map calculations using *SYBYL* (Tripos Associates, Inc., 1988) have shown that conformations that have N(4)···N(16) distances between 8·25 and 9·0 Å are accessible without obvious increases in molecular energy (P. Van Roey, unpublished work). Therefore, although (I) differs substantially in structure from other inhibitors, it could bind in a similar manner as (III) and (IV).

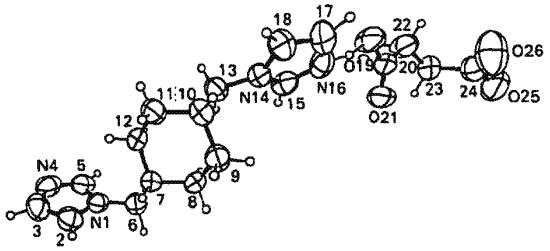


Fig. 2. Structure of the succinic acid complex of (I), showing the numbering scheme used in the text. Thermal ellipsoids are shown at 50% probability levels.

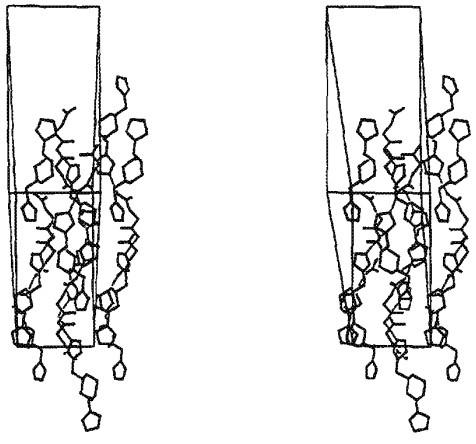


Fig. 3. Stereo packing diagram of the succinic acid complex of (I) viewed approximately down the *a* axis. The *c* axis is vertical and the *b* axis is horizontal. Note the helical strings of alternating donor and acceptor molecules parallel with the *c* axis.

UM00012435
NOVARTIS EXHIBIT 1017
Novartis v. Regents, IPR2023-01346
Page 1181 of 4460

Research supported in part by the Ciba–Geigy Corporation and by grant RR-05716 from the National Institutes of Health, DHHS.

References

ABRAHAMS, S. C. & KEVE, E. T. (1971). *Acta Cryst.* A27, 157–165.

BANTING, L., SMITH, H. J., JAMES, M., JONES, G., NAZARETH, W., NICHOLLS, P. J., HEWLINS, M. J. E. & ROWLANDS, M. G. (1988). *J. Enzyme Inhib.* 2, 215–229.

BLESSING, R. H. (1987). *Crystallogr. Rev.* 1, 3–57.

BULLION, K. A., OSAWA, Y. & BRAUN, D. G. (1990). *Endocrinol. Res.* 16, 255–267.

Enraf–Nonius (1979). *Structure Determination Package*. Enraf–Nonius, Delft, The Netherlands.

GERMAIN, G., MAIN, P. & WOOLFSON, M. M. (1971). *Acta Cryst.* A27, 368–376.

JOHNSON, C. K. (1976). *ORTEPII*. Report ORNL-5138. Oak Ridge National Laboratory, Tennessee, USA.

SANTEN, R. J., SANTNER, S., DAVIS, B., VELDHUIS, J., SAMOJLIK, E. & RUBY, E. (1978). *J. Clin. Endocrinol. Metab.* 47, 1257–1265.

SCHIAVO, D. M., GREEN, J. D., TRIANA, V. M., SPAET, R. & ZAIDI, I. (1988). *Fundam. Appl. Toxicol.* 10, 329–334.

SHAW, M. A., NICHOLLS, P. J. & SMITH, H. J. (1988). *J. Steriod Biochem.* 31, 137–146.

STEELE, R. E., MELLER, L. B., SAWYER, W. K. & BROWN, L. J. (1987). *Steroids*, 50, 147–161.

STOUT, G. H. & JENSEN, L. H. (1968). *X-ray Structure Determination*, pp. 457. New York: Macmillan.

Tripos Associates, Inc. (1988). *SYBYL*. A molecular modeling program. Tripos Associates, Inc., St Louis, Missouri, USA.

VAN ROEY, P., BULLION, K. A., OSAWA, Y., BOWMAN, R. M. & BRAUN, D. G. (1991). *Acta Cryst.* C47, 829–832.

VAN ROEY, P, BULLION, K. A., OSAWA, Y., BROWNE, L. J., BOWMAN, R. M. & BRAUN, D. G. (1990). *J. Enzyme Inhibit.* In the press.

Acta Cryst. (1991). C47, 1018–1021

Structure of Sodium 1,2,3,4-Thiatriazole-5-thiolate Dihydrate and 5-Benzoylthio-1,2,3,4-thiatriazole

BY CRAIG A. PERMAN AND W. B. GLEASON*

Corporate Research Laboratories, 3M Company, 3M Center, St Paul, MN 55144, USA

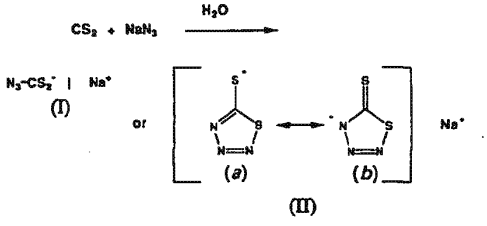
(*Received* 5 *January* 1990; *accepted* 28 *August* 1990)

Abstract. Sodium 1,2,3,4-thiatriazole-5-thiolate (*A*) dihydrate, $Na^+.CS_2N_3^-.2H_2O$, $M_r = 177{\cdot}18$, monoclinic, $P2_1/n$, $a = 5{\cdot}821\ (2)$, $b = 18{\cdot}494\ (7)$, $c = 6{\cdot}786\ (3)$ Å, $\beta = 114{\cdot}84\ (3)°$, $V = 663{\cdot}0$ Å^3, $Z = 4$, $D_x = 1{\cdot}77$ g cm^{-3}, λ(Mo $K\alpha$) = 0·71073 Å, $\mu = 7{\cdot}6$ cm^{-1}, $F(000) = 360$, $T = 173\ (1)$ K, $R = 0{\cdot}024$ for 1160 observed reflections. 5-Benzoylthio-1,2,3,4-thiatriazole (*B*), $C_8H_5N_3OS_2$, $M_r = 223{\cdot}28$, triclinic, $P\bar{1}$, $a = 7{\cdot}420\ (3)$, $b = 11{\cdot}115\ (2)$, $c = 5{\cdot}642\ (1)$ Å, $\alpha = 91{\cdot}50\ (2)$, $\beta = 98{\cdot}42\ (2)$, $\gamma = 79{\cdot}68\ (2)°$, $V = 452{\cdot}8$ Å^3, $Z = 2$, $D_x = 1{\cdot}64$ g cm^{-3}, λ(Mo $K\alpha$) = 0·71073 Å, $\mu = 5{\cdot}3$ cm^{-1}, $F(000) = 228$, $R = 0{\cdot}026$ for 1435 observed reflections. The structure of the reaction product of sodium azide and carbon disulfide is unequivocally established as (*A*). The exocyclic C—S bond length is 1·704 (1) Å in contrast with the bond length of 1·580 Å predicted by MNDO methods [Conti, Franco & Trsic (1986). *Inorg. Chim. Acta*, 113, 71–74]. Benzoylation of (*A*) is established to occur at the exocyclic S atom rather than at an N atom of the thiatriazole ring, yielding (*B*).

* To whom correspondence should be addressed: Department of Biochemistry, University of Minnesota, Minneapolis, MN 55455, USA.

0108-2701/91/051018-04$03.00 © 1991 International Union of Crystallography

Introduction. Brown & Hoel (1922) reported the reaction of carbon disulfide and sodium azide to give what was thought to be an azidodithiocarbamate (I). From infrared spectroscopic measurements Lieber, Pilli, Ramachandran & Hites (1957) concluded that the reaction product was actually the 1,2,3,4-thiatriazole-5-thiolate anion (II). Discussion has continued concerning the structure of (II) and its protonated form as to whether the thiol (II*a*) or the thione (II*b*) structure is the major resonance contributor (Lieber, Oftedahl & Rao, 1961; Christopherson & Holm, 1971); L'abbe, Toppet, Willocx & Mathys, 1977). Recently the MNDO method has been applied to the problem and Conti, Franco &



(II)

UM00012436
NOVARTIS EXHIBIT 1017
Novartis v. Regents, IPR2023-01346
Page 1182 of 4460

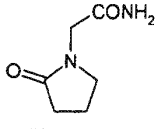
Crystal engineering of pharmaceutical co-crystals from polymorphic active pharmaceutical ingredients†

Peddy Vishweshwar,[a] Jennifer A. McMahon,[a] Matthew L. Peterson,[b] Magali B. Hickey,[b] Tanise R. Shattock[a] and Michael J. Zaworotko*[a]

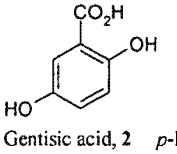
Received (in Columbia, MO, USA) 25th January 2005, Accepted 18th July 2005
First published as an Advance Article on the web 15th August 2005
DOI: 10.1039/b501304f

The carboxylic acid–primary amide supramolecular heterosynthon is exploited for the generation of pharmaceutical co-crystals that contain two active pharmaceutical ingredients that are polymorphic in their pure forms.

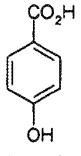
That crystal engineering has matured into a form of supramolecular synthesis is the consequence of several decades of research focused upon gaining a better understanding of the forces that sustain and direct crystal structures.[1] The fundamental precept of crystal engineering is that crystals are in effect "supermolecules",[2] the result of a series of directional, and therefore predictable, molecular recognition events or supramolecular synthons.[3] A salient feature of crystal engineered structures is that they are designed from first principles and can therefore consist of a diverse range of chemical components as exemplified by coordination polymers (*i.e.*, metals and organic ligands),[4] polymers sustained by organometallic linkages[5] and hydrogen bonded organic networks.[1d,e,6] Active pharmaceutical ingredients, APIs, are extremely valuable materials so it is perhaps surprising that crystal engineering has only recently addressed APIs *via* development of a fourth class of API, pharmaceutical co-crystals.[7] Whereas co-crystals have long been known as *addition compounds*[8] or *organic molecular compounds*[9] the Cambridge Structural Database, CSD,[10] indicates that they remain relatively unexplored with very few entries prior to 1960 and even now there are only *ca.* 1450 hydrogen bonded co-crystals *vs.* almost 35,000 hydrates. The potential benefits of co-crystals include the generation of novel NLO materials,[11] solvent-free organic synthesis,[12] modification of photographic films[13] and formulation of APIs,[7,14] which is the focus of this contribution.



Piracetam, **1**



Gentisic acid, **2**



p-Hydroxybenzoic acid, **3**

Pharmaceutical co-crystals, *i.e.*, co-crystals that are formed between an API and a co-crystal former that is a solid under ambient conditions, represent a new paradigm in API formulation that might address important intellectual and physical property issues in the context of drug development and delivery. In this contribution we demonstrate how the carboxylic acid–primary amide supramolecular heterosynthon[7c] can be exploited to generate pharmaceutical co-crystals of a polymorphic API, piracetam, **1**,[15] in which the co-crystal formers are also polymorphic and APIs in their own right: gentisic acid, **2**,[16] and *p*-hydroxybenzoic acid, **3**.[17]

Piracetam, (2-oxo-1-pyrrolidinyl)acetamide, **1**, is a nootropic drug that works to boost intelligence by stimulating the central nervous system.[18] Four polymorphic forms of **1** have been reported[15] although only three, refcode BISMEV, have been deposited in the CSD. No co-crystals, solvates or hydrates have been reported although one study suggests that **1** may exhibit as many as 6 polymorphs.[19] Gentisic acid, 2,5-dihydroxybenzoic acid, **2**, is an aspirin metabolite that exhibits NSAID activity.[20] Gentisic acid exhibits two polymorphic forms[21] and forms co-crystals with piperazine-2,5-dione and L-proline.[22] Single crystals of the 1:1 co-crystal of piracetam and gentisic acid, **4**, were obtained *via* slow evaporation from acetonitrile. Co-crystal **4** can also be prepared *via* grinding or slurrying in water. Co-crystal **4** was characterized by IR, melting point, DSC, PXRD and single crystal X-ray diffraction.[23] The carboxylic acid–amide supramolecular heterosynthon has been long documented[24] and 71 of the 153 structures in the CSD that contain both a carboxylic acid and a primary amide are sustained by this interaction. It would therefore be unsurprising if the acid–amide supramolecular heterosynthon were to occur in **4** and, as revealed by Fig. 1a, this is indeed the case. The remaining H-bond donors are satisfied as follows: the 2-hydroxy group of gentisic acid forms an intramolecular hydrogen bond and acts an acceptor to the *anti*-oriented NH of the primary amide; the 5-hydroxy group of gentisic acid serves as a hydrogen bond donor to the ring carbonyl of piracetam (Fig. 1b). The resulting network exhibits 4,4-topology and it is 2-fold interpenetrated (Fig. 1c).

Piracetam also forms a 1:1 co-crystal with *p*-hydroxybenzoic acid, **5**. Co-crystal **5** can be crystallized from acetonitrile *via* slow evaporation. Co-crystal **5** can also be prepared *via* grinding or slurrying in water. The crystal structure of **5**[25] reveals the presence of the acid–amide supramolecular heterosynthon which in turn dimerizes to form a tetrameric motif sustained by N–H···O hydrogen bonding (Fig. 2). This tetrameric motif is found in 10 (14%) of the 71 structures in the CSD that contain acid–amide supramolecular heterosynthons.[26] The ring carbonyl of piracetam molecules and the hydroxy group of **3** H-bond each tetramer to four others, thereby affording a 3-fold interpenetrated network.

[a]*Department of Chemistry, University of South Florida, SCA 400, 4202 E. Fowler Avenue, Tampa, Florida, USA. E-mail: xtal@usf.edu; Fax: +1 813 974 3203; Tel: +1 813 974 4129*
[b]*TransForm Pharmaceuticals, Inc., 29 Hartwell Avenue, Lexington, Massachusetts, 02421, USA*
† Electronic supplementary information (ESI) available: Experimental details of solvent drop grinding, PXRD spectra and interpenetration in **5**. See http://dx.doi.org/10.1039/b501304f

This journal is © The Royal Society of Chemistry 2005

UM00012437
NOVARTIS EXHIBIT 1017
Novartis v. Regents, IPR2023-01346
Page 1183 of 4460

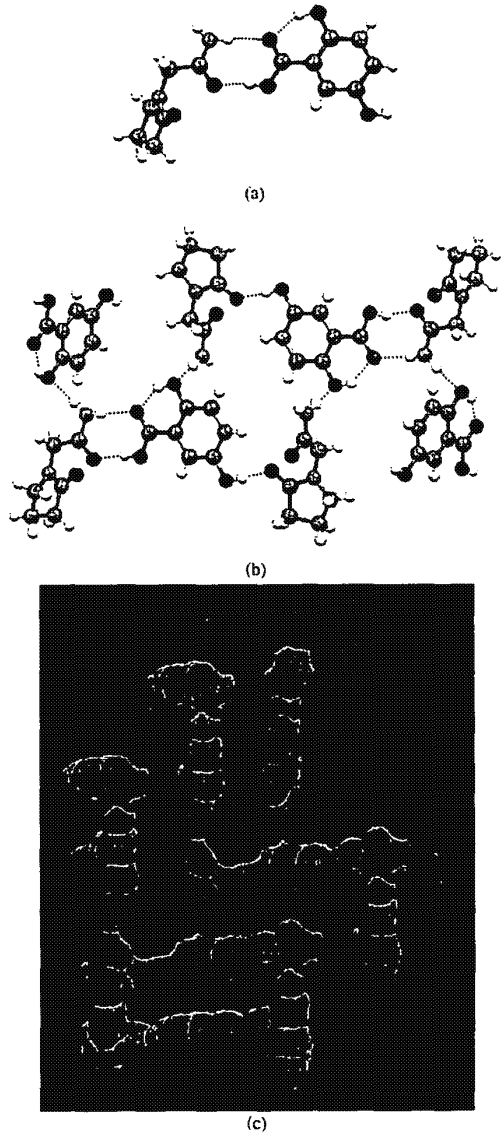


Fig. 1 (a) The carboxylic acid–amide supramolecular heterosynthon in the 1:1 co-crystal of piracetam and gentisic acid, **4**. Structural parameters: $O–H_{acid}\cdots O$ = 2.590(15) Å, $N–H_{syn}\cdots O$ = 2.907(18) Å, $N–H_{anti}\cdots O$ = 2.944(19) Å. (b) A portion of the hydrogen bond network in **4**. (c) A space-filling model of the 2-fold interpenetration that occurs in **4**.

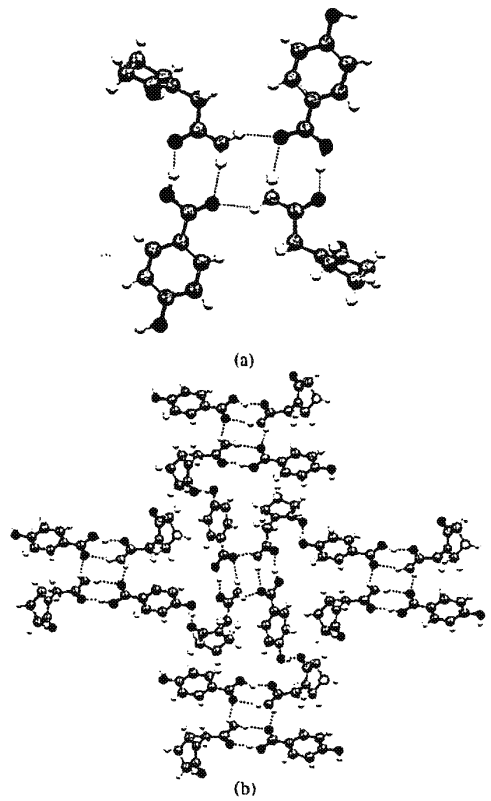


Fig. 2 (a) The carboxylic acid–amide supramolecular heterosynthon in the tetrameric motif that sustains **5**. Structural parameters: $O–H_{acid}\cdots O$ = 2.598(3)Å, $N–H_{syn}\cdots O$ = 2.955(3) Å, $N–H_{anti}\cdots O$ = 2.908(3) Å. (b) A portion of the hydrogen bond network in **5**.

That APIs are promiscuous in the context of polymorphism is a critical issue for the pharmaceutical industry:[27] from a regulatory perspective it has been established that bioactivity can change between forms; from an intellectual property perspective, polymorphic forms are established in law as discrete materials and new forms can be patented. We have therefore investigated the general occurrence of polymorphism in existing co-crystals. A CSD search revealed only eleven examples of polymorphism in hydrogen bonded co-crystals for which coordinates are available for two or more forms.[28] Interestingly, the polymorphism in these eleven co-crystals can be attributed to conformational flexibility or different packing between layers, *i.e.*, the hydrogen bonded supramolecular synthons are consistent. Co-crystals **4** and **5** were therefore screened for the existence of polymorphs using solvent-drop grinding, a technique that has been shown to be able to generate and control polymorphism.[29] Mechanical grinding experiments were conducted in reaction vessels by adding gentisic acid or *p*-hydroxybenzoic acid to solid piracetam form A. A group of 23 solvents (water, acetone, methanol, ethanol, ethyl acetate, *n*-hexane, toluene, acetonitrile, tetrahydrofuran, isopropyl acetate, benzyl alcohol, nitromethane, dimethyl amine, 2-butanol, ethyl formate, acetic acid, methyl ethyl ketone, methyl *tert*-butyl ether, chlorobenzene, *N*-methyl pyrrolidone, 1,2-dichloroethane, dimethyl sulfoxide and dimethoxyethane) was evaluated by adding a different solvent to each well. The samples were ground for 20 minutes and characterized using powder X-ray diffraction. Co-crystals **4** and **5** were also obtained by slurrying 0.62 mmol of piracetam and 0.62 mmol of gentisic acid or *p*-hydroxybenzoic acid in water (100μL) for 60 or 16 hours, respectively. Co-crystals **4** or **5** were obtained from all grinding and slurrying reactions as a mixture with one or both of the starting materials, *i.e.*, co-crystals **4** and **5** do not exhibit polymorphism based on a series of solvent-mediated grinding experiments (See ESI for experimental details and PXRD spectra†).

In summary, we address herein the use of supramolecular heterosynthons, in particular the carboxylic acid–primary amide

This journal is © The Royal Society of Chemistry 2005

UM00012438
NOVARTIS EXHIBIT 1017
Novartis v. Regents, IPR2023-01346
Page 1184 of 4460

dimer, to crystal engineer pharmaceutical co-crystals from pairs of APIs that are polymorphic in their pure forms. An analysis of the CSD and evaluation of new pharmaceutical co-crystals suggests that these co-crystals are robust enough to be prepared *via* solution, slurry or solid-state methods and that they appear to be less prone to polymorphism than the corresponding single component APIs. However, it should be stressed that the amount of data available concerning the extent of polymorphism in co-crystals remains minimal and that one will not be able to make definitive conclusions even if exhaustive high throughput screenings are conducted.

Notes and references

‡ See http://dx.doi.org/10.1039/b501304f for crystallographic data in CIF or other electronic format.

1 (*a*) G. M. J. Schmidt, *Pure Appl. Chem.*, 1971, **27**, 647; (*b*) F. H. Allen, O. Kennard and R. Taylor, *Acc. Chem. Res.*, 1983, **16**, 146; (*c*) G. R. Desiraju, *Crystal Engineering: the Design of Organic Solids*, Elsevier, Amsterdam, 1989; (*d*) M. C. Etter, *Acc. Chem. Res.*, 1990, **23**, 120; (*e*) C. B. Aakeröy, *Acta Crystallogr., Sect. B: Struct. Sci.*, 1997, **53**, 569.

2 J. D. Dunitz, *Perspect. Supramol. Chem.*, 1996, **2**, 1.

3 G. R. Desiraju, *Angew. Chem., Int. Ed. Engl.*, 1995, **34**, 2311.

4 (*a*) B. Moulton and M. J. Zaworotko, *Chem. Rev.*, 2001, **101**, 1629; (*b*) B. F. Hoskins and R. Robson, *J. Am. Chem. Soc.*, 1990, **112**, 1546; (*c*) M. Eddaoudi, D. B. Moler, H. L. Li, B. L. Chen, T. M. Reineke, M. O'Keeffe and O. M. Yaghi, *Acc. Chem. Res.*, 2001, **34**, 319; (*d*) S. Kitagawa, R. Kitaura and S. Noro, *Angew. Chem. Int. Ed.*, 2004, **43**, 2334; (*e*) C. Janiak, *Dalton Trans.*, 2003, 2781; (*f*) S. L. James, *Chem. Soc. Rev.*, 2003, 276.

5 M. Oh, G. B. Carpenter and D. A. Sweigart, *Angew. Chem. Int. Ed.*, 2003, **42**, 2026.

6 M. W. Hosseini, *Coord. Chem. Rev.*, 2003, **240**, 157.

7 (*a*) Ö. Almarsson and M. J. Zaworotko, *Chem. Commun.*, 2004, 1889; (*b*) R. B. Walsh, M. W. Bradner, S. Fleischman, L. A. Morales, B. Moulton, N. Rodriguez-Hornedo and M. J. Zaworotko, *Chem. Commun.*, 2003, 186; (*c*) S. G. Fleischman, S. S. Kuduva, J. A. McMahon, B. Moulton, R. D. B. Walsh, N. Rodriguez-Hornedo and M. J. Zaworotko, *Cryst. Growth Des.*, 2003, **3**, 909; (*d*) J. A. McMahon, J. A. Bis, P. Vishweshwar, T. R. Shattock, O. L. McLaughlin and M. J. Zaworotko, *Z. Kristallogr.*, 2005, **220**, 340; (*e*) J. F. Remenar, S. L. Morissette, M. L. Peterson, B. Moulton, J. M. MacPhee, H. R. Guzman and Ö. Almarsson, *J. Am. Chem. Soc.*, 2003, **125**, 8456; (*f*) S. L. Morissette, Ö. Almarsson, M. L. Peterson, J. F. Remenar, M. J. Read, A. V. Lemmo, S. Ellis, M. J. Cima and C. R. Gardner, *Adv. Drug Delivery Rev.*, 2004, **56**, 275; (*g*) S. L. Childs, L. J. Chyall, J. T. Dunlap, V. N. Smolenskaya, B. C. Stahly and P. G. Stahly, *J. Am. Chem. Soc.*, 2004, **126**, 13335; (*h*) G. Bettinetti, M. R. Caira, A. Callegari, M. Merli, M. Sorrenti and C. Tadini, *J. Pharm. Sci.*, 2000, **89**, 478; (*i*) J. A. Zerkowski, J. C. MacDonald and G. M. Whitesides, *Chem. Mater.*, 1997, **9**, 1933.

8 J. S. Buck and W. S. Ide, *J. Am. Chem. Soc.*, 1931, **53**, 2784.

9 (*a*) A. R. Ling and J. L. Baker, *J. Chem. Soc. Trans.*, 1893, **63**, 1314; (*b*) J. S. Anderson, *Nature*, 1937, **140**, 583.

10 F. H. Allen and O. Kennard, *Chemical Design Automation News*, 1993, **8**, 31.

11 K. Huang, D. Britton, M. C. Etter and S. R. Byrn, *J. Mater. Chem.*, 1997, **7**, 713.

12 (*a*) K. Tanaka and F. Toda, *Chem. Rev.*, 2000, **100**, 1025; (*b*) J. N. Gamlin, R. Jones, M. Leibovitch, B. Patrick, J. R. Scheffer and J. Trotter, *Acc. Chem. Res.*, 1996, **29**, 203; (*c*) G. W. V. Cave, C. L. Raston and J. L. Scott, *Chem. Commun.*, 2001, 2159; (*d*) K. Tanaka, *Solvent-free Synthesis*, Wiley-VCH, Weinheim, 2003.

13 A. S. Cannon and J. C. Warner, *Cryst. Growth Des.*, 2002, **2**, 255.

14 (*a*) Ö. Almarsson, M. B. Hickey, M. L. Peterson, S. L. Morissette, C. McNulty, S. Soukasene, M. Tawa, M. MacPhee and J. F. Remenar, *Cryst. Growth Des.*, 2003, **3**, 927; (*b*) S. Datta and D. J. W. Grant, *Nat. Rev. Drug Discovery*, 2004, **3**, 42; (*c*) I. D. H. Oswald, D. R. Allen, P. A. McGregor, W. D. S. Motherwell, S. Parsons and C. R. Pulham, *Acta Crystallogr., Sect. B: Struct. Sci.*, 2002, **58**, 1057.

15 (*a*) C. Giurgea, F. E. Moeyersoons and A. C. Evraerd, *Arch. Int. Pharmacodyn.*, 1967, **166**, 238; (*b*) G. Admiraal, J. C. Eikelenboom and A. Vos, *Acta Crystallogr., Sect. B: Struct. Crystallogr. Cryst. Chem.*, 1982, **38**, 2600; (*c*) D. Louder, M. Louder, V. A. Dzyabchenko, V. Agafonov and R. Ceolin, *Acta Crystallogr., Sect. B: Struct. Sci.*, 1995, **51**, 182; (*d*) F. P. A. Fabbiania, D. R. Allan, S. Parsons and C. R. Pulham, *CrystEngComm*, 2005, **7**, 179.

16 (*a*) E. Ginoulhiac, F. Semenza and L. Mainardi, *Boll. Soc. Ital. Biol. Sper.*, 1950, **26**, 583; (*b*) A. Pavlova, K. Konstantinova, H. Daskalov and A. Georgiev, *Pharmazie*, 1983, **38**, 634.

17 B. M. Kariuki, C. L. Bauer, K. D. M. Harris and S. J. Teat, *Angew. Chem. Int. Ed.*, 2000, **39**, 4485.

18 K. Scheuer, A. Rostock, R. Bartsch and W. E. Müller, *Pharmacopsychiatry*, 1999, **32**, 10.

19 M. Kuhnert-Brandstaetter, A. Burger and R. Voellenklee, *Sci. Pharm.*, 1994, **62**, 307.

20 (*a*) A. Lorico, P. Masturzo, S. Villa, M. Salmona, N. Semeraro and G. De Gaetano, *Biochem. Pharmacol.*, 1986, **35**, 2443; (*b*) M. Ohsako, C. Nakamura and O. Tsuzuki, *Yakuzaigaku*, 1995, **55**, 261; (*c*) J. F. Cunha, F. D. Campestrini, J. B. Calixto, A. Seremin and N. Paulino, *Braz. J. Med. Biol. Res.*, 2001, **34**, 381.

21 M. Haisa, S. Kashino, S. I. Hanada, K. Tanaka, S. Okazaki and M. Shibagaki, *Acta Crystallogr., Sect. B: Struct. Crystallogr. Cryst. Chem.*, 1982, **38**, 1480 (CSD refcodes: BESKAL, BESKAL01).

22 (*a*) T. J. M. Luo and G. T. R. Palmore, *Cryst. Growth Des.*, 2002, **2**, 337; (*b*) C. B. Aäkeroy, G. S. Bahra, C. R. Brown, P. B. Hitchcock, Y. Patell and K. R. Seddon, *Acta Chem. Scand.*, 1995, **49**, 762.

23 Crystal data for **4**: $C_{13}H_{16}N_2O_6$, M = 296.28, monoclinic, a = 27.896(3), b = 5.1762(5), c = 19.7879(18) Å, β = 101.090(2)°, V = 2803.9(4) Å^3, T = 100 K, space group $C2/c$, Z = 8, ρ_{calc} = 1.404 g cm^{-3}, μ(Mo-K$_\alpha$) = 0.112 mm^{-1}, 7622 reflections measured, 2873 unique reflections, 2417 observed reflections [$I > 2\sigma(I)$], R_1 obs = 0.043, wR_2 obs = 0.108. CCDC 262605.‡ Microcrystals of **4** can also be obtained by grinding **1** and **2** in a 1:1 ratio for four minutes in a ball mill or by melting the two components.

24 (*a*) S. Harkema, J. W. Bats, A. M. Weyenberg and D. Feil, *Acta Crystallogr., Sect B: Struct. Crystallogr. Cryst. Chem.*, 1972, **28**, 1646; (*b*) L. Leiserowitz and F. Nader, *Acta Crystallogr., Sect B: Struct. Crystallogr. Cryst. Chem.*, 1977, **33**, 2719.

25 Crystal data for **5**: $C_{13}H_{16}N_2O_5$, M = 280.28, monoclinic, a = 14.780(3), b = 5.5029(12), c = 17.068(4) Å, β = 109.557(4)°, V = 1308.0(5) Å^3, T = 100 K, space group $P2_1/n$, Z = 4, ρ_{calc} = 1.423 g cm^{-3}, μ(Mo-K$_\alpha$) = 0.11 mm^{-1}, 4995 reflections measured, 2220 unique reflections, 1753 observed reflections [$I > 2\sigma(I)$], R_1 obs = 0.048, wR_2 obs = 0.109. CCDC 262606.‡ Microcrystals of **5** can also be obtained by grinding **1** and **3** in a 1:1 ratio for four minutes in a ball mill or by melting the two components.

26 CSD refcodes: AJALAY, FURAOX, NEMTEE, RAHGEM, UNEZIW, UNEZOC, UNEZUI, UROXAM, XEWTIC and ZODWIY.

27 (*a*) S. L. Morissette, S. Soukasene, D. Levinson, M. J. Cima and Ö. Almarsson, *Proc. Natl. Acad. Sci. U. S. A.*, 2003, **100**, 2180; (*b*) J. Bernstein, *Polymorphism in Molecular Crystals*, Oxford University Press, Oxford, 2002.

28 CSD refcodes: AJAJEA, EXUQUJ, HADKUT, JICTUK, MACCID, MUROXA, PDTOMS10, PTZTCQ, QUIDON, TECCAF01 and ZIGPAG.

29 (*a*) A. V. Trask, W. D. S. Motherwell and W. Jones, *Chem. Commun.*, 2004, 890; (*b*) A. V. Trask, N. Shan, W. D. S. Motherwell, W. Jones, S. Feng, R. B. H. Tan and K. J. Carpenter, *Chem. Commun.*, 2005, 880; (*c*) A. V. Trask, W. D. S. Motherwell and W. Jones, *Cryst. Growth Des.*, 2005, **5**, 1013.

UM00012439
NOVARTIS EXHIBIT 1017
Novartis v. Regents, IPR2023-01346
Page 1185 of 4460

Recurrence of Carboxylic Acid−Pyridine Supramolecular Synthon in the Crystal Structures of Some Pyrazinecarboxylic Acids

Peddy Vishweshwar,[†] Ashwini Nangia,*[,†] and Vincent M. Lynch[‡]

School of Chemistry, University of Hyderabad, Hyderabad 500 046, India, and Department of Chemistry and Biochemistry, University of Texas, Austin, Texas 78712

ansc@uohyd.ernet.in

Received October 30, 2001

X-ray crystal structures of pyrazinic acid **1** and isomeric methylpyrazine carboxylic acids **2**−**4** are analyzed to examine the occurrence of carboxylic acid−pyridine supramolecular synthon **V** in these heterocyclic acids. Synthon **V**, assembled by (carboxyl)O−H···N(pyridine) and (pyridine)-C−H···O(carbonyl) hydrogen bonds, controls self-assembly in the crystal structures of pyridine and pyrazine monocarboxylic acids. The recurrence of acid−pyridine heterodimer **V** compared to the more common acid−acid homodimer **I** in the crystal structures of pyridine and pyrazine monocarboxylic acids is explained by energy computations in the RHF 6-31G* basis set. Both the O−H···N and the C−H···O hydrogen bonds in synthon **V** result from activated acidic donor and basic acceptor atoms in **1**−**4**. Pyrazine 2,3- and 2,5-dicarboxylic acids **10** and **11** crystallize as dihydrates with a (carboxyl)O−H···O(water) hydrogen bond in synthon **VII**, a recurring pattern in the diacid structures. In summary, the carboxylic acid group forms an O−H···N hydrogen bond in pyrazine monocarboxylic acids and an O−H···O hydrogen bond in pyrazine dicarboxylic acids. This structural analysis correlates molecular features with supramolecular synthons in pyridine and pyrazine carboxylic acids for future crystal engineering strategies.

Introduction

The retrosynthesis of crystal structures from multifunctional molecules may be carried out with supramolecular synthons,[1] defined as structural units within supermolecules that can be assembled by hydrogen bonds and/or intermolecular interactions. Thus, crystal engineering[2] is a kind of supramolecular (noncovalent) synthesis of target crystal structures with hydrogen bonding as the key recognition element between molecules.[1,3] O−H···O, O−H···N, and N−H···O hydrogen bonds[4] are frequently used to construct crystalline architectures[5] because of their strength and directionality. Supramolecular synthons assembled with weak hydrogen bonds (C−H···O, C−H···N)[6] and heteroatom interactions (Br···Br, I···O, I···N)[7] have emerged in complementary strategies.[8] These studies have advanced our understanding of hydrogen bonding and heteroatom interactions for the construction of target nanostructures with desired architectures and functions. Some applications of supramolecular chemistry in organic synthesis include enantioselective reactions in a chiral host lattice,[9] catalysis in the constrained microenvironment,[10] and stereospecific topochemical reactions[11] between molecules aligned in the crystal.

* To whom correspondence should be addressed. Phone: +91 40 3011338. Fax: +91 40 3010567.

[†] University of Hyderabad.

[‡] University of Texas.

(1) Desiraju, G. R. *Angew. Chem., Int. Ed. Engl.* **1995**, *34*, 2311.

(2) Desiraju, G. R. *Crystal Engineering. The Design of Organic Solids*; Elsevier: Amsterdam, 1989.

(3) (a) Whitesides, G. M.; Simanek, E. E.; Mathias, J. P.; Seto, C. T.; Chin, D. N.; Mammen, M.; Gordon, D. M. *Acc. Chem. Res.* **1995**, *28*, 37. (b) Fyfe, M. C. T.; Stoddart, J. F. *Acc. Chem. Res.* **1997**, *30*, 393. (c) Prins, L. J.; Reinhoudt, D. N.; Timmerman, P. *Angew. Chem., Int. Ed.* **2001**, *40*, 2382. (d) Nangia, A. *Curr. Opin. Solid State Mater. Sci.* **2001**, *5*, 115.

(4) (a) Jeffrey, G. A.; Saenger, W. *Hydrogen Bonding in Biological Structures*; Springer-Verlag: Berlin, 1991. (b) Jeffrey, G. A. *An Introduction to Hydrogen Bonding*; Oxford University Press: New York, 1997.

(5) (a) Zerkowski, J. A.; Whitesides, G. M. *J. Am. Chem. Soc.* **1994**, *116*, 4298. (b) Endo, K.; Sawaki, T.; Koyanagi, M.; Kobayashi, K.; Masuda, H.; Aoyama, Y. *J. Am. Chem. Soc.* **1995**, *117*, 8341. (c) MacGillivray, L. R.; Atwood, J. L. *J. Am. Chem. Soc.* **1997**, *119*, 6931. (d) Ashton, P. R.; Collins, A. N.; Fyfe, M. C. T.; Menzer, S.; Stoddart, J. F.; Williams, D. J. *Angew. Chem., Int. Ed. Engl.* **1997**, *36*, 735. (e) Simanek, E. A.; Tsoi, A.; Wang, C. C. C.; Whitesides, G. M.; McBride, M. T.; Palmore, G. T. R. *Chem. Mater.* **1997**, *9*, 1954. (f) Biradha, K.; Dennis, D.; MacKinnon, V. A.; Sharma, C. V. K.; Zaworotko, M. J. *J. Am. Chem. Soc.* **1998**, *120*, 11894. (g) Ranganathan, D.; Lakshmi, C.; Karle, I. L. *J. Am. Chem. Soc.* **1999**, *121*, 6103. (h) Hanessian, S.; Saladino, R.; Margarita, R.; Simard, M. *Chem. Eur. J.* **1999**, *5*, 2169. (i) Yue, W.; Bishop, R.; Craig, D. C.; Scudder, M. L. *Tetrahedron* **2000**, *56*, 6667. (j) Mak, T. C. W.; Xue, F. *J. Am. Chem. Soc.* **2000**, *122*, 9860. (k) Jetti, R. K. R.; Xue, F.; Mak, T. C. W.; Nangia, A. *J. Chem. Soc., Perkin Trans. 2* **2000**, 1223. (l) Holman, K. T.; Martin, S. M.; Parker, D. P.; Ward, M. D. *J. Am. Chem. Soc.* **2001**, *123*, 4421. (m) Zaman, M. B.; Tomura, M.; Yamashita, Y. *J. Org. Chem.* **2001**, *66*, 5987.

(6) Desiraju, G. R.; Steiner, T. *The Weak Hydrogen Bond in Structural Chemistry and Biology*; Oxford University Press: Oxford, 1999.

(7) (a) Desiraju, G. R.; Parthasarthy, R. *J. Am. Chem. Soc.* **1989**, *111*, 8725. (b) Navon, O.; Bernstein, J.; Khodorkovsky, V. *Angew. Chem., Int. Ed. Engl.* **1997**, *36*, 601. (c) Robinson, J. M. A.; Philp, D.; Harris, K. D. M.; Kariuki, B. M. *New J. Chem.* **2000**, *24*, 799. (d) Chu, Q.; Wang, Z.; Huang, Q.; Yan, C.; Zhu, S. *J. Am. Chem. Soc.* **2001**, *123*, 11069.

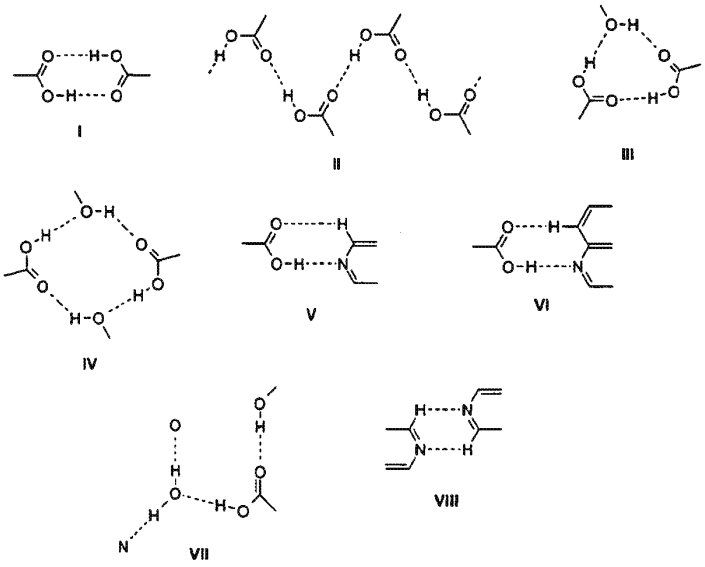
(8) (a) Langley, P. J.; Hulliger, J.; Thalmattam, R.; Desiraju, G. R. *New J. Chem.* **1998**, *22*, 1307. (b) Jetti, R. K. R.; Thallapally, P. K.; Xue, F.; Mak, T. C. W.; Nangia, A. *Tetrahedron* **2000**, *56*, 6707. (c) Tanaka, K.; Fujimoto, D.; Oeser, T.; Irngartinger, H.; Toda, F. *Chem. Commun.* **2000**, 413. (d) Tanaka, K.; Fujimoto, D.; Altruether, A.; Oeser, T.; Irngartinger, H.; Toda, F. *J. Chem. Soc., Perkin Trans. 2* **2000**, 2115. (e) Jetti, R. K. R.; Nangia, A.; Xue, F.; Mak, T. C. W. *Chem. Commun.* **2001**, 919. (f) Thaimattam, R.; Sharma, C. V. K.; Clearfield, A.; Desiraju, G. R. *Cryst. Growth. Des.* **2001**, *1*, 103. (g) Marjo, C. E.; Bishop, R.; Craig, D. E.; Scudder, M. L. *Eur. J. Org. Chem.* **2001**, 863. (h) Ohkita, M.; Suzuki, T.; Nakatani, K.; Tsuji, T. *Chem. Commun.* **2001**, 1454. (i) McGee, B. J.; Sherwood, L. J.; Greer, M. L.; Blackstock, S. C. *Org. Lett.* **2001**, *2*, 1181.

(9) (a) Soai, K.; Osanai, S.; Kadowaki, K.; Yonekubo, S.; Shibata, T.; Sato, I. *J. Am. Chem. Soc.* **1999**, *121*, 11235. (b) Tanaka, K.; Toda, F. *Chem. Rev.* **2000**, *100*, 1025 and references therein.

10.1021/jo0162484 CCC: $22.00 © 2002 American Chemical Society
Published on Web 12/29/2001

UM00012440
NOVARTIS EXHIBIT 1017
Novartis v. Regents, IPR2023-01346
Page 1186 of 4460

Scheme 1. Hydrogen Bond Synthons of Carboxylic Acid Discussed in This Paper



Hydrogen bond patterns of carboxylic acids in the solid state[12] are summarized in Scheme 1. Carboxylic acids are well known to form centrosymmetric dimer **I** as the dominant recognition motif; however, hydrogen bond catemer (or chain) **II** and single- and double-bridged aggregation motifs **III** and **IV** incorporating one and two alcohol (or water) molecules, respectively, are also known.[12d] There is a one-to-many relationship between the functional group present in the molecule and supramolecular synthons observed in the crystal structure, even for a strong O−H···O hydrogen bonding group like CO_2H. From a supramolecular retrosynthesis perspective, only those synthons that occur repeatedly in crystal structures, namely, robust synthons,[13] are useful in crystal design. In this context, the occurrence frequencies of 75 common ring motifs assembled with O/N−H···O/N hydrogen bonds in the Cambridge Structural Database (CSD, October 1996, ca. 160 000 entries) were classified recently.[14] Carboxylic acids are the second most common category of molecules archived in the CSD, with an occurrence frequency of 33% for dimer **I** formation. Furthermore, the probability increases to 96% in monocarboxylic acids when competing donor and acceptor groups are absent, making synthon **I** a robust and reliable crystal design element.

A perusal of supramolecular synthon schemes[1,13,14] shows that there are examples of bimolecular motifs with two strong hydrogen bonds or with two weak hydrogen bonds, but motifs with one strong and one weak bond are rare. However, as more crystal structures are deposited in the CSD (April 2001, 233 218 entries), new hydrogen bond patterns are discovered. A very recent database study[15] on carboxyl donors shows that recognition of CO_2H with pyridine is favored 10 times more through an O−H···N hydrogen bond compared to dimer **I** and catemer **II** motifs with itself. The participation of a weak C−H···O hydrogen bond between the pyridine and the acid results in heterodimer ring motif **V**. To our knowledge, synthon **V** is the only example of a mixed strong−weak hydrogen bonded motif, O−H···N and C−H···O, that has been systematically exploited in the crystal engineering of molecular complexes by a number of research groups.[16] These studies indicate that an acid−acid dimer (O−H···O) does not generally form when the pyridine functional group is present. However, both O−H···N and N^+−H···O^- hydrogen bondings are possible depending on the acidity of the CO_2H group and the basicity of the pyridyl moiety. For example, adducts of formic acid with pyridine crystallize as a 1:1 molecular complex and a 4:1 ionic salt.[17] In a variation to synthon **V**, and yet containing one strong and one weak hydrogen bond, supramolecular assemblies of predictable one- and two-dimensional arrays were constructed using cocrystals of carboxylic acids with phenazine (synthon **VI**).[18] Car-

(10) (a) Aoyama, Y. *Top. Curr. Chem.* **1998**, *198*, 131 and references therein. (b) Nakash, M.; Clyde-Watson, Z.; Feeder, N.; Davies, J. E.; Teat, S. J.; Sanders, J. K. M. *J. Am. Chem. Soc.* **2000**, *122*, 5286.

(11) (a) Ramamurthy, V.; Venkatesan, K. *Chem. Rev.* **1987**, *87*, 433 and references therein. (b) Kane J. J.; Liao, R.-F.; Lauher, J. W.; Fowler, F. W. *J. Am. Chem. Soc.* **1995**, *117*, 12003. (c) Coates, G. W.; Dunn, A. R.; Henling, L. M.; Ziller, J. W.; Lobkovsky, E. B.; Grubbs, R. H. *J. Am. Chem. Soc.* **1998**, *120*, 3641. (d) Xiao, J.; Yang, M.; Lauher, J. W.; Fowler, F. W. *Angew. Chem., Int. Ed.* **2000**, *39*, 2132. (e) MacGillivray, L. R.; Reid, J. L.; Ripmeester, J. A. *J. Am. Chem. Soc.* **2000**, *122*, 7817. (f) Feast, W. J.; Lövenich, P. W.; Puschmann, H.; Taliani, C. *Chem. Commun.* **2001**, 505. (g) Scheffer, J. R.; Scott, C. *Science* **2001**, *291*, 1712. (h) Irie, M.; Kobatake, S.; Horichi, M. *Science* **2001**, *291*, 1769. (i) Yang, Z.; Ng, D.; Garcia-Garibay, M. A. *J. Org. Chem.* **2001**, *66*, 4468.

(12) (a) Leiserowitz, L. *Acta Crystallogr.* **1976**, B*32*, 775. (b) Ref 2, pp 129−132. (c) Bernstein, J.; Etter, M. C.; Leiserowitz, L. In *Structure Correlation*; Bürgi, H.-B., Dunitz, J. D., Eds.; VCH: Weinheim, 1994; Vol. 2. (d) Kolotuchin, S. V.; Fenlon, E. E.; Wilson, S. R.; Loweth, C. J.; Zimmerman, S. C. *Angew. Chem., Int. Ed. Engl.* **1995**, *34*, 2654.

(13) Nangia, A.; Desiraju, G. R. *Top. Curr. Chem.* **1998**, *198*, 57.

(14) Allen, F. H.; Motherwell, W. D. S.; Raithby, P. R.; Shields, G. P.; Taylor, R. *New J. Chem.* **1999**, *23*, 25.

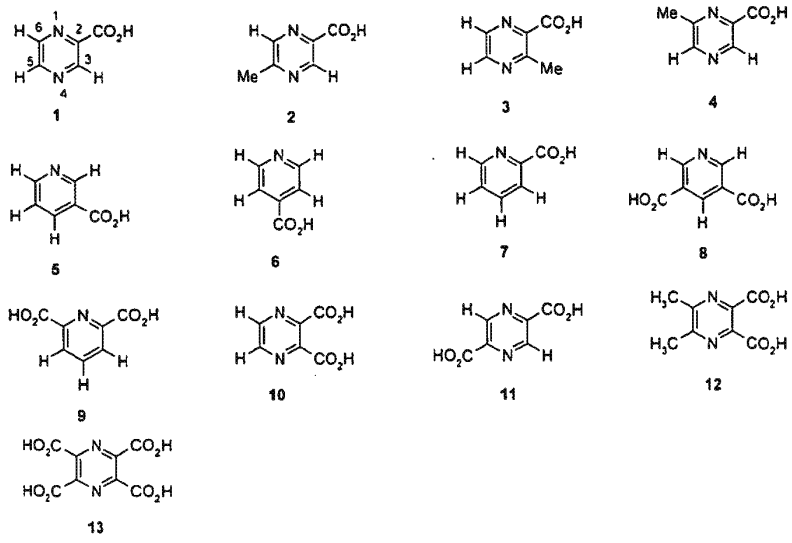
(15) Steiner, T. *Acta Crystallogr.* **2001**, *B57*, 103.

(16) (a) Sharma, C. V. K.; Zaworotko, M. J. *Chem. Commun.* **1996**, 2655. (b) Palmore, G. T. R.; McBride, M. T. *Chem. Commun.* **1998**, 145. (c) Ferguson, G.; Glidewell, C.; McManus, G. D.; Meehan, P. R. *Acta Crystallogr.* **1998**, C*55*, 418. (d) Pedireddi, V. R.; Chaterjee, S.; Ranganathan, A.; Rao, C. N. R. *Tetrahedron* **1998**, *54*, 9457. (e) Lough, A. J.; Wheatley, P. S.; Ferguson, G.; Glidewell, C. *Acta Crystallogr.* **2000**, *B56*, 261. (f) Aakeröy, C. B.; Beatty, A. M.; Tremayne, M.; Rowe, D. M.; Seaton, C. C. *Cryst. Growth Des.* **2001**, *1*, 377. (g) Lynch, D. E.; McClenaghan, I. *Acta Crystallogr.* **2001**, *C57*, 830. (h) Ishida, H.; Rahman, B.; Kashino, S. *Acta Crystallogr.* **2001**, *C57*, 876.

(17) Wiechert, D.; Mootz, D. *Angew. Chem., Int. Ed.* **1999**, *38*, 1974.

UM00012441
NOVARTIS EXHIBIT 1017
Novartis v. Regents, IPR2023-01346
Page 1187 of 4460

Scheme 2. Pyridine and Pyrazine Carboxylic Acids Analyzed in This Paper. Pyrazine Ring Atoms Are Numbered as Shown in 1, and the CH_3 Group is C7



boxylic acids that are insoluble in conventional solvents can be crystallized from pyridine as solvates[19] on the basis of the enthalpic advantage of multipoint recognition during crystallization.[20]

The examples cited above relate to molecular complexes. While binary crystals are excellent systems to study new synthons and their robustness, difficulties in obtaining a particular cocrystal because of mismatched solubility between the two components is a vexing problem. For example, Jones and co-workers[18] were interested in mixed crystals of terephthalic acid with phenazine to synthesize molecular tapes but instead had to use malonic acid because solubility considerations favored complexation with the latter acid. Generally, the more soluble component dictates the choice of complementary molecules in cocrystallization experiments. On the other hand, single-component crystals can be recrystallized from a wide variety of solvents depending on the solubility profile of that particular molecule. Therefore, one can systematically study crystal packing characteristics in a family of structures with the same functional group (e.g., CO_2H, $CONH_2$, OH) and different substituents (e.g., alkyl, phenyl, halogen), or with the same substituent in isomeric positions. Crystal engineering studies that deal with functional group ➡ supramolecular synthon correlation in closely related structures continue to elicit interest from organic and supramolecular chemists.[5,8,21] By modifying the nature of donor and acceptor groups in a graded manner through chemical synthesis, it is possible to probe the supramolecular behavior of a particular synthon in the crystal. The idea in these studies is to find out the extent to which one can perturb the molecule and still obtain the same or similar crystal packing and also the limit at which a different hydrogen bond pattern is adopted.

Pyrazine carboxylic acids (Scheme 2), exemplified by pyrazinic acid **1**, are a rare category of molecules in the CSD.[22] In methylpyrazine carboxylic acids **2**–**4**, the CO_2H group and the pyridine moiety are covalently linked, thus overcoming the necessity of preparing molecular complexes as a route to studying synthon **V**. Crystal packing in some simple pyridine and pyrazine mono- and dicarboxylic acids may be summarized in the following manner:[23] acids **1**,[23d] **5**,[23f] **6**,[23e] and **8**[23b] contain synthon **V**; **9**[23a] and **10**[23c] crystallize as dihydrates via motif **VII**. In view of the structural diversity observed in the published crystal structures,[23] further studies on hydrogen bond patterns in pyrazine mono- and dicarboxylic acids will be useful in crystal engineering. The structures of acids **2**–**4** and diacid **11** were determined by single-crystal X-ray diffraction with the following objectives: (1) To find out the occurrence of synthon **V** in the family of substituted pyrazinic acids. This crystallographic study will complement earlier reports on molecular complexes. (2) To examine the formation of O–H···N and C–H···O hydrogen bonds in competing situations of donor acidity and acceptor basicity in the same crystal structure. (3)

(18) (a) Pedireddi, V. R.; Jones, W.; Chorlton, A. P.; Docherty, R. *Chem. Commun.* **1996**, 997. (b) Batchelor, E.; Klinowski, J.; Jones, W. *J. Mater. Chem.* **2000**, *10*, 839.

(19) Anthony, A.; Desiraju, G. R. *Supramol. Chem.* **2001**, *13*, 11.

(20) Nangia, A.; Desiraju, G. R. *Chem. Commun.* **1999**, 605.

(21) (a) Schwiebert, K. E.; Chin, D. N.; MacDonald, J. C.; Whitesides, G. M. *J. Am. Chem. Soc.* **1996**, *118*, 4018. (b) Bhyrappa, P.; Wilson, S. R.; Suslick, K. S. *J. Am. Chem. Soc.* **1997**, *119*, 8492. (c) Kuduva, S. S.; Craig, D. C.; Nangia, A.; Desiraju, G. R. *J. Am. Chem. Soc.* **1999**, *121*, 1936. (d) Kuduva, S. S.; Bläser, D.; Boese, R.; Desiraju, G. R. *J. Org. Chem.* **2001**, *66*, 1621.

(22) Allen, F. H.; Kennard, O. *Chem. Des. Automat. News* **1993**, *8*, 31. The Cambridge Structural Database (April 2001, 233 218 entries) was searched for synthon **V** from good quality ($R < 0.10$) organic crystal structures in the normal distance–angle range: O–H···N (1.4–2.3 Å, 130–180°), C–H···O (2.0–3.0 Å, 110–180°), and the O–H and C–H distance was neutron normalized. Out of the 45 hits retrieved, 10 structures are single-component crystals and 35 are molecular complexes. The only example of a pyrazine carboxylic acid with synthon **V** in the database is **1**.

(23) (a) Takusagawa, F.; Hirotsu, K.; Shimada, A. *Bull. Chem. Soc. Jpn.* **1973**, *46*, 2020. (b) Takusagawa, F.; Hirotsu, K.; Shimada, A. *Bull. Chem. Soc. Jpn.* **1973**, *46*, 2292. (c) Takusagawa, F.; Shimada, A. *Chem. Lett.* **1973**, 1121. (d) Takusagawa, F.; Higuchi, T.; Shimada, A.; Tamura, C.; Sasada, Y. *Bull. Chem. Soc. Jpn.* **1974**, *47*, 1409. (e) Takusagawa, F.; Shimada, A. *Acta Crystallogr.* **1976**, *B32*, 1925. (f) Kutoglu, A.; Scheringer, C. *Acta Crystallogr.* **1983**, *C39*, 232. (g) Hamazaki, H.; Hosomi, H.; Takeda, S.; Kataoka, H.; Ohba, S. *Acta Crystallogr.* **1988**, *C54*, e49.

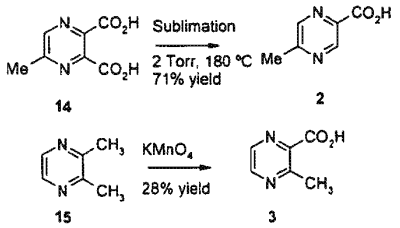
UM00012442
NOVARTIS EXHIBIT 1017
Novartis v. Regents, IPR2023-01346
Page 1188 of 4460

Table 1. Crystallographic Data and Structure Refinement Parameters

	2	3	4	11
empirical formula	$C_6H_6N_2O_2$	$C_6H_6N_2O_2$	$C_6H_6N_2O_2$	$C_6H_4N_2O_4 \cdot 2H_2O$
fw	138.13	138.13	138.13	204.14
crystal system	monoclinic	monoclinic	orthorhombic	triclinic
crystallization solvent	ethanol/water	hexane/EtOAc	hexane/EtOAc	20% aqueous HCl
space group	$P2_1/n$	$P2_1/c$	$Pca2_1$	$P\bar{1}$
a [Å]	4.1037(8)	5.0546(2)	14.494(3)	5.2101(2)
b [Å]	11.597(2)	13.2795(6)	3.8090(8)	6.8261(2)
c [Å]	13.556(3)	9.1067(4)	11.269(2)	6.8713(2)
α [deg]	90	90	90	119.144(2)
β [deg]	93.34(3)	95.315(3)	90	99.808(2)
γ [deg]	90	90	90	99.927(2)
Z	4	4	4	1
volume [Å^3]	644.0(2)	608.64(5)	622.1(2)	200.85(1)
λ [Å]	0.71073	0.71073	0.71073	0.71073
D_{calc} [g/cm^3]	1.425	1.507	1.475	1.688
μ [mm^{-1}]	0.110	0.116	0.114	0.153
2θ [°]	4.62–59.92	7.60–54.98	7.24–55.06	6.9–54.86
range h	0 to 5	−6 to 6	−18 to 18	−6 to 5
range k	0 to 16	−17 to 16	−4 to 4	−8 to 7
range l	−18 to 18	−11 to 11	−14 to 14	−8 to 8
reflections collected	1870	8509	3793	1268
unique reflections	1870	1392	1399	875
observed reflections	1265	1174	1346	781
R_1 [$I > 2\sigma(I)$][a]	0.063	0.040	0.027	0.032
wR_2 [all]	0.176	0.114	0.070	0.091
T[K]	293(2)	123(2)	173(2)	153(2)
Diffractometer	Nonius CAD4	Nonius CCD	Nonius CCD	Nonius CCD
C_k* [%][b]	69.5	74.3	72.7	77.1

[a] R_1, crystallographic reliability index. [b] C_k*, packing fraction calculated with PLATON.[46]

Scheme 3. Synthesis of Methylpyrazine Carboxylic Acids



To calculate the energy of heterodimer **V** and homodimer **I** in order to explain the preference for synthon **V** in the crystal structures of pyridine and pyrazine monocarboxylic acids. (4) The crystal structure of pyrazine-2,5-dicarboxylic acid **11** contains synthon **VII**, a new motif common to pyrazine diacids.

Results and Discussion

Acid **2** was obtained by vacuum sublimation of diacid **14** with concomitant decarboxylation.[24a] Acids **3** and **4** were synthesized by mono-oxidation of the corresponding dimethyl pyrazine with $KMnO_4$ (Scheme 3).[24b] Recrystallization of **2** from 4:1 EtOH/H_2O and of **3** and **4** from *n*-hexane/EtOAc afforded diffraction quality single crystals. Diacid **11** was recrystallized from 20% aqueous HCl. Details of X-ray data collection on crystals of **2**–**4** and **11** are listed in Table 1. The arrangement of molecules and hydrogen bonding interactions (Table 2) in these structures are analyzed and compared, specifically with reference to synthons **V** and **VII**.

(24) (a) Leonard, F.; Spoerri, P. E. *J. Am. Chem. Soc.* **1946**, *68*, 526. (b) Pitre, D.; Boveri, S.; Grabitz, E. B. *Chem. Ber.* **1966**, *99*, 364. (c) For preparation of pyrazine dicarboxylic and related acids, see: Jones, R. G.; McLaughlin, K. C. *Organic Syntheses, Coll. Vol. 4*, 1963, 824.

Table 2. Geometrical Parameters of Hydrogen Bonds

acid	H-bond	d (Å)[a]	D (Å)	θ (deg)
1[b]	O–H···N[c]	1.68	2.66	173.4
	C3–H···O[c]	2.32	3.10	127.2
	C5–H···O	2.33	3.16	132.7
	C6–H···O	2.76	3.68	143.2
	C5–H···N	2.51	3.53	157.2
2	O–H···N[c]	1.70	2.683(1)	174.3
	C3–H···O[c]	2.49	3.294(2)	129.9
	C6–H···O	2.72	3.805(2)	172.1
	C6–H···N	2.43	3.158(2)	122.7
3	O–H···N[c]	1.67	2.655(1)	176.4
	C5–H···O[c]	2.42	3.227(1)	130.1
	C6–H···O	2.37	3.458(1)	175.5
	(Me)C7–H···O	2.76	3.633(1)	137.5
	C6–H···N	2.53	3.224(1)	120.6
4	O–H···N[c]	1.69	2.680(2)	177.5
	C3–H···O[c]	2.39	3.225(2)	132.3
	(Me)C7–H···O	2.54	3.540(2)	152.9
	(Me)C7–H···O	2.49	3.536(2)	160.1
	C5–H···N	2.62	3.658(2)	158.4
11	O–H···O(H_2O)[d]	1.54	2.514(1)	170.3
	(H_2O)O–H···O[d]	1.88	2.802(1)	153.5
	(H_2O)O–H···N[d]	1.88	2.849(2)	165.8
	C3–H···O	2.49	3.452(2)	146.3
12[e]	O–H···O(H_2O)[d]	1.55	2.527(1)	167.2
	(H_2O)O–H···O[d]	1.92	2.874(1)	162.4
	(H_2O)O–H···N[d]	1.97	2.896(1)	155.1
13[e]	O–H···O(H_2O)[d]	1.50	2.479(1)	170.3
	(H_2O)O–H···O[d]	1.74	2.701(1)	162.6
	(H_2O)O–H···N[d]	2.01	2.939(2)	156.1

[a] O–H and C–H distances are neutron-normalized to 0.983 and 1.083 Å. [b] Ref 23d. [c] Hydrogen bonds in synthon **V**. [d] Hydrogen bonds in synthon **VII**. [e] Ref 29.

The ORTEP plots of acids **2**–**4** (see Supporting Information for figures) show that the assignment of isomers in the literature is incorrect. Decarboxylation of diacid **14** afforded the 5-methyl isomer **2** and not the 6-methyl isomer **4**, as described in the preparation.[24a] The melting point of **2** is in agreement with the value reported in a later report.[24b] 6-Methyl isomer **4** was prepared in the

UM00012443
NOVARTIS EXHIBIT 1017
Novartis v. Regents, IPR2023-01346
Page 1189 of 4460

same way as **3** by $CH_3 \rightarrow CO_2H$ oxidation (see Experimental Section for details).

Crystal Packing in Acids 1–4. 5-Methylpyrazine-2-carboxylic acid **2** crystallizes in the space group $P2_1/n$ ($Z = 4$). Screw axis related molecules form a zigzag, hydrogen bonded tape along [010] with synthon **V**. The metrics of O–H···N and C–H···O hydrogen bonds are 1.70 Å, 174.3° and 2.49 Å, 129.9°, respectively. O–H and C–H distances are normalized to the neutron diffraction value of 0.983 and 1.083 Å, respectively.[25] The hydrogen bonded tapes of synthon **V** are connected through C–H···N dimer **VIII** (2.43 Å, 122.7°) and C–H···O bond (2.72 Å, 172.1°) to produce a lamellar structure in the $(10\bar{2})$ plane (Figure 1a). It is difficult to assess whether the C–H···N or the C–H···O interaction is more significant in the bifurcated motif[26] of C6–H (atom numbering as in acid **1**, Scheme 2), because the former has a short-bent geometry while the latter is long-linear. It is likely that the layered structure of **2** is stabilized by a combination of synthon **V** and C–H···O/N hydrogen bonds; the sheets are in turn stacked with slight offset through van der Waals interactions (Figure 1b). Six molecules of **2** assemble in a brick-shaped array, with the hydrophobic core occupied by methyl groups of inversion-related molecules (Figure 1c). In 3-methylpyrazine-2-carboxylic acid **3** (space group $P2_1/c$, $Z = 4$), the layers are assembled with linear tapes of acid–pyridine synthon **V** and C–H···N dimer **VIII** (Figure 2, see Table 2 for hydrogen bond metrics). Compared to the brick pattern of **2**, hydrogen bonded molecules of **3** produce a hexagonal core that is occupied by methyl groups. The occurrence of C–H···N synthon **VIII** in these crystal structures is not surprising because this recognition motif was identified in a recent analysis of some pyrazine crystal structures.[27]

6-Methylpyrazine-2-carboxylic acid **4** crystallizes in the polar space group $Pca2_1$ ($Z = 4$). Zigzag tapes of 2_1-related molecules connected by synthon **V** (1.69 Å, 177.5°; 2.39 Å, 132.3°) along [001] extend into a pleated sheet through (pyrazine)C–H···N and (methyl)C–H···O (2.62 Å, 158.4°; 2.54 Å, 152.9°) hydrogen bonds (Figure 3). Cyclic C–H···N synthon **VIII** is not possible in **4** because ortho substituents flank the second N-atom. (Me)C–H···O and (pyrazine)C–H···N hydrogen bond chains run in opposite directions within a pleated layer. Significantly, adjacent layers stack in a parallel fashion resulting in the noncentrosymmetric, polar crystal structure. In centrosymmetric structures **2** and **3**, the layers stack with the more common antiparallel alignment. The arrangement of molecules and hydrogen bonding motifs in **4** are similar to the crystal structure of pyrazinic acid **1** ($Pna2_1$, $Z = 4$, $a = 11.35$ Å, $b = 7.36$ Å, $c = 6.45$ Å).[23d] In **1**, C5–H is involved in a bifurcated C–H···O/N motif while C6–H makes a long contact (Table 2, Figure 4). In methyl-substituted acid **4**, C5–H is engaged in a C–H···N interaction and the C6 position is occupied by a methyl group. Thus, replacement of H with Me at the position on the pyrazine ring that is only weakly C–H···O bonded results in minimal structural perturbation. A minor difference between these structures is that the layer is flat in **1** but pleated in **4**, a structural adjustment that accommodates the bulkier Me group in place of the H atom. The above analysis also explains why crystal structures of isomeric acids **2** and **3** are very different and adopt centrosymmetric packing in $P2_1/n$ and $P2_1/c$ space groups. Replacement of H with Me at the C3 or C5 position of **1** results in global structural changes

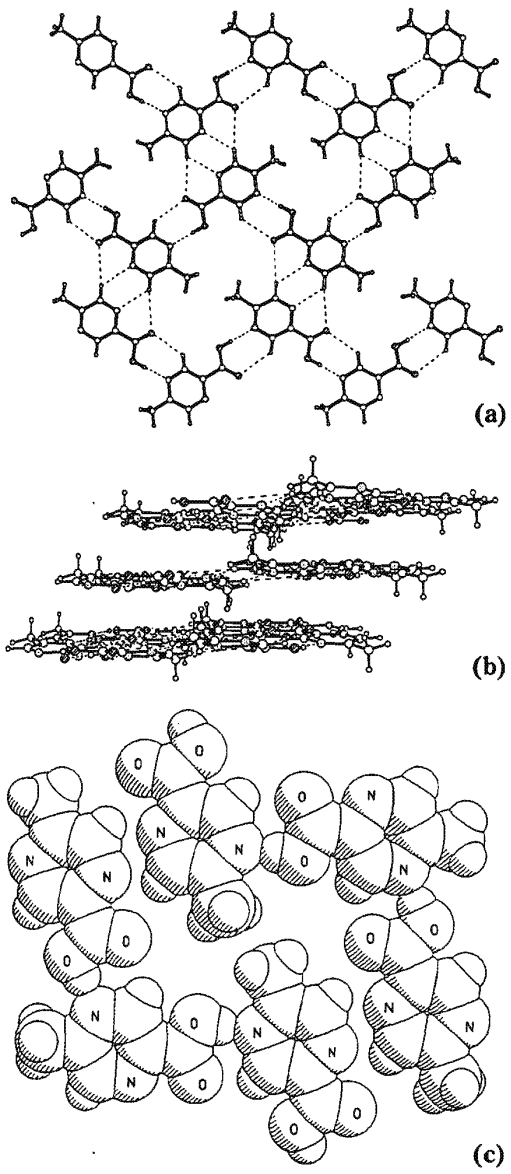


Figure 1. (a) Zigzag hydrogen bonded tapes mediated by synthon **V** along [010] in 5-methylpyrazine-2-carboxylic acid **2**. Inversion-related tapes (shaded differently) are connected by C–H···O/N hydrogen bonds (synthon **VIII**). (b) Interlayer region with a slight offset is stabilized by van der Waals interactions. (c) Space-filling representation of six molecules of **2** to show the rectangular array of 7.4 × 12.8 Å. Methyl groups fill the internal hydrophobic core.

(25) Since H-atom positions are systematically underestimated and cannot be determined accurately by X-ray diffraction, D–H bonds are uniformly normalized to the neutron distance so that comparison of hydrogen bond geometry in different crystal structures is more reliable.

(26) If there are two acceptors bonded to the same H-atom, the motif is a bifurcated hydrogen bond. For a recent paper on bifurcated hydrogen bonds, see: Parra, R. D.; Zeng, H.; Zhu, J.; Zheng, C.; Zeng, X. C.; Gong, B. *Chem. Eur. J.* **2001**, *7*, 4352.

(27) Thalladi, V. R.; Gehrke, A.; Boese, R. *New J. Chem.* **2000**, *24*, 463.

UM00012444
NOVARTIS EXHIBIT 1017
Novartis v. Regents, IPR2023-01346
Page 1190 of 4460

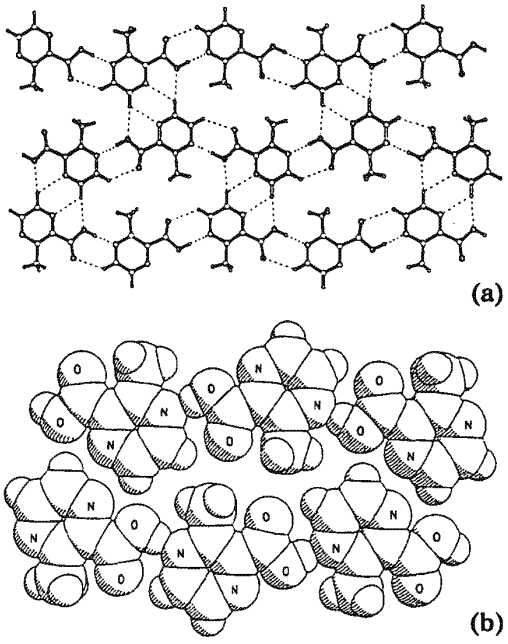


Figure 2. (a) Linear tapes of synthon **V** in 3-methylpyrazine-2-carboxylic acid **3**. Inversion-related tapes produce the layer structure in (101). (b) Space-filling view of the hexagonal array formed by six molecules of **3**.

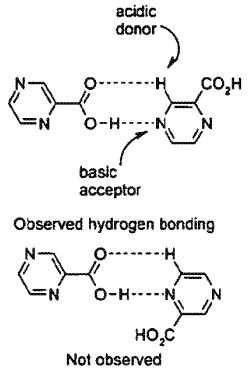
because these H atoms are intimately involved in hydrogen bonding.

Analysis of Synthon V in Acids 1−4. The recurrence of synthon **V** in the crystal structure of pyrazinic acids **1−4** confirms the robustness of this recognition motif. Since synthon **V** can result from more than one O−H···N hydrogen bond orientation in pyrazinic acids, the nature of acceptor group in these crystal structures was scrutinized. It is known that hydrogen bond strength increases with the acidity of the donor atom and the basicity of the acceptor group.[28] In acids **1−4**, the carboxyl O−H bonds to the more basic (electronegative) pyridine moiety, namely, the N-atom adjacent to the H/Me group, and not the N-atom ortho to the electron-withdrawing CO_2H group. Furthermore, this preference is observed even for the weak C−H···O hydrogen bond in pyrazinic acids **1** and **4**. The C3−H donor, activated by the ortho CO_2H group, forms the C−H···O bond that is part of synthon **V**, and not C5−H. Thus, both the CO_2H group and the H−C=N moiety form the best combination of O−H···N and C−H···O hydrogen bonds (synthon **V**) in pyrazinic acids **1−4** (Scheme 4). These results imply that not only the strong O−H···N (7−8 kcal/mol) but also the weak C−H···O (1−2 kcal/mol) hydrogen bond contribute to the stability of synthon **V**. This issue is substantiated by computation of charges on donor/acceptor atoms in pyrazinic acid **1** and energies of synthons **I**, **V**, and **VIII** later in this paper.

Hydrogen Bonding in Pyrazinic and Related Acids. We now compare crystal structures of pyrazinic acids **1−4** with pyridine carboxylic acids and pyrazine dicarboxylic acids, molecules that are less and more densely functionalized, respectively, than the title acids.

(28) (a) Ref 4b, pp 11−16. (b) Ref 6, pp 50−56.

Scheme 4. Selectivity in Hydrogen Bonding between the CO_2H Group and the Chemically Activated H−C=N Moiety



Acid−pyridine synthon **V** is present in nicotinic acid **5**,[23f] isonicotinic acid **6**,[23c] and dinicotinic acid **8**;[23b] picolinic acid **7**[23g] has a complex hydrogen bonding network between neutral and zwitterionic molecules. Pyrazine-2,3-dicarboxylic acid **10**[23c] crystallizes as a dihydrate with motif **VII**. A reason for the absence of synthon **V** in **10** could be either the inclusion of a water molecule that opens the possibility for a strong (carboxyl)-O−H···O(water) motif or because the *ortho* CO_2H group deactivates the pyrazine N-atom as the O−H···N acceptor. In any case, acid−acid homodimer **I** is not formed in pyrazine mono- and dicarboxylic acids. Since **10** is the only pyrazine diacid in the CSD, we determined the X-ray crystal structure of pyrazine-2,5-dicarboxylic acid **11**.

Pyrazine-2,5-diacid crystallizes as a dihydrate, **11**·2(H_2O) (space group $P\bar{1}$). The structure contains a (carboxyl)O−H···O(water) hydrogen bond (1.54 Å, 170.3°) that is part of motif **VII**. The carbonyl oxygen accepts a hydrogen bond from a water molecule (O−H···O=C: 1.88 Å, 153.5°), and the water molecule is polarized because it donates to the pyrazine N-atom (1.88 Å, 165.8°), resulting in a cyclic cooperative array (Figure 5). Crystals of **10**[23c] and **11**, as well as related compounds diacid **12**[29] and tetraacid **13**,[29] are hydrated because these molecules are rich in hydrogen bond acceptor groups (CO_2H, N-atom). The inclusion of water, a donor-rich molecule, compensates for this imbalance and completes the hydrogen bond network in these crystal structures.[30] The (carboxyl)O−H···O(water) hydrogen bond is short and linear compared to isolated hydrogen bonds of synthon **VII** in diacids **11−13** (Table 2). We have recently ascribed the unusual shortening of (carboxyl)O−H···O(water) (1.50 Å, O···O 2.479(1) Å, 170.3°) in pyrazine tetraacid **13** into the short hydrogen bond regime (O···O < 2.5 Å) to the cumulative stabilization from σ- and π-bond cooperativity in the extended array **VII**.[29]

A comparison of hydrogen bonding in closely related crystal structures gives an idea of the molecular features that favor the recurrence of a particular synthon and also of the factors that result in different crystal packing motifs. In the present case, acid−pyridine synthon **V** is

(29) Vishweshwar, P.; Nangia, A.; Lynch, V. M. *Chem. Commun.* **2001**, 179.

(30) (a) Desiraju, G. R. *J. Chem. Soc., Chem. Commun.* **1991**, 426. (b) Krygowski, T. M.; Grabowski, S. J.; Konarski, J. *Tetrahedron* **1998**, *54*, 11311. (c) Vishweshwar, P.; Nangia, A.; Lynch, V. M. *Acta Crystallogr.* **2000**, *C56*, 1512.

UM00012445
NOVARTIS EXHIBIT 1017
Novartis v. Regents, IPR2023-01346
Page 1191 of 4460

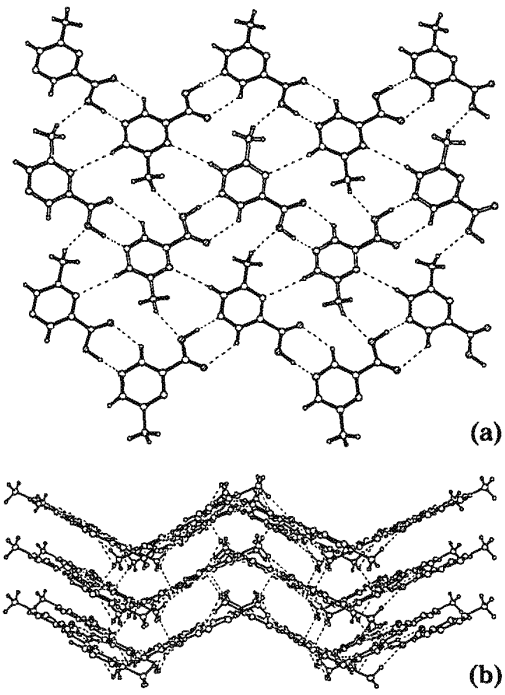


Figure 3. (a) Zigzag tapes of 6-methylpyrazine-2-carboxylic acid **4** assembled with synthon **V** along [001]. Translation-related tapes are connected by C−H···O/N hydrogen bonds into a pleated sheet structure. Note that synthon **VIII** is not possible here. (b) Stacking of pleated sheets with (Me)-C−H···O interactions between the layers.

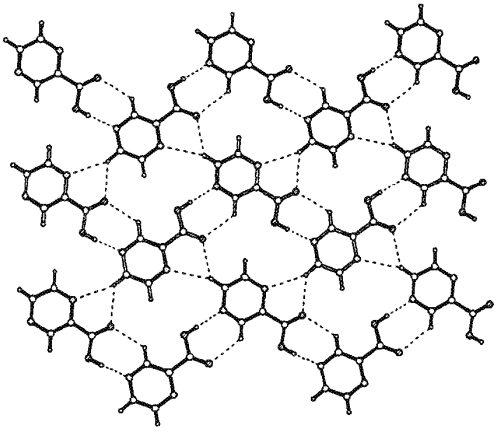


Figure 4. Laminated sheet parallel to (001) in pyrazinecarboxylic acid **1**. Note the similarity with Figure 3a. The layer in **1** is flat, while it is pleated in **4**.

a recurring (robust) structural pattern in pyridine and pyrazine monocarboxylic acids, while di- and tetraacids adopt motif **VII** in hydrate crystal structures (Table 3).[31] Such a molecule → synthon correlation is an essential exercise for the rational supramolecular synthesis of

(31) However, if a CO_2H group is present ortho to the pyridine/pyrazine N-atom (e.g., **7**, **10**, and **11**), then the likelihood of O−H···N hydrogen bonding is diminished because the adjacent electron-withdrawing group weakens the basicity of the N-acceptor.

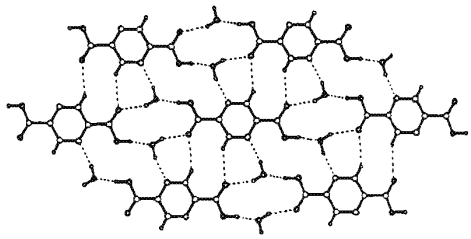


Figure 5. Lamellar structure parallel to $(1\bar{2}1)$ mediated by synthon **VII** in pyrazine-2,5-dicarboxylic acid **11**. Note that the extended hydrogen bond array O−H···O=C−O−H···OH_2···O/N is stabilized through cooperativity and polarization resulting in the short (strong) (carboxyl)O−H···O(water) hydrogen bond.

Table 3. Dominant Synthon in Some Pyridine and Pyrazine Carboxylic Acids

molecule	synthon	molecule	synthon
1	**V**	**8**	**V**
2	**V**	**9**	**VII**
3	**V**	**10**	**VII**
4	**V**	**11**	**VII**
5	**V**	**12**	**VII**
6	**V**	**13**	**VII**

target crystal structures from functionalized molecules.[13] While establishing such relationships, it may be noted that carboxylic acids participate in a variety of hydrogen bond motifs depending on the presence of other functional groups,[12d] activated C−H donors,[21c] and heterocyclic rings.[32] Therefore, reliable correlation is possible only within families of homogeneous crystal structures. As the structural diversity is expanded to cover the entire database,[14] the probability of the occurrence of the synthon is reduced.

RHF Computation of Charge and Energy. The next step in our study was to compute the energy of acid−pyridine synthon **V**, acid−acid synthon **I**, and pyridine dimer **VIII**.[33] Energies of these synthons were calculated in the Restricted Hartree−Fock (RHF) 6-31G* basis set using Spartan Pro 1.0.[34] The molecules selected for energy calculation are the 1:1 CH_3CO_2H−pyridine adduct and isonicotinic acid **6**, so that energies of these synthons may be compared in two types of chemical systems, molecular complexes, and in single-component crystals. The energy of the synthon was computed by calculating the difference between the minimized energy of the hydrogen bonded complex and that of the isolated molecules. For example, the energy of synthon **V** was calculated by optimizing the energy of CH_3CO_2H−pyridine complex and subtracting from this value the energy of CH_3CO_2H and pyridine molecules. The computed energy of synthons **I**, **V**, and **VIII** is listed in Table 4. The hydrogen bond geometry in the computed configuration was found to be in the normal distance−angle

(32) Pyrazole-4-carboxylic acid forms ribbons of O−H···N and N−H···O hydrogen bonds in the solid state: Foces-Foces, C.; Echevarria, A.; Jagerovic, N.; Alkorta, I.; Elguero, J.; Langer, U.; Klein, O.; Minguet-Bonvenhí, M.; Limbach, H.-H. *J. Am. Chem. Soc.* **2001**, *123*, 7898.

(33) For recent papers on hydrogen bond energy computations, see: (a) Vargas, R.; Garza, J.; Dixon, D. A.; Hay, B. P. *J. Am. Chem. Soc.* **2000**, *122*, 4750. (b) Kobko, N.; Paraskevas, L.; del Rio, E.; Dannenberg, J. J. *J. Am. Chem. Soc.* **2001**, *123*, 4348. (c) Raymo, F. M.; Bartberger, M. D.; Houk, K. N.; Stoddart, J. F. *J. Am. Chem. Soc.* **2001**, *123*, 9264.

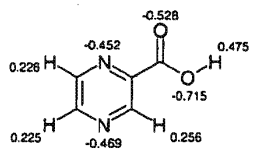
(34) *Spartan Pro 1.0.*; Wave Function, Inc.: 18401 von Karman Avenue, Suite 370, Irvine, CA 92612.

UM00012446
NOVARTIS EXHIBIT 1017
Novartis v. Regents, IPR2023-01346
Page 1192 of 4460

Table 4. Energy of Synthons Calculated in RHF 6-31G* (in kcal/mol)

	CH_3CO_2H–pyridine	isonicotinic acid
synthon V	−9.95	−9.97
synthon I	−15.54	−15.62
synthon VIII	−2.50	−2.67

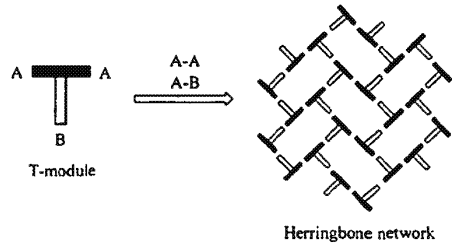
Scheme 5. Mulliken Charges on Donor and Acceptor Atoms in Pyrazinecarboxylic Acid 1



range for these interactions. From these data, it is clear that crystallization through heterodimer **V** (2 × −9.97 = −19.94 kcal/mol) is energetically favored compared to a combination of O−H···O and C−H···N homodimers **I** and **VIII** [−(15.62 + 2.67) = −18.29 kcal/mol] by −1.65 kcal/mol in isonicotinic acid **6**. Similarly, the CH_3CO_2H–pyridine molecular complex formation is favored over acid–acid and pyridine–pyridine hydrogen bonded aggregates by −1.86 kcal/mol. Thus, the recurrence of mixed strong–weak hydrogen bonded synthon **V** in crystal structures is explained by energy considerations. The calculated Mulliken charge (RHF 6-31G*) on donor/acceptor atoms in pyrazinic acid **1** is displayed in Scheme 5. It is clear that the more basic N-acceptor (electronegative) and the more acidic C−H donor (electropositive) participate in the hydrogen bonds of synthon **V**. These charges are in agreement with the selectivity for the synthon formation summarized in Scheme 4.

It has been suggested in a recent paper[35] that formation of acid–pyridine synthon **V** may be rationalized by the formation of an O−H···N hydrogen bond between the best donor (CO_2H) and the best acceptor (pyridine N-atom) in the crystal. The electronegativity of the C=O oxygen is moderately better than the pyridine nitrogen in **1** on the basis of Mulliken charge (−0.528, −0.469 e). Our computations suggest that hydrogen bonding of carboxylic acid O−H group is equally likely with both C=O oxygen and pyridine N for electrostatic and basicity reasons. However, self-assembly of molecules in the crystal is favored via synthon **V** compared to synthon **I** because of energetic factors. Furthermore, depending on the pK_a of the carboxylic acid and pyridine, O−H···N hydrogen bonding will result when $\Delta pK_a < 3.75$ and proton transfer (hence salt formation) when $\Delta pK_a > 3.75$.[16g,36] The pK_a of pyrazinic acid **1** is 2.92[37] and that of pyridine is 5.23,[36,38] giving ΔpK_a of 2.31, a value that is in agreement with the O−H···N hydrogen bonding observed in these crystal structures. Since different atoms in different chemical environments are the potential acceptors, namely, C=O and pyridine−N, the final outcome in terms of the O−H···O vs O−H···N hydrogen bonding is determined by a combination of electronegativity and basicity factors. A hydrogen bond is a three-center, four-electron multicomponent interaction, and a dissection of the various contributions to the total energy is not trivial. Tables of hydrogen bond acidity and basicity constants for aliphatic, aromatic, and heterocyclic compounds published recently[39] should aid in our further understanding of hydrogen bonding in multifunctional molecules.

Scheme 6. Self-Assembly of a T-Module into a Herringbone Network



Herringbone Network in 5-Methylpyrazine-2-carboxylic Acid. The description of crystal structures as networks may be carried out by representing the molecules as nodes and the intermolecular interactions between them as node connectors.[40] The network representation facilitates the understanding of three-dimensional architectures and the comparison of structures assembled with the same or different molecular constituents. The topology of metal–organic crystal structures, or coordination polymers, is frequently described in terms of chain, ladder, brick wall, square grid, rhombus grid, and hexagonal networks.[41] Self-assembly of a T-module with recognition sites A, A, and B produces a herringbone network through one A−A and two A−B type metal–ligand or metal–metal bonding, or through hydrogen bonding in the case of an organic molecule (Scheme 6). For example, $[Cd_2(azpy)_3(NO_3)_4]$ (azpy = 4,4′-azopyridine) **16** is a T-shaped molecule in which pyridine rings of azpy B are nearly coplanar, while pyridine rings in azpy A have a dihedral angle of 65°. Recrystallization from ethanol/acetone afforded **16**·2Me_2CO, which exhibits a herringbone-type two-dimensional network[41,42] (Figure 6) with rectangular cavities of 23 × 11 Å. Acetone molecules are included in the voids of the triple-interpenetrated three-dimensional structure.

In the nomenclature of Scheme 6, acid **2** may be viewed as a T-shaped molecule (Figure 7a) with pyridyl groups making A-type hydrogen bonding and a carboxylic acid representing B-type recognition site. In the crystal structure of **2**, two acid–pyridine synthons **V** and one pyridine dimer **VIII** at each molecule (node) produce the herringbone network in the $(10\bar{2})$ plane (Figure 7b). Similarly, acid **3** exhibits a hexagonal network (Figure 7c). It may be noted that Cd···N bonding with A- and B-type azpy ligands in **16**·2Me_2CO is replaced by synthons **V** and **VIII** in **2**. In effect, the two-dimensional network formed by an organic molecule and a metal–

(35) Aakeröy, C. B.; Beatty, A. M.; Helfrich, B. A. *Angew. Chem., Int. Ed.* **2001**, *40*, 3240.
(36) Johnson, S. L.; Rumon, K. A. *J. Phys. Chem.* **1965**, *69*, 74.
(37) The Merck Index, 11th ed.; Merck & Co.: Rahway, 1989; p 1266.
(38) The pK_a of pyridinium ion is 5.23 (ref 36). This is taken as the approximate pK_a for the protonated form of pyrazine N4 in **1**.
(39) Abraham, M. H.; Platts, J. A. *J. Org. Chem.* **2001**, *66*, 3484.
(40) (a) Desiraju, G. R. *Chem. Commun.* **1997**, 1475. (b) Zaworotko, M. J. *Chem. Commun.* **2001**, 1.
(41) Kondo, M.; Shimamura, M.; Noro, S.; Minakoshi, S.; Asami, A.; Seki, K.; Kitagawa, S. *Chem. Mater.* **2000**, *12*, 1288.
(42) For other examples of two-dimensional herringbone networks, see: (a) Ref 40b. (b) Dong, Y.-B.; Layland, R. C.; Pschirer, N. G.; Smith, M. D.; Bunz, U. H. F.; Loye, H.-C. *Chem. Mater.* **1999**, *11*, 1413. (c) Carlucci, L.; Ciani, G.; Proserpio, D. M. *J. Chem. Soc., Dalton Trans.* **1999**, 1799. (d) Masse, R.; Nicoud, J.-F.; Bagieu-Beucher, M.; Bourgogne, C. *Chem. Phys.* **1999**, *245*, 365. (e) Withersby, M. A.; Blake, A. J.; Champness, N. R.; Coole, P. A.; Hubberstey, P.; Schröder, M. *New. J. Chem.* **1999**, *23*, 573.

UM00012447
NOVARTIS EXHIBIT 1017
Novartis v. Regents, IPR2023-01346
Page 1193 of 4460

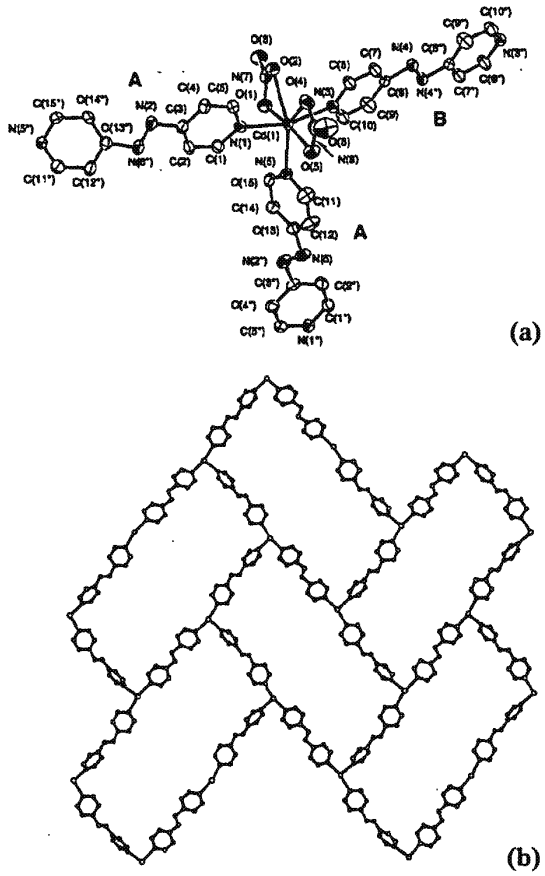


Figure 6. (a) ORTEP plot of T-shaped molecule **16** to show the A, A, and B sites. (b) Herringbone two-dimensional network formed by one A−A and two A−B type Cd···N interactions. (Adapted from ref 41.)

organic clathrate is identical. Such a topological comparison of crystal structures and their connectivity is possible only through the network representation. To our knowledge, acid **2** is the first example of an organic crystal structure with a herringbone network. Staircase-type networks have been recently identified in some organic structures.[11f,16e,30c]

Conclusions

We have studied hydrogen bonding supramolecular synthons in a family of crystalline pyrazine carboxylic acids by X-ray diffraction. Strong−weak O−H···N and C−H···O hydrogen bonded synthon **V** is a robust recognition motif that is largely insensitive to the substitution and placement of functional groups in pyridine and pyrazine monocarboxylic acids. However, a pyridyl N with an ortho CO_2H group is sufficiently deactivated that it does not form synthon **V**. Pyrazine dicarboxylic acids crystallize as dihydrates with a (carboxyl)O−H···O(water) hydrogen bond as the strong and dominant interaction in synthon **VII**. Our structural analysis shows that pyrazine mono- and dicarboxylic acids exhibit distinct hydrogen bonding patterns. The recurrence of acid−pyridine synthon **V** compared to the more common acid−

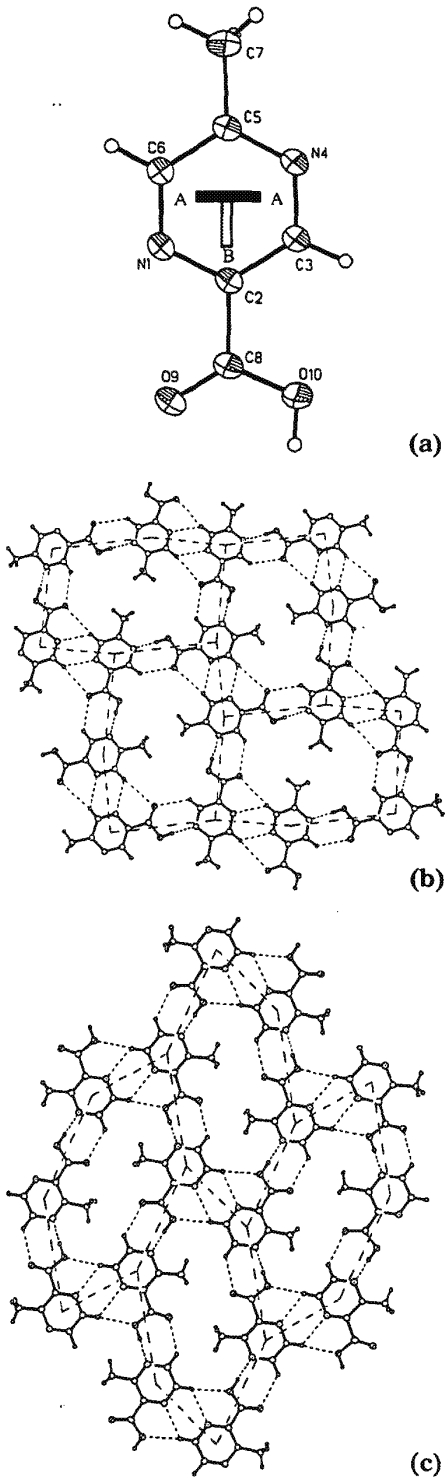


Figure 7. (a) ORTEP plot of 5-methylpyrazine-2-carboxylic acid **2** to show the A, A, and B hydrogen bonding sites. (b) Self-assembly of the T-shaped molecule **2** into a two-dimensional herringbone network via two A−B (synthon **V**) and one A−A (synthon **VIII**) type interactions. (c) Hexagonal network in 3-methylpyrazine-2-carboxylic acid **3**.

UM00012448
NOVARTIS EXHIBIT 1017
Novartis v. Regents, IPR2023-01346
Page 1194 of 4460

acid dimer **I** in these crystal structures is supported by ab initio computations. Synthon V results from hydrogen bonding between activated acidic donor and basic acceptor atoms.

Previous studies on molecular complexes of acid and pyridine derivatives have focused on the construction of one-dimensional tape and two-dimensional layer architectures from simple molecular building blocks. The lamellar and pleated architectures of pyrazinic acids discussed in this paper provide a novel system for the design of nanostructures from tailored molecules. The present study on pyrazine mono- and dicarboxylic acids examines crystal packing in complex and competing chemical environments and hence provides a better understanding of a useful supramolecular synthon in crystal engineering.

Experimental Section

Synthesis: 5-Methylpyrazine-2-carboxylic Acid 2.[24a] 5-Methylpyrazine-2,3-dicarboxylic acid **14** (250 mg, 1.4 mmol) was placed in a vacuum sublimation apparatus and decarboxylated by heating to 175−185 °C at 2 Torr. Yield: 130 mg (71%) of acid **2**. Mp: 167−8 °C (166−167 °C).[24b] ^{1}H NMR (DMSO-d_6): δ 2.59 (s, 3H), 8.68 (s, 1H), 9.06 (s, 1H). IR (cm^{-1}): 3450, 2507, 1892, 1734, 1273, 1184.

3-Methylpyrazine-2-carboxylic Acid 3.[24b] To 1 mL (9.3 mmol) of 2,3-dimethylpyrazine **15** in 10 mL of water at 70−75 °C was added 3.3 g (20.9 mmol) of $KMnO_4$ in 50 mL of water. After decolorization of a purple color, the MnO_2 cake was filtered and washed with water several times. The filtrate was acidified to pH 1.5 with HNO_3 and the solution heated to 50 °C briefly, cooled to room temperature, and extracted with EtOAc. Workup afforded 350 mg (28%) of acid **3**. Mp: 170−1 °C. ^{1}H NMR (DMSO-d_6): δ 2.65 (s, 3H), 2.66 (s, 1H), 2.75 (s, 1H). IR (cm^{-1}): 3749, 1684, 1508, 1413, 1288, 1103.

6-Methylpyrazine-2-carboxylic Acid 4.[24b] Compound **4** was prepared in 21% yield using the above procedure starting from 2,6-dimethylpyrazine. Mp: 200−1 °C (201−202 °C). ^{1}H NMR (DMSO-d_6): δ 2.59 (s, 3H), 8.85 (s, 1H), 9.05 (s, 1H). IR (cm^{-1}): 3435, 1732, 1383, 1296, 1257, 1018.

Pyrazine-2,5-dicarboxylic Acid 11. Pyrazine-2,5-dicarboxylic acid 11 (dihydrate) was purchased from Acros Chemicals and used as received for crystallization.

Single crystals of acid **2** were obtained from 4:1 EtOH/H_2O; **3** and **4** from *n*-hexane/EtOAc; and **11** from 20% aqueous HCl.

X-ray Diffraction. Reflections were collected on an Enraf-Nonius CAD-4 diffractometer (for acid **2**) and on a Nonius Kappa CCD diffractometer (for acids **3**, **4**, and **11**). The incident radiation is Mo Kα X-ray (λ = 0.71073 Å) on both instruments. Data on the crystal of **2** was collected at 293 K, and crystals of **3**, **4**, and **11** were cooled with an Oxford Cryostream device attached to the CCD machine. Data reductions were performed using Xtal 3.5 (CAD-4) and DENZO−SMN (CCD).[43] Structures were solved by direct methods using the SHELXS-97 program and refined by full-matrix least-squares refinement on F^2 with anisotropic displacement parameters for the non-H atoms using the SHELXL-97 program.[44] The function $\Sigma w(|F_o|^2 - |F_c|^2)^2$ was minimized, where $w = 1/[(\sigma(F_o))^2 + (0.0415*P)^2 + (0.9360*P)]$ and $P = (|F_o|^2 + 2|F_c|^2)/3$. Equations for calculating $R(F)$, $R_w(F^2)$, and the goodness of fit, S, are given below. Neutral atom scattering factors and values used to calculate the linear absorption coefficient are taken from the International Tables for X-ray Crystallography.[45] Geometrical analysis was carried out in PLATON[46] on a Silicon Graphics Octane2 workstation. Details of cell parameters, data collection, and structure refinement are summarized in Table 1. Hydrogen bond metrics are listed in Table 2. $R_w(F^2) = \{\Sigma w(|F_o|^2 - |F_c|^2)^2/\Sigma w(|F_o|)^4\}^{1/2}$, where w is the weight given to each reflection. $R(F) = \Sigma(|F_o| - |F_c|)/\Sigma|F_o|\}$ for reflections with $F_o > 4(\Sigma(F_o))$. $S = [\Sigma w(|F_o|^2 - |F_c|^2)^2/(n - p)]^{1/2}$, where n is the number of reflections and p is the number of refined parameters.

Acknowledgment. A.N. thanks the Department of Science and Technology (Project No. SP/S1/G-29/98) for research funding on nanostructures. The CAD-4 diffractometer at UH is supported by DST. P.V. thanks the CSIR for SRF. V.M.L. thanks the National Science Foundation (Project No. CHE-9807702) for funding.

Supporting Information Available: X-ray data with details of refinement procedures (cif files) and ORTEP plots of acids **2**−**4** and **11**. This material is available free of charge via the Internet at http://pubs.acs.org.

JO0162484

(43) (a) *Xtal3.5*. Reference Manual; Hall, S. R., Flack, H. D., Stewart, J. M., Eds.; University of Western Australia: Australia, Geneva, Switzerland and MD, USA; 1995. (b) *DENZO−SMN*. Otwinowski, Z.; Minor, W. In *Methods in Enzymology*; Macromolecular Crystallography, Part A; Carter, C. W., Jr., Sweets, R. M., Eds.; Academic Press: New York, 1997; Vol. 276.

(44) *SHELX97 Program for the Refinement and Solution of Crystal Structures*; Sheldrick, G. M.; University of Göttingen: Göttingen, Germany, 1997.

(45) *International Tables for X-ray Crystallography*; Wilson, A. J. C., Ed.; Kluwer Academic Press: Boston, 1992; Vol. C, Tables 4.2.6.8 and 6.1.1.4.

(46) *PLATON*; Spek, A. L.; Bijvoet Center for Biochemical Research, Vakgroep Kristal-en Structure-Chemie, University of Utrecht: The Netherlands.

UM00012449
NOVARTIS EXHIBIT 1017
Novartis v. Regents, IPR2023-01346
Page 1195 of 4460

COMMUNICATION

ChemComm www.rsc.org/chemcomm

Supramolecular synthons based on N–H···N and C–H···O hydrogen bonds. Crystal engineering of a helical structure with 5,5-diethylbarbituric acid

Peddy Vishweshwar,[a] Ram Thaimattam,[b] Mariusz Jaskólski*[b] and Gautam R. Desiraju*[a]

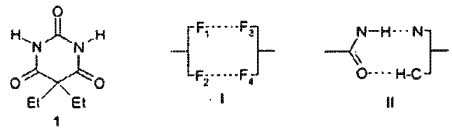
[a] *School of Chemistry, University of Hyderabad, Hyderabad 500 046, India. E-mail: desiraju@uohyd.ernet.in; Fax: +91 40 3010567*

[b] *Center for Biocrystallographic Research, IBCh, Polish Academy of Sciences and Department of Crystallography, Faculty of Chemistry, A. Mickiewicz University, Grunwaldzka 6, 60-780 Poznan, Poland. E-mail: mariuszj@amu.edu.pl*

Received (in Columbia, MO, USA) 7th May 2002, Accepted 3rd July 2002
First published as an Advance Article on the web 18th July 2002

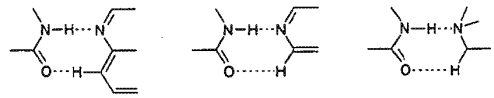
5,5-Diethylbarbituric acid is a convenient molecular precursor for a newly identified N–H···N/C–H···O synthon, which is robust enough for the design of a helix architecture.

The central aim of crystal engineering is a general protocol for the construction of crystal structures from molecular structures.[1] Since there is no direct correspondence between molecular functional groups (F_n) and crystal packing features, a realistic approach to crystal engineering is to identify particular combinations of molecular functionality that preferentially yield particular supramolecular synthons, which in turn are more easily related to the packing features.[2] Along these lines, several groups of investigators have identified two-point hydrogen bonded synthons with the general structure **I**. A number of these have been identified by Allen *et al.* from the Cambridge Structural Database (CSD),[3] while Jones and coworkers have shown that a strong/weak combination† such as O–H···N/C–H···O for $F_1\cdots F_3/F_2\cdots F_4$ is sufficiently reliable in crystal design.[4] Other related examples of strong/weak synthons are well known.[5] In this communication, we show that 5,5-diethylbarbituric acid, **1** (barbital),‡ is an effective tecton in the generation of the hitherto unreported N–H···N/C–H···O strong/weak supramolecular synthon **II**, which is endowed with sufficient robustness for effective crystal engineering.



1 I II

When barbital and acridine were taken in an equimolar ratio in EtOAc, crystals of the 1:2 molecular complex (mp 175 °C, *C2/c*), § shown in Fig. 1, were obtained. Notice the 'bifurcated' arrangement of two acridine molecules about the central barbital molecule and the two-fold symmetry equivalent synthons **IIa** (N–H···N: 1.92 Å, 177°; C–H···O: 2.49 Å, 157°). Similarly, when equimolar amounts of 1 and 1,10-phenanthroline were taken in EtOAc, the result was the 1:1 molecular complex (mp 160 °C, $P2_1/c$)§ shown in Fig. 2. Here too the N–H···N/C–H···O arrangement is seen (as synthon **IIb**, N–H···N: 1.83 Å, 172°; C–H···O: 2.85 Å, 114°), but additionally there is a centrosymmetric N–H···O dimer (1.83 Å, 176°) that effectively acts as a spacer. Why acridine gives the 1:2 complex with 1 while 1,10-phenanthroline gives the 1:1 complex is another matter because equimolar amounts of the components were taken for recrystallisation in both experiments, and there appeared to be no special problem with compound solubility in either case. Perhaps the approach of two molecules of phenanthroline towards the barbital molecule is sterically disfavoured. In any event, what is significant is the formation of the N–H···N/C–H···O synthon **II** in both cases.



IIa IIb IIc

The CSD was now examined to find out the generality of occurrence of heterosynthon **II**. The April 2002 version (5.23, 257162 entries, screens 85, 88, 153) contains 10323 hits with the (C=O)NH fragment. Using accepted ranges for N–H···N (1.5–2.4 Å, 120–180°) and C–H···O (2.0–3.1 Å, 110–180°) hydrogen bonds,[6] we obtained 140 occurrences of synthon **II** containing either 0, 1 and 2 atoms in the tether between the N-atom and the C–H group. Among these, synthon **II** occurs as part of a larger three-point recognition motif in 62 hits. These larger synthons contain not only N–H···N and C–H···O hydrogen bonds but also a third, generally stronger hydrogen bond. Accordingly, these 62 hits were removed so as to obtain 78 genuine occurrences of the two-point synthon **II**. Computations on the model system succinimide–pyridine (Spartan RHF/6-31G*) showed that the stabilisation energy for synthon **IIb** is −8.2 kcal mol^{-1}, which is comparable to the stabilisation

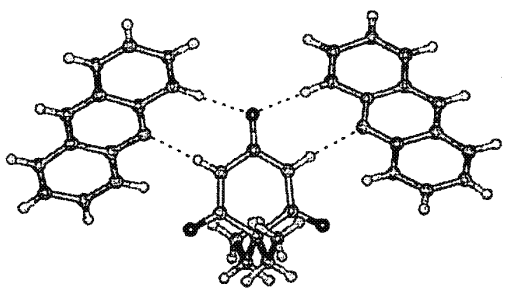


Fig. 1 Barbital and acridine 1:2 complex. Notice synthon **II**.

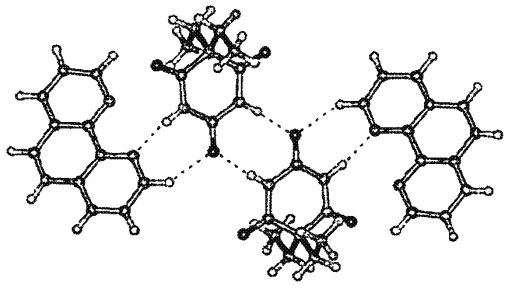


Fig. 2 Barbital and 1,10-phenanthroline 1:1 complex. Notice synthon **II** and the central N–H···O dimer.

DOI: 10.1039/b204388b

 This journal is © The Royal Society of Chemistry 2002

UM00012450
NOVARTIS EXHIBIT 1017
Novartis v. Regents, IPR2023-01346
Page 1196 of 4460

provided by a single O–H···O hydrogen bond. These CSD and computational results show that synthon **II** is a reasonably viable structural unit for crystal design.

The next step in the crystal engineering exercise was to test the robustness of synthon **II** in a new system. The molecule selected for co-crystallisation with barbital was urotropine (hexamethylenetetramine). An equimolar mixture of the two components taken in EtOAc yielded a 1 : 1 molecular complex (Fig. 3). Notice that both barbital and urotropine can be supramolecularly bifunctional with respect to synthon **IIc**. Further, the rigid geometry of both molecules leads *via* the intermediacy of this synthon (N–H···N: 1.88 Å, 169°, 1.84 Å, 168°; C–H···O: 2.50 Å, 124°, 2.89 Å, 115°) to a helix with a pitch of 13.3 Å. The space group is centrosymmetric (*Pbca*) and so both left and right-handed helices are present in the crystal structure. The helix topology is a current target in crystal engineering strategies,[7] but very few all-organic helix structures have been reported.[8] What makes the present example noteworthy is that the helix may be anticipated from the robustness of the N–H···N/C–H···O synthon **II**, the shapes of the constituent molecules, barbital and urotropine, and the firm scaffolding provided by both molecules.

Finally, it is worthwhile to observe that variations of synthon **II** with an overall stabilisation of only around −8 kcal mol^{-1} occur repeatedly in molecular complexes of barbital. As seen from our computations, such stabilisation is comparable to what is provided by a single strong hydrogen bond such as O–H···O or N–H···O. We estimate that the N–H···N hydrogen bond is worth around −6 kcal mol^{-1} and that the C–H···O bond is correspondingly weak. A combination of a moderate to strong interaction and a weak interaction therefore seems to be sufficient to achieve synthon robustness. Such robustness almost surely arises from the two-point nature of synthon **II**. All this augurs well for the reliability of other strong/weak interaction combinations in crystal engineering because of the concomitant predictability of the design exercise.

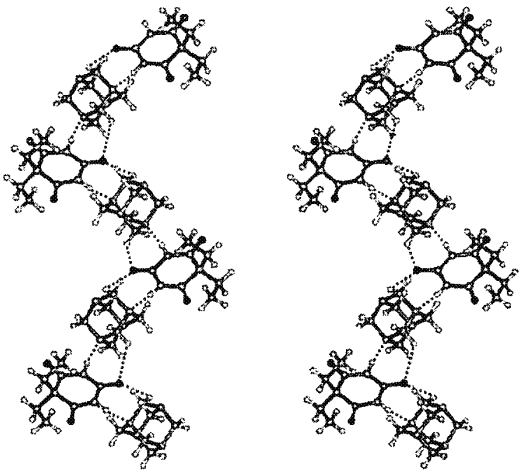


Fig. 3 Stereoview of the helix structure in 1 : 1 complex of barbital and urotropine.

P. V. thanks the CSIR, New Delhi for the award of an SRF. G. R. D. and M. J. thank the DST-KBN for a collaborative grant (INT/POL/008/00). The research of M. J. was partially supported by the HHMI. G. R. D. acknowledges continuing cooperation from the Cambridge Crystallographic Data Centre and Accelrys Inc.

Notes and references

† While there is some subjectivity in the use of the terms 'strong' and 'weak' as applied to hydrogen bonds, the convention used here is as described in ref. 6.

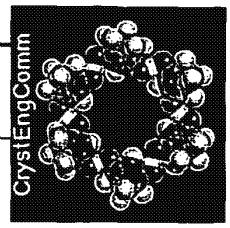
‡ The compounds were purchased and used as such in the complexation experiments.

§ *Crystal data*: **1**·acridine: $C_8H_{12}N_2O_3{\cdot}2(C_{13}H_9N)$, M = 542.62, monoclinic, space group $C2/c$, a = 18.249(4), b = 16.260(3), c = 10.053(2) Å, β = 111.47(3)°, V = 2776.0(10) Å^3, Z = 4, D_c = 1.298 Mg m^{-3}, T = 100 K, 3138 unique reflections, $R1$ = 0.043, $wR2$ = 0.106. CCDC 186035. **1**·1,10-phenanthroline: $C_8H_{12}N_2O_3{\cdot}C_{12}H_8N_2$, M = 364.40, monoclinic, space group $P2_1/c$, a = 12.656(3), b = 7.014(1), c = 20.665(4) Å, β = 98.31(3)°, V = 1815.1(6) Å^3, Z = 4, D_c = 1.333 Mg m ^{3}, T = 100 K, 4096 unique reflections, $R1$ = 0.060, $wR2$ = 0.124. CCDC 186036. **1**·urotropine: $C_8H_{12}N_2O_3{\cdot}C_6H_{12}N_4$, M = 324.39, orthorhombic, space group $Pbca$, a = 10.866(2), b = 13.263(3), c = 22.634(5) Å, V = 3262.0(11) Å^3, Z = 8, D_c = 1.321 Mg m^{-3}, T = 100 K, 3736 unique reflections, $R1$ = 0.065, $wR2$ = 0.119. CCDC 186037. See http://www.rsc.org/suppdata/cc/b2/b204388b/ for crystallographic data in .cif or other electronic format. KUMA CCD detector, ω scan mode. Structure solution and refinement with standard methods (SHELX97); H-atoms refined isotropically.

1 G. R. Desiraju, in *Stimulating concepts in chemistry*, eds. F. Vögtle, J. F. Stoddart and M. Shibasaki, Wiley-VCH, 2000, pp. 293–306.
2 G. R. Desiraju, *Angew. Chem., Int. Ed. Engl.*, 1995, **34**, 2311.
3 F. H. Allen, W. D. S. Motherwell, P. R. Raithby, G. P. Shields and R. Taylor, *New J. Chem.*, 1999, 25.
4 (*a*) V. R. Pedireddi, W. Jones, A. P. Chorlton and R. Docherty, *Chem. Commun.*, 1996, 997; (*b*) E. Batchelor, J. Klinowski and W. Jones, *J. Mater. Chem.*, 2000, **10**, 839.
5 (*a*) C. V. K. Sharma and M. J. Zaworotko, *Chem. Commun.*, 1996, 2655; (*b*) A. Anthony and G. R. Desiraju, *Supramolecular Chemistry*, 2001, **13**, 11; (*c*) C. B. Aakeröy, A. M. Beatty and B. A. Helfrich, *Angew. Chem., Int. Ed.*, 2001, **40**, 3240.
6 G. R. Desiraju and T. Steiner, *The Weak Hydrogen Bond in Structural Chemistry and Biology*, Oxford University Press, Oxford, 1999.
7 (*a*) J. E. Field and D. Venkataraman, *Chem. Commun.*, 2002, 306; (*b*) P. I. Coupar, C. Glidewell and G. Ferguson, *Acta Crystallogr., Sect. B*, 1997, **53**, 521 and references cited therein.
8 S. J. Geib, C. Vicent, E. Fan and A. D. Hamilton, *J. Am. Chem. Soc.*, 1993, **32**, 119.

UM00012451
NOVARTIS EXHIBIT 1017
Novartis v. Regents, IPR2023-01346
Page 1197 of 4460

Supramolecular synthons in phenol–isonicotinamide adducts



Paper

Peddy Vishweshwar,[a] Ashwini Nangia*[a] and Vincent M. Lynch[b]

[a]*School of Chemistry, University of Hyderabad, Hyderabad 500 046, India. E-mail: ansc@uohyd.ernet.in*
[b]*Department of Chemistry and Biochemistry, University of Texas, Austin, Texas 78712, USA*

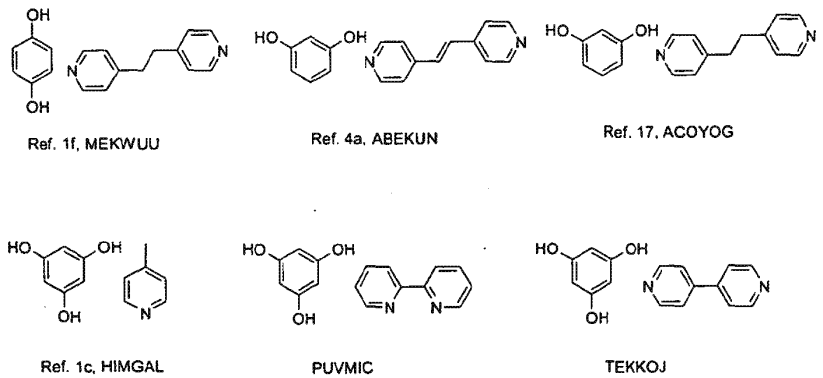
Received 14th April 2003, Accepted 8th May 2003
First published as an Advance Article on the web 20th May 2003

Molecular complexes of four phenols (hydroquinone, resorcinol, phloroglucinol and 4-hydroxybenzoic acid) with isonicotinamide are characterized by X-ray diffraction. (Hydroquinone)$_{0.5}$·(isonicotinamide) **1** and (resorcinol)·(isonicotinamide)$_2$ **2** have tapes of O–H···N and amide N–H···O dimer synthons. In (phloroglucinol)·(isonicotinamide)$_2$·(H$_2$O)$_2$ **3**, six component self-assembly results in stacked dimers with four O–H···N and four amide N–H···O hydrogen bonds and the third phenol OH aggregates with two water molecules in a supramolecular chair cyclohexane array. Phenol···pyridine and amide N–H···O dimers are robust synthons in **1–3** for the self-assembly of 0D discrete aggregates and infinite 1D chains. Hydrogen bonding of amide dimers *via* N–H···O$_{phenol/water}$ is ascribed to cooperative effects. The crystal structure of (4-hydroxybenzoic acid)·(isonicotinamide) **4** establishes the robustness of phenol···pyridine hydrogen bonding in the presence of carboxylic acid groups. Molecular components in **4** are arranged as zigzag tapes of O–H···N hydrogen bonds and acid···amide heterodimers. Supramolecular synthesis with phenol–isonicotinamide adducts expands the versatility of isonicotinamide as a co-crystallizing agent in crystal engineering.

Introduction

Crystallization of phenol with pyridine (O–H···N hydrogen bond) has been examined to build structures with intricate supramolecular architectures,[1] for non-linear optics,[2] to synthesize host–guest complexes,[3] and as a supramolecular template to direct topochemical reactions.[4] Proton transfer in a very short O–H···N hydrogen bond in pentachlorophenol–4-methylpyridine has been studied by variable temperature neutron diffraction.[5] Supramolecular organization is controlled by the strong and directional O–H···N hydrogen bond in co-crystals of diverse phenol molecules with various pyridine derivatives, some of which are displayed in Scheme 1. However, co-crystallization of phenols with isonicotinamide is not reported. Perusal of recent literature shows that carboxylic acids have been co-crystallized with isonicotinamide.[6] We reasoned that bis- and tris-phenols would hydrogen bond with the pyridine moiety of isonicotinamde and the amide group would extend the hydrogen bond aggregate *via* dimer synthon. Another reason for studying phenol–isonicotinamide co-crystals is to better understand hydrogen bond competition and interplay between O–H···O, O–H···N and N–H···O hydrogen bonds in binary systems.

We report and discuss in this paper X-ray crystal structures of (hydroquinone)$_{0.5}$·(isonicotinamide) **1**, (resorcinol)·(isonicotinamide)$_2$ **2**, (phloroglucinol)·(isonicotinamide)$_2$·(H$_2$O)$_2$ **3**, and (4-hydroxybenzoic acid)·(isonicotinamide) **4**. Crystals **1** and **2** have predictable 1D chains assembled *via* O–H···N hydrogen bond **I** and amide dimer **II** (Scheme 2). The chains are infinite in **1** and **2** whereas in **3** phenol–isonicotinamide recognition results in finite stacked dimers of synthons **I** and **II** that extend *via* the third OH group of phloroglucinol as dihydrate. Competition between four functional groups in co-crystallization of **4** results in zigzag tapes of phenol···pyridine O–H···N hydrogen bond **I** and acid···amide heterodimer **III**. The fact that synthon **I** prevails in the presence of COOH

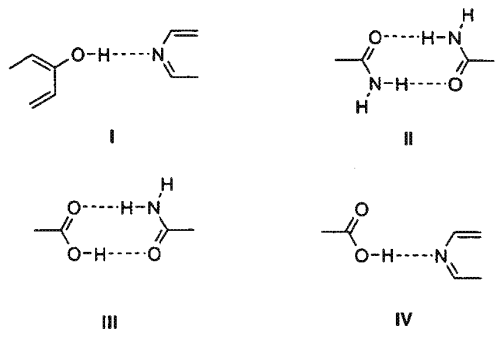


Scheme 1 Some examples of phenol–pyridine co-crystals found in the Cambridge Structural Database (CSD).

 DOI: 10.1039/b304078j

This journal is © The Royal Society of Chemistry 2003

UM00012452
NOVARTIS EXHIBIT 1017
Novartis v. Regents, IPR2023-01346
Page 1198 of 4460



Scheme 2 Hydrogen bond synthons discussed in this paper.

groups suggests that phenol···pyridine hydrogen bonding is specific and strong. Supramolecular synthons[7] are structural units that direct self-assembly in crystal structures.

Experimental

Chemicals were purchased from Lancaster and used as such for the crystallization. In all co-crystallization experiments the components were finely ground manually and dissolved in appropriate solvents in the stoichiometry mentioned below.

(Hydroquinone)$_{0.5}$·(isonicotinamide) 1. Hydroquinone (0.022 g, 0.20 mmol) and isonicotinamide (0.05 g, 0.40 mmol) were dissolved in hot EtOH. Colorless, needle-shaped crystals were formed after a few days upon evaporation of the solvent. mp: 155 °C.

(Resorcinol)·(isonicotinamide)$_2$ 2. A 1 : 2 mixture of resorcinol (0.025 g, 0.23 mmol) and isonicotinamide (0.055 g, 0.46 mmol) was dissolved in hot EtOAc. Needle shaped, light brown crystals were obtained after a few days. mp: 155 °C.

(Phloroglucinol)·(isonicotinamide)$_2$·(H$_2$O)$_2$ 3. Phloroglucinol (0.017 g, 0.14 mmol) and isonicotinamide (0.05 g, 0.42 mmol) were ground and dissolved in acetone. Colorless crystals of the dihydrate were obtained the next day after evaporation of solvent. mp: 144 °C.

(4-Hydroxybenzoic acid)·(isonicotinamide) 4. Colorless, plate like crystals of the 1 : 1 complex were obtained upon crystallization of 4-hydroxybenzoic acid (0.028 g, 0.205 mmol) and isonicotinamide (0.025 g, 0.205 mmol) from hot MeOH. mp: 195 °C.

X-Ray diffraction

Reflections were collected on a Nonius Kappa CCD diffractometer at 153(2) K using incident X-ray radiation Mo-Kα (λ = 0.71073 Å). Crystals were cooled with an Oxford Cryosystem device attached to the CCD machine. Data reductions were performed using DENZO-SMN.[8] Structures were solved by direct methods using SHELXS-97[9] and refined by full-matrix least-squares refinement on F^2 with anisotropic displacement parameters for non-H atoms using SHELXL-97.[9] The function, $\Sigma w(|F_o|^2 - |F_c|^2)^2$, was minimized, where $w = 1/[(\sigma(F_o))^2 + (aP)^2 + (bP)]$, $P = (|F_o|^2 + 2|F_c|^2)/3$, and parameters a and b are suggested by the refinement results. Neutral atom scattering factors and values used to calculate the linear absorption coefficient are taken from the International Tables for X-ray Crystallography. Geometrical analysis was carried out in PLATON.[10] Details of cell parameters, data collection and structure refinement are summarized in Table 1. Hydrogen bond metrics (Table 2) are neutron normalized because the H atoms were only located with limited accuracy by X-ray diffraction.

CCDC reference numbers 208482–208485.

See http://www.rsc.org/suppdata/ce/b3/b304078j/ for crystallographic data in CIF or other electronic format.

Results and discussion

In the crystal structure of **1** hydroquinone resides around a crystallographic inversion center at ½, ½, ½ in space group $P2_1/c$. The molecules aggregate as linear tapes along [1 −2 1] through O–H···N hydrogen bond **I** (1.73 Å, 2.693(2) Å, 165.1°) and centrosymmetric amide N–H···O dimer **II** (1.93 Å, 2.932(2) Å, 171.7°), as shown in Fig. 1. The primary amide does not extend through the normal 5.1 Å translation[11] but instead hydrogen bonds with the phenol O atom of a screw axis related tape (N–H···O$_{phenol}$: 2.11 Å, 3.110(2) Å, 169.1°). A search of the Cambridge Structural Database[12] (ConQuest 1.5, November 2002 update) for motif **V** wherein the amide dimer is hydrogen bonded to OH groups shows that it is present in five crystal structures and motif **VI** occurs in one structure.[13]

Table 1 Crystallographic data and structure refinement parameters[a]

	1	2	3	4
Chemical formula	$(C_6H_6O_2)_{0.5}\cdot(C_6H_6N_2O)$	$(C_6H_6O_2)\cdot(C_6H_6N_2O)_2$	$(C_6H_6O_3)\cdot(C_6H_6N_2O)_2\cdot(H_2O)_2$	$(C_7H_6O_3)\cdot(C_6H_6N_2O)$
Formula weight	177.18	354.36	406.40	260.25
Crystal system	Monoclinic	Triclinic	Triclinic	Monoclinic
Space group	$P2_1/c$	$P\bar{1}$	$P\bar{1}$	$P2_1/n$
a/Å	14.2811(4)	7.0307(1)	7.4967(1)	6.0729(1)
b/Å	5.4136(2)	10.7052(2)	8.8748(1)	9.4013(2)
c/Å	11.9110(3)	11.9562(2)	15.2793(3)	20.6723(4)
α/°	90.0	87.755(1)	95.1886(6)	90.0
β/°	111.934(1)	82.735(1)	97.4790(6)	95.287(1)
γ/°	90.0	73.835(1)	105.7701(7)	90.0
Z	4	2	2	4
V/Å^3	854.21(5)	857.36(2)	961.50(3)	1175.23(4)
D_{calc}/g cm^{-3}	1.378	1.373	1.404	1.471
μ/mm^{-1}	0.100	0.100	0.110	0.111
Reflns. collected	3354	7843	6903	4946
Unique reflns.	1933	4462	4275	2684
Observed reflns.	1277	3324	3583	1952
R_1 [$I > 2\sigma(I)$]	0.044	0.041	0.036	0.041
wR_2 [all]	0.113	0.115	0.098	0.105
Goodness-of-fit	1.040	1.070	1.051	1.029

[a] $R_w(F^2) = \{\Sigma w(|F_o|^2 - |F_c|^2)^2/\Sigma w(|F_o|)^4\}^{1/2}$ where w is the weight given to each reflection. $R(F) = \Sigma(|F_o| - |F_c|)/\Sigma|F_o|$ for reflections with $F_o > 4(\sigma(F_o))$. $S = [\Sigma w(|F_o|^2 - |F_c|^2)^2/(n - p)]^{1/2}$, where n is the number of reflections and p is the number of refined parameters.

UM00012453
NOVARTIS EXHIBIT 1017
Novartis v. Regents, IPR2023-01346
Page 1199 of 4460

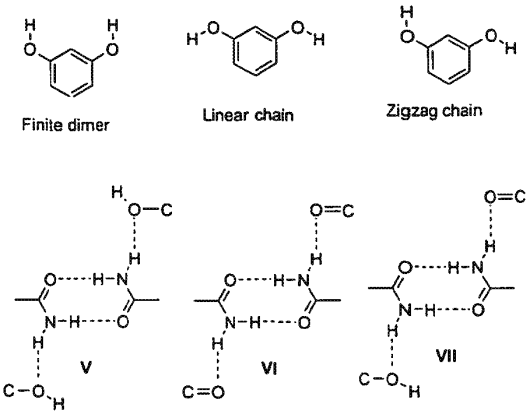
Table 2 Geometrical parameters of hydrogen bonds[a]

Co-crystal	H-bond	d/Å	D/Å	θ/°
1	O–H···N	1.73	2.6936(16)	165.1
	N–H···O	1.93	2.9321(19)	171.7
	N–H···O	2.11	3.1100(20)	169.1
	C–H···O	2.30	3.3270(20)	156.9
	C–H···O	2.51	3.1370(20)	115.5
2	O–H···N	1.75	2.7225(14)	168.7
	O–H···N	1.78	2.7198(15)	159.0
	N–H···O	1.87	2.8764(15)	176.2
	N–H···O	1.95	2.8657(15)	149.8
	N–H···O	2.02	3.0208(15)	168.6
	N–H···O	2.14	3.1202(15)	162.4
	C–H···O	2.36	3.2262(17)	135.4
	C–H···O	2.67	3.5682(17)	140.1
	C–H···O	2.75	3.5815(17)	133.2
3	O–H···O	1.65	2.6275(14)	173.0
	O–H···O	1.81	2.7899(15)	170.3
	O–H···O	1.81	2.7967(14)	178.2
	O–H···O	1.83	2.8172(14)	175.3
	O–H···O	1.94	2.8878(14)	160.1
	O–H···N	1.77	2.7555(14)	174.5
	O–H···N	1.81	2.7953(14)	179.2
	N–H···O	1.91	2.9128(15)	174.1
	N–H···O	1.92	2.9292(15)	176.2
	N–H···O	2.14	3.0464(16)	148.5
	N–H···O	2.48	3.3096(16)	138.6
	C–H···O	2.44	3.2249(16)	128.4
	C–H···O	2.48	3.5438(17)	166.9
	C–H···O	2.65	3.4998(17)	134.5
	C–H···O	2.70	3.7749(17)	170.0
	C–H···N	2.48	3.2895(17)	130.2
	C–H···N	2.67	3.4132(16)	125.6
4	O–H···O	1.61	2.5796(15)	168.5
	O–H···N	1.78	2.7459(17)	165.2
	N–H···O	1.98	2.9760(17)	168.2
	N–H···O	2.46	3.2931(17)	139.3
	N–H···O	2.47	3.1334(17)	122.6
	C–H···O	2.44	3.2060(20)	126.8
	C–H···O	2.51	3.5050(20)	152.4
	C–H···O	2.61	3.4670(20)	135.0
	C–H···O	2.73	3.5171(18)	129.3

[a] O–H, N–H and C–H bond lengths are neutron-normalized.

We note the similarity of hydrogen bonding in **1** with 4-hydroxybenzamide monohydrate (JIXCOI, $P2_1/a$)[14] in which amide dimers hydrogen bond with the OH group of a 2_1-related molecule (N–H···O: 2.08 Å, 168.4°).

The crystal structure of **2** in space group $P\bar{1}$ contains one molecule of resorcinol and two molecules of isonicotinamide. Of the three possible conformations of resorcinol OH groups, the divergent form that leads to a linear tape is present in **2** (synthon **I**: (i) 1.78 Å, 2.719(2) Å, 159.0°; (ii) 1.75 Å, 2.722(2) Å, 168.7°). Symmetry-independent isonicotinamide molecules extend the chain along [2 1 −1] *via* dimer **II** (Fig. 2; N–H···O: (iii) 1.87 Å, 2.876(2) Å, 176.2°; (iv) 2.02 Å, 3.020(2) Å, 168.6°). The second NH of the amide groups hydrogen bonds with amide and phenol O atoms of inversion-related tapes (N–H···O_{amide} (v) 1.95 Å, 2.865(2) Å, 149.8°; N–H···O_{phenol} (vi) 2.14 Å, 3.120(2) Å, 162.4°) to produce a 2D sheet parallel to (−1 2 0). The amide donor with the shorter N–H···O bond in synthon **II** (iii) has a longer second contact (vi) and *vice versa* (iv and v). There are no examples in the CSD of primary amides with symmetry-independent dimers **II** that hydrogen bond to different acceptor groups, C=O and OH (motif **VII**). Generally, carbonyl oxygen is the preferred acceptor for H atoms in primary amides. The cooperative hydrogen bond array[15] in motif N–H···O_{phenol}–H···N perhaps polarizes the acceptor and makes it comparable to an amide C=O group.



Crystallization of phloroglucinol and isonicotinamide in a 1 : 3 ratio afforded dihydrate **3**, (phloroglucinol)·(isonicotinamide)$_2$·$(H_2O)_2$. Six-component self-assembly involving two phloroglucinol and four isonicotinamide molecules produce a stacked dimer of 1 : 2 stoichiometry ($P\bar{1}$, Fig. 3). Two phenol groups hydrogen bond with the symmetry independent isonicotinamide molecules (O–H···N **I**: (i) 1.77 Å, 2.755(2) Å, 174.5°; (ii) 1.81 Å, 2.795(2) Å, 179.2°) that are in turn bonded *via* symmetry-independent amide dimer **II** (N–H···O: (iii) 1.92 Å, 2.929(2) Å, 176.2°; (iv) 1.91 Å, 2.912(2) Å, 174.1°). These stacked dimer units constructed from inversion-related phloroglucinol and isonicotinamide molecules are hydrogen bonded along [0 1 2] *via* the third phenol and two water molecules. Phenol to water hydrogen bond (O–H···O: (v) 1.65 Å, 2.627(2) Å, 173.0°) is shorter than H-bonds from water ((vi) 1.81 Å, 2.796(2) Å, 178.2°; (vii) 1.81 Å, 2.789(2) Å, 170.3°), as expected. Two phenol and four water molecules form a supramolecular chair cyclohexane with O–H···O hydrogen

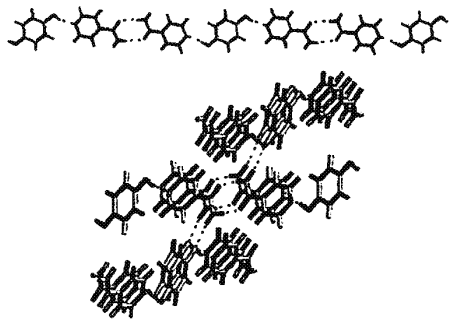


Fig. 1 (a) Linear tape of O–H···N synthon I and amide dimer II in (hydroquinone)$_{0.5}$·(isonicotinamide) **1**. Click here to access a 3D representation. (b) N–H···O_{phenol} hydrogen bond between 2_1 related tapes.Click here to access a 3D representation. See text for metrics of H-bonds.

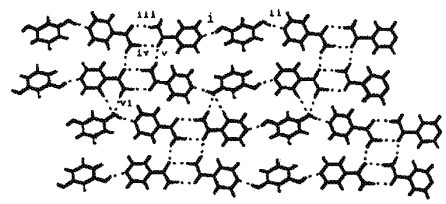


Fig. 2 Linear tapes of O–H···N synthon I and amide dimer II in (resorcinol)·(isonicotinamide)$_2$ **2**. Synthon **II** is between symmetry-independent amide molecules. Inversion-related tapes are connected *via* N–H···O_{amide} and N–H···O_{phenol} H-bonds into 2D sheets parallel to (−1 2 0). See text for metrics of H-bonds i, ii, iii, *etc.*Click here to access a 3D representation.

UM00012454
NOVARTIS EXHIBIT 1017
Novartis v. Regents, IPR2023-01346
Page 1200 of 4460

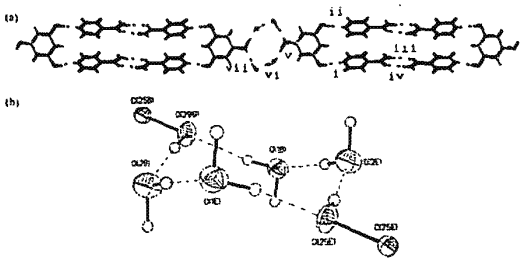


Fig. 3 (a) Six component self-assembly in (phloroglucinol)·(isonicotinamide)$_2$·(H$_2$O)$_2$ 3 through eight hydrogen bonds of synthons I and II. The third OH of phloroglucinol is hydrogen bonded to water molecules. See text for metrics of H-bonds i, ii, iii, *etc*.Click here to access a 3D representation. (b) Supramolecular chair cyclohexane of O–H···O hydrogen bonds from two phenol and four water molecules.

bonds.[16] The six O atoms are related by a center of symmetry, the most common (81%) torsion pattern in R6 water clusters.[16a] The left over amide NH hydrogen bond with phenol and water oxygen acceptors (N–H···O$_{water}$: 2.14 Å, 3.046(2) Å, 148.5°; N–H···O$_{phenol}$: 2.48 Å, 3.309(2) Å, 138.6°) through interactions at the long (weak) distance range. It may be noted that the N–H···O$_{amide}$ hydrogen bond formed from the dimer aggregate is replaced by N–H···O$_{phenol/water}$ in this series of co-crystals.

Three types of supramolecular organization are possible for 1,3/1,4-bis- and 1,3,5-tris-phenols: infinite chain,[1f] finite dimer[1d] and trigonal motif.[1c] When π–π stacking stabilizes the strong hydrogen bond assembly, finite dimers are preferred over infinite chains in adducts with resorcinol.[4a] The placement of an electronegative Cl atom in resorcinol steers the infinite chain motif towards a finite stacked dimer.[17] In light of these observations we feel that weak π–π stacking (3.9–4.0 Å) of the pyridyl rings appears to tip the structure towards a discrete dimer in 3 compared to an infinite chain in 2. Another reason for the 1D chain in 2 could be that this motif promotes crystal growth through strong hydrogen bonds. The 0D discrete dimer in 3 is able to use the third phenol group for assembly into larger aggregates through water molecules. Our results supplement structural trends in phenol–pyridine co-crystals with O–H···N synthon I (Scheme 1). Hydrogen bonding of an amide group to a OH acceptor is a new recurring motif in these crystal structures.

The 1 : 1 co-crystal of (4-hydroxybenzoic acid)·(isonicotinamide) 4 ($P2_1/n$) is a multi-functional system suited to study hydrogen bond competition between phenol, acid, pyridine and amide groups (Fig. 4). Phenol···pyridine and acid···amide synthons I and III (O–H···N: 1.78 Å, 2.745(2) Å, 165.2°; O–H···O: 1.61 Å, 2.579(2) Å, 168.5°; N–H···O: 1.98 Å, 2.976(2) Å, 168.2°) assemble *n*-glide related molecules as zigzag tapes. Such inversion related tapes are connected by

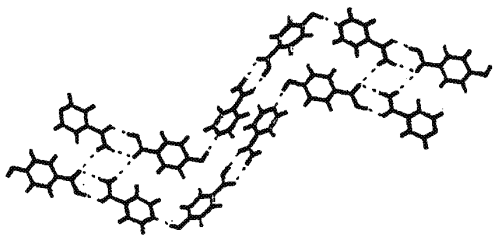


Fig. 4 Zigzag tapes of alternating phenol···pyridine I and acid···amide III in (4-hydroxybenzoic acid)·(isonicotinamide) 4. The tapes are connected by N–H···O$_{acid}$ H-bonds. Note that the crystal structure is stabilized by heterosynthons. See text for metrics of H-bonds.Click here to access a 3D representation.

amide-to-acid N–H···O hydrogen bonds (2.46 Å, 3.293(2) Å, 139.3°) and weak C–H···O interactions (Table 2). There are at least two other supramolecular organization modes possible in 4. (1) In the crystal structure of (3,5-dihydroxybenzoic acid)$_2$·(4,4-bipyridine)$_3$ (space group $P\bar{1}$)[1d] both phenol OH and COOH groups are hydrogen bonded to a pyridine acceptor *via* O–H···N hydrogen bonds I and IV. (2) The crystal structure of (3-hydroxybenzoic acid)·(isonicotinamide) (1 : 1, $C2/c$)[6h] is stabilized by acid···pyridine and amide···amide hydrogen bonds IV and II. The occurrence of different combinations of synthons I–IV in a given molecular adduct involving hydrogen bonding between the same functional groups implies that their energy is comparable. We are computing hydrogen bond energies in experimental crystal structures and also other possible structures that are not observed. Co-crystal 4 is the first example of a carboxylic acid–isonicotinamide adduct with phenol···pyridine and acid···amide synthons I and III. On the other hand, over a dozen structures with acid···pyridine and amide···amide synthons IV and II have been published under the banner of high-yield supramolecular reactions.[6b] Desiraju[18] has emphasized the need to report low yield supramolecular reactions also because they provide new information about molecular recognition and hydrogen bond preferences. In the present context, isolation of minor product 4 leads to the question: are there other carboxylic acid–isonicotinamide co-crystals with the same synthon and furthermore what chemical modification will favor this motif?

Conclusions

Crystal engineering[19] with complementary multi-functional systems requires a proper understanding of the factors that control supramolecular organization when different hydrogen bond synthons are in competition. Crystal structures 1–3 of phenol–isonicotinamide adducts have recurring O–H···N synthon I and amide dimer II. The OH group of phenol/water appears to be a better hydrogen bond acceptor for the amide NH than C=O, perhaps because of cooperative effects in the former motif. The change from infinite chains in 2 to stacked dimers in 3 is ascribed to stabilization from weak π···π stacking in the latter structure. The 'low-yield' adduct 4 provides the first example of a carboxylic acid–isonicotinamide co-crystal with acid···amide synthon III without acid···pyridine recognition IV. Phenol···pyridine synthon I is a persistent recognition pattern in the present family of co-crystals. To conclude, some novel hydrogen bonding features in the supramolecular organization of phenol–isonicotinamide adducts are observed that could not have been anticipated from hydrogen bond synthons in phenol–pyridine and carboxylic acid–isonicotinamide co-crystals.

Acknowledgements

A. N. thanks the CSIR (01/1738/02/EMR-II) for research funding. P. V. thanks the CSIR for fellowship support. V. M. L. thanks the National Science Foundation (Project No. CHE-9807702) for funding.

References and notes

1 (*a*) A. C. Bényei, P. I. Coupar, G. Ferguson, C. Glidewell, A. J. Lough and P. R. Meehan, *Acta Crystallogr., Sect. C*, 1998, 54, 1515; (*b*) T. L. Nguyen, A. Scott, B. Dinkelmeyer, F. W. Fowler and J. W. Laugher, *New J. Chem.*, 1998, 22, 129; (*c*) K. Biradha and M. J. Zaworotko, *J. Am. Chem. Soc.*, 1998, 120, 6431; (*d*) P. S. Wheatley, A. J. Lough, G. Ferguson and C. Glidewell, *Acta Crystallogr., Sect. C*, 1999, 55, 1489; (*e*) G. Ferguson, C. Glidewell, R. M. Gregson and E. S. Lavender, *Acta Crystallogr., Sect. B*, 1999, 55, 573; (*f*) E. Corradi, S. V. Meille, M. T. Messina, P. Metrangolo and G. Resnati, *Angew. Chem., Int.*

UM00012455
NOVARTIS EXHIBIT 1017
Novartis v. Regents, IPR2023-01346
Page 1201 of 4460

Ed., 2000, **39**, 1782; (*g*) C. M. Zakaria, G. Ferguson, A. J. Lough and C. Glidewell, *Acta Crystallogr., Sect. C*, 2002, **58**, o1.
2 K.-S. Huang, D. Britton, M. C. Etter and S. R. Byrn, *J. Mater. Chem.*, 1997, **7**, 713.
3 (*a*) M. R. Caira, A. Horne, L. R. Nassimbeni and F. Toda, *J. Mater. Chem.*, 1997, **7**, 2145; (*b*) G. Ferguson, C. Glidewell, A. J. Lough, G. D. McManus and P. R. Meehan, *J. Mater. Chem.*, 1998, **8**, 2339; (*c*) L. R. MacGillivray, J. L. Reid and J. A. Ripmeester, *CrystEngComm*, 1999, **1**, 1; (*d*) L. R. MacGillivray, J. L. Reid and J. A. Ripmeester, *Chem. Commun.*, 2001, 1034; (*e*) B.-Q. Ma, Y. Zhang and P. Coppens, *Cryst. Growth Des.*, 2001, **1**, 271; (*f*) J. Scott, M. Asami and K. Tanaka, *New J. Chem.*, 2002, **26**, 1822; (*g*) B.-Q. Ma, Y. Zhang and P. Coppens, *Cryst. Growth Des.*, 2002, **2**, 7; (*h*) S. Hoger, D. L. Morrison and V. Enkelman, *J. Am. Chem. Soc.*, 2002, **124**, 6734.
4 (*a*) L. R. MacGillivray, J. L. Reid and J. A. Ripmeester, *J. Am. Chem. Soc.*, 2000, **122**, 7817; (*b*) L. R. MacGillivray, *CrystEngComm*, 2002, **4**, 37.
5 T. Steiner, I. Majerz and C. C. Wilson, *Angew. Chem., Int. Ed.*, 2001, **40**, 2651.
6 (*a*) C. B. Aakeröy, A. M. Beatty and B. A. Helfrich, *Angew. Chem., Int. Ed.*, 2001, **40**, 3240; (*b*) C. B. Aakeröy, A. M. Beatty and B. A. Helfrich, *J. Am. Chem. Soc.*, 2002, **124**, 14425; (*c*) C. B. Aakeröy, A. M. Beatty, B. A. Helfrich and M. Nieuwenhuyzen, *Cryst. Growth Des.*, 2003, **3**, 159.
7 G. R. Desiraju, *Angew. Chem., Int. Ed. Engl.*, 1995, **34**, 2311.
8 Z. Otwinowski and W. Minor, DENZO-SMN, in *Methods in Enzymology, Macromolecular Crystallography, Part A*, eds. C. W. Carter, Jr. and R. M. Sweets, Academic Press, New York, 1997, **vol. 276**.
9 G. M. Sheldrick, SHELX-97, Package for Crystal Structure Solution and Refinement, University of Göttingen, Germany, 1997.
10 A. L. Spek, PLATON, Bijvoet Center for Biochemical Research, University of Utrecht, The Netherlands, 2002.
11 (*a*) L. Leiserowitz and G. M. J. Schmidt, *J. Chem. Soc. A*, 1969, 2372; (*b*) L. Leiserowitz and M. Tuval, *Acta Crystallogr., Sect. B*, 1978, **34**, 1230.
12 F. H. Allen, *Acta Crystallogr., Sect. B*, 2002, **58**, 380.
13 The CSD (ConQuest 1.5, November 2002) contains 225 hits with $CONH_2$ and COH fragments having $R \leqslant 0.10$ and 3D coordinates determined. Of these, 27 structures contain amide dimer II, five structures contain motif V (CERNIW, JIXCOI, OHPHXD, RUJVAT, WEGYEM), and one structure has motif VI (MEGLOZ) in the distance–angle range $1.5 < H\cdots O < 2.4$ Å (HNORM) and $130 < \angle N\text{–}H\cdots O < 180°$.
14 S. Kashimo, S. Tateno, H. Tanabe, M. Haisa and Y. Katsube, *Acta Crystallogr., Sect. C*, 1991, **47**, 2236.
15 (*a*) G. A. Jeffrey, *An Introduction to Hydrogen Bonding*, Oxford University Press, New York, 1997; (*b*) P. Vishweshwar, A. Nangia and V. M. Lynch, *Chem. Commun.*, 2001, 179; (*c*) B. R. Bhogala, P. Vishweshwar and A. Nangia, *Cryst. Growth Des.*, 2002, **2**, 325.
16 (*a*) L. Infantes and S. Motherwell, *CrystEngComm*, 2002, **4**, 454; (*b*) R. Ludwig, *Angew. Chem., Int. Ed.*, 2001, **40**, 1808; (*c*) R. Custelcean, C. Afloroaei, M. Vlassa and M. Polverejan, *Angew. Chem., Int. Ed.*, 2000, **39**, 3094; (*d*) J. N. Moorthy, R. Natarajan and P. Venugopalan, *Angew. Chem., Int. Ed.*, 2002, **41**, 3417; (*e*) K.-M. Park, R. Kuroda and T. Iwamoto, *Angew. Chem., Int. Ed. Engl.*, 1993, **32**, 884.
17 G. S. Papaefstathiou and L. R. MacGillivray, *Org. Lett.*, 2001, **3**, 3835.
18 P. K. Thallapally, A. K. Katz, H. L. Carrell and G. R. Desiraju, *CrystEngComm*, 2003, **5**, 87.
19 G. R. Desiraju, *Crystal Engineering: The Design of Organic Solids*, Elsevier, New York, 1989.

UM00012456
NOVARTIS EXHIBIT 1017
Novartis v. Regents, IPR2023-01346
Page 1202 of 4460

Evie Sun

From: Rick Gyory
Sent: Monday, September 15, 2003 6:46 AM
To: Chris Moore; Truc Tran; Evie Sun
Subject: FW: TPI Conference call: Galantamine flux work
Importance: High

I may need to call in separately, and may not be able to call in at all.

We ARE NOT USING THE CONFERENCE BRIDGE. sEE THE CONTACT NUMBER BELOW.

Rick
-----Original Message-----
From: Yates, Barbara [mailto:Barbara.Yates@Alza.com]
Sent: Thursday, September 11, 2003 5:14 PM
To: Audett, Jay; TFP: Gyory, Rick; TFP: Moore, Chris; Goldman, Eli; Wen, Jack; Nedberge, Diane; Van Osdol, Bill [ALZUS]
Cc: Imbert, Delphine
Subject: TPI Conference call: Galantamine flux work
Importance: High

When: Monday, September 15, 2003 1:00 PM-2:00 PM (GMT-08:00) Pacific Time (US & Canada); Tijuana.
Where: Dial in # below; not bridge line

~~*~*~*~*~*~*~*~*~*

Conference Call Information
Toll-Free Number 866-222-0917
International, Caller Paid 803-477-2000

Participant Code 879688
Customer Care 888-864-5656 or 205-791-4402

UM00012457
NOVARTIS EXHIBIT 1017
Novartis v. Regents, IPR2023-01346
Page 1203 of 4460

Barbiturates and Adenine Derivatives. Molecular Structure of a Hydrogen-Bonded Complex

Donald Voet and Alexander Rich*

Contribution from the Department of Biology, Massachusetts Institute of Technology, Cambridge, Massachusetts 02139. *Received January 7, 1972*

Abstract: A crystalline 1:1 intermolecular complex has been formed between 9-ethyladenine and 5-isopropyl-5-bromoallylbarbituric acid. The complex crystallizes in a triclinic unit cell, the molecular structure of which has been solved by X-ray diffraction analysis. It was found that the molecules form linear hydrogen-bonded arrays in which the adenine derivative forms a pair of hydrogen bonds with one barbituric acid molecule using the Watson–Crick bonding that is found in DNA. In addition, the adenine forms another pair of hydrogen bonds with a second barbituric acid molecule using the imidazole bonding that has often been observed in crystalline complexes of derivatives of adenine and uracil. Each molecule in the complex thus participates in four different hydrogen bonds.

Barbiturates have diverse actions in biological systems. In addition to their widely known sedative effects, they are also regarded as general metabolic depressants because they inhibit a large number of enzyme systems, including those involved in oxidative phosphorylation.[1] A great deal of information concerning the complex pharmacological activities of the barbiturates has been accumulated, but very little is known concerning the molecular basis of their activities.

The barbiturates are derivatives of uracil. Solution studies of the specificity of hydrogen bonding among purines, pyrimidines, and barbiturates have shown that the barbiturates have a selective affinity for forming strongly hydrogen-bonded complexes with a variety of adenine derivatives. This strong association has been demonstrated by infrared studies,[2] and by the formation of a number of crystalline intermolecular complexes containing derivatives of adenine and the barbiturates.[3] The molecular basis of the extremely varied pharmacological effects of the barbiturates might therefore be understood in terms of the strong association of the barbiturates with adenine-containing coenzymes as well as with molecules, such as cyclic AMP, that play an important role in controlling various metabolic activities. Thus, it is of considerable interest to determine the detailed molecular geometry of the complexes between barbiturates and adenine derivatives.

The crystallographic analysis of one complex containing two molecules of an adenine derivative and one of a barbiturate has previously been reported.[4] In the present report we describe the structure of an intermolecular complex containing a commercially available barbiturate, 5-isopropyl-5-bromoallylbarbituric acid, and 9-ethyladenine. In this 1:1 complex the two types of molecules are organized into infinite ribbons of alternating adenine and barbiturate residues in which adjacent adenine and barbiturate molecules interact through a pair of hydrogen bonds.

9-Ethyladenine (Cyclo Chemical Corp.) and 5-isopropyl-5-bromoallylbarbituric acid (Riedel-deHaen, A. G., Hanover, West Germany) were mixed together in equimolar amounts and dissolved in 50% aqueous ethanol. The solution was allowed to evaporate to dryness, yielding a number of flat prismatic crystals with well-developed faces approximately 0.2–0.4 mm in diameter. The ultraviolet spectrum of an aqueous solution of one of these crystals revealed that the adenine and the barbiturate derivative were present in the crystal in equimolar amounts.

Precession and Weissenberg X-ray diffraction photographs showed that the complex crystallized in a triclinic lattice. The unit cell parameters of this lattice, as measured on a four-circle diffractometer, are presented in Table I. The buoyant density of the crystals was measured in a CCl_4–cyclohexane mixture. A statistical analysis of the diffraction data revealed that the space group contained a center of symmetry. Therefore, the space group of the crystal is $P\bar{1}$ and the asymmetric unit of the unit cell contains two sets of complexed molecules. Diffraction data were collected with a G.E. XRD-490 automatic diffractometer, using the stationary counter–stationary crystal method and Cu $K\alpha$ X-radiation. Observable reflections (1718) were measured out to a value of $2\theta = 120°$.[5] After correcting the intensities for the Lorentz polarization factors, a three-dimensional sharpened Patterson function was calculated. The position of the bromine

Table I. Unit Cell and Space Group Data for 9-Ethyladenine–5-Isopropyl-5-bromoallylbarbituric Acid[a]

a = 9.094 (6) Å	α = 107.05 (5)°
b = 10.056 (8) Å	β = 106.71 (5)°
c = 14.271 (7) Å	γ = 114.08 (5)°
Space group, $P\bar{1}$	
$Z = 2$	
Density (obsd) = 1.501 g/cm³	Density (calcd) = 1.496 g/cm³

[a] The quantities in parentheses are the estimated standard deviations of the least significant figure of the tabulated values.

(1) S. K. Sharpless in "The Pharmacological Basis of Therapeutics," 3rd ed, L. S. Goodman and A. Gilman, Ed., Macmillan, New York, N. Y., 1965, p 105.
(2) Y. Kyogoku, R. C. Lord, and A. Rich, *Nature (London)*, 218, 69 (1968).
(3) D. Voet, S. H. Kim, and A. Rich, unpublished results.
(4) S. H. Kim and A. Rich, *Proc. Nat. Acad. Sci.*, 60, 402 (1968).

(5) Structure factors and thermal parameters will appear following these pages in the microfilm edition of this volume of the journal. Single copies may be obtained from the Business Operations Office, Books and Journals Division, American Chemical Society, 1155 Sixteenth St., N.W., Washington, D. C. 20036, by referring to code number JACS-72-5888. Remit check or money order for $3.00 for photocopy or $2.00 for microfiche.

UM00012458
NOVARTIS EXHIBIT 1017
Novartis v. Regents, IPR2023-01346
Page 1204 of 4460

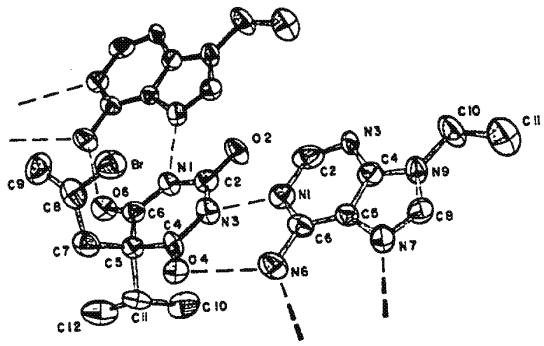


Figure 1. A perspective drawing of the hydrogen-bonded intermolecular complex 9-ethyladenine–5-isopropyl-5-bromallylbarbituric acid. The atoms are represented as thermal ellipsoids of a size such that the centers of the vibrating atoms have a 50% probability of being found within them.[7] The numbering system for the two molecules is shown in the figure.

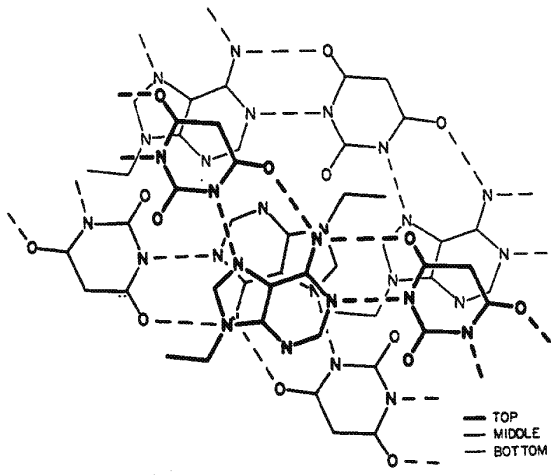


Figure 2. A projection of the crystal structure onto the plane of the aromatic rings. This shows the packing relationship among the adenine and the barbiturate rings. The side groups of the barbiturate which do not lie in the plane have been left out for the sake of clarity.

atom was located directly from analysis of the Patterson map. This information was used with the Woolfson weighting technique[6] to determine the phases and the amplitudes of the Fourier coefficients of an electron density map. This heavy-atom Fourier map revealed all 28 nonhydrogen atoms in the asymmetric unit of the unit cell. The structure was refined using full-matrix least-squares refinement, initially employing isotropic temperature factors and finally anisotropic temperature factors. The data converged to a final error residual of $R = 0.097$. Hydrogen atoms were not evident in the final difference Fourier map.

The structure of the complex together with the atomic numbering scheme used here is shown by the perspective drawing in Figure 1.[7] It can be seen that each barbiturate molecule participates in a cyclic dimer of hydrogen bonds with two neighboring adenine molecules. Thus, adenine atoms N-1 and N-6 hydrogen bond with barbituric acid atoms N-3 and O-4, respectively. This pair of hydrogen bonds resembles the Watson–Crick pairing between adenine and thymine in DNA. The second set of hydrogen bonds associates the imidazole nitrogen, N-7, and the amino group, N-6, on the second adenine molecule with barbituric acid atoms N-1 and O-6, respectively. The two adenine molecules are related by a unit cell translation. Thus, the structure forms an infinite hydrogen-bonded array of alternating adenine and barbiturate residues.

Many crystalline intermolecular complexes of adenine and uracil derivatives have been found in which the adenine forms a hydrogen-bonded cyclic dimer utilizing either its N-1 or its N-7 position as the hydrogen bond acceptor.[8] Only in the cases in which the stoichiometry of the complex is two uracil derivatives to one adenine derivative are both hydrogen bonding sites used.[8] The present structure is the only intermolecular complex of 1:1 stoichiometry reported to date in which both adenine sites are occupied. This is made possible because the barbituric acid derivative has a proton rather than some other substituent at the N-1 position, and this gives it the capability of forming a second pair of hydrogen bonds. In this respect barbituric acid derivatives are somewhat analogous to pseudouridine, a nucleoside that is found in all transfer RNA molecules. In pseudouridine the uracil ring is connected to ribose with a carbon–carbon bond to uracil atom C-5, leaving atom N-1 of the ring free to form a second set of hydrogen bonds. The barbiturate molecule in the present structure could thus be considered to be a model for a pseudouridine molecule in transfer RNA because both have the potential of forming a pair of hydrogen bonds to two different adenine bases. In the intermolecular complex of phenobarbital with two molecules of 8-bromo-9-ethyladenine[4] the barbiturate ring forms two sets of hydrogen bonds to two crystallographically independent adenine derivatives. In that crystal structure the formation of an additional pair of hydrogen bonds between symmetry-related adenine molecules exhausts the hydrogen bonding capability of the complex.

Figure 2 illustrates the mode of packing of successive layers in the lattice. As is shown in this figure, the arrays of hydrogen-bonded adenine–barbiturate complexes form an elongated flat zigzag chain. These are packed side by side in the crystal to form a layer structure. The hydrogen-bonded array at one level lies largely over and under the spaces between neighboring linear arrays of hydrogen-bonded molecules in the adjacent levels. The side chains of the barbiturate derivatives project above and below the plane of the hydrogen-bonded array to fill the space between neighboring layers in adjacent levels.

In the perspective drawing of Figure 1 the atoms are represented as thermal ellipsoids with a size such that the centers of the vibrating atoms have a 50% probability of being found within them.[7] The thermal ellipsoids are therefore indicative of the mobility of the different parts of the molecule in the crystalline lattice. It can be seen that the amino group (N-6) and the ethyl

(6) M. M. Woolfson, *Acta Crystallogr.*, 9, 804 (1956).
(7) C. K. Johnson, "ORTEP: A Fortran Thermal-Ellipsoid Plot Program for Crystal Structure Illustrations," ORNL-3794, Oak Ridge National Laboratory, Oak Ridge, Tenn., 1965.
(8) D. Voet and A. Rich, *Progr. Nucl. Acid Res. Mol. Biol.*, 10, 183 (1970).

UM00012459
NOVARTIS EXHIBIT 1017
Novartis v. Regents, IPR2023-01346
Page 1205 of 4460

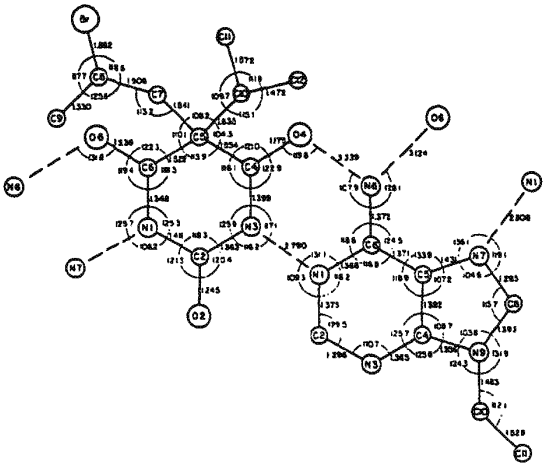


Figure 3. A schematic drawing of the complex showing the bond distances (in ångströms) and the bond angles (in degrees). Hydrogen bonds are represented by dashed lines.

group (C-10–C-11) of adenine vibrate in a direction out of the plane of the purine ring. In a similar fashion, the isopropyl group of the barbiturate (C-10, C-11, C-12) can be seen to vibrate about the C-5–C-11 bond.

The atomic coordinates of the intermolecular complex are listed in Table II. The bond distances and angles are given in Figure 3. The estimated standard deviations of these quantities are 0.02 Å and 1.0°, respectively. The bond distances and angles are generally similar to those which have been obtained from averaging the corresponding quantities in a number of crystal structures containing adenine or barbiturate derivatives.[8] An exception is found in those bonds involving atom C-10 in the barbiturate. Since no significant peaks could be detected in the difference Fourier map in that region, it is likely that the least-squares refinement did not position this atom appropriately. It has been noted by Hughes[9] that the estimated standard deviations obtained from least-squares refinement are often underestimates.

Table II. Atomic Parameters in Fractions of a Unit Cell Edge of the Crystal Structure 9-Ethyladenine–5-Isopropyl-5-bromoallylbarbituric Acid[a]

Atom	x	y	z
	9-Ethyladenine		
N-1	0.0240	0.2102	0.3869
C-2	0.0557	0.3408	0.4744
N-3	−0.0070	0.3405	0.5452
C-4	−0.1136	0.1832	0.5265
C-5	−0.1618	0.0403	0.4389
C-6	−0.0937	0.0541	0.3657
N-7	−0.2775	−0.0965	0.4493
C-8	−0.2918	−0.0315	0.5340
N-9	−0.1964	0.1403	0.5873
N-6	−0.1299	−0.0770	0.2768
C-10	−0.1743	0.2598	0.6888
C-11	−0.2802	0.1741	0.7411
	5-Isopropyl-5-Bromoallylbarbituric Acid		
N-1	0.5198	0.5584	0.3245
C-2	0.4017	0.4917	0.3668
N-3	0.2778	0.3258	0.3119
C-4	0.2496	0.2137	0.2128
C-5	0.3804	0.2857	0.1664
C-6	0.5155	0.4724	0.2303
O-2	0.4054	0.5818	0.4499
O-4	0.1385	0.0719	0.1683
O-6	0.6167	0.5469	0.1969
C-7	0.2654	0.2330	0.0441
C-8	0.1824	0.3329	0.0300
C-9	0.2260	0.4375	−0.0113
Br	−0.0050	0.2998	0.0699
C-10	0.4922	0.1932	0.1705
C-11	0.6001	0.2337	0.2934
C-12	0.6095	0.2239	0.1166

[a] The numbering system is the same as that shown in Figure 1. Carbonyl oxygen and amino nitrogen atoms have the same number as the carbon atom to which they are covalently bound.

Both the adenine and the barbiturate rings are very close to being planar. The root-mean-square deviation from planarity of the adenine atoms, excluding the side-chain atom C-11, is 0.022 Å. The corresponding quantity for the barbiturate molecule is 0.037 Å, excluding the side-chain atoms. The dihedral angle between these planes is 10.5°. In intermolecular complexes of this type, the hydrogen-bonded molecules usually have dihedral angles which are less than 5°.[8] However, the majority of these hydrogen-bonded purine–pyrimidine complexes contain only two molecules and do not form infinite chains. The small size of such a hydrogen-bonded complex may enable it to act as a more rigid unit in response to crystal packing forces than is possible for an infinite hydrogen-bonded array. Thus it seems likely that in the present case the deviation of the rings from coplanarity is the result of a compromise between the tendency of the infinite arrays of hydrogen-bonded molecules to be perfectly coplanar and the requirement that the bulky substituents of the barbiturate molecules be efficiently packed in a regular crystalline lattice.

Adjoining levels in the layered structure are separated by a distance of 3.2 Å. This is somewhat shorter than the 3.4 Å which is the van der Waals thickness of aromatic rings.[10] However, as is seen in Figure 2, there is very little overlapping of the rings in successive layers so that a closer approach is possible between successive layers of the structure than if there had been more overlap.

The two NH–N hydrogen bond lengths (2.790, 2.808 Å) are in the normal range, whereas the two NH–O hydrogen bonds (3.124, 3.339 Å) are significantly longer than normal.[6,10] The reason for these longer hydrogen bonds is not entirely clear. Model building studies show that the two adenine molecules that are hydrogen bonded to a single barbiturate residue could not be parallel if all of their hydrogen bonds were of normal length. However, since these adenine molecules are related by the translational symmetry of the unit cell, they must be parallel. Hence the increased length of the longer hydrogen bonds may be due to constraints arising from the packing of molecules in the unit cell.

The closest nonbonding intermolecular approaches are between barbiturate atom O-2 and atoms O-2 and C-2 of the barbiturate molecule related to the first by a center of symmetry. These distances, which are 3.159 and 3.165 Å, respectively, are slightly larger than the minimal van der Waals contact for such interactions.[10]

(9) E. W. Hughes, "Structural Chemistry and Molecular Biology," A. Rich and N. Davidson, Ed., W. A. Freeman, San Francisco, Calif., 1968, p 628.

(10) L. Pauling, "The Nature of the Chemical Bond," Cornell University Press, Ithaca, N. Y., 1960.

UM00012460
NOVARTIS EXHIBIT 1017
Novartis v. Regents, IPR2023-01346
Page 1206 of 4460

Our interest in intermolecular complexes between derivatives of purines and pyrimidines is related to the central role of hydrogen bonding in the transfer of information in biological systems. In the present case, however, the intermolecular complexes between adenine derivatives and the barbiturates are of interest because these interactions may provide some insight into the varied and profound biochemical effects of the barbiturates when they are present in biological systems. The present structure shows a somewhat unusual and extensive system of hydrogen bonding which is a reflection in the solid state of the highly selective hydrogen bonding affinity that is observed between the barbiturates and adenine-containing compounds.

Acknowledgment. This research was supported by grants from the National Science Foundation and the National Institutes of Health. We thank the General Electric Corporation for allowing us to use their XRD-490 diffractometer and are grateful to Mr. Howard Pickett for his assistance with that instrument.

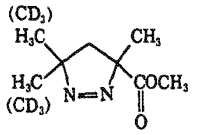
Communications to the Editor

Decomposition of Azo Compounds *via* Cationic Intermediates. Elucidation of the Mechanism of Ionization and Nitrogen Elimination

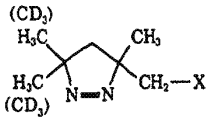
Sir:

Recently we reported the first two cases of azo compounds which eliminate nitrogen by mechanisms involving cationic intermediates.[1] The results clearly showed that for a structurally suitable system the –N=N– group anchimerically assists ionization.[1] However, the preliminary work did not provide for a definitive mechanistic description of nitrogen loss. This has stimulated us to begin a general investigation of the scope and mechanistic details of such reactions. In this communication we wish to report the acetolysis of the new system IIb-OBs and a detailed analysis of ionization–nitrogen elimination for this reaction.

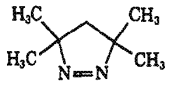
Addition of 2-diazopropane[2] to methyl methacrylate afforded I in excellent yield, bp 67–73° (1.5 mm).[3]



I



IIa, X = OH
b, X = OBs
c, X = OAc

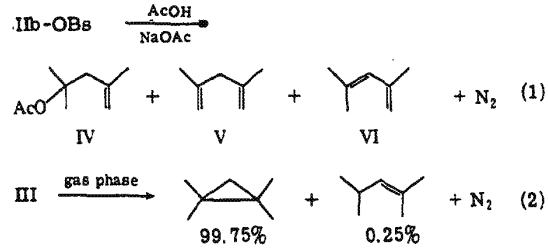


III

Reduction of I with lithium aluminum hydride followed by oxidation with yellow mercuric oxide gave IIa-OH, bp 88–90° (1.2 mm).[3] Reaction of IIa-OH with sodium hydride followed by treatment with *p*-bromobenzenesulfonyl chloride produced IIb-OBs, mp 109–110°. 2-Diazopropane-d_6[4] was converted in an analogous manner to IIb-OBs-d_6. Treatment of IIa-OH with acetic anhydride and pyridine afforded IIc-OAc.

Azo *p*-bromobenzenesulfonate IIb-OBs was solvolyzed in dry acetic acid buffered with sodium acetate. Rate measurements were made by the usual sealed ampoule technique. Titration of the developing *p*-bromobenzenesulfonic acid was performed with a Metrohm Potentiograph Model E-436 high-precision automatic titrator. All of the rate constants were nicely first order. The kinetic data are summarized in Table I. A reactivity comparison of IIb-OBs acetolysis with the gas-phase thermolysis of structurally related III also is included. Another reactivity comparison was made by subjecting IIc-OAc to the acetolysis conditions at 130°. The azo acetate was stable for at least 25 acetolysis half-lives of IIb-OBs.

p-Bromobenzenesulfonate IIb-OBs produced a quantitative yield of nitrogen and a mixture of the acetate and dienes shown in eq 1; no IIc-OAc was detected.



Product identification was based on glpc and nmr comparisons with authentic samples of IV,[5] V,[6] and VI.[7] Product yields and ratios are summarized in Table II. Equations 1 and 2 compare the products of IIb-OBs acetolysis and the gas-phase thermolysis of III.[8]

The best available evidence indicates that decomposition of III occurs by a mechanism which involves a

(1) E. L. Allred and C. R. Flynn, *J. Amer. Chem. Soc.*, 92, 1064 (1970).
(2) A. C. Day, P. Raymond, R. M. Southam, and M. C. Whiting, *J. Chem. Soc. C*, 467 (1966).
(3) Satisfactory elemental analyses were obtained for all of the new compounds. The nmr, ir, and uv spectral data were in complete agreement with the structural assignments.
(4) 2-Diazopropane-d_6 was prepared from acetone-d_6 of 99.5% minimum isotopic purity.[2] Nmr analysis showed I-d_6 and II-d_6 to be of greater than 98% deuterium incorporation.
(5) Prepared from 2,4-dimethyl-4-penten-2-ol obtained from Chemical Samples Co.
(6) Obtained from Chemical Samples Co.
(7) T. L. Jacobs and R. A. Meyers, *J. Amer. Chem. Soc.*, 86, 5244 (1964).
(8) R. J. Crawford and A. Mishra, *ibid.*, 88, 3963 (1966).

UM00012461
NOVARTIS EXHIBIT 1017
Novartis v. Regents, IPR2023-01346
Page 1207 of 4460

The Crystal and Molecular Structure of the Intermolecular Complex 9-Ethyladenine–5,5-Diethylbarbituric Acid[1]

Donald Voet

Contribution from the Department of Chemistry, and the Laboratory for Research on the Structure of Matter, University of Pennsylvania, Philadelphia, Pennsylvania 19104. *Received March 22, 1972*

Abstract: The X-ray crystal structure of the intermolecular complex 9-ethyladenine–5,5-diethylbarbituric acid has been determined. The two types of molecules associate by forming extended planar sequences of mutually hydrogen-bonded barbiturate and adenine rings. The mode of hydrogen bonding in these sequences alternates between the Watson–Crick and the Hoogsteen types of base pairing. In both of these pairings the N–H···O contacts are anomalously long. The planes of hydrogen-bonded molecules form stacks of parallel layers that are held together by dipole–dipole interactions. The strengths of these interactions appear to be related to the strengths of the N–H···O hydrogen bonds.

Barbiturates are general metabolic depressants that appear to act as competitive inhibitors in oxidative metabolism.[2] Barbiturate derivatives that are physiologically effective as sedative–hypnotic agents are substituted at their 5 position by two nonpolar groups of at least the size of ethyl groups.[2] These hydrophobic side groups increase the solubility of the barbiturate ring in nonpolar environments and decrease it in aqueous media. Nerve tissue is quite lipid rich in comparison with other tissues such as muscle or blood. Hence, the marked effect of barbiturates on the central nervous system is due, at least in part, to their selective solubility in nerve tissue.

The nature of the barbiturate receptor site is largely unknown. Barbiturates, as do other uracil derivatives, have a selective affinity for hydrogen bonding to adenine derivatives. This has been demonstrated by infrared and nmr spectroscopy[3,4] and by the formation of a number of crystalline intermolecular complexes containing both adenine and barbiturate derivatives.[5,6] An attractive hypothesis concerning the nature of the barbiturate receptor site is that it involves adenine containing effectors or coenzymes, such as 3′,5′-cyclic AMP, ATP, FAD, and NAD. It has been postulated that the barbiturate molecules selectively hydrogen bond to these receptor molecules, thereby interfering with their normal function.[3,5] It is therefore of great interest to determine the crystal structure of a number of adenine–barbiturate complexes as this may shed light on the detailed molecular architecture of the barbiturate receptor site.

This article describes the structural determination of the crystalline intermolecular complex 9-ethyladenine–5,5-diethylbarbituric acid (I). In this structure the adenine and the barbiturate derivatives associate by the formation of extended hydrogen-bonded strips that contain adenine and barbiturate residues in alternating order. The layers of hydrogen-bonded strips appear to be held together by a series of stacked dipoles. It is shown that the strengths of these dipolar interactions and those of the N–H···O hydrogen bonds appear to be closely interrelated.

(1) This paper was presented, in part, at the American Crystallographic Association Winter Meeting, Columbia, S. C., Jan 1971, Abstract L4.
(2) S. K. Sharpless in "The Pharmacological Basis of Therapeutics," 3rd ed, L. S. Goodman and A. Gilman, Ed., Macmillan, New York, N. Y., 1965, p 105.
(3) Y. Kyogoku, R. C. Lord, and A. Rich, *Nature (London)*, 218, 69 (1968).
(4) Y. Kyogoku and B. S. Yu, *Chem-Biol. Interactions*, 2, 117 (1970).
(5) S.-H. Kim and A. Rich, *Proc. Nat. Acad. Sci. U. S.*, 60, 402 (1968).
(6) D. Voet and A. Rich, *J. Amer. Chem. Soc.*, 94, 5888 (1972).

Experimental Section

9-Ethyladenine (Cyclo Chemical) and 5,5-diethylbarbituric acid (Merck and Co.) were dissolved in equimolar amounts in dimethyl sulfoxide. The resulting solution was evaporated to dryness at ~80°, yielding a number of small colorless crystals with the shape of flattened parallelepipeds. The ultraviolet spectrum and the paper chromatographic analysis of an aqueous solution of one of these crystals indicated that both 9-ethyladenine and 5,5-diethylbarbituric acid were present in the crystals in approximately equimolar amounts.

A small crystal (0.45 × 0.30 × 0.08 mm) was sealed inside a glass capillary tube. Preliminary Weissenberg and precession photographs of the crystal revealed that it had triclinic lattice symmetry. All subsequent X-ray measurements were made using a Picker FACS-1 diffractometer employing Ni-filtered Cu radiation (λ(Cu Kα) = 1.5418 Å). The reduced unit cell parameters as determined by the least-squares analysis of the angular positions of 12 independent reflections are given in Table I. The buoyant density of the crystals was measured by flotation in a mixture of CCl_4 and cyclohexane.

Table I. Crystal Data[a]

a = 7.520 (1) Å	α = 95.88 (1)°
b = 10.455 (2) Å	β = 102.35 (1)°
c = 12.255 (1) Å	γ = 115.48 (1)°
Space Group $P\bar{1}$	
Z = 2	
Density (obsd) = 1.393 g/cm³	
Density (calcd) = 1.391 g/cm³	

[a] The quantities in parentheses are the estimated standard deviations of the least significant figure of the tabulated data.

X-Ray diffraction peak counts, C, were measured using the θ–2θ scan mode, a scan rate of 1°/min, a scan range of 1.2°, and a take-off angle of 3°. Stationary background counts, B_1 and B_2, of 10-sec duration each, were taken at the limits of each scan. A total of 2464 unique reflections were measured to the limit 2θ = 125°. All computer calculations were performed using an IBM 360-75 computer.

Structure Determination and Refinement. The intensities, $I(h,k,l)$, were calculated according to the equation

$$I = [C - t(B_1 + B_2)]/Lp$$

where t is the ratio of the peak counting time to the total background

UM00012462
NOVARTIS EXHIBIT 1017
Novartis v. Regents, IPR2023-01346
Page 1208 of 4460

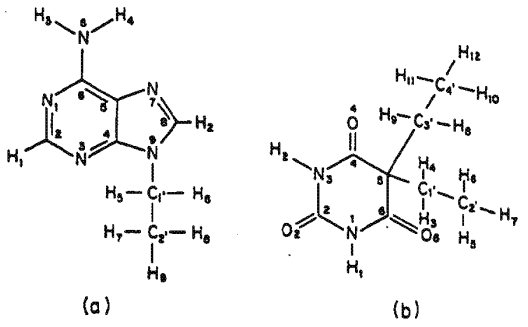


Figure 1. The molecular formulas and atomic numbering schemes for (a) 9-ethyladenine and (b) 5,5-diethylbarbituric acid.

counting time, L is the Lorentz factor, and p is the polarization factor. The standard deviation of these intensities, $\sigma(I)$, is defined as

$$\sigma(I) = [C + t(B_1 + B_2) + (kI)^2]^{1/2}/Lp$$

where k is a factor that accounts for instrumental instabilities.[7] In the present structural determination, k was assigned a value of 0.030. A total of 43 reflections had $I < 2.33\sigma(I)$ and hence were considered to be unobserved. (The rest are observed at the 98% confidence level.) It was not considered necessary to correct the intensities for absorption effects due the small size of the crystal.

The amplitudes of the normalized structure factors, E, were calculated according to the equation

$$E^2(h,k,l) = I(h,k,l)/\epsilon\langle I\rangle$$

where $\langle I\rangle$ is the average value of the intensity at the same (sin θ/λ) value as that of the (h,k,l) reflection and ϵ is a small positive integer, the value of which depends on the symmetry class of the reflection.[8] For triclinic symmetry, ϵ is unity for all reflections.

The values of $\langle I\rangle$ were calculated according to the equation

$$\ln\langle I\rangle = \sum_{n=0}^{N}\alpha_n(\sin\theta/\lambda)^n$$

The coefficients, α_n, of the above polynomial are determined as follows. The reflections are ordered in increasing (sin θ/λ) and the resulting list is divided into a small number of equally populated intervals. The average values of I and (sin θ/λ) are computed for each interval. The α_n values are then fitted to these averages by the method of polynomial regression.[9] The degree of the final polynomial, N, is that integer such that there is no statistical improvement of fit of the equation to the data when $n = N + 1$. In the present case N was found to be 3 when the list of reflections was divided into 25 intervals.

The statistical distribution of the normalized structure factors,[10] which is shown in Table II, indicated that the unit cell had centric

Table II. Experimental and Theoretical Values of the Normalized Structure Factors

	Obsd	Centric	Acentric
$\langle E^2\rangle$	0.994	1.000	1.000
$\langle\|E\|\rangle$	0.797	0.798	0.886
$\langle E^2 - 1\rangle$	0.979	0.968	0.736
$\|E\| \geq 3.0$	0.50%	0.30%	0.01%
$\|E\| \geq 2.0$	4.46	5.00	1.80
$\|E\| \geq 1.0$	30.66	32.00	36.80

(7) G. H. Stout and L. H. Jensen, "X-Ray Structure Determination," Macmillan, New York, N. Y., 1968.
(8) A. J. C. Wilson, *Acta Crystallogr.*, 2, 318 (1949).
(9) System 360 Scientific Subroutine Package (360 A-CM-03X), Version III, Programmers Manual, I.B.M. Manual H20-0205-3, White Plains, N. Y., 1968, pp 408–412.
(10) H. Hauptman and J. Karle, "Solution of the Phase Problem I. The Centrosymmetric Crystal," A. C. A. Monograph No. 3, Polycrystal Book Service, Pittsburgh, Pa., 1953.

symmetry and hence that its space group was $P\bar{1}$. This finding was corroborated by the zero moment test[11] and was subsequently confirmed by the successful refinement of the structure. The above method of computing normalized structure factors, and also the Wilson plot[12] and the centrosymmetry tests, were carried out by the program STATISTX which was written by the author.

The structure was solved by the reiterative application of the Sayre equation[13] using a modified version of the program REL.[14] The positions of all of the expected nonhydrogen atoms except those of the barbiturate ethyl groups were evident in an E map based on the 310 (phased) reflections with $|E| > 1.5$. The positions of the remaining four ethyl carbon atoms were found in a Fourier map in which the phases of the observed structure factors were based on the positions of the 21 located atoms. The structure was refined by the method of full matrix least squares. The quantity minimized in this process was $\Sigma w(|F|_o - |F|_c)^2$ where $w = 1/\sigma^2(I)$. The initial scale factor and the initial overall isotropic temperature factor were those determined by Wilson's method.[12] The atomic scattering factors were taken from the International Tables for Crystallography.[15] After three cycles of refinement of the scale factor, the atomic positions and the isotropic temperature factors, the discrepancy index, R $(= \Sigma\,||F_o| - |F_c||/\Sigma|F_o|)$, was 0.132. An additional cycle of refinement employing anisotropic temperature factors reduced the discrepancy index to $R = 0.098$. A difference Fourier map based on the structure at this stage of refinement revealed the positions of all 21 unique hydrogen atoms at their expected positions. However, the hydrogen atoms about one of the barbiturate methyl carbon atoms, C-2′, were very poorly resolved from each other.

The positions and the isotropic temperature factors of the hydrogen atoms were refined for two cycles yielding a discrepancy index of $R = 0.074$. The full structure was then refined for three cycles using isotropic temperature factors for the hydrogen atoms and anisotropic temperature factors for the nonhydrogen atoms. The refinement process converged at a final discrepancy index of $R = 0.063$ based on 2421 reflections.[16] The final parameter shifts were, with three exceptions, all less than the estimated standard deviations of these parameters.

Results

The atomic numbering scheme used in this article is presented in Figure 1. Table III contains the final fractional coordinates and thermal parameters for all atoms in the asymmetric unit together with their standard deviations as estimated from the variance–covariance matrix of the final cycle of the least-squares refinement.[17]

Most of the thermal parameters are within the normal ranges for these quantities. However, the thermal parameters for barbiturate hydrogen atoms H-5, H-6, and H-7 are considerably larger than those of the other atoms in the crystal. Furthermore, the estimated standard deviations of the atomic parameters of these hydrogen atoms are significantly larger than those of any other atom in the structure. These hydrogen atoms form a methyl group with barbiturate atom C-2′, which itself has the largest thermal parameters of any nonhydrogen atom in the structure. Three of the

(11) E. R. Howells, D. C. Phillips, and D. Rogers, *Acta Crystallogr.*, 3, 210 (1950).
(12) A. J. C. Wilson, *Nature (London)*, 150, 151 (1942).
(13) D. Sayre, *Acta Crystallogr.*, 5, 60 (1952).
(14) R. E. Long, *Diss. Abstr.*, 26, 3651 (1966).
(15) "International Tables for Crystallography," Vol. III, The Kynoch Press, Birmingham, England, 1968, p 201.
(16) The observed and calculated structure factors for 9-ethyladenine–5,5-diethylbarbituric acid will appear following these pages in the microfilm edition of this volume of the journal. Single copies may be obtained from the Business Operations Office, Books and Journals Division, American Chemical Society, 1155 Sixteenth St., N.W., Washington, D. C. 20036, by referring to code number JACS-72-8213. Remit check or money order for $4.00 for photocopy or $2.00 for microfiche.
(17) It has been noted by Hughes that the estimated standard deviations obtained from a least-squares refinement are often underestimates (E. W. Hughes in "Structural Chemistry and Molecular Biology," A. Rich and N. Davidson, Ed., W. H. Freeman, San Francisco, Calif., 1968, p 628).

UM00012463
NOVARTIS EXHIBIT 1017
Novartis v. Regents, IPR2023-01346
Page 1209 of 4460

Table III. Final Atomic Coordinates and Thermal Parameters[a]

Atom[b]	x	y	z	β_{11} or B	β_{22}	β_{33}	β_{12}	β_{13}	β_{23}
AN 1	0.2922 (3)	0.2873 (2)	0.0503 (2)	0.0232 (6)	0.0097 (3)	0.0066 (2)	0.0096 (3)	0.0026 (2)	0.0012 (2)
AC 2	0.3044 (4)	0.3011 (3)	−0.0562 (2)	0.0244 (7)	0.0101 (4)	0.0067 (2)	0.0095 (4)	0.0027 (3)	0.0017 (2)
AN 3	0.2979 (3)	0.2064 (2)	−0.1397 (2)	0.0249 (6)	0.0093 (3)	0.0060 (2)	0.0095 (3)	0.0027 (2)	0.0018 (2)
AC 4	0.2754 (3)	0.0839 (3)	−0.1047 (2)	0.0169 (6)	0.0090 (4)	0.0054 (2)	0.0074 (4)	0.0016 (2)	0.0011 (2)
AC 5	0.2608 (3)	0.0542 (3)	0.0005 (2)	0.0165 (6)	0.0091 (4)	0.0054 (2)	0.0071 (4)	0.0019 (2)	0.0015 (2)
AC 6	0.2701 (4)	0.1640 (3)	0.0825 (2)	0.0177 (6)	0.0105 (4)	0.0051 (2)	0.0079 (4)	0.0016 (2)	0.0010 (2)
AN 7	0.2394 (3)	−0.0833 (2)	0.0047 (2)	0.0235 (6)	0.0087 (3)	0.0060 (2)	0.0087 (3)	0.0025 (2)	0.0017 (2)
AC 8	0.2424 (4)	−0.1329 (3)	−0.0970 (2)	0.0226 (7)	0.0089 (4)	0.0061 (2)	0.0083 (4)	0.0024 (3)	0.0014 (2)
AN 9	0.2630 (3)	−0.0385 (2)	−0.1675 (2)	0.0218 (5)	0.0091 (3)	0.0055 (2)	0.0083 (3)	0.0024 (2)	0.0008 (2)
AN 6	0.2615 (4)	0.1505 (4)	0.1891 (2)	0.0338 (8)	0.0132 (4)	0.0058 (2)	0.0128 (5)	0.0043 (3)	0.0018 (2)
AC 1′	0.2770 (5)	−0.0583 (4)	−0.2851 (2)	0.0286 (8)	0.0131 (5)	0.0056 (2)	0.0113 (5)	0.0041 (3)	0.0012 (2)
AC 2′	0.0918 (5)	−0.0706 (5)	−0.3717 (3)	0.0337 (10)	0.0177 (6)	0.0055 (2)	0.0128 (6)	0.0018 (4)	0.0014 (3)
BN 1	0.1967 (3)	0.7189 (2)	0.1502 (2)	0.0267 (6)	0.0093 (3)	0.0051 (2)	0.0101 (3)	0.0035 (2)	0.0016 (2)
BC 2	0.2190 (4)	0.6059 (3)	0.0986 (2)	0.0186 (6)	0.0088 (4)	0.0052 (2)	0.0070 (4)	0.0016 (3)	0.0010 (2)
BN 3	0.2309 (3)	0.5087 (3)	0.1632 (2)	0.0254 (6)	0.0095 (3)	0.0058 (2)	0.0100 (4)	0.0038 (2)	0.0015 (2)
BC 4	0.2065 (4)	0.5079 (3)	0.2696 (2)	0.0220 (7)	0.0103 (4)	0.0054 (2)	0.0082 (4)	0.0027 (3)	0.0018 (2)
BC 5	0.1481 (4)	0.6176 (3)	0.3209 (2)	0.0273 (7)	0.0108 (4)	0.0052 (2)	0.0108 (4)	0.0034 (3)	0.0014 (2)
BC 6	0.1840 (4)	0.7413 (3)	0.2598 (2)	0.0194 (6)	0.0096 (4)	0.0056 (2)	0.0074 (4)	0.0021 (3)	0.0005 (2)
BO 2	0.2301 (3)	0.5939 (2)	0.0005 (1)	0.0268 (5)	0.0113 (3)	0.0050 (1)	0.0097 (3)	0.0033 (2)	0.0010 (1)
BO 4	0.2205 (4)	0.4154 (2)	0.3194 (2)	0.0453 (8)	0.0142 (3)	0.0075 (2)	0.0177 (4)	0.0068 (3)	0.0043 (2)
BO 6	0.1923 (3)	0.8558 (2)	0.3018 (2)	0.0334 (6)	0.0103 (3)	0.0077 (2)	0.0114 (3)	0.0048 (2)	0.0006 (2)
BC 1′	0.2526 (5)	0.6718 (4)	0.4497 (2)	0.0346 (10)	0.0165 (5)	0.0060 (2)	0.0136 (6)	0.0027 (4)	0.0007 (3)
BC 2′	0.4856 (7)	0.7526 (7)	0.4780 (4)	0.0329 (12)	0.0266 (9)	0.0102 (4)	0.0128 (8)	0.0003 (5)	0.0008 (5)
BC 3′	−0.0961 (5)	0.5223 (4)	0.2966 (3)	0.0277 (8)	0.0130 (5)	0.0078 (3)	0.0092 (5)	0.0049 (4)	0.0024 (3)
BC 4′	−0.2017 (6)	0.5998 (5)	0.3442 (3)	0.0289 (9)	0.0193 (6)	0.0103 (3)	0.0131 (6)	0.0070 (4)	0.0041 (4)
AH 1	0.326 (5)	0.896 (4)	−0.073 (3)	3.1 (8)					
AH 2	0.232 (5)	−0.229 (4)	−0.119 (3)	2.9 (8)					
AH 3	0.252 (5)	0.219 (4)	0.231 (3)	3.6 (8)					
AH 4	0.237 (6)	0.068 (5)	0.216 (3)	3.4 (1.0)					
AH 5	0.299 (4)	−0.144 (4)	−0.301 (2)	2.4 (7)					
AH 6	0.408 (6)	0.025 (4)	−0.288 (3)	3.9 (9)					
AH 7	−0.037 (6)	−0.165 (4)	−0.375 (3)	4.7 (9)					
AH 8	0.081 (6)	0.019 (5)	−0.356 (3)	5.2 (1.0)					
AH 9	0.117 (5)	−0.072 (4)	−0.444 (3)	3.8 (8)					
BH 1	0.204 (4)	0.789 (3)	0.106 (2)	1.3 (6)					
BH 2	0.257 (5)	0.439 (4)	0.129 (3)	2.2 (7)					
BH 3	0.211 (7)	0.578 (5)	0.486 (4)	5.5 (1.1)					
BH 4	0.182 (6)	0.738 (5)	0.476 (4)	5.2 (1.0)					
BH 5	0.539 (10)	0.821 (8)	0.548 (6)	12.0 (2.1)					
BH 6	0.525 (13)	0.824 (9)	0.437 (7)	16.9 (3.2)					
BH 7	0.553 (13)	0.693 (9)	0.476 (7)	14.2 (3.0)					
BH 8	−0.118 (5)	0.430 (4)	0.340 (3)	3.7 (8)					
BH 9	−0.157 (4)	0.486 (3)	0.211 (3)	2.3 (6)					
BH 10	−0.349 (7)	0.528 (4)	0.332 (3)	4.9 (1.0)					
BH 11	−0.183 (7)	0.690 (5)	0.300 (4)	7.0 (1.2)					
BH 12	−0.148 (5)	0.621 (4)	0.434 (3)	3.5 (7)					

[a] The positional parameters are expressed as fractions of unit cell edges. Anisotropic temperature parameters are expressed as $T = \exp[-(h^2\beta_{11} + k^2\beta_{22} + l^2\beta_{33} + 2hk\beta_{12} + 2hl\beta_{13} + 2kl\beta_{23})]$. Isotropic temperature factors for hydrogen atoms are of the form $\exp(-B \sin^2\theta/\lambda^2)$. Standard deviations, as determined from the variance–covariance matrix of the final cycle of least-squares refinement, are given in parentheses and refer to the least significant digits of their corresponding parameters. [b] The prefix A refers to the 9-ethyladenine molecule and the prefix B refers to the 5,5-diethylbarbituric acid molecule. The atomic numbering scheme is the same as that given in Figure 1.

six highest peaks in the final difference Fourier map were in the region about this methyl group. These peaks had heights in the range 0.10–0.15 e/Å^3. Hence it is concluded that this methyl group either can rotate rather freely or is rotationally disordered about the barbiturate C-1′–C-2′ bond.

The Molecular Structure

Table IV shows the bond distance and the bond angles found in I together with their standard deviations as estimated from the least-squares refinement.[17] These standard deviations are abnormally large for those bonds that involve barbiturate hydrogen atoms H-5, H-6, and H-7 due to the previously discussed disorder. The covalent bond distances and bond angles are, for the most part, well within the ranges normally found for these quantities.[18] The twofold molecular symmetry of the barbiturate ring is preserved almost to within experimental error. However, the methyl groups, especially the one involving barbiturate atom C-2′, appear to be somewhat distorted. This is not surprising in view of the disorder mentioned above and because of the difficulty of accurately determining the positions of hydrogen atoms in an X-ray structure determination.

The only other significant deviations from the expected covalent bond parameters in the structure are the barbiturate C-5–C-3′ bond length, which is at least 0.05 Å longer than is expected for a carbon–carbon single bond, and the barbiturate C-4–C-5–C-3′ bond angle, which is 7.3° smaller than the nominally expected tetrahedral angle. The highest feature in the final differ-

(18) D. Voet and A. Rich, *Progr. Nucl. Acid Res. Mol. Biol.*, 10, 183 (1970).

UM00012464
NOVARTIS EXHIBIT 1017
Novartis v. Regents, IPR2023-01346
Page 1210 of 4460

Table IV. Bond Lengths and Angles[a]

1. 9-Ethyladenine

	Å		Å
N-1–C-2	1.345 (3)	C-2–H-1	0.99 (4)
C-2–N-3	1.326 (3)	C-8–H-2	0.98 (4)
N-3–C-4	1.345 (3)	N-6–H-3	0.87 (4)
C-4–C-5	1.372 (3)	N-6–H-4	0.92 (4)
C-5–C-6	1.413 (4)	C-1′–H-5	0.98 (4)
C-6–N-1	1.338 (3)	C-1′–H-6	1.01 (4)
C-5–N-7	1.384 (3)	C-2′–H-7	1.03 (4)
N-7–C-8	1.309 (3)	C-2′–H-8	0.98 (4)
C-8–N-9	1.358 (3)	C-2′–H-9	0.95 (4)
N-9–C-4	1.379 (3)		
N-9–C-1′	1.468 (3)		
C-1′–C-2′	1.506 (4)		
	Deg		Deg
C-6–N-1–C-2	119.5 (2)	N-1–C-2–H-1	115 (2)
N-1–C-2–N-3	128.8 (3)	N-3–C-2–H-1	116 (2)
C-2–N-3–C-4	110.2 (2)	N-7–C-8–H-2	123 (2)
N-3–C-4–C-5	127.6 (2)	N-9–C-8–H-2	124 (2)
C-4–C-5–C-6	117.0 (2)	C-6–N-6–H-3	117 (2)
C-5–C-6–N-1	117.0 (2)	C-6–N-6–H-4	125 (2)
N-3–C-4–N-9	127.0 (2)	H-3–N-6–H-4	117 (3)
C-6–C-5–N-7	132.1 (2)	N-7–C-1′–H-5	109 (2)
C-5–N-7–C-8	103.8 (2)	N-7–C-1′–H-6	108 (2)
N-7–C-8–N-9	113.8 (3)	H-5–C-1′–H-6	104 (3)
C-8–N-9–C-4	106.0 (2)	C-2′–C-1′–H-5	112 (2)
N-9–C-4–C-5	105.4 (2)	C-2′–C-1′–H-6	112 (2)
C-4–C-5–N-7	111.0 (2)	C-1′–C-2′–H-7	110 (2)
N-1–C-6–N-6	119.8 (3)	C-1′–C-2′–H-8	109 (2)
C-5–C-6–N-6	123.2 (3)	C-1′–C-2′–H-9	109 (2)
C-4–N-9–C-1′	126.3 (2)	H-7–C-2′–H-8	116 (3)
C-8–N-9–C-1′	127.7 (2)	H-7–C-2′–H-9	110 (3)
N-9–C-1′–C-2′	112.4 (2)	H-8–C-2′–H-9	103 (3)

2. 5,5-Diethylbarbituric Acid

	Å		Å
N-1–C-2	1.374 (3)	N-1–H-1	0.95 (3)
C-2–N-3	1.371 (3)	N-3–H-2	0.92 (4)
N-3–C-4	1.356 (3)	C-1′–H-3	1.07 (5)
C-4–C-5	1.519 (4)	C-1′–H-4	1.10 (4)
C-5–C-6	1.513 (4)	C-2′–H-5	0.94 (7)
C-6–N-1	1.370 (3)	C-2′–H-6	0.93 (9)
C-2–O-2	1.219 (3)	C-2′–H-7	0.96 (9)
C-4–O-4	1.225 (3)	C-3′–H-8	1.11 (4)
C-6–O-6	1.225 (3)	C-3′–H-9	1.01 (4)
C-5–C-1′	1.528 (4)	C-4′–H-10	1.11 (5)
C-1′–C-2′	1.520 (5)	C-4′–H-11	1.06 (3)
C-5–C-3′	1.608 (4)	C-4′–H-12	1.00 (4)
C-3′–C-4′	1.510 (4)		
	Deg		Deg
C-6–N-1–C-2	125.5 (2)	C-6–N-1–H-1	120 (2)
N-1–C-2–N-3	116.7 (2)	C-2–N-1–H-1	114 (2)
C-2–N-3–C-4	125.8 (2)	C-2–N-3–H-2	115 (2)
N-3–C-4–C-5	118.2 (2)	C-4–N-3–H-2	119 (2)
C-4–C-5–C-6	113.2 (2)	C-5–C-1′–H-3	107 (2)
C-5–C-6–N-1	117.4 (2)	C-5–C-1′–H-4	103 (2)
N-1–C-2–O-2	121.5 (2)	C-2′–C-1′–H-3	108 (2)
N-3–C-2–O-2	121.8 (2)	C-2′–C-1′–H-4	115 (2)
N-3–C-4–O-4	121.1 (2)	H-3–C-1′–H-4	111 (3)
C-5–C-4–O-4	121.6 (2)	C-1′–C-2′–H-5	109 (4)
C-5–C-6–O-6	123.0 (2)	C-1′–C-2′–H-6	110 (5)
N-1–C-6–O-6	119.5 (2)	C-1′–C-2′–H-7	116 (5)
C-4–C-5–C-1′	111.1 (2)	H-5–C-2′–H-6	93 (6)
C-6–C-5–C-1′	112.1 (2)	H-5–C-2′–H-7	113 (6)
C-4–C-5–C-3′	102.2 (2)	H-6–C-2′–H-7	114 (7)
C-6–C-5–C-3′	107.7 (2)	C-5–C-3′–H-8	106 (2)
C-1′–C-5–C-3′	110.1 (2)	C-5–C-3′–H-9	107 (2)
C-5–C-1′–C-2′	112.4 (3)	C-4′–C-3′–H-8	107 (2)
C-5–C-3′–C-4′	115.4 (3)	C-4′–C-3′–H-9	111 (2)
		H-8–C-3′–H-9	111 (3)
		C-3′–C-4′–H-10	109 (2)
		C-3′–C-4′–H-11	107 (2)
		C-3′–C-4′–H-12	107 (2)
		H-10–C-4′–H-11	113 (3)
		H-10–C-4′–H-12	100 (3)
		H-11–C-4′–H-12	120 (3)

UM00012465
NOVARTIS EXHIBIT 1017
Novartis v. Regents, IPR2023-01346
Page 1211 of 4460

Table IV (*Continued*)

3. Intramolecular Contacts

(a) Hydrogen Bonds			
	—Å—		—Å—
AN-1-BN-3	2.832 (3)	AN-1-BH-2	1.91 (4)
AN-6-BO-4	3.218 (4)	BO-4-AH-3	2.35 (4)
AN-7-BN-1a	2.827 (3)	AN-7-BH-1a	1.89 (3)
AN-6-BO-6a	3.387 (4)	BO-6a-AH-4	2.47 (4)
	—Deg—		—Deg—
AC-2-AN-1-BN-3	112.2 (2)	AC-2-AN-1-BH-2	113 (1)
AC-6-AN-1-BN-3	126.9 (2)	AC-6-AN-1-BH-2	127 (1)
BC-2-BN-3-AN-1	114.0 (2)	AN-1-BH-2-BN-3	176 (3)
BC-4-BN-3-AN-1	120.1 (2)	BC-4-BO-4-AH-3	123 (1)
AC-6-AN-6-BO-4	111.8 (2)	AN-6-AH-3-BO-4	172 (3)
BC-4-BO-4-AN-6	120.6 (2)	AC-5-AN-7-BH-1a	140.(1)
AC-5-AN-7-BN-1a	142.8 (2)	AC-8-AN-7-BH-1a	116 (1)
AC-8-AN-7-BN-1a	113.4 (2)	AN-7-BH-1a-BN-1a	171 (3)
BC-2a-BN-1a-AN-7	108.3 (2)	BC-6a-BO-6a-AH-4	129 (1)
BC-6a-BN-1a-AN-7	125.7 (2)	AN-6-AH-4-BO-6a	176 (3)
AC-6-AN-6-BO-6a	127.4 (2)		
BC-6a-BO-6a-AN-6	129.3 (2)		
(b) Dipole–Dipole Interactions	—Å—		
BC-2-BO-2b	2.983 (4)		
BC-2-BC-2b	3.288 (5)		
BO-2-BO-2b	3.156 (4)		
BC-2-AC-2c	3.458 (3)		
BC-2-AN-3c	3.192 (3)		
BO-2-AC-2c	3.073 (3)		
BO-2-AN-3c	3.190 (3)		
	—Deg—		
BC-2-BO-2-BC-2b	93.4 (2)		
BC-2-BO-2-BO-2b	70.7 (2)		
BC-2-BO-2-AC-2c	97.9 (2)		
BO-2-BC-2-AN-3c	78.9 (2)		
AC-2c-AN-3c-BC-2	90.1 (2)		
AN-3c-AC-2c-BO-2	82.8 (2)		
(c) C–H···O Hydrogen Bond-Like Interaction	—Å—		—Å—
AC-8-BO-2a	3.180 (4)	BO-2a-AH-2	2.47 (4)
	—Deg—		—Deg—
AN-7-AC-8-BO-2a	85.4 (2)	BC-2a-BO-2a-AH-2	125 (2)
AN-9-AC-8-BO-2a	160.4 (2)	AC-8-AH-2-BO-2a	129 (2)
AC-8-BO-2a-BC-2a	109.2 (2)		
(d) Closest Stacking Contacts	—Å—		
AC-6-AN-7d	3.437 (4)		
AC-6-AC-5d	3.483 (4)		
AN-1-AN-7d	3.493 (3)		
AN-6-AN-9d	3.538 (4)		
AN-6-AC-4d	3.544 (4)		
AN-6-AC-8d	3.634 (4)		
AC-8-AC-5e	3.361 (3)		
AN-7-AC-8e	3.403 (3)		
AN-7-AN-9e	3.434 (3)		
AN-7-AN-7e	3.573 (4)		
AN-7-AC-4e	3.595 (3)		
AN-7-AC-5e	3.653 (3)		
(e) Other Close Contacts	—Å—		—Å—
BO-2-BC-3'b	3.496 (4)	BO-2-AH-1	2.60 (4)
BO-2-AC-2	3.372 (4)		

[a] The bond lengths are uncorrected for thermal motion. Standard deviations as determined from the final cycle of least-squares refinement are given in parentheses and refer to the least significant digit of their corresponding parameter. The prefix A refers to the 9-ethyladenine molecule and the prefix B refers to the 5,5-diethylbarbituric acid molecule. The atomic numbering scheme is that given in Figure 1. Lower case letters accompanying the atom numbers refer to atoms related to those in Table III by the following symmetry operations: (a) $x, -1 + y, z$; (b) $-x, 1 - y, -z$; (c) $1 - x, 1 - y, -z$; (d) $-x, -y, -z$; (e) $1 - x, -y, -z$.

ence Fourier map has a peak height of 0.21 e/Å.[3] It is located at the point (0.030, 0.605, 0.395) which is near barbiturate atoms C-5, C-1', and C-3'. This peak appeared in all of the difference Fourier maps that were calculated in the latter stages of the structure refinement. It is likely that it is symptomatic of a small amount of disorder, that is most probably due to a different puckering conformation of the barbiturate ring at atom C-5. Such disorder could easily account for the apparent distortions in the above-mentioned bond parameters.

The adenine and the barbiturate molecules are highly planar as is shown in Table V. The planes of the molecules are very nearly parallel to the crystals' (2, 0,0) planes. The only large deviations of the atoms of the rings out of the least-squares planes are those of barbiturate atoms C-5 and O-6 from plane 2. This "flap" conformation of the barbiturate ring, in which atom C-5 and one or both of the carbonyl oxygen atoms O-4 and O-6 are displaced to opposite sides of the planar barbiturate ring by 0.1–0.4 Å, has been observed quite often in crystal structures of barbiturates.[18]

UM00012466
NOVARTIS EXHIBIT 1017
Novartis v. Regents, IPR2023-01346
Page 1212 of 4460

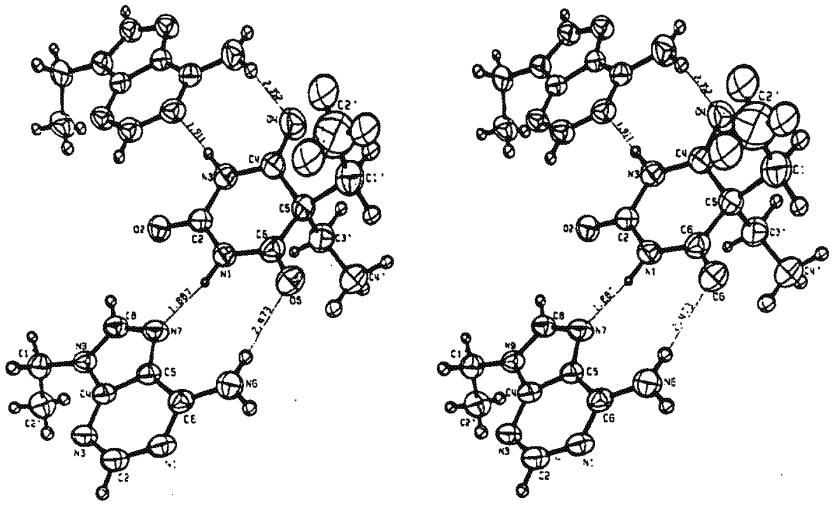


Figure 2. A stereodrawing depicting a section of the extended hydrogen-bonded chain in the crystalline intermolecular complex 9-ethyladenine-5,5-diethylbarbituric acid. The nonhydrogen atoms are represented as thermal ellipsoids of a size such that the vibrating atoms have a 50% probability of being found within them. The hydrogen atoms are represented as spheres of a size such that the atoms have a 25% probability of being found within them.

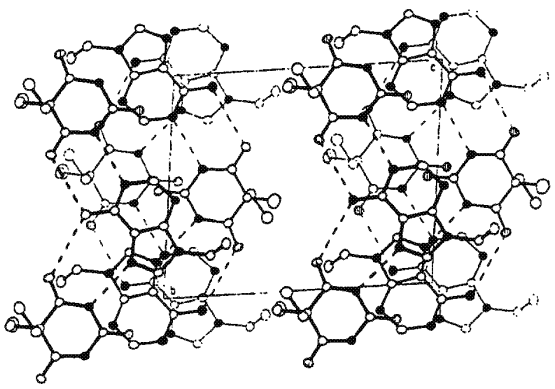


Figure 3. A projection of three consecutive hydrogen-bonded layers of the crystal structure onto the (1, 0, 0) plane of the crystal. This illustrates the stacking relationships in the structure. Hydrogen bonds are represented as dashed lines. Carbon atoms are depicted as open ellipsoids, nitrogen atoms are filled ellipsoids, and oxygen atoms are shaded ellipsoids. Hydrogen atoms have been omitted for the sake of clarity.

Table V. Deviations, in Ångstroms, of Nonhydrogen Atoms from the Least-Squares Planes through the Adenine Atoms (Plane 1), the Barbiturate Atoms (Plane 2), and the Adenine–Barbiturate Complex (Plane 3)

Atom	Plane 1[b]	Plane 2[c]	Plane 3[d]
	Adenine		
N-1	0.001		0.284
C-2	−0.003		0.299
N-3	−0.005		0.181
C-4	−0.009		0.028
C-5	−0.008		−0.007
C-6	−0.003		0.131
N-7	−0.009		−0.176
C-8	−0.005		−0.233
N-9	−0.009		−0.121
N-6	0.023		0.139
C-1′	0.028		−0.111
	Barbiturate		
N-1		−0.006	−0.141
C-2		0.000	−0.063
N-3		0.037	0.026
C-4		−0.038	−0.062
C-5		−0.266[a]	−0.370[a]
C-6		0.012	−0.148
O-2		−0.012	−0.057
O-4		0.006	0.032
O-6		0.188[a]	−0.039[a]
rms deviation	0.012	0.021	0.150

[a] Atoms not included in the least-squares fit. [b] The equation of plane 1 is: $10.2183x - 1.0118y + 0.6551z = 1.6989$. [c] The equation of plane 2 is: $6.0830x + 0.8305y + 0.7024z = 1.9049$. [d] The equation of plane 3 is: $6.3054x + 0.2671y + 0.6161z = 1.6663$.

However, there are also many crystal structures reported in which the barbiturate ring assumes some other conformation such as that of coplanarity.[18] As has been pointed out by Voet and Rich[18] and also by Gatehouse and Craven,[19] there seems to be no reliable correlation between the mode of barbiturate ring puckering and the nature of the substituents at atom C-5. Indeed, the mode of barbiturate ring puckering varies quite significantly among the six crystal structures containing 5,5-diethylbarbituric acid that have been reported.[20-23] This suggests that little energy is required to cause small distortions of the barbiturate ring from its equilibrium conformation. Therefore, in the solid state the mode of barbiturate ring puckering must be largely directed by crystal packing forces.

The two ethyl groups substituent to the barbiturate have quite different conformations relative to the barbiturate ring as can be seen in Figures 2–4. Atom C-1′ is in a nearly equatorial position with respect to the barbiturate ring whereas atom C-3′ is almost axial.

(19) B. M. Gatehouse and B. M. Craven, *Acta Crystallogr., Sect. B*, 27, 1337 (1971).
(20) B. M. Craven, E. A. Vizzini, and M. M. Rodrigues, *ibid., Sect. B*, 25, 1978 (1969).
(21) B. M. Craven and E. A. Vizzini, *ibid., Sect. B*, 27, 1917 (1971).
(22) B. M. Craven and G. L. Gartland, *J. Pharm. Sci.* 59, 1666 (1970).
(23) S. Kiryu, *ibid.*, 60, 699 (1971).

UM00012467
NOVARTIS EXHIBIT 1017
Novartis v. Regents, IPR2023-01346
Page 1213 of 4460

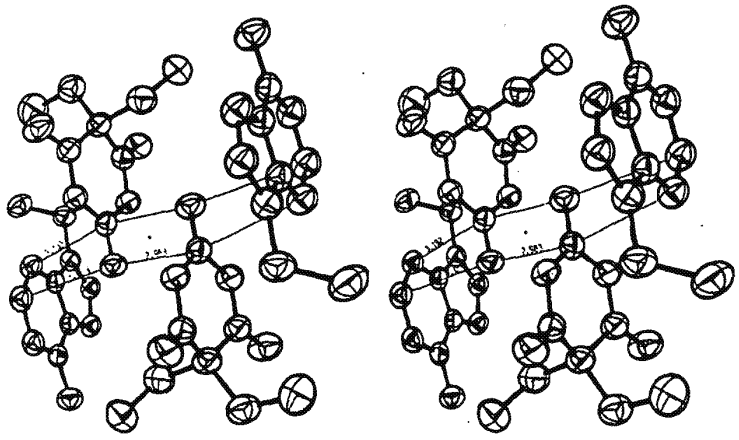


Figure 4. A stereodrawing illustrating the dipole–dipole interactions among the adenine and the barbiturate rings in four consecutive layers of the crystal structure. The atoms are represented as thermal ellipsoids of such a size that the vibrating atoms have a 50% probability of being found within them. Hydrogen atoms have been omitted for the sake of clarity.

The C-1′–C-2′ bond has a trans configuration with respect to the bond sequence C-2′–C-1′–C-5–C-3′. Thus the C-1′–C-2′ ethyl group is pointed back over the barbiturate ring in a manner that is quite common among 5-substituent ethyl groups in barbiturates. However, the C-3′–C-4′ bond assumes a gauche configuration with respect to the C-4′–C-3′–C-5–C-1′ bond sequence and thus is pointed away from the ring. This latter conformation is quite unusual among 5-substituent ethyl groups in barbiturates.

The Intermolecular Associations

The most striking structural feature of the crystalline adenine–barbiturate complex (I) is that it forms extended planar sequences of alternating adenine and barbiturate rings. These are held together by cyclic dimers of hydrogen bonds as is shown in Figure 2.[24,25] The hydrogen-bonded ribbons are organized side by side to form planar sheets. These in turn stack to form a layered structure. This is illustrated in Figure 3.[24] Alternate layers in this arrangement are related to each other by centers of symmetry located between the layers.

If barbiturates are considered to be derivatives of uracil, then it can be seen in Figure 2 that one of the two types of hydrogen-bonded cyclic dimers present in the structure has the Watson–Crick base pairing configuration and the other has the Hoogsteen (imidazole) configuration.[18] The bond lengths and the bond angles of these hydrogen bonds are given in Table IV. It can be seen that the two N–H···N hydrogen bonds have parameters within the normal ranges for these quantities.[18,26] However, the two N–H···O hydrogen bonds are extremely long. Indeed, the one involving barbiturate atom O-6 has an O···H distance of 2.47 Å. This is just slightly shorter than the O···H van der Waals contact distance of 2.6 Å[27] and hence the interaction energy of this hydrogen bond must be extremely weak.[28]

The best planes through the adenine ring and through the barbiturate ring (planes 1 and 2 in Table V) are related by a dihedral angle of 10.2°. This is a rather large dihedral angle relating planar hydrogen-bonded base pairs.[18] However, there are considerably less degrees of freedom for efficiently packing extended hydrogen-bonded sequences of rigidly coplanar bases into a crystalline lattice than there are for the more usual complexes consisting of two coplanar hydrogen-bonded molecules. Thus it seems reasonable to attribute the large dihedral angle between the best planes through the adenine and the barbiturate rings to crystal packing forces.

An extremely interesting feature of the crystalline complex is the close contact made between two symmetry related barbiturate carbonyl groups, C-2–O-2. These groups lie in neighboring planes of hydrogen-bonded rings as is shown in Figures 3 and 4.[24,25] The noncovalent C-2···(O-2)′ contact is 2.983 Å which is somewhat less than the C···O van der Waals contact distant of 3.1 Å.[27] Such short intermolecular C···O contacts are not uncommon in crystal structures of conjugated ring molecules that have several substituent carbonyl groups.[29]

Each barbiturate C-2–O-2 carbonyl group is also in very close contact with atoms C-2 and N-3 of an adenine ring located in a neighboring layer but on the side of the barbiturate ring opposite the close carbonyl–carbonyl contact. This interaction, which can also be seen in Figures 3 and 4, has two intermolecular contacts that are slightly shorter than generally accepted van der Waals contact distances. These are the BC-2–AN-3 distance which is 3.192 Å and the BO-2–AC-2 distance which is 3.073 Å. The minimum van der Waals distances for C···N and C···O contacts are 3.2 and 3.1 Å, respectively.[27]

(24) C. K. Johnson, "ORTEP: A FORTRAN Thermal Ellipsoid Plot Program for Crystal Structure Illustrations," Oak Ridge National Laboratory, Oak Ridge, Tenn., 1965, ORNL-3794.

(25) Inexpensive glasses that give the stereo effect with this figure may be purchased from Taylor Merchant Corp., New York, N. Y. 10036, or from Hubbard Scientific Co., Northbrook, Ill. 60062.

(26) J. Donohue in "Structural Chemistry and Molecular Biology," A. Rich and N. Davidson, Ed., W. H. Freeman, San Francisco, Calif., 1968, p 443.

(27) L. Pauling, "The Nature of the Chemical Bond," Cornell University Press, Ithaca, N. Y., 1960.

(28) W. C. Hamilton and J. A. Ibers, "Hydrogen Bonding in Solids," W. A. Benjamin, New York, N. Y., 1968, p 182.

(29) W. Bolton, *Nature (London)*, 201, 987 (1964).

UM00012468
NOVARTIS EXHIBIT 1017
Novartis v. Regents, IPR2023-01346
Page 1214 of 4460

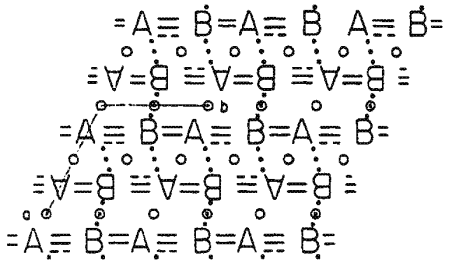


Figure 5. A schematic representation of the hydrogen bonding and the dipole-dipole interactions found in the structure of the complex 9-ethyladenine-5,5-diethylbarbituric acid: A, 9-ethyladenine; B, 5,5-diethylbarbituric acid; solid line, N-H···N or N-H···O hydrogen bond; dashed line, C-H···O hydrogen bond-like interaction; dotted line, dipole-dipole interaction; open circle, center of symmetry.

Bolton[29] has attributed close carbonyl-carbonyl contacts to electrostatic attractions between activated dipoles on the interacting carbonyl groups. This hypothesis was tested by a CNDO/2 molecular orbital calculation[30,31] on 5,5-diethylbarbituric acid using the atomic coordinates found in Table III. The total atomic charges calculated for the barbiturate molecule are given in Table VI. This table shows that the two-fold symmetry of the barbiturate molecule is maintained to within 0.01 electron unit with the exception of the disordered, and therefore distorted, methyl group. It can be seen that the charge separation on the C-2-O-2 carbonyl group is 15% greater than those on the other carbonyl groups.

Table VI. Total Atomic Charges, in Electron Units, of the 5,5-Diethylbarbituric Acid Molecule as Determined Using the CNDO/2 Method of Calculating Molecular Orbitals[a]

Atom	Charge	Atom	Charge
N-1	−0.24	H-1	0.14
C-2	0.47	H-2	0.14
N-3	−0.24	H-3	0.01
C-4	0.39	H-4	0.01
C-5	−0.08	H-5	0.04
C-6	0.38	H-6	0.04
O-2	−0.37	H-7	0.03
O-4	−0.34	H-8	0.01
O-6	−0.33	H-9	0.01
C-1′	−0.03	H-10	0.03
C-2′	−0.10	H-11	0.02
C-3′	−0.03	H-12	0.03
C-4′	−0.05		

[a] The calculations were based on the atomic coordinates found in Table III.

A CNDO/2 calculation on adenine that was calculated by Geissner-Prettre and Pullman[32] predicts that ring atoms N-1 and N-3 are the most negatively charged positions of the adenine molecule. They have total net charges of −0.26 electron unit each. In addition, atom C-2, with a total net charge of 0.21 electron unit, is second to atom C-6 (with 0.27 electron unit) as the most positively charged atom of the adenine molecule.

(30) J. A. Pople and G. A. Segal, *J. Chem. Phys.*, 43, S136 (1965).
(31) G. A. Segal, A CNDO/2 Program, Carnegie Institute of Technology, Pittsburgh, Pa., 1966.
(32) C. Geissner-Prettre and A. Pullman, *Theor. Chim. Acta*, 9, 279 (1968).

Thus, the close contact between the barbiturate carbonyl group C-2-O-2 and the adenine ring atoms C-2-N-3 can also be attributed to a strongly attractive dipole–dipole interaction.

Barbiturate atom O-2 appears to take part in a hydrogen bond-like interaction with the C-H group at atom C-8 of the adenine ring making the Hoogsteen pair with the barbiturate. The C···O contact for this interaction is 3.180 Å and the H···O contact is 2.47 Å. These distances are significantly less than the normal van der Waals contacts for these quantities of 3.6 and 2.6 Å, respectively.[27] Such close C-H···O contacts are commonly observed between oxygen atoms and the C-8 position of purines.[18]

The short C-H···O contact involves the carbonyl group that takes part in the dipole–dipole interaction. Through the center of symmetry, there are two short C-H···O contacts surrounding the interacting carbonyl groups. Considering the supposed electrostatic nature of C-H···O interactions, it seems likely that the C-H···O and the dipole–dipole interactions found in the structure mutually stabilize each other. Hence, a second feature that has major responsibility in maintaining the stereochemistry of the crystal structure is the sequence of four stacked dipoles, flanked by two C-H···O hydrogen bond-like interactions. The entire assembly of molecules that are associated through hydrogen bonds and dipole–dipole interactions is schematically depicted in Figure 5.

Each adenine ring contacts two other adenine rings. As can be seen in Figure 3, these contacting adenine rings are in adjoining layers and are related by centers of symmetry. The data in Table IV show that the closest of these adenine–adenine interatomic distances are greater than 3.35 Å. Hence, these are normal stacking interactions.[18] As can be seen in Figure 3, there is remarkably little overlap of rings in neighboring layers. This manner of packing parallel rings is not uncommon in crystal structures of purines and pyrimidines.[33]

The ethyl groups of the adenine and the barbiturate molecules are gathered together above and below the assembly represented in Figure 5 so as to form continuous bands of closely associated ethyl groups. Thus, as can be seen in Figure 3, the crystal structure consists of these bands interspersed with the regions containing the stacks of associated rings. This type of structural feature, in which groups of atoms with similar polarities are closely associated, is often found in crystal structures of organic molecules.

Discussion

The basic structural features of I closely resemble those of the crystalline complex 9-ethyladenine–5-isopropyl-5-bromoallylbarbituric acid[6] (II). The hydrogen bonding patterns of the two complexes are almost identical. Both have two N-H···N hydrogen bonds of normal length, two abnormally long N-H···O hydrogen bonds and a short AC-8···BO-2 contact. However, in II the N-H···O hydrogen bonds are about 0.2 Å shorter and the AC-8···BO-2 contact is about 0.1 Å longer than the corresponding contacts in I. In both crystalline complexes the barbiturate C-2-O-2

(33) C. E. Bugg, J. M. Thomas, M. Sundaralingham, and S. T. Rao, *Biopolymers*, 10, 175 (1971).

UM00012469
NOVARTIS EXHIBIT 1017
Novartis v. Regents, IPR2023-01346
Page 1215 of 4460

carbonyl group has a close contact with a centrosymmetrically related C-2–O-2 group, but in II the intermolecular C-2···(O-2)′ distance of 3.165 Å is 0.182 Å longer than in I.

In the structure of the crystalline complex phenobarbital–(8-bromo-9-ethyladenine)$_2$ (III), the phenobarbital molecule forms a separate Watson–Crick type base pair with each of two crystallographically independent adenine rings.[5] The N–H···O distance for the hydrogen bond involving the barbiturate atom O-2 is 2.97 Å, whereas the analogous N–H···O distance involving barbiturate atom O-4 is 3.19 Å. This latter N–H···O contact is also considerably longer than usual.

There are eight reported crystal structures of adenine–uracil complexes that contain N–H···O hydrogen bonds involving atom N-6 of the adenine derivative and atom O-4 of the uracil derivative.[18] None of these N–H···O hydrogen bonds have lengths outside the normal range for such interactions. Yet in the three reported adenine–barbiturate complexes (I–III), all five N–H···O bonds involving barbiturate atom O-4 (or its chemical equivalent, O-6) are anomalously long. The forces stabilizing hydrogen bonds are believed to be largely electrostatic in character.[27] Yet Table VI shows that the net atomic charges on all three barbiturate carbonyl oxygen atoms should be approximately equal in the isolated barbiturate molecule. In addition a comparison of the values in Table VI with the net atomic charges on thymine, as calculated by Geissner-Prettre and Pullman[32] using the CNDO/2 method, reveals that analogous positions in 5,5-diethylbarbituric acid and thymine should have almost identical net atomic charges. This suggests that the interaction between adenine and barbiturate derivatives somehow polarizes the barbiturate ring so as to reduce the charges on atoms O-4 and O-6.

The data in Table VI and that of Geissner-Prettre and Pullman[32] suggest that the C-2–O-2 carbonyl groups in both barbiturates and uracil derivatives have strong dipole moments. Nevertheless, dipole–dipole interactions between carbonyl groups are rather uncommon phenomena in the crystal structures of dialkylbarbiturates and have not been observed in crystal structures of uracil derivatives.[18] Thus it appears that such dipole–dipole interactions occur only when the dipoles are "activated"[29] in some manner.

It has been observed that adenine and barbiturate derivatives form highly specific hydrogen-bonded complexes which, in chloroform solutions, have association constants that are an order of magnitude greater than those of adenine–uracil complexes.[3] The nature of this hydrogen bonding specificity, which has been termed "electronic complementarity,"[34] is not understood. However, the foregoing discussion suggests that the immediate result of the "electronically complementarity" adenine–barbiturate association is a redistribution of the bonding electron density on the barbiturate ring so as to reduce the electrostatic charge on atoms O-4 and O-6 and to enhance the dipole moment on the C-2–O-2 carbonyl group.

In light of its apparently greater charge, it may appear surprising that barbiturate atom O-2 is not a member of one of the N–H···O hydrogen bonds in I and II. However, in the crystal structure of alloxan[35] (5-oxobarbituric acid), each molecule has the potential to participate in four intermolecular hydrogen bonds. It should therefore be expected that this number of hydrogen bonds will form.[26] Yet none are observed. Rather the structure is held together by a number of carbonyl–carbonyl dipolar interactions. This demonstrates that if dipolar interactions are sufficiently strong, they can form at the expense of hydrogen bonding interactions.

In II, the requirement of efficiently packing the barbiturate's bulky bromoallyl and isopropyl side groups into the crystalline lattice probably prevents the adenine rings from closely approaching the C-2–O-2 carbonyl groups as they do in I. It is quite likely that the additional dipole–dipole interactions in I provided by the proximity of the adenine C-2–N-3 bonds to the barbiturate C-2–O-2 carbonyl groups enhance the charge polarization in the barbiturate ring. Thus it is not surprising that anomalies in N–H···O hydrogen bond lengths and carbonyl–carbonyl contacts are more extreme in I than in II.

Voet and Rich[6] explained the long N–H···O hydrogen bonds in II as being due to the packing forces in the crystal that maintain the translational equivalence of all adenine (and barbiturate) molecules in the same layer. This would force the N–H···O hydrogen bonds to lengthen because if they were all of normal length, alternate molecules in the hydrogen-bonded sequence could not be parallel. The present study sheds more light on the molecular forces underlying these distortions and suggests why the dipole–dipole interactions appear to form at the expense of the N–H···O hydrogen bonding strength.

In the solid state, the C–H bonds at the C-8 position of purines are commonly observed to participate in close C–H···O contacts. It is known that the C–H groups at these positions are considerably more acidic than is usually the case for C–H groups.[36,37] Therefore, a close C–H···O contact may be symptomatic of an unusually large electrostatic charge difference between the oxygen atom and the C–H hydrogen atom. If this is the basis of close C–H···O contacts, it follows that if the charge on the oxygen atom were increased, the C–H···O contact distance should decrease. As was explained above, the close approach of the adenine C-2–N-3 bond to the barbiturate C-2–O-2 carbonyl group in I appears to induce a greater negative charge on atom BO-2 than would otherwise be the case. Thus the AC-8···BO-2 contact in I might be expected to be significantly shorter than the analogous contact in II. This is what is observed.

There has been some controversy concerning the nature of close C–H···O contacts.[26,28,38] Their C–H–O angles appear to have much greater departures from linearity[26,38] than has been found for the analogous angles in normal N–H···O, N–H···N, and O–H···O hydrogen bonds.[18,26] This suggests that C–H···O interactions have a lesser covalent character

(34) Y. Kyogoku, R. C. Lord, and A. Rich, *Proc. Nat. Acad. Sci. U. S.*, 57, 250 (1967).

(35) W. Bolton, *Acta Crystallogr.*, 17, 147 (1964).

(36) P. O. P. Ts'o, N. S. Kondo, M. P. Schweitzer, and D. P. Hollis, *Biochemistry*, 8, 997 (1969).

(37) M. P. Schweitzer, S. I. Chan, G. K. Helmkamp, and P. O. P. Ts'o, *J. Amer. Chem. Soc.*, 86, 696 (1964).

(38) D. J. Sutor, *Nature (London)*, 195, 68 (1962).

UM00012470
NOVARTIS EXHIBIT 1017
Novartis v. Regents, IPR2023-01346
Page 1216 of 4460

than is true of normal hydrogen bonds. Normal hydrogen bonds are directly observable by a number of physical–chemical techniques such as infrared and nmr spectroscopy. So far, C–H···O interactions in molecules such as purines and pyrimidines have not been observed using these techniques.[39] Therefore, although the reality of C–H···O interactions in the solid state can no longer be denied,[18,22,40] they must be placed in a class apart from normal hydrogen-bonding interactions until it can be shown that they exhibit similar physical characteristics. Hence in this report short C–H···O contacts are referred to as hydrogen bond-*like* interactions.

There is no direct evidence to support the hypothesis that adenine–barbiturate base pairing has biological significance. Nevertheless, the great specificity and binding strength of this interaction[3] makes this hypothesis seem extremely plausible. The biological significance, if any, of the stacked dipoles found in I and II is less clear. In aqueous media, the free energies of such interactions are insignificant as are those of hydrogen bonds between bases. However, as was previously explained, it is quite likely that the barbiturate receptor site is in a nonpolar environment. The low dielectric constant of such a medium would stabilize any dipole–dipole interactions present. Hence, it may be that the barbiturate receptor site contains a group of atoms forming a strong dipole. This could be aligned so as to form an attractive interaction with the C-2–O-2 dipole of the barbiturate when it forms a hydrogen-bonded base pair with the adenine residue supposed to be at the receptor site. Such an interaction would enhance the strength of the adenine–barbiturate base pair and would therefore increase the already large specificity and binding strength of the barbiturate with its receptor site.

(39) G. C. Pimentel and A. C. McClellan, "The Hydrogen Bond," W. H. Freeman, San Francisco, Calif., 1960, p 197.
(40) N. C. Seeman, J. L. Sussman, and S.-H. Kim, *Nature (London), New Biol.*, 233, 90 (1971).

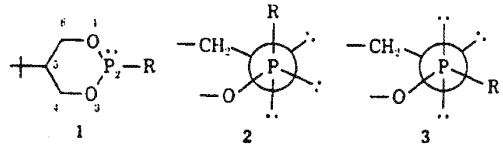
Acknowledgments. This work was supported by the National Institutes of Health (Grant No. GM18632) and by the Advanced Research Projects Agency, Office of the Secretary of Defense.

Communications to the Editor

Conformations of Saturated Phosphorus Heterocycles. Possible p_π–d_π Overlap Effects on the Apparent Conformational Energies of the Dimethylamino Group and the Influence of Phosphorus Lone-Pair Orientation on $^3J_{H_{eq}P}$

Sir:

Earlier work[1] has demonstrated that 2-R-5-*tert*-butyl-1,3,2-dioxaphosphorinanes **1** prefer to be in chair con-

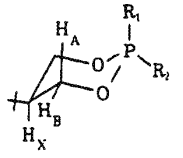


1 2 3

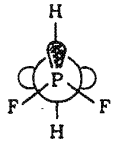
formations with the substituent on phosphorus *axial* rather than *equatorial* (for R = Cl,[1b] MeO,[1b] Me,[1a] *i*-Pr,[2] Ph[1c]). Consequently, the cis isomers (*t*-Bu equatorial, R axial) have been found to be more stable than the trans species. Thus, conformation about phosphorus is not determined primarily by 1,3-steric interactions but rather by the balance of vicinal interactions[3] between adjacent phosphorus and oxygen ring atoms and the substituent R (compare sturctures **2** and **3**).

We now report evidence that the dimethylamino group on phosphorus is more stable in the equatorial position with the consequence that *trans-2-dimethylamino-5-tert-butyl-1,3,2-dioxaphosphorinane* (**4a**) *is more stable than its cis isomer* **4b**.[4] This finding is quite surprising in that the Me_2N should have similar steric requirements to those of the isopropyl group[5] and also could impart to the system with axial Me_2N the stabilization usually ascribed to the anomeric effect.[6] In addition, results are presented that very strongly suggest that *the size of* $^3J_{H_{eq}P}$ *is greatly dependent on the axial or equatorial orientation of the lone pair on phosphorus.*

Compound 4 was synthesized by reaction of 2-*tert*-



4a, R_1 = e⁻ pair; R_2 = Me_2N
b, R_1 = Me_2N; R_2 = e⁻ pair
5a, R_1 = O; R_2 = Me_2N
b, R_1 = Me_2N; R_2 = O



6

(1) (a) W. G. Bentrude, K. C. Yee, R. D. Bertrand, and D. M. Grant, *J. Amer. Chem. Soc.*, 93, 797 (1971); (b) W. G. Bentrude and J. H. Hargis, *ibid.*, 92, 7136 (1970); (c) W. G. Bentrude and K. C. Yee, *Tetrahedron Lett.*, 3999 (1970).
(2) W. G. Bentrude, H. W. Tan, and K. C. Yee, unpublished results.
(3) The so-called *gauche effect* may be operative: S. Wolfe, *Accounts Chem. Res.*, 5, 102 (1972).
(4) This conclusion has been reached on the basis of independent evidence from a study of the *meso*-2-dimethylamino-4,6-dimethyl-1,3,2-dioxaphosphorinane system: J. A. Mosbo and J. G. Verkade, *J. Amer. Chem. Soc.*, 94, 8224 (1972).
(5) J. A. Hirsch, *Top. Stereochem.*, 1, 199 (1967). This review quotes a best value for the conformational energy of *i*-Pr in cyclohexane of 2.15 kcal/mol and a value for Me_2N of 2.1 kcal/mol (80% methyl Cellosolve).
(6) For recent discussions and references to the anomeric effect, see: H. Booth and R. U. Lemieux, *Can. J. Chem.*, 49, 777 (1971); S. Wolfe, A. Rauk, L. M. Tel, and I. G. Csizmadia, *J. Chem. Soc. B*, 136 (1971); F. W. Nader and E. L. Eliel, *J. Amer. Chem. Soc.*, 92, 3050 (1970).

UM00012471
NOVARTIS EXHIBIT 1017
Novartis v. Regents, IPR2023-01346
Page 1217 of 4460

The Structure of an Intermolecular Complex between Cytosine and 5-Fluorouracil

Donald Voet and Alexander Rich

Contribution from the Department of Biology, Massachusetts Institute of Technology, Cambridge, Massachusetts 02139.
Received October 15, 1968

Abstract: Crystals of an intermolecular complex containing cytosine and 5-fluorouracil in 1:1 molar ratio have been isolated from an aqueous solution containing these components. The structure of the crystal has been determined using single-crystal X-ray diffraction techniques. The crystals belong to the space group $P\bar{1}$ with one molecule each of cytosine and 5-fluorouracil in the asymmetric unit. The two molecules are joined together by two hydrogen bonds to form a cyclic dimer. These cyclic dimers are in turn joined by hydrogen bonds across centers of symmetry to other such cyclic dimers to form infinite sheets so that the crystal is a layered structure. In each unit cell of this structure there is a centrosymmetric cavity that contains two disordered water molecules.

The properties of purines and pyrimidines are determined to a great extent by their ability to form hydrogen bonds. Hydrogen bonds between purines and pyrimidines are responsible for the specificity that is believed to be the basis of intracellular information transfer in biological systems. In the double helical form of DNA, adenine forms hydrogen bonds with uracil and guanine with cytosine. This specificity of hydrogen bonding can be seen both in the solid state and in solution. A large number of intermolecular complexes have been formed between purines and pyrimidines in which specific interactions are found that are related to those occurring in the double helical form of DNA. Several adenine derivatives have been crystallized with uracil or thymine derivatives,[1-5] and likewise, derivatives of guanine and cytosine have been crystallized together.[6,7] Infrared[8,9] and proton nmr[10] studies in solution have shown the existence of selective hydrogen bonding between the naturally occurring purines and pyrimidines that have substituents on the glycosidic nitrogen. Thus, adenine derivatives have a high association constant for hydrogen bonding with uracil or thymine derivatives but do not form hydrogen bonds with guanine or cytosine derivatives. The latter pair, however, associate strongly with each other. This selective affinity has been described as being due to an electronic complementarity which is a property of the individual purine and pyrimidine molecules. However, it is of considerable interest to look for other kinds of interactions between the purines and pyrimidines. In the present work, we have discovered that it is possible to make a hydrogen-bonded one-to-one intermolecular complex between two pyrimidines, cytosine and 5-fluorouracil (see Figure 1). The structure of this complex has been solved by X-ray diffraction analysis. The molecules crystallize in a layer structure involving a complex system of hydrogen bonding. The lattice is somewhat unusual in that it contains a cavity that is partially filled with water molecules in a disordered state.

(1) K. Hoogsteen, *Acta Cryst.*, 16, 907 (1963).
(2) L. Katz, K. Tomita, and A. Rich, *ibid.*, 21, 754 (1966).
(3) K. Tomita, L. Katz, and A. Rich, *J. Mol. Biol.*, 30, 545 (1967).
(4) H. M. Sobell, *ibid.*, 18, 1 (1966).
(5) L. L. Labana and H. M. Sobell, *Proc. Natl. Acad. Sci. U. S.*, 57, 459 (1967).
(6) H. M. Sobell, K. Tomita, and A. Rich, *ibid.*, 49, 885 (1963).
(7) E. J. O'Brien, *Acta Cryst.*, 23, 92 (1967).
(8) Y. Kyogoku, R. C. Lord, and A. Rich, *Science* 154, 518 (1966).
(9) E. Küchler and J. Derkosch, *Z. Naturforsch.*, 21B, 209 (1966).
(10) L. Katz and S. Penman, *J. Mol. Biol.*, 15, 220 (1966).

Experimental Section

Materials. 5-Fluorouracil was obtained as a gift of the Hoffman La Roche Co. The cytosine was purchased from the Cyclo Chemical Co. Crystals of the intermolecular complex were obtained by preparing an aqueous solution of the two materials in 1:1 molar ratio and allowing this solution to evaporate to dryness at room temperature. Only one class of needle-shaped crystals appeared in the beaker, suggesting that the two materials had cocrystallized. Single crystals were isolated from the beaker and dissolved in water. The ultraviolet absorption spectrum of the resulting solution suggested that both cytosine and 5-fluorouracil were present in 1:1 molar ratio. The solution was also analyzed by paper chromatography using an aqueous phosphate–ammonium sulfate solvent, pH 6.8.[11] This analysis showed that both materials were in the solution in approximately 1:1 molar ratio.

A chemical analysis of the crystals, carried out by Dr. S. Nagy, showed that the best empirical formula that could be written for the crystals involved cytosine and 5-fluorouracil in 1:1 molar ratio plus an added molecule of water.

Anal. Calcd for $C_8N_5O_4FH_{10}$: C, 37.07; N, 27.02; F, 7.33; H, 3.89; O, 24.69. Found: C, 37.05; N, 27.40; F, 7.15; H, 3.77; O (by difference), 24.63.

Crystallographic Analysis. A suitable crystal, which measured 0.5 mm along its needle axis and 0.2 mm in cross-section, was mounted along the needle axis (*a* axis). The absence of any diffraction symmetry other than Friedel symmetry implied that the Bravais lattice of the crystal was triclinic. The unit cell parameters were determined from an *0kl* Weissenberg photograph that had been calibrated with superimposed Al powder lines and from *hk*0 and *h*0*l* precession photographs. The unit cell parameters were found to be $a = 4.29 \pm 0.02$, $b = 9.59 \pm 0.01$, and $c = 15.14 \pm 0.02$ Å; $\alpha = 111.8 \pm 0.2$, $\beta = 98.0 \pm 0.2$, and $\gamma = 101.3 \pm 0.2°$.

The bouyant density of the crystals in a CCl_4–$CHCl_3$ solution was found to be 1.594 g/cm³. The calculated density for the crystal, if it contains the complex cytosine–5-fluorouracil–water, with two such complexes in the unit cell, is 1.560 g/cm³.

Weissenberg intensity photographs were made using the multiple film technique. The levels *hkl* were collected for $0 \leq h \leq 3$ using Cu Kα ($\lambda = 1.5418$ Å) X-rays. Data for correlating the individual levels were recorded with timed exposures of precession photographs employing Mo Kα radiation ($\lambda = 0.7107$ Å). For this latter set of data the levels *hkl* for $0 \leq k \leq 2$ were collected. The intensities of the diffracted spots were estimated visually using a calibrated film strip that was made using the same crystal from which the intensity data were collected. Lorentz-polarization corrections were applied and the intensities from individual films within each level were placed on the same scale using the program

(11) Pabst Laboratory Circular OR-10, Pabst Brewing Co., Milwaukee, Wis., 1956.

UM00012472
NOVARTIS EXHIBIT 1017
Novartis v. Regents, IPR2023-01346
Page 1218 of 4460

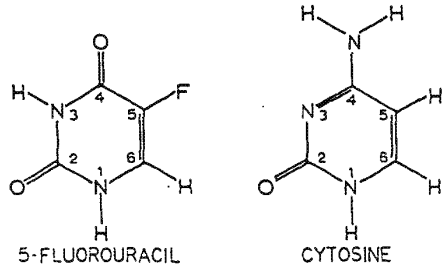


Figure 1.

XRDP1.[11] The intensities determined from the Weissenberg films were corrected for spot-shape distortion by the method of Phillips.[13] All the intensities were then placed on a common scale using the method of Simpson.[12] All computer calculations were performed using an IBM 7094 computer.

Structure Determination and Refinement

A total of 1730 unique reflections were collected. Of these, 1218 were considered intense enough to have been accurately estimated. The absolute scale factor and mean isotropic temperature factor were found by Wilson's method[14] to be $k = 1.080$ and $B = 1.84$, respectively. The statistics of the normalized structure factors,[15] normalized to $\langle E^2 \rangle = 1.00$, were found to be as shown in Table I. The results indicated that the crystal structure is centric; therefore the space group of the crystal is $P\bar{1}$. This result was subsequently confirmed by the successful refinement of the structure.

Table I

	Exptl	Centric	Acentric
$\langle E^2 - 1 \rangle$	1.050	0.968	0.736
$\langle \lvert E \rvert \rangle$	0.718	0.798	0.886
$\lvert E \rvert \geq 3.0$, %	0.99	0.30	0.01
$\lvert E \rvert \geq 2.0$, %	4.70	5.00	1.80
$\lvert E \rvert \geq 1.0$, %	27.54	32.00	37.00

Initial attempts were made to solve the structure by direct methods using the Σ_2 relationship.[16] This attempt was unsuccessful, probably due to the effect of the lack of symmetry in the unit cell in limiting the number of vectors with known phases. Accordingly, Patterson methods were employed to solve the crystal structure. The $1\bar{2}2$ reflection was by far the most intense reflection in the diffraction pattern. Its corresponding interplanar spacing of 3.45 Å suggested that the complex between cytosine and 5-fluorouracil crystallized in a layer structure because this spacing is very close to the thickness of the pyrimidine ring. The sharpened Patterson map with the origin partially removed was calculated. The $1\bar{2}2$ section of this map showed an extremely well-resolved and extensive hexagonal pattern that served to confirm our initial assignment of the $1\bar{2}2$ plane as the molecular plane.

The structure was solved by a consideration of the packing properties of the pyrimidines. If the pyrimidines crystallize with a center of symmetry, they often do so by forming infinite chains of hydrogen-bonded molecules that are organized into cyclic dimers across a center of symmetry. It also seemed reasonable to assume that the cytosine and 5-fluorouracil molecules were forming a hydrogen-bonded pair. There are eight possible ways of forming a hydrogen-bonded cyclic dimer between cytosine and 5-fluorouracil that incorporate the necessary centers of symmetry. From the Patterson map the orientation of the six-membered rings was evident. Accordingly, there are six different orientations of the structures which could be considered, making a total of 48 possible packing configurations. Only one of these possible structures was found to have the translational symmetry which is required for proper packing into the unit cell. From the coordinates of the atoms in this model the structure factors of a trial structure were calculated using the 12 ring atoms of the cytosine and 5-fluorouracil rings. In this initial calculation all atoms were assumed to be carbon atoms. The residual, $R = \Sigma \| F_o \| - |F_c| / \Sigma |F_o|$, of this initial structure factor calculation was 0.58. Two more iterations of Fourier map calculations brought out the remaining five cytosine and 5-fluorouracil atoms. When all 17 of these atoms were used in the structure factor calculation the value of the residual became $R = 0.44$.

The least-squares refinement of the structure was carried out employing the program ORFLS[17] using the Hughes weighting scheme.[18] The atomic scattering factors were taken from the International Tables for X-Ray Crystallography.[19] The 16 most intense reflections in the diffraction pattern were not used in the refinement because it was considered that their intensities could not be accurately estimated. In later stages of refinement those reflections with $\sigma(F_c)/F_o > 10$, 13 reflections in total, were deleted so that a total of 1189 reflections were used in the final refinement.[20] Two cycles of isotropic temperature refinement reduced the residual to $R = 0.34$. A difference Fourier map that was subsequently calculated showed a large diffuse peak, elongated in the direction parallel to the a axis, located between the molecular planes in an apparent cavity in the structure. This peak appeared to be caused by the presence of a water molecule. Accordingly, an oxygen atom, atom A, was added to the model of the structure being refined at the position of the maximum of this peak. Two more cycles of isotropic temperature refinement reduced the residual to $R = 0.24$. Two cycles of anisotropic temperature refinement then reduced the residual to $R = 0.17$. However, during the anisotropic temperature refinement the temperature factor, β_{11}, for oxygen atom A appeared to increase without limit. The difference Fourier map at this stage of refinement showed two poorly resolved peaks, one

(12) P. G. Simpson, Ph.D. Thesis, Harvard University, 1963.
(13) D. C. Phillips, *Acta Cryst.*, 7, 746 (1954).
(14) A. J. C. Wilson, *Nature*, 150, 152 (1942).
(15) J. Karle and H. Hauptman, *Acta Cryst.*, 9, 635 (1956).
(16) I. L. Karle and J. Karle, *ibid.*, 16, 969 (1963).
(17) W. R. Busing, K. O. Martin, and H. A. Levy, "A FORTRAN Crystallographic Least Squares Program" ORNL-TM-305, Oak Ridge National Laboratory, Oak Ridge, Tenn., 1962.
(18) E. W. Hughes, *J. Amer. Chem. Soc.*, 63, 1737 (1941).
(19) "International Tables for X-Ray Crystallography," Vol. III, The Kynoch Press, Birmingham, England, 1952.
(20) Observed and calculated structure factors have been deposited as Document No. NAPS-00312 with the ASIS National Auxiliary Publications Service, % CCM Information Sciences, Inc., 22 West 34th St. New York, N. Y. 10001. A copy may be secured by citing the document number and by remitting $1.00 for microfiche or $3.00 for photocopies. Advance payment is required. Make checks or money orders payable to: ASIS-NAPS.

UM00012473
NOVARTIS EXHIBIT 1017
Novartis v. Regents, IPR2023-01346
Page 1219 of 4460

of which was near the position of oxygen atom A. A second oxygen atom, atom B, was therefore added to the model of the structure at the position of the second peak and the refinement was continued with the occupancy factors of both oxygen atoms A and B allowed to vary. Two cycles of anisotropic temperature refinement brought the residual to its final value of $R = 0.162$. In the final cycle of refinement the shifts of the atomic position parameters, except for those of atoms O–A and O–B, were all less than one-fourth of their standard deviations. The same situation was true of the thermal parameters except for those of 5-fluorouracil atoms C(4) and C(5), cytosine atom N(6), and water-oxygen atoms O–A and O–B. The probable reason for these exceptions will be discussed below. The final occupancy factors for partial water-oxygen atoms A and B were 0.76 ± 0.11 and 0.26 ± 0.08, respectively. The refinement program was not constrained in terms of determining the total occupancy of the two sites of the water molecules. However, the fact that the sum of these two partial occupancies is close to unity suggests, in addition to the data previously mentioned, that the crystal is a monohydrate with one water of crystallization for each cytosine–5-fluorouracil pair. It is quite clear that the water molecules are present in the structure since refining the structure without them leads to a final residual of $R = 0.26$.

Results

The final fractional coordinates for all the atoms in the asymmetric unit are given in Table II together with the maximum value of the standard deviation, σ, for each atom type. Table III contains the final anisotropic temperature factors for all unique atoms together with the maximum value of their standard deviations for each atom type. The final anisotropic temperature factors for oxygen atom A can be seen to be very large. These values correspond to root-mean-square thermal displacements of oxygen atom A from its atomic center of 0.81 Å parallel to the a axis, 0.40 Å parallel to the b axis, and 0.41 Å parallel to the c axis.[21] The temperature factors of oxygen atom B are also rather large. Such displacements are much too large to be satisfactorily accounted for by thermal vibrations. It should also be noted that the final water–oxygen atom refinement parameters have very large standard deviations (Tables II and III), whereas the final standard deviations of the parameters describing the atoms of the cytosine and the 5-fluorouracil molecules are all small. This result must be taken as evidence of extreme disorder of the water molecules within the cavity in the crystal structure. This disorder was readily evident in the difference map since the electron density of the water molecule appeared to be very large and diffuse compared with that of a normal oxygen atom. Thus, the existence of water–oxygen atom sites A and B does not imply that the water molecule occupies two discrete sites in the crystal structure but rather, suggests that there is a continuum of sites, some of which have a relatively high probability of occupancy. This continuum is only poorly approximated by the model of discrete atoms held in a harmonic potential field implicit in the functional form of the thermal parameters (see footnote a of Table III).

The values of the anisotropic temperature factors of the atoms of the cytosine and 5-fluorouracil molecules, although somewhat scattered, are mostly within the normal range for these parameters. However, the

Table II. The Atomic Positions in Fractions of a Unit Cell Edge and the Deviation from the Mean Molecular Plane in Ångström Units

Atom	x	y	z	Δ
C-N(1)	−1.1933	0.0082	0.6011	−0.04
C-C(2)	−0.9705	0.1577	0.6394	−0.02
C-N(3)	−0.9599	0.2530	0.7349	0.00
C-C(4)	−1.1384	0.2049	0.7887	0.07
C-C(5)	−1.3742	0.0520	0.7515	0.04
C-C(6)	−1.3802	−0.0435	0.6545	0.02
C-O(2)	−0.8173	0.2000	0.5898	−0.11
C-N(4)	−1.1059	0.3070	0.8796	0.09
U-N(1)	0.4652	0.4634	0.1990	−0.05
U-C(2)	0.4639	0.3513	0.1087	0.09
U-N(3)	0.2360	0.2043	0.0794	0.10
U-C(4)	0.0287	0.1664	0.1353	0.02
U-C(5)	0.0640	0.2932	0.2304	−0.08
U-C(6)	0.2773	0.4325	0.2606	−0.10
U-O(2)	0.6308	0.3762	0.0566	0.15
U-O(4)	−0.1713	0.0370	0.1030	−0.01
U-F(5)	−0.1326	0.2613	0.2859	−0.17
O-A	0.1131	0.4208	0.5147	
O-B	0.3973	0.4162	0.5017	

The Maximum Value of σ for Atomic Positions in Fractions of a Unit Cell Edge

Atom type	Δx	Δy	Δz
C	0.0028	0.0011	0.0008
N	0.0022	0.0010	0.0007
O[a]	0.0020	0.0008	0.0006
F	0.0017	0.0007	0.0005
O[b]	0.0231	0.0043	0.0025

[a] Ring substituent. [b] Water.

Table III. The Anisotropic Thermal Parameters[a] (× 10^4)

Atom	β_{11}	β_{22}	β_{33}	β_{12}	β_{13}	β_{23}
C-N(1)	198	58	50	−22	23	18
C-C(2)	154	37	32	−18	34	8
C-N(3)	297	53	30	−16	60	8
C-C(4)	137	37	24	38	41	7
C-C(5)	154	68	30	−12	28	7
C-C(6)	109	78	38	−8	50	11
C-O(2)	490	61	35	−9	113	5
C-N(4)[b]	224	105	16	−24	68	9
U-N(1)	253	48	33	23	42	4
U-C(2)	63	60	28	−7	33	13
U-N(3)	179	60	40	−11	13	14
U-C(4)[b]	−3	68	33	−26	26	14
U-C(5)[b]	107	92	26	14	72	12
U-C(6)	336	59	38	52	22	6
U-O(2)	333	90	39	−2	75	8
U-O(4)	419	56	21	−50	51	−5
U-F(5)	445	100	39	−58	114	2
O-A	5195	352	139	75	55	122
O-B	139	153	86	33	97	70

The Maximum Value of σ for Thermal Parameters (× 10^4)

Atom type						
C	83	13	7	24	17	7
N	64	11	6	19	15	7
O[c]	60	10	4	18	13	5
F	52	9	4	16	11	5
O[d]	1439	71	31	219	127	38

[a] The thermal parameters are in the form $\exp[-(h^2\beta_{11} + k^2\beta_{22} + l^2\beta_{33} + 2hk\beta_{12} + 2hl\beta_{13} + 2kl\beta_{23})]$. [b] The matrix of this quantity is not positive definite. [c] Ring substituent. [d] Water.

(21) D. W. J. Cruickshank, *Acta Cryst.*, 9, 747 (1956).

UM00012474
NOVARTIS EXHIBIT 1017
Novartis v. Regents, IPR2023-01346
Page 1220 of 4460

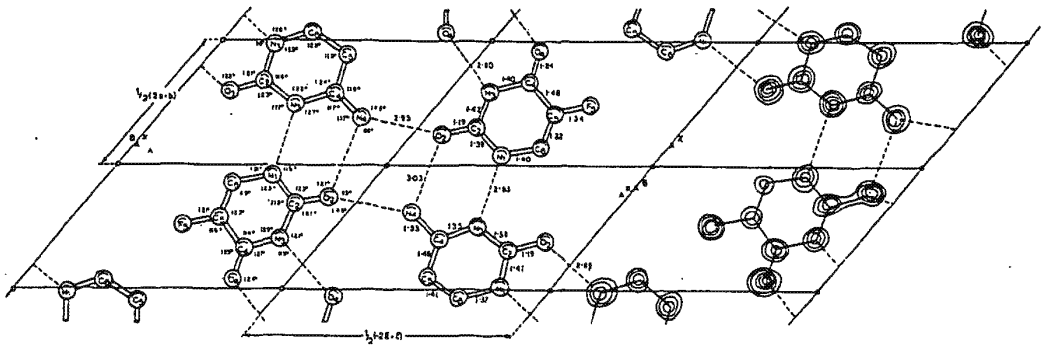


Figure 2. The 1 $\bar{2}$ 2 section of the electron-density map together with a schematic drawing of the molecular structure indicating the atomic numbering scheme, the bond lengths (in ångström units) and the bond angles. Hydrogen bonds are indicated by dashed lines. The positions of the partial water oxygen atoms, A and B, as projected along the *a* axis onto the 1 $\bar{2}$ 2 plane, are indicated by ×'s.

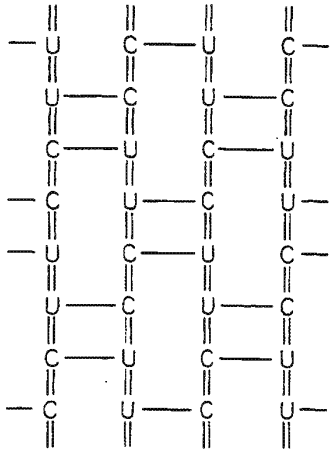


Figure 3. A schematic representation of the hydrogen bonding in the crystal. Here C represents cytosine, U represents 5-fluorouracil, and a solid line represents a single hydrogen bond.

matrices of the anisotropic temperature factors for 5-fluorouracil atoms C(4) and C(5) and cytosine atom N(4) are not positive definite quantities, a situation that is not physically meaningful. It is likely that this situation, together with the large shifts in the thermal parameters for these atoms, is due to the disorder of the water molecule which has a distribution that does not fit the model of discrete atoms assumed in the refinement procedure. This disorder is undoubtedly also responsible for the slightly high value of the residual after the final refinement.

Figure 2 shows the 1$\bar{2}$2 section of the electron density map together with a schematic drawing that illustrates the hydrogen bonds between the 5-fluorouracil and the cytosine molecules. The atomic numbering scheme and the bond angles and distances are also shown in this figure together with the relationship of the molecular structure to the unit cell. The standard deviations of the cytosine and the 5-fluorouracil bond lengths and bond angles as determined from the errors in the unit cell parameters and from the variance–covariance matrix of the final refinement are all very close to 0.01 Å and 1°, respectively.

The 122 section of the electron density map is very close to the molecular plane but not exactly through it. The equation of the mean molecular plane through all the atoms of the cytosine and the 5-fluorouracil residues as determined by the method of least squares is given by the equation $x - 1.955y + 1.924z = -0.041$, where x, y, and z are the fractional coordinates of the unit cell. The deviations of the atoms of the cytosine and the 5-fluorouracil molecules from this plane are given in Table II. The root-mean-square deviation of these 17 atoms out of the mean molecular plane is 0.027 Å. The maximum deviation out of this plane, which is that of 5-fluorouracil atom F(5), is 0.17 Å. The interplanar spacing between these mean molecular planes is 3.50 Å, a figure which is very close to the value cited above of 3.45 Å for the 1$\bar{2}$2 plane. In Figure 2 it was convenient to draw the structure in the 1$\bar{2}$2 plane. However, this action resulted in a slight deviation of a portion of the 5-fluorouracil molecule from the plane of the drawing. For example, the electron density peaks of atoms C(6), C(5), and F(5) of the 5-fluorouracil molecule are slightly out of the plane of Figure 2 which causes these peaks to appear somewhat smaller in the electron density map of this figure than they actually are at their maxima.

The 5-fluorouracil and cytosine molecules are organized into a hydrogen-bonded net as is shown in Figure 2. In the vertical direction of this figure there are infinite chains of molecules held together by two hydrogen bonds between each pyrimidine molecule. These chains consist of the pair 5-fluorouracil–cytosine followed by the pair cytosine–5-fluorouracil. The former pair is related to the latter pair by a center of symmetry. This hydrogen-bonding scheme forms an alternating double repetition of cytosine and 5-fluorouracil residues. These infinite chains are cross linked by single hydrogen bonds between cytosine and 5-fluorouracil residues. This scheme is illustrated schematically in Figure 3 in which the lines between the symbols for cytosine (C) and 5-fluorouracil (U) stand for the number of hydrogen bonds connecting them. It can be seen that adjacent vertical columns have the alternating sequence of two cytosine and two 5-fluorouracil residues out of phase in such a way that they are held together by single hydrogen bonds between the cytosine and the 5-fluorouracil residues in the horizontal

UM00012475
NOVARTIS EXHIBIT 1017
Novartis v. Regents, IPR2023-01346
Page 1221 of 4460

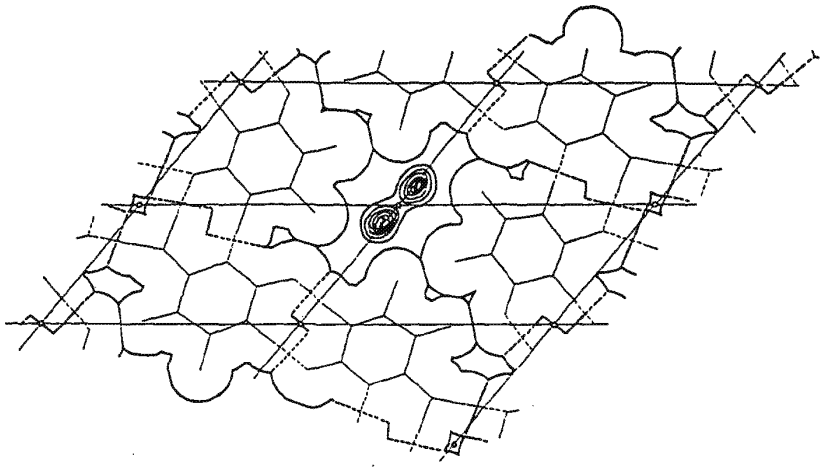


Figure 4. The van der Waals packing diagram in the 122 plane shown in Figure 2. The contours represent the electron-density distribution of the water molecules projected along the a axis onto the $1\bar{2}2$ plane. The positions of the partial water–oxygen atoms, A and B, are indicated by ×'s.

direction. The open areas without hydrogen bonds in Figure 3 are schematic representations of the cavity that contains the disordered water molecules. This elongated cavity is also illustrated in Figure 2 which has ×'s over the positions of partial water–oxygen atoms A and B as projected along the a axis.

The bond lengths and angles listed in Figure 2 are similar to those which have been observed in crystal structure analyses of other cytosine or uracil derivatives. The hydrogen bond distances shown in Figure 2 are all within the normal range,[22] the only exception being a slightly long hydrogen bond of length 3.03 Å between the amino group, N(4), of cytosine and the carbonyl oxygen atom, O(2), of 5-fluorouracil.

The van der Waals packing of the cytosine–5-fluorouracil complex in the $1\bar{2}2$ plane is shown in Figure 4. As can be seen in this figure, the pyrimidine rings fit together quite well with no abnormally short intermolecular contacts in forming the hydrogen-bonded net but they leave empty a flattened and somewhat elongated cavity which is shown in the middle of the figure. In Figure 4 the electron-density distribution of the water molecules is projected along the a axis onto the molecular plane producing the contours shown. The position of partial water oxygen atoms A and B are indicated by ×'s in Figure 4. Figure 5 shows the electron-density map between the molecular planes. This section, which is part of the plane $y = 0.433$, is taken through the water peak. It shows the diffuseness of the water peak and the position of the two partial water–oxygen atoms A and B. It can be seen that peak B is located just below the midline between the two molecular planes, whereas peak A is far above it. An identical electron density peak, related to the peak shown in Figure 5 by a center of symmetry, lies 1.15 Å away in the plane $y = 0.567$.

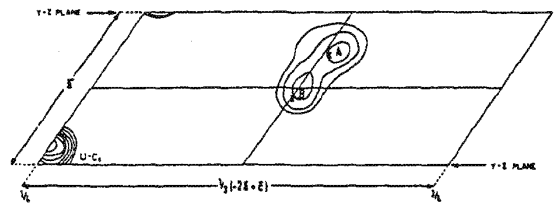


Figure 5. A portion of the section $y = 0.433$ of the electron-density map in the vicinity of the water molecules. The positions of the partial water–oxygen atoms, A and B, are indicated by ×'s.

Discussion

The cavity in the cytosine–5-fluorouracil crystal is quite narrow in the molecular plane; if an oxygen atom were located at the level of the plane it would be quite crowded. Accordingly, the water molecules adopt positions in between the two molecular levels. The walls of the cavity are lined with atoms with which it is unlikely that a water molecule would have any significant interaction. The only exceptions to this statement are the four symmetry-related cytosine O(2) atoms which are located at the ends of the flattened crevice. However, the approach to the only available position on each of these oxygen atoms which is most likely to take part in strong hydrogen bonding is completely blocked by the hydrogen atom which is covalently bonded to 5-fluorouracil atom C(6) adjacent to the atom under consideration. The closest approach of any of the symmetry-related cytosine O(2) atoms surrounding a particular cavity to the positions of partial oxygen atom A is 2.77 Å, about the distance one would expect for a strong O–H···O hydrogen bond.[22] However, it is also about the distance one would expect for an O···O van der Waals contact.[22] It could be argued that the relative orientations of cytosine carbonyl oxygen atom O(2) and the closest of the two water molecules centered at the two symmetry related positions, O–A, are unfavorable for hydrogen bonding but this argument is, at best, tenuous.[23] However, it is to be expected that if the water molecule were hydrogen bonded to cytosine atom O(2) it would be strongly

(22) L. Pauling, "The Nature of the Chemical Bond," Cornell University Press, Ithaca, N. Y., 1960.

(23) J. Donahue in "Structural Chemistry and Molecular Biology," A. Rich and N. Davidson, Ed., W. H. Freeman and Co., San Francisco, Calif., 1968.

UM00012476
NOVARTIS EXHIBIT 1017
Novartis v. Regents, IPR2023-01346
Page 1222 of 4460

localized near that atom but, as mentioned above, the water molecules are extremely disordered within the cavity. Thus it appears unlikely that a water molecule at position O–A, and similarly, one at position O–B, hydrogen bonds to any of the symmetry-related cytosine O(2) atoms. Therefore it seems reasonable to argue that there are only very small, if any, attractive forces between the water molecules and the atoms lining the cavity wall and that the observed stoichiometry of the crystal is simply a reflection of the fact that the total volume of the cavity is such that it will accommodate only two water molecules.

The cytosine–5-fluorouracil structure has an interesting four-membered hydrogen-bonded ring. As can be seen in Figure 2, this ring involves two amino groups and two carbonyl groups so that, in effect, two sets of cytosine and 5-fluorouracil molecules each held together with two hydrogen bonds are then joined with two additional symmetry related hydrogen bonds to make a cyclic tetramer. Arrangements of this type have been found in other crystal structures involving purines and pyrimidines. In the intermolecular complex of 1-methyl-5-bromocytosine and 9-ethylguanine[4] the two base pairs are organized into a cyclic tetramer with a set of hydrogen bonds similar to that observed in the present structure. A similar ring is also found in the structure of cytosine-5-acetic acid[24] in which the cytosine derivative itself occupies all four sides of the hydrogen-bonded ring. A third example is found in the closely related structure of 1-methylcytosine–5-fluorouracil.[25] The occurrence of this type of hydrogen-bonded tetramer in which pairs of bases are brought together is of some interest because of the frequent occurrence of hydrogen-bonded pairs of bases in the double-helical form of the nucleic acids. These structures provide a kind of structural rationale for believing that cyclic tetramers of bases in polynucleotide structures may form in configurations which are transiently stabilized.[26] This phenomenon might be of direct relevance in the phenomenon of genetic crossing over which involves the participation of two double-helical molecules of DNA.

The molecular structure of the complex between 1-methylcytosine and 5-fluorouracil[25] is very closely related to present structure. In both crystals the network of hydrogen-bonded cytosine and uracil derivatives are identical, including the cyclic tetramer described above, except that the structure containing 1-methylcytosine is blocked by the methyl group from forming a cyclic dimer between the two cytosine derivatives. The similarity between the two structures is remarkable considering that the crystal structures of the two complexes are completely different. The space group of the crystal containing 1-methylcytosine is Pbca which causes the rings to pack into a herring-bond pattern, whereas the rings in the present structure are packed into a layered array. We must therefore conclude that there is some type of specificity between the bases which is common to the two structures.

A survey of reported crystal structures containing self-bonding uracil derivatives revealed nine such additional structures.[27–35] In eight of these nine structures, those of uracil,[27] 1-methyluracil,[28] 1-methylthymine,[29] the complex 5-fluorouracil–9-ethylhypoxánthine,[30] 5-ethyl-6-methyluracil,[31] 2,4-dithiouracil,[32] 5-nitrouracil monohydrate,[33] and the photodimer of 1-methylthymine,[34] a cyclic dimer is formed between the uracil residues which is identical with that formed between the uracil residues in the structure of cytosine–5-fluorouracil. Only in the structure of thymine monohydrate[35] does a different cyclic dimer form. In that case atom O(4) is hydrogen bonded to a water molecule. The frequent occurence of the type of cyclic dimer found between the uracil residues in the structure of cytosine–5-fluorouracil suggests that its association constant is far greater than those of the two other possible cyclic dimers which might exist between uracil derivatives. When such a cyclic dimer is formed between two 5-fluorouracil molecules there are only two ways of forming a cyclic dimer with cytosine using the available hydrogen-bonding sites. However, only one of these ways can be used to form a cyclic dimer with 1-methylcytosine. It is interesting that the cyclic dimer which is possible with both cytosine derivatives is the only one which allows the formation of the above-mentioned cyclic tetramer. It is likely that the formation of the cyclic tetramer confers additional stability on the crystal structure.

Only in the present structure has the mode of self-complexing between cytosine molecules shown in Figures 2 and 4 been found. In two of the other three known structures in which a neutral cytosine derivative forms a self-complex, those of cytosine[36] and cytosine monohydrate,[37] an unsymmetrical cyclic dimer is formed utilizing, respectively, as the hydrogen donor and acceptor atoms, atoms N(1) and O(2) on one molecule and atoms N(4) and N(3) on the other molecule. In the remaining reported structure in which a neutral cytosine derivative forms a self-complex, that of 1-methylcytosine[38] atom N(1) is blocked by a methyl group. The molecule forms a hydrogen-bonded pair with itself through a centrosymmetric cyclic dimer utilizing atoms N(3) and N(4) in each molecule as the hydrogen-acceptor and -donor atoms, respectively. The limited data above do not suggest that the cyclic dimer formed between cytosine molecules in the present structure is especially favorable energetically since all three possible types of cyclic dimers which can be formed between two neutral cytosine molecules do occur. Thus it is likely that the strength of the cyclic dimer formed between the 5-fluorouracil molecules in the present structure and in that of the complex 1-methylcytosine–5-fluorouracil[25] and the formation of the cyclic tetramers mentioned above are the energetically controlling factors in these structures.

(24) R. E. Marsh, R. Bierstadt, and E. L. Eichorn, *Acta Cryst.*, 15, 310 (1962).
(25) S. H. Kim and A. Rich, *J. Mol. Biol.*, in press.
(26) O. Siddiqi, "The Nucleic Acids," Sree Sarawaty Press Ltd., Calcutta, 1965, p 175.
(27) (a) G. S. Parry, *Acta Cryst.*, 7, 313 (1954); (b) R. F. Stewart, and L. H. Jensen, *ibid.*, 23, 1102 (1967).
(28) D. W. Green, F. S. Mathews, and A. Rich, *J. Biol. Chem.*, 237, 3573 (1962).
(29) K. Hoogsteen, *Acta Cryst.*, 16, 28 (1963).
(30) S. H. Kim and A. Rich, *Science*, 158, 1046 (1967).
(31) G. N. Reeke and R. E. Marsh, *Acta Cryst.*, 20, 703 (1966).
(32) E. Shefter and H. G. Mautner, *J. Amer. Chem. Soc.*, 89, 1249 (1967).
(33) B. M. Craven, *Acta Cryst.*, 23, 376 (1967).
(34) J. R. Einstein, J. L. Hossau, J. W. Longworth, R. O. Rahn, and C. H. Wei, *Chem. Commun.*, 1063 (1967).
(35) R. Gerdil, *Acta Cryst.*, 14, 333 (1961).
(36) D. L. Barker and R. E. Marsh, *ibid.*, 17, 1581 (1964).
(37) G. A. Jeffrey, and Y. Kinoshita, *ibid.*, 16, 20 (1963).
(38) F. S. Mathews, and A. Rich, *Nature*, 201, 179 (1964).

UM00012477
NOVARTIS EXHIBIT 1017
Novartis v. Regents, IPR2023-01346
Page 1223 of 4460

The present structure is an intermolecular complex involving cytosine and a derivative of uracil. It appears to go against the rule of electronic complimentarity described above, since infrared studies of derivatives of these molecules have shown that there is no selective affinity for hydrogen bonding between uracil and cytosine derivatives.[8] Similarly, 1-methyl-5-fluorouracil forms a crystalline complex with 9-ethyladenine[8] but does not form one with cytosine derivatives.[39] However, it is important to note that the molecules involved in the present structure do not have side chains on their glycosidic nitrogen atoms. Instead, atom N(1) is protonated in both molecules and, of course, plays an important role in developing the hydrogen bonding system which stabilizes the entire crystal. Thus, it is likely that the electronic distributions in the pyrimidines are modified somewhat when they are substituted on the N(1) position so that their hydrogen-bonding properties are altered. Of course, in the present crystal structure, and that of the complex 1-methylcytosine–5-fluorouracil, the hydrogen bonding between the cytosine derivatives and 5-fluorouracil involves the atom N(1) of 5-fluorouracil. Such a mode of hydrogen bonding would be impossible if a substituent were present on this atom.

(39) A. Rich, unpublished observations.

Acknowledgments. We wish to thank Dr. S.-H. Kim for his assistance in pointing out the existence of the complex. This work was supported by grants from the National Institutes of Health, the U. S. Public Health Service, and the National Aeronautics and Space Agency.

Synthesis of Carbocyclic Analogs of Purine Ribonucleosides[1]

Y. Fulmer Shealy and Joe D. Clayton

Contribution from the Kettering-Meyer Laboratory, Southern Research Institute, Birmingham, Alabama 35205. *Received November 8, 1968*

Abstract: The racemic forms of the carbocyclic (cyclopentane) analogs of adenosine, inosine, 6-mercaptopurine ribonucleoside, and 6-(methylthio)purine ribonucleoside were synthesized from (±)-4β-amino-2α,3α-dihydroxy-1β-cyclopentanemethanol. This amine was synthesized by two routes from 2α,3α-diacetoxy-1β,4β-cyclopentanedicarboxylic acid *via* its anhydride and monoamide. The two routes differed in the order in which the amino group was introduced by a Hofmann reaction and the hydroxymethyl group, by metal hydride reduction of an ester or acid chloride group. The stereochemistry of the starting cyclopentane was fixed by the preparation of this compound from *exo-cis*-5-norbornene-2,3-diol, which was prepared by *cis*-dihydroxylation of norbornadiene. The structure of the norbornenediol was confirmed by chemical means and by nmr analysis.

It is now well estaolished that alterations of either the furanose or the base moiety of naturally occurring purine and pyrimidine nucleosides may produce derivatives that exert interesting and powerful biological effects.[2] Replacement of the furanose oxygen atom of nucleosides with a methylene group would produce carbocyclic (cyclopentane) analogs in which the hydroxyl groups occupy the same positions, have the same *cis–trans* relationships, and may be expected to assume similar conformations.[4] The carbocyclic analogs have the potential, therefore, either to mimic or to antagonize the functions of the naturally occurring nucleosides and nucleotides. Unlike the nucleosides, the carbon–nitrogen bond joining the heterocyclic base to the cyclopentane ring should be comparable in stability to that of a simple alkyl derivative and should, therefore, be much less susceptible to enzymatic fission than the analogous bond of nucleosides. For these reasons we have synthesized the carbocyclic analogs (racemic forms) of the naturally occurring nucleosides adenosine and inosine and of two biologically active purine nucleosides. A preliminary account of our synthesis of the adenosine analog (C-Ado, **28**) has appeared;[3] subsequently, Kishi and coworkers[5] reported in a preliminary communication that X-ray analysis revealed the structure of a recently isolated antibiotic[6] to be an optically active form of C-Ado (**28**). Earlier, Murdock

(1) This investigation was supported by the Cancer Chemotherapy National Service Center, National Cancer Institute, National Institutes of Health, Contract No. PH43-64-51 and by the C. F. Kettering Foundation.

(2) References to some of the large number of publications in this field may be found in the following reviews: J. A. Montgomery and H. J. Thomas, *Advan. Carbohydrate Chem.*, 17, 301 (1962); J. J. Fox, K. A. Watanabe, and A. Bloch, *Progr. Nucl. Acid Res. Mol. Biol.*, 5, 251 (1966); S. S. Cohen, *ibid.*, 5, 1 (1966); C. Heidelberger, *Ann. Rev. Pharmacol.*, 7, 101 (1967); J. A. Montgomery, *Progr. Med. Chem.*, in press; *cf.* references cited in ref 3.

(3) Y. F. Shealy and J. D. Clayton, *J. Amer. Chem. Soc.*, 88, 3885 (1966).

(4) The preferred conformations of simple substituted cyclopentanes are the puckered envelope and half-chair forms [K. S. Pitzer and W. E. Donath, *ibid.*, 81, 3213 (1959); F. V. Brutcher, Jr., T. Roberts, S. J. Barr, and N. Pearson, *ibid.*, 81, 4915 (1959); M. Hanack, "Conformation Theory," Academic Press, New York, N. Y., 1965, pp 72–78; E. L. Eliel, N. L. Allinger, S. J. Angyal, and G. A. Morrison, "Conformational Analysis," John Wiley & Sons, Inc., New York, N. Y., 1965. In crystalline purine and pyrimidine nucleosides and nucleotides either C2′ or C3′ is displaced (either *endo* or *exo* to the base moiety) from the mean plane of the other four furanose-ring atoms by 0.5–0.6 Å; see the following publications and references cited therein: M. Sundaralingam, *J. Amer. Chem. Soc.*, 87, 599 (1965); M. Sundaralingam and L. H. Jensen, *J. Mol. Biol.*, 13, 930 (1965); A. E. V. Haschemeyer and A. Rich, *ibid.*, 27, 369 (1967); P. Tollin, H. R. Wilson, and D. W. Young, *Nature*, 217, 1148 (1968). There is evidence, however, of some difference in the stabilities of the preferred conformers of comparably substituted cyclopentanes and tetrahydrofurans [H. R. Buys, C. Altona, and E. Havinga, *Tetrahedron*, 24, 3019 (1968)].

(5) T. Kishi, M. Muroi, T. Kusaka, M. Nishikawa, K. Kamiya, and K. Mizuno, *Chem. Commun.*, 852 (1967).

(6) T. Kusaka, H. Yamamoto, M. Shibata, M. Muroi, T. Kishi, and K. Mizuno, *J. Antibiot.* (Tokyo), 21, 255 (1968).

UM00012478
NOVARTIS EXHIBIT 1017
Novartis v. Regents, IPR2023-01346
Page 1224 of 4460

This Page is Inserted by IFW Indexing and Scanning Operations and is not part of the Official Record

BEST AVAILABLE IMAGES

Defective images within this document are accurate representations of the original documents submitted by the applicant.

Defects in the images include but are not limited to the items checked:

- ☐ BLACK BORDERS
- ☐ IMAGE CUT OFF AT TOP, BOTTOM OR SIDES
- ☐ FADED TEXT OR DRAWING
- ☐ BLURRED OR ILLEGIBLE TEXT OR DRAWING
- ☐ SKEWED/SLANTED IMAGES
- ☐ COLOR OR BLACK AND WHITE PHOTOGRAPHS
- ☐ GRAY SCALE DOCUMENTS
- ☐ LINES OR MARKS ON ORIGINAL DOCUMENT
- ☐ REFERENCE(S) OR EXHIBIT(S) SUBMITTED ARE POOR QUALITY
- ☐ OTHER: _____

IMAGES ARE BEST AVAILABLE COPY.

As rescanning these documents will not correct the image problems checked, please do not report these problems to the IFW Image Problem Mailbox.

of orally administered digoxin may be due to variation in gastric pH, which would modify the composition of digoxin species available for absorption (12). The catalytic effect of montmorillonite will accentuate this problem. Therefore, the concomitant administration of drug products containing digoxin and montmorillonite should be avoided.

A similar catalytic effect may also occur with other neutral drugs that degrade by acid hydrolysis and should be considered in the formulation of clay-containing drug products or their coadministration with other drugs.

REFERENCES

(1) L. S. Porubcan, C. J. Serna, J. L. White, and S. L. Hem, *J. Pharm. Sci.*, 67, 1081 (1978).

(2) W. F. Bradley, *J. Am. Chem. Soc.*, 67, 975 (1945).

(3) D. M. C. MacEwan, *Trans. Faraday Soc.*, 44, 349 (1948).

(4) B. K. G. Theng, "The Chemistry of Clay-Organic Reactions," Adam Hilger, London, England, 1974, pp. 206–210.

(5) D. D. Evans, in "Methods of Soil Analysis, Part 2," C. A. Black, Ed., American Society of Agronomy, Madison, Wis., 1965, chap. 57.

(6) M. L. Carvalhas and M. A. Figueira, *J. Chromatogr.*, 86, 254 (1973).

(7) R. Greene-Kelley, *Trans. Faraday Soc.*, 51, 412 (1955).

(8) J. L. White, *ACS Symp. Ser.*, 29, 208 (1976).

(9) M. Cruz, J. L. White, and J. D. Russell, *Isr. J. Chem.*, 6, 315 (1968).

(10) R. L. Ledoux and J. L. White, *J. Colloid Interface Sci.*, 21, 127 (1966).

(11) K. Kasahara and A. Ruily-Torres, *Klin. Wochenschr.*, 47, 1109 (1969).

(12) J. Kuhlmann, U. Abshagen, and N. Rietbrock, *Naunyn-Schmiedebergs Arch. Pharmacol.*, 276, 149 (1973).

(13) M. H. Gault, J. D. Charles, D. L. Sugden, and D. C. Kepkay, *J. Pharm. Pharmacol.*, 29, 27 (1977).

(14) L. A. Sternson and R. D. Shaffer, *J. Pharm. Sci.*, 67, 327 (1978).

(15) N. T. Coleman and C. McAuliffe, in "Proceedings of the Third National Conference on Clays and Clay Minerals," W. V. Milligan, Ed., National Academy of Sciences–National Research Council, Washington, D.C., 1955, pp. 282–289.

(16) J. D. Russell, M. Cruz, J. L. White, G. W. Bailey, W. R. Payne, Jr., J. D. Pope, Jr., and J. I. Teasley, *Science*, 160, 1340 (1968).

ACKNOWLEDGMENTS

Supported in part by The Upjohn Co.

This report is Journal Paper 7215, Purdue University Agricultural Experiment Station, West Lafayette, IN 47907.

Digoxin was kindly supplied by the Burroughs-Wellcome Co.

NOTES

Crystal Structure of 1:1 Complex of Barbital with 1-Methylimidazole

ALBERT WANG and B. M. CRAVEN ×

Received May 8, 1978, from the *Crystallography Department, University of Pittsburgh, Pittsburgh, PA 15260.* Accepted for publication August 9, 1978.

Abstract □ The prediction of a strong hydrogen-bonding interaction between barbital and 1-methylimidazole was confirmed. Two crystal complexes were obtained, 1:1 and 2:1, and the X-ray structure was determined for the 1:1 complex, which is monoclinic, space group $P2_1/c$, with $a = 12.236(3)$ Å, $b = 11.332(4)$ Å, $c = 12.495(4)$ Å, and $\beta = 120.67(1)°$. The structure contains disk-shaped hydrogen-bonded tetramers with two molecules of each kind. There is a short NH···N hydrogen bond (2.82 Å) in which barbiturate provides the NH donor.

Keyphrases □ Barbital—complex with 1-methylimidazole, crystal structure determined □ 1-Methylimidazole—complex with barbital, crystal structure determined □ Complexes—barbital with 1-methylimidazole, crystal structure determined □ Crystal structure—determined for complex of barbital with 1-methylimidazole

Barbiturate drugs behave as strong hydrogen-bonding donors through their two NH groups but are weak acceptors through their three carbonyl oxygen atoms. These conclusions were derived from the hydrogen-bonding arrangements and interatomic distances observed in the crystal structures of a series of complexes of barbital with other small molecules representative of biological systems (1, 2). Thus, barbiturate drug receptor sites are likely to involve strongly electronegative hydrogen-bonding acceptor groups, such as the nitrogen atoms of adenine (3, 4), the imidazole ring in histidine or histamine (2), or the phosphoryl oxygen atoms of phospholipids (5).

These studies indicated that a strong hydrogen-bonding interaction would occur between barbital (5,5-diethylbarbituric acid) and 1-methylimidazole (Fig. 1), which might lead to crystal complexation. Indeed, 1-methylimidazole was a powerful solvent for barbital. The high viscosity of this solution made direct crystallization impractical. However, two crystal complexes were obtained from an ethanol solution; in one complex (1:1), crystal structure determination confirmed a short hydrogen bond NH···N (2.82 Å) in which barbital is the donor and 1-methylimidazole is the acceptor.

EXPERIMENTAL

Crystals of the 1:1 and 2:1 complexes were obtained from the same ethanolic solution, which was saturated at 60° with respect to both barbital and 1-methylimidazole, and slowly cooled in a sealed vial. Space groups and approximate cell data for these complexes were determined from X-ray precession photographs[1].

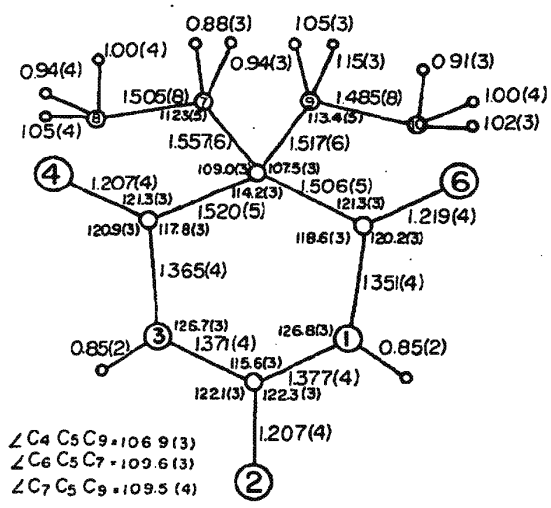
Crystals of the 1:1 complex, which dissociate at 96°, are monoclinic, space group $P2_1/c$, with $a = 12.236(3)$ Å, $b = 11.332(4)$ Å, $c = 12.495(4)$ Å, and $\beta = 120.67(1)°$. The crystal density (1.190 g/cm³) determined by

[1] No further work is planned on the 2:1 complex of barbital and 1-methylimidazole. These crystals are monoclinic, space group $P2_1/c$, with $a = 16.7$ Å, $b = 12.1$ Å, $c = 12.4$ Å, and $\beta = 102°$. There are eight barbital and four 1-methylimidazole molecules per unit cell.

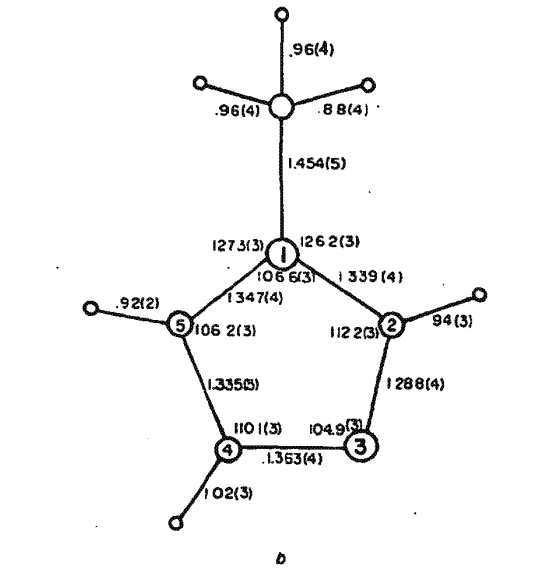
0022-3549/79/0300-0361$01.00/0

© 1979, American Pharmaceutical Association

UM00012480
NOVARTIS EXHIBIT 1017
Novartis v. Regents, IPR2023-01346
Page 1226 of 4460



a



b

Figure 1—*Bond lengths (angstroms) and angles (degrees) for barbital (a) and 1-methylimidazole (b). Estimated standard deviations are given in brackets. Circles of decreasing size represent oxygen, nitrogen, carbon, and hydrogen atoms, in that order.*

flotation in carbon tetrachloride–benzene agrees with the calculated density (1.187 g/cm³), assuming that the unit cell contains four molecules of each kind.

The cell data and the X-ray intensities were measured at room temperature using a four-circle computer-controlled diffractometer[2] with graphite-monochromated MoKα-radiation (λ = 0.7093 Å). The crystal (0.32 × 0.22 × 0.20 mm) was mounted with the c-axis almost along the diffractometer Φ-axis. Integrated intensities for 2625 nonsymmetry related reflections were measured by θ/2θ scans. The variance in an integrated intensity was assumed to be $\sigma^2(I) = \sigma^2 + (0.02I)^2$, where σ^2 is the variance due to counting statistics. There were 1887 reflections with an intensity greater than $2\sigma(I)$. No corrections were made for X-ray absorption or extinction.

The phase problem was solved by direct methods, using symbolic addition and tangent refinement procedures (6). The nonhydrogen atomic parameters obtained from an E-map were refined initially by block-diagonal least-squares methods. Nine of the 18 hydrogen atoms were readily found in a difference Fourier map. The remainder, which consisted mostly of terminal methyl hydrogen atoms, were found near the end of a full matrix least-squares refinement.

The function minimized by least squares was $\Sigma w_H \Delta_H^2$, where $\Delta_H = |F_{obs}| - |F_{calc}|$ and $w_H = 1/\sigma^2(F_{obs})$. Atomic scattering factors were those of Cromer and Waber (7) for nonhydrogen and of Stewart *et al.* (8) for hydrogen. The data were suspected to be subject to X-ray extinction since reflections with strong intensities and large d-spacings gave calculated structure amplitudes systematically larger than the observed values. In the final refinement, seven such reflections were omitted. The final R-

[2] Enraf-Nonius CAD-4.

Table I—Atomic Positional Parameters for the 1-Methylimidazole–Barbital Complex[a]

	x	y	z
	Nonhydrogen Atoms[b]—Barbital		
N(1)	5936 (2)	4106 (2)	6423 (2)
C(2)	4719 (3)	4016 (2)	6211 (3)
O(2)	3818 (2)	4452 (2)	5313 (2)
N(3)	4602 (2)	3424 (2)	7104 (2)
C(4)	5557 (3)	2909 (3)	8153 (3)
O(4)	5346 (2)	2439 (2)	8896 (2)
C(5)	6881 (3)	2908 (3)	8328 (3)
C(6)	6995 (3)	3611 (3)	7367 (3)
O(6)	8013 (2)	3727 (2)	7421 (2)
C(7)	7843 (4)	3384 (6)	9651 (4)
C(8)	7617 (5)	4663 (6)	9802 (4)
C(9)	7199 (4)	1635 (5)	8222 (5)
C(10)	6312 (5)	1093 (4)	6997 (5)
	Nonhydrogen Atoms[b]—1-Methylimidazole		
N(1)	1138 (2)	2571 (2)	7773 (2)
C(1)	807 (4)	1866 (4)	8538 (4)
C(2)	2204 (3)	2479 (3)	7728 (3)
N(3)	2230 (2)	3217 (2)	6957 (2)
C(4)	1116 (3)	3825 (3)	6476 (3)
C(5)	443 (3)	3436 (3)	6974 (3)
	Hydrogen Atoms[c]—Barbital		
H(1)	595 (2)	453 (2)	587 (2)
H(3)	386 (2)	340 (2)	700 (2)
H(71)	870 (3)	335 (3)	984 (2)
H(72)	773 (3)	301 (2)	1020 (3)
H(81)	786 (3)	519 (3)	931 (3)
H(82)	827 (4)	491 (3)	1059 (4)
H(83)	675 (3)	481 (3)	977 (3)
H(91)	715 (3)	118 (3)	893 (3)
H(92)	819 (3)	158 (3)	834 (3)
H(101)	659 (3)	34 (3)	701 (3)
H(102)	609 (3)	145 (3)	618 (3)
H(103)	535 (3)	100 (3)	653 (3)
	Hydrogen Atoms[c]—1-Methylimidazole		
H(11)	0 (3)	165 (3)	814 (3)
H(12)	84 (3)	242 (3)	913 (3)
H(13)	140 (3)	127 (3)	903 (3)
H(2)	283 (2)	192 (2)	821 (2)
H(4)	92 (2)	446 (2)	583 (2)
H(5)	966 (2)	363 (2)	684 (2)

[a] Positional parameters are given as fractions of the lattice translations. Estimated standard deviations given in parentheses refer to the least-significant figures in parameter values. [b] Positional parameters × 10^4. [c] Positional parameters × 10^3.

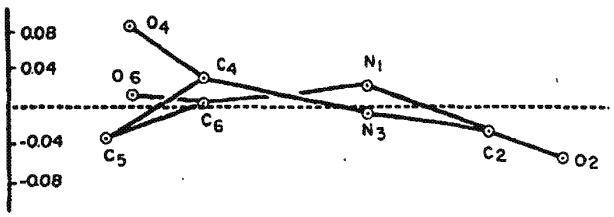


Figure 2—*Barbital ring. The dashed line is the trace of the best least-squares plane through the ring atoms. Atomic displacements from this plane (angstroms) are shown on a vertical scale eight times greater than the horizontal scale.*

UM00012481
NOVARTIS EXHIBIT 1017
Novartis v. Regents, IPR2023-01346
Page 1227 of 4460

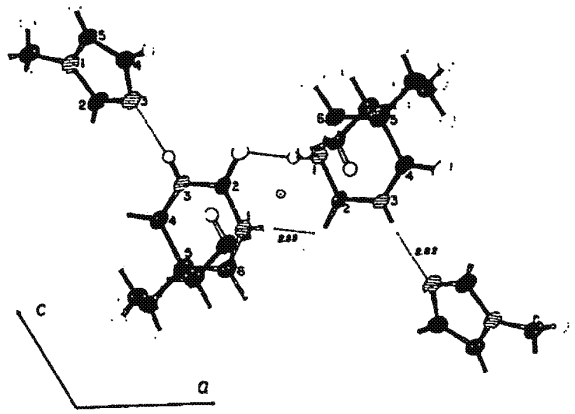


Figure 3—*Hydrogen-bonded tetramer. Thermal ellipsoids are shown that have 50% probability of enclosing each vibrating atom. Nitrogen atom ellipsoids are hatched, and carbon atom ellipsoids are cross-hatched. Hydrogen-bonded N···O and N···N distances (angstroms) are shown.*

factors were $R = \Sigma_H|\Delta_H|/\Sigma_H F_{obs} = 0.077$ and $R_w = [\Sigma_H(w\Delta_H)^2/\Sigma_H(wF_{obs})^2]^{1/2} = 0.034$. A list of observed and calculated structure factors and a table of anisotropic temperature factors for nonhydrogen atoms were compiled[3]. Final atomic positional parameters are given in Table 1.

DISCUSSION

Bond lengths and angles (Fig. 1) agree with those in the barbital–imidazole complex (2) within the limits of experimental error. The barbital ring atoms are in an almost coplanar conformation (Fig. 2) similar to that observed in a number of other barbiturate crystal structures (Fig. 3 in Ref. 9). The ethyl group carbon atoms and the ring atom C(5) in barbital are almost coplanar, with atom C(2) having the largest displacement (0.065 Å) from the least-squares plane. This coplanar group and the ring plane make a dihedral angle of 91.7°. In 1-methylimidazole, the imidazole ring atoms and the 1-methyl carbon atom are coplanar.

The most interesting feature in the structure is the formation of hydrogen-bonded tetramers consisting of two molecules of each kind (Fig. 3). Two barbital molecules related by a crystallographic center of symmetry form N(1)H···O(2) hydrogen bonds with N···O distance (2.85 Å). This distance is within the range (2.8–3.0 Å) observed for other hydrogen bonds between barbiturates (1). The other barbital N(3)H donor group forms a very short hydrogen bond (N···N, 2.82 Å) with the nitrogen acceptor atom of 1-methylimidazole (2). The NH···N angle is 172°. The barbiturate and imidazole rings of molecules that form a tetramer are at dihedral angles of 19.1°. The tetramers are thus disk shaped, with nonpolar groups forming most of the outer surface. There is an unusual CH···O interaction between tetramers (C···O distance, 3.31 Å; CH···O angle 154.1°) involving the 1-methylimidazole C(5)–H(5) group and barbiturate atom O(6). This interaction is not considered to be a hydrogen bond because the C···O distance is too long.

The hydrogen-bonding arrangement is quite different from that of the imidazole complex with barbital. In that complex, barbitals dimerize through NH···O hydrogen bonds involving O(6) rather than O(2). These dimers are cross-linked by hydrogen bonds formed at opposite sides of imidazole molecules to make infinite ribbons through the crystal structure. The important feature common to both crystal complexes is the short NH···N hydrogen bond (N···N distance, 2.78 Å in the imidazole complex) in which barbiturate is the donor.

Thus, the present crystal structure fits a pattern of behavior in which barbiturate NH groups form strong hydrogen bonds with acceptor groups in other molecules.

[3] Available on request from authors.

REFERENCES

(1) G. L. Gartland and B. M. Craven, *Acta Crystallogr.*, **B30**, 980 (1974).

(2) I. N. Hsu and B. M. Craven, *ibid.*, B30, 988 (1974).

(3) S. H. Kim and A. Rich, *Proc. Natl. Acad. Sci. USA*, 60, 402 (1968).

(4) D. Voet, *J. Am. Chem. Soc.*, 94, 8213 (1972).

(5) I. N. Hsu and B. M. Craven, *Acta Crystallogr.*, **B30**, 1299 (1974).

(6) J. Karle and I. L. Karle, *ibid.*, 21, 849 (1966).

(7) D. T. Cromer and J. T. Waber, *ibid.*, 18, 104 (1965).

(8) R. F. Stewart, E. R. Davidson, and W. T. Simpson, *J. Chem. Phys.*, 43, 3175 (1965).

(9) B. M. Craven, C. Cusatis, G. L. Gartland, and E. A. Vizzini, *J. Mol. Struct.*, 16, 331 (1973).

ACKNOWLEDGMENTS

Supported by Grant GM-22548 from the U.S. Public Health Service, National Institutes of Health.

UM00012482
NOVARTIS EXHIBIT 1017
Novartis v. Regents, IPR2023-01346
Page 1228 of 4460

This Page is Inserted by IFW Indexing and Scanning Operations and is not part of the Official Record

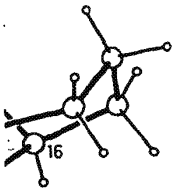
BEST AVAILABLE IMAGES

Defective images within this document are accurate representations of the original documents submitted by the applicant.

Defects in the images include but are not limited to the items checked:

- ☐ BLACK BORDERS
- ☐ IMAGE CUT OFF AT TOP, BOTTOM OR SIDES
- ☐ FADED TEXT OR DRAWING
- ☐ BLURRED OR ILLEGIBLE TEXT OR DRAWING
- ☐ SKEWED/SLANTED IMAGES
- ☐ COLOR OR BLACK AND WHITE PHOTOGRAPHS
- ☐ GRAY SCALE DOCUMENTS
- ☐ LINES OR MARKS ON ORIGINAL DOCUMENT
- ☐ REFERENCE(S) OR EXHIBIT(S) SUBMITTED ARE POOR QUALITY
- ☐ OTHER: _____

IMAGES ARE BEST AVAILABLE COPY.
As rescanning these documents will not correct the image problems checked, please do not report these problems to the IFW Image Problem Mailbox.



Cryst.Struct.Comm. (1976). *5*, 207.

2,5-O-METHYLENE-D-MANNITOL SODIUM-CHLORIDE, $C_7H_{14}O_6.NaCl$

R.A. Wood and V.J. James*

School of Physics, University of New South Wales, P.O. Box 1, Kensington 2033, Australia

J.A. Mills

Division of Chemical Technology, C.S.I.R.O., P.O. Box 310, South Melbourne 3205, Australia

PRELIMINARY INFORMATION

2,5-O-Methylene-D-mannitol (Ness, Hann and Hudson, 1943) was found to form a crystalline complex with sodium chloride, and several facts prompted a structure determination. It is very stable, unaffected by being heated to 250° (2,5-O-methylene-D-mannitol melts at 174°), and is less soluble in water than its components (about 13 g in 100 ml at 25°). Paper electrophoresis showed no evidence of complex-formation in aqueous solution between 2,5-O-methylene-D-mannitol and a number of metal cations. There are several possible conformations for the seven-membered ring of this acetal in solution (Stoddart and Szarek, 1971).

The compound was recrystallised from water and freed of adhering mother liquor by centrifugation of the wet crystals under chloroform.

UM00012484
NOVARTIS EXHIBIT 1017
Novartis v. Regents, IPR2023-01346
Page 1230 of 4460

CRYSTAL DATA

From oscillation and Weissenberg photographs and single-crystal diffractometry (CuKα, λ = 1.54178 Å), $\underline{a}$ = 6.839 (5), $\underline{b}$ = 11.474 (5), $\underline{c}$ = 13.328 (5)Å, Z = 4 (the basic asymmetric unit contains only half of the molecule), D_{obs} = 1.61 g cm^{-3}, D_{calc} = 1.60 g cm^{-3}, space group: $C222_1$.

INTENSITY DATA, STRUCTURE DETERMINATION AND REFINEMENT

The intensities of 597 reflections with $\theta < 70°$ were measured on a Siemens automatic single-crystal diffractometer using the method of Hoppe (1965). The scanning procedure utilized the moving-crystal, moving-detector method (θ-2θ scan) (Arndt and Willis, 1966). Lorentz, polarisation and absorption corrections were applied to the data. The position of the chloride ion was determined from a Patterson map, and subsequent Fourier difference syntheses revealed the remaining atoms. A full-matrix least-squares refinement, incorporating anisotropic temperature factors for non-hydrogen atoms while the thermal parameters of hydrogen atoms were kept equal to those of the atoms with which they were most closely associated, resulted in a conventional R of 0.044. The co-ordinate of the two hydroxyl hydrogens in the basic asymmetric unit repeatedly refined to values that gave O-H bond lengths of approximately 0.6 Å, whereas the co-ordinates of the associated peaks on the difference map gave bond lengths of approximately 0.9 Å. Consequently, only fractional shifts were applied to these hydrogens in the refinement.

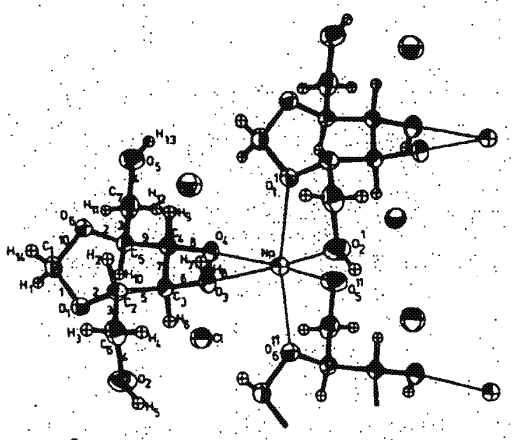
UM00012485
NOVARTIS EXHIBIT 1017
Novartis v. Regents, IPR2023-01346
Page 1231 of 4460

hs and single-
= 6.839 (5),
ic asymmetric
= 1.61 g cm^{-3},

'INEMENT
< 70° were
diffracto-
canning pro-
ctor method
plied to the
ermined from
ence syntheses
east-squares
ure factors
eters of
atoms with
ted in a
ne two
t repeatedly
f approximately
ted peaks on
imately 0.9 Å.
ied to these

Atomic co-ordinates (×10^4 for non-hydrogen and ×10^3 for hydogen atoms)

	x/a (σ)	y/b (σ)	z/c (σ)		x/a(σ)	y/b(σ)	z/c(σ)
Cl	2757(1)	0	0	O(3)	711(2)	332(1)	3491(1)
Na	0	2044(1)	2500	H(1)	57(4)	613(2)	194(2)
C(1)	0	6580(3)	2500	H(2)	-16(4)	804(2)	384(2)
C(2)	1056(3)	8211(2)	3501(2)	H(3)	256(5)	764(2)	457(2)
C(3)	863(3)	9314(2)	2869(2)	H(4)	266(4)	891(2)	474(2)
C(6)	2656(4)	8266(2)	4279(2)	H(5)	531(4)	877(3)	417(2)
O(1)	1586(2)	7272(1)	2824(1)	H(6)	216(4)	938(2)	256(2)
O(2)	4491(2)	8377(2)	3777(1)	H(7)	- 3(5)	21(2)	398(2)



Bond distances (Å)		Bond angles (°)		Torsional angles (°)	
1	1.412(2)	10,1	111.6(2)	10,1,2	47.4(1)
2	1.452(3)	1,2	114.6(1)	1,2,5	-97.1(2)
3	1.508(3)	2,3	106.1(2)	2,5,7	67.6(2)
4	1.428(3)	3,4	108.6(2)	5,7,9	-47.9(3)
5	1.526(3)	3,5	114.0(2)	6,7,8	62.1(3)
6	1.436(3)	5,6	111.2(2)		
7	1.538(4)	5,7	114.8(1)		
		6,7	108.3(1)		

UM00012486
NOVARTIS EXHIBIT 1017
Novartis v. Regents, IPR2023-01346
Page 1232 of 4460

COMMENTS

Each sodium ion is coordinated, with Na-O distances of 2.388(1), 2.314(2), 2.417(2) Å, to six oxygen atoms, comprising O(3) and O(4) from one molecule of 2,5-O-methylene-D-mannitol, O(1) and O(2) from a second molecule, and O(5) and O(6) from a third. The sodium ions and cyclic acetal molecules form sheets, with the chloride ions arranged between. The conformation of the seven-membered ring of the acetal is essentially a twist-chair (TCl) that was considered to be one of the most probable for this compound and its derivatives in solution (Stoddart and Szarek, 1971). The cyclic acetal is symmetrical about a two-fold axis through C(1) and the sodium ion lies on this axis. The highly symmetrical arrangement and efficient six-fold coordination of sodium ions without incorporation of water molecules account for the stability of the crystalline complex, although the acetal lacks the structural features that seem to be most favourable for complexing of carbohydrates with cations in solution (Angyal, 1972).

REFERENCES

Angyal, S.J. (1972). *Austral. J. Chem.* 25, 1957.

Arndt, V.W. and Willis, B.T.M. (1966). *Single Crystal Diffractometry*, Cambridge University Press, 265.

Hoppe, W. (1965). *Angew, Chem.* 77, 484.

Ness, A.T., Hann, R.M. and Hudson, C.S. (1943) *J.Amer.Chem.Soc.* 65, 2215.

Stoddart, J.F. and Szarek, W.A. (1971) *J. Chem. Soc.(B)* 437.

Received: 10 December 1975

UM00012487
NOVARTIS EXHIBIT 1017
Novartis v. Regents, IPR2023-01346
Page 1233 of 4460

This Page is Inserted by IFW Indexing and Scanning Operations and is not part of the Official Record

BEST AVAILABLE IMAGES

Defective images within this document are accurate representations of the original documents submitted by the applicant.

Defects in the images include but are not limited to the items checked:

- ☐ BLACK BORDERS
- ☐ IMAGE CUT OFF AT TOP, BOTTOM OR SIDES
- ☐ FADED TEXT OR DRAWING
- ☐ BLURRED OR ILLEGIBLE TEXT OR DRAWING
- ☐ SKEWED/SLANTED IMAGES
- ☐ COLOR OR BLACK AND WHITE PHOTOGRAPHS
- ☐ GRAY SCALE DOCUMENTS
- ☐ LINES OR MARKS ON ORIGINAL DOCUMENT
- ☐ REFERENCE(S) OR EXHIBIT(S) SUBMITTED ARE POOR QUALITY
- ☐ OTHER: _____

IMAGES ARE BEST AVAILABLE COPY.
As rescanning these documents will not correct the image problems checked, please do not report these problems to the IFW Image Problem Mailbox.

ELSEVIER

Polymer 42 (2001) 3867–3874

polymer

www.elsevier.nl/locate/polymer

Effect of composition distribution on miscibility and co-crystallization phenomena in the blends of low density polyethylene with conventional and metallocene-based ethylene–butene copolymers

Junting Xu[a,*], Xurong Xu[a], Linsen Chen[a], Linxian Feng[a], Wei Chen[b]

[a]*Department of Polymer Science & Engineering, Zhejiang University, Hangzhou 310027, People's Republic of China*
[b]*Research Institute of Petroleum Processing, SINOPEC, Beijing 100083, People's Republic of China*

Received 27 June 2000; received in revised form 15 August 2000; accepted 19 September 2000

Abstract

Three ethylene–butene copolymers (two metallocene-based and one conventional) having different composition distributions were blended with low density polyethylene (LDPE) in a wide proportion range. The miscibility of the blend melts was studied with the rheological method. It is found that zero-shear viscosity of all the blends does not obey the logarithmic additivity rule, indicating the immiscible state of the blend melts. The blends were rapidly quenched from the melts and co-crystallization phenomena were investigated by differential scanning calorimetry (DSC). The obtained results show that composition distribution has a great influence on co-crystallization. In the blends of the conventional ethylene–butene copolymer, which has a broad composition distribution, part of the co-crystals may segregate from the crystals of both LDPE and ethylene copolymer and exist as a separated population. This suggests that there exist three phases in the melts. In contrast, the blends of the metallocene-based ethylene–butene copolymers with a narrow composition distribution are only composed of two phases together with some exchange between the two components. It is also observed that broader composition distribution leads to more ethylene–butene copolymer transferred into LDPE. © 2001 Elsevier Science Ltd. All rights reserved.

Keywords: Composition distribution; Miscibility; Co-crystallization

1. Introduction

Co-crystallization phenomenon is frequently observed in the blends of different types of polyethylene [1–9]. It is believed that co-crystallization is produced due to the thermodynamically miscible parts of two components in the blends having similar crystallization rate [10–12]. This means that the miscibility of the components in melt plays an important role in the co-crystallization phenomenon, though it is a kinetic process. The miscibility of the blend melt and the crystallization rate strongly depend on the molecular structure of the polymers such as branch content, molecular shape and molecular weight [13–18]. Among these factors, the branch content of ethylene copolymers may be the most important one. As a result, when one of the components is composed of a series of fractions with different branch contents, i.e. the intermolecular composition distribution is inhomogeneous, the composition distribution may have a great influence on co-crystallization [19,20]. In fact, the ethylene/α-olefin copolymers produced with Ziegler–Natta catalysts generally have a broad composition distribution [21], even though the structure of the copolymers from metallocene catalysts is also not very homogeneous [22,23]. Tashiro et al. observed different co-crystallization degrees in the blends of high density polyethylene (HDPE) with two linear low density polyethylene (LLDPE) samples (LLDPE1 and LLDPE2) having a close composition [16]. No explanation was given for this phenomenon. However, it could be seen from this paper that these two LLDPE samples were prepared by two different methods: one from the hydrogenation of polybutadiene and the other with heterogeneous Ziegler–Natta catalyst. The DSC melting curves of the former were much narrower than the latter, indicating a more homogeneous composition distribution [16]. To our knowledge, most of the ethylene copolymers used in the literature for the study of co-crystallization were not well characterized in the composition distribution, and there has been no systematic report about the influence of composition distribution on co-crystallization.

For the blends of LDPE with HDPE, it is often observed

* Corresponding author. Tel./fax: +86-571-795-2400.
E-mail address: xujt@ipsm.zju.edu.cn (Junting Xu).

0032-3861/01/$ - see front matter © 2001 Elsevier Science Ltd. All rights reserved.
PII: S0032-3861(00)00756-4

UM00012489
NOVARTIS EXHIBIT 1017
Novartis v. Regents, IPR2023-01346

Table 1
Some characteristics of polymer samples

Samples	Branches content (CH/1000C)		Density (g/cm^3)	M_w ($\times 10^{-4}$)	M_w/M_n
	Short[a]	Long[b]			
A	1.9	0	0.947	11.10	2.28
B	5.8	0	0.931	8.01	2.72
C	2.9	0	0.949	13.86	6.49
LDPE	11.7	1.6	0.923	9.65	4.85

[a] Branches containing ≤8 carbon atoms (via ^{13}C-NMR).
[b] Branches containing >8 carbon atoms (via ^{13}C-NMR).

that the linear part of LDPE is incorporated into the crystals of HDPE and co-crystallization occurs in HDPE crystals, leading to the decrease in the melting temperatures of both LDPE and HDPE [24]. However, co-crystallization can also occur in other forms. For example, co-crystals may segregate from both HDPE and LDPE and exist as a separate part (showing a third intermediate melting peak between the melting temperatures of two pure components) [25]. Recently, Wignall et al. reported that co-crystals can also occur within the LDPE lamellae by incorporating HDPE molecules [26]. Therefore, two questions are raised: Why can co-crystallization occur in different forms? How do the polymer structure and crystallization conditions affect the forms of co-crystallization? So far, no answer has been given to these two questions in the publications.

In the present work, ethylene–butene copolymers with different composition distributions, which were prepared with metallocene and conventional Ziegler–Natta catalysts, were blended with LDPE in a wide range of blending ratios. The miscibility in the melt of the blends and the co-crystallization phenomena were studied and the observed differences between these copolymers were correlated to their composition distributions.

2. Experimental procedure

2.1. Materials

LDPE was blended with three different ethylene–butene copolymers. Some characteristics of these polymers are listed in Table 1. Samples A and B prepared with metallocene catalyst were donated by RIPP SINOPEC. Sample C, which was prepared with heterogeneous Ziegler–Natta catalyst, was supplied by Qilu Petrochemical Corporation. LDPE prepared by free radical polymerization under high pressure was commercially purchased.

2.2. Preparative temperature rising elution fractionation (TREF)

Preparative TREF apparatus was used to collect a sufficient amount of polymer fractions. About 2 g of polymer was dissolved in xylene at a concentration of 0.005 g/ml at 130°C. This solution was deposited on an inert support, sea sand (particle diameter: 0.3–0.6 mm) packed in a steel column. The length and the internal diameter of the column are 1.0 and 40 mm, respectively. The column was cooled to room temperature at a rate of 1.5°C/h. Then, the deposited polymer was heated stepwise and eluted with xylene. The polymer fractions were recovered by evaporating the xylene solvent and drying in a vacuum oven. Because a small amount of antioxidant 1010 had been added, the total recovery of polymer was around 105%.

2.3. Characterization of composition distribution with DSC

The samples of ethylene–butene and LDPE were first heated to 170°C and kept for 10 min, then were quickly transferred into an oil bath of 140°C. The temperature of the oil bath decreases stepwise, and at each temperature the samples were maintained for 12 h under nitrogen gas atmosphere. The temperatures of the oil bath were 140, 135, 130, 125, 120, 115, 105, 100, 95, 90, 85 and 80°C. Then, the treated samples were scanned with DSC at a heating rate of 5°C/min.

2.4. Dynamic rheological testing

The polymer samples were molded into 2 mm thick disks with a diameter of 30 mm under 160°C and 15 MPa. The dynamic rheological properties were carried out on a Rheometric Science ARES-9A rheometer. Parallel plates with gap 1.0 mm and diameter 25 mm were used. The temperatures for testing were 170°C and the angular frequency range was from 0.1 to 300 rad/s. The strain and time sweeps were first performed before dynamic testing to ensure that the frequency sweeps were within the linear viscoelastic and stable region.

2.5. Preparation of the blends

LDPE and ethylene–butene copolymers were dissolved in xylene (1% w/v) at 130°C and stirred for 2 h. Then, the hot xylene solution of the polymer blends was poured into a large amount of ethanol to precipitate the blends, followed by filtering and drying under vacuum at 60°C for two days. The pure components went through the same procedure. For

UM00012490
NOVARTIS EXHIBIT 1017
Novartis v. Regents, IPR2023-01346
Page 1236 of 4460

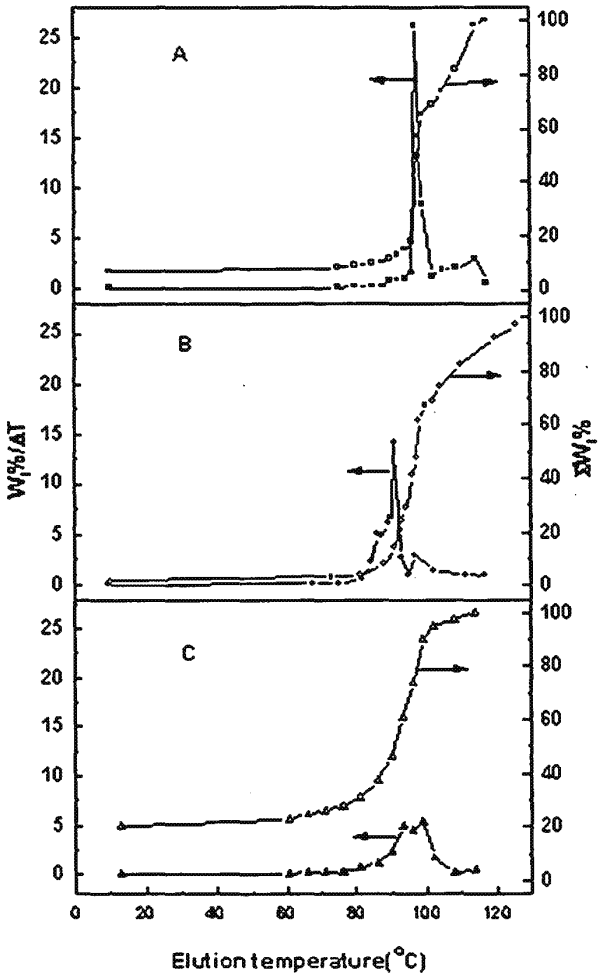


Fig. 1. TREF curves of various ethylene–butene copolymers.

the purpose of convenience, all blends were designated with a letter and a number, which referred to ethylene–butene copolymers and the proportion of the ethylene copolymers, respectively.

2.6. Thermal treatments and DSC measurement

The blends were weighted and wrapped in aluminum pans for DSC measurement. The aluminum pans were sealed in glass tubes full of N_2 and placed into an oil bath at 170°C for 30 min, then rapidly quenched with liquid nitrogen. The melting curves of the thermally treated samples were recorded on a Perkin–Elmer DSC-7 calorimeter. The heating rate applied was 10°C/min, and the temperature was calibrated with standard substance Indium at the same heating rate.

3. Results and discussion

3.1. Composition distribution of pure components

Fig. 1 illustrates the TREF curves of samples A, B and C. TREF fractionates the ethylene copolymers based on comonomer content [27,28]. The higher the comonomer content, the lower the elution temperature. From the peak height, peak width and peak number in $W_i\%/\Delta T$–T curves of Fig. 1, one can compare the composition distribution of these three samples. The higher and narrower peaks, and the smaller number of peaks suggest a narrower composition distribution. It is observed that the peak height decreases in the order A > B > C whereas the peak width exhibits a reverse order A < B < C. This result shows that the metallocene-based ethylene–butene copolymers A and B have a more homogeneous composition distribution than the

UM00012491
NOVARTIS EXHIBIT 1017
Novartis v. Regents, IPR2023-01346
Page 1237 of 4460

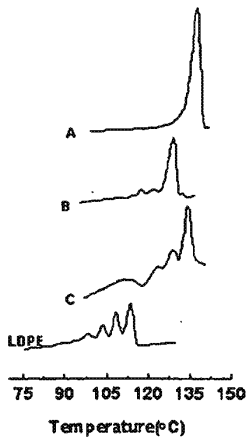


Fig. 2. Melting curves of different pure components after stepwise crystallization.

conventional sample C. Moreover, it is found from the cumulative curves in Fig. 1 that as high as 20 wt% of sample C is eluted at room temperature, and this quantity is much higher than that of samples A and B, indicating that sample C contains more highly branched fractions than samples A and B.

The composition distribution of ethylene copolymers can also be qualitatively investigated by DSC and this method shows better resolution than TREF [22,29]. Fig. 2 shows the DSC melting curves of various pure components after stepwise crystallization from 140 to 70°C at an interval of 5°C. Under this crystallization condition, the crystallization of ethylene copolymers is mainly controlled by the composition (thermodynamic factor) instead of kinetic factors, thus the polymer fractions with different comonomer contents

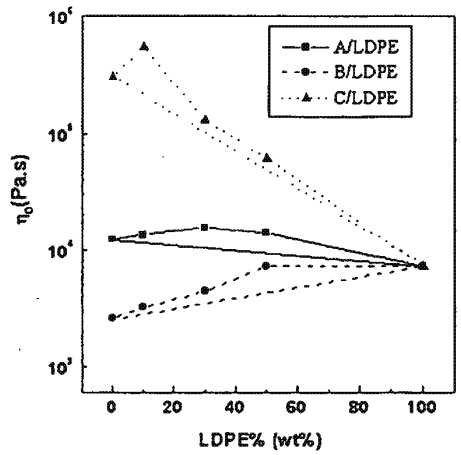


Fig. 3. The plot of logarithmic zero-shear viscosity versus the proportion of LDPE in the blends.

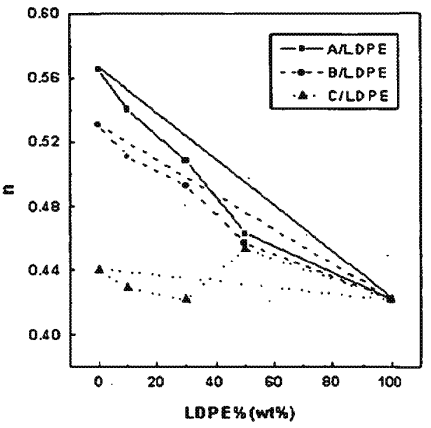


Fig. 4. The plot of values of n versus the proportion of LDPE in the blends.

will not co-crystallize. The larger the comonomer content, the lower the crystallization and melting temperatures. Only a single peak appears in the melting curve of sample A, indicating a relatively homogeneous composition distribution of this polymer. In the melting curve of sample C it is observed that four peaks distribute in a wide temperature range (from 100 to 135°C). This shows that sample C has a much broader composition distribution than sample A, though they have similar densities. Sample B has an intermediate composition distribution between sample A and C, since there exist several small peaks besides a major peak in its melting curve. The result obtained with the DSC method is in accordance with that of TREF. The DSC curve of LDPE reveals that the molecular structure of LDPE is also inhomogeneous.

3.2. Rheological results

The complex viscosity (η) of various blends at different frequencies was determined with a dynamic rheometer under 170°C. It is found that all experimental data can be fitted by the Cross model [30]:

$$\eta = \frac{\eta_0}{[1 + \tau^* \gamma]^{1-n}}, \tag{1}$$

where η_0 is the zero-shear viscosity, τ^* a representative relaxation time and n an exponent.

It is generally accepted that the zero-shear viscosity of a miscible blend without specific interactions or free volume variation should obey the logarithmic additivity rule defined as [31]:

$$\log \eta_0 = \sum w_i \log \eta_0^i. \tag{2}$$

Fig. 3 is the plot of $\log \eta_0$ versus the proportion of LDPE in the blends. It is observed that the zero-shear viscosity of all the blends exhibits a positive deviation from the logarithmic additivity rule, indicating the immiscible state of

UM00012492
NOVARTIS EXHIBIT 1017
Novartis v. Regents, IPR2023-01346
Page 1238 of 4460

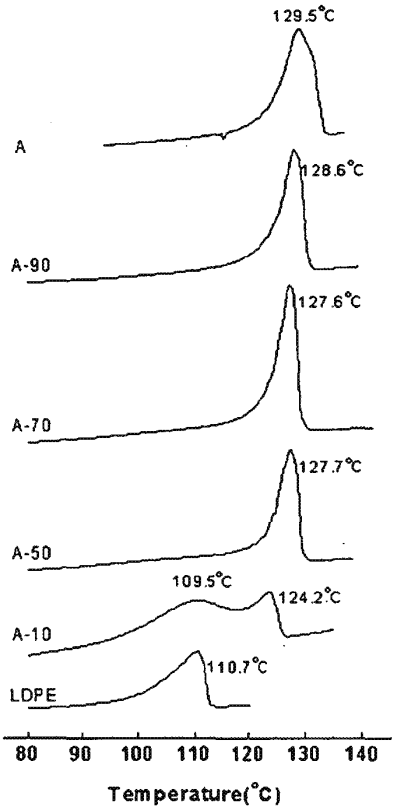


Fig. 5. Melting curves of rapidly quenched A/LDPE blends.

these blend melts. The obtained values of n are also plotted versus the proportion of LDPE in the blends (Fig. 4). All the blends show a negative deviation except for the blend C-50. This unusual change will be discussed together with the result of co-crystallization.

3.3. The occurrence of co-crystallization

The blends were heated to 170°C and then rapidly quenched with liquid nitrogen. This thermal treatment was applied for two purposes. Firstly, in such a procedure the crystallization is mainly controlled by kinetic factors and co-crystallization phenomena can be readily observed. Secondly, the morphology of the blend melt is solidified and the co-crystallization behavior can be correlated with the phase behavior of the melt [19]. Figs. 5–7 show the melting curves of the rapidly quenched blends, and the data of melting temperature and fusion heat are listed in Table 2.

In the rapidly quenched blends of LDPE with samples A and B, it is found that the melting temperatures of both components are lower than that of pure LDPE and those of ethylene–butene copolymers, respectively. This indicates that the most linear part of LDPE is incorporated into the lamellae of ethylene–butene copolymers, thus reducing the stability of the lamellae of ethylene–butene copolymers and leaving more branched parts in the LDPE [9]. On the other hand, crystallization kinetics experiments have revealed that the crystallization of the ethylene–butene copolymers becomes faster after blending with LDPE [32]. This was attributed to the transfer of the highly branched fractions of ethylene–butene copolymers into LDPE. The above results show that samples A and B are not completely immiscible with LDPE, though the presence of liquid–liquid phase separation is evidenced by rheological experiment. There are some exchanges between LDPE and these two ethylene copolymers, i.e. some less branched fractions of LDPE were incorporated into ethylene copolymers and a part of the highly branched ethylene copolymers is transferred into LDPE.

In contrast, a broad melting peak is observed at the low temperature region in the blend C-70, and in the blend C-50 this peak is further separated into two melting peaks at 106.3 and 115.5°C. Moreover, it is found that the high melting peak temperatures of the blends C-90, C-70 and C-50 are higher than that of the pure sample C, while the low peak temperatures are lower than that of pure LDPE. It is strange that the melting peak temperature becomes higher after blending, and this phenomenon is rarely reported. From the third intermediate melting peak between the melting peaks of LDPE and sample C, we can judge that a part of the co-crystals segregate from the crystals of both sample C and LDPE and exist as a separated population in the blend C-50.

Since the samples in Figs. 5–7 are directly quenched from the melt state, the co-crystallization behavior of these blends can be correlated with the miscibility of their melts. Only two melting peaks are observed in the blends of LDPE with samples A and B, indicating two phases in the melts of these blends. On the contrary, three endotherms appear in some of the blends of LDPE with sample C (for instance, C-50), which correspond to LDPE crystals, segregated co-crystals and ethylene–butene copolymer crystals. This shows that there exist three phases in the melt of the blend of LDPE with sample C at certain proportions. As reported above, it is observed that in the blend containing 50 wt% sample C, the value of n in the rheological experiment suddenly changes from the usual negative deviation to positive deviation at this proportion (Fig. 5(b)). This unusual change may also imply the presence of ternary phases in this blend. Therefore, the metallocene-based and conventional ethylene–butene copolymers exhibit different miscibility with LDPE. This difference may originate from their different composition distributions and can be illustrated as in Scheme 1. Scheme 1 shows the exchange between LDPE and ethylene–butene (E–B) copolymers. Both LDPE and E–B copolymer are viewed as compositionally heterogeneous and the stacks in this scheme are designated for differently branched fractions. LDPE and the metallocene-based

UM00012493
NOVARTIS EXHIBIT 1017
Novartis v. Regents, IPR2023-01346
Page 1239 of 4460

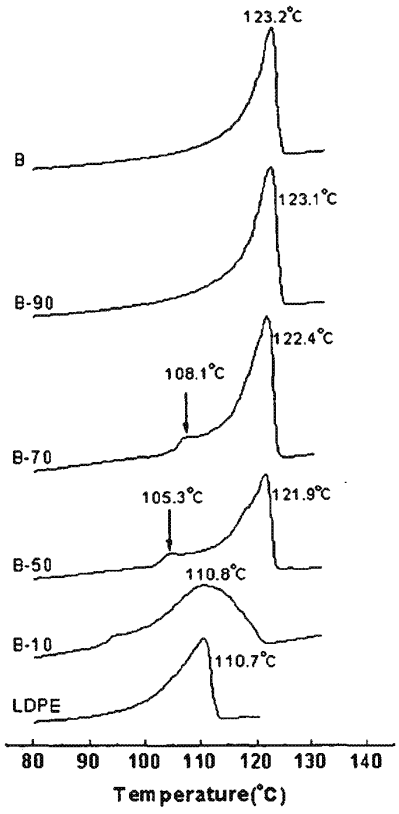


Fig. 6. Melting curves of rapidly quenched B/LDPE blends.

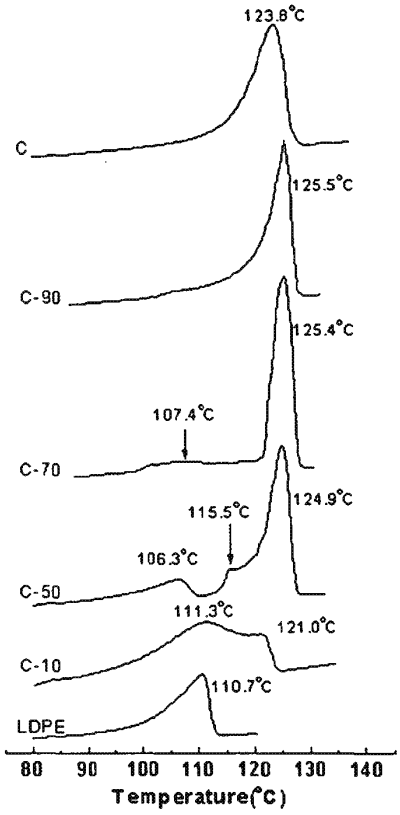


Fig. 7. Melting curves of rapidly quenched C/LDPE blends.

samples A and B can be considered to consist of two parts for simplicity: L1 (highly branched part) and L2 (less branched part) for LDPE, and H1 (highly branched part) and H2 (less branched part) for samples A and B. There are two phases, in the blend melts of LDPE with samples A and B, which are composed of L1 and H1, L2 and H2, respectively, due to the exchange between the two components (Scheme 1(a)). Nevertheless, in the blends of sample C with LDPE both components must be viewed to be composed of three parts for simplicity, and the blend melts (at least for the blend C-50) are ternary blend systems [15,33,34] instead of a binary blend system (Scheme 1(b)). The highly branched fractions (L1), intermediately branched fractions (L2) and the less branched fractions (L3) of LDPE are miscible with the corresponding fractions H1, H2 and H3 of sample C, respectively. After the blends are quenched, they exhibit different co-crystallization phenomena because of the difference in miscibility. Based on these analyses, it is very clear that the composition distribution of the components has a great influence on the form of occurrence of co-crystallization, though only three ethylene copolymers are used to blend with LDPE in the present work and definite conclusions cannot be drawn.

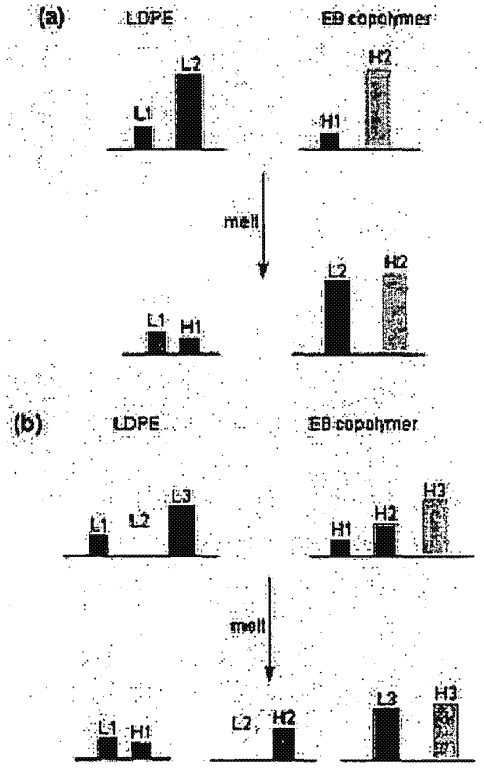
The TREF result has revealed that sample C contains much more highly branched fractions than the metallocene-based samples A and B. These highly branched fractions can severely interfere with the crystallization of the less branched fractions [35]. After blending with LDPE, these highly branched fractions are transferred into the separated co-crystals and the crystals of LDPE. The loss of these fractions leads to the disappearance of the interference effect, and thus the melting temperatures of the sample C increase accordingly. On the contrary, the metallocene-based copolymers A and B contain few highly branched fractions and the interference to the crystallization of the less branched fractions is not remarkable. The transfer of the highly branched fractions of samples A and B into LDPE hardly change the melting temperature of the high temperature peaks. In fact, the melting temperatures of the high temperature peaks for the quenched blends of samples A and B are always lower than that of corresponding pure ethylene copolymers due to the concentration dilution effect [36].

UM00012494
NOVARTIS EXHIBIT 1017
Novartis v. Regents, IPR2023-01346
Page 1240 of 4460

Table 2
DSC data of the quenched samples (the superscripts H and L denote high temperature peak and low temperature peak, respectively)

Samples	T_m^L/T_m^H (°C)	$\Delta T_m^{La}/\Delta T_m^{Hb}$ (°C)	$\Delta H_f^L/\Delta H_f^H$ (J/g)		$\Delta(\Delta H_f^H)^c$ (J/g)
			Experimental	Calculated[d]	
LDPE	110.7/–	0/–	81.8/0	–	–
A	–/129.5	–/0	–/152.7	–	–
A-90	–/128.6	–/–0.9	0/145.3	8.2/137.4	7.9
A-70	–/127.6	–/–1.9	0/134.2	24.5/106.9	27.3
A-50	–/127.7	–/–1.8	0/112.0	40.9/76.4	35.6
A-10	109.5/124.2	–1.2/–5.3	75.1/–[e]	73.6/15.3	–
B	–/123.2	–/0	–/128.7	–	–
B-90	–/123.1	–/–0.1	0/128.1	8.2/115.8	12.3
B-70	108.1/122.4	–2.6/–0.8	2.2/106.2	24.5/90.1	15.9
B-50	105.3/121.9	–5.4/–1.3	3.1/98.2	40.9/64.4	33.8
B-10	110.8/–	+0.1/–[e]	62.1/–[e]	73.6/12.9	–
C	–/123.8	–/0	–/162.2	–	–
C-90	105.8/125.5	–4.9/+1.7	0.2/153.0	8.2/146.0	7.0
C-70	105.6/125.4	–5.1/+1.6	9.9/121.1	24.5/113.5	7.6
C-50[f]	106.3/124.9	–4.4/+1.2	22.4/110.7	40.9/81.1	29.7
C-10	111.0/121.0	+0.3/–2.8	85.1/–[e]	73.6/16.2	–

[a] Difference between the melting temperatures of low peak and pure LDPE.
[b] Difference between the melting temperatures of high peak and pure ethylene copolymer.
[c] Difference between the experimental and calculated ΔH_f^H.
[d] Calculated assuming completely segregated crystals.
[e] It was not determined because of not well-separated peaks, and the fusion enthalpy was included in low temperature peak.
[f] The fusion enthalpy of the intermediate peak at 115.5°C was included in the high temperature peak.



Scheme 1.

3.4. Semi-quantitative estimation of the exchange of the components

The exchange of the components in the blends can be semi-quantitatively estimated from the change of the fusion enthalpy. It is found that the experimental data of fusion enthalpy corresponding to the high temperature peaks (ΔH_f^H) are invariably larger than the theoretical values calculated assuming completely segregated crystals. The differences between the experimental and calculated data of the high temperature peaks ($\Delta(\Delta H_f^H)$) are approximate to the theoretical values of fusion enthalpy corresponding to the low temperature peaks. This indicates that most of the LDPE is incorporated into the crystals of ethylene copolymers.

On the other hand, the values of fusion enthalpy for the low temperature peaks increase in the order A < B < C at any proportion, which is the same as the composition distributions. The fusion enthalpy of the low temperature peaks is contributed by two parts: the highly branched part of LDPE (L1) and the highly branched part of ethylene copolymer (H1). Since most of the LDPE is transferred into the ethylene copolymers, the contribution of the highly branched part of LDPE is very small and the highly branched part of ethylene copolymer is mainly responsible for the lower temperature peaks. Therefore, one can see that the quantity of ethylene–butene copolymer transferred into LDPE rises as the composition distribution becomes broader. This result is easily understandable. The broader the composition distribution, the more the highly branched fractions in the

UM00012495
NOVARTIS EXHIBIT 1017
Novartis v. Regents, IPR2023-01346
Page 1241 of 4460

ethylene–butene copolymers, thus more ethylene–butene is incorporated into the crystals of LDPE.

Acknowledgements

This work was financially supported by National Natural Science Foundation of China (Grant No.: 59703002).

References

[1] Clampitt BH. J Polym Sci A 1965;3:671.
[2] Sato T, Takahashi M. J Appl Polym Sci 1969;13:2655.
[3] Norton D, Keller A. J Mater Sci 1984;19:447.
[4] Hu SR, Kyu T, Stein RS. J Polym Sci, Polym Phys Ed 1987;25:71.
[5] Kyu T, Hu SR, Stein RS. J Polym Sci, Polym Phys Ed 1987;25:89.
[6] Vadhar P, Kyu T. Polym Engng Sci 1987;27:202.
[7] Alamo RG, Glaser RH, Mandelkern L. J Polym Sci, Polym Phys Ed 1988;26:2169.
[8] Conde Brafla MT, Iragorri Sainz JI, Terselius B, Gedde UW. Polymer 1989;30:410.
[9] Puig CC. Polym Bull 1997;38:715.
[10] Tashiro K, Izuchi M, Kaneuchi F, Jin C, Kobayashi M, Stein RS. Macromolecules 1994;27:1240.
[11] Tashiro K, Imanishi K, Izumi Y, Kobayashi M, Satoh M, Stein RS. Macromolecules 1995;28:8477.
[12] Galante MJ, Mandelkern L, Alamo RG. Polymer 1998;39:5105.
[13] Hill MJ, Barham PJ, Keller A. Polymer 1992;33:2530.
[14] Hill MJ, Barham PJ, van Ruiten J. Polymer 1993;34:2975.
[15] Hill MJ. Polymer 1994;35:1991.
[16] Tashiro K, Stein RS, Hsu SL. Macromolecules 1992;25:1801.
[17] Alamo RG, Londono JD, Mandelkern L, Stehling FC, Wignall GD. Macromolecules 1994;27:411.
[18] Graessley WW, Krishnamoorti R, Balsara NP, Fetters LJ, Lohse DJ, Schulz DN, Sissano JA. Macromolecules 1994;27:2574.
[19] Morgan RL, Hill MJ, Barham PJ. Polymer 1999;40:337.
[20] Agamalian MM, Alamo RG, Londono JD, Mandelkern L, Stehling FC, Wignall GD. Polym Mater Sci Engng 1998;78:74.
[21] Hosoda S. Polym J 1988;20:383.
[22] Starck P. Polym Int 1996;40:111.
[23] Fu Q, Chiu FC, McCreight KW, Guo M, Tseng WW, Cheng SZD, Keating YK, Hsieh ET, DesLauriers P. J Macromol Sci, Phys 1997;B36:41.
[24] Tashiro K, Izuchi M, Kobayashi M, Stein RS. Macromolecules 1994;27:1228.
[25] Reckinger C, Larbi FC, Rault J. J Macromol Sci, Phys 1985;B23:511.
[26] Wignall GD, Londono JD, Lin JS, Alamo RG, Galante MJ, Mandelkern L. Macromolecules 1995;28:3156.
[27] Wild L. Adv Polym Sci 1990;98:1.
[28] Xu JT, Feng LX. Eur Polym J 2000;36:867.
[29] Xu JT, Xu XR, Feng LX. Eur Polym J 2000;36:685.
[30] Hieber CA, Chiang HH. Polym Engng Sci 1992;32:931.
[31] Utracki LA, Schlund B. Polym Engng Sci 1987;27:1512.
[32] Xu XR, Xu JT, Chen LS, Liu RW, Feng LX, Chen W. J Appl Polym Sci 2000 (in press).
[33] Hill MJ, Puig CC. J Appl Polym Sci 1997;65:1921.
[34] Hill MJ, Barham PJ. Polymer 1994;35:1802.
[35] Xu JT, Xu XR, Feng LX. J Mater Sci Lett 2000;19:1541.
[36] Puig CC, Hill MJ, Odell JA. Polymer 1993;34:3402.

UM00012496
NOVARTIS EXHIBIT 1017
Novartis v. Regents, IPR2023-01346
Page 1242 of 4460

ELSEVIER

Polyhedron 21 (2002) 715–719

POLYHEDRON

www.elsevier.com/locate/poly

Cocrystallization of a dinuclear platinum complex as a monomer and a one-dimensional polymer

Jeongsoo Yoo [a,b,*], Young-Kyu Han [b], Yoon Sup Lee [b], Youngkyu Do [b,*]

[a] *Division of Radiological Sciences, Washington University School of Medicine, Box 8225, Mallinckrodt Institute of Radiology, 510 South Kingshighway, St. Louis, MO 63110, USA*

[b] *Department of Chemistry, School of Molecular Science-BK21 and Center for Molecular Design and Synthesis, Korea Advanced Institute of Science and Technology, Daejeon 305-701, Republic of Korea*

Received 30 June 2001; accepted 3 December 2001

Abstract

The reaction of $Pt(DMB)Cl_2$ (DMB = 3,3′-dihydroxymethyl-2,2′-bipyridine) with AgF_3CSO_3 in H_2O yielded a dimeric platinum complex, $[\{Pt(DMB)(\mu\text{-}OH)\}_2](F_3CSO_3)_4 \cdot 2H_2O$. X-ray structure reveals that two conformational isomers are self-assembled by different hydrogen bonding motifs in one crystal, resulting in a new type of co-crystal of monomer and its polymer. One conformer is self-assembled into the one-dimensional polymeric chain by strong hydrogen bonds, while the other conformer of which possible hydrogen bond donors/acceptors are blocked by two triflate anions exists as an isolated molecule itself. DFT calculations show that the strong hydrogen bonds and crystal packing force might compensate for the energy gap of ~ 14 kcal mol^{-1} between two conformers and the conformational energetics are dominated by the energies of the coordinated ligands rather than those of hydroxo-bridged platinum cores. © 2002 Published by Elsevier Science Ltd.

Keywords: Cocrystallization; Dinuclear platinum complexes; One-dimensional polymers

1. Introduction

Molecular self-assembly employing hydrogen bonding and its significance in crystal engineering are of considerable interest [1]. Hydrogen bonding is known to play an important role in governing the crystal packing of molecules due to its moderately strong interaction and high degree of directionality [2]. Recently, the incorporation of transition metal into supramolecular chemistry triggered the development of new molecular architecture, and several elegant examples for the combination of coordination and hydrogen bonding in self-assembly are published [3].

Some coordination or organometallic complexes which possess conformational flexibility or possible hydrogen bond donor/acceptor, could crystallize in two or more different crystal systems containing each conformational isomer or differently self-assembled molecule, respectively, by tuning crystallization conditions precisely, i.e. co-crystallization with other molecules [4] or different solvent pairs [5]. To the best of our knowledge, we are not aware, however, of any previous examples in which two differently self-assembled conformational isomers co-crystallize in one asymmetric unit.

Herein, we report a new example of the self-assembly of a platinum dinuclear complex $[\{Pt(DMB)(\mu\text{-}OH)\}_2](F_3CSO_3)_4 \cdot 2H_2O$ into a co-crystal containing a dinuclear monomer and a hydrogen-bonded one-dimensional chain of the dinuclear monomer.

2. Experimental

2.1. General procedures

K_2PtCl_4 was purchased from Strem. All other reagents were purchased from Aldrich and used without further purification. Solvents were of reagent grade and

* Corresponding authors. Tel.: +1-314-362-8636; fax: +1-314-362-9940 (J.Y.); tel.: +82-42-869-2829; fax: +82-42-869-2810 (Y.D.).

E-mail addresses: yooj@mir.wustl.edu (J. Yoo), ykdo@kaist.ac.kr (Y. Do).

0277-5387/02/$ - see front matter © 2002 Published by Elsevier Science Ltd.
PII: S0277-5387(02)00838-0

UM00012497
NOVARTIS EXHIBIT 1017
Novartis v. Regents, IPR2023-01346
Page 1243 of 4460

were dried by standard methods. $Pt(DMB)Cl_2$ (DMB = 3,3′-dihydroxymethyl-2,2′-bipyridine) was prepared according to the published procedure [6].

^1H and $^{13}C\{^1H\}$ NMR spectra were measured on a Bruker AM 300 spectrometer and were referenced to internal solvent peaks. IR spectra were recorded in KBr discs on a Bruker Equinox 55 FT–IR spectrometer. C, H and N elemental analyses were carried out at the Seoul Branch Analytical Laboratory, Korea Basic Science Institute, on an Elementar Analysensysteme GmbH Vario EL elemental analyzer.

2.2. Synthesis of $[\{Pt(DMB)(\mu\text{-}OH)\}_2]_2$-$(F_3CSO_3)_4\cdot 2H_2O$ (1)

To a water solution (30 ml) of $Pt(DMB)Cl_2$ (190 mg, 0.40 mmol) was added a twofold amount of solid AgF_3CSO_3 (210 mg, 0.80 mmol). The reaction mixture was warmed to 55 °C and was allowed to stir for 20 h in the absence of light. The precipitated AgCl was filtered off by a membrane filter. The slow evaporation of the solvent from the yellow filtrate at room temperature gave yellow crystalline product **1**, which was collected over glass frit, washed with a small amount of cold water and dried in air (120 mg, 52%). *Anal.* Found: C, 26.85; H, 2.42; N, 4.77. Calc. for $C_{52}H_{56}F_{12}N_8O_{26}Pt_4S_4$: C, 26.63; H, 2.41; N, 4.78%. ^1H NMR (300 MHz, DMF-d_7, 273 K): δ 8.73 (dd, $J = 5.5$, 1.2 Hz, 4H), 8.67 (dd, $J = 8.0$, 1.2 Hz, 4H), 8.13 (dd, $J = 8.0$, 5.5 Hz, 4H), 6.00 (t, $J = 5.8$ Hz, 4H), 5.92 (s, 2H), 4.74 (d, $J = 5.8$ Hz, 8H). $^{13}C\{^1H\}$ NMR (75 MHz, DMF-d_7, 297 K): δ 155.0, 148.1, 143.5, 143.3, 127.2, 61.5. IR (KBr, cm^{-1}): 3425 (br m, OH stretch), 1029 (s, OH bend), 575 (m, PtO stretch).

2.3. X-ray structure determination

Yellow crystals of **1** suitable for X-ray diffraction study were grown by slow evaporation of solvent from an aqueous solution. A crystal was mounted on a glass fiber tip. Crystal data were collected on an Enraf–Nonius CAD4 diffractometer equipped with graphite monochromated Mo Kα radiation. Cell dimensions and orientation matrix for data collection were obtained from least-squares refinement, using the setting angles of 25 centered reflections. Intensity data were collected in the $\omega-\theta$ scan mode to a maximum 2θ of 50°. Data were corrected for Lorentz and polarization effects, and an empirical absorption correction was applied.

The structure was solved by using the SHELXS-86 system [7] and refined by full-matrix least-squares on F^2 (SHELXL-93) [8]. The non-hydrogen atoms were refined anisotropically and all hydrogen atom positions, except those of μ-OH hydrogen, were initially calculated and then refined using a riding model. Geometrical restraint was applied for four triflates using SADI in SHELXL-93. The detailed crystallographic data are listed in Table 1.

Table 1
Crystallographic data for **1**

Empirical formula	$C_{52}H_{56}N_8O_{26}F_{12}S_4Pt_4$
Formula weight	2345.7
Crystal system	triclinic
Space group	$P\bar{1}$ (No. 2)
Unit cell dimensions	
a (Å)	15.692(3)
b (Å)	15.758(3)
c (Å)	17.953(6)
α (°)	64.17(3)
β (°)	65.58(2)
γ (°)	62.83(2)
V (Å^3)	3424.8(16)
Z	2
D_{calc} (g cm^{-3})	2.275
Absorption coefficient (mm^{-1})	8.385
Radiation (Å)	0.71073
Temperature (K)	293
R_1 [$I \geq 2\sigma(I)$] [a]	0.0432
wR_2 [$I \geq 2\sigma(I)$] [b]	0.1166

[a] $R_1 = \Sigma||F_o|-|F_c||/\Sigma|F_o|$.
[b] $wR_2 = [\Sigma[w(F_o^2-F_c^2)^2]/\Sigma[w(F_o^2)^2]]^{1/2}$.

2.4. Computational method

The B3LYP calculations [9] were carried out with GAUSSIAN98 program [10]. Single point energy evaluations were performed using the experimental geometries. A pseudopotential was used to replace 60 core electrons while a (8s7p6d)/[6s5p3d] basis set was used to describe the valence orbitals of Pt [11]. The 6-31G** basis set was used for the other elements. The 6-31++G* and 6-311++G** basis sets were also applied for the calculation of four residues, but there was no noticeable discrepancy between energy values.

3. Results and discussion

3.1. Crystal structure of 1

ORTEP representation of **1** is shown in Fig. 1 and selected bond distances and angles are summarized in Table 2. X-ray structure determination of **1** has revealed that the asymmetric unit contains two independent conformational isomers, **1a** and **1b**, of a dinuclear $[Pt(DMB)(\mu\text{-}OH)]_2^{2+}$ unit. The crystal and molecular structures with the numbering schemes of the conformers **1a** and **1b** are shown in Figs. 2 and 3, respectively.

The conformer **1a** is a dinuclear monomer and has the expected hydroxymethyl conformation in which two hydroxymethyl substituents are oriented as far as possible to minimize steric interaction between themselves as seen in the structure of $Pt(DMB)Cl_2$ [6]. The

UM00012498
NOVARTIS EXHIBIT 1017
Novartis v. Regents, IPR2023-01346
Page 1244 of 4460

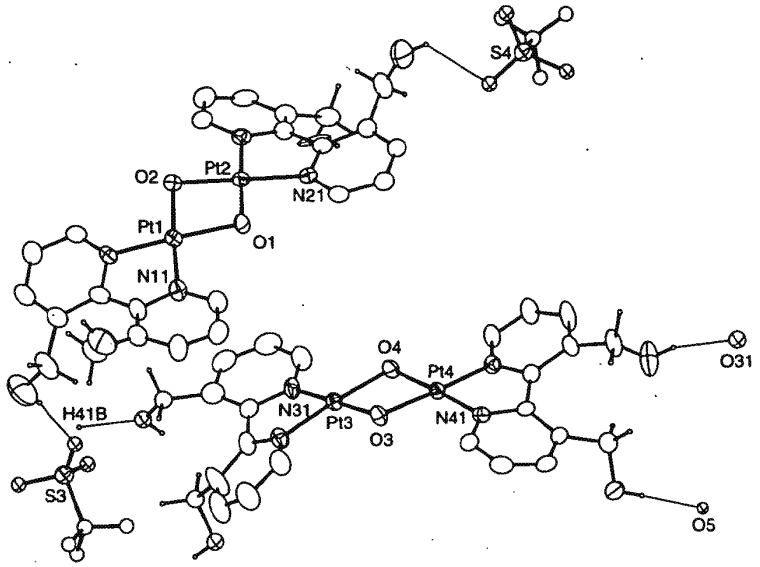


Fig. 1. ORTEP drawing of 1 showing the atom numbering scheme. Two triflates and one solvated water, which show no intermolecular interaction with two $[\{Pt(DMB)(\mu\text{-}OH)\}_2]_2$ complexes, are omitted for clarity.

Table 2
Selected bond distances (Å) and angles (°) for 1

Bond lengths			
Pt(1)–Pt(2)	3.1283(14)	Pt(1)–N(11)	1.997(8)
Pt(1)–N(11′)	1.977(9)	Pt(1)–O(1)	2.038(6)
Pt(1)–O(2)	2.063(7)	Pt(2)–N(21)	1.970(8)
Pt(2)–N(21′)	1.991(8)	Pt(2)–O(1)	2.048(6)
Pt(2)–O(2)	2.042(7)	O(11)···O(312^{i})	2.759(7)
O(21)···O(411^{ii})	2.840(6)	Pt(3)–Pt(4)	3.1275(12)
Pt(3)–N(31)	1.974(9)	Pt(3)–N(31′)	2.013(9)
Pt(3)–O(3)	2.050(7)	Pt(3)–O(4)	2.023(6)
Pt(4)–N(41)	1.979(8)	Pt(4)–N(41′)	1.970(8)
Pt(4)–O(3)	2.032(6)	Pt(4)–O(4)	2.033(6)
O(41)···O(5^{iv})	2.649(5)	O(41′)···O(31^{ii})	2.689(3)
Bond angles			
N(11′)–Pt(1)–N(11)	80.5(4)	O(1)–Pt(1)–O(2)	79.0(2)
N(21)–Pt(2)–N(21′)	80.8(3)	O(2)–Pt(2)–O(1)	79.2(3)
Pt(1)–O(1)–Pt(2)	99.9(3)	Pt(2)–O(2)–Pt(1)	99.3(3)
O(11)–H(11A)···O(312^{i})	167.1(5)	O(21)–H(21A) ···O(411^{ii})	107.7(2)
N(31)–Pt(3)–N(31′)	81.7(4)	O(4)–Pt(3)–O(3)	79.0(3)
N(41′)–Pt(4)–N(41)	80.2(3)	O(3)–Pt(4)–O(4)	79.1(3)
Pt(4)–O(3)–Pt(3)	100.0(3)	Pt(3)–O(4)–Pt(4)	100.9(3)
O(41)–H(41A) ···O(5^{iv})	158.5(8)	O(41′)–H(41B) ···O(31^{ii})	160.8(2)

two OH groups in *trans* position (relative to the plane which contains two Pt atoms and is perpendicular to the Pt_2O_2 plane) is hydrogen bonded to the oxygen atom of two triflates, which prevents the approach of other molecules for further hydrogen bonding. The O···O distances in hydrogen-bonded OH···O are 2.76 and 2.84 Å and the O–H···O angles are 167° and 108°. The

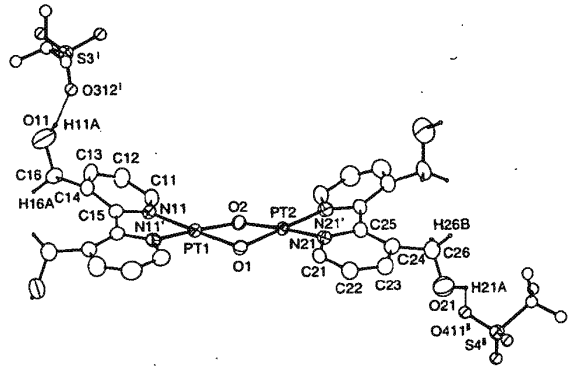


Fig. 2. Crystal and molecular structure of the conformer **1a**. Hydrogen atoms of hydroxymethyl group are only seen for clarity. Symmetry operation: (i) $x, y, -1+z$; (ii) $1-x, 1-y, 1-z$.

extreme disparity of the hydrogen bond angle from 180° may be attributed to the effect of crystal packing force [12].

In contrast to **1a**, the conformer **1b** exists as a hydrogen-bonded one-dimensional chain of the dinuclear unit and has a completely different pattern of crystal packing. The orientations of the oxygen atoms of hydroxymethyl groups are directed toward the same direction, resulting in the unfavorable interactions of C(36′)···O(31) [3.07 Å] and C(46)···O(41′) [3.08 Å]. Furthermore, the conformer **1b** self-assembles to form a one-dimensional linear polymer through the formation of intermolecular hydrogen bonding between the two hydroxymethyl OH groups of neighboring monomers. Two OH groups in **1b** involved in the connection of

UM00012499
NOVARTIS EXHIBIT 1017
Novartis v. Regents, IPR2023-01346
Page 1245 of 4460

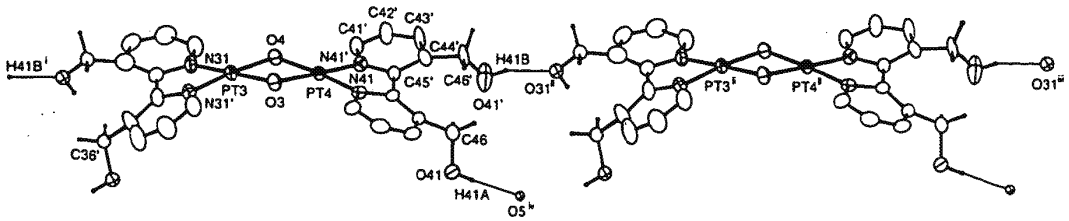


Fig. 3. Crystal and molecular structure of conformer **1b**. Hydrogen bonds are represented by thin lines. Symmetry operation: (i) $x, y, 1+z$; (ii) $x, y, -1+z$; (iii) $x, y, -2+z$; (iv) $1-x, 1-y, -z$.

building blocks are situated in *cis* position. The intermolecular O(41′)···O(31) distance of 2.69 Å and O(41′)–H(41B)···O(31) angle of 161° shows that the hydrogen bond between donor OH and acceptor O is reasonably strong [13]. One OH hydrogen atom (H41A) of the two remaining hydroxymethyl groups in **1b** is also strongly hydrogen-bonded to a crystal water [O(41)···O(5) 2.65 Å].

Perspective view of **1** clearly shows the different orientations of hydroxymethyl groups of ligands (Fig. 1). Two hydroxymethyl oxygen atoms in DMB residues of **1a** are directed to the opposite side, up and down, but those of **1b** are all oriented to the lower direction. The structures around the platinum cores of the two conformers are of close similarity. The coordination geometries of the two platinum centers are approximately square planar. Two least-squares planes of N_2PtO_2 in **1a** and **1b** are not coplanar but tilted by 15.5° and 12.2°, respectively.

3.2. Calculations

The B3LYP calculations, summarized in Table 3, indicate that the conformer **1a** is more stable than **1b**, as expected, by 13.8 kcal mol^{-1}. The stability of two conformers was further analyzed by carrying out calculations on four coordinated DMB residues using the same method. The residue *n* refers to DMB coordinated to Pt*n* ($n = 1$–4). Surprisingly, the residue 4 is more stable than the residues 1, 2 and 3 by +1.6, +2.0, and +15.6 kcal mol^{-1}, respectively. These somewhat unexpected results could be rationalized by close examination of dihedral angle between the average pyridyl planes of DMB units and torsional angles in each residue (Table 4). The dihedral angle of two least-squares pyridine planes in residue 4 is 24.1° that is smaller than 28.1° for residue 3, indicating that the residue 4 is expected to be more stable because the better π-conjugation between the two pyridyl rings can be achieved as the dihedral angle decreases [14]. The dihedral angle of 24.9° in the residue 1 is comparable with that of the residue 4 and there is no close interaction between two hydroxymethyl groups. However, torsional angles of C13–C14–C16–O11 (35.7°) and C13′–C14′–C16′–O11′ (43.7°) for the residue 1 are far from 60° of the ideal *gauche* conformation, which makes the residue 1 unstable due to torsional strain. No steric repulsion between two substituents and the favorable torsional angles of C23–C24–C26–O21 (46.8°) and C23′–C24′–C26′–O21′ (50.0°) in the residue 2 compensate less overlap of π-conjugation between the two pyridyl rings (dihedral angle: 28.2°). The energy difference of 13.6 kcal mol^{-1} [*E*(residue 3 and 4)–*E*(residue 1 and 2)] is comparable to 13.8 kcal mol^{-1} derived from intact **1a** and **1b**. This implies that the conformational energetics of **1a** and **1b** are dominated by the energies of the coordinated ligands, residue 1–4 rather than those of two hydroxo-bridged platinum cores, $N_2PtO_2PtN_2$.

Table 3
Summary of B3LYP calculations with 6-31G** basis set on the relative stability of the conformational isomers, **1a** and **1b** and DMB residues

Entries	Energy (a.u.)	Relative difference [a] (kcal mol^{-1})
1a	−1838.81907657	0.0
1b	−1838.79703584	13.8
Residue 1	−724.1657956	1.6
Residue 2	−724.1651554	2.0
Residue 3	−724.1435419	15.6
Residue 4	−724.1683875	0.0

[a] Unit conversion: a.u. × 627.51 = kcal mol^{-1}. Relative differences are referenced to **1a** and the residue 4 for the comparison of the conformers and the residues, respectively.

Table 4
Dihedral angles (°) of the two least-squares pyridine planes and selected torsional angles (°) for **1**

Residue 1	24.91 (0.53)	Residue 2	28.19 (0.53)
Residue 3	28.14 (0.36)	Residue 4	24.08 (0.52)
C13–C14–C16–O11	−35.7	C13′–C14′–C16′–O11′	−43.7
C23–C24–C26–O21	46.8	C23′–C24′–C26′–O21′	50.0
C33–C34–C36–O31	69.6	C33′–C34′–C36′–O31′	−56.6
C43–C44–C46–O41	49.7	C43′–C44′–C46′–O41′	−68.3

UM00012500
NOVARTIS EXHIBIT 1017
Novartis v. Regents, IPR2023-01346
Page 1246 of 4460

4. Conclusions

Two different hydrogen bonding patterns involving *cis*- and *trans*-positioned OH groups stabilize each conformational isomer, yielding a new co-crystal of the dinuclear monomer terminated by two triflates (**1a**) and the self-assembled infinite one-dimensional polymer (**1b**). This work provides a new type of co-crystal containing two differently self-assembled conformational isomers in one crystal system. This is also a good example of the important role of hydrogen bonding in self-assembly and of the usefulness of flexible molecule in studying the nature of forces controlling the molecular structure in the crystal. The strong hydrogen bonds and crystal force seem to compensate for ~ 14 kcal mol^{-1} of energy gap between two conformers.

5. Supplementary material

Crystallographic data for the structural analysis have been deposited with the Cambridge Crystallographic Data Centre, CCDC No. 166378 for compound **1**. Copies of this information may be obtained free of charge from The Director, CCDC, 12 Union Road, Cambridge, CB2 1EZ, UK (fax: +44-1223-336033; e-mail: deposit@ccdc.cam.ac.uk or www: http://www.ccdc.cam.ac.uk).

Acknowledgements

We gratefully acknowledge the financial support provided by Non-Directed Research Fund, Korea Research Foundation, 1998. We also thank the KISTI Supercomputing center for the use of CRAY C90.

References

[1] (a) J.L. Atwood, J.E.D. Davies, D.D. MacNicol, F. Vögtle, Comprehensive Supramolecular Chemistry, Pergamon, Oxford, 1996;
(b) D. Braga, F. Grepioni, G.R. Desiraju, Chem. Rev. 98 (1998) 1375.

[2] (a) R. Taylor, O. Kennard, Acc. Chem. Res. 17 (1984) 320;
(b) D. Braga, F. Grepioni, P. Sabatino, Organometallics 13 (1994) 3532.

[3] (a) J.A.R. Navarro, B. Lippert, Coord. Chem. Rev. 185 (1999) 653;
(b) M.-C. Tse, K.-K. Cheung, M.C.-W. Chan, C.-M. Che, Chem. Commun. (1998) 2295;
(c) V.Y. KuKushkin, T. Nishioka, D. Tudela, K. Isobe, I. Kinoshita, Inorg. Chem. 36 (1997) 6157;
(d) D. Walther, T. Klettke, A. Schmidt, Organometallics 15 (1996) 2314;
(e) P.J. Davies, N. Veldman, D.M. Grove, A.L. Spek, B.T.G. Lutz, G. van Koten, Angew. Chem., Int. Ed. Engl. 35 (1996) 1959;
(f) S.L. James, G. Verspui, A.L. Spek, G. van Koten, Chem. Commun. (1996) 1309;
(g) M.M. Chowdhry, D.M.P. Mingos, A.J.P. White, D.J. Williams, Chem. Commun. (1996) 899;
(h) A.D. Burrows, D.M.P. Mingos, A.J.P. White, D.J. Williams, J. Chem. Soc., Dalton Trans. (1996) 149;
(i) S.B. Copp, K.T. Holman, J.O.S. Sangster, S. Subramanian, M.J. Zaworotko, J. Chem. Soc., Dalton Trans. (1995) 2233.

[4] (a) F. Cervantes-Lee, H.K. Sharma, K.H. Pannell, A. Derecskei-Kovacs, D.S. Marynick, Organometallics 17 (1998) 3701;
(b) D. Braga, F. Grepioni, C.M. Martin, E. Parisini, Organometallics 13 (1994) 2170.

[5] (a) D. Braga, F. Grepioni, Acc. Chem. Res. 27 (1994) 51;
(b) Z. Qin, H.A. Jenkins, S.J. Coles, K.W. Muir, R.J. Puddephatt, Can. J. Chem. 77 (1999) 155;
(c) T. Ishida, R. Manabe, Y. In, H. Takashima, K. Kitamura, A. Wakahara, Bull. Chem. Soc. Jpn. 72 (1999) 947;
(d) S.B. Sembiring, S.B. Colbran, R. Bishop, D.C. Craig, A.D. Rae, Inorg. Chim. Acta 228 (1995) 109.

[6] J. Yoo, J.-H. Kim, Y.S. Shon, Y. Do, Inorg. Chim. Acta 263 (1997) 53.

[7] G.M. Sheldrick, SHELXS 86. Program for Crystal Structure Determination, University of Göttingen, Göttingen, Germany, 1986.

[8] G.M. Sheldrick, SHELXL 93. Program for Crystal Structure Refinement, University of Göttingen, Göttingen, Germany, 1993.

[9] (a) A.D. Becke, J. Chem. Phys. 98 (1993) 5648;
(b) C. Lee, W. Yang, R.G. Parr, Phys. Rev. B 37 (1988) 785.

[10] M.J. Frisch, G.W. Trucks, H.B. Schlegel, G.E. Scuseria, M.A. Robb, J.R. Cheeseman, V.G. Zakrzewski, J.A. Montgomery, R.E. Stratmann, J.C. Burant, S. Dapprich, J.M. Millam, A.D. Daniels, K.N. Kudin, M.C. Strain, O. Farkas, J. Tomasi, V. Barone, M. Cossi, R. Cammi, B. Mennucci, C. Pomelli, C. Adamo, S. Clifford, J. Ochterski, G.A. Petersson, P.Y. Ayala, Q. Cui, K. Morokuma, D.K. Malick, A.D. Rabuck, K. Raghavachari, J.B. Foresman, J. Cioslowski, J.V. Ortiz, B.B. Stefanov, G. Liu, A. Liashenko, P. Piskorz, I. Komaromi, R. Gomperts, R.L. Martin, D.J. Fox, T. Keith, M.A. Al-Laham, C.Y. Peng, A. Nanayakkara, C. Gonzalez, M. Challacombe, P.M.W. Gill, B.G. Johnson, W. Chen, M.W. Wong, J.L. Andres, M. Head-Gordon, E.S. Replogle, J.A. Pople, Gaussian 98 (Revision A.7), Gaussian, Inc., Pittsburgh, PA, 1998.

[11] P. Schwerdtfeger, M. Dolg, W.H.E. Schwarz, G.A. Bowmaker, P.D.W. Boyd, J. Chem. Phys. 91 (1989) 1762.

[12] P. Dauber, A.T. Hagler, Acc. Chem. Res. 13 (1980) 105.

[13] (a) P. Gilli, V. Bertolasi, V. Ferretti, G. Gilli, J. Am. Chem. Soc. 116 (1994) 909;
(b) G.M. Kapteijn, P.J. Baesjou, P.L. Alsters, D.M. Grove, W.J.J. Smeets, H. Kooijman, A.L. Spek, G. van Koten, Chem. Ber. 130 (1997) 35.

[14] V.M. Miskowski, V.H. Houlding, C.-M. Che, Y. Wang, Inorg. Chem. 32 (1993) 2518.

UM00012501
NOVARTIS EXHIBIT 1017
Novartis v. Regents, IPR2023-01346
Page 1247 of 4460

Lists of structure factors, anisotropic displacement parameters, H-atom coordinates and complete geometry have been deposited with the IUCr (Reference: CR1112). Copies may be obtained through The Managing Editor, International Union of Crystallography, 5 Abbey Square, Chester CH1 2HU, England.

References

Bailey, C. L., Bereman, R. D., Rillema, D. P. & Nowak, R. (1984). *Inorg. Chem.* **23**, 3956–3960.

Cotton, F. A. & Czuchajowska, J. (1990). *Polyhedron*, **9**, 2553–2566.

Cutler, A. R., Alleyne, C. S. & Dolphin, D. (1985). *Inorg. Chem.* **24**, 2281–2286.

Enraf–Nonius (1977). *CAD-4 Operations Manual*. Enraf–Nonius, Delft, The Netherlands.

Fair, C. K. (1990). *MolEN. An Interactive Intelligent System for Crystal Structure Analysis*. Enraf–Nonius, Delft, The Netherlands.

Goedken, V. L., Pluth, J. J., Peng, S. M. & Bursten, B. (1976). *J. Am. Chem. Soc.* **98**, 8014–8020.

Johnson, C. K. (1976). *ORTEPII*. Report ORNL-5138. Oak Ridge National Laboratory, Tennessee, USA.

Main, P., Fiske, S. J., Hull, S. E., Lessinger, L., Germain, G., Declercq, J.-P. & Woolfson, M. M. (1980). *MULTAN80. A System of Computer Programs for the Automatic Solution of Crystal Structures from X-ray Diffraction Data*. Univs. of York, England, and Louvain, Belgium.

North, A. C. T., Phillips, D. C. & Mathews, F. S. (1968). *Acta Cryst.* A**24**, 351–359.

Uhrhammer, R., Black, D. G., Gardner, T. G., Olsen, J. D. & Jordan, R. F. (1993). *J. Am. Chem. Soc.* **115**, 8493–8494.

Zachariasen, W. H. (1963). *Acta Cryst.* **16**, 1139–1144.

Acta Cryst. (1995). C**51**, 1857–1859

A 2:1 Molecular Complex of Theophylline and 5-Fluorouracil as the Monohydrate

SHYUICHI ZAITU, YOSHIHISA MIWA AND TOORU TAGA

Faculty of Pharmaceutical Sciences, Kyoto University, Sakyo-ku, Kyoto 606-01, Japan

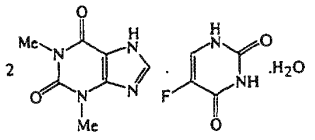
(*Received* 13 *January* 1995; *accepted* 6 *March* 1995)

Abstract

Theophylline, 5-fluorouracil and water molecules are packed in parallel sheets in the crystal structure of the title compound, 3,7-dihydro-1,3-dimethyl-1*H*-purine-2,6-dione–5-fluoro-2,4(1*H*,3*H*)-pyrimidinedione–water (2/1/1), $2C_7H_8N_4O_2.C_4H_3FN_2O_2.H_2O$. The planar molecules are held together within the sheets by hydrogen bonds which include C—H···O interactions. Short linear N—CH_3···F and N—CH_3···O contacts are also found between molecules within the sheets.

Comment

Theophylline has the ability to form molecular complexes with various aromatic compounds, and several crystal structures of these complexes have been studied (*e.g.* Shefter, 1969; Shefter & Sackman, 1971; Nakao, Fujii, Sakaki & Tomita, 1977; Aoki, Ichikawa, Koinuma & Iitaka, 1978). The complexing properties of 5-fluorouracil and its derivatives have also been studied extensively through the determination of the structures of purine–pyrimidine hydrogen-bonded complexes (*e.g.* Kim & Rich, 1967; Tomita, Katz & Rich, 1967; Mazza, Sobell & Kartha, 1969). We report here the crystal structure of the title 2:1 complex of theophylline and 5-fluorouracil as the monohydrate, (I), obtained from aqueous solution.



(I)

The bond distances and angles in the two crystallographically independent theophylline molecules in the asymmetric unit are in good agreement, and are similar to those reported previously for theophylline (Sutor, 1958; Koo, Shin & Oh, 1978). The bond distances and angles in the 5-fluorouracil molecule are also similar to those in 5-fluorouracil itself (Fallon, 1973). The 5-fluorouracil molecule is bonded to the one theophylline molecule by two N—H···O hydrogen bonds [N(20)···O(33) 2.772 (4), N(29)···O(26) 2.785 (4) Å], and the two independent theophylline molecules are linked together by an N—H···N hydrogen bond [N(7)···N(22) 2.903 (5) Å] (Fig. 1). The three molecules are approximately coplanar: the largest deviation from the least-squares plane through the 35 non-H atoms is 0.37 Å for F(35). The water O atom also lies on this plane with a deviation of 0.66 Å. The crystal structure consists of these molecules packed in parallel sheets perpendicular to the *ac* plane (Fig. 2).

The water molecule is hydrogen bonded to two 5-fluorouracil molecules within the same sheet [N(27)···O(36) 2.702 (5), O(36)···O(34)(x, $-1+y$, z) 2.829 (4) Å] and is also hydrogen bonded to a theophylline molecule in an adjacent sheet [O(36)···N(9)($-x$, $-1-y$, $-z$) 2.980 (5) Å]. Short C_{sp^2}—H···O_{sp^2} contacts are also found for C(8)—H···O(24)(x, $-1+y$, z) [C···O 3.226 (5), H···O 2.25 (3) Å, C—H···O 159 (3)°] and C(21)—H···O(24)(x, $-1+y$, z) [C···O 3.298 (5), H···O 2.35 (4) Å, C—H···O 171 (3)°]. These C—H···O hydrogen bonds stabilize the sheet structure.

There are also close intermolecular contacts within the sheets between the methyl groups of the theophylline molecules and F and O atoms. The short N—CH_3···F contacts are C(10)···F(35)($1+x$, $\frac{1}{2}-y$, $-\frac{1}{2}+z$) 3.107 (6) Å [N—C···F 170.0 (3)°] and C(12)···F(35)($1+x$, $-\frac{1}{2}-y$, $-\frac{1}{2}+z$) 3.246 (7) Å [N—C···F

©1995 International Union of Crystallography
Printed in Great Britain – all rights reserved

UM00012502
NOVARTIS EXHIBIT 1017
Novartis v. Regents, IPR2023-01346
Page 1248 of 4460

BEST AVAILABLE COPY

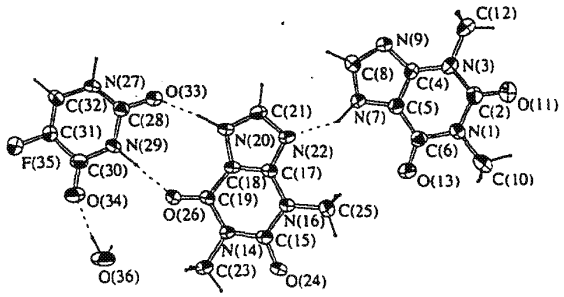


Fig. 1. Perspective view of the molecules with the atom-numbering scheme. Displacement ellipsoids are drawn at the 50% probability level.

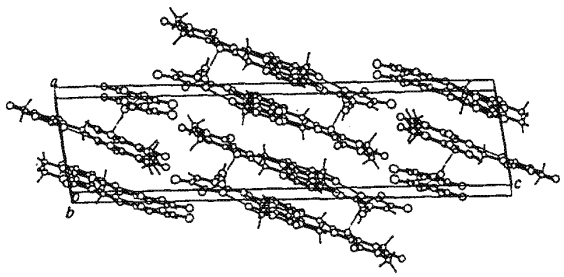


Fig. 2. Perspective view of the unit cell.

141.6 (4)°], which are similar to the linear N—$CH_3\cdots$F contacts observed in 1,3-dimethyl-5-fluorouracil (Taga, Yamamoto & Machida, 1989) and the 1:1 adduct of hexafluorobenzene and *N,N*-dimethylaniline (Dahl, 1977). Short N—$CH_3\cdots$O contacts are also found between theophylline molecules in the same plane: C(23)$\cdots$O(33)(x, 1 + y, z) 3.263 (5) Å [N—C$\cdots$O 165.0 (3)°] and C(25)$\cdots$O(13) 3.178 Å [N—C$\cdots$O 150.6 (3)°]. Similar N—$CH_3\cdots$O hydrogen-bond like contacts have been observed in 1,3-dimethyluracil (Banerjee, Dattagupta, Saenger & Rabczenko, 1977). These N—$CH_3\cdots X$ interactions may also stabilize the sheet structure.

Experimental

Crystals of the title complex were grown from a solution prepared by dissolving equimolar theophylline and 5-fluorouracil in water. The crystal density D_m was measured by flotation.

Crystal data

$2C_7H_8N_4O_2.C_4H_3FN_2O_2.H_2O$	Cu $K\alpha$ radiation
M_r = 508.43	λ = 1.54178 Å
Monoclinic	Cell parameters from 25 reflections
$P2_1/c$	θ = 17.54–25.85°
a = 7.640 (1) Å	μ = 0.901 mm^{-1}
b = 8.804 (1) Å	T = 295 K
c = 32.126 (2) Å	Prism
β = 98.28 (1)°	0.40 × 0.30 × 0.30 mm
V = 2138.4 Å^3	Colorless
Z = 4	
D_x = 1.579 Mg m^{-3}	
D_m = 1.58 Mg m^{-3}	

Data collection

Rigaku AFC-5*RU* diffractometer	R_{int} = 0.015
$\theta/2\theta$ scans	θ_{max} = 60°
Absorption correction: none	h = 0 → 8
3533 measured reflections	k = 0 → 10
3269 independent reflections	l = −36 → 36
2697 observed reflections [$F > 3\sigma(F)$]	3 standard reflections monitored every 150 reflections
	intensity decay: <3%

Refinement

Refinement on F	$(\Delta/\sigma)_{max}$ = 0.27
R = 0.059	$\Delta\rho_{max}$ = 0.44 e Å^{-3}
wR = 0.072	$\Delta\rho_{min}$ = −0.53 e Å^{-3}
S = 1.19	Extinction correction: none
2697 reflections	Atomic scattering factors from *International Tables for X-ray Crystallography* (1974, Vol. IV, Table 2.2B)
389 parameters	
Only coordinates of H atoms refined	
$w = 1/[\sigma^2(F) + 0.023F^2]$	

Table 1. *Fractional atomic coordinates and equivalent isotropic displacement parameters* (Å^2)

$B_{eq} = (4/3)\Sigma_i\Sigma_j\beta_{ij}\mathbf{a}_i.\mathbf{a}_j$.

	x	y	z	B_{eq}
N(1)	0.5909 (4)	0.0416 (4)	−0.1740 (1)	3.2 (2)
C(2)	0.6050 (5)	−0.1007 (5)	−0.1928 (1)	3.4 (2)
N(3)	0.5526 (5)	−0.2248 (4)	−0.1717 (1)	3.4 (2)
C(4)	0.4839 (5)	−0.2043 (4)	−0.1348 (1)	3.0 (2)
C(5)	0.4701 (5)	−0.0638 (4)	−0.1177 (1)	2.7 (2)
C(6)	0.5255 (5)	0.0713 (5)	−0.1359 (1)	3.1 (2)
N(7)	0.3973 (4)	−0.0891 (4)	−0.0816 (1)	3.0 (2)
C(8)	0.3709 (6)	−0.2392 (5)	−0.0797 (1)	3.5 (2)
N(9)	0.4223 (5)	−0.3152 (4)	−0.1113 (1)	3.6 (2)
C(10)	0.6478 (7)	0.1739 (6)	−0.1963 (2)	4.4 (2)
O(11)	0.6618 (4)	−0.1134 (4)	−0.22623 (9)	4.7 (2)
C(12)	0.5770 (8)	−0.3769 (6)	−0.1878 (2)	4.9 (2)
O(13)	0.5215 (4)	0.1999 (3)	−0.12208 (9)	4.2 (2)
N(14)	0.1710 (4)	0.4364 (3)	0.05166 (9)	2.7 (2)
C(15)	0.2310 (5)	0.4580 (4)	0.0131 (1)	2.9 (2)
N(16)	0.2691 (4)	0.3308 (3)	−0.00869 (9)	2.8 (2)
C(17)	0.2393 (5)	0.1898 (4)	0.0073 (1)	2.6 (2)
C(18)	0.1707 (5)	0.1730 (4)	0.0437 (1)	2.6 (2)
C(19)	0.1343 (5)	0.2966 (4)	0.0692 (1)	2.9 (2)
N(20)	0.1598 (4)	0.0188 (4)	0.0495 (1)	3.0 (2)
C(21)	0.2215 (6)	−0.0462 (5)	0.0172 (1)	3.2 (2)
N(22)	0.2736 (4)	0.0539 (3)	−0.0098 (1)	2.9 (2)
C(23)	0.1447 (7)	0.5748 (5)	0.0755 (1)	3.7 (2)
O(24)	0.2503 (4)	0.5861 (3)	−0.00026 (8)	3.7 (2)
C(25)	0.3357 (7)	0.3442 (6)	−0.0490 (1)	3.8 (2)
O(26)	0.0805 (4)	0.2906 (3)	0.10337 (8)	4.0 (2)
N(27)	−0.1092 (5)	−0.1668 (4)	0.1725 (1)	3.1 (2)
C(28)	−0.0496 (5)	−0.0706 (4)	0.1450 (1)	2.9 (2)
N(29)	−0.0350 (4)	0.0785 (4)	0.1577 (1)	3.0 (2)
C(30)	−0.0740 (5)	0.1373 (5)	0.1953 (1)	3.2 (2)
C(31)	−0.1310 (6)	0.0227 (5)	0.2221 (1)	3.3 (2)
C(32)	−0.1492 (6)	−0.1223 (5)	0.2109 (1)	3.2 (2)
O(33)	−0.0091 (4)	−0.1130 (3)	0.11126 (8)	3.8 (2)

UM00012503
NOVARTIS EXHIBIT 1017
Novartis v. Regents, IPR2023-01346
Page 1249 of 4460

BEST AVAILABLE COPY

O(34)	−0.0612 (4)	0.2726 (3)	0.20315 (9)	4.3 (2)
F(35)	−0.1661 (4)	0.0704 (3)	0.25983 (8)	5.7 (2)
O(36)	−0.1613 (5)	−0.4648 (4)	0.1548 (1)	5.3 (2)

Table 2. *Selected geometric parameters* (Å, °)

N(1)—C(2)	1.402 (5)	N(16)—C(17)	1.375 (4)
N(1)—C(6)	1.412 (5)	N(16)—C(25)	1.463 (5)
N(1)—C(10)	1.466 (7)	C(17)—C(18)	1.357 (5)
C(2)—N(3)	1.375 (5)	C(17)—N(22)	1.358 (5)
C(2)—O(11)	1.220 (5)	C(18)—C(19)	1.414 (5)
N(3)—C(4)	1.376 (5)	C(18)—N(20)	1.374 (5)
N(3)—C(12)	1.457 (7)	C(19)—O(26)	1.227 (4)
C(4)—C(5)	1.364 (5)	N(20)—C(21)	1.329 (5)
C(4)—N(9)	1.359 (5)	C(21)—N(22)	1.337 (5)
C(5)—C(6)	1.417 (6)	N(27)—C(28)	1.349 (5)
C(5)—N(7)	1.375 (5)	N(27)—C(32)	1.370 (5)
C(6)—O(13)	1.218 (5)	C(28)—N(29)	1.374 (5)
N(7)—C(8)	1.339 (6)	C(28)—O(33)	1.227 (4)
C(8)—N(9)	1.322 (5)	N(29)—C(30)	1.385 (5)
N(14)—C(15)	1.394 (5)	C(30)—C(31)	1.434 (6)
N(14)—C(19)	1.399 (4)	C(30)—O(34)	1.219 (5)
N(14)—C(23)	1.468 (5)	C(31)—C(32)	1.328 (6)
C(15)—N(16)	1.374 (5)	C(31)—F(35)	1.346 (5)
C(15)—O(24)	1.223 (4)		
C(2)—N(1)—C(6)	126.7 (3)	C(15)—N(16)—C(17)	119.1 (3)
C(2)—N(1)—C(10)	116.9 (4)	C(15)—N(16)—C(25)	120.8 (3)
C(6)—N(1)—C(10)	116.3 (4)	C(17)—N(16)—C(25)	120.1 (3)
N(1)—C(2)—N(3)	116.9 (3)	N(16)—C(17)—C(18)	121.7 (3)
N(1)—C(2)—O(11)	121.4 (4)	N(16)—C(17)—N(22)	126.3 (3)
N(3)—C(2)—O(11)	121.8 (4)	C(18)—C(17)—N(22)	111.9 (3)
C(2)—N(3)—C(4)	119.7 (3)	C(17)—C(18)—C(19)	123.2 (3)
C(2)—N(3)—C(12)	119.6 (4)	C(17)—C(18)—N(20)	105.2 (3)
C(4)—N(3)—C(12)	120.7 (4)	C(19)—C(18)—N(20)	131.4 (3)
N(3)—C(4)—C(5)	121.8 (3)	N(14)—C(19)—C(18)	112.1 (3)
N(3)—C(4)—N(9)	126.2 (3)	N(14)—C(19)—O(26)	120.7 (3)
C(5)—C(4)—N(9)	112.0 (3)	C(18)—C(19)—O(26)	127.2 (3)
C(4)—C(5)—C(6)	123.4 (3)	C(18)—N(20)—C(21)	106.5 (3)
C(4)—C(5)—N(7)	104.9 (3)	N(20)—C(21)—N(22)	113.3 (4)
C(6)—C(5)—N(7)	131.7 (3)	C(17)—N(22)—C(21)	103.0 (3)
N(1)—C(6)—C(5)	111.5 (3)	C(28)—N(27)—C(32)	123.4 (3)
N(1)—C(6)—O(13)	121.3 (4)	N(27)—C(28)—N(29)	115.2 (3)
C(5)—C(6)—O(13)	127.2 (3)	N(27)—C(28)—O(33)	122.6 (3)
C(5)—N(7)—C(8)	106.3 (3)	N(29)—C(28)—O(33)	122.2 (3)
N(7)—C(8)—N(9)	113.6 (4)	C(28)—N(29)—C(30)	126.7 (3)
C(4)—N(9)—C(8)	103.2 (3)	N(29)—C(30)—C(31)	112.5 (4)
C(15)—N(14)—C(19)	126.1 (3)	N(29)—C(30)—O(34)	121.7 (4)
C(15)—N(14)—C(23)	115.9 (3)	C(31)—C(30)—O(34)	125.9 (3)
C(19)—N(14)—C(23)	118.0 (3)	C(30)—C(31)—C(32)	122.9 (3)
N(14)—C(15)—N(16)	117.5 (3)	C(30)—C(31)—F(35)	116.0 (4)
N(14)—C(15)—O(24)	120.6 (3)	C(32)—C(31)—F(35)	121.1 (4)
N(16)—C(15)—O(24)	121.8 (3)	N(27)—C(32)—C(31)	119.4 (4)

Table 3. *Hydrogen-bonding geometry* (Å, °)

D—H···*A*	H···*A*	*D*···*A*	*D*—H···*A*
N(7)—H(N7)···N(22)	2.05 (4)	2.903 (5)	162 (2)
N(20)—H(N20)···O(33)	1.87 (4)	2.772 (4)	170 (2)
N(27)—H(N27)···O(36)	1.83 (4)	2.702 (5)	174 (2)
N(29)—H(N29)···O(26)	1.90 (4)	2.785 (4)	172 (2)
O(36)—H(O36A)···O(34^{i})	1.99 (5)	2.829 (4)	168 (4)
O(36)—H(O36B)···N(9^{ii})	2.21 (5)	2.980 (5)	163 (6)

Symmetry codes: (i) $x, y-1, z$; (ii) $-x, -1-y, -z$.

All H atoms were located from a difference Fourier map. Data collection and cell refinement: *MSC/AFC Diffractometer Control Software* (Molecular Structure Corporation, 1988). Program(s) used to solve structure: *MULTAN*88 (Main *et al.*, 1988). Program(s) used to refine structure: *KPPXRAY* (Taga, Masuda, Higashi & Iizuka, 1991) including a modified version of *ORFLS* (Busing, Martin & Levy, 1962). Molecular graphics: *KPPXRAY*. Software used to prepare material for publication: *EDCIF-J* (Osaki & Taga, 1993).

©1995 International Union of Crystallography
Printed in Great Britain – all rights reserved

Lists of structure factors, anisotropic displacement parameters, H-atom coordinates, bond distances and angles involving non-H atoms, and torsion angles have been deposited with the IUCr (Reference: AS1172). Copies may be obtained through The Managing Editor, International Union of Crystallography, 5 Abbey Square, Chester CH1 2HU, England.

References

Aoki, K., Ichikawa, T., Koinuma, Y. & Iitaka, Y. (1978). *Acta Cryst.* B34, 2333–2336.
Banerjee, A., Dattagupta, J. K., Saenger, W. & Rabczenko, A. (1977). *Acta Cryst.* B33, 90–94.
Busing, W. R., Martin, K. O. & Levy, H. A. (1962). *ORFLS*. Report ORNL-TM-305. Oak Ridge National Laboratory, Tennessee, USA.
Dahl, T. (1977). *Acta Cryst.* B33, 3021–3024.
Fallon, L. III (1973). *Acta Cryst.* B29, 2549–2556.
Kim, S.-H. & Rich, A. (1967). *Science*, **158**, 1046–1048.
Koo, C. H., Shin, H. S. & Oh, S. S. (1978). *J. Korean Chem. Soc.* **22**, 86–94.
Main, P., Hull, S. E., Lessinger, L., Germain, G., Declercq, J.-P. & Woolfson, M. M. (1988). *MULTAN*88. *A System of Computer Programs for the Automatic Solution of Crystal Structures from X-ray Diffraction Data*. Univs. of York, England, and Louvain, Belgium.
Mazza, F., Sobell, H. M. & Kartha, G. (1969). *J. Mol. Biol.* **43**, 407–422.
Molecular Structure Corporation (1988). *MSC/AFC Diffractometer Control Software*. MSC, 3200 Research Forest Drive, The Woodlands, TX 77381, USA.
Nakao, S., Fujii, S., Sakaki, T. & Tomita, K. (1977). *Acta Cryst.* B33, 1373–1378.
Osaki, K. & Taga, T. (1993). *J. Crystallogr. Soc. Jpn*, **35**, 223–224.
Shefter, E. (1969). *J. Pharm. Sci.* **58**, 710–714.
Shefter, E. & Sackman, P. (1971). *J. Pharm. Sci.* **60**, 282–286.
Sutor, D. J. (1958). *Acta Cryst.* **11**, 83–87.
Taga, T., Masuda, K., Higashi, T. & Iizuka, H. (1991). *KPPXRAY. Kyoto Program Package for X-ray Crystal Structure Analysis*. Kyoto Univ., Kyoto, Japan.
Taga, T., Yamamoto, N. & Machida, K. (1989). *Bull. Chem. Soc. Jpn*, **62**, 354–357.
Tomita, K., Katz, L. & Rich, A. (1967). *J. Mol. Biol.* **30**, 545–549.

Acta Cryst. (1995). C51, 1859–1861

(2*R*,3*S*,4*S*)-3-Hydroxy-4-methyl-1-[(1*S*)-1-phenylethyl]pyrrolidine-2-methanol

ANGÈLE CHIARONI, CLAUDE RICHE AND LANGLOIS NICOLE

Institut de Chimie des Substances Naturelles, CNRS, 91198 Gif sur Yvette CEDEX, France

(*Received* 11 *October* 1994; *accepted* 26 *May* 1994)

Abstract

The crystal structure determination of the title compound, $C_{14}H_{21}NO_2$, established the absolute configuration of the *N*-phenylethyl chain. The pyrrolidine ring

UM00012504
NOVARTIS EXHIBIT 1017
Novartis v. Regents, IPR2023-01346
Page 1250 of 4460

Acta Crystallographica Section C
Crystal Structure Communications
ISSN 0108-2701

Linear hydrogen-bonded molecular tapes in the cocrystals of squaric acid with 4,4′-dipyridylacetylene and 1,2-bis(4-pyridyl)ethylene

Md. Badruz Zaman,[a]† Masaaki Tomura[a]* and Yoshiro Yamashita[b]

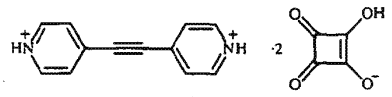
[a]Institute for Molecular Science, Myodaiji, Okazaki 444-8585, Japan, and [b]Department of Electronic Chemistry, Interdisciplinary Graduate School of Science and Engineering, Tokyo Institute of Technology, Nagatsuta, Midori-ku, Yokohama 226-8502, Japan
Correspondence e-mail: tomura@ims.ac.jp

Received 5 January 2001
Accepted 28 February 2001

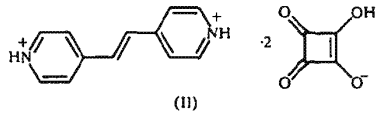
The title compounds, 4,4′-(ethyne-1,2-diyl)dipyridinium bis(squarate), $C_{12}H_{10}N_2^{2+}\cdot 2C_4HO_4^-$, and 4,4′-(ethene-1,2-diyl)dipyridinium bis(squarate), $C_{12}H_{12}N_2^{2+}\cdot 2C_4HO_4^-$, are isomorphous and crystallize in space group $P\bar{1}$. The cocrystals contain linear hydrogen-bonded molecular tape structures along the [120] direction. The squarate monoanions form a ten-membered dimer linked by two intermolecular O—H···O hydrogen bonds. Each component molecule forms a segregated stack along the *c* axis. The bond lengths of the squarate monoanion indicate delocalization of the enolate anion.

Comment

Squaric acid (3,4-dihydroxy-3-cyclobutene-1,2-dione) is a very strong dibasic acid and has been studied for potential application to xerographic photoreceptors, organic solar cells and optical recording (Seitz & Imming, 1992; Liebeskind *et al.*, 1993). From the viewpoint of crystal engineering, squaric acid is also a useful tool for constructing crystalline architectures, because of its rigid and flat four-membered ring framework, and its proton donating and accepting capabilities for hydrogen bonding (Braga *et al.*, 1999; Reetz *et al.*, 1994). We have recently shown that the simple combination of chloranilic acid and various dipyridyl-type ligands can create a variety of supramolecular architectures involving an infinite one-dimensional molecular tape structure (Zaman *et al.*, 1999, 2000). In the course of our crystal-engineering studies on the combination of squaric acid and dipyridyl-type ligands, we have obtained cocrystals of 4,4′-dipyridylacetylene–squaric acid (1/2), (I), and 1,2-bis(4-pyridyl)ethylene–squaric acid (1/2), (II), where a rare ten-membered hydrogen-bonded dimer of a squarate monoanion is formed. We report here the structures of the resulting hydrogen-bonded molecular tapes.



(I)



(II)

Cocrystals (I) and (II) are isomorphous and crystallize in space group $P\bar{1}$, with one molecule of squaric acid and half a molecule of the dipyridyl-type ligand in the asymmetric unit. The molecular structures of (I) and (II) are shown in Figs. 1 and 2, respectively, and selected geometric parameters are listed in Tables 1 and 2, respectively. The coordinates in (I) can be related to those in (II) by the transformation $(1-x, \frac{1}{2}-y, \frac{1}{2}-z)$ subject to a permutation of the O labels; O1–O4 in (I) correspond to O2–O4 and O1, respectively, in (II). The molar ratio of the dipyridinium dication and the monoanion of squaric acid is 1:2 in both (I) and (II). The bond lengths in the squarate monoanion display delocalization of the enolate anion. Thus, the average bond lengths in the four-membered squarate frameworks are 1.421 (5) (C1—C4, C3—C4) and 1.494 (5) Å (C1—C2, C2—C3) for (I), and 1.429 (2) (C1—C2, C1—C4) and 1.495 (2) Å (C2—C3, C3—C4) for (II). The bond lengths of O1—C1 [1.255 (4) Å] and O3—C3 [1.240 (4) Å] in (I), and O2—C2 [1.245 (2) Å] and O4—C4 [1.244 (2) Å] in (II), are intermediate between a double and single bond. Such bond-length distribution has been found in cobalt and nickel squarate octahydrates (Brach *et al.*, 1987)

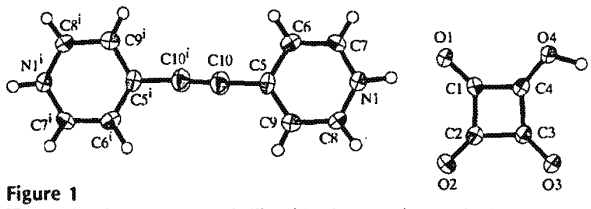


Figure 1
The molecular structure of (I) with the atomic numbering scheme. Displacement ellipsoids are drawn at the 50% probability level and H atoms are shown as small spheres of arbitrary radii [symmetry code: (i) $1-x, 2-y, 3-z$].

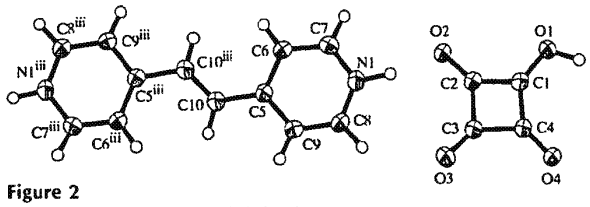


Figure 2
The molecular structure of (II) with the atomic numbering scheme. Displacement ellipsoids are drawn at the 50% probability level and H atoms are shown as small spheres of arbitrary radii [symmetry code: (iii) $1-x, -1-y, -2-z$].

† Present address: Department of Chemistry and Biochemistry, University of South Carolina, 631 Sumter Street, Columbia, SC 29208, USA.

 © 2001 International Union of Crystallography · Printed in Great Britain – all rights reserved

UM00012505
NOVARTIS EXHIBIT 1017
Novartis v. Regents, IPR2023-01346
Page 1251 of 4460

and in L-argininium hydrogen squarate (Angelova *et al.*, 1996). The dipyridinium dications of (I) and (II) lie in a plane, with maximum deviations of 0.003 (3) Å for (I) and 0.004 (1) Å for (II). The bond lengths in the dipyridinium moieties are similar to the literature values [Cambridge Structural Database (CSD), Version 5.20; Allen *et al.*, 1987].

Figs. 3 and 4 show the packing diagrams of (I) and (II), respectively, viewed along the *c* axis. The squarate monoanions and the dipyridinium dications form an infinite one-dimensional molecular tape structure along the [120] direction and are connected *via* an intermolecular N—H···O hydrogen bond [N1—H1···O1 2.636 (4) Å for (I) and N1—H1···O2 2.655 (2) Å for (II); see Tables 3 and 4]. The conformation of these molecular tapes is flat and almost linear. The squarate monoanions and the pyridine rings of the dipyridinium dications are almost coplanar [the dihedral angles between the two ring planes are 8.9 (2)° for (I) and 10.2 (1)° for (II)].

The most remarkable feature of the molecular tapes is the existence of a ten-membered hydrogen-bonded dimer of the squarate monoanions within the tapes. The two squarate monoanions are linked by two intermolecular O—H···O hydrogen bonds [O4—H4···O3^{ii} 2.511 (3) Å for (I) and O1—H1*A*···O4^{iv} 2.503 (2) Å for (II); symmetry codes: (ii) $2-x, -y, 1-z$; (iv) $-x, 1-y, -z$] and are coplanar. The dimensions of the squarate dimer fit those of the dipyridyl-type ligands, as shown in Figs. 3 and 4. The squarate monoanion dimer is rare, and we have found only eight examples in the CSD (Angelova *et al.*, 1996; Bernardinelli *et al.*, 1989; Bock *et al.*, 1998; Braga *et al.*, 1999; Braga & Grepioni, 1998; Kanters *et al.*, 1991; Karle *et al.*, 1996; MacLean *et al.*, 1999). In all other squarate structures, the squarate monoanions are linked by a single intermolecular O—H···O hydrogen bond and no ten-membered rings are formed.

Each component molecule forms a segregated stack along the *c* axis. The interstack distances of the squarate plane and the dipyridinium plane for (I) and (II) are 3.21 (1) and 3.40 (1) Å, respectively. The flat conformation of the molecular tapes is favourable for close packing of the tapes and of the segregated stack.

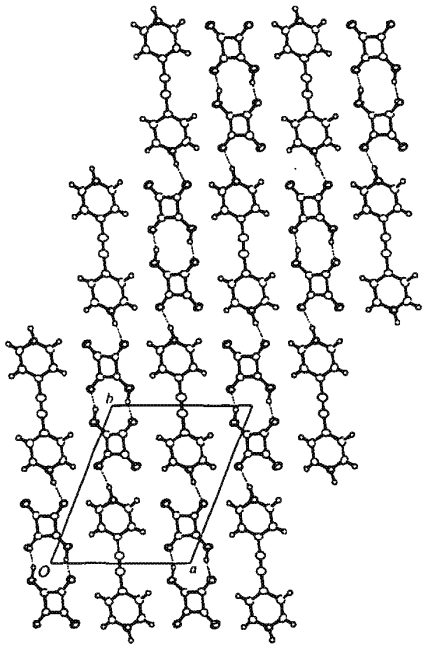


Figure 3
The packing diagram of (I) viewed along the *c* axis. Dotted lines show the intermolecular hydrogen bonds.

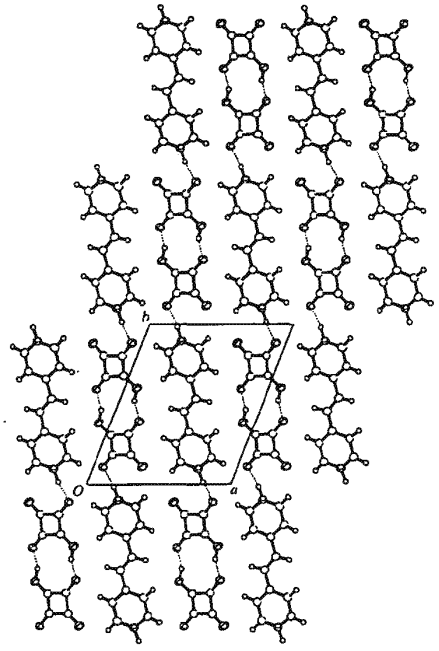


Figure 4
The packing diagram of (II) viewed along the *c* axis. Dotted lines show the intermolecular hydrogen bonds.

In conclusion, the supramolecular synthon (Desiraju, 1995) formed by a combination of squaric acid and dipyridyl-type ligands has been successfully used in the construction of linear hydrogen-bonded molecular tapes. The strong resemblance between the crystal structures of (I) and (II) suggests the robustness and reproducibility of this supramolecular synthon. Studies of the characterization of the physical properties of the cocrystals (I) and (II), and of the construction of new molecular architectures using squaric acid and other dipyridyl-type ligands, are now in progress.

Experimental

4,4′-Dipyridylacetylene was prepared according to the literature method of Tanner & Ludi (1980). Squaric acid and 1,2-bis(4-pyridyl)ethylene were commercially available and were purified by standard methods. Slow evaporation of a solution of squaric acid (0.05 mmol) and the dipyridyl-type ligand (0.05 mmol) in methanol–water (1:1, 20 ml) gave crystals of (I) or (II) suitable for X-ray analysis.

UM00012506
NOVARTIS EXHIBIT 1017
Novartis v. Regents, IPR2023-01346
Page 1252 of 4460

Compound (I)

Crystal data

$C_{12}H_{10}N_2^{2+}\cdot 2C_4HO_4^-$
M_r = 408.32
Triclinic, $P\overline{1}$
a = 10.221 (2) Å
b = 12.325 (3) Å
c = 3.7951 (9) Å
α = 97.24 (2)°
β = 98.49 (2)°
γ = 67.649 (18)°
V = 436.06 (18) Å^3
Z = 1
D_x = 1.555 Mg m^{-3}
Mo $K\alpha$ radiation
Cell parameters from 25 reflections
θ = 13.1–14.8°
μ = 0.12 mm^{-1}
T = 296 (2) K
Prismatic, gold
0.22 × 0.15 × 0.05 mm

Data collection

Rigaku AFC-7R diffractometer
$\omega/2\theta$ scans
2101 measured reflections
1992 independent reflections
788 reflections with $I > 2\sigma(I)$
R_{int} = 0.048
θ_{max} = 27.5°
$h = 0 \rightarrow 13$
$k = -14 \rightarrow 15$
$l = -4 \rightarrow 4$
3 standard reflections
every 150 reflections
intensity decay: 0.8%

Refinement

Refinement on F^2
$R[F^2 > 2\sigma(F^2)]$ = 0.045
$wR(F^2)$ = 0.141
S = 0.92
1992 reflections
160 parameters
All H-atom parameters refined
$w = 1/[\sigma^2(F_o^2) + (0.0564P)^2]$ where $P = (F_o^2 + 2F_c^2)/3$
$(\Delta/\sigma)_{max}$ = 0.001
$\Delta\rho_{max}$ = 0.24 e Å^{-3}
$\Delta\rho_{min}$ = −0.26 e Å^{-3}

Compound (II)

Crystal data

$C_{12}H_{12}N_2^{2+}\cdot 2C_4HO_4^-$
M_r = 410.33
Triclinic, $P\overline{1}$
a = 10.2606 (9) Å
b = 12.2942 (17) Å
c = 3.7749 (13) Å
α = 97.845 (17)°
β = 98.444 (13)°
γ = 67.259 (8)°
V = 432.75 (17) Å^3
Z = 1
D_x = 1.575 Mg m^{-3}
Cu $K\alpha$ radiation
Cell parameters from 22 reflections
θ = 13.9–42.6°
μ = 1.06 mm^{-1}
T = 296 (2) K
Prismatic, yellow
0.25 × 0.10 × 0.08 mm

Data collection

Enraf–Nonius CAD-4 diffractometer
$\omega/2\theta$ scans
Absorption correction: ψ scan (North *et al.*, 1968)
T_{min} = 0.778, T_{max} = 0.920
2052 measured reflections
1771 independent reflections
1468 reflections with $I > 2\sigma(I)$
R_{int} = 0.009
θ_{max} = 74.2°
$h = -12 \rightarrow 12$
$k = -15 \rightarrow 15$
$l = 0 \rightarrow 4$
3 standard reflections
frequency: 120 min
intensity decay: 2.9%

Refinement

Refinement on F^2
$R[F^2 > 2\sigma(F^2)]$ = 0.044
$wR(F^2)$ = 0.133
S = 1.02
1771 reflections
164 parameters
All H-atom parameters refined
$w = 1/[\sigma^2(F_o^2) + (0.0919P)^2 + 0.0683P]$ where $P = (F_o^2 + 2F_c^2)/3$
$(\Delta/\sigma)_{max} < 0.001$
$\Delta\rho_{max}$ = 0.24 e Å^{-3}
$\Delta\rho_{min}$ = −0.30 e Å^{-3}

Table 1
Selected geometric parameters (Å, °) for (I).

O1—C1	1.255 (4)	C2—C3	1.505 (5)
O2—C2	1.215 (4)	C3—C4	1.427 (5)
O3—C3	1.240 (4)	C5—C6	1.383 (4)
O4—C4	1.306 (4)	C5—C9	1.397 (4)
N1—C7	1.328 (4)	C5—C10	1.436 (5)
N1—C8	1.329 (4)	C6—C7	1.367 (5)
C1—C4	1.415 (4)	C8—C9	1.377 (5)
C1—C2	1.483 (5)	C10—C10^{i}	1.181 (6)
C7—N1—C8	122.3 (3)	O4—C4—C3	136.5 (3)
O1—C1—C4	136.6 (3)	C1—C4—C3	93.5 (3)
O1—C1—C2	133.3 (3)	C6—C5—C9	119.4 (3)
C4—C1—C2	90.0 (2)	C6—C5—C10	119.2 (3)
O2—C2—C1	135.0 (3)	C9—C5—C10	121.4 (3)
O2—C2—C3	137.3 (3)	C7—C6—C5	119.1 (3)
C1—C2—C3	87.7 (3)	N1—C7—C6	120.4 (3)
O3—C3—C4	138.2 (3)	N1—C8—C9	120.3 (3)
O3—C3—C2	133.1 (3)	C8—C9—C5	118.4 (3)
C4—C3—C2	88.7 (2)	C10^{i}—C10—C5	176.2 (6)
O4—C4—C1	130.0 (3)		

Symmetry code: (i) $1-x, 2-y, 3-z$.

Table 3
Selected geometric parameters (Å, °) for (II).

O1—C1	1.3138 (19)	C2—C3	1.491 (2)
O2—C2	1.2453 (19)	C3—C4	1.499 (2)
O3—C3	1.215 (2)	C5—C9	1.394 (2)
O4—C4	1.2440 (19)	C5—C6	1.400 (2)
N1—C7	1.340 (2)	C5—C10	1.470 (2)
N1—C8	1.342 (2)	C6—C7	1.369 (2)
C1—C2	1.425 (2)	C8—C9	1.378 (2)
C1—C4	1.432 (2)	C10—C10^{iii}	1.320 (3)
C7—N1—C8	121.94 (13)	O4—C4—C3	133.73 (14)
O1—C1—C2	130.32 (14)	C1—C4—C3	88.84 (12)
O1—C1—C4	136.15 (14)	C9—C5—C6	118.14 (14)
C2—C1—C4	93.53 (12)	C9—C5—C10	119.34 (14)
O2—C2—C1	136.23 (14)	C6—C5—C10	122.51 (14)
O2—C2—C3	134.37 (14)	C7—C6—C5	119.41 (15)
C1—C2—C3	89.40 (12)	N1—C7—C6	120.71 (14)
O3—C3—C2	135.13 (15)	N1—C8—C9	119.52 (14)
O3—C3—C4	136.64 (15)	C8—C9—C5	120.27 (14)
C2—C3—C4	88.22 (11)	C10^{iii}—C10—C5	125.34 (19)
O4—C4—C1	137.42 (14)		

Symmetry code: (iii) $1-x, -1-y, -2-z$.

Table 2
Hydrogen-bonding geometry (Å, °) for (I).

D—H···A	D—H	H···A	D···A	D—H···A
N1—H1···O1	0.98 (4)	1.68 (4)	2.636 (4)	165 (3)
O4—H4···O3^{ii}	1.04 (5)	1.52 (5)	2.511 (3)	157 (4)

Symmetry code: (ii) $2-x, -y, 1-z$.

Table 4
Hydrogen-bonding geometry (Å, °) for (II).

D—H···A	D—H	H···A	D···A	D—H···A
O1—H1A···O4^{iv}	0.99 (2)	1.56 (2)	2.5033 (17)	156 (2)
N1—H1···O2	1.02 (3)	1.64 (3)	2.6546 (17)	170 (2)

Symmetry code: (iv) $-x, 1-y, -z$.

UM00012507
NOVARTIS EXHIBIT 1017
Novartis v. Regents, IPR2023-01346
Page 1253 of 4460

All H atoms in both (I) and (II) were located in the Fourier map and were refined isotropically; the C—H ranges are 0.91 (3)–0.95 (4) and 0.96 (2)–0.99 (2) Å for (I) and (II), respectively.

For compound (I), data collection: *MSC/AFC Diffractometer Control Software* (Molecular Structure Corporation, 1988); cell refinement: *MSC/AFC Diffractometer Control Software*. For compound (II), data collection: *CAD-4 EXPRESS* (Enraf–Nonius, 1995); cell refinement: *CAD-4 EXPRESS*. For both compounds, data reduction: *TEXSAN* (Molecular Structure Corporation, 1995); program(s) used to solve structure: *SHELXS97* (Sheldrick, 1997); program(s) used to refine structure: *SHELXL97* (Sheldrick, 1997); molecular graphics: *ORTEP*II (Johnson, 1976); software used to prepare material for publication: *SHELXL97*.

MBZ thanks the Institute for Molecular Science for post-doctoral fellowships. This work was supported by a Grant-in-Aid for Scientific Research on Priority Areas from the Ministry of Education, Culture, Sports, Science and Technology, Japan.

Supplementary data for this paper are available from the IUCr electronic archives (Reference: GD1134). Services for accessing these data are described at the back of the journal.

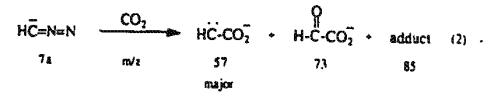
References

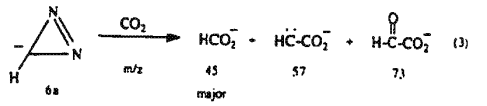
Allen, F. H., Kennard, O., Watson, D. G., Brammer, L., Orpen, A. G. & Taylor, R. (1987). *J. Chem. Soc. Perkin Trans.* 2, pp. S1–19.
Angelova, O., Velikova, V., Kolev, T. & Radomirska, V. (1996). *Acta Cryst.* C**52**, 3252–3256.
Bernardinelli, G., Deguenon, D., Soules, R. & Castan, P. (1989). *Can. J. Chem.* **67**, 1158–1165.
Bock, H., Schodel, H., Van, T. T. H., Dienelt, R. & Gluth, M. (1998). *J. Prakt. Chem.* **340**, 722–732.
Brach, I., Rozière, J., Anselment, B. & Peters, K. (1987). *Acta Cryst.* C**43**, 458–460.
Braga, D., Bazzi, C., Maini, L. & Grepioni, F. (1999). *CrystEngComm*, No. 5.
Braga, D. & Grepioni, F. (1998). *Chem. Commun.* pp. 911–912.
Desiraju, G. R. (1995). *Angew. Chem. Int. Ed. Engl.* **34**, 2311–2327.
Enraf–Nonius (1995). *CAD-4 EXPRESS*. Version 5.1. Enraf–Nonius, Delft, The Netherlands.
Johnson, C. K. (1976). *ORTEP*II. Report ORNL-5138. Oak Ridge National Laboratory, Tennessee, USA.
Kanters, J. A., Schouten, A., Kroon, J. & Grech, E. (1991). *Acta Cryst.* C**47**, 807–810.
Karle, I. L., Ranganathan, D. & Haridas, V. (1996). *J. Am. Chem. Soc.* **118**, 7128–7133.
Liebeskind, L. S., Yu, M. S., Yu, R. H., Wang, J. & Hager, K. S. (1993). *J. Am. Chem. Soc.* **115**, 9048–9055.
MacLean, E. J., Wheatley, P. S., Ferguson, G. & Glidewell, C. (1999). *Acta Cryst.* C**55**, 1892–1896.
Molecular Structure Corporation (1988). *MSC/AFC Diffractometer Control Software*. MSC, 3200 Research Forest Drive, The Woodlands, TX 77381, USA.
Molecular Structure Corporation (1995). *TEXSAN*. Version 1.7-2. MSC, 3200 Research Forest Drive, The Woodlands, TX 77381, USA.
North, A. C. T., Phillips, D. C. & Mathews, F. S. (1968). *Acta Cryst.* A**24**, 351–359.
Reetz, M. T., Höger, S. & Harms, K. (1994). *Angew. Chem. Int. Ed. Engl.* **33**, 181–183.
Seitz, G. & Imming, P. (1992). *Chem. Rev.* **92**, 1227–1260.
Sheldrick, G. M. (1997). *SHELXS97* and *SHELXL97*. University of Göttingen, Germany.
Tanner, M. & Ludi, A. (1980). *Chimica*, **34**, 23–24.
Zaman, M. B., Tomura, M. & Yamashita, Y. (1999). *Chem. Commun.* pp. 999–1000.
Zaman, M. B., Tomura, M. & Yamashita, Y. (2000). *Org. Lett.* **2**, 273–275.

UM00012508
NOVARTIS EXHIBIT 1017
Novartis v. Regents, IPR2023-01346
Page 1254 of 4460

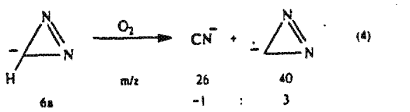
orbital calculations,[13] we conclude that the product is indeed the diazirinyl anion (**6a**).

Consistent with this assignment is the observation that **6a** exchanges one hydrogen for deuterium upon reaction with ND_3. Likewise one might expect the diazirinyl anion to react similarly to the diazomethyl anion, and this is the case with CO_2 (eqs 2 and 3).[10] Both ions lead to the formation of a carbene (m/z 57)

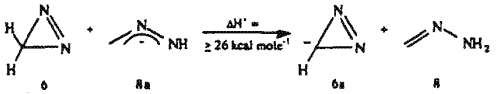




and a glyoxylate ion (m/z 73), but the latter also leads to the formation of a small amount of an adduct (15%)[10] while the former gives rise to a formal hydride ion transfer product (~80%). Given the greater basicity of the diazirinyl anion, one might also expect it to be more reactive than **7a**. Indeed, the diazomethyl anion is inert to O_2, whereas **6a** undergoes a rapid reaction affording two product ions (eq 4). The structure of the m/z 40 ion (P − 2, $CN_2^{\cdot-}$) is intriguing. Three possibilities, cyclic, C–N–N, and N–C–N, exist, and an independent preparation of the two acyclic ions via the reaction of $O^{\cdot-}$ with cyanamide and diazomethane has enabled us to conclude that the reaction product is cyclic. This assignment is based on the different reactivities of the P − 2 ions and indicates that the C–H bond in **6a** is quite weak (≤49 kcal mol^{-1}).[14]



Having established the structure of the diazirinyl anion, we are in a position to address the question of its stability. In this regard, it is of interest to compare **6a** to its acyclic analogue (**8a**, eq 5). The reaction enthalpy is the difference in acidity between **6** and **8**. The latter quantity has not been measured, but the proton affinity of 3-methyl-1-azaallyl anion, 375 ± 3 kcal mol^{-1},[15] can be taken as an upper limit. The acyclic ion is clearly the more stable isomer. This is consistent with the notion of antiaromaticity, but can also be accounted for by the charge repulsion in a constrained allylic system.[16]



Recently Zhou and Parr[17] described the use of relative and absolute hardness in determining the stability and reactivity of cyclic conjugated systems. Their model predicts that the diazirinyl anion should be nonaromatic.[18] This is consistent with more detailed ab initio molecular orbital calculations[13] and suggests that **6a** will be a viable species in solution. Investigations to test this hypothesis are currently underway and will be reported in due course.

Acknowledgment. Kraig Anderson carried out the initial experiments that led to this work, and Professors Steven Bachrach and Joel Liebman read this manuscript and made helpful suggestions. Financial support from the National Science Foundation (CHE-8907198); the donors of the Petroleum Research Fund, administered by the American Chemical Society; a research award from the American Society for Mass Spectrometry; and a McKnight Professorship administered by the University of Minnesota are gratefully acknowledged.

Design of Organic Structures in the Solid State: Hydrogen-Bonded Molecular "Tapes" [1]

Jonathan A. Zerkowski, Christopher T. Seto, Derk A. Wierda, and George M. Whitesides*

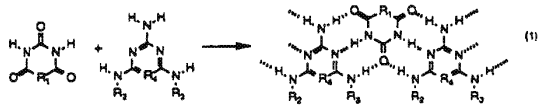
Department of Chemistry, Harvard University Cambridge, Massachusetts 02138

Received August 27, 1990

We have begun a program whose objective is to develop methods to predict the packing of organic molecules in crystalline and noncrystalline solids, starting from the atomic structures of these molecules.[2] The ability to relate molecular and crystalline structure for organic solids will clarify the interactions that underlie molecular recognition and self-assembly, simplify the preparation of optically or electronically active organic solids, and help to rationalize the macroscopic properties of organic materials in terms of microscopic, molecular structures.

One problem that has frustrated efforts to relate molecular and crystalline structures is the very large number of orientations the molecules can, in principle, adopt: calculating relative energies of all possible packing structures is currently impractical. To limit the scope of the problem, we wish to constrain the possible orientations of the molecules in the solid state. We are developing systems in which strong, directional hydrogen bonds provide the required constraint.

Using the network proposed for melamine/cyanuric acid as a model,[3,4] we are examining the structures of 1:1 cocrystals of derivatives of melamine (M) and barbituric acid (B), functionalized in patterns that break up the sheet structure but permit the formation of hydrogen bonds that yield "tapes" (eq 1). Tapes are likely to pack with their axes parallel. This enforced parallelism will, we believe, significantly simplify the computational analysis of these solid-state structures.



Here we summarize evidence that this strategy is successful in generating a family of closely related solid-state structures and that these structures can be classified according to a hierarchy of elementary structural features (Figure 1). The two components, M and B, form tapes with an alternating sequence, ···M·B·M·B···; the tapes pack into sheets with their long axes parallel; the sheets stack and form three-dimensional solids. Table I summarizes crystallographic data for the structures we have examined; complete data will follow in a full paper. We believe that this system has sufficient simplicity to be the object of a systematic study of the influence of molecular structure on crystal structure.

(14) We thank one of the referees for pointing this out to us. The bond dissociation energy of O_2-H (49 kcal mol^{-1}) is taken from ref 9.
(15) Dahlke, G. D.; Kass, S. R., unpublished results.
(16) Streitwieser et al. have shown that as the central bond angle of an allylic anion is reduced, the energy rapidly increases. Boerth, D. W.; Streitwieser, A., Jr. *J. Am. Chem. Soc.* **1978**, *100*, 750.
(17) Zhou, Z.; Parr, R. G. *J. Am. Chem. Soc.* **1989**, *111*, 7371.
(18) Absolute hardness (η) is given by $\eta = (\epsilon_{LUMO} - \epsilon_{HOMO})/2$, where the dividing line between aromatic ($\eta > -0.25\beta$) and antiaromatic ($\eta < -0.15\beta$) compounds is about -0.2β. For the diazirinyl anion, $\eta = -0.21\beta$ (HOMO α -0.46β; LUMO α -0.89β).

(1) Supported by the National Science Foundation, Grant CHE-88-12709 to G.M.W. and Grant DMR-89-20490 to the Harvard University Materials Research Laboratory.
(2) Desiraju, G. R. *Crystal Engineering: The Design of Organic Solids*; Elsevier: New York, 1989. Etter, M. C. *Acc. Chem. Res.* **1990**, *23*, 120. Hagler, A. T.; Dauber, P. *Acc. Chem. Res.* **1980**, *13*, 105.
(3) Seto, C.; Whitesides, G. M. *J. Am. Chem. Soc.* **1980**, *112*, 6409.
(4) We have not yet been able to obtain diffraction-quality single crystals from cocrystallizations of derivatives of melamine and cyanuric acid.

0002-7863/90/1512-9025$02.50/0 © 1990 American Chemical Society

UM00012509
NOVARTIS EXHIBIT 1017
Novartis v. Regents, IPR2023-01346
Page 1255 of 4460

Table I. Summary of Structures of Cocrystals of Derivatives of Barbituric Acid and Melamine (Eq 1, R_4 = N)

R_1	$R_2 = R_3$	T	S	θ, deg	data[a]	temp,[b] °C	space group	R factor, %	goodness of fit
CEt_2	C_6H_5	1	2	0	a	−80	$Pnma$	6.5	1.21
	p-ClC_6H_4	1	2	0	b	23	$P\bar{1}$	9.9	1.44
	p-BrC_6H_4	1	1	0	b	23	$P\bar{1}$	7.2	1.91
	p-IC_6H_4	1	1	0	b	23	$P2_1/n$	4.5	1.39
	p-MeC_6H_4	1	1	0	a	−10	$P2_1/n$	10.3[c]	1.50
	m-MeC_6H_4	1	1	0	b	23	$P\bar{1}$	5.5	1.54
	tert-butyl	2	2	0	d	20	$Pna2_1$	3.7	1.19
	m-ClC_6H_4	2	1	0	a	0	$C2/c$	4.9	0.80
$C(CH_2C_6H_4$-p-$Br)_3$	1-naphthyl	1	2	0	c	23	$P2_1/n$	6.8	2.09
	p-$MeOC_6H_4$	1	2	0	c	−120	$P2_1/n$	8.6	2.39
CBr_2	H	1	1	0	a	0	$Ccm2_1$	4.0	1.05
CH_2		1	1	90	a	−10	$Ccc2$	4.1	2.79

[a] Data code: a = data collected and structure solved by us; b = data collected by Molecular Structure Corporation (MSC) and solved by us; c = the complete structure determination was performed by MSC; d = the complete structure determination was performed by Crystalytics, Inc. [b] All temperatures correct to ±1 °C. [c] Further refinement is in progress.

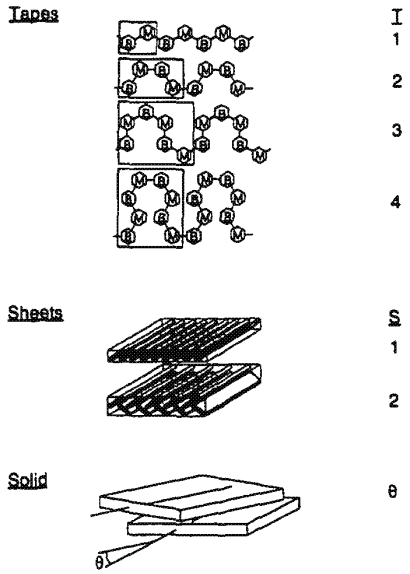


Figure 1. Classification of features characterizing solid-state structures of 1:1 cocrystals of derivatives of melamine (M) and barbituric acid (B). T = the number of B·M units that constitute a translational repeat unit along a tape (boxed); S = the number of tapes that constitute a translational repeat unit in a sheet. This figure shows representative examples of possible geometries, not an exhaustive list.

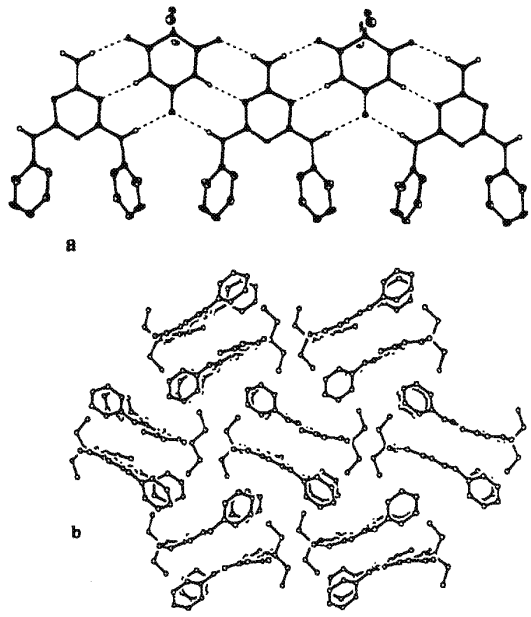


Figure 2. Plots of the packing patterns of *N,N'*-diphenylmelamine/5,5-diethylbarbituric acid complex. (a) Individual tape, ORTEP plot along the [001] direction showing 30% ellipsoids. Non-hydrogen-bonding hydrogen atoms have been omitted for clarity. (b) End-on packing view down the long tape axes, [010] direction. All hydrogen atoms have been omitted for clarity.

We offer two general observations concerning these structures. First, all follow some variant on the motif: tape; sheet; solid. Second, although 1:1 compound formation seems to be general, this system is not yet ideally convenient for studying the physical-organic chemistry of the solid state, because the crystals that grow are often too small for single-crystal X-ray structure determination. Figure 2 shows one representative structure.[5] Most (10 of 12) of the tapes follow the simple motif shown in this structure (T = 1), although we have observed two "crinkled" tapes (T = 2). We have not encountered structures in which T = 3 or 4.

Others have described hydrogen-bonded chains in the solid state.[6-9] In particular, Leiserowitz and co-workers[7] have examined patterns in amides in detail. While many of these structures consisted of hydrogen-bonded tapes, a variety of other structural motifs were also identified. Shimizu[8] and Lehn[9] have studied structures related to those reported here. We believe that the 1:1 compounds based on the barbituric acid/melamine structure offer predictable stoichiometry and simplicity in packing, while still affording (through variation in R_{1-4}) ample opportunity to vary details of tape–tape and sheet–sheet interactions.

Acknowledgment. We acknowledge the support of the National Science Foundation through Grant CHE 80-00670 for the purchase of the Siemens X-ray diffractometer.

Supplementary Material Available: Brief synthetic outline, details of X-ray data collection, tables of crystal data and atomic positional parameters and an ORTEP drawing for *N,N'*-diphenylmelamine/5,5-diethylbarbituric acid, and table of lattice parameters for all structures (9 pages). Ordering information is given on any current masthead page.

(5) Crystal data for *N,N'*-diphenylmelamine/5,5-diethylbarbituric acid: $(C_{15}H_{14}N_6)(C_8H_{12}N_2O_3)$; a = 12.940 (3) Å, b = 9.982 (5) Å, c = 17.377 (3) Å, V = 2245 (1) Å^3, D_{calcd} = 1.37 g/cm^3, Z = 4 (four M·B pairs).

(6) O'Brien, E. J. *J. Mol. Biol.* **1966**, *22*, 377. Voet, D. *J. Am. Chem. Soc.* **1972**, *94*, 8213.
(7) Leiserowitz, L.; Hagler, A. T. *Proc. R. Soc. London* **1983**, *A388*, 133.
(8) Shimizu, N.; Nishigaki, S.; Osaki, K. *Acta Crystallogr.* **1982**, *B38*, 2309.
(9) Lehn, J.-M.; Mascal, M.; DeCian, A.; Fischer, J. *J. Chem. Soc., Chem. Commun.* **1990**, 479.

UM00012510
NOVARTIS EXHIBIT 1017
Novartis v. Regents, IPR2023-01346
Page 1256 of 4460

J. Am. Chem. Soc. 1994, *116*, 2382–2391

Design of Organic Structures in the Solid State: Molecular Tapes Based on the Network of Hydrogen Bonds Present in the Cyanuric Acid·Melamine Complex

Jonathan A. Zerkowski, John C. MacDonald, Christopher T. Seto, Derk A. Wierda, and George M. Whitesides*

Contribution from the Department of Chemistry, Harvard University, Cambridge, Massachusetts 02138

Received August 11, 1992. Revised Manuscript Received January 10, 1994[⊕]

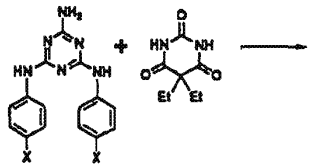
Abstract: This paper describes the single-crystal X-ray structures of 1:1 complexes between seven *N,N'*-bis(4-X-phenyl)melamines (X = H, F, Cl, Br, I, CH_3, and CF_3) and 5,5-diethylbarbituric acid. These complexes crystallize as infinite tapes having components joined by triads of hydrogen bonds; the tapes pack with their long axes parallel. The crystalline architecture of these complexes—parallel tapes—serves as a structurally constrained framework with which to study physical–organic relationships between the structures of the crystals and the molecules of which they are composed. The complex with X = Br exists in polymorphic forms. One of the polymorphs is isomorphous to the X = Cl complex; the other is related to the X = I complex.

Introduction

We are interested in three complementary problems in the organic solid state: rationalizing the structures of organic crystals based on the structures of their component molecules; predicting the structures of new molecular crystals; and designing molecules that crystallize in designed arrays. An understanding of intermolecular interactions that is sufficiently detailed to accomplish these objectives would be useful throughout materials science and would contribute to molecular recognition and molecular self-assembly.

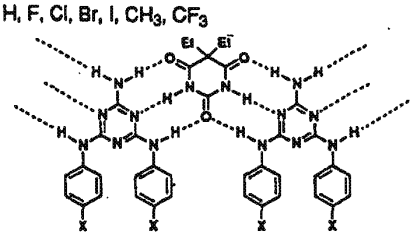
The problem of understanding and predicting the packing of organic molecules in crystals, considered in its full generality, is complicated: a very large number of possible arrangements of molecules in the crystal need to be considered, the differences in energy between crystal forms may be small, and there are no search routines to identify the most stable of these forms.[1] We simplify the problem by reducing the number of orientations open to each molecule by forcing them to form "tapes" (which might also be called "rods" or "ribbons") connected by networks of hydrogen bonds (eq 1). We expect tapes to pack with their long axes parallel, a geometric arrangement likely to minimize free volume.[2] Packing of hydrogen-bonded tapes with axes parallel would necessarily limit their constituent molecules to a set of arrangements in space that is substantially reduced relative to that available, in principle, to molecules with no constraints on their packing.

We have based our design for tapes on the network of hydrogen bonds present in the 1:1 complex of cyanuric acid and melamine (CA-M). We and others believe that this material has the structure shown in Figure 1, although it has not been possible to grow single crystals of this compound large enough for X-ray diffraction.[3-5] By interrupting the hydrogen bonds (either by replacement of two of the NH_2 groups of melamine with NHR groups, by substitution of NH groups in cyanuric acid with CR_2 or NR groups, or by more complex structural modifications) it is possible to construct at least two types of tape ("linear" and "crinkled", Figure 1) that preserve the three hydrogen bonds between the two components.[6,7] The objective of the research reported in this paper was to establish the correctness of the hypothesis that molecules of types Mel(4-X-Ph)$_2$ and Bar(Et)$_2$ would form 1:1 complexes with tape structures in the solid state. An additional goal was to define the generality of tape formation for a range of substituents on melamines and barbiturates. Our immediate interest was to define structures of a series of molecular crystals differing only in substitution at one position. This set of structures might serve as a starting point for a systematic physical–organic analysis of the relation of molecular to crystal structure.



Mel(4-X-Ph)$_2$ Bar(Et)$_2$

X = H, F, Cl, Br, I, CH_3, CF_3



(1)

* Abstract published in *Advance ACS Abstracts*, February 15, 1994.

(1) Promising approaches for predicting packing have been reported by: Gavezzotti, A. *J. Am. Chem. Soc.* 1991, *113*, 4622. Perlstein, J. *J. Am. Chem. Soc.* 1992, *114*, 1955.

(2) We relate our argument for parallel packing of tapes to the similar packing of long-chain alkanes. For a summary, see: Kitaigorodskii, A. I. *Molecular Crystals and Molecules*; Academic Press: New York, 1973.

(3) Seto, C. T.; Whitesides, G. M. *J. Am. Chem. Soc.* 1990, *112*, 6409.

(4) There is probably substantial disorder in samples of CA-M, and it is difficult to control its nucleation and subsequent crystal growth.

(5) We consider a crystal to be big enough to warrant investigation using a rotating anode X-ray generator if its smallest dimension is at least 0.05 mm. A crystal referred to in the text as "good" or "usable" or "diffraction quality" was in this size range and was free of cracks or visible twinning under a microscope.

(6) Zerkowski, J. A.; Seto, C. T.; Whitesides, G. M. *J. Am. Chem. Soc.* 1992, *114*, 5473.

(7) Figure 1 indicates that a possible geometry for a 1:1 complex of Mel(4-X-Ph)$_2$ and Bar(Et)$_2$ could also be a cyclic structure (Mel(4-X-Ph)$_2$)$_3$·(Bar(Et)$_2$)$_3$. For X = C(CH_3)$_3$, we have observed this disk shape as a crystallographic motif.[6]

0002-7863/94/1516-2382$04.50/0 © 1994 American Chemical Society

UM00012511
NOVARTIS EXHIBIT 1017
Novartis v. Regents, IPR2023-01346
Page 1257 of 4460

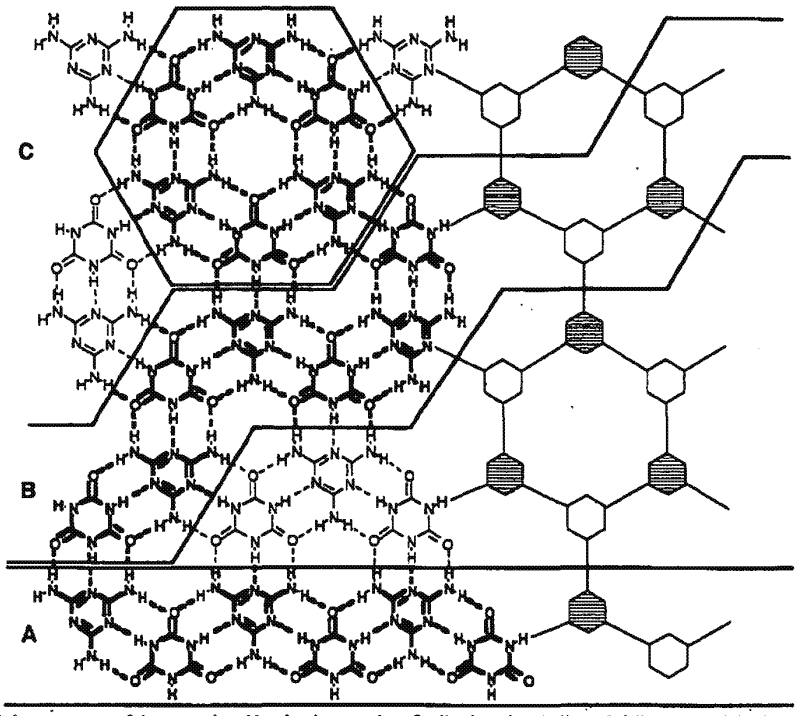


Figure 1. Proposed sheet structure of the cyanuric acid·melamine complex. Outlined sections indicate (A) linear tape, (B) crinkled tape, and (C) cyclic hexamer.

Advantages to the Use of Hydrogen Bonding of Melamines and Barbiturates in Crystal Engineering. Hydrogen bonds are well suited for use in the design of molecular solids for two reasons: they are directional, and their formation is reversible at room temperature. Using nondirectional forces (e.g. van der Waals and ionic interactions), it is difficult to predict geometries relating adjacent molecules in a crystal. Statistical studies of hydrogen bonds in organic crystals have shown that, for many hydrogen-bonding moieties, bond angles and distances involving the hydrogen atoms and donor and acceptor heteroatoms cluster in a small spread of values.[8] Measurements of the enthalpy of formation of hydrogen bonds in purine and pyrimidine bases—compounds similar to cyanuric acid, barbituric acid, and melamine—and in other compounds give a range of values,[9] but regardless of the precise energetics, hydrogen bonds will be important intermolecular interactions in the solid state.[10] Etter has suggested that strong hydrogen bond donors and acceptors will always engage in hydrogen bonding in organic solids.[11] Given the directional preferences and strength of hydrogen bonds and the complementary donor/acceptor pattern of melamines and barbiturates, we expect our tapes to assemble reliably.

A further advantage of compounds of the type Mel(4-X-Ph_2) and Bar$(Et)_2$ is that their heterocyclic core is rigid. Thus, the bidirectional hydrogen bonding necessary for construction of extended solid-state structures is not dependent on conformations of flexible linkers.[12] Their simple trigonal shapes also require consideration of only a few orientations of hydrogen-bonding moieties; this symmetry simplifies predictions of packing.

The syntheses of Mel(4-X-$Ph)_2$ and Bar$(Et)_2$ are straightforward. We have used barbiturates rather than isocyanurates[13] because the latter have not yielded crystals suitable for single-crystal X-ray analysis.[5,14] The barbiturates seem to be more soluble than isocyanurates in common organic solvents, and the two sites for substitution in the 5-position allow more opportunity for modification.

(8) Taylor, R.; Kennard, O. *Acc. Chem. Res.* **1984**, *17*, 320. Murray-Rust, P.; Glusker, J. P. *J. Am. Chem. Soc.* **1984**, *106*, 1018. Taylor, R.; Kennard, O.; Versichel, W. *Acta Crystallogr.* **1984**, *B40*, 280. Vedani, A.; Dunitz, J. D. *J. Am. Chem. Soc.* **1985**, *107*, 7653.

(9) Calorimetric measurements of association of guanosine and cytidine (derivatized at the 3′- and 5′-positions with triisopropylsilyl groups) in *o*-dichlorobenzene: $\Delta H = -2.2$ kcal/mol H-bonds. Williams, L. D.; Chawla, B.; Shaw, B. R. *Biopolymers* **1987**, *26*, 591. Monte-Carlo calculations on G·C base-pair formation in CCl_4: $\Delta E = -5.9$ kcal/mol H-bonds. Pohorille, A.; Burt, S. K.; MacElroy, R. D. *J. Am. Chem. Soc.* **1984**, *106*, 402. Spectrophotometric measurement by van't Hoff analysis of cyclic intramolecular hydrogen bonding in an amide: $\Delta H = -1.4$ to -1.6 kcal/mol H-bonds. Gellman, S. H.; Dado, G. P.; Liang, G.-B.; Adams, B. R. *J. Am. Chem. Soc.* **1991**, *113*, 1164. Calculations using thermodynamic cycles based on estimates for translational and rotational entropies: $\Delta H \approx -2.9$ kcal/mol H-bonds (mean in CCl_4) and -1.0 kcal/mol H-bonds (mean in H_2O). Doig, A. J.; Williams, D. H. *J. Am. Chem. Soc.* **1992**, *114*, 338. Measurements of differential binding of substrates to enzymes in the presence and absence of hydrogen-bonding groups: $\Delta G = -0.5$ to -1.8 kcal/mol H-bonds. Fersht, A. R. *Trends Biochem. Sci.* **1987**, *12*, 301.

(10) Desiraju, G. R. *Crystal Engineering: The Design of Organic Solids*; Elsevier: New York, 1989.

(11) Etter, M. C. *J. Am. Chem. Soc.* **1982**, *104*, 1095. There are exceptions to this guideline; see the structure of alloxan, which engages in only weak, bifurcated hydrogen bonds: Swaminathan, S.; Craven, B. M.; McMullan, R. K. *Acta Crystallogr.* **1985**, *B41*, 113.

(12) Garcia-Tellado, F.; Geib, S. J.; Goswami, S.; Hamilton, A. D. *J. Am. Chem. Soc.* **1991**, *113*, 9265. Etter, M. C.; Adamond, D. A. *J. Chem. Soc., Chem. Commun.* **1990**, 589.

(13) Isocyanurates are N-alkylated; cyanurates are O-alkylated. Following this convention, the parent molecule as its trishydroxy tautomer should be named cyanuric acid, even though it is known to exist almost exclusively as the triketo form. Our examination of the literature suggests that the name isocyanuric acid is rarely used, however, so we will continue to refer to the triketo form as cyanuric acid.

(14) We suspect that the greater acidity of isocyanurates relative to barbiturates may lead to stronger hydrogen bonding along one developing crystalline axis in the former case and hence to rapid and uncontrollable crystal growth. Isocyanurates were also more difficult to synthesize. Perrin, D. D. *Dissociation Constants of Organic Bases in Aqueous Solution*; Butterworths: London, 1965.

UM00012512
NOVARTIS EXHIBIT 1017
Novartis v. Regents, IPR2023-01346
Page 1258 of 4460

Precedent for Crystal Engineering of Hydrogen-Bonded Structures. Infinite chains based on hydrogen bonds have been observed and studied previously, notably in monocomponent crystals of amides and carboxylic acids. Leiserowitz and colleagues have produced comprehensive catalogues of crystalline features arising from hydrogen bonding of these functionalities.[15] The relationships between the molecular structures of alicyclic diols and their packing motifs have been investigated by Bishop and Dance.[16] Etter's work provides useful structural generalizations and predictive guidelines for patterns of solid-state hydrogen-bonded networks.[17] Several hydrogen-bonded dimers of barbiturates have been reported by Craven,[18] and Shimizu has observed a hydrogen-bonded chain of barbital cocrystallized with adenine.[19] Lehn has examined a molecular tape similar to ours[20] and has used hydrogen bonds to design other kinds of systems.[21]

Guide to the Work. The data presented below support our hypothesis that threefold hydrogen bonding leads to the formation of crystalline tapes. These tapes consist of a structurally constant backbone and variable periphery that can be altered by substitution on Mel(4-X-Ph)$_2$ and barbiturates. The packing of the tapes is sensitive to small perturbations on the molecular composition. In at least two cases (X = Br and CF$_3$) polymorphism occurs, allowing packing of a complex in more than one phase.[22] Despite the complexity introduced by polymorphism, we believe that this system of linear, hydrogen-bonded tapes is an excellent one with which to study the physical–organic chemistry of organic molecular solids. Its most serious shortcomings at present are that numerous crystallization efforts may be required to obtain single crystals large enough for X-ray analysis, that polymorphism complicates interpretation, and that difficulties may be encountered in forming single crystals containing certain polar substituents.

Results

Crystallizations. We have not yet developed a single crystallization procedure that produces diffraction-quality single crystals of tapes. An acicular crystal habit was the one most frequently obtained. The most common reason for rejecting a batch of crystals was that the needles were too thin.[5] We suggest that the crystals grow rapidly in the direction of faces that expose hydrogen bonds. A solvent capable of both donating and accepting hydrogen bonds should, in principle, bind well to the crystal face exposing polar hydrogen-bonding moieties and should slow growth in this direction, while allowing growth to continue on faces with exposed alkyl or aryl substituents.[23] Crystals that are less acicular are in fact obtained from methanol and ethanol, while solvents of lesser hydrogen-bonding ability gave whiskers. Thus one guideline that we can offer is that hydrogen-bonding solvents work best for crystallizations of solutes of this sort.[24] Indexing of crystal faces, to allow correlation of the tape packing direction with the shape of the crystal, has been performed in only one case (on the Mel(4-F-Ph)$_2$Bar(Et)$_2$ complex). The long needle axis did correspond with the long tape axis, along the crystallographic *b* direction, in that case.[25]

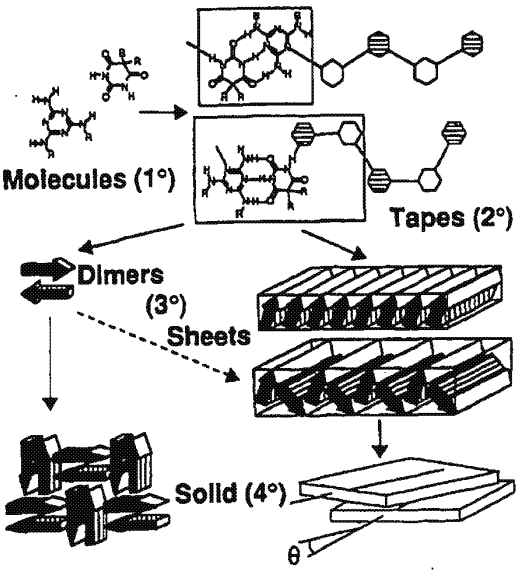


Figure 2. Hierarchies of structural elements, or crystalline architecture, in crystals of the 1:1 complexes of *N,N'*-bis(4-X-phenyl)melamines and 5,5-diethylbarbituric acid. Levels of structural organization are suggested schematically: primary = 1°, molecules; secondary = 2°, tapes; tertiary = 3°, arrays of tapes with parallel axes; quaternary = 4°, full solid, axes of tapes may be nonparallel.

Structural Generalizations. As background for the experimental results, we summarize two limitations (summarized graphically in Figure 2) to the types of structures considered. First, we consider only linear tapes; crinkled tapes have also been observed.[6] Limiting consideration to the linear tapes allows us to focus on the structural features common to them. Second, we further restrict the scope of this paper to small structural perturbations generated by a series of substituents in the *para* position of the phenyl rings of *N,N'*-diphenylmelamines: H, F, Cl, Br, I, CH$_3$, and CF$_3$. For all of these structures, θ (Figure 2, bottom) is zero: that is, all the tapes pack with their long axes parallel.[26] A conglomerate view of all these substituents, showing their relative van der Waals radii, is presented in Figure 3.

Solid-State Structures of Complexes Mel(4-X-Ph)$_2$Bar(Et)$_2$. Figures 4–11 summarize the structures of 1:1 cocrystals between 5,5-diethylbarbituric acid (Bar(Et)$_2$) and derivatives of diphen-

(15) Leiserowitz, L.; Hagler, A. T. *Proc. R. Soc. London* **1983**, *A388*, 133. Leiserowitz, L. *Acta Crystallogr.* **1976**, *B32*, 775.
(16) Bishop, R.; Dance, I. G. in *Inclusion Compounds*; Atwood, J. L., MacNicol, D. D., Davies, J. E. D., Eds.; Academic Press: London, 1991; Vol. IV.
(17) Etter, M. C. *Acc. Chem. Res.* **1990**, *23*, 120.
(18) Hsu, I.; Craven, B. M. *Acta Crystallogr.* **1974**, *B30*, 974.
(19) Shimizu, N.; Nishigaki, S.; Nakai, Y.; Osaki, K. *Acta. Crystallogr.* **1982**, *B38*, 2309.
(20) Lehn, J.-M.; Mascal, M.; DeCian, A.; Fischer, J. *J. Chem. Soc., Perkin Trans. 2* **1992**, 461.
(21) Lehn, J.-M. *Angew. Chem., Int. Ed. Engl.* **1990**, *29*, 1304.
(22) A systematic study of the crystal packing of organic molecules must take polymorphism into consideration. We have found that at least two members of this family of complexes, Mel(4-Br-Ph)$_2$Bar(Et)$_2$ and Mel(4-CF$_3$-Ph)$_2$Bar(Et)$_2$, display polymorphism. For X = Br, we observe three polymorphs. The structures of two are reported here, but we have been unable to obtain large enough crystals of the third for single-crystal analysis. For X = CF$_3$, we observe two polymorphs; the one for which we have obtained good crystals is described here. A full investigation of the alternative packing modes of the *para* series of complexes, relying on X-ray powder diffraction and solid-state NMR, will be presented in a separate publication.
(23) Berkovitch-Yellin, Z.; van Mil, J.; Addadi, L.; Idelson, M.; Lahav, M.; Leiserowitz, L. *J. Am. Chem. Soc.* **1985**, *107*, 3111. Wireko, F. C.; Shimon, L. J. W.; Frolow, F.; Berkovitch-Yellin, Z.; Lahav, M.; Leiserowitz, L. *J. Phys. Chem.* **1987**, *91*, 472. Wang, J.-L.; Leiserowitz, L.; Lahav, M. *J. Phys. Chem.* **1992**, *96*, 15.
(24) Broader generalizations on the techniques we have used will be published at a later time. The crystals discussed in this work, except for the fluorine-containing complexes, were comparatively readily grown; that is, they did not require many trial-and-error-based crystallization attempts. We have not been able to crystallize melamines with polar substituents (e.g. CO$_2$H, CONH$_2$, or CN). After several attempts, we could only obtain microcrystals, at best. We suspect that the need for these substituents to hydrogen bond may be geometrically incompatible with close packing of tapes.
(25) The data collected from the particular crystal that was indexed gave a crystallographic solution that could not be refined below an *R*-factor of 0.20. Since a recollection of data from another crystal gave an essentially identical solution (and good refinement), we do believe that the tape/needle correspondence is real.
(26) Strong interactions between tapes might, however, make $\theta \neq 0$. This is the case in the complex between melamine and barbituric acid, where three-dimensional hydrogen bonding of tapes twists θ to almost 90°. Zerkowski, J. A.; Whitesides, G. M. Unpublished results.

UM00012513
NOVARTIS EXHIBIT 1017
Novartis v. Regents, IPR2023-01346
Page 1259 of 4460

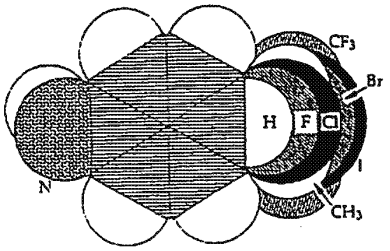


Figure 3. Comparative van der Waals sizes of the phenyl substituents used in this work. The van der Waals radii used are listed in ref 29. The NH group *para* to the substituents is attached to the triazine ring.

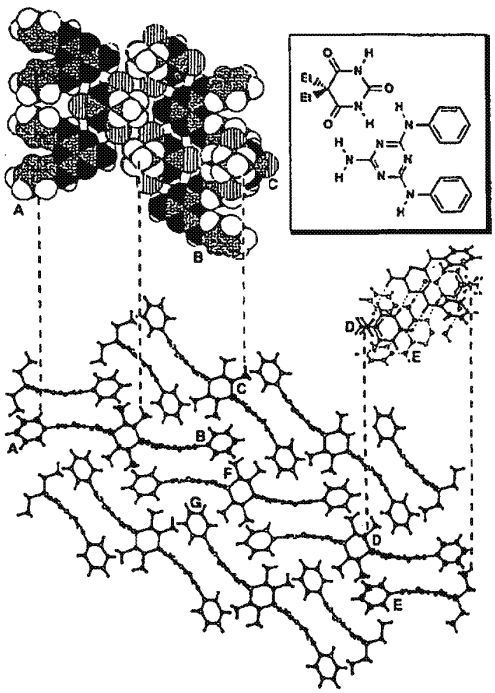


Figure 4. Views of the Mel(4-H-Ph)$_7$Bar(Et)$_2$ complex.

ylmelamine substituted in the *para* position with substituents X (Mel(4-X-Ph)$_2$). These figures show several views of packing at once and are intended to provide the information needed to discuss packing. We are primarily concerned here with *inter*molecular interactions. We have not yet found a single representation of the crystal structure that provides the information needed to visualize intertape, contacting van der Waals surfaces. Stereoscopic views are not helpful. The sets of composite views given in Figures 4–11, while complicated, represent the most useful way we have developed to describe packing and to show close, nonbonded contacts between molecules.

The central portion of each figure shows an end-on view, looking down the long axes of the tapes. This view illustrates the major stacking motifs of the tapes. Both the van der Waals section and the remaining ball-and-stick picture(s) are views looking down on selected tapes (indicated in the end-on view with thermal ellipsoids). The vertical dotted lines identify tapes that appear in more than one view. The letters also identify corresponding structures in different views. The ball-and-stick top-down view shows how various portions of the tapes overlap. For simplicity, the only noncovalent interactions illustrated (dotted lines) are hydrogen bonds.

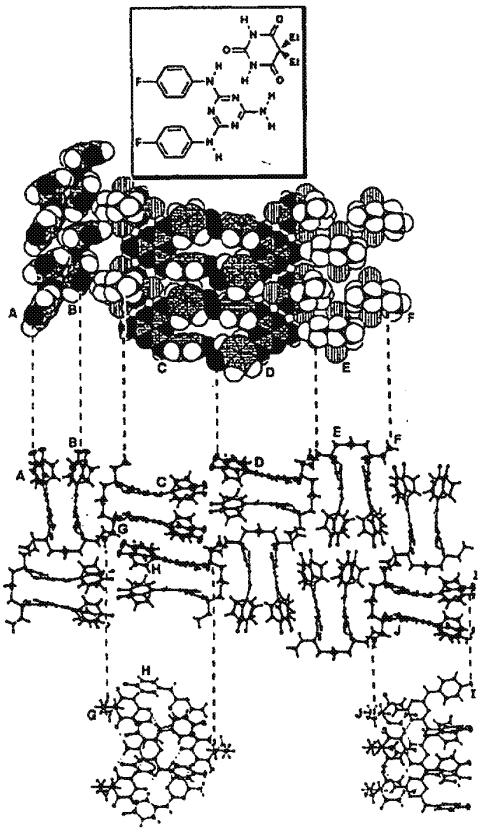


Figure 5. Views of the Mel(4-F-Ph)$_7$Bar(Et)$_2$ complex.

To summarize the registry of the tapes along their long axes, we introduce the symbolism shown in Figure 12. We choose one tape (A, Figure 12), arbitrarily as a reference, and represent its orientation in the crystal by an arrow attached to an open circle. All the other tapes represented by open circles are related to the reference tape by simple translation perpendicular to the long axis of the tape. The relation of any other tape (B, Figure 12) to the reference tape is determined by the manipulations that must be performed to superimpose it on the reference tape. First, we move tape B along the tape axis (and in the positive direction of the parallel crystallographic axis) by a distance λ (see Figure 12) until its melamine and barbituric acid groups (but not necessarily the substituents on these groups)[27] line up with those of the reference tape. To convert the fraction λ/L (where L is the repeat distance along a tape axis, Figure 13) to a graphic symbol, we multiply by 2π radians and represent the resulting angle φ on the circle attached to the arrow representing tape B. Other manipulations of tape B required to superimpose it on tape A—reflections of melamine and barbiturate units across a mirror plane perpendicular or parallel to the long axis—are also indicated in Figure 12.

The most important information summarized in Figure 12 is the relative positions and orientations of the tapes. Thus, for example, X = Cl and X = Br (form I) are isomorphous,[28] and

(27) Since the angles at the melamine nitrogens linking the phenyl ring to the triazine ring are greater than 120° (Figure 13) and are not equal to each other, the phenyl rings splay out and the intramolecular separation of the *para* substituents is greater than the width of the triazine ring. Thus depending on the crystallographic relationship of two tapes, superimposing their backbones might not superimpose their substituents.

UM00012514
NOVARTIS EXHIBIT 1017
Novartis v. Regents, IPR2023-01346
Page 1260 of 4460

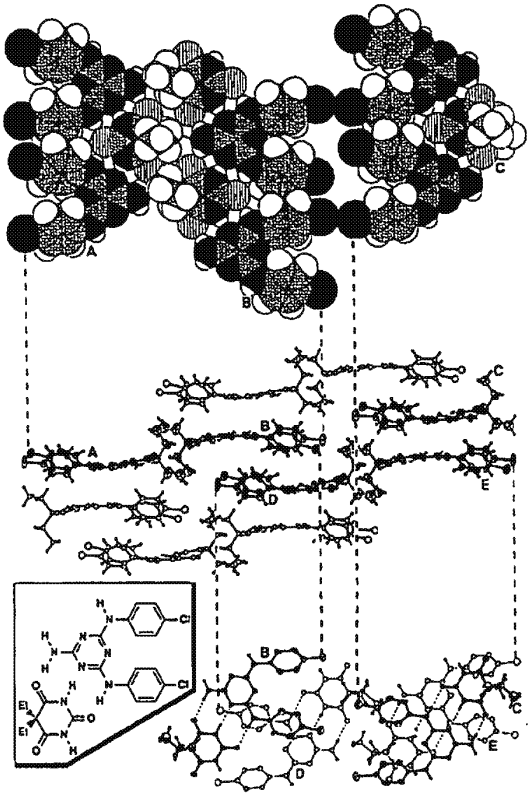


Figure 6. Views of the Mel(4-Cl-Ph)$_2$Bar(Et)$_2$ complex. Only one orientation of the disordered ethyl groups of barbital is shown.

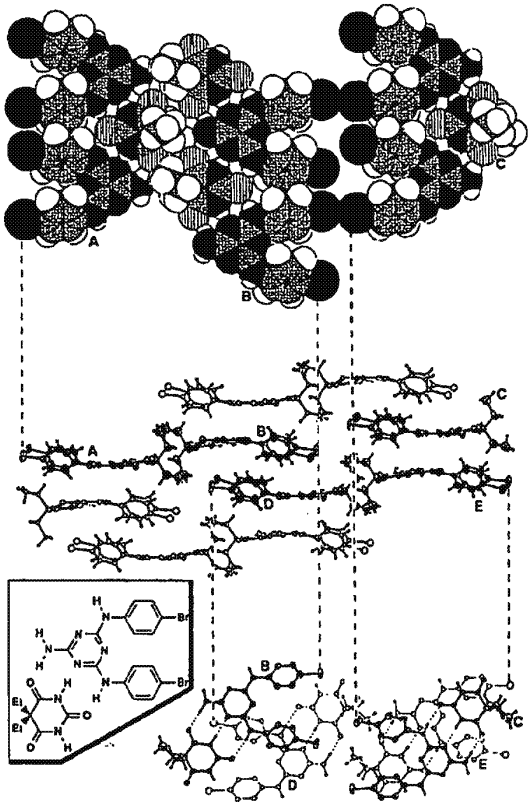


Figure 7. Views of the Mel(4-Br-Ph)$_2$Bar(Et)$_2$ (form I) complex. Only one orientation of the disordered ethyl groups of barbital is shown.

X = I, X = CH_3, and X = Br (form II) are a closely related set. Head-to-tail dimers occur in four structures (H, Cl, Br (form I), and CF_3). The tape with X = F is unique in its architecture. Table 1 lists some pertinent crystallographic data.

***N,N'*-Diphenylmelamine/barbital (Mel(4-H-Ph)$_2$Bar(Et)$_2$).** The phenyl and ethyl substituents on adjacent, stacked tapes dovetail: tapes D and E (a centrosymmetric dimer) in Figure 4 show how the phenyl groups of one tape in an inversion-related pair of tapes tilt to form a small pocket into which an ethyl group from the partner tape can fit. This kind of accommodation is repeated between nonparallel tapes, as between tapes B and C in Figures 4 and 14. There are no intertape phenyl–phenyl interactions, such as in a stacking or edge-to-face arrangement.

***N,N'*-Bis(4-fluorophenyl)melamine/barbital (Mel(4-F-Ph)$_2$Bar(Et)$_2$).** There are two dimers in the asymmetric unit of this complex. The packing is built up from both centrosymmetric, or head-to-tail dimers (tapes G and H in Figure 5), and parallel head-to-head dimers (tapes C and G). The interplanar separations between the head-to-head tapes are smaller than those for the head-to-tail tapes (3.3–3.5 vs 4.2–4.4 Å). There are no fluorine–fluorine contacts, but there is a hydrogen–fluorine contact: one fluorine atom in tape C is 2.44 Å away from a *meta*-phenyl hydrogen in tape D ($\Sigma_{vdW} \approx 2.67$ Å).[29-31] One of the ethyl groups is disordered, with the methyl group occupying two different positions in approximately a 2:1 ratio.

***N,N'*-Bis(4-chlorophenyl)melamine/barbital and *N,N'*-Bis(4-bromophenyl)melamine/barbital (Mel(4-Cl-Ph)$_2$Bar(Et)$_2$ and Mel(4-Br-Ph)$_2$Bar(Et)$_2$ (Form I)).** These complexes are isomorphous. The centrosymmetric dimer is again a principal motif. Both ethyl groups of barbital are disordered. In both complexes, there are no halogen–halogen contacts at or under the sum of the van der Waals radii.

***N,N'*-Bis(4-iodophenyl)melamine/barbital and *N,N'*-Bis(4-bromophenyl)melamine/barbital (Mel(4-I-Ph)$_2$Bar(Et)$_2$) and Mel(4-Br-Ph)$_2$Bar(Et)$_2$ (Form II)).** The halogen–halogen interactions are more extensive in these complexes than in those for which X = F, Cl, and Br (form I) and are clearly less than the sum of van der Waals radii: for iodine, $\Sigma_{vdW} \approx 4.0$ Å, I---I contacts at 3.76 and 3.81 Å; for bromine, $\Sigma_{vdW} \approx 3.7$ Å, Br---Br contacts at 3.75 and 3.50 Å. These interactions occur between tapes. The packing has changed to a format based on sheets.

***N,N'*-Bis(4-methylphenyl)melamine/barbital (Mel(4-CH$_3$-Ph)$_2$Bar(Et)$_2$).** The packing of this complex is very similar to that of Mel(4-I-Ph)$_2$Bar(Et)$_2$ and Mel(4-Br-Ph)$_2$Bar(Et)$_2$ (form II), although none of the three are in fact crystallographically

(28) "Crystals in which the atomic positions are essentially the same but differ only in the nature of the atoms that occupy these positions are called isomorphous; ...they are recognized by their similar cell dimensions, same space group, and similar diffraction patterns." Dunitz, J. D. *X-Ray Analysis and the Structure of Organic Molecules*; Cornell University Press: Ithaca, NY, 1979; p 123.

(29) We are using isotropic van der Waals radii: H, 1.20 Å; C, 1.70 Å, N, 1.55 Å; O, 1.52 Å; F, 1.47 Å; Cl, 1.75 Å; Br, 1.85 Å; I, 1.98 Å. Bondi, A. *J. Phys. Chem.* **1964**, *68*, 441. For anisotropic van der Waals radii, see: Nyburg, S. C.; Faerman, C. H. *Acta Crystallogr.* **1985**, *B41*, 274.

(30) Since we placed all the hydrogen atoms in calculated positions for determining intermolecular contacts, we will only propose that specific contacts involving hydrogens are suggested and will not put too much emphasis on the precise distances of these contacts. Most of the contacts that we comment upon in the text are at least 0.1 Å less than the sum of van der Waals radii of the interacting atoms. We believe, however, that even if a hydrogen–heteroatom contact is slightly over the sum of van der Waals radii, it will still probably play some role in guiding packing.

(31) All aliphatic and aromatic C–H bonds were set to 1.08 Å, and all N–H bonds to 1.00 Å.

UM00012515
NOVARTIS EXHIBIT 1017
Novartis v. Regents, IPR2023-01346
Page 1261 of 4460

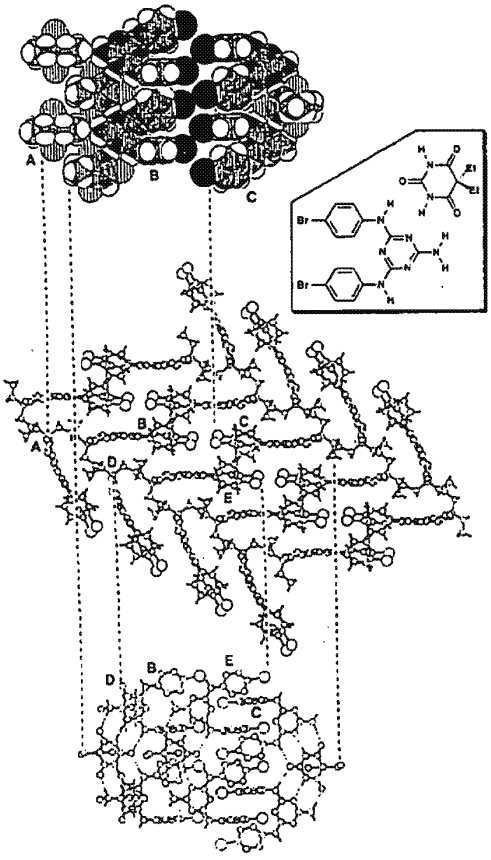


Figure 8. Views of the Mel(4-Br-Ph)$_2$·Bar(Et)$_2$ (form II) complex.

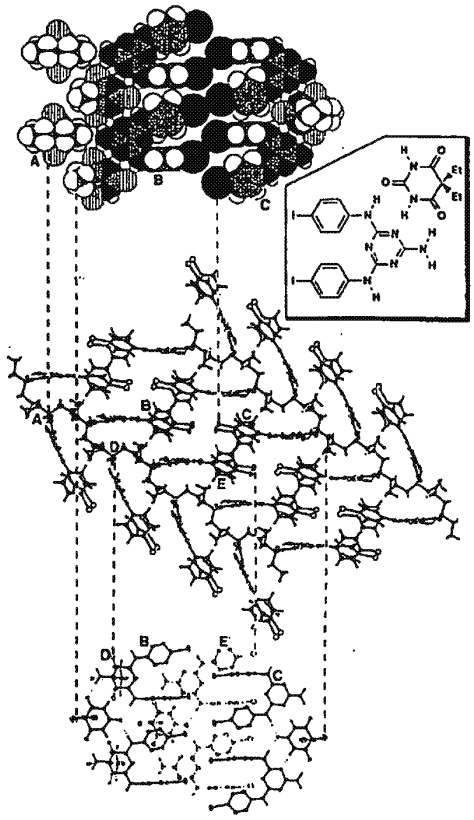


Figure 9. Views of the Mel(4-I-Ph)$_2$·Bar(Et)$_2$ complex.

isomorphous. Between the methyl groups, there are no intertape contacts analogous to the halogen–halogen interactions of the preceeding two Mel(4-X-Ph)$_2$·Bar(Et)$_2$ complexes.

***N,N'*-Bis(4-trifluoromethylphenyl)melamine/barbital (Mel(4-CF$_3$-Ph)$_2$·Bar(Et)$_2$).** There is rotational disorder around the F$_3$C–C$_{aryl}$ bond. Intertape fluorine–hydrogen contacts at 2.41, 2.45, and 2.51 Å ($\Sigma_{vdW} \approx 2.67$ Å) exist between the fluorines of tape D and the barbital CH$_3$ hydrogens of tape C in Figure 11, although the disorder cautions against overinterpreting those contacts. There are no fluorine–fluorine interactions.

Packing Fractions. Table 1 lists the packing fractions, C_k*,[32] for all the complexes. The packing fraction, which is a measure of the efficiency of space filling in a crystal, is defined by eq 2, where V_m is the molecular volume, N is the number of molecules

$$C_k = N(V_m/V_c) \qquad (2)$$

in the unit cell (which is not necessarily equal to Z, the number of asymmetric units), and V_c is the volume of the unit cell. The molecular volumes were calculated by putting crystallographic coordinates into MacroModel.[33] All C–H and N–H bond lengths were set to conventional values.[31] The MacroModel volume-calculating facility was used without alteration, so these values, while in the acceptable range for organic compounds, are not intended for comparison to previous literature values for C_k.[34] We have therefore employed a modified label, C_k*, for the packing fraction. Furthermore, strict comparisons should only be made for structures done at the same temperature (X = F, Cl, Br (forms I and II), I, and CF$_3$).

Regarding the two X = Br polymorphs, Kitaigorodskii's close-packing principle would suggest that the form I polymorph should be the more thermodynamically stable, since it fills space more efficiently and since there are no strong directional intertape interactions.[2,10] The disordered ethyl groups should also favor this polymorph by raising the entropy of the crystal. A complete discussion of the relative energetics of these two polymorphs must await detailed calculations.[22]

The lowest packing coefficient, that for Mel(4-CF$_3$-Ph)$_2$·Bar-(Et)$_2$, is consistent with the existence of rotational disorder in the

(32) Kitaigorodskii, A. I. *Organic Chemical Crystallography*; Consultants Bureau: New York, 1961.

(33) Still, W. C., *et al. MacroModel V3.0*; Department of Chemistry, Columbia University: New York, 1990.

(34) We calculated some molecular volumes using published crystallographic coordinates to compare our MacroModel-derived packing fractions to literature values (compound and reference for crystallographic coordinates, literature value for C_k and reference, our MacroModel value for C_k*): hexanitrobenzene (ref 34a), 0.64 (ref 2), 0.68; hexacyanobenzene (ref 34b), 0.56 (ref 10), 0.61; resorcinol, α-form (ref 34c), 0.67 (ref 32), 0.68; acridine (ref 34d), 0.71 (ref 32), 0.73. (a) Akopyan, Z. A.; Struchkov, Yu. T.; Dashevskii, V. G. *Zh. Strukt. Khim.* **1966**, *7*, 408. (b) Drück, U.; Kutoglu, A. *Acta Crystallogr.* **1983**, *C39*, 638. (c) Robertson, J. M. *Proc. R. Soc.* **1936**, *A157*, 79. (d) Phillips, D. C. *Acta Crystallogr.* **1956**, *9*, 237. The values of C_k that come from Kitaigorodskii's work[2,10] were almost certainly calculated from tables of average volume increments, since Kitaigorodskii developed and promoted that method. Obvious drawbacks to his approach are that some functional groups may not have tabulated values and that different volume contributions may be inferred from different molecular environments. While some of these pairs of C_k and C_k* values may not be as close to each other as is desirable, the relative ease of calculating molecular volumes using MacroModel or some other widely accessible program recommends our procedure. As long as the programs use the same set of van der Waals radii,[28] comparisons should be valid. We hope that this approach, rather than the use of potentially antiquated or incomplete tables of volume increments for functional groups,[2,32] may induce wider reporting of packing fractions.

UM00012516
NOVARTIS EXHIBIT 1017
Novartis v. Regents, IPR2023-01346
Page 1262 of 4460

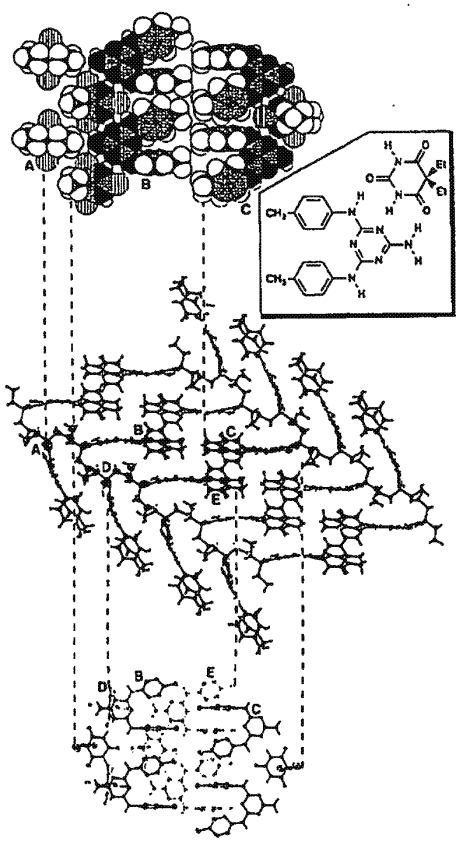


Figure 10. Views of the Mel(4-CH_3-Ph)$_2$-Bar(Et)$_2$ complex.

CF_3 groups. If packing is loose, there may be enough free space to permit molecular motion in the crystal.[35] There is no correlation between substituent size and tightness of packing.

Discussion

The eight structures described here confirm the hypothesis that suitably designed 1:1 cocrystals of N,N′-disubstituted melamines and dialkylbarbituric acids form linear tapes in the solid state. These structures all have relatively small, nonpolar substituents in the 4-position of the phenyl groups of *N,N′*-diphenylmelamine. Larger, nonpolar substituents (CO_2CH_3, *tert*-butyl) lead to different structures (crinkled tapes or cyclic "rosettes"); these structures have been described in a separate paper.[6] We have not yet been able to prepare cocrystals suitable for single-crystal X-ray diffraction when the substituent in the 4-position is polar (CO_2H, CN, $CONH_2$).

The limitation to the formation of linear tapes in the structural class of cocrystals explored here appears to be unfavorable steric interactions between the substituents in the 4-positions of phenyl groups of *adjacent* melamines (Figure 13, Table 2).. The intermolecular separation of substituents (*d* in Figure 13) is always smaller than the intramolecular separation (*d′*). This feature reflects the fact that the angle at the melamine nitrogen connecting the phenyl and triazine rings (Φ in Figure 13) is greater than 120°. For the larger X groups CH_3 and CF_3, *d* is smaller than

(35) A reviewer has pointed out that it is the *local*, not the overall, packing efficiency near a disordered group that is relevant to its disorder. Nonetheless, it seems reasonable to expect that local regions of loose packing may contribute to a reduced overall packing fraction.

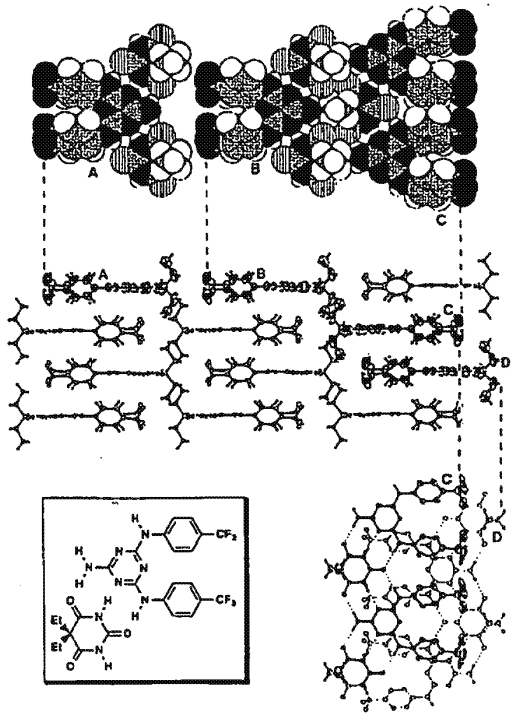


Figure 11. Views of the Mel(4-CF_3-Ph)$_2$-Bar(Et)$_2$ complex. Only one orientation of the disordered trifluoromethyl group is shown.

the van der Waals diameter of X. Since these diameters assume a semicircular cross section, they probably imply a potential for steric repulsion that is greater than that existing between real, noncylindrical CH_3 or CF_3 groups. Any increase in the size of X beyond the values of these larger substituents would lead to repulsive interactions and prevent formation of a linear tape.[7] The quantity $d + d'$ is constant at about 10 Å, and this value is greater than the translational repeat distance within a tape (9.70–9.98 Å, Table 1; *L* in Figure 13). This extra separation is attained by a distortion of the phenyl rings above or below the mean planes of the hydrogen-bonded backbones.

When the *para* substituent is bromine, which comes toward the middle of the range of sizes spanned by substituents H to CF_3 (Table 2), two alternative packing arrangements (at least)[22] are energetically accessible at ambient conditions. Complexes with the smaller substituents H, F, and Cl adopt a packing that is based on dimers of tapes (Figure 2), although the architecture of the case with X = F is unique and complicates this simplified picture. Complexes with the larger substituents CH_3 and I adopt a packing that is sheet-like, although, again, the fluorinated complex with X = CF_3 does not fit into this picture, since it packs with head-to-tail dimers that are further stacked into sheets (see, however, footnote 22). The complexes with the intermediate-sized X = Br substituents can adopt either a dimer-based (Figure 7) or a sheet-based (Figure 8) packing. Thus, as we have observed with bulkier substituents,[6] the steric properties of the substituents in the *para* positions of these diphenylmelamine complexes appear to be critical to determining both secondary and tertiary crystalline architecture.

The overall quality of these structures (as measured by the crystallographic *R*-index) varies from 0.04 to 0.09. An independent measure of the reliability of the structures comes from examination of the geometries of the triazine, phenyl, and barbital groups. These fragments would be expected to be approximately constant in geometry, and errors in the crystal structures might

UM00012517
NOVARTIS EXHIBIT 1017
Novartis v. Regents, IPR2023-01346
Page 1263 of 4460

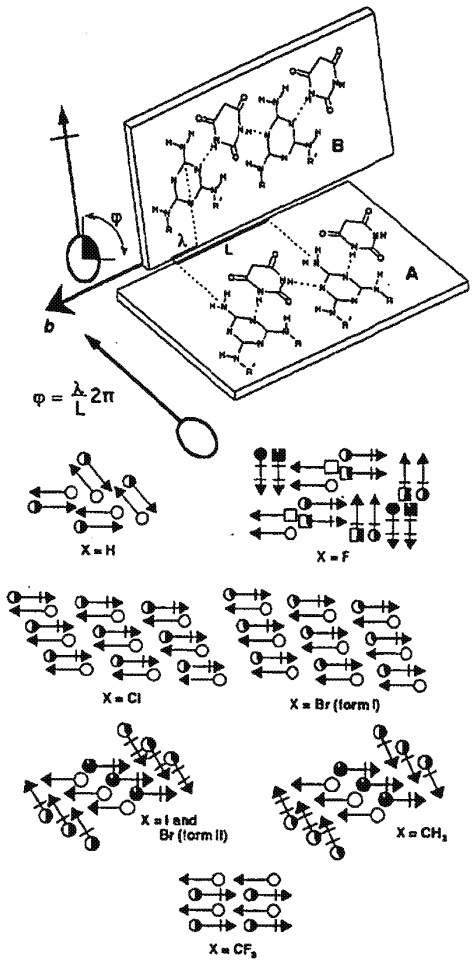


Figure 12. Top: Schematic diagram summarizing the packing of tapes. Tape B is moved in the positive direction along its long axis until the atoms of the tape backbones in the two tapes have (in this example) the same y coordinate. φ (radians) is the fraction of the repeat distance in a tape (L) that tape B must be moved to line up with tape A (open circle). The arrows with circles attached represent end-on views of the tapes, looking down their long axes. Bottom: All the tapes with partially filled circles are related to the reference tapes by at least a rotation around an axis parallel to the long tape axis. A crossbar near the arrowhead indicates that a reflection across a mirror plane perpendicular to the long axes must also be done (as in the picture at the top); a crossbar near the circle indicates the same for a mirror plane parallel to the long axes. The reference unit in the X = F case is a dimer (one circle and one square), since there are two independent tapes in that complex. The offset amount φ is rounded to the nearest twelfth for clarity of the filled circles. This rounding exaggerates the difference between the isomorphous structures X = Cl and Br (form I).

be expected to appear as distortions from the anticipated geometries. In fact the observed geometries are sensibly constant.

Conclusions

The objective of this work was to develop a class of organic crystals that would exist in a limited set of crystalline architectures but would allow the kind of variation in structure useful in physical-organic studies of structure–property relationships. These 1:1 cocrystalline tapes have many of the desired characteristics. Their components are easily synthesized and can be

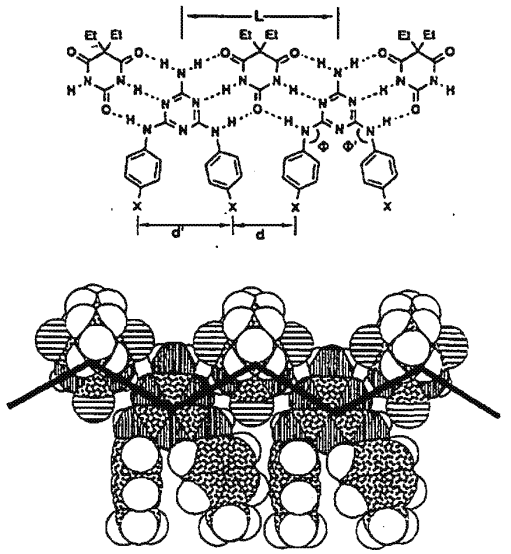


Figure 13. Intratape measurements listed in Table 2. L is the crystallographic repeat in a tape.

varied widely over a range of structures. The observation that linear tapes are frequently obtained, and that these tapes pack with their long axes parallel, has the potential to simplify the analysis of solid-state structure significantly (relative to crystals in which the constituent molecules can, in principle, adopt many conformations with respect to one another).

The system also has three disadvantages: growing crystals of the quality and size suitable for single-crystal X-ray diffraction requires patience; the system has not yet proved amenable to the introduction of polar substituents (perhaps because of competition of these substituents for hydrogen bonding sites); and at least some of the crystals can apparently exist in several crystalline forms. The issue of polymorphism is probably the one with the most far-reaching consequences.[22] Nonetheless, the important feature of our system is that it does tolerate small changes in molecular structure while maintaining a consistent solid-state motif. We have, thus, demonstrated a system that allows systematic investigation into crystalline architecture.

Experimental Section

General Methods. Cyanuric chloride (Fluka), barbital (Fisher Scientific), and all anilines (Aldrich) were used as received without purification. Solvents were reagent grade and were used without purification unless otherwise indicated; THF was distilled from sodium benzophenone ketyl. Melting points were determined on a Mel-Temp apparatus and are uncorrected.

2-Amino-4,6-dichloro-1,3,5-triazine.[36] Ammonia from a cylinder was slowly bubbled into a round-bottomed flask containing a slurry of cyanuric chloride (36.88 g, 0.2 mol) in 200 mL of dioxane and 30 mL of diglyme cooled in an ice–water bath. The temperature of the reaction was not allowed to rise above 10 °C. Addition of the gas was continued until 6.8 g (0.4 mol) had been taken up by the mixture, which took about 1 h. Nitrogen was blown through the reaction flask to remove excess NH_3. The mixture was filtered, and the precipitate was washed well with THF (300 mL). The collected solutions were concentrated by rotary evaporation (first at aspirator pressure and then at 1 Torr), and the solid residue was dried under vacuum at 0.1 Torr overnight, yielding 28.34 g (0.172 mol, 86%) of a white powder, mp 228–231 °C (lit.[36] 235–236 °C). This material decomposed slowly in the presence of atmospheric moisture; it was stored in a desiccator. To obtain fresh aminodichlorotriazine for a

(36) This preparation is a modification of that found in: Thurston, J. T.; Dudley, J. R.; Kaiser, D. W.; Hechenbleikner, I.; Schaefer, F. C.; Holm-Hansen, D. *J. Am. Chem. Soc.* **1951**, *73*, 2981.

UM00012518
NOVARTIS EXHIBIT 1017
Novartis v. Regents, IPR2023-01346
Page 1264 of 4460

Table 1. Crystallographic Data for Cocrystals of *N,N'*-Bis(*para*-X-phenyl)melamines and 5,5-Diethylbarbituric acid (Mel(4-X-Ph)$_2$Bar(Et)$_2$)[a]

X	space group	*a* (Å)	*b* (Å)	*c* (Å)	*α* (deg)[b]	*β* (deg)[b]	*γ* (deg)[b]	*R*[c]	C_k[a,d]	density (g/cm^3)[e]	crystallization solvent
H	*Pnma*	12.940	9.982	17.377				0.063	0.72	1.369	CH_2Cl_2
F	$P2_1/n$	31.627	15.470	9.700		90.08		0.044	0.69	1.395	CH_3CN
Cl	$P\bar{1}$	9.822	13.650	9.228	92.86	95.14	92.57	0.084	0.70	1.436	MeOH
Br (form I)	$P\bar{1}$	9.826	13.742	9.389	93.67	95.11	93.30	0.061	0.71	1.636	MeOH
Br (form II)	$P2_1/n$	9.735	31.396	8.417		90.47		0.044	0.68	1.602	$(CH_3)_2C{=}O$
I	$P2_1/n$	8.656	31.412	9.735		90.73		0.045	0.69	1.792	MeOH
CH_3	$P2_1/n$	9.747	8.226	31.982		95.46		0.093	0.68	1.276	MeOH
CF_3	$P2/n$	8.673	16.186	9.740		92.80		0.071	0.66	1.455	2:1 pyridine/H_2O

[a] The underlined cell dimensions represent the repeat distance in a tape, or *L* in Figure 13. [b] A blank means that the angle is constrained to be 90°. [c] This value is the crystallographic reliability index, $R = \sum|(F_o - F_c)|/\sum F_o$. [d] This value is the packing coefficient calculated using molecular volumes obtained from MacroModel[33] (see the Results section and footnote 34 for a discussion of the relationship between C_k and the "classical" packing coefficient, C_k). [e] Calculated.

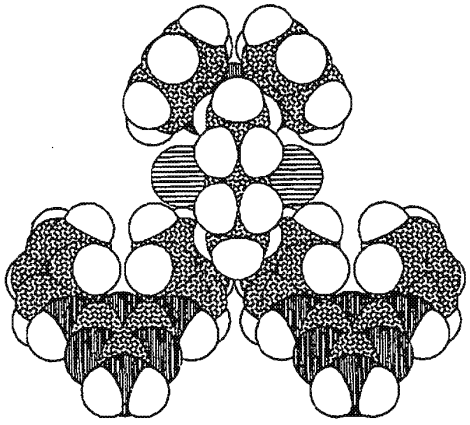


Figure 14. Complementary packing between phenyl and ethyl substituents in the Mel(4-H-Ph)$_2$Bar(Et)$_2$ complex. The top melamine belongs to tape B in Figure 4, the barbital to tape F, and the bottom melamines to tape G.

Table 2. Intratape Measurements[a]

	X in Mel(4-X-Ph)$_2$Bar(Et)$_2$						
	H	F[b]	Cl	Br[c]	I	CH_3	CF_3
intermolecular distance, *d* (Å)	4.45	3.70 4.14	3.70	3.85 4.30	4.38	4.25	4.33
intramolecular distance, *d'* (Å)	5.53	6.34 5.76	6.32	6.09 5.59	5.47	5.69	5.48
d + *d'* (Å)	9.98	10.04 9.90	10.02	9.94 9.89	9.85	9.94	9.81
van der Waals diameter of X (Å)	2.40	2.94	3.50	3.70	3.96	4.44[d]	5.46[d]

[a] See Figure 13 for depictions of parameters. [b] There are two melamines in the asymmetric unit of this complex. [c] The first and second lines give the values for the form I and form II polymorphs, respectively. [d] The diameters listed for CH_3 and CF_3 are calculated assuming a circular cross section for these groups. The value for CF_3 is therefore approximately 1.1 Å greater than *d*, but since a fluorine of one CF_3 group may be able to cogwheel with two fluorines on an adjacent group, steric repulsion is not necessarily as large as these diameters imply.

reaction, the stored material was stirred with dry diethyl ether (about 10 mL/g), the slurry was filtered at reduced pressure, and the solvent was removed by rotary evaporation at aspirator pressure to yield pure aminodichlorotriazine.

General Procedure for Synthesis of 2-Amino-4,6-bis(arylamino)-1,3,5-triazines (*N,N'*-Diphenylmelamines). Method A.[37] A 0.1 M solution of 2-amino-4,6-dichloro-1,3,5-triazine was prepared in freshly distilled THF and heated to 40–50 °C in an oil bath. To the solution in the oil bath was added a THF solution of 1 equiv of the desired aniline (0.1 M) and 1 equiv of diisopropylethylamine (DIEA) via a dropping funnel over the course of about 30 min with magnetic stirring. Conversion to the 2-amino-4-anilino-6-chloro-1,3,5-triazine was usually complete by the end of the addition, as shown by TLC, but heating could be continued as necessary until the reaction was complete. At that point, another equivalent of aniline was added, along with another of DIEA, in THF. The temperature of the heating bath was raised to about 100–105 °C. As the THF boiled off, 2:1 dioxane/H_2O was added to keep the amount of solvent approximately constant, and a reflux condenser was attached. Reaction was usually continued for 3–5 h at 100–105 °C, but it could be prolonged as necessary, while the progress of the reaction was monitored by TLC. At completion, the reaction was cooled and poured into about 150–200 mL of H_2O. The precipitated product was collected by vacuum filtration. After being dried under vacuum at 0.1 Torr, the melamine was purified by flash chromatography on silica gel.

Method B.[37] A 0.1 M solution of cyanuric chloride was prepared in freshly distilled THF and cooled in an ice–water bath. A THF solution of 1 equiv of the desired aniline (0.1 M) and 1 equiv of DIEA was added via a dropping funnel over the course of 15–30 min with magnetic stirring. When the addition was complete, the mixture was allowed to warm to room temperature, and stirring was continued for another hour. The mixture was then heated to 40–50 °C in an oil bath, and another equivalent of aniline and base was added. Heating was continued for several hours, or until TLC showed no further change. At this stage, the intermediate 2-chloro-4,6-diamino-1,3,5-triazine was usually pure enough, as determined by TLC, that it could be isolated by filtering the reaction mixture and removing solvent by rotary evaporation at aspirator pressure. The crude product was usually used directly in the next step. Flash chromatography on silica could be performed if necessary.

The 2-chloro-4,6-diamino-1,3,5-triazine (dissolved in ~5–8 mL of dioxane or THF) and a magnetic stirrer were placed in a 15-mL pressure bottle. Approximately 3–5 mL of 30% NH_4OH was added, and the bottle was capped and heated (CAUTION: **behind a safety shield**) to 100–105 °C in an oil bath. Heating was continued for 5–8 h, after which the vial could be cooled and opened to monitor reaction progress by TLC. If an unacceptable amount of starting material remained, an additional aliquot of 30% NH_4OH (2–3 mL) was added, and the vial was recapped and reheated as necessary. When reaction was judged to be complete, the solution was poured into 150–200 mL of H_2O, and the precipitated product was collected by vacuum filtration. After drying under vacuum at 0.1 Torr, the crude melamine was purified by flash chromatography on silica gel.

The following summary lists the melamine (X in Mel(4-X-Ph)$_2$), the method used, and the melting point of the product: H, A, 214–6 °C (lit. mp 219–20 °C[37]); F, B, 191–3 °C dec; Cl, B, 202–4 °C; Br, A, 243–5 °C dec; I, B, 267–70 °C dec; CH_3, A, 282–4 °C dec (lit. mp 289–90 °C[38]); CF_3, B, 218–9 °C. For spectroscopic details and elemental analyses on new compounds, see the supplementary material.

Preparation of Complexes. Equimolar amounts of the melamine and barbital were dissolved together (in one flask) in THF. The solvent was removed by rotary evaporation at aspirator pressure, and the composition of the complex was checked by ^{1}H NMR spectroscopy. If integration of peaks indicated that one component was present in excess, the other component was added to bring their ratio to 1:1. The melting points of the complexes were as follows: Mel(4-H-Ph)$_2$Bar(Et)$_2$, 234–237 °C; Mel(4-F-Ph)$_2$Bar(Et)$_2$, 238–243 °C dec; Mel(4-Cl-Ph)$_2$Bar(Et)$_2$, 268–270 °C; Mel(4-Br-Ph)$_2$Bar(Et)$_2$ (form I), 272–275 °C dec, (form II),

(37) This preparation is a modification of that found in: Kaiser, D. W.; Thurston, J. T.; Dudley, J. R.; Schaefer, F. C.; Hechenbleikner, I.; Holm-Hansen, D. *J. Am. Chem. Soc.* **1951**, *73*, 2984.

(38) Honda, I. *Yuki Gosei Kagaku Kyokaishi* **1962**, *20*, 460; *Chem. Abstr.* **1963**, *58*, 4568c.

UM00012519
NOVARTIS EXHIBIT 1017
Novartis v. Regents, IPR2023-01346
Page 1265 of 4460

278–280 °C dec; Mel(4-I-Ph)$_2$·Bar(Et)$_2$, 280–283 °C dec; Mel(4-CH$_3$-Ph)$_2$·Bar(Et)$_2$, 270–277 °C dec; Mel(4-CF$_3$-Ph)$_2$·Bar(Et)$_2$, 264–266 °C. The melting point of barbital is 190–192 °C.

Crystallization of Complexes. A. **Mel(4-H-Ph)$_2$·Bar(Et)$_2$.** Crystals were grown by room-temperature evaporation of a solution of the complex in CH_2Cl_2 in a 1-dram screw-top vial with the lid resting on top of the vial.

B. **Mel(4-F-Ph)$_2$·Bar(Et)$_2$, Mel(4-CH$_3$-Ph)$_2$·Bar(Et)$_2$, and Mel(4-CF$_3$-Ph)$_2$·Bar(Et)$_2$.** Crystals were grown by allowing a solution of the complex in boiling CH_3CN, MeOH, or 2:1 pyridine/H_2O, respectively, to cool over the course of at least 24 h to room temperature by enclosing it in a corked Dewar flask.

C. **Mel(4-Cl-Ph)$_2$·Bar(Et)$_2$, Mel(4-Br-Ph)$_2$·Bar(Et)$_2$ (both forms), and Mel(4-I-Ph)$_2$·Bar(Et)$_2$.** Crystals were grown by room-temperature evaporation of a solution of the complex in CH_3OH in a 5-mL screw-top vial with the lid resting on top of the vial.

X-Ray Crystallography. For details of X-ray data collection and structure solution and refinement, see the supplementary material. Data were collected on complexes Mel(4-H-Ph)$_2$·Bar(Et)$_2$ and Mel(4-CH$_3$-Ph)$_2$·Bar(Et)$_2$ at Harvard on a Siemens P3 diffractometer. Data on the other complexes were collected by Molecular Structure Corporation, The Woodlands, TX, on a Rigaku AFC5R diffractometer equipped with a rotating anode generator. All structures were solved and refined at Harvard using the Siemens SHELXTL-PLUS package of programs.

Acknowledgment. We acknowledge the support of the National Science Foundation through Grants CHE-91-22331, to G.M.W., DMR CHE-89-20490, to the Harvard University Materials Research Laboratory, and CHE-80-00670, for the purchase of the Siemens X-ray diffractometer. J.C.M. acknowledges the Merck Corporation for financial assistance. We thank Professor Jack Dunitz for helpful comments, especially concerning polymorphism.

Supplementary Material Available: Techniques of crystallization, experimental details for substituted diphenylmelamines, table of hydrogen bond lengths, table of intermolecular contacts, crystallographic details including tables of atomic positional parameters and bond lengths and angles (134 pages); tables of observed and calculated structure factors (108 pages). This material is contained in many libraries on microfiche, immediately follows this article in the microfilm version of the journal, and can be ordered from the ACS; see any current masthead page for ordering information.

UM00012520
NOVARTIS EXHIBIT 1017
Novartis v. Regents, IPR2023-01346
Page 1266 of 4460

Investigations into the Robustness of Secondary and Tertiary Architecture of Hydrogen-Bonded Crystalline Tapes

Jonathan A. Zerkowski, John C. MacDonald, and George M. Whitesides*

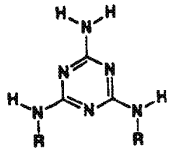
Department of Chemistry, Harvard University, Cambridge, Massachusetts 02138

*Received May 6, 1994. Revised Manuscript Received June 10, 1994**

Five crystal structures of hydrogen-bonded complexes (*N*-(*p*-iodophenyl)-*N'*-(*p*-cyanophenyl)-melamine·barbital, *N,N'*-diphenylmelamine·5,5-dimethylbarbituric acid, 2-amino-4-((*m*-bromophenyl)amino)-6-chloro-1,3,5-triazine·barbital, melamine·5,5-dibromobarbituric acid, and melamine·barbituric acid) are presented. These particular components represent perturbations on the molecules that were previously used to construct crystallographic hydrogen-bonded tapes (Zerkowski, J. A.; MacDonald, J. C.; Seto, C. T.; Wierda, D. A.; Whitesides, G. M. *J. Am. Chem. Soc.* **1994**, *116*, 2382). Four of the complexes pack in the solid state as linear tapes, while the diphenylmelamine·dimethylbarbituric acid complex packs as a crinkled tape due to the closer stacking of tapes permitted by the small methyl substituents. The triad of hydrogen bonds that forms tapes is apparently robust to this sort of variation, even though some of the substituents introduce noncovalent intertape interactions, such as halogen–nitrogen contacts, ionic forces, and other hydrogen bonds. The potential of such intertape interactions for designing crystalline architecture is discussed.

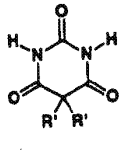
Introduction

To probe the modifiability and robustness of hydrogen-bonded cocrystalline "tapes", we have begun investigating the effects that major structural changes have on the formation and packing of tapes. We have shown that crystalline architecture[1] could be constructed and rationalized from complexes of **1** and **2**. In particular, by varying



1

Mel(R)$_2$

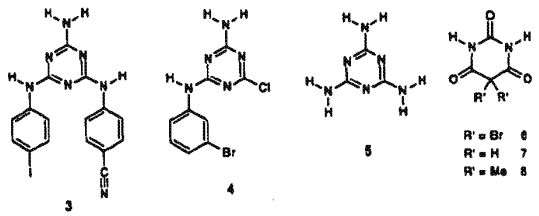


2

Bar(R')$_2$

the steric properties of the substituents R of **1**, we have obtained three structural motifs. When R was a phenyl ring substituted in the para position with CF_3 or a smaller group, we obtained linear tapes.[2] When the para substituent on the phenyl group was CO_2Me,[3] the meta substituent was Cl or Br,[4] or when R was *tert*-butyl,[5] crinkled tapes were obtained. When the para substituent was *tert*-butyl, a pseudo-C_3 cyclic structure (a "rosette") was obtained.[3] **Bar(Et)$_2$** (barbital) has been the barbiturate that we used most frequently, although other substituents on the barbiturate have also generated crystalline tapes.[5]

In the research presented in this paper, we examined the influence of larger variations in the structures of both components on the structure of the 1:1 cocrystals. With an unsymmetrically substituted melamine (**3**, R_1 = *p*-iodophenyl, R_2 = *p*-cyanophenyl), a non-melamine (**4**), *un*substituted melamine (**5**), or significantly truncated substituents on the barbiturate (R' = Br (**6**) or H (**7**)), linear tapes are still obtained. With the seemingly minor perturbation of shortening the ethyl groups of **Bar(Et)$_2$** to methyl groups (**8**), the secondary architecture switched from a linear to a crinkled motif. We were also interested in surveying how substitution patterns of these kinds might be used to control intertape orientation, or tertiary crystalline architecture.



Results

Figures 1–5 are conglomerate pictures of the sort we introduced in previous work. These pictures show several

* Abstract published in *Advance ACS Abstracts*, August 15, 1994.

(1) To analyze the packing of these complexes, we define hierarchical levels of crystalline architecture: the *primary* level is composition and sequence (formation of 1:1 chains or rings with alternation of melamine and barbituric acid components); the *secondary* level consists of the *motif* describing the 1:1 aggregates (for example linear or crinkled tapes and rosettes); the *tertiary* level consists of the organization and packing of the tapes in the crystal (for example, as sheetlike or dimeric structures).

(2) Zerkowski, J. A.; MacDonald, J. C.; Seto, C. T.; Wierda, D. A.; Whitesides, G. M. *J. Am. Chem. Soc.* **1994**, *116*, 2382.

(3) Zerkowski, J. A.; Seto, C. T.; Whitesides, G. M. *J. Am. Chem. Soc.* **1992**, *114*, 5473.

(4) Zerkowski, J. A.; Mathias, J. P.; Whitesides, G. M. *J. Am. Chem. Soc.* **1994**, *116*, 4305.

(5) Zerkowski, J. A.; Whitesides, G. M. *J. Am. Chem. Soc.* **1994**, *116*, 4298.

0897-4756/94/2806-1250$04.50/0 © 1994 American Chemical Society

UM00012521
NOVARTIS EXHIBIT 1017
Novartis v. Regents, IPR2023-01346
Page 1267 of 4460

Table 1. Crystallographic Data[a]

complex	space group	a (Å)	b (Å)	c (Å)	α (deg)[b]	β (deg)[b]	γ (deg)[b]	R[c]	C_k[cd]	density (g/cm³)[e]	crystallization solvent
Mel(*p*-I-Ph)(*p*-CN-Ph)·Bar(Et)₂	*Fdd2*	30.603	35.760	9.711				0.052	0.68	1.534	EtOH
4·Bar(Et)₂	*P*$\bar{1}$	7.424	9.944	13.599	97.34	91.25	95.41	0.059	0.72	1.625	MeOH
Mel·Bar(Br)₂	*Ccm2₁*	7.207	9.740	17.072				0.035	0.81	2.284	H_2O
MelH⁺·BarH⁻	*Ccc2*	5.052	12.221	15.742				0.045	0.79	1.737	H_2O
Mel(Ph)₂·Bar(Me)₂	*P2₁/a*	9.295	16.911	13.520		96.16		0.058	0.70	1.366	MeOH

[a] The underlined cell dimensions represent the repeat distance in a linear tape. [b] A blank indicates that the angle is constrained to be 90°. [c] This value is the crystallographic reliability index, $R = \sum|(F_o - F_c)|/\sum F_o$. [d] This value is the packing coefficient based on molecular volumes calculated using MacroModel (see Results). For a comparison of our modified, MacroModel-derived C_k* values to "classical" C_k values, see ref 2. [e] Calculated.

different views of the packing of the complexes. Table 1 lists crystallographic data and some geometric parameters describing the packing of tapes.

N-(*p*-Iodophenyl)-N′-(*p*-cyanophenyl)melamine·Barbital, Mel(*p*-I-Ph)(*p*-CN-Ph)·Bar(Et)₂ (Figure 1). This complex was investigated to determine whether interactions between iodine and nitrile groups could be used to guide the formation of tertiary architecture. Although –CN and –I have similar linear sizes,[6] the crystal is well ordered with alternating nitrile and iodide moieties along the edge of each tape.[7] Despite abundant evidence for interaction between nitrile groups and the halogen atoms of organic iodides and bromides in the solid state,[8] neither linear nor lateral I- - -NC contacts is important. The closest I- - -N distance involving nitrile groups is that occurring intermolecularly between adjacent melamines within a tape, with a magnitude of 4.0 Å (Σ_{vdW} ~ 3.5 Å).[9] There is, however, a contact at 3.4 Å between perpendicular tapes involving an iodine in tape A in Figure 1 and an NH_2 nitrogen of a melamine in tape B (see Figure 6 for a closeup view of this contact).[10] There are no iodine–iodine contacts.

***N,N′*-Diphenylmelamine·5,5-Dimethylbarbituric Acid, Mel(Ph)₂·Bar(Me)₂ (Figure 2).** We investigated this complex to study the influence that the protruding ethyl groups of $Bar(Et)_2$ exert on the packing of tapes. Although we assumed that the replacement of ethyl with methyl groups would have no effect on the secondary architecture, the complex packs as a crinkled tape, rather than the linear tape observed for **Mel(Ph)₂·Bar(Et)₂**.[2] One of the phenyl groups is almost coplanar with the melamine ring, while the other is more twisted out of the plane (torsion angles 11° and 28°, respectively). With no substituents extending very far out of the hydrogen-bonded plane of the tape (relative to tapes with ethyl groups or phenyl groups with larger torsion angles), these crinkled tapes appear "flat" (see the end-on view in Figure 2) and can stack closely on top of each other. Conversely, there are no contacts between adjacent stacks of tapes (e.g., between tapes B and C in Figure 2). There are two intratape CH- - -O contacts under the sum of the van der Waals radii (~2.7 Å).[9] One involves an ortho proton on the nearly in-plane phenyl ring and the neighboring barbituric acid. The other contact involves a meta proton on the other, more twisted phenyl ring and the barbituric acid three units away in the tape (see the top of Figure 2). Both H- - -O distances are ~2.55 Å.

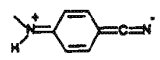
2-Amino-4-((*m*-bromophenyl)amino)-6-chloro-1,3,5-triazine·Barbital, 4·Bar(Et)₂ (Figure 3). This melamine analogue (a triazine) was chosen primarily because it has only two amine groups. Chlorine is one of many substituents that might go in the remaining ring position, and the *m*-bromophenyl ring fortuitously gave good crystals; neither of these substituents was chosen to test a specific hypothesis. The linear tape motif is preserved, even though one hydrogen bond has been deleted relative to complexes constructed from melamines. The chlorine and oxygen that occupy the space of the former hydrogen bond are just at van der Waals contact (distance = 3.3 Å, Σ_{vdW} = 3.3 Å). With the removal of one of the NHR groups, the phenyl group of the remaining NHR has room to lie almost coplanar with the triazine ring: the mean planes of the two rings differ by only approximately 3°. Due to this orientation of the phenyl ring, one *ortho*-hydrogen is positioned close to a barbital oxygen at 2.5 Å.

Melamine·5,5-Dibromobarbituric Acid, Mel·Bar(Br)₂ (Figure 4). This substituted barbituric acid (and barbituric acid itself, Figure 5) was examined to determine the influence of replacing the ethyl groups of barbital by smaller but more polarizable and/or reactive substituents. The bromine atoms of **Bar(Br)₂** are involved in several intertape contacts with nitrogen atoms of melamine at 2.7 and 2.8 Å (Σ_{vdW} = 3.4 Å, see Figure 7 for a closeup view). These intertape interactions are reflected in the high value of C_k* (Table 1).

Melamine·Barbituric Acid, MelH⁺·BarH⁻ (Figure 5). Proton transfer from the CH_2 of barbituric acid to a ring nitrogen of melamine has occurred. This complex

(6) The C_{phenyl}–I bond length in this structure is 2.09 Å; the C_{phenyl}–N distance (skipping over the nitrile carbon) is 2.52 Å.

(7) The bond lengths of the cyanophenyl group do not indicate a significant contribution from the dipolar quinonoid resonance structure i. In particular, the HN-C_{phenyl} bond (1.418 Å) is unchanged from the analogous bonds we have observed in other para substituted diphenylmelamines, which ranged from 1.389 to 1.441 Å.[2]



i

(8) For a review of halogen–nitrile interactions, see: Desiraju, G. R.; Harlow, R. L. *J. Am. Chem. Soc.* 1989, *111*, 6757. Carter, V. B.; Britton, D. *Acta Crystallogr.* 1972, *B28*, 945. Britton, D. *Persp. Str. Chem.* 1967, *1*, 109. For general halogen–nitrogen contacts, see: Xu, K.; Ho, D. M.; Pascal, R. A., Jr. *J. Am. Chem. Soc.* 1994, *116*, 105.

(9) The van der Waals radii we are using are isotropic: H 1.20 Å; C 1.70 Å; N 1.55 Å; O 1.52 Å; F 1.47 Å; Cl 1.75 Å; Br 1.85 Å; I 1.98 Å. Bondi, A. *J. Phys. Chem.* 1964, *68*, 441.

(10) Intuition suggests that the van der Waals radius of an atom should be dependent, to some extent, upon its hybridization state and the identity of the atoms to which it is covalently attached. There is evidence supporting this idea: Bondi[9] cites data purporting that the nitrogen in a nitrile group has a van der Waals radius of 1.4 Å parallel to the CN axis and 1.7 Å perpendicular to it. Some interesting work has appeared on anisotropic van der Waals radii suggesting that halogens in particular undergo "polar flattening" parallel to the C–X axis and expansion perpendicular to it: Nyburg, S. C.; Faerman, C. H. *Acta Crystallogr.* 1985, *B41*, 274, and Nyburg, S. C.; Faerman, C. H.; Prasad, L. *Acta Crystallogr.* 1987, *B43*, 106. Nonetheless, many solid-state chemists seem to prefer Bondi's isotropic radii as simple, consistent (and successful) approximations, in the absence of comprehensive studies of different hybridization classes of each element. For a discussion, see: Desiraju, G. R. *Crystal Engineering: The Design of Organic Solids*; Elsevier: New York, 1989.

UM00012522
NOVARTIS EXHIBIT 1017
Novartis v. Regents, IPR2023-01346
Page 1268 of 4460

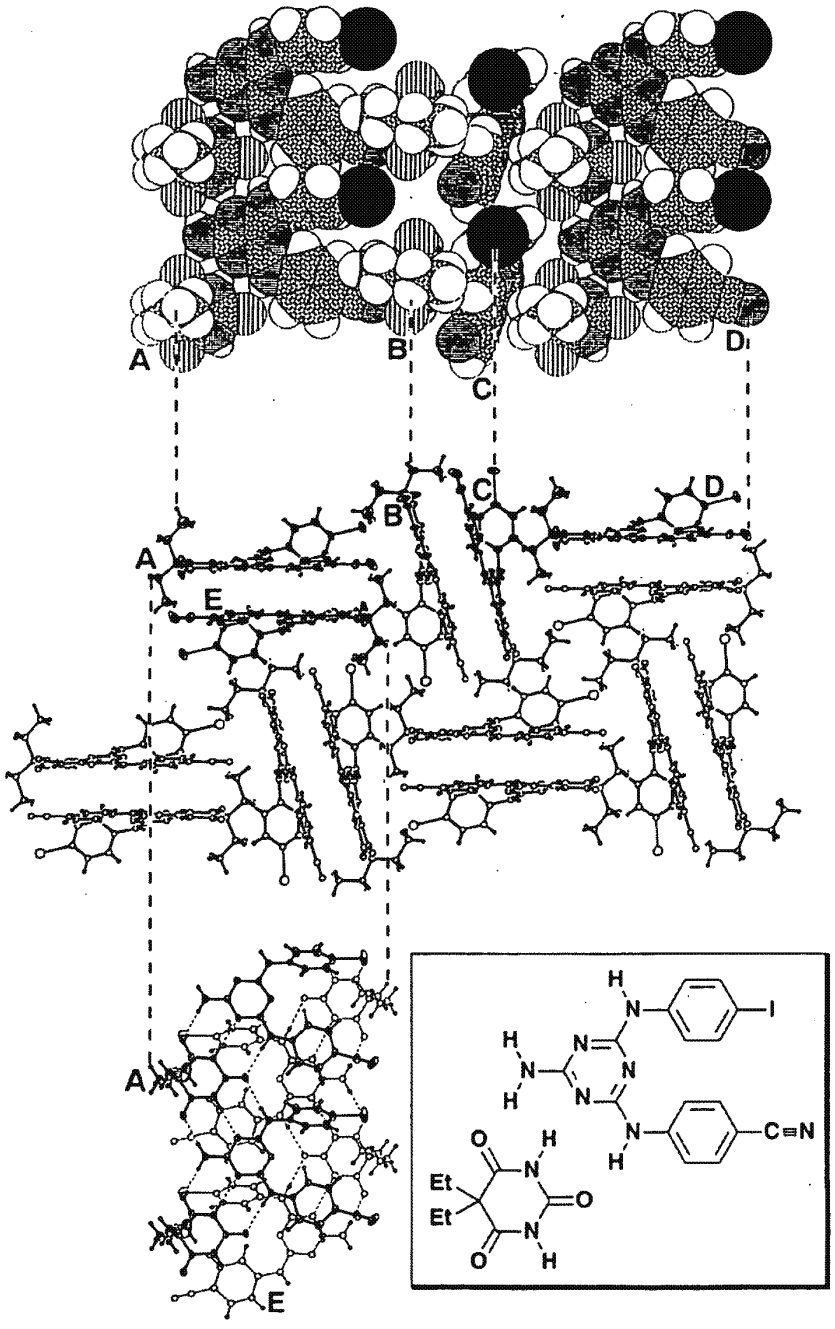


Figure 1. Views of the **MeI(*p*-I-Ph)(*p*-CN-Ph)·Bar(Et)$_2$** complex.

also has a high value of C_k*. The crystallographically infinite hydrogen-bonded axes of the tapes are parallel within a stack of tapes, but adjacent stacks are twisted by 78° with respect to each other. This structure is the first in which we have observed nonparallel tapes.

Packing Fractions. The values of C_k*[11] for the complexes incorporating **Bar(Br)$_2$** and **BarH$^-$** are higher than normal for organic molecular crystals.[12] The value for **MeI·Bar(Br)$_2$** is the highest we have observed in any tape. This increase in the efficiency of space filling is probably due to two factors. The first is the presence of

(11) $C_k = NV_{mol}/V_{cell}$, where N is the number of molecules in a unit cell, V_{mol} is the molecular volume, and V_{cell} is the volume of the unit cell. Kitaigorodsky, A. I. *Organic Chemical Crystallography*; Consultants Bureau: New York, 1961. For a discussion of the relationship between our modified C_k* values and traditionally calculated C_k values, see ref 2.

(12) Values of C_k usually range from roughly 0.65 to 0.77: Desiraju, G. R. *Crystal Engineering: The Design of Organic Solids*; Elsevier: New York, 1989; Chapter 2. Some of the highest values listed by Kitaigorodsky[11] are 0.785 (*p*-quaterphenyl), 0.781 (1,2-anthraquinone), and 0.805 (perylene). The value for graphite is 0.887, which can probably be considered an effective upper limit.

UM00012523
NOVARTIS EXHIBIT 1017
Novartis v. Regents, IPR2023-01346
Page 1269 of 4460

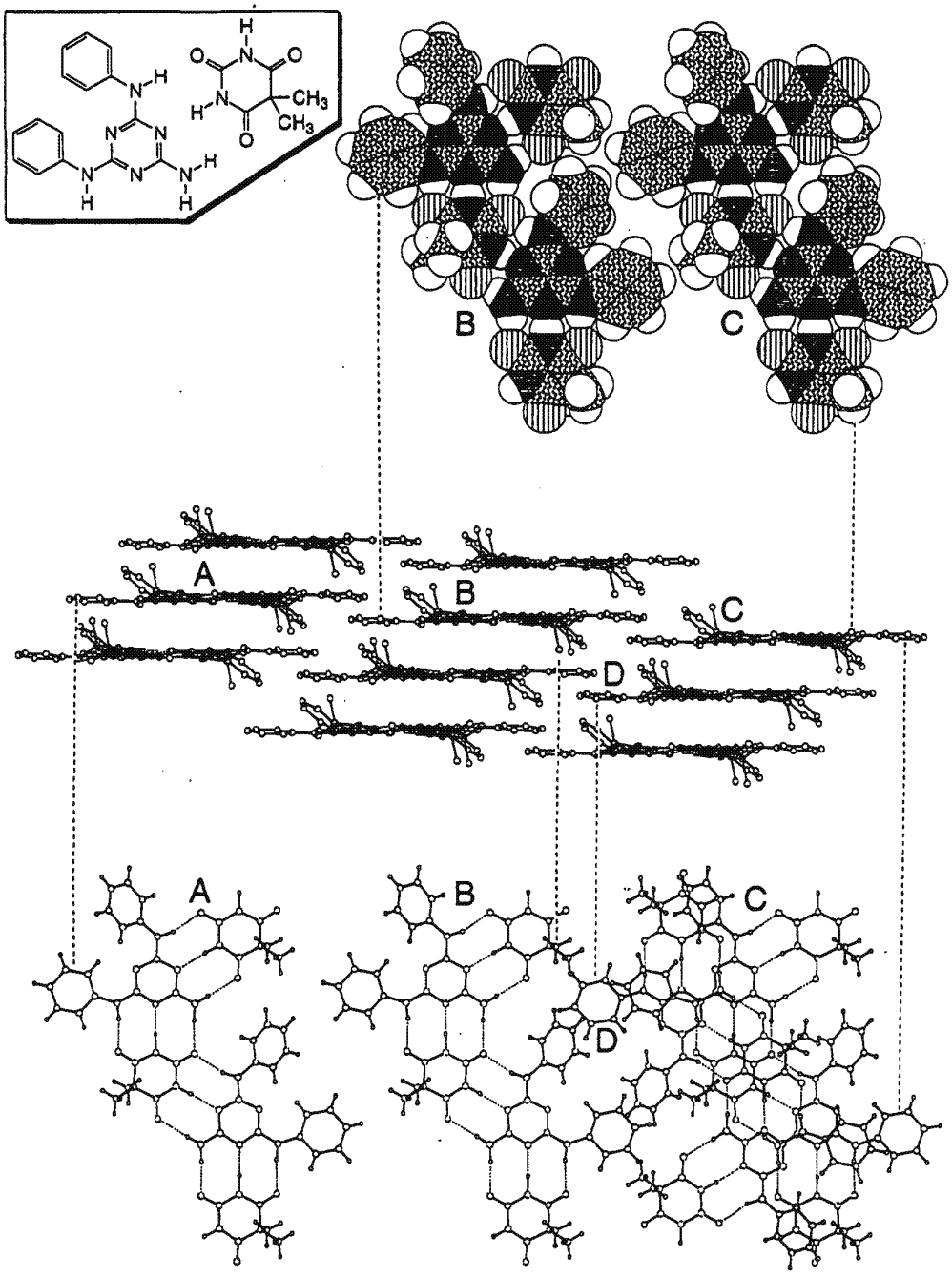


Figure 2. Views of the **MeI(Ph)$_2$·Bar(Me)$_2$** complex. Hydrogen atoms have been omitted from the central, end-on view for clarity.

strong electrostatic intertape forces such as those between bromine and nitrogen atoms in **MeI·Bar(Br)$_2$** and the ionic interactions in **MeIH$^+$·BarH$^-$**. Ionic interactions in crystals of the latter compound cause them to have a high density (1.737 g/cm^3) for a material containing only C, H, O, and N.[13] The second factor is geometric: the individual molecules are flatter than melamines and barbiturates substituted with phenyl or ethyl groups; this shape allows the tapes to stack with little empty space between them.

Discussion

The complex of **MeI(*p*-I-Ph)(*p*-CN-Ph)** with **Bar(Et)$_2$** was investigated because it represented a preliminary experiment in the control of tertiary architecture. We hypothesized that this complex might pack analogously to the **MeI(*p*-I-Ph)$_2$·Bar(Et)$_2$** complex (Figure 8).[2] There were extensive I- - -I contacts between tapes in that complex; we thought that replacing one iodine with a nitrile group would allow for virtually isostructural packing and

UM00012524
NOVARTIS EXHIBIT 1017
Novartis v. Regents, IPR2023-01346
Page 1270 of 4460

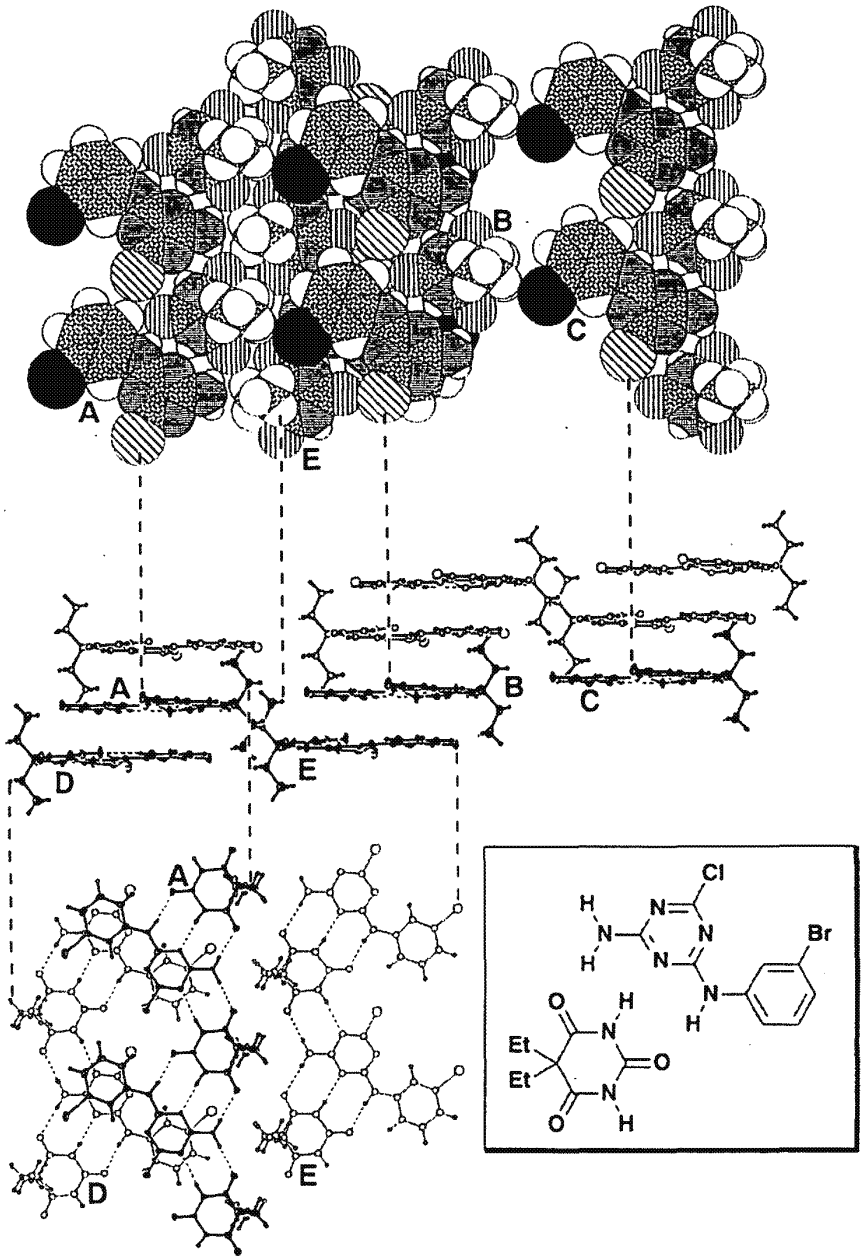


Figure 3. Views of the 4·**Bar(Et)$_2$** complex.

the introduction of I- - -CN interactions.[7,14] Instead, a different kind of packing arrangement occurred, namely, the head-to-tail dimeric orientation of tapes that we have observed in many complexes.[2,4] In this structure, an iodine- - -nitrogen interaction different from the one we expected was formed (Figure 6). This contact, which is only about 0.1 Å under the sum of van der Waals radii, is probably weak, but it may help to stabilize the perpendicular orientation of tapes.[15,16] The intended packing arrangement shown at the bottom of Figure 8 may have

(13) Extensive hydrogen bonding in the solid state can lead to high densities in organic crystals. For example, the density of cyanuric acid is 1.82 g/cm^3 (Dietrich, H.; Scheringer, C.; Meyer, H.; Schulte, K.-W.; Schweig, A. *Acta Crystallogr.* 1979, *B35*, 1191); oxalic acid = 1.91 g/cm^3 (Derissen, J. L.; Smit, P. H. *Acta Crystallogr.* 1974, *B30*, 2240); oxamide = 1.67 g/cm^3 (Ayerst, E. M.; Duke, J. R. C. *Acta Crystallogr.* 1954, *7*, 588); octahydroxycyclobutane = 1.98 g/cm^3 (Bock, C. M. *J. Am. Chem. Soc.* 1968, *90*, 2748); squaric acid = 1.90 g/cm^3 (Semmingsen, D.; Hollander, F. J.; Koetzle, T. F. *J. Chem. Phys.* 1977, *66*, 4405).

(14) We have previously observed an iodine-nitrile interaction in the *N,N'*-bis(*m*-iodophenyl)melamine-barbital-acetonitrile crystalline solvate.[4]

(15) Since the iodine atoms in the **Mel(*p*-I-Ph)$_2$-Bar(Et)$_2$** complex were involved in interactions among themselves, they did not engage in short contacts with nitrogen in that complex.[2]

(16) We have not searched for polymorphs of this complex (nor of any of the structures presented in this paper); other packing arrangements, perhaps even the proposed one shown in Figure 8, could of course occur for this complex.

UM00012525
NOVARTIS EXHIBIT 1017
Novartis v. Regents, IPR2023-01346
Page 1271 of 4460

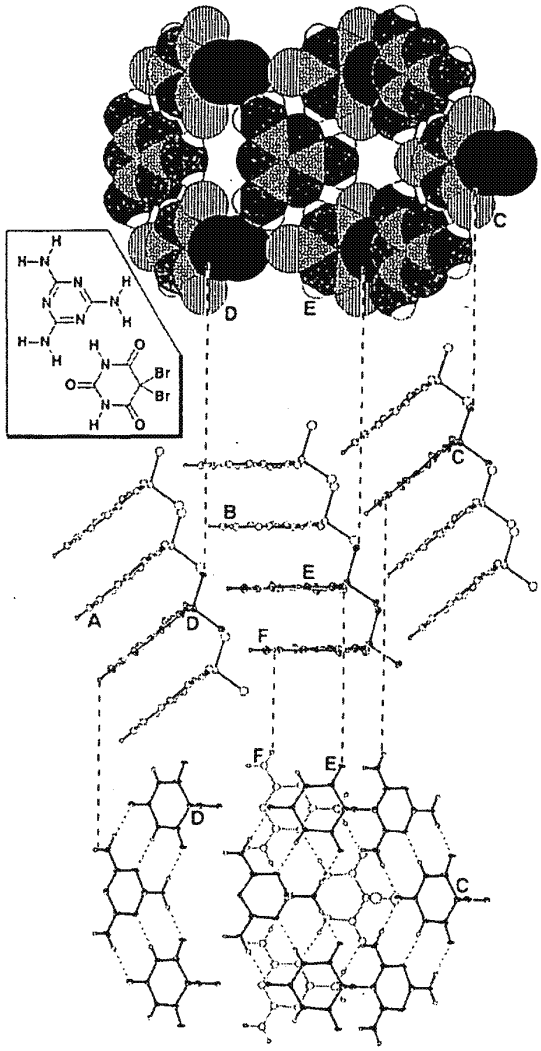


Figure 4. Views of the **Mel·Bar(Br)$_2$** complex. The extensive Br- - -N interactions have been omitted from all these views for clarity; see Figure 7 for a closeup of these interactions.

failed to form because the strong dipoles of the nitriles would have been too close to each other in an unfavorable head-to-head orientation.[17]

The difference between hypothesized and observed structures emphasizes that it is still difficult to predict solid-state structures, even when the prediction is based on a relatively modest change to a known structure.

The hypothesis motivating our study of the **Mel-(Ph)$_2$·Bar(Me)$_2$** complex was that small alkyl substituents on the barbiturate component would permit close stacking of tapes. The **Mel(Ph)$_2$·Bar(Et)$_2$** complex packs as linear tapes, its tertiary architecture consisting of dimers of tapes arranged in a herringbone pattern.[2] We suspected that replacement of ethyl groups with methyl groups might alter this dimer-based packing to a sheetlike arrangement, similar to that observed in **4·Bar(Et)$_2$** (Figure 3) or **Mel·Bar(Br)$_2$** (Figure 4), where all the tape backbones in a given stack are parallel.

(17) Gavezzotti, A. *J. Phys. Chem.* 1990, *94*, 4319.

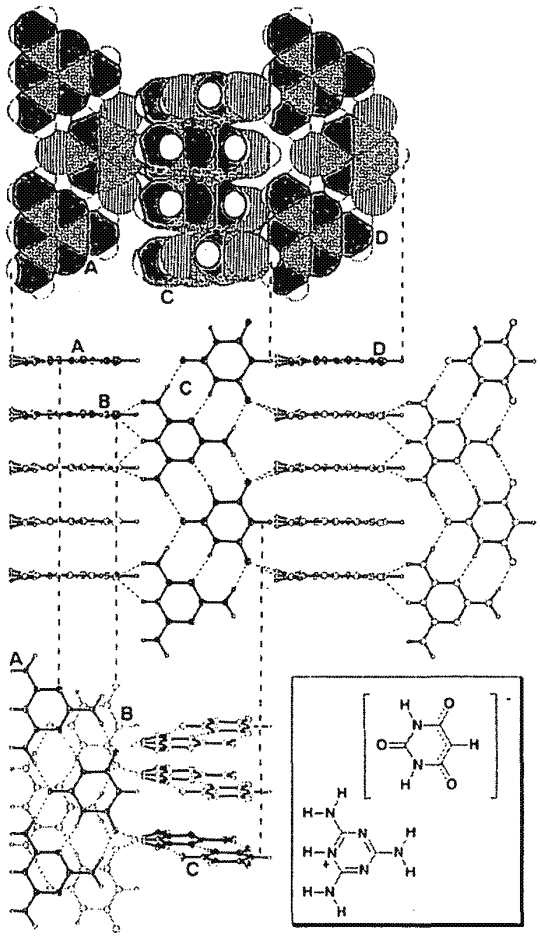


Figure 5. Views of the **MelH$^+$·BarH$^-$** complex.

While the crinkled tape that resulted does display some of the close-stacking features that small barbiturate substituents should allow, the crossover to a crinkled motif was entirely unexpected. On closer examination, however, the factors that favor adoption of a crinkled motif become clearer. One of the phenyl rings of **Mel(Ph)$_2$** is nearly coplanar to the triazine ring. It thus protrudes into the region of space that phenyl groups on a neighboring melamine in a linear tape would need to occupy. The flat, in-plane orientation of this phenyl group is favored by stacking interactions between two tapes (e.g., C and D in Figure 2) involving both the heterocyclic, hydrogen-bonded backbone rings and the aromatic substituents. The intended close stacking of tapes arising from a reduction in the ratio of alkyl to aryl surface area has therefore occurred, but maximal close packing of flat, aromatic and heterocyclic surfaces at the *tertiary* level is apparently energetically favorable enough to dictate the motif of *secondary* architecture that is adopted.

The **4·Bar(Et)$_2$** complex was investigated to see if 3-fold hydrogen bonding is essential to the construction of cocrystalline tapes between barbiturates and derivatives of triazines. Evidently, it is not. We do not know if the approach of the chlorine to the oxygen atom is energetically favorable or repulsive. If repulsive, it is apparently not strong enough to overwhelm the favorable tape-forming

UM00012526
NOVARTIS EXHIBIT 1017
Novartis v. Regents, IPR2023-01346
Page 1272 of 4460

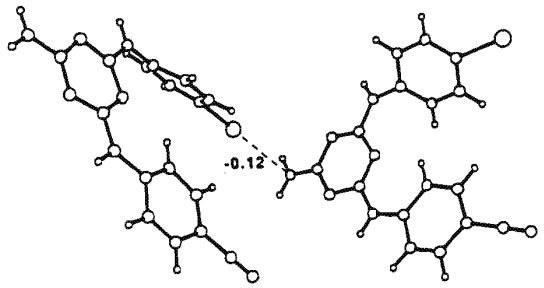


Figure 6. Closeup of the iodine-nitrogen interaction between two perpendicular melamines in **MeI(*p*-I-Ph)(*p*-CN-Ph)·Bar(Et)$_2$**. The melamine on the left belongs to tape A in Figure 1; the melamine on the right belongs to tape B. The number adjacent to the dashed line that indicates this interaction represents the value of the distance of the contact minus the sum of the van der Waals radii (in angstroms).

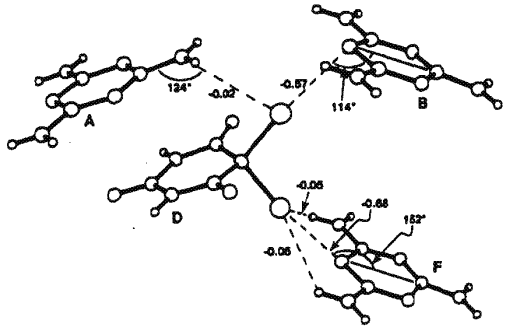


Figure 7. Closeup of the intermolecular interactions involving bromines in **MeI·Bar(Br)$_2$**. The letters indicate to which tape in Figure 4 the molecules belong. The numbers adjacent to the dashed lines that indicate these interactions represent the value of the distance of the contact minus the sum of the van der Waals radii (in angstroms). The hydrogen atoms were placed in calculated positions for crystallographic refinement, with a N–H bond length of 0.9 Å.

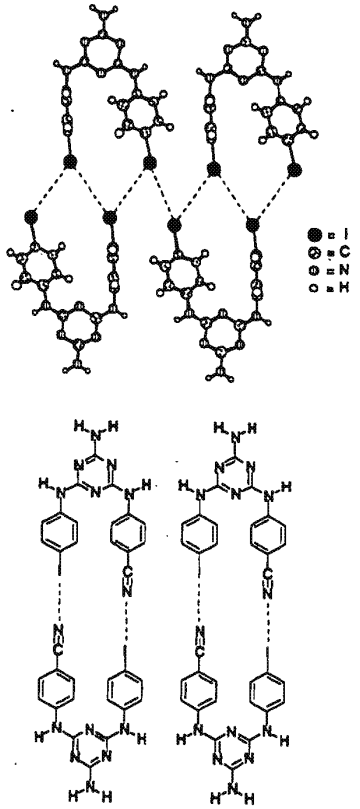


Figure 8. Back-to-back orientations of two tapes linked by noncovalent interactions between substituents in the para positions of the diphenylmelamines. At the top is the *observed* structure of the **MeI(*p*-I-Ph)$_2$·Bar(Et)$_2$** complex.[3] At the bottom is the *hypothetical* structure that we predicted (incorrectly) might result by replacing one iodine with a nitrile group. The observed structure is given in Figure 1.

hydrogen bonds.[18] In a structural sense, we have "mutated" the symmetrically substituted melamine component that we have usually employed for constructing tapes into this kind of chlorotriazine by replacing one NHR group (R = alkyl or aryl) with a chlorine atom.[19] As a result, an indentation or hole has been generated along the periphery of the linear tape (see Figure 3).[20] Note that a nearly coplanar orientation of the bromophenyl and triazine groups can be accommodated by the linear motif when the other substituent on the triazine ring is small (chlorine in 4 compared to NHPh in **MeI(Ph)$_2$**).

The key feature of both complexes incorporating melamine is that some of the hydrogen-bonding sites of the melamine remain unutilized by the formation of linear tapes. That is, one edge of the planar melamine molecule, representing a donor–acceptor–donor triad (HN–N–NH), is uncomplexed. It is therefore free to engage in intertape interactions that can direct tertiary architecture. The occurrence of several close contacts involving bromine and nitrogen atoms in the **Bar(Br)$_2$** complex (Figure 7) is due to the availability of these melamine sites for participation in electrostatic interactions.[8]

In the **MeIH$^+$·BarH$^-$** complex, the uncomplexed state of one ring nitrogen of melamine permits proton transfer from the CH_2 group of barbituric acid. Protonation creates ionic interactions between **MeIH$^+$** and **BarH$^-$** both within and between tapes, and the hydrogen-bonding network throughout the crystal is three-dimensional. To maximize the influence that these strong forces can provide and thereby minimize the lattice energy, stacks of the tapes twist with respect to each other. This crystal structure is the only one in which we have observed tapes with nonparallel axes. We hypothesize that in the absence of such strong intertape forces, the arrangement of tapes that permits the closest possible packing (reflected in a high C_k*) is one in which the hydrogen-bonded axes of all tapes are parallel.

Conclusions

The crystal structures presented in this paper demonstrate that hydrogen-bonded cocrystalline tapes are robust to a wide range of structural variations. Even variations that preclude formation of the full triad of hydrogen bonds, such as replacement of a melamine by a chlorotriazine, do

(18) The retention of the *linear* motif cannot be ascribed to the Cl···O contact, since a crinkled tape or a rosette would also contain this contact.
(19) In a synthetic sense, the transformation is in the opposite direction: the chlorotriazine is a precursor to the melamine.
(20) Tapes of this general shape may be useful for inducing back-to-back packing of tapes through a knob-into-hole approach; a protruding substituent, perhaps appended to the para position of the phenyl ring, might dovetail efficiently into the cleft on a neighboring tape.

UM00012527
NOVARTIS EXHIBIT 1017
Novartis v. Regents, IPR2023-01346
Page 1273 of 4460

not disrupt the tape motif. Interactions between tapes involving bromine–nitrogen contacts, ionic forces, or hydrogen bonds can lead to close packing of tapes and to high densities. Intertape stacking interactions appear to be able to cause a switch from a linear to a crinkled motif. This phenomenon runs counter to our previous hypothesis that intratape steric effects are most likely to force adoption of a crinkled motif.[5] On the other hand, we have also noted that electrostatic interactions (e.g., CH- - -O contacts) or the packing of tapes around trapped solvent molecules may play a role in crinkling.[4] The **Mel(Ph)$_2$·Bar(Me)$_2$** complex can be viewed as combining these two effects: the immediate cause leading to crinkling is intratape (secondary) steric repulsion involving flat phenyl groups, but the underlying cause is favorable intertape (tertiary) stacking of these groups and the heterocyclic tape backbones. These initial forays into controlling tertiary architecture show that moieties that are capable of engaging in noncovalent interactions can be appended to the peripheries of tapes. Directing those interactions in a specific manner, however, remains a challenge.

Experimental Section

General Methods. *N*-(*p*-Iodophenyl)-*N'*-(*p*-cyanophenyl)-melamine (**Mel(*p*-I-Ph)(*p*-CN-Ph)**), 2-amino-4-((*m*-bromophenyl)amino)-6-chloro-1,3,5-triazine (**4**), *N,N'*-diphenylmelamine (**Mel(Ph)$_2$**), and 5,5-dimethylbarbituric acid (**Bar(Me)$_2$**) were prepared according to previously published procedures.[2,4,5] The supplementary material contains spectroscopic details and elemental analyses (see paragraph at end of paper). Melamine and dibromobarbituric acid were obtained from Aldrich Chemicals, barbital from Fisher Scientific, and barbituric acid from Alfa Products. Solvents were reagent grade and were used as received without purification.

Crystallizations. Mel(*p*-I-Ph)(*p*-CN-Ph)·Bar(Et)$_2$, 4·Bar(Et)$_2$, and Mel(Ph)$_2$·Bar(Me)$_2$. These 1:1 complexes were prepared according to procedures described previously.[2,4,5] Crystals of the first two complexes were obtained by room-temperature evaporation of solutions of the complexes in ethanol and methanol, respectively, in 1-dram screw-top vials with the lids resting loosely on top of the vials. Crystals of **Mel(Ph)$_2$·Bar(Me)$_2$** were obtained by room-temperature evaporation of a solution of the complex in methanol in a glass beaker with a watchglass resting on top of the beaker.

Mel·Bar(Br)$_2$ and MelH$^+$·BarH$^-$. Solutions of melamine and the barbituric acid (both 0.1 M) were prepared in distilled H_2O and heated on a steam bath. When the temperature of the solutions was approximately 70 °C, they were combined in an Erlenmeyer flask. This flask was loosely capped and was placed in a Dewar flask that contained approximately 25 mL of water that had also been heated to about 70 °C on a steam bath. The Dewar flask was corked and allowed to rest undisturbed for at least 24 h as it cooled to room temperature. Crystals of the complex developed during this cooling period.

X-ray Crystallography. Data on the **Mel(*p*-I-Ph)(*p*-CN-Ph)·Bar(Et)$_2$** and **Mel(Ph)$_2$·Bar(Me)$_2$** complexes were collected on a Rigaku AFC5R diffractometer equipped with a rotating anode generator by Molecular Structure Corp., The Woodlands, TX. Data on the other complexes were collected on a Siemens P3 diffractometer at Harvard. All structures were solved and refined at Harvard using the SHELXTL-PLUS, SHELXS-86, and SHELXL-93 package of programs. For details of data collection, structure solution, and refinement, see the supplementary material.

Acknowledgment. We acknowledge the support of the National Science Foundation through Grants CHE-91-22331 to G.M.W. and CHE-80-00670 to the Department of Chemistry for the purchase of the Siemens X-ray diffractometer. We thank Dr. Derk Wierda for helpful discussions. J.C.M. acknowledges the Merck Corp. for partial support of this work.

Supplementary Material Available: Experimental details for **Mel(*p*-I-Ph)(*p*-CN-Ph)** and **4** and crystallographic details including tables of atomic positional parameters and bond lengths and angles (56 pages); tables of observed and calculated structure factors (36 pages). Ordering information is given on any current masthead page.

UM00012528
NOVARTIS EXHIBIT 1017
Novartis v. Regents, IPR2023-01346
Page 1274 of 4460

New Varieties of Crystalline Architecture Produced by Small Changes in Molecular Structure in Tape Complexes of Melamines and Barbiturates

Jonathan A. Zerkowski, John P. Mathias, and George M. Whitesides*

Contribution from the Department of Chemistry, Harvard University, Cambridge, Massachusetts 02138

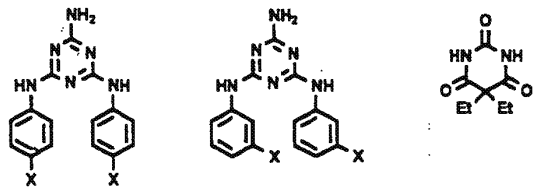
Received October 9, 1992. Revised Manuscript Received March 2, 1994•

Abstract: This paper describes the crystal structures of a series of seven 1:1 complexes between *N,N'*-bis(*m*-X-phenyl)-melamine and 5,5-diethylbarbituric acid (X = H, F, Cl, Br, I, CH_3, and CF_3). This series provides small perturbations on the structures of molecules (*N,N'*-bis(*p*-X-phenyl)melamines) used in a previous study (Zerkowski, J. A.; MacDonald, J. C.; Seto, C. T.; Wierda, D. A.; Whitesides, G. M. *J. Am. Chem. Soc.* In press). Both the *meta* and *para* complexes crystallize as hydrogen-bonded "tapes". With the phenyl substituent in the *meta* position, however, the melamines can adopt a greater number of molecular conformations; this feature leads to a greater variety of orientations of packing. The *meta* series packs in both linear and crinkled tape motifs, and four of the seven complexes are solvates. By contrast, the *para* series, which used the same set of phenyl substituents, always yielded linear tapes and crystals without solvent in the lattice. Inclusion of solvent increases the packing coefficients of members of the *meta* series to values approximately equal to those of the *para* series. The multiplicity of molecular conformations available to the *meta* series is probably largely responsible for the clathration of solvent, which does not rely upon specific non-covalent interactions except in the case of the *m*-iodo complex with acetonitrile. The wider range of crystalline architecture in the *meta* series attests only to the kinetic accessibility of these packing formats; polymorphic phases of greater thermodynamic stability may occur. Polymorphism has not been investigated in the series of *meta*-substituted compounds.

Introduction

To expand our understanding of the physical–organic chemistry of the solid state, we are continuing to develop a system of co-crystallized derivatives of melamine and of barbituric acid.[1–4] Hydrogen bonding between these components affords crystallographically infinite 1:1 solid-state complexes in the form of "tapes" that pack with their long axes parallel. The constrained packing of tapes allows systematic study of the relationships of crystalline architecture to molecular structure. Formation of the triad of hydrogen bonds that links the components of the tapes withstands variation of the substituents at the periphery of the tapes. We have found that steric properties of the substituents can be controlled to induce selectively the formation of three different crystalline motifs: linear tape (for small substituents),[3] crinkled tape (for medium-sized substituents),[2,4] or cyclic pseudo-C_3 "rosette" structures (for large substituents).[2] These motifs can be thought of as abbreviated segments of the infinite hydrogen-bonded sheet structure of the 1:1 complex between cyanuric acid and melamine (CA·M). We have used the network of hydrogen bonds in the CA·M lattice as the conceptual template for the design of crystallographic motifs[1,3] and solution-phase structures.[5,6]

Our most extensive investigations have focused on a series of *para*-substituted diphenylmelamines complexed with 5,5-diethylbarbituric acid (barbital, **Bar(Et)$_2$**).[3] The principal result from that work was that all the tapes were linear when the *para* substituent was CF_3 or smaller.[7] An important inference from X-ray powder diffraction was that polymorphism occurred for some of the complexes.[3,8] In the work reported in this paper, we changed the position of substituents on the phenyl rings of the melamine component of the tapes from *para* to *meta*, so that we could explore a structurally closely related series of compounds. We employed the same set of substituents (H, F, Cl, Br, I, CH_3, and CF_3) in our investigations of both the *para*- and *meta*-substituted series of complexes so that comparisons between the two series could be as straightforward as possible. The barbiturate component was held constant as **Bar(Et)$_2$** in both series.



Mel(*p*-X-Ph)$_2$ **Mel(*m*-X-Ph)$_2$** **Bar(Et)$_2$**

X = H, F, Cl, Br, I, CH_3, CF_3

While these changes in the pattern of substitution on the diphenylmelamines are geometrically well-defined, they are not necessarily *simple*. For example, the number of conformers obtainable by rotation around the *N*-phenyl bond in the melamine, which affects both steric and electrostatic features of the molecules, is greater for the *meta* series than for the *para* series.[9] Thus the orientational options for packing the molecules are substantially more complicated for the *meta*- than for the *para*-substituted compounds.

Our overall aim in this work was to survey the crystalline architecture (either new varieties or modified versions of those

• Abstract published in *Advance ACS Abstracts*, April 1, 1994.

(1) Zerkowski, J. A.; Seto, C. T.; Wierda, D. A.; Whitesides, G. M. *J. Am. Chem. Soc.* **1990**, *112*, 9025.

(2) Zerkowski, J. A.; Seto, C. T.; Whitesides, G. M. *J. Am. Chem. Soc.* **1992**, *114*, 5473.

(3) Zerkowski, J. A.; MacDonald, J. C.; Seto, C. T.; Wierda, D. A.; Whitesides, G. M. *J. Am. Chem. Soc.* **1994**, *116*, 2382.

(4) Zerkowski, J. A.; Whitesides, G. M. *J. Am. Chem. Soc.* Previous paper in this issue.

(5) Seto, C. T.; Whitesides, G. M. *J. Am. Chem. Soc.* **1991**, *113*, 712.

(6) Seto, C. T.; Whitesides, G. M. *J. Am. Chem. Soc.* **1993**, *115*, 1321.

(7) In two complexes with larger substituents (X = CO_2Me and $C(CH_3)_3$), the tapes were sterically forced to adopt either the crinkled or rosette format.[2]

(8) MacDonald, J. C.; Zerkowski, J. A. Unpublished data.

(9) We are describing an effective rotation: when the phenyl groups are adjacent to each other as they are in both linear and crinkled tapes, a *meta* substituent would be expected to hinder rotation around the *N*-phenyl bond relative to a *para* substituent. Different conformations must instead be accessed when the melamine is free in solution (or only partially complexed) and rotation around the *N*-triazine bond has separated the phenyl groups.

0002-7863/94/1516-4305$04.50/0 © 1994 American Chemical Society

UM00012529
NOVARTIS EXHIBIT 1017
Novartis v. Regents, IPR2023-01346
Page 1275 of 4460

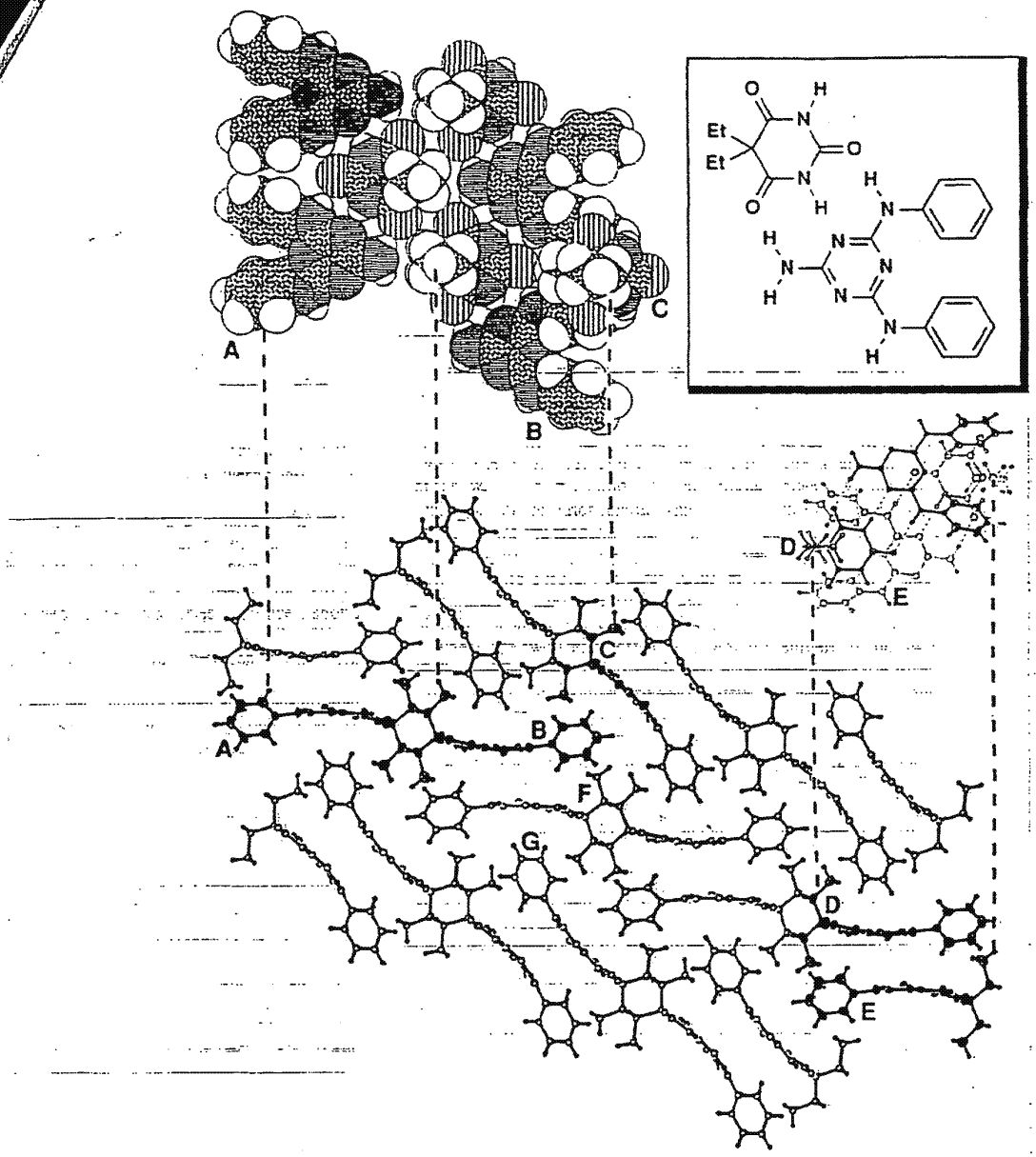


Figure 1. Views of the Mel(Ph)$_2$-Bar(Et)$_2$ complex.

previously observed) in these *meta*-substituted compounds and to establish the types of structural changes that can accompany a relatively small perturbation on molecular structure.

Results

To give an overview of the important packing interactions in these co-crystals, we will continue to use the conglomerate pictures (Figures 2–7) that we introduced in previous papers.[3,4] These pictures show several different views of the structure. The complex in which the phenyl substituent is hydrogen (Figure 1, *N,N'*-diphenylmelamine/barbital, or Mel(Ph)$_2$-Bar(Et)$_2$) was discussed fully in an earlier paper.[3] It is included here for comparison to the *meta* series, since it could be considered a member of either the *meta* or *para* series. Table 1 lists crystallographic data and some geometric parameters describing the packing of tapes.

N,N'-Bis(*m*-fluorophenyl)melamine/Barbital, Mel(*m*-F-Ph)$_2$-Bar(Et)$_2$ (Figure 2). The packing of this complex is similar to that of the Mel(Ph)$_2$-Bar(Et)$_2$ complex, although the arrangement of the phenyl groups is significantly different: the melamine molecule does not sit on a mirror plane as it did in Mel(Ph)$_2$-Bar-(Et)$_2$. One fluorophenyl group is disordered, with 60:40 occupancy of sites related by a 180° rotation of the phenyl ring around the FC$_6$H$_4$–N bond. The corresponding *p*-F complex was also a nonsolvated[10] linear tape, but there were two tapes in its asymmetric unit.

N,N'-Bis(*m*-chlorophenyl)melamine/Barbital and *N,N'*-Bis(*m*-bromophenyl)melamine/Barbital, Mel(*m*-Cl-Ph)$_2$-Bar(Et)$_2$ and Mel(*m*-Br-Ph)$_2$-Bar(Et)$_2$ (Figures 3 and 4). These two structures

(10) We will use the term *solvate* to refer to a specific kind of *clathrate* in which the *host* is the tape complex and the *guest* is the solvent from which it was crystallized. For a proposed scheme of definitions of the varieties of clathrates, see: Weber, E. In *Molecular Inclusion and Molecular Recognition—Clathrates I*; Weber, E., Ed.; Springer-Verlag: Berlin, 1987 (*Top. Curr. Chem.*, Vol. 140).

UM00012530
NOVARTIS EXHIBIT 1017
Novartis v. Regents, IPR2023-01346
Page 1276 of 4460

Table 1. Crystallographic Data for Cocrystals of *N,N'*-Bis(*m*-X-phenyl)melamine and 5,5-Diethylbarbituric Acid, **Mel(*m*-X-Ph)$_2$Bar(Et)$_2$**[a]

X	solvate	space group	*a* (Å)	*b* (Å)	*c* (Å)	α (deg)[b]	β (deg)[b]	γ (deg)[b]	*R*[c]	density (g/cm^3)[d]	crystallization solvent	dev from planarity[e] (Å)	tape motif[f]
H		*Pnma*	12.940	9.982	17.377				0.063	1.369	CH_2Cl_2	0.14	L
F		$P2_1/n$	9.724	18.715	13.068		93.18		0.085	1.394	CH_3CN	0.17	L
Cl	$^1/_2$THF	$C2/c$	27.319	16.656	13.335		119.09		0.044	1.422	THF	0.41	C
Br	$^1/_2Me_2CO$	$C2/c$	27.283	16.470	13.340		118.14		0.060	1.632	acetone	0.39	C
I	CH_3CN	$P2_1/c$	13.095	11.575	19.212		96.52		0.033	1.734	CH_3CN	0.61	L
CH_3		$P\bar{1}$	11.273	12.117	9.730	98.35	110.86	81.45	0.054	1.333	EtOH	0.18	L
CF_3	CH_3CN	$P2_1/n$	14.268	9.824	22.377		108.18		0.074	1.426	CH_3CN	0.14	L

[a] The underlined cell dimensions represent the repeat distance in a linear tape. [b] A blank indicates that the angle is constrained to be 90°. [c] This value is the crystallographic reliability index, $R = \sum||(F_o - F_c)|/\sum F_o$. [d] Calculated. [e] Deviation from planarity of the hydrogen-bonded backbone (see the text). The average deviation of linear tapes in ref 3 (*para* series) is 0.14 Å. [f] L = linear, C = crinkled.

are isomorphous. The tapes of the complexes are crinkled. There is a CH---O contact (H---O = 2.5 Å, $\sum_{vdW_{H---O}} = 2.7$ Å) between a proton in the *meta* position of one phenyl ring and a barbital oxygen in the same tape.[11] Both *meta* complexes are solvates.[12] The crystals of the corresponding *para*-substituted compounds were also isomorphous to each other (for one polymorph of the *p*-X = Br complex), but both of those complexes were nonsolvated linear tapes.

***N,N'*-Bis(*m*-iodophenyl)melamine/Barbital, Mel(*m*-I-Ph)$_2$Bar(Et)$_2$ (Figure 5).** The linear tapes of this complex pack as head-to-tail dimers that are further stacked into sheets. The tapes deviate from planarity (Table 1) to a greater extent than any of the linear tapes we observed in the *para* series.[3] Figure 8 shows this deviation in a side-on view of a tape. Solvent (CH_3CN) is included in the lattice. There is a contact between the nitrogen of acetonitrile and an iodine atom (3.3 Å, $\sum_{vdW} \sim 3.5$ Å).[13] In the *p*-I complex, which was not a solvate (even when crystallized from acetonitrile), there were extensive I---I contacts under the sum of the van der Waals radii; no such contacts occur in the *m*-I complex.

***N,N'*-Bis(*m*-methylphenyl)melamine/Barbital, Mel(*m*-CH_3-Ph)$_2$Bar(Et)$_2$ (Figure 6).** These linear tapes pack in head-to-tail dimers that then stack into sheets. The *p*-CH_3 analogue was also a nonsolvated linear tape.

***N,N'*-Bis(*m*-(trifluoromethyl)phenyl)melamine/Barbital, Mel(*m*-CF_3-Ph)$_2$Bar(Et)$_2$ (Figure 7).** The tapes of this complex are linear and pack as head-to-tail dimers. Molecules of solvent (CH_3CN) are included in the lattice in discrete channels between the dimers. This structure is the first example of a channel clathrate that we have observed in crystals of tapes. There are no fluorine–fluorine contacts under the sum of van der Waals radii. There is, however, a region of high fluorine density between tapes B and D in Figure 7. The *p*-CF_3 complex also consisted of linear tapes but was not a solvate.

Packing Fractions (Table 2). The *meta* complexes that crystallize as solvates would have lower packing fractions than their *para* congeners if the volume of the solvent molecule were not included in the calculation of C_k*.[14] In fact, two of the solvates (*m*-I and CF_3) would have values lying outside the range accepted as normal for organic molecular crystals.[15] Inclusion of the solvent leads to more efficient packing as measured by minimization of void spaces and maximization of contact of van der Waals surfaces. We comment on the values of C_k* in the Discussion section.

(11) We do not know if this contact is attractive or repulsive. For a discussion of CH---O contacts, see: Desiraju, G. R. *Acc. Chem. Res.* **1991**, *24*, 290.

(12) For **Mel(*m*-Cl-Ph)$_2$Bar(Et)$_2$**, the solvent is an ordered molecule of THF; for **Mel(*m*-Br-Ph)$_2$Bar(Et)$_2$**, the solvent is a disordered molecule of acetone.

(13) For an investigation of nitrile–iodine interactions, see: Desiraju, G. R.; Harlow, R. L. *J. Am. Chem. Soc.* **1989**, *111*, 6757.

(14) $C_k = N \cdot V_{mol}/V_{cell}$, where N is the number of molecules in a unit cell, V_{mol} is the molecular volume, and V_{cell} is the volume of the unit cell. Kitaigorodsky, A. I. *Organic Chemical Crystallography*; Consultants Bureau: New York, 1961. For a discussion of our modified parameter C_k* (calculated using MacroModel), see ref 3.

(15) Values of C_k usually range from roughly 0.65 to 0.77. Desiraju, G. R. *Crystal Engineering: The Design of Organic Solids*; Elsevier: New York, 1989; Chapter 2.

Discussion

Crystalline Architecture in the *Meta* Series. This series of complexes presents examples of several new varieties of the architecture of packing of tapes, as well as modifications of some types that we have observed before. Five of the seven structures (*m*-X = H, F, I, CH_3, and CF_3) consist of linear tapes, while the other two (*m*-X = Cl and Br) are crinkled tapes. We have not searched for polymorphism, which was important in the *para* series.[16] Polymorphism may, in fact, also turn out to be crystallographically important in the *meta* series; the greater variety of architecture already observed for complexes of *meta*-substituted diphenylmelamines might suggest that the existence of polymorphs of these complexes is likely.

There are two sets of crystals in which members of the *meta* and *para* series have similar although not isomorphous structures. First, the *m*-CH_3 complex adopts a structure analogous to that of the *p*-Cl and *p*-Br (form I) complexes.[3] All three crystallize in space group $P\bar{1}$ and consist of stacked head-to-tail dimers of tapes. Second, the crinkled tapes of *m*-Cl and *m*-Br pack similarly to the crinkled tape[2] of *p*-CO_2Me in space group $C2/c$, with solvent included between stacks of tapes.

Another similarity occurs in the packing of the **Mel(Ph)$_2$Bar(Et)$_2$** and **Mel(*m*-F-Ph)$_2$Bar(Et)$_2$** complexes. In this pair, steric effects seem uppermost in determining packing, since a large change in the dipoles of the substituents does not alter the secondary or tertiary architecture. In addition, the disorder of one of the *m*-fluorophenyl moieties demonstrates the rough steric equivalence of H and F. By contrast, a different result is obtained on going from **Mel(Ph)$_2$Bar(Et)$_2$** to **Mel(*p*-F-Ph)$_2$Bar(Et)$_2$**. Those two complexes pack with different tertiary architecture.[3]

The adoption of a crinkled tape motif in the *meta* series is not due to the bulk of the substituents. Larger substituents (CH_3 and I) afford linear tapes, while smaller ones (Cl and Br) afford crinkled tapes. It is, however, not clear what factors do determine whether a member of the *meta* series adopts a linear or a crinkled motif. The observation of a particular motif might, in fact, turn out to be a manifestation of polymorphism. In other words, different conditions of crystallization may yield alternative crystalline architectures (such as a crinkled *m*-I or a linear *m*-Br structure).

The **Mel(*m*-I-Ph)$_2$Bar(Et)$_2$** complex has a tape backbone that is abnormally deformed, or wavy, for a linear tape (Table 1 and Figure 8). We hypothesize that the deformation of the tapes of this complex reflects association of CH_3CN and iodine, and not steric properties of the substituent.[13] The tapes incorporating the substituents *m*-CH_3 and *m*-CF_3 (both of which have larger cross sections than I) deviate from planarity to about the same extent as the tapes containing the small substituent *m*-F (see Table 1).

Importance of Solvent to Packing. Four of the seven complexes of the *meta* series are solvates: two of the linear tapes (*m*-I and

(16) The principal reason that we have not yet looked for alternative phases of these complexes is that we lack an experimental setup capable of preventing desolvation while investigating the powder diffraction patterns of clathrates. Non-solvated polymorphs could of course occur, however.

UM00012531
NOVARTIS EXHIBIT 1017
Novartis v. Regents, IPR2023-01346
Page 1277 of 4460

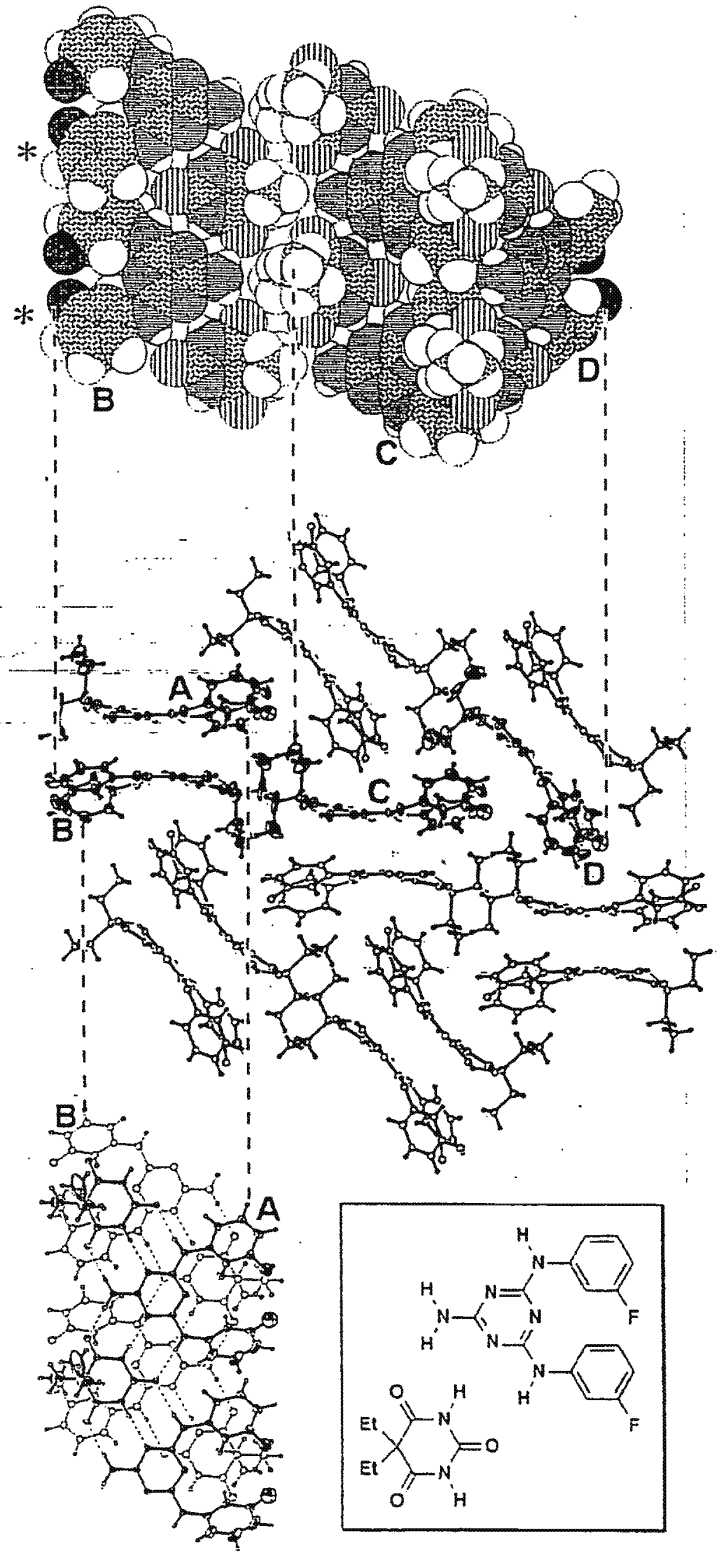


Figure 2. Views of the $MeI(m\text{-}F\text{-}Ph)_2Bar(Et)_2$ complex. One fluorophenyl group (indicated with an asterisk) is disordered; only one position (the one with the more populated fractional site occupancy) is shown for the fluorine in this group.

m-CF_3) and both of the crinkled tapes (*m*-Cl and *m*-Br). By contrast, none of the crystals of linear tapes in the *para*-substituted series contained solvent. All of these solvated crystals decomposed through the loss of solvent at room temperature in the open

UM00012532
NOVARTIS EXHIBIT 1017
Novartis v. Regents, IPR2023-01346
Page 1278 of 4460

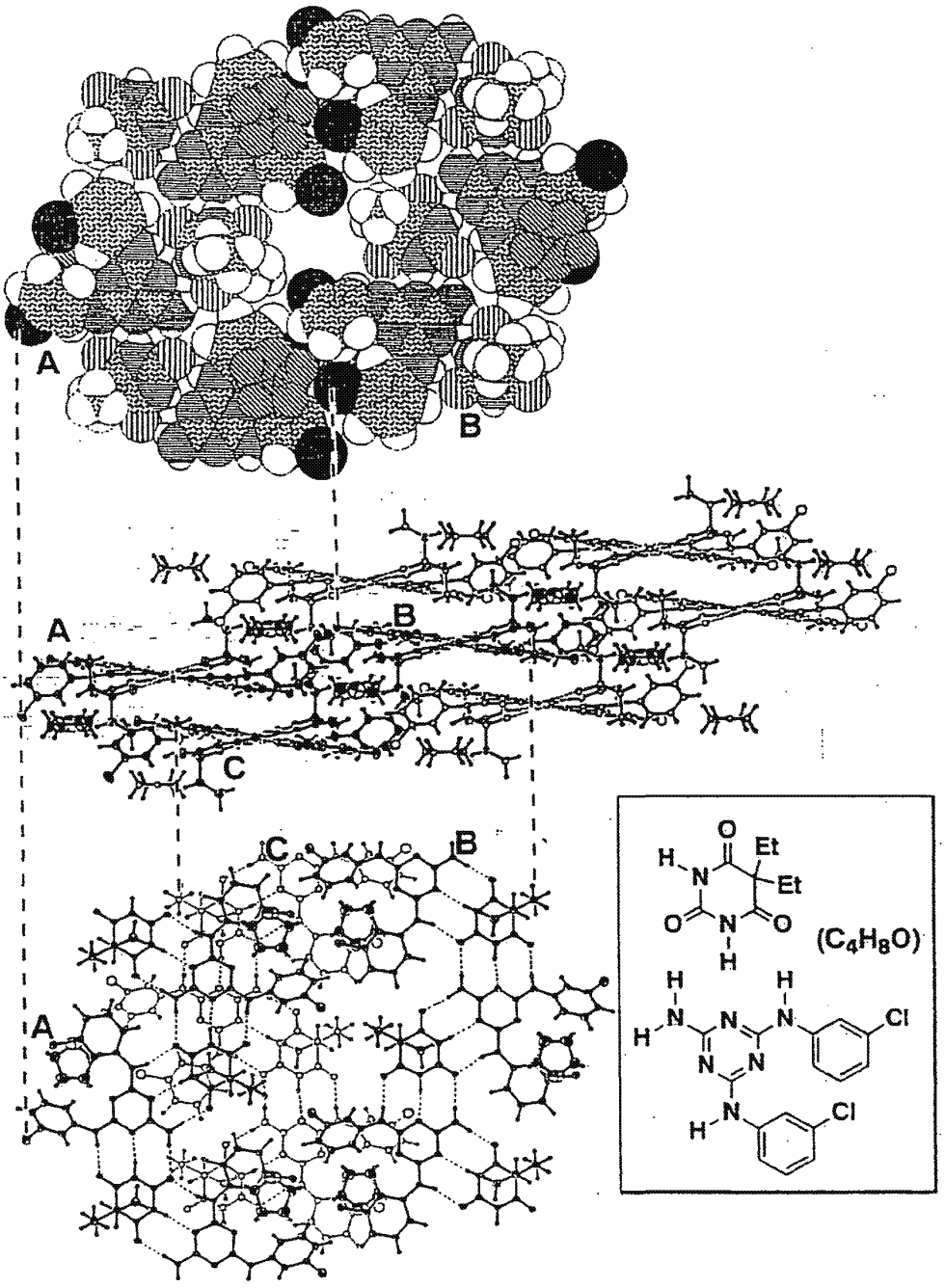


Figure 3. Views of the **MeI(m-Cl-Ph)$_2$-Bar(Et)$_2$-0.5THF** complex.

atmosphere, as evidenced by their transformation from clear to opaque and by the development of fractures. The m-CF_3 complex desolvated in a matter of hours, m-Cl and Br in about a day, and m-I over the course of several days. For clathrates, the guest is an integral part of the lattice. It might be most accurate, therefore, to describe these crystals as three-component systems composed of melamine, barbital, and solvent molecules. Solvent seems to play an important role in determining the packing of these tapes (probably more important than that it plays in crystallizations of nonsolvates).

The precise influence of solvent in determining the packing of the *meta* structures remains obscure. The m-I solvate is the only structure that has a specific non-covalent interaction (CN---I) between solvent and host. The crinkled solvates, m-Cl and m-Br, have contacts between hydrogen atoms of the solvent and halogen atoms (in the range of 2.9 to 3.0 Å) that are just at the limit of van der Waals contact (approximately 2.95 to 3.05 Å), but these interactions are probably weak. Since voids in these two isomorphous crystals are filled by different solvents (THF and acetone), we infer that shape specificity of host for guest is minimal. In the m-CF_3 case, there is no host–guest contact, but there is a H---N contact (2.5 Å, $\Sigma_{vdw} \sim 2.7$ Å) between adjacent solvent molecules, creating a crystallographically infinite chain that may be held together by weak hydrogen bonds. We have

UM00012533
NOVARTIS EXHIBIT 1017
Novartis v. Regents, IPR2023-01346
Page 1279 of 4460

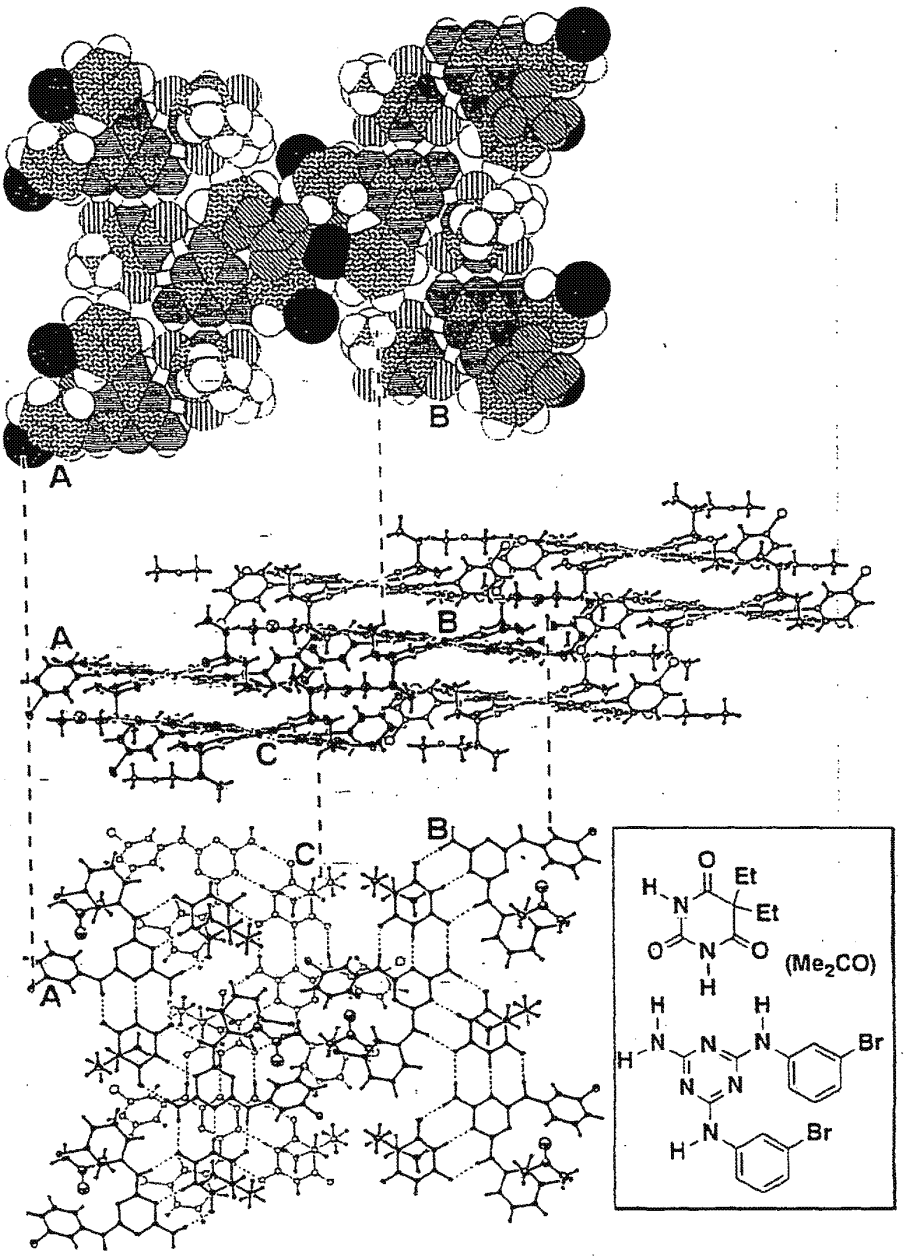


Figure 4. Views of the Mel(*m*-Br-Ph)$_2$-Bar(Et)$_2$·0.5(Me_2CO) complex. Only one orientation of the disordered acetone molecule is shown.

not yet investigated the contribution of solvent by attempting to crystallize these complexes (especially the solvates) from different solvents.

For the *para* series, we searched for polymorphism by performing X-ray powder diffraction (XPD) on crystals of the complexes grown from different solvents. While polymorphism occurred unambiguously for *p*-Br and *p*-CF_3, there was never a special relationship between solvent and crystalline phase in the sense that polymorph X was only obtainable from solvent X or that solvent Y yielded only polymorph Y.[17] In particular, there appeared to be no specific interaction between CH_3CN and the *p*-I complex when it was grown from that solvent.[8] The crystals were not solvates, and they had the same structure (according to XPD) as crystals grown from other solvents. Similarly, neither *p*-Cl grown from THF nor *p*-Br grown from acetone were solvates, unlike their *meta* analogues. Observation of solvent-dependent polymorphism in the *meta* series would therefore constitute a marked difference from the *para* series.

Table 2 compares values of the packing coefficient, C_k*, for the *para* and *meta* series. In most cases, the value for the *meta* complexes is the same or only slightly larger than that for the *para* complexes. The exception is the pair of CH_3-substituted complexes. The *meta*-CH_3 complex has a higher value of C_k* and is also more dense. The space-filling of the *meta* series is

(17) Polymorphism of the *p*-Br complex (and perhaps of the *para*-CF_3 complex) appeared to be more sensitive to the rate of crystal growth by solvent evaporation, or to factors influencing nucleation (such as vibrations or dust particles) over which we exercised little or no control, than to the solvent from which the crystals formed (MacDonald, J. C.; Weissbecker, C.; Zerkowski, J. A. Unpublished data).

UM00012534
NOVARTIS EXHIBIT 1017
Novartis v. Regents, IPR2023-01346
Page 1280 of 4460

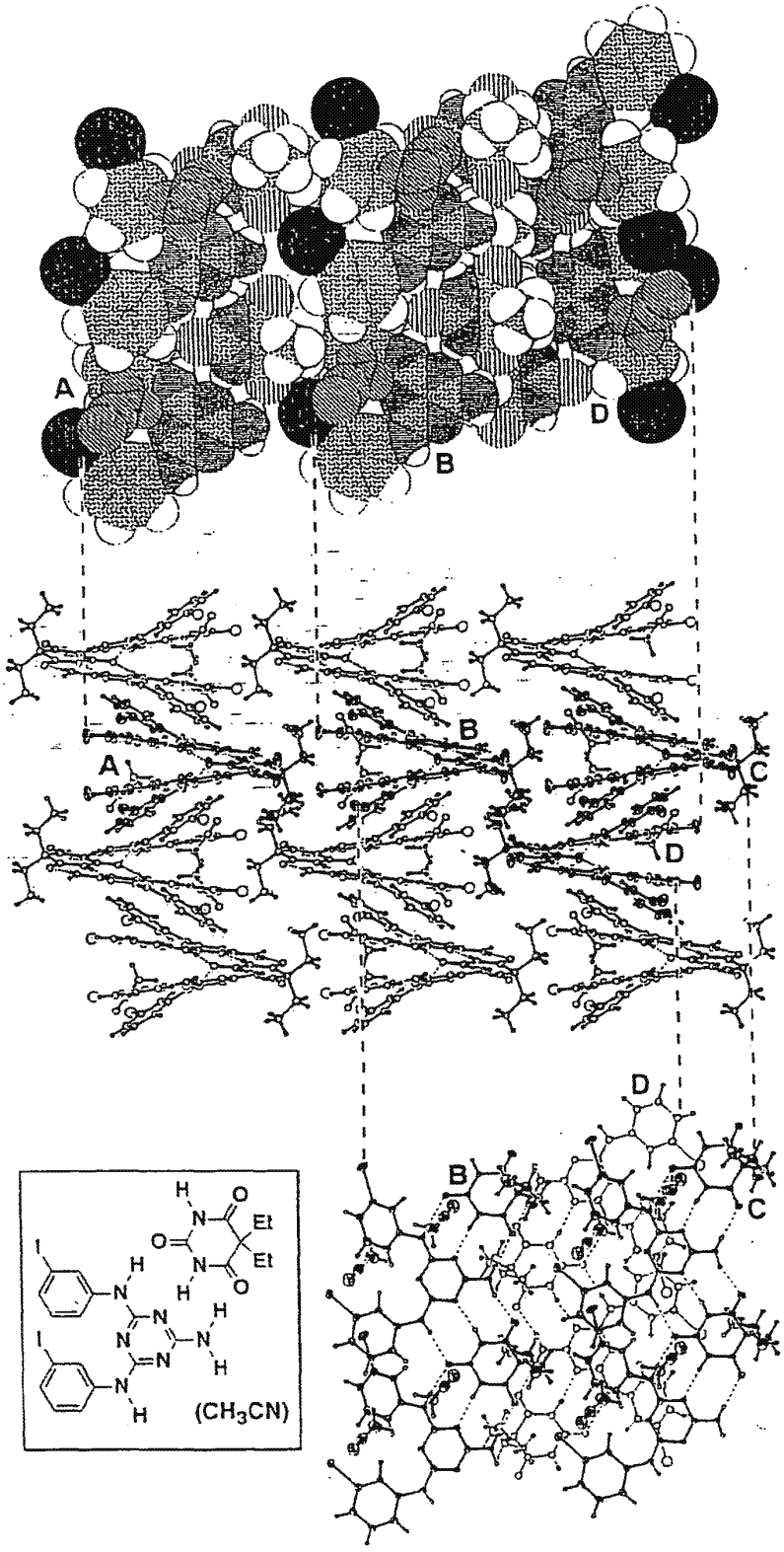


Figure 5. Views of the Mel(m-I-Ph)$_2$·Bar(Et)$_2$·CH_3CN complex.

therefore, not necessarily less efficient than that of the *para* series. Table 2 also includes a listing of *hypothetical* C_k* values for the *meta* solvates with solvent removed. It is interesting that inclusion of solvent increases the efficiency of space-filling for the *meta* series only to values roughly equal to those of the *para* series.

UM00012535
NOVARTIS EXHIBIT 1017
Novartis v. Regents, IPR2023-01346
Page 1281 of 4460

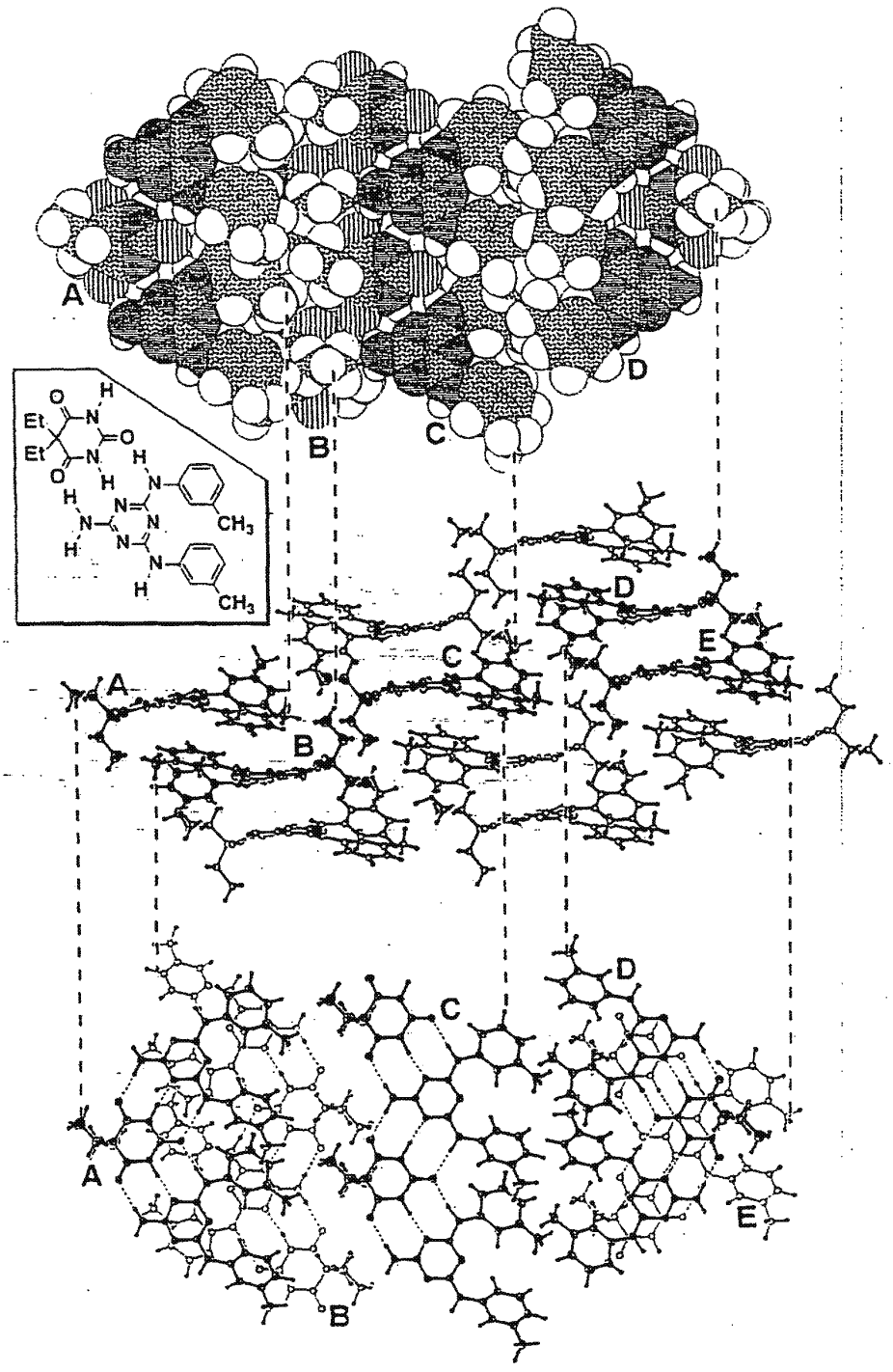


Figure 6. Views of the Mel(m-CH_3-Ph)$_2$-Bar(Et)$_2$ complex.

Conclusions

A comparison of the series of *meta*-substituted diphenylmelamines complexed with barbital presented in this paper to the *para*-substituted series[3] shows that small changes in molecular structure can be accompanied by significant changes in crystalline architecture. For example, switching a chlorine substituent from a *para* to a *meta* position on a phenyl ring results in a change in the tape motif from linear to crinkled. We emphasize, however, that we do not know whether this change reflects thermodynamic or kinetic factors (or both). Without extensive studies of polymorphism, the observation of these two particular chlorine-containing structures shows only that both are *accessible*, not that they are thermodynamically preferred relative to other structures.

The *meta* series provides new examples of the varieties of crystalline architecture that tapes, particularly linear ones, can

UM00012536
NOVARTIS EXHIBIT 1017
Novartis v. Regents, IPR2023-01346
Page 1282 of 4460

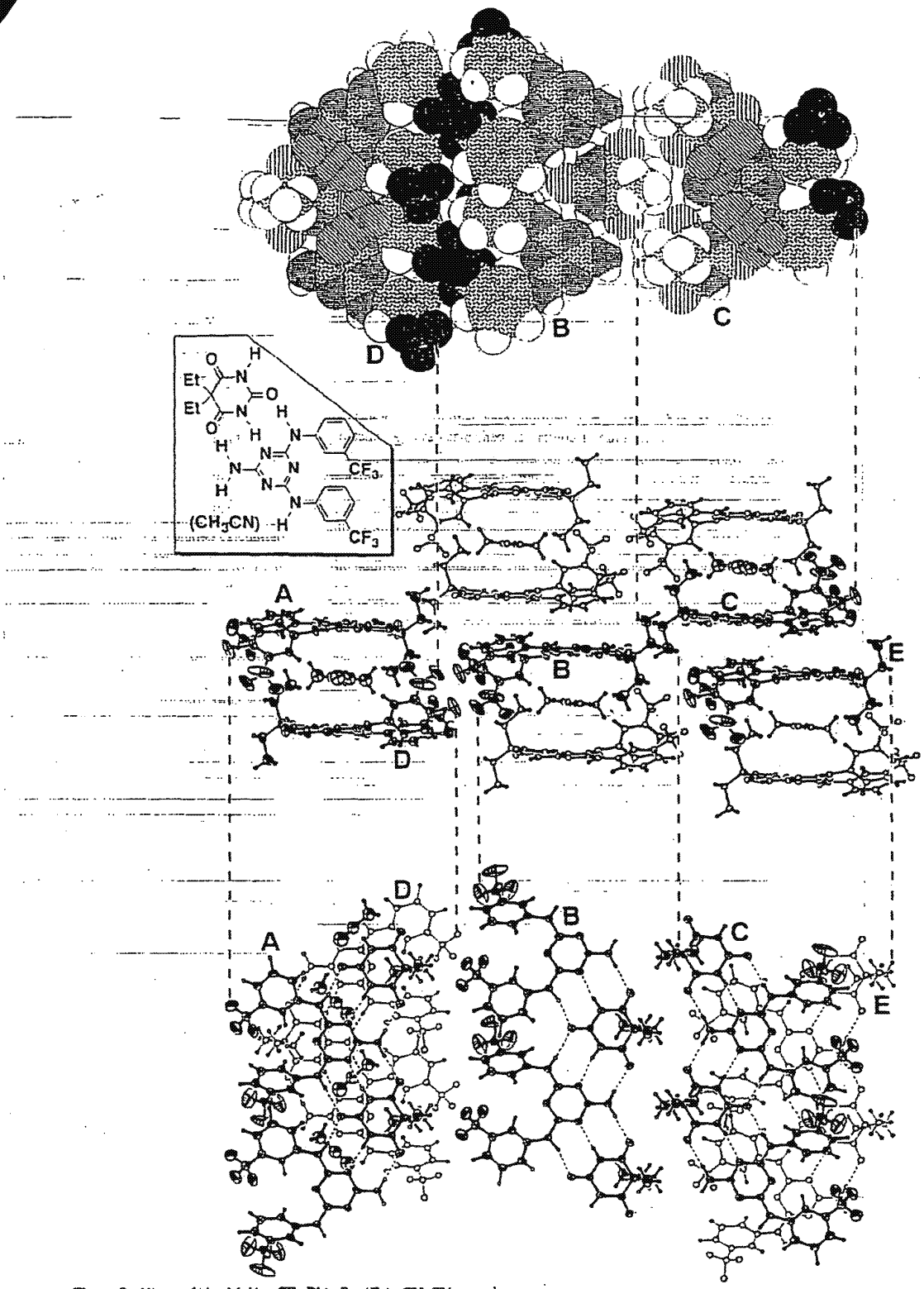


Figure 7. Views of the $Mel(m\text{-}CF_3\text{-}Ph)_2Bar(Et)_2\text{-}CH_3CN$ complex.

adopt. Tapes can accommodate solvent in the lattice in several ways. First, crinkled tapes (such as *m*-Cl and Br) can pack to give pockets between stacks of tapes that solvent can fill. Second, linear tapes (*m*-I) can deform from planarity (become "wavy") to allow a solvent molecule to engage in a close, specific contact with a tape substituent. Third, linear tapes ($m\text{-}CF_3$) can pack with channels of solvent between them. In each of these cases, inclusion of solvent increased the efficiency of space-filling of the

UM00012537
NOVARTIS EXHIBIT 1017
Novartis v. Regents, IPR2023-01346
Page 1283 of 4460

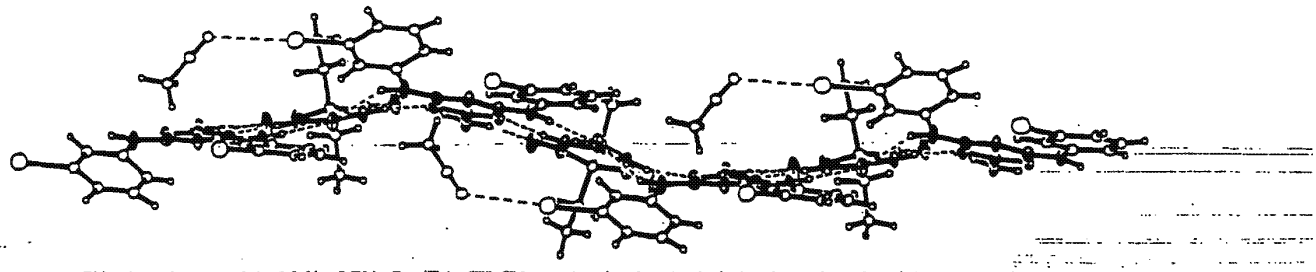


Figure 8. Side view of a tape of the Mel(*m*-I-Ph)$_2$Bar(Et)$_2$·CH$_3$CN complex showing the deviation from planarity of the tape backbone. The contact between acetonitrile and iodine is indicated by a dashed line. The atoms of the tape backbone are shown as thermal ellipsoids.

Table 2. Comparison of Packing Coefficients for the *Meta* and *Para* Series[a]

X	C_k* for *p*-X[b]	C_k* for *m*-X: with solvent if present	C_k* for *m*-X: *hypothetical*, without solvent[c]
H	0.72	0.72	
F	0.69	0.69	
Cl ($^1/_2$THF)	0.70	0.70	0.65
Br ($^1/_2$Me$_2$CO)	0.71 (form I)	0.71	0.67
	0.69 (form II)		
I (CH$_3$CN)	0.69	0.70	0.63
CH$_3$	0.68	0.71	
CF$_3$ (CH$_3$CN)	0.66	0.67	0.61

[a] These packing coefficients are based on molecular volumes calculated with MacroModel. See ref 3 for a discussion of the relationship between C_k* and the packing coefficient calculated in a traditional way, C_k.[14] [b] Taken from ref 3. [c] This value is a hypothetical one that excludes the contribution to volume from the included solvent molecule.

meta series to values approximately equivalent to those of the *para* series. Only the *m*-I complex relies clearly upon a specific host–solvent contact to favor clathration.

We suspect that nonspecific clathration of solvent may arise principally as an effect of polymorphism. For example, since the linear motif can accommodate *meta* substituents with large diameters (I, CH$_3$, CF$_3$), there should be no steric barrier to the *m*-Br or *m*-Cl complexes adopting a linear motif. Thus there could well be other (yet unobserved) polymorphs, such as linear *m*-Br and *m*-Cl tapes, that pack to fill space more completely but that are not solvates. These phases might occur if crystals were grown from a solvent that for some reason (probably steric) could not be included in a lattice of tapes. Kinetic effects leading to packing arrangements that are local minima in free energy should become more important as conformational multiplicity increases.[18] Computational modeling and energy calculations will be required to make comparisons between alternative packing orientations.

The *meta* series of complexes has important structural similarities to the corresponding *para* series, and to other related 1:1 co-crystalline complexes that we have investigated. In particular, members of this series preserve the triad of hydrogen bonds between melamine and barbituric acid components as the dominant structure-determining element in the solid state and crystallize in both the linear and crinkled tape motifs observed previously. Our initial investigations into this series suggest to us, however, that crystals based on *meta*-substituted diphenylmelamines are less suitable than other series we have examined (specifically, crystals based on *para*-substituted diphenylmelamines[3] and on *N*,*N*′-di(*tert*-butyl)melamine[4]) as the basis for a systematic physical–organic study. This unsuitability arises because of the greater number of varieties of packing adopted by the *meta* series than by the *para* series. We hypothesize that this range of architectures may be attributable to the variability of molecular conformation of *meta*-substituted diphenylmelamines,[18] while the limited architecture of the *para* series and the *N*,*N*′-di(*tert*-butyl)melamine series is a result of the reduced conformational multiplicity of those molecules.

(18) Desiraju, G. R. *Crystal Engineering: The Design of Organic Solids*; Elsevier: New York, 1989; Chapter 10.

Experimental Section

General. All anilines were obtained from Aldrich Chemicals. General procedures were performed as previously published.[3]

General Procedure for Synthesis of 2-Amino-4,6-bis(arylamino)-1,3,5-triazines (*N*,*N*′-Diphenylmelamines).[19] A 0.1 M solution of cyanuric chloride was prepared in freshly distilled THF and cooled in an ice-water bath. A THF solution of 1 equiv of the aniline (0.1 M) and 1 equiv of diisopropylethylamine as base was added from a dropping funnel over the course of 15–30 min with magnetic stirring of the reaction mixture. When the addition was complete, the mixture was allowed to warm to room temperature, and stirring was continued for another hour. The mixture was heated to 40–50 °C in an oil bath, and another equivalent each of aniline and base (in THF) was added. Heating was continued for several hours. At this stage, the intermediate 2-chloro-4,6-diamino-1,3,5-triazine was pure enough, as determined by TLC, that it could be isolated by filtering the reaction mixture through a short plug of silica gel. The silica gel was washed with solvent (ethyl acetate or THF) and the combined organic solutions were concentrated to dryness by rotary evaporation at aspirator pressure. An alternative procedure was to remove the solvent from the reaction mixture by rotary evaporation, dissolve the residue in ethyl acetate and wash it several times with H$_2$O, and then remove the ethyl acetate by rotary evaporation. The crude product was used directly in the next step.

The 2-chloro-4,6-diamino-1,3,5-triazine (dissolved in approximately 5–8 mL of 1,4-dioxane or THF) and a magnetic stirrer were placed in a 15-mL pressure bottle. Approximately 3–5 mL of 30% NH$_4$OH was added, and the bottle was capped and heated (**CAUTION: behind a safety shield**) to 100–105 °C in an oil bath. Heating was continued for 5–8 h, after which the vial was cooled and opened to measure the progress of the reaction by TLC. If an unacceptable amount of starting material remained, an additional portion of 30% NH$_4$OH (2–3 mL) was added, and the vial was recapped and reheated. When reaction was judged to be complete by TLC, the solution was poured into 150–200 mL of H$_2$O, and the precipitated product was collected by vacuum filtration. After drying under vacuum at 0.1 Torr, the crude melamine was purified by flash chromatography on silica gel.

The melting points of the melamines were the following: Mel(*m*-F-Ph)$_2$, 178–80 °C; Mel(*m*-Cl-Ph)$_2$, 181–84 °C; Mel(*m*-Br-Ph)$_2$, 192–95 °C; Mel(*m*-I-Ph)$_2$, 188–91 °C; Mel(*m*-CH$_3$-Ph)$_2$, 138–40 °C (lit.[20] mp 139–40 °C); Mel(*m*-CF$_3$-Ph)$_2$, 70–75 °C. For spectroscopic details and elemental analyses on new compounds see the supplementary material.

Preparation of Complexes. Equimolar amounts of the melamine and barbital were dissolved together (in one flask) in THF. The solvent was removed by rotary evaporation at aspirator pressure, and the composition of the complex was checked by ^{1}H NMR spectroscopy. If integration of peaks indicated that one component was present in excess, the other component was added to bring their ratio to 1:1. The melting points of the complexes were the following: Mel(*m*-F-Ph)$_2$Bar(Et)$_2$, 230–32 °C;

(19) This procedure is a modification of that found in: Kaiser, D. W.; Thurston, J. T.; Dudley, J. R.; Schaefer, F. C.; Hechenbleikner, I.; Holm-Hansen, D. *J. Am. Chem. Soc.* **1951**, *73*, 2984.

(20) Honda, I. *Yuki Gosei Kagaku Kyokai Shi* **1962**, *20*, 460; *Chem. Abstr.* **1963**, *58*, 4568e.

UM00012538
NOVARTIS EXHIBIT 1017
Novartis v. Regents, IPR2023-01346
Page 1284 of 4460

Mel(*m*-Cl-Ph)$_2$·Bar(Et)$_2$,[21] 210–12 °C dec; **Mel(*m*-Br-Ph)$_2$·Bar(Et)$_2$**,[21] 191–94 °C; **Mel(*m*-I-Ph)$_2$·Bar(Et)$_2$**,[21] 197–202 °C; **Mel(*m*-CH$_3$-Ph)$_2$·Bar(Et)$_2$**, 198–200 °C; **Mel(*m*-CF$_3$-Ph)$_2$·Bar(Et)$_2$**,[21] 178–81 °C. The melting point of barbital is 190–92 °C.

Crystallization of Complexes: Mel(*m*-CH$_3$-Ph)$_2$·Bar(Et)$_2$. Crystals were grown by room-temperature evaporation of a solution of the complex in EtOH. A slow rate of evaporation (approximately 2 weeks for complete evaporation of solvent from a 1-mL sample of solution) was achieved by enclosing a loosely capped 1-dram screw-top vial containing the solution inside a 10-mL vial that was also loosely capped.

Mel(*m*-F-Ph)$_2$·Bar(Et)$_2$, Mel(*m*-I-Ph)$_2$·Bar(Et)$_2$, and Mel(*m*-CF$_3$-Ph)$_2$·Bar(Et)$_2$. Crystals were grown by allowing a solution of the complex in boiling CH_3CN to cool over the course of at least 24 h to room temperature. A slow rate of cooling was achieved by enclosing a round-bottomed flask containing the solution in a corked Dewar flask. After it was observed that crystals of the *m*-I and *m*-CF$_3$ complexes were solvates, these crystals were stored in contact with mother liquor.

Mel(*m*-Cl-Ph)$_2$·Bar(Et)$_2$ and Mel(*m*-Br-Ph)$_2$·Bar(Et)$_2$. Crystals were grown by room-temperature evaporation of solutions of the complexes in THF and acetone, respectively, in loosely capped 25-mL round-bottomed flasks. Once suitable single crystals had formed, as determined by observation under a microscope, the flasks were tightly stoppered to retain a small amount of solvent and prevent decomposition of the solvated crystals.

(21) The crystalline samples used for melting point analyses of these complexes had been grown from the solvent that afforded the solvated crystals studied by single-crystal diffraction, but they had desolvated prior to the melting point analysis. If solvated samples had been used, they probably would have desolvated (even in a sealed capillary) during the melting point analysis.

X-ray Crystallography. For details of X-ray data collection and structure solution and refinement, see the supplementary material. Data were collected on complexes of **Mel(*m*-Cl-Ph)$_2$·Bar(Et)$_2$** and **Mel(*m*-Br-Ph)$_2$·Bar(Et)$_2$** at Harvard on a Siemens P3 diffractometer. Data on the other complexes were collected by Molecular Structure Corp., The Woodlands, TX, on a Rigaku AFC5R diffractometer equipped with a rotating anode generator. All structures were solved and refined at Harvard using the Siemens SHELXTL-PLUS package of programs.

Acknowledgment. We acknowledge the support of the National Science Foundation through Grants CHE-91-22331 to G.M.W. and CHE-80-00670 to the Department of Chemistry for the purchase of the Siemens X-ray diffractometer. J.P.M. acknowledges support from a SERC/NATO postdoctoral fellowship, 1991–93. We thank Dr. Derk Wierda for helpful discussions.

Supplementary Material Available: Experimental details for melamines, crystallographic details including tables of atomic positional parameters and bond lengths and angles (95 pages); tables of observed and calculated structure factors (85 pages). This material is contained in many libraries on microfiche, immediately follows this article in the microfilm version of the journal, and can be ordered from the ACS; see any current masthead page for ordering information.

UM00012539
NOVARTIS EXHIBIT 1017
Novartis v. Regents, IPR2023-01346
Page 1285 of 4460

This Page is Inserted by IFW Indexing and Scanning Operations and is not part of the Official Record

BEST AVAILABLE IMAGES

Defective images within this document are accurate representations of the original documents submitted by the applicant.

Defects in the images include but are not limited to the items checked:

- ☐ BLACK BORDERS
- ☐ IMAGE CUT OFF AT TOP, BOTTOM OR SIDES
- ☐ FADED TEXT OR DRAWING
- ☐ BLURRED OR ILLEGIBLE TEXT OR DRAWING
- ☐ SKEWED/SLANTED IMAGES
- ☐ COLOR OR BLACK AND WHITE PHOTOGRAPHS
- ☐ GRAY SCALE DOCUMENTS
- ☐ LINES OR MARKS ON ORIGINAL DOCUMENT
- ☐ REFERENCE(S) OR EXHIBIT(S) SUBMITTED ARE POOR QUALITY
- ☐ OTHER: _____

IMAGES ARE BEST AVAILABLE COPY.

As rescanning these documents will not correct the image problems checked, please do not report these problems to the IFW Image Problem Mailbox.

Polymorphic Packing Arrangements in a Class of Engineered Organic Crystals

Jonathan A. Zerkowski, John C. MacDonald, and George M. Whitesides*

Department of Chemistry, Harvard University, Cambridge, Massachusetts 02138

Received December 4, 1996. Revised Manuscript Received April 16, 1997®

Polymorphism occurs in the family of engineered cocrystals that form from *N,N'*-bis(*p*-X-phenyl)melamines (X = H, F, Cl, Br, I, CH_3, and CF_3) and barbital. X-ray powder diffraction indicates that only one crystalline phase formed for X = Cl, F, and CH_3, that primarily one phase occurred for X = H and I, but that a small contribution from an alternative phase or phases was possibly also present, and that at least two different polymorphs exist for both X = Br and CF_3. Agreement of *positions* of peaks in experimental XPD traces and reflections calculated from single-crystal data is good, while agreement in *intensities* is good in some cases but only fair in others. Reasons for this disagreement are likely to include the physical design of the diffractometer and preferred orientation of crystallites in the sample. Two of the polymorphic forms of X = Br are converted to a third on annealing at 140 °C. Steric effects seem the most probable origin of the polymorphism: the bromine-substituted diphenylmelamine crystallizes in several polymorphs, and the bromine substituent is intermediate in size for the family of substituents examined. This cocrystal forms one polymorph that is formed by cocrystals having larger substituents (I and CH_3) and one that packs similarly to a cocrystal having a smaller substituent (Cl).

Introduction

Successful design of crystalline organic solids requires control over molecular packing. As part of our studies of the engineering (that is, the design and preparation) of organic molecular crystals,[1–4] we are concerned with the occurrence of multiple patterns of packing—polymorphism—for compounds of interest. The widespread occurrence of polymorphism in organic crystals makes the packing of organic molecules especially difficult to rationalize and predict. As Desiraju has rhetorically asked in his important overview of organic solids, "does the existence of polymorphism negate ... the very concept of crystal engineering?".[5]

Truly rational solid-state design will not be possible until polymorphism is understood and controlled.[6] Almost all approaches to understanding the structure of crystals focuses on their thermodynamics: the first question is always "what is the most stable crystal form?" The occurrence of polymorphs often reflects the kinetic factors that determine the rates of nucleation and growth of crystals and is even more difficult to understand than the thermodynamics of the most stable crystal.[7] Since the crystal that forms in some circumstances is not necessarily the most stable crystal, it is especially difficult to work out structure–stability relations of the sort on which physical-organic chemistry is based.[8] Complicating this issue is the fact that many polymorphs differ in energy only slightly (for example, by less than 10 or 12 kJ/mol, according to compilations of heats of transition between polymorphs).[9,10]

A further difficulty is that conformational polymorphism[11] will always be a theoretical possibility for molecules that have multiple conformational isomers accessible energetically: every different conformation is a different molecular shape and can, in principle, form its own crystalline polymorph (or polymorphs). Even molecules constrained to pack in geometrically simple aggregates through the use of directional intermolecular forces—the class of interest in our work—can show conformational isomerism and polymorphism. Evidence of the present difficulty in rationalizing and controlling polymorphism is the fact that an experimental examination for polymorphs usually involves an almost undirected, empirical search across the many parameters—solvent, temperature, mass transport, nucleation—that influence crystallization.[12]

The study of polymorphism can be valuable for several reasons.[13] It can yield information about the interplay between molecular conformation and intermolecular interactions. It will contribute to the determination of the stable thermodynamic form of a molecular crystal. It also has technological ramifications: polymorphism is an important consideration in the design of acentric

* Abstract published in *Advance ACS Abstracts*, June 1, 1997.

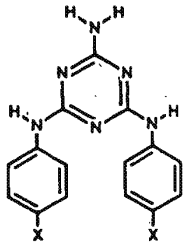
(1) Zerkowski, J. A.; MacDonald, J. C.; Seto, C. T.; Wierda, D. A.; Whitesides, G. M. *J. Am. Chem. Soc.* **1994**, *116*, 2382.
(2) Zerkowski, J. A.; Whitesides, G. M. *J. Am. Chem. Soc.* **1994**, *116*, 4298.
(3) Zerkowski, J. A.; Mathias, J. P.; Whitesides, G. M. *J. Am. Chem. Soc.* **1994**, *116*, 4305.
(4) Zerkowski, J. A.; MacDonald, J. C.; Whitesides, G. M. *Chem. Mater.* **1994**, *6*, 1250.
(5) Desiraju, G. *Crystal Engineering: The Design of Organic Solids*; Elsevier: New York, 1989; Chapter 10.
(6) Bernstein, J. *J. Phys. D: Appl. Phys.* **1993**, *26*, B66.
(7) Saito, K. *J. Phys. D: Appl. Phys.* **1993**, *26*, B77.
(8) Dunitz, J. D. *Pure Appl. Chem.* **1991**, *63*, 177.
(9) Burger, A.; Ramberger, R. *Mikrochim. Acta (Wien) II* **1979**, 273.
(10) Royer, J.; Décoret, C.; Tinland, B.; Perrin, M.; Perrin, R. *J. Phys. Chem.* **1989**, *93*, 3393.
(11) Bernstein, J. In *Organic Solid State Chemistry*; Desiraju, G., Ed.; Elsevier: Amsterdam, 1987.
(12) Etter, M. C.; Kress, R. B.; Bernstein, J.; Cash, D. J. *J. Am. Chem. Soc.* **1984**, *106*, 6921.
(13) (a) McCrone, W. C. In *Physics and Chemistry of the Organic Solid State*; Fox, D., Labes, M. M., Weissberger, A., Eds.; Interscience: New York, 1965; Vol. II. (b) Haleblian, J. K. *J. Pharm. Sci.* **1975**, *64*, 1269.

S0897-4756(95)00566-7 CCC: $14.00 © 1997 American Chemical Society

UM00012541
NOVARTIS EXHIBIT 1017
Novartis v. Regents, IPR2023-01346
Page 1287 of 4460

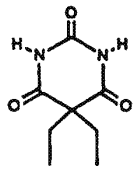
phases for nonlinear optical materials,[14] in explaining solid-state reactivity,[15] in stabilizing bioavailability in pharmaceutical applications where rates of dissolution of a drug can differ among polymorphs,[16] and in controlling the physical properties (packing, pourability, triboelectrical effects) of crystalline solids.[17-19]

We have previously demonstrated that 1:1 cocrystals of melamines and barbiturates serve as a model system for the study of packing in organic molecular crystals in which molecular structure can be correlated with crystal structure (at least to some extent).[1-4] One class of this system, composed of *N,N'*-bis(*p*-X-phenyl)-melamines and barbital (where X = H, F, Cl, Br, I, CH_3, and CF_3), clearly exhibited polymorphism (see ref 1 for the crystal structures of this series of complexes). Here we present a study of the polymorphism of this family of complexes, using X-ray powder diffraction and solid-state NMR spectroscopy. Although techniques such as differential scanning calorimetry (DSC), thermogravimetric analysis (TGA), solid-state IR spectroscopy, and optical microscopy have been used to study polymorphism, we have focused on XPD since this technique provides information about the packing of molecules in crystal lattices. We have not attempted to address the use of XPD as a method for ab initio determination of crystalline structure. Rather, a major objective of this work was to demonstrate, on a representative class of designed crystals, that XPD is the most convenient tool to use for rapid yet comprehensive screening for polymorphism in organic solids and that a survey for this phenomenon is crucial to rational crystal engineering.



N,N'-bis(para-X-phenyl)melamine

X = H, F, Cl, Br, I, CH_3, CF_3



barbital

Results and Discussion

Detection of Polymorphs using X-ray Powder Diffraction (XPD). We rely upon XPD for information about polymorphism in polycrystalline samples. This technique provides qualitative results quickly, and it characterizes the average structure of a sample of crystals generated by a given set of crystallization conditions, not just the structure of a few selected single crystals suitable for single-crystal X-ray diffraction. In contrast to spectroscopic methods, which characterize the local environment of individual atoms or functional groups, XPD provides a fingerprint, or diagnostic pattern, of any crystalline lattice that is present in a polycrystalline sample; that is, it characterizes the three-dimensional organization of molecules in a solid, not just the environment of single molecules.

For these studies, we have examined only the influence of solvent on crystallization;[20] all crystallizations were carried out at room temperature. Figures 1-3 show XPD traces for complexes containing the seven substituents used to construct this family. Each set of traces includes a calculated trace, generated using the Siemens program XPOW or the MSI program Cerius·2 from the data obtained from single-crystal diffraction studies. These calculated traces consider only the intensities of the reflections, the unit-cell dimensions, and the lattice symmetry; no explicit allowance is made for disorder of the molecules in the crystalline lattice, crystal morphology, or X-ray absorbance.[21] Experimental traces were obtained from crystals that had been ground for several minutes with a mortar and pestle. Crystals were grown from several solvents, not just the solvent used to obtain single crystals for diffraction.

Comparison of the experimental traces to the calculated trace suggests that these seven complexes can be separated into three classes. The first class (X = Cl, CH_3, and F) has, in our opinion, satisfactory agreement between experimental and calculated traces. By this judgment, we mean that the positions of the observed peaks (their 2θ values) do not deviate, within the experimental error of the technique (approximately ±0.2°), from the calculated values. Furthermore, the relative intensities are also in general agreement with calculations, although some peaks clearly are weaker or stronger than calculations predict. We discuss our investigation of potential causes for disagreement between calculated and experimental diffraction traces below.

The second class (X = H and I) is intermediate in agreement between experiment and calculation. The positions of peaks, especially the most intense ones, are in satisfactory agreement, but in some traces the relative intensities of experimental peaks agree less well with the relative intensities of calculated peaks than they do in the first class (X = Cl, F, and CH_3). Additional low-intensity peaks may appear, suggesting that other polymorphs may be present. Alternatively, some peaks expected from calculation may be weak or virtually absent. This diminution is most apparent in several traces of X = H that have only broad, ill-defined peaks, which may be indicative of poor crystallinity.

(14) Oliver, S. N.; Pantelis, P.; Dunn, P. L. *Appl. Phys. Lett.* **1990**, *56*, 307.
(15) Cohen, M. D.; Schmidt, G. M. J.; Sonntag, F. I. *J. Chem. Soc.* **1964**, 2000.
(16) (a) Byrn, S. R.; Pfeiffer, R. R.; Stephenson, G.; Grant, D. J. W.; Gleason, W. B. *Chem. Mater.* **1994**, *6*, 1148. (b) Byrn, S. R. *Solid-State Chemistry of Drugs*; Academic Press: New York, 1982.
(17) For food behavior, see: (a) Walstra, P. In *Food Structure and Behavior*; Blanshard, J. M. V., Lillford, P., Eds.; Academic Press: London; 1987. (b) Craig, S. R.; Roberts, K. J.; Sherwood, J. N.; Sato, K.; Hayashi, Y.; Iwahashi, M.; Cernik, R. J. *J. Cryst. Growth* **1993**, *128*, 1263. (c) Davey, R. J.; Richards, J. *J. Cryst. Growth* **1985**, *71*, 597.
(18) For polymorphism of clathrate lattices, see: Weber, E.; Skobridis, K.; Wierig, A.; Nassimbeni, L. R.; Johnson, L. *J. Chem. Soc., Perkin Trans. 2* **1992**, 2123.
(19) For polymorphism in organic conductors, see: Shibaeva, R. P.; Kaminskii, V. F.; Yagubskii, E. B. *Mol. Cryst. Liq. Cryst.* **1985**, *119*, 361.
(20) A number of techniques can be employed, such as vapor diffusion, sublimation, or melt crystallization. Experimental conditions such as temperature or rate of evaporation of the solvent can also be varied. Historically, attempts to crystallize neutral organic compounds have relied most frequently on changes of solvent. Ellern, A.; Bernstein, J.; Becker, J. Y.; Zamir, S.; Shahal, L.; Cohen, S. *Chem. Mater.* **1994**, *6*, 1378.
(21) Inasmuch as these factors do affect the observed reflection data in single-crystal studies, they will also make a contribution to a calculated powder trace based on those data. It is unknown, however, whether they would affect experimental powder diffraction data to the same extent.

UM00012542
NOVARTIS EXHIBIT 1017
Novartis v. Regents, IPR2023-01346
Page 1288 of 4460

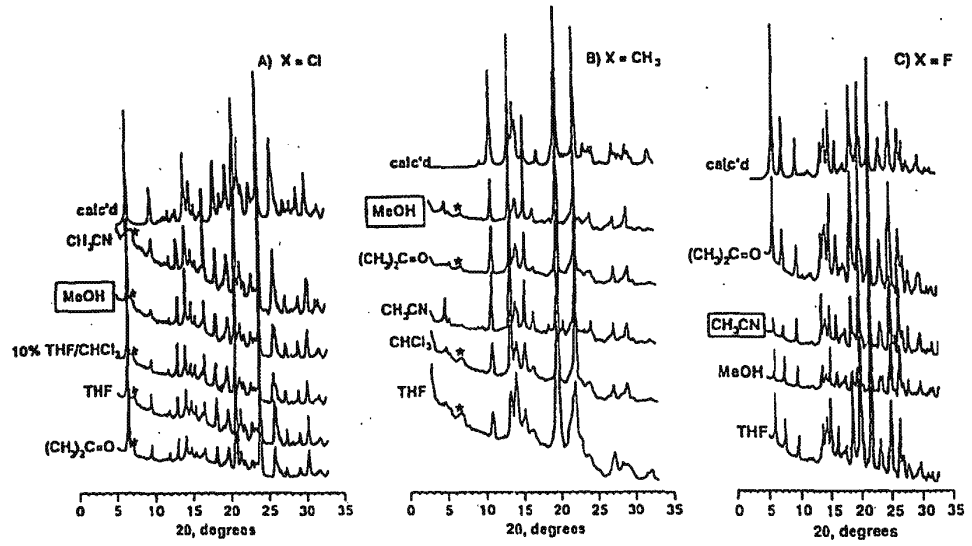


Figure 1. Experimental X-ray powder diffraction traces for X = Cl, CH_3, and F, and comparison with traces calculated from single-crystal coordinates. Agreement between experimental and calculated patterns is considered good. The boxed solvent is that used to grow the crystal studied by single-crystal diffraction. The starred peak that appears in many of the traces may be due to the fiberboard sample holder[23] or to an unknown contaminant; it is neither barbital nor the substituted diphenylmelamine in uncomplexed form.

The third class (X = Br and CF_3) obviously lacks even partial agreement between observed and calculated traces. We conclude that the single crystals used for structure determination were a different polymorph from the powdered bulk samples investigated by XPD. We will label the single-crystal phase as polymorph I, and the new phase detected as polymorph II.

After detecting the presence of polymorphs of X = Br and X = CF_3 by XPD, we made repeated attempts at crystallization, varying experimental conditions such as solvent and rate of evaporation and were able to grow single crystals of polymorph II for X = Br. For X = CF_3, however, we could not obtain single crystals of polymorph II or a powder sample consisting predominantly of polymorph I, as judged by XPD.[22] Figure 4 shows comparisons between calculated and observed XPD traces for the X = Br polymorphs (calculated traces for both polymorphs are based on single-crystal data); agreement is satisfactory, especially between the 2θ values of the calculated and experimental peaks, as it was for the X = Cl, CH_3, and F complexes described above.

In addition to these first two polymorphs for X = Br, we obtained a third polymorph, no single crystal of which could be grown (Table 1 lists the conditions that yielded each polymorph). The XPD result for this third polymorph (Figure 4) is unusual: only one dominant diffraction peak appears, with few separate small peaks. The presence of one very intense reflection may indicate that the constituent molecules pack in flat, parallel layers in this phase. In fact, the value of 2θ of this reflection, 21.9°, corresponds to a spacing of lattice planes of 4.05 Å, a reasonable value for the distance between adjacent molecular layers.

(22) For an overview of "disappearing polymorphs", see: Dunitz, J. D.; Bernstein, J. *Acc. Chem. Res* **1995**, *28*, 193.

Table 1. Crystallization Parameters and Crystal Data for X = Br Polymorphs I–III

polymorph	solvent(s)[a]	crystal morphology	density[b] (g/cm³)
I	MeOH	plates	1.636
	THF		
	1:1 CH_3CN/THF		
II	$(CH_3)_2C=O$	needles	1.602
	EtOAc		
	MeOH		
	CH_3CN		
	5:95 THF/$CHCl_3$		
III	THF (fast evap)[c]	prisms	
	2:5 CH_3CN/THF		
	1:1 $CHCl_3$/THF		

[a] All evaporations of solvent took several days from a closed vessel unless otherwise noted. The underlined solvent was the one used to grow single crystals. [b] Calculated from single-crystal results. [c] Evaporation was complete in several hours from an uncovered beaker.

This third polymorph of the X = Br complex is unlikely to be a partially amorphous solid, where poor crystallinity could be caused by desolvation of a lattice with trapped solvent, leading to a comparatively featureless XPD trace of this sort. First, there is no evidence of even trace amounts of residual solvent in an NMR spectrum of the redissolved solid. Second, a decrease in crystallinity should be accompanied by broadening of the diffraction peaks, whereas the major peak of polymorph III is no broader than intense peaks in the other polymorphs. Similarly, resonances in the solid-state ^{13}C NMR are not broadened relative to resonances for the other polymorphs (see below). Finally, heating polymorph III transforms it to one of the polymorphs with known structure (see below).

Influence of Sample Preparation on XPD Traces. There are significant differences in the intensities of observed and calculated peaks in the data summarized in Figures 1–3; the peaks at 2θ = 6° in Figure 1c and

UM00012543
NOVARTIS EXHIBIT 1017
Novartis v. Regents, IPR2023-01346
Page 1289 of 4460

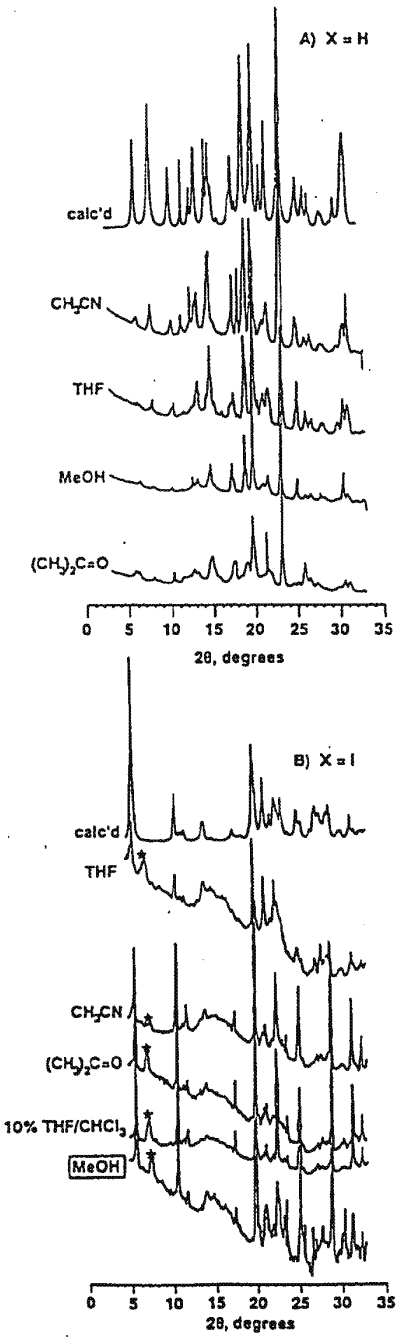


Figure 2. Experimental X-ray powder diffraction traces for X = H and I. Agreement with the calculated traces is only fair: although the peaks in the calculated trace are present in the observed traces, additional peaks are also observed and the agreement in intensities is poor. The boxed solvent is that used to grow the crystal studied by single-crystal diffraction (for X = H, the solvent for growth of single crystals was dichloromethane). The starred peak may be due to the sample holder or to a contaminant as in Figure 1.

$2\theta = 31°$ in Figure 2a provide examples. Effects associated with the geometry of the diffractometer are likely to be responsible for intensity differences at low values of 2θ.[23,24] In fact, attempts to solve crystal structures from powder data might discard from the calculations diffraction peaks at low angles[25] or at least apply a correction factor,[26] for this reason. The explanation is as follows: a divergence slit of fixed width (in our case, 0.5°) will bathe a wider area with X-rays at

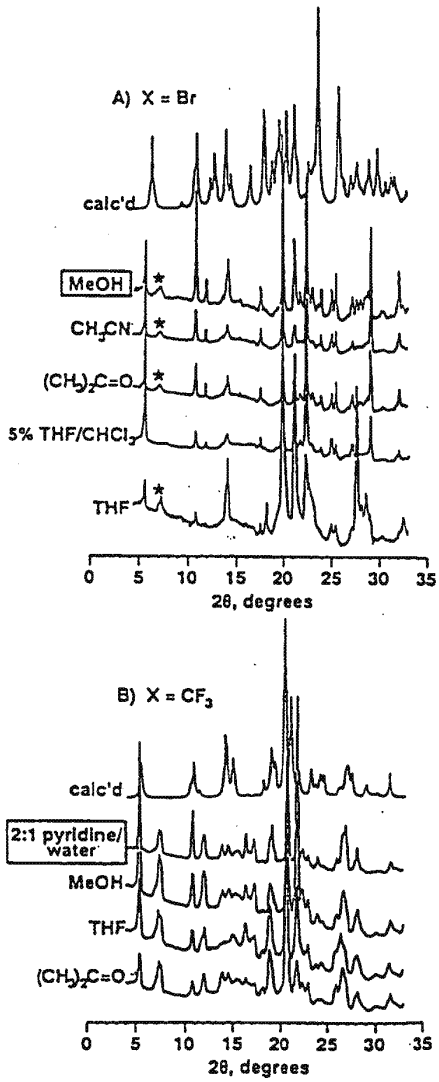


Figure 3. Experimental X-ray powder diffraction traces for X = Br and CF_3; the disagreement between experimental and calculated traces indicates that the single-crystal and powder data were obtained on different polymorphs. The boxed solvent is that used to grow the crystal studied by single-crystal diffraction. The starred peak may be due to the sample holder or to a contaminant as in Figure 1.

(23) *Modern Powder Diffraction*; Bish, D. L., Post, J. E., Eds.; Mineralogical Society of America: Washington, DC, 1989.
(24) Parrish, W.; Mack, M.; Taylor, J. *J. Sci. Instrum.* **1966**, *43*, 623.
(25) Masciocchi, N.; Moret, M.; Cairati, P.; Sironi, A.; Ardizzoia, G. A.; La Monica, G. *J. Am. Chem. Soc.* **1994**, *116*, 7668.
(26) Petit, S.; Coquerel, G.; Perez, G.; Louër, D.; Louër, M. *Chem. Mater.* **1994**, *6*, 116.

UM00012544
NOVARTIS EXHIBIT 1017
Novartis v. Regents, IPR2023-01346
Page 1290 of 4460

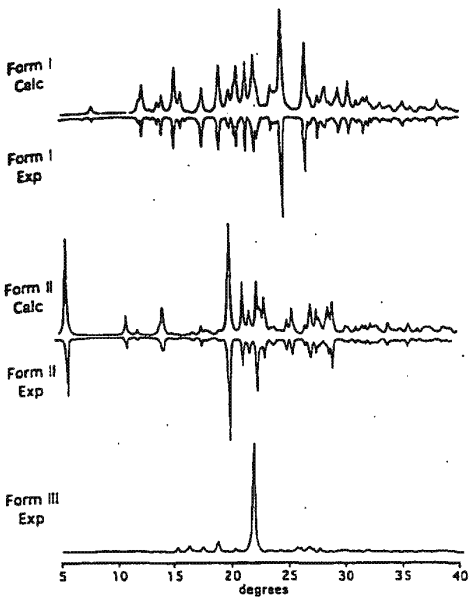


Figure 4. Comparison of experimental X-ray powder diffraction traces for three polymorphs of the X = Br complex with traces calculated from the solved crystal structures. There is no calculated trace for the third polymorph, since no single crystal suitable for X-ray diffraction could be grown.

low 2θ than at high 2θ. Equation 1, taken from ref 24,

$$L = R \tan \alpha / \sin \theta \qquad (1)$$

details this relationship for a point X-ray source (an approximation that will serve for demonstration purposes). For example, with α, the angular slit width, equal to 0.5°, and R, the distance from the source to the sample, equal to 170 mm, the irradiated area L is 10 mm wide (the size of our sample) at $2\theta = 17°$. For $2\theta = 5°$, the area is 34 mm wide. In effect, the sample will then be sensing only a fraction of the total X-ray intensity of the beam, so diffraction from crystallite planes below about 17° in our experimental setup is correspondingly weaker. In addition, at low angles there will be a contribution from scattering due to the sample holder, which can give rise to a small peak at low 2θ.[23] We suspect that this background scattering is the origin of the small peaks that are starred in Figures 1–3, as well as the broad hump from approximately 13–18° in Figure 2b.

Effects associated with sample preparation could also be important. In general, we propose that some combination of two experimental features—preferred orientation and crystallite size—could produce powders that are not sufficiently isotropic to yield experimental XPD data in good agreement with idealized traces calculated only from unit-cell information and the molecular structure of the asymmetric unit.

We first considered preferred orientation, which is known to cause a weakening of some reflections experimentally.[27,28] Crystals composed of linear hydrogen-bonded tapes, when ground for XPD studies, probably afford crystallites with high aspect ratios due to the anisotropy of the intermolecular forces.[29] Fracture should thus be easier parallel, rather than perpendicular, to the tapes. Alignment of these microneedles with their long axes parallel seems likely, although we do not have independent experimental evidence (such as electron micrographs) for this effect.

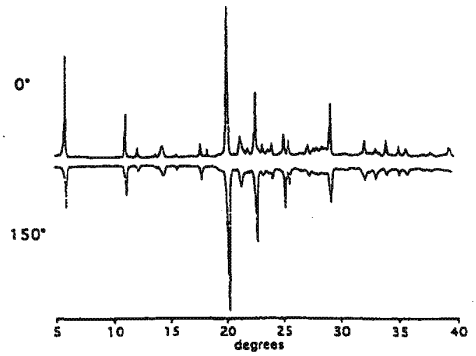


Figure 5. Comparison of two XPD traces performed on the same sample showing the effect of rotation of the sample holder in the diffractometer. The initial orientation is arbitrarily labeled 0°. The change in relative intensities of peaks, especially at low 2θ, could be an indication of preferred orientation of crystallites in the sample or of variations in the beam width due to the geometry of the diffractometer (see text).

We tested for preferred orientation by rotating a sample (polymorph II of the X = Br complex in all cases) in the diffractometer by 30° increments about the axis perpendicular to the horizontal sample holder.[30] Figure 5 shows the diffraction traces obtained at two such orientations; the biggest change occurs in the relative intensity of the peak at about 6°. These results suggest that preferred orientation might be occurring in these samples, although considering the small effects in relative intensity in primarily one region of the spectrum (at low 2θ, where the beam-width problems discussed above are also operative), it is probably not responsible for all the discrepancies between calculated and observed traces.[31]

A second factor could be incomplete grinding of the sample, leaving large crystallites; this situation could lead to a poorly isotropic distribution of crystal planes in the X-ray beam.[32,33] To test for the effects that a broad distribution of crystallite size might have, we ground samples for varying lengths of time. Grinding

(27) Klug, H. P.; Alexander, L. E. *X-ray Diffraction Procedures for Polycrystalline and Amorphous Materials*, 2nd ed.; Wiley: New York, 1974.

(28) (a) Nakata, K.; Sugihara, H.; Mori, S.; Yamaguchi, H.; Takaki, Y. *Bull. Chem. Soc. Jpn.* **1984**, *57*, 3395. (b) Nakata, K.; Takaki, Y. *Bull. Chem. Soc. Jpn.* **1987**, *60*, 1168.

(29) Macroscopically, these complexes do frequently yield needle-shaped crystals. The plate morphology that also regularly occurs can also lead to orientation problems of crystallites.[28]

(30) The sample for this experiment was ground for 5–8 min in an agate mortar and pestle. This method was the one we commonly used to prepare all our powdered samples, so we believe that this search for preferred orientation is based on a representative class of powders.

(31) Note, however, that by rotating the sample and sample holder only around one axis, we would only be able to detect preferred orientation in one plane (the plane of the sample holder). Tilting the sample holder (which is essentially impossible in our diffractometer) should also be performed to test for a horizontal packing of needle-shaped crystallites.

(32) Large crystallites can give anomalously intense spikes for some reflections.[23] We speculate that some of the peaks in the X = I complex (Figure 2b) could arise in this manner.

UM00012545
NOVARTIS EXHIBIT 1017
Novartis v. Regents, IPR2023-01346
Page 1291 of 4460

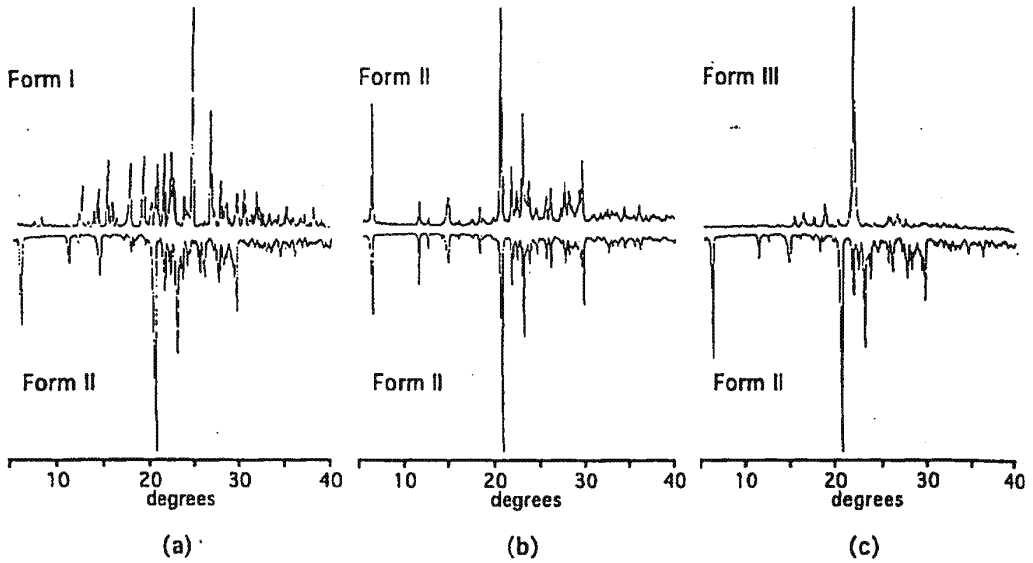


Figure 6. XPD traces of three polymorphs of the X = Br complex before (above) and after (below) thermal annealing at 140 °C for 6 days. Forms I and III have been converted to form II.

samples 10 min longer than usual (for a total of 15–18 min) led to small changes in the relative intensities of peaks at 6° and 11° (data not shown), on the order of magnitude of the changes seen above for rotating the sample. Visual inspection of crystalline samples showed that individual crystals did not become opaque or develop fractures with the passage of time (over a period of at least several days), indicating that they were not solvates. Grinding was therefore unlikely to be responsible for any changes in crystallinity associated with desolvation of the lattice (none of the members of this para series of complexes were ever found to contain solvent in the lattice).[1]

Our conclusion is that disagreement between calculated and observed traces, especially at low 2θ, are likely to be due primarily to the physical design of the diffractometer.[34] This contention is consistent with the fact that even for those complexes where agreement is satisfactory (X = Cl, CH_3, and F), agreement is *least* good at low 2θ. An auxilliary reason for the disagreement could be heterogeneity and anisotropy over the region probed by the diffractometer, caused by preferred orientation and/or crystallite size. The magnitudes of these effects associated with sample preparation, as determined by tests intended to check for their presence, seem too small to explain the discrepancies fully.[35]

Annealing of the X = Br Polymorphs. Annealing powders of the three polymorphs at 140 °C for 6 days demonstrated that both forms I and III convert to form II (see Figure 6). The relative intensities of the peaks in form II itself change slightly. These results indicate that form II is thermodynamically the most stable (at 140 °C) of these three polymorphs. We do not know which polymorph is the thermodynamically stable one *at room temperature*, although one rule of thumb holds that the denser polymorph (in this case polymorph I) will be the more stable.[36,37] Polymorph I also has a higher packing density, 0.72 vs 0.68 for polymorph II.[1]

Differential scanning calorimetry (DSC) was attempted on forms I–III. Separate runs were conducted for each sample during which the rate of heating was varied from 1 to 10 °C/min. In each case, the samples began to turn brown and decompose in the range 240–260 °C. Each sample showed a broad melting endotherm in the range 270–280 °C. None of the samples gave a detectable endotherm/exotherm prior to melting that indicated a phase transition under the conditions reported above. For melting points of the complexes, see ref 1.

Comparison of Packing in Single Crystals of Br Polymorphs I and II. Figures 7 and 8 show several views of the molecular packing in polymorphs I and II

(33) For a demonstration that differences in crystallite size and shape can lead to powder diffraction traces that can be mistakenly interpreted as arising from different polymorphs, see: Potts, G. D.; Jones, W.; Bullock, J. F.; Andrews, S. J.; Maginn, S. J. *J. Chem. Soc., Chem. Commun.* **1994**, 2565.

(34) Other problems associated with the setup of the diffractometer, e.g., inconsistent filling of the sample holder, could also make a contribution. Furthermore, the very act of grinding a sample could generate enough heat or mechanical stress to initiate a polymorphic phase transition. There seem to be few ways around this dilemma, except perhaps by employing a gradual increase in grinding time or vigor while remaining aware of the problems mentioned in footnotes 32 and 33.

(35) For studies that demonstrate the difficulty of reproducing peak intensities exactly, see: (a) Chrzanowski, F. A.; Fegely, B. J.; Sisco, W. R.; Newton, M. P. *J. Pharm. Sci* **1984**, *73*, 1448. (b) Kidd. W. C.; Varlashkin, P.; Li, C. *Powder Diffraction* **1993**, *8*, 180. (c) Davey, R. J.; Maginn, S. J.; Andrews, S. F.; Black, S. N.; Buckley, A. M.; Cottier, D.; Dempsey, P.; Plowman, R.; Rout, J. E.; Stanley, D. R.; Taylor, A. *J. Chem. Soc., Faraday Trans.* **1994**, *90*, 1003. (d) Davey, R. J.; Maginn, S. J.; Andrews, S. F.; Black, S. N. *Mol. Cryst. Liq. Cryst.* **1994**, *242*, 79. These last two papers demonstrate an important but subtle point: different polymorphs may have XPD patterns that appear virtually indistinguishable from each other.

(36) Burger, A.; Ramberger, R. *Mikrochim. Acta (Wien) II* **1979**, 259.

(37) In the absence of calorimetric measurements, we cannot tell whether forms I and II are enantiotropic or monotropic.[38] The fact that the thermally produced samples of form II did not revert to their initial identity (forms I and III, respectively) is not proof that form II is the thermodynamically stable polymorph at room temperature. Metastable phases can be trapped well below the temperature of phase transition: (a) Yang, Q.-C.; Richardson, M. F.; Dunitz, J. D. *Acta Crystallogr.* **1989**, *B45*, 312. (b) Richardson, M. F.; Yang, Q.-C.; Novotny-Bregger, E.; Dunitz, J. D. *Acta Crystallogr.* **1990**, *B46*, 653.

UM00012546
NOVARTIS EXHIBIT 1017
Novartis v. Regents, IPR2023-01346
Page 1292 of 4460

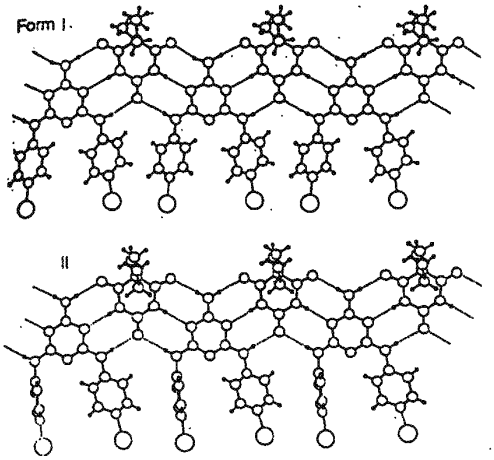


Figure 7. Comparison of tape geometry for two X = Br polymorphs. The disorder of the ethyl groups in form I is *not* shown in this figure; the torsion angles of one ethyl group cause it to appear skewed in this top-down view of the tapes.

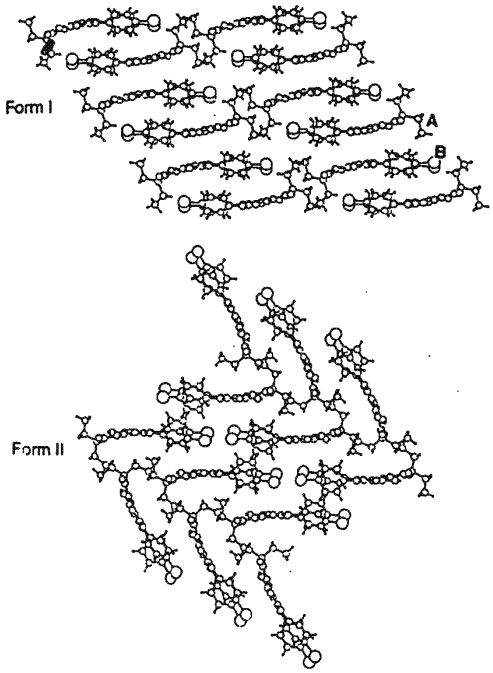


Figure 8. End-on packing views of two X = Br polymorphs.

of the X = Br complex (both of these structures were described in a previous paper on the family of complexes built from para-substituted diphenylmelamines).[1] Both polymorphs adopt the same kind of secondary architecture, namely, the linear tape motif. Differences arise instead at the tertiary level of architecture. Polymorph I exhibits dimer-based packing (illustrated by tapes A and B in Figure 8), while polymorph II adopts a sheetlike architecture. There are also differences in molecular conformation (Figure 9). The torsion angles of the phenyl groups differ: they are 42° and −136° in polymorph I, and 156° and −93° in polymorph II.

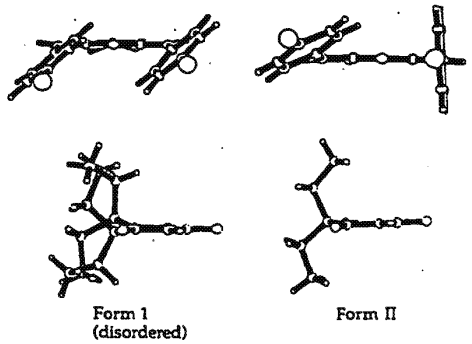


Figure 9. Comparison of the molecular geometry in two polymorphs of the X = Br complex. The ethyl groups in form I are statistically disordered in a ratio of about 2:1; the minor component has essentially the same torsion angles, but with trans and gauche conformations switched as though the molecule were flipped upside-down.

Polymorph I is statistically disordered in the Et groups of barbital, and the torsion angles of these groups also differ: they are 38° (roughly a gauche conformation) and 178° in polymorph I, and −180° and −174° in polymorph II (both groups extended and trans).

^{13}C Solid-State NMR of Br Polymorphs I, II, and III. We also used ^{13}C CP/MAS NMR to characterize the three polymorphs. Solid-state NMR should be useful for studies on polymorphism. The characteristics that define a molecule in alternative polymorphs, such as its conformation, thermal motion, and near-neighbor contacts, will also affect the isotropic chemical shifts of each carbon atom in the solid state.[38] In practice, however, routine one-dimensional spectra provide little specific information about three-dimensional packing.[39] We use the technique primarily in a fingerprinting sense to confirm the composition of the solid and to show that solvent is not included in the lattice.

Figure 10 shows solution and solid-state NMR spectra of all three polymorphs. The only significant statement we can make is that polymorph III is qualitatively different from the other two, especially in the aliphatic region, in that it has three methylene resonances. We cannot, however, determine what structural features might cause this spectroscopic result: for example, the ethyl groups could be crystallographically disordered, or there could be multiple molecules in the crystallographic asymmetric unit.

Conclusions

Figures 1–3 indicate that, considering only a limited range of crystallization conditions, polymorphism is not equally likely across this closely related family of complexes. Three complexes (X = Cl, CH_3, F) adopt only one packing arrangement, two (X = H, I) adopt primarily one arrangement but may have a small contribution from an alternative phase or phases, and two complexes

(38) Changes in van der Waals contacts, charge-transfer interactions, ionic field effects, or dipolar interactions that arise from alternative packing arrangements can lead to differences between solution-phase and solid-phase chemical shift values of up to 3 ppm. Larger differences of up to 10 ppm are likely to be associated with changes in molecular conformation from solution to solid.

(39) For solid-state studies using sophisticated NMR techniques, see: Edwards, A. J.; Burke, N. J.; Dobson, C. M.; Prout, K.; Heyes, S. J. *J. Am. Chem. Soc.* **1995**, *117*, 4637.

UM00012547
NOVARTIS EXHIBIT 1017
Novartis v. Regents, IPR2023-01346
Page 1293 of 4460

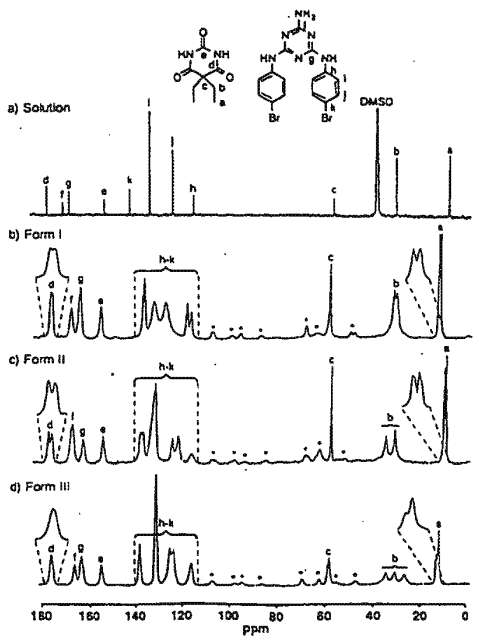


Figure 10. Solution and solid-state ^{13}C NMR spectra of X = Br polymorphs. Spinning sidebands are starred.

(X = Br, CF_3) adopt at least two packing arrangements. Given the polymorphism of the X = Br and CF_3 complexes, the single-crystal diffraction studies that we *initially* performed on those complexes only provided an incomplete picture of the packing preferences of these molecules.[1] In other words, the particular polymorph that was first described reflected a subjective choice of a crystallographer who simply selected the single crystals of diffraction quality. In the case of the X = Br complex, this choice amounts to a preference for polymorph I (plates) over polymorph II (needles; see Table 1). These studies reinforce the idea clearly stated by Desiraju,[5] Dunitz,[40] and Aakeroy and Seddon[41] that single-crystal studies should not form the basis for generalizations about molecular packing preferences in the absence of XPD studies (or other studies that explore polymorphism). Arguably, in studies directed toward crystal engineering, XPD studies that survey polymorphism should precede single-crystal studies.

In making connections to our previous work on crystalline architecture, we can draw only limited conclusions, since we have found only one complex that yields two polymorphs as single crystals. We note, however, that the differences between polymorphs occur at the levels of molecular conformation and tertiary packing, or aggregates of tapes; the secondary motif (linear tapes) is unchanged. This consistency in the secondary motif is expected considering our previous work: there are no steric or electronic reasons to force a change in the secondary motif, since the molecular composition has not changed.[1-3]

Furthermore, we speculate that the Br substituent, coming approximately at the midpoint of the size range

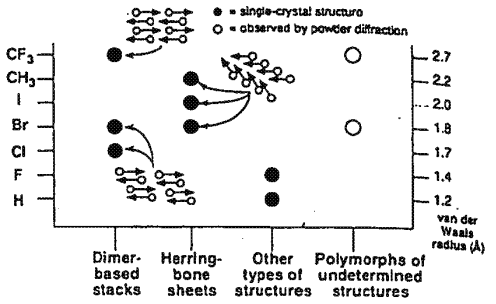


Figure 11. Relationship between the size of the substituent and the motif of tertiary crystalline architecture in complexes built from *N,N'*-bis(*p*-X-phenyl)melamines. Two varieties of dimer-based stacks and one of herringbone sheets are shown schematically. Arrows with circles attached represent end-on views of the tapes.

spanned by these substituents (from H to CF_3), can crystallize in one of two alternative, polymorphic packing arrangements (see Figure 11). Phase II is isostructural to the packing adopted by the larger substituents X = I and CH_3, while phase I is isostructural to the packing of the smaller substituent X = Cl. We do not understand why the cocrystal with X = CF_3 has the structure it does. In other studies we have also found that fluorinated compounds show behavior that is anomalous based on steric arguments, but the origin of the anomalies remains undefined.[42] It remains to be seen whether the steric component to polymorphism turns out to be a general phenomenon that occurs in other families of organic crystals.

Experimental Section

General. Preparation of the complexes and single-crystal diffraction studies on them were described previously.[1]

X-ray Powder Diffraction Studies. Crystallizations to search for alternative polymorphs were performed by dissolving the complexes and placing the solution in a loosely closed vessel, such as a beaker or a crystallization dish covered with the lid of a crystallization dish. Evaporation proceeded at room temperature, usually over the course of several days. The crystalline solids obtained after evaporation was complete were ground by hand with an agate mortar and pestle, routinely for 5–8 min. The resulting powders were loaded into a fiberboard holder that had a 1 cm by 1 cm depression for the sample. The top of the powder was smoothed with a metal spatula to be flush with the top of the fiberboard holder. Thermal annealing of powder samples was performed in a drying oven.

Powder diffraction traces were obtained on both Phillips Model PW1010 and Scintag model XDS-2000 diffractometers with Cu Kα radiation (λ = 1.4506 Å). Scans were begun at 2θ = 3° and run to 33° or 43° in 0.1° step sizes with 40 s of counting at each step. Output files (intensity vs 2θ) were generated using the plotting program Kaleidagraph.

^{13}C CP/MAS NMR. Spectra of forms I–III of *N,N'*-bis(*p*-bromophenyl)melamine-barbital were collected at Eli Lilly Corp., Indianapolis, IN, on a Varian Unity 400 spectrometer operating at a carbon frequency of 100.577 MHz and equipped with a Varian solid-state NMR probe. Typical conditions for measurements utilized a 3.4 ms 90° proton radio frequency pulse, 1 ms contact time, 10 ms pulse-repetition time, 7 ± 0.2 kHz MAS frequency (rate of spinning), 50 kHz spectral width, and 50 ms acquisition time. The ^{13}C chemical shifts were referenced to the methyl resonance of hexamethylbenzene (δ = 17.3 ppm) by replacing the sample. Powders were prepared by grinding samples in an agate mortar and pestle for 5 min.

(40) Dunitz, J. D. *X-ray Analysis and the Structure of Organic Molecules*; Cornell University Press: Ithaca, NY, 1979.
(41) Aakeroy, C. B.; Seddon, K. R. *Chem. Soc. Rev.* **1993**, *23*, 397.
(42) Schwiebert, K.; Chin, D.; Whitesides, G. M. Unpublished data.

UM00012548
NOVARTIS EXHIBIT 1017
Novartis v. Regents, IPR2023-01346
Page 1294 of 4460

Calculation of XPD Traces. The Siemens programs XPOW and XFOG in the SHELXTL-PLUS package of programs and the MSI package Cerius·2 were used to calculate XPD traces. XPOW (which uses observed single-crystal intensity data) and XFOG (which calculates intensity data based on an input molecular model and space group) gave identical calculated traces.

Acknowledgment. We acknowledge the support of the National Science Foundation through Grants CHE-91-22931 to G.M.W., DMR CHE-89-20490 to the Harvard University Materials Research Laboratory, and CHE-80-00670 for the purchase of the Siemens X-ray diffractometer. J.C.M. acknowledges the Merck Corporation for financial assistance. We thank Dr. Susan M. Reutzel for obtaining the solid-state NMR spectra.

Supporting Information Available: X-ray diffraction data (3 pages). Ordering information is given on any current masthead page.

CM9505660

UM00012549
NOVARTIS EXHIBIT 1017
Novartis v. Regents, IPR2023-01346
Page 1295 of 4460

C-4 and also in that due to C-3, indicating formation of 6β-hydroxytropine with the labeling pattern 9A plus 9B, identical with that found in the experiment with [1,2-$^{13}C_2$]acetate. Incorporation of an intact C_3 unit (9G), as observed in the case of *N*-methylpelletierine,[2] would have resulted in a doublet of doublets in the signal due to the CHOH group, C-3. Since the pattern of incorporation of ^{13}C from [1,2,3,4-$^{13}C_4$]acetoacetate was identical with that from [1,2-$^{13}C_2$]acetate, the acetoacetate had cleaved to acetate before incorporation of the label. Thus, the C_3 unit, C-2–4, was generated from two discrete acetate units, as demanded by the "cocaine mechanism"[1] (2 → 3 → 4, Scheme I), and not from an intact acetoacetate-derived C_3 unit, as demanded by the "pelletierine mechanism"[2] (2 → → 5, Scheme I).

Secondly, entry of the side chain into 2 may take place stereospecifically, eventually leading to a uniquely labeled tropine (7), but the hydroxylation whereby the 6β-OH group is introduced into the ornithine-derived moiety of the tropine unit of hyoscyamine (8), while diastereospecific, is not enantiospecific with respect to the tropine unit, forming a pair of diastereomers, (3*S*,6*S*)-6β-hydroxyhyoscyamine (10) and (3*R*,6*R*)-6β-hydroxyhyoscyamine (also known as 7β-hydroxyhyoscyamine), from which a pair of enantiomeric molecules, 9A plus 9C or 9B plus 9D, is generated on hydrolysis.

This explanation of the labeling pattern requires that the biosynthetic sample of 6β-hydroxytropine be a racemate, consisting of the (3*S*,6*S*) isomer (9) (see also 9A and 9B) and the (3*R*,6*R*) isomer (occasionally referred to erroneously as 3α,7β-dihydroxytropane,[15] i.e., 7β-hydroxytropine) (9C and 9D). Esters of both enantiomers of 6β-hydroxytropine occur in plants of the genus Solanaceae, including several species of *Datura*, but no racemates have been reported, and the enzymic hydroxylation process whereby the 6β-hydroxy group is introduced into one of the alkaloids, (−)-hyoscyamine (8), is stereospecific[8] as well as substrate specific.[9] Furthermore, in the instances when diastereomeric alkaloids, namely, the *O*-3 (−)-(*S*)-tropic acid esters of (3*S*,6*S*)-dihydroxytropane ((−)-6β-hydroxyhyoscyamine) (10) and of (3*R*,6*R*)-dihydroxytropane ((−)-7β-hydroxyhyoscyamine), were isolated from the same plant, the latter compound was much less abundant than the former.[15,16] It is unlikely that hydrolysis of a mixture of ester alkaloids should fortuitously yield an equimolar mixture of the two enantiomeric dihydroxytropanes. This explanation of the incorporation pattern is thus unlikely.[17]

Thirdly, addition of the acetate-derived side chain to the *N*-methyl-Δ^1-pyrrolinium ion[5] (2) may take place by the "cocaine mechanism"[1] (analogous to route C in ref 2), yielding an equimolar mixture of (*R*)- and (*S*)-*N*-methylpyrrolidineacetoacetate (4), both of which are then further elaborated into tropine (7) either via (*R*)- and (*S*)-hygrine[7] (5) or directly. The mixture of (*R*)- and (*S*)-4 can originate either by racemization[14] of a chiral species, namely (*R*)-4 which is originally generated,[6] or less probably can be formed directly by nonstereospecific entry of the side chain into 2.

A third experiment, with *N*-methyl-Δ^1-[2-^{2}H]pyrrolinium chloride (500 mg, 98% ^{2}H; prepared from DL-[2-^{2}H]proline by Eschweiler–Clarke methylation,[18] followed by heating with $POCl_3$[19]) as the substrate, provides evidence for the implication of racemic intermediates between 2 and 6. This experiment gave a sample of 6β-hydroxytropine (ca. 3 mg, % enrichment 0.3%) whose ^{2}H NMR spectrum (76 MHz, 16 000 scans) indicated the presence of deuterium, equimolar within the limits of detection, at each of the two bridgehead sites (δ = 3.0, 3.6 ppm)[15] of the molecule, which thus consisted of an equimolar mixture of 9E and 9F. This result disposes of any scheme that does not accommodate the involvement of both enantiomers of *N*-methylpyrrolidineacetoacetate (4) (or of hygrine[7] (5)). Any mechanism that involves chiral intermediates (e.g., (*R*)-4 and (*R*)-5) would have produced 9E as the sole product rather than an equimolar mixture of 9E and 9F.

The evidence here presented leads to the inference that, contrary to conventional wisdom, the non-ornithine-derived moiety of the tropane ring system of 6β-hydroxytropine in *D. stramonium* does not originate from acetoacetate but by stepwise incorporation of acetate, whose nonregiospecific distribution within the C_3 unit implies the involvement of a racemic intermediate on the pathway.

Registry No. 9, 41164-06-1; acetate, 64-19-7.

(15) Ishimaru, K.; Shimomura, K. *Phytochemistry* **1989**, *28*, 3507.
(16) Shimomura, K.; Sauerwein, M.; Ishimaru, K. *Phytochemistry* **1991**, *30*, 2275. Sauerwein, M.; Shimomura, K. *Phytochemistry* **1991**, *30*, 3277.
(17) The labeled samples of 6β-hydroxytropine isolated from our feeding experiments were of inadequate weight and chemical purity to permit determination of reliable $[\alpha]_D$ values.
(18) Clarke, H. T.; Gillespie, H. B.; Whitehouse, S. Z. *J. Am. Chem. Soc.* **1933**, *55*, 4571.
(19) Dean, R. T.; Padgett, H. C.; Rapoport, H. *J. Am. Chem. Soc.* **1976**, *98*, 7448.

Solid-State Structures of "Rosette" and "Crinkled Tape" Motifs Derived from the Cyanuric Acid–Melamine Lattice[1]

Jonathan A. Zerkowski, Christopher T. Seto, and George M. Whitesides*

Department of Chemistry
Harvard University
Cambridge, Massachusetts 02138

Received February 21, 1992

We are using the pattern of hydrogen bonds present in the 1:1 complex formed from cyanuric acid and melamine (CA·M) as the basis for the design of self-assembling structures.[2-5] We have described a solid-state structure based on a "linear" tape motif taken from this lattice (3, Figure 1),[3] and we have inferred the existence of cyclic aggregates containing three melamine and three isocyanurate moieties in solution.[4,5] Here we report solid-state structures of a new type of tape format (a "crinkled tape", 4) and a cyclic structure (a "rosette", 5), both obtained by combination of *N*,*N*′-bis(*p*-substituted phenyl)melamine (1) and 5,5-diethylbarbituric acid (2). We believe that the three solid-state structures 3–5 are the most plausible structural motifs that can be derived from the CA·M lattice: other, more collapsed tape or cyclic structures (e.g., 6 and 7, and larger cyclic structures containing these units) are destabilized by nonbonded steric interactions (indicated by arrows in Figure 1). These two new structures, together with the structure of a linear tape (X = H) already described,[3] serve as paradigms for use in the design of self-assembling structures based on the CA·M lattice and provide structural parameters applicable to evaluation of the energetics of these structures using molecular mechanics.[6]

Figure 2 (middle) shows the structure of the 1:1 complex of **1a** (X = CO_2CH_3) and 2.[7] This crinkled format occurs commonly: of 15 structures we have determined in the series of cocrystals incorporating substituted diphenylmelamines and 2, three are crinkled tapes. The complex **1a**·2 crystallizes from

(1) Supported by the National Science Foundation, Grant CHE-88-12709 to G.M.W., Grant DMR-89-20490 to the Harvard University Materials Research Laboratory, and Grant CHE 80-00670 for the purchase of the Siemens X-Ray diffractometer.
(2) Whitesides, G. M.; Mathias, J. P.; Seto, C. T. *Science* **1991**, *254*, 1312.
(3) Zerkowski, J. A.; Seto, C. T.; Wierda, D. A.; Whitesides, G. M. *J. Am. Chem. Soc.* **1990**, *112*, 9025.
(4) Seto, C. T.; Whitesides, G. M. *J. Am. Chem. Soc.* **1990**, *112*, 6409.
(5) Seto, C. T.; Whitesides, G. M. *J. Am. Chem. Soc.* **1991**, *113*, 712.
(6) Desiraju, G. R. *Crystal Engineering: The Design of Organic Solids*; Elsevier: New York, 1989. Wright, J. D. *Molecular Crystals*; Cambridge University Press: Cambridge, 1987.
(7) Crystal data for **1a**·2 (X = CO_2CH_3): $(C_{19}H_{11}N_6O_4)(C_8H_{12}N_2O_3)$-$C_3H_7CH_2OH$; space group $C2/c$; a = 23.95 (3) Å, b = 16.95 (4) Å, c = 14.59 (1) Å, β = 94.4 (1)°, V = 5905 (2) Å^3, D_{calcd} = 1.302 g/cm^3 without a contribution from included solvent, 1.405 g/cm^3 with the solvent; Z = 8 1·2 pairs; R = 0.14 (further refinement to model the disordered solvent molecule is underway).

0002-7863/92/1514-5473$03.00/0 © 1992 American Chemical Society

UM00012550
NOVARTIS EXHIBIT 1017
Novartis v. Regents, IPR2023-01346
Page 1296 of 4460

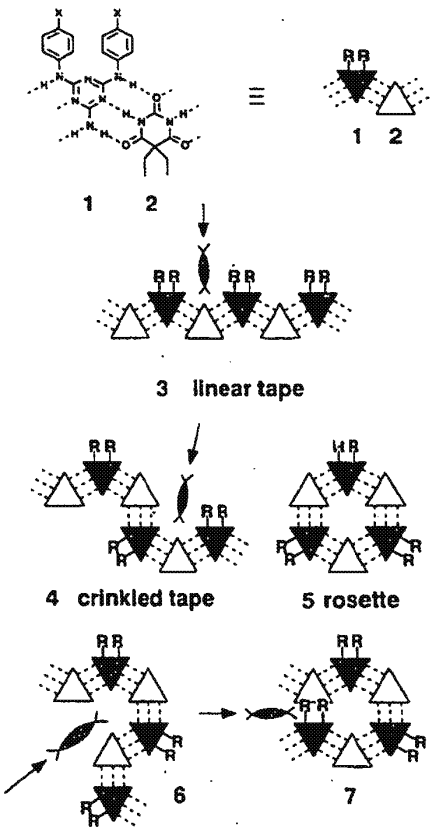


Figure 1. Schematic representation of structures based on repeating units of 1·2. Melamines are represented by filled triangles, diethylbarbituric acid is represented by open triangles, and the triad of hydrogen bonds is represented by the three connecting dotted lines. Regions of unfavorable steric interactions are indicated by the arrows. The structure of 7 superimposes one pair of R groups on a unit of 2 to show the steric strain.

ethanol as a solvate.[8] Figure 2 (lower) shows the structure of **1b** (X = $C(CH_3)_3$) and 2.[9] The mean planes of all the rosettes in the crystal are parallel: that is, they do not adopt a herringbone packing motif. No solvent of crystallization is included in the lattice.

We hypothesize that a competition between nonbonded steric interactions between the X groups and a tendency for a high packing coefficient[10] in the crystal is important in determining which structural motif is adopted by a 1:1 cocrystal of 1 and 2. We assume that any structure must retain the triad pattern of hydrogen bonds. The linear tape 3 is observed for a number of groups X that are small (F, Cl, Br, I, CH_3). When X becomes larger than CF_3 or I,[11] unfavorable lateral nonbonding interactions between X groups on adjacent melamines (Figure 1) are relieved in going to the crinkled structure 4, but are replaced by unfavorable interactions with the ethyl groups of 2 (Figure 2, bottom).[12] The crinkled structure is sufficiently loosely packed to accommodate one ethanol per dimer unit of **1a**·2.[8] Both types of steric interactions are relieved in the rosette 5.

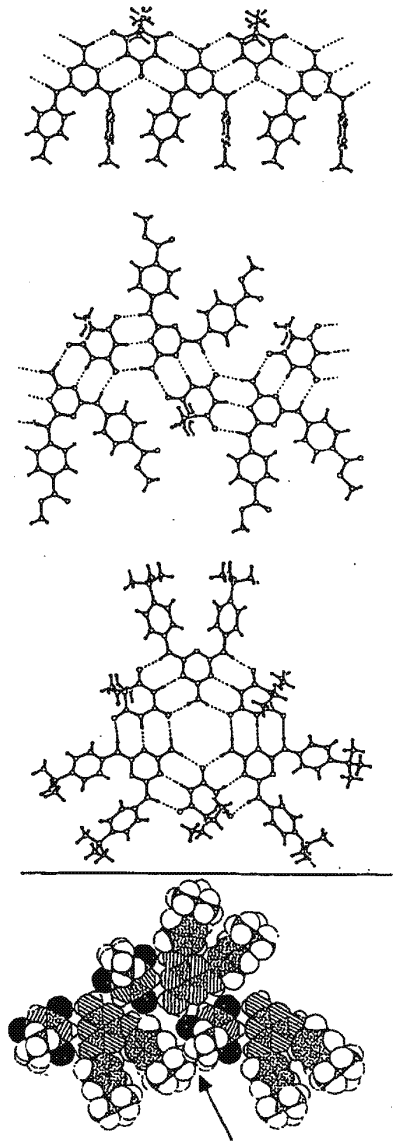


Figure 2. Top: crystal structures of linear tape (X = CH_3),[3] crinkled tape (X = CO_2CH_3), and rosette (X = $C(CH_3)_3$) motifs. The crinkled tape crystal contains disordered ethanol that has been deleted from this view for clarity; it is located above and below the planes of the phenyl rings. Bottom: hypothetical space-filling model generated by replacing the ester groups in the crinkled tape with *tert*-butyl groups, without changing any other nuclear positions. The arrow indicates regions of unfavorable steric interaction between the *tert*-butyl group and the ethyl groups of the diethylbarbituric acid.[12]

The structures reported here demonstrate that simple modifications in the molecular structures of a self-assembling system can lead to changes in crystalline architecture that can be rationalized (at least qualitatively) using steric arguments. By

(8) All three of the crinkled diphenylmelamine structures we have observed are solvates.

(9) Crystal data for **1b**·2 (X = $C(CH_3)_3$): $(C_{21}H_{20}N_6)_2(C_8H_{12}N_2O_3)_2$; space group $P\bar{1}$; a = 16.471 (3) Å, b = 19.930 (2) Å, c = 15.410 (4) Å, α = 95.10 (1)°, β = 99.79 (2)°, γ = 97.01 (1)°, V = 4917 (2) Å^3, D_{calcd} = 1.165 g/cm^3, Z = 2 rosettes (6 1·2 pairs); R = 0.112 (four of the *tert*-butyl groups are disordered; we are continuing to refine the structure with alternative positions for the CH_3 groups).

(10) Kitaigorodsky, A. I. *Molecular Crystals and Molecules*; Academic Press: New York, 1973.

(11) Zerkowski, J. A.; Seto, C. T.; Wierda, D. A.; Whitesides, G. M. Unpublished work.

(12) We have not examined these systems for crystalline polymorphism and have not excluded the possibility that some of these structures are kinetically determined, rather than being thermodynamic minima.

UM00012551
NOVARTIS EXHIBIT 1017
Novartis v. Regents, IPR2023-01346
Page 1297 of 4460

varying the steric demands of substituents around the periphery of our hydrogen-bonded components, we expect to be able to select from among alternative geometrical isomers of hydrogen-bonded assemblies in the solid state.

Supplementary Material Available: Brief synthetic outline, details of X-ray data collection, tables of crystal data and atomic positional parameters, and ORTEP drawings for both complexes (23 pages). Ordering information is given on any current masthead page.

β-Cyclodextrin/Pyridine Gel Systems. The Crystal Structure of a First β-Cyclodextrin–Pyridine–Water Compound

Colette de Rango,*,† Pierrette Charpin,† Jorge Navaza,† Nelly Keller,‡ Ioannis Nicolis,† Françoise Villain,† and Anthony W. Coleman†

CNRS UPR 180, Centre Pharmaceutique Université de Paris Sud, Châtenay-Malabry, France
CNRS URA 331, SCM-DPhG-CEN Saclay 91191 Gif sur Yvette, France

Received February 20, 1992

General models for gel structure involve a dynamic interlocking three-dimensional network of solvent and "gelant" held together by ordered regions.[1-3] We report here the crystal structure of a compound in the β-cyclodextrin–pyridine–water gel system, which evidences such an interlocking network of β-cyclodextrin (β-CD) and solvent.

Isotropic physical gels are obtained from solutions of rigorously anhydrous β-CD in dry pyridine. For concentrations up to 2.5 × 10^{-1} M, melting points vary linearily with temperature; at higher concentrations the gels become sensitive to rapid temperature increases, with formation of a microcrystalline solid and free pyridine. Slow syneresis with formation of anhydrous needles[4] within the gel has been observed, although samples may be stable for several years. Ternary gels exist with toluene, chloroform, or tetrahydrofuran, with the cosolvent in the isotropic phase.

The ^{2}H NMR signals of pyridine-d_5 have line widths (10–15 Hz), in the melt and gel, typical for solution samples, implying the pyridine is in an isotropic fluid state. Solution technique ^{13}C NMR spectra of molten and gel samples show narrow line widths, requiring some β-CD molecules to be in an isotropic state. On going from liquid to gel, the intensity of the β-CD ^{13}C signals decreases considerably with respect to the signals of pyridine, due to a percentage of molecules becoming fixed in ordered junction zones as observed for agarose gels.[5] Addition of water by slow diffusion through the gel from $CuSO_4 \cdot 5H_2O$ yields a crystalline form, corresponding to the title compound.[6]

The structure is a novel packing of β-CD monomers that is less compact (2300 Å^3 per β-CD) than known monomeric (~1500–1750 Å^3) or dimeric (~1800 Å^3) structures. Monomers have been described either as the "herringbone" packing for hydrates[7] and inclusion[8] and cationic insertion[9] compounds or as arranged in sheets in the "brick" packing model.[10] Dimeric layers of inclusion compounds form C-centered layers in four classes of molecular packing.[11] In contrast to all of these compounds formed in aqueous solutions, in our pyridine medium, water was introduced under strict control.

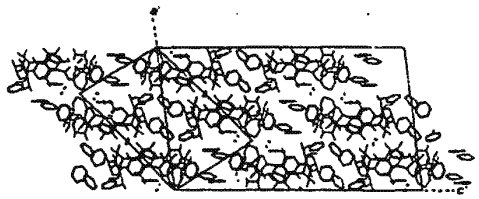


Figure 1. Projection of the structure along the *b* axis showing the packing of cyclodextrin layers in the triple unit cell: $a' = a + c = 23.641$, $b' = -b = 14.742$, $c' = 2a - c = 40.03$ Å, $\beta = 96.57°$ (similarly transformed anhydrous form: $a' = 22.135$, $b' = 15.224$, $c' = 39.94$ Å, $\beta = 95.83°$).

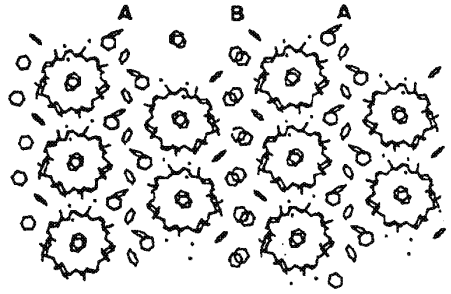


Figure 2. Section of the structure in the (1, 0, 2) plane, isolating a monomeric layer.

The crystal structure was solved using a new molecular replacement package.[12,13] Eight pyridine molecules per β-CD are located in inter- and intramolecular channels (Figure 1), and three water molecules are outside the cavity. One pyridine is included within the β-CD cavity, and a second is located at the primary hydroxyl level. Six others are present within two channels (A and B), both along the crystallographic 2-fold screw axis.

Sheets of β-CD molecules stacked nearly parallel to the *b* axis (inclination ≈ 10°) form an open arrangement of nonoverlapping β-CD monomers. The overall packing consists of layers, formed of pyridine and β-CD units, appearing with a 3-fold translational periodicity along $a' = a + c$; water molecules are located interlayer.

The interlayer distance (7.88 Å) is within the previously observed range; in the layers, β-CD molecules are packed more openly in a pseudo-C-centered arrangement (unit area 620 Å^2) than in dimer structures (unit area 460 Å^2). Each layer (Figure 2) contains two alternative symmetry-related rows of β-CD, each

† Université de Paris Sud.
‡ SCM-DPhG-CEN Saclay.

(1) Hoffmann, H.; Ebert, G. *Angew. Chem., Int. Ed. Engl.* **1988**, *27*, 902–12.
(2) Atkins, E. D. T. *Comprehensive Polymer Science*; Allen, G., Ed.; Pergamon Press: Oxford, 1989; Vol. 1, pp 613–50.
(3) Watase, M.; Nishinara, K.; Williams, P. A.; Phillips, G. O. *Polym. J.* **1990**, *22*, 991–9.
(4) Crystal parameters (crystallogenesis under investigation): $a = 14.551$ (1), $b = 15.224$ (3), $c = 20.854$ (2) Å; $\beta = 104.96$ (1)°, $V = 4463$ (1) Å^3; monoclinic $P2_1$, $Z = 2$.
(5) Nicolaisen, F. M.; Meyland, I.; Schaumberg, K. *Acta Chem. Scand.* **1980**, *B34*, 579–583.
(6) Crystal data: formula $C_{92}H_{116}O_{58}N_8$; cell constants $a = 14.700$ (3), $b = 14.742$ (6), $c = 21.784$ (4) Å; $\beta = 101.87$ (2)°, $V = 4620$ (6) Å^3; monoclinic $P2_1$, $Z = 2$. Least-squares refinement based on 3783 unique observed reflections (Mo Kα, λ = 0.71073 Å). Final $R = 0.100$; anisotropic thermal parameters for all hydroxyl oxygen atoms, pyridine molecules as rigid groups, hydrogen atoms, except those of water molecules and hydroxyl groups, were in ideal positions.
(7) Lindner, K.; Saenger, W. *Carbohydr. Res.* **1982**, *99*, 103–115. Betzel, C.; Saenger, W.; Hingerty, B. E.; Brown, G. M. *J. Am. Chem. Soc.* **1984**, *106*, 7545–7557. Zabel, V.; Saenger, W.; Mason, S. A. *J. Am. Chem. Soc.* **1986**, *108*, 3663–3673.
(8) Tokuoka, R.; Abe, M.; Fujiwara, T.; Tomita, K.; Saenger, W. *Chem. Lett.* **1980**, 491–494. Lindner, K.; Saenger, W. *Carbohydr. Res.* **1982**, *107*, 7–16. Harata, K.; Kawano, K.; Fukunaga, K.; Ohtani, Y. *Chem. Pharm. Bull. Jpn.* **1983**, *31*, 1428–1430. Harata, K. *Bull. Chem. Soc. Jpn.* **1984**, *57*, 2596–2599. Harata, K.; Uekama, K.; Otagiri, M.; Hirayama, F.; Ohtani, Y. *Bull. Chem. Soc. Jpn.* **1985**, *58*, 1234–1238.
(9) Charpin, P.; Nicolis, I.; Villain, F.; de Rango, C.; Coleman, A. W. *Acta Crystallogr.* **1991**, *C47*, 1829–1833.
(10) Harata, K. *Bull. Chem. Soc. Jpn.* **1982**, *55*, 2315–2320.
(11) Le Bas, G.; Rysanek, N. *Cyclodextrins and Their Industrial Uses*; Editions de la Santé: Paris, 1987; pp 107–130. Le Bas, G.; Rysanek, N.; Tsoucaris, G. *Proc. 5th Int. Symp. Cyclodextrins*, Paris 1990; pp 114–119. Mentzafos, D.; Mavridis, M.; Le Bas, G.; Tsoucaris, G. *Acta Crystallogr.* **1991**, *B47*, 746–757.
(12) Navaza, J. *Acta Crystallogr.* **1987**, *A43*, 645–653.
(13) Castellano, E.; Oliva, G.; Navaza, J. *J. Appl. Crystallogr.* **1992**, *25*, 281–284.

0002-7863/92/1514-5475$03.00/0 © 1992 American Chemical Society

UM00012552
NOVARTIS EXHIBIT 1017
Novartis v. Regents, IPR2023-01346
Page 1298 of 4460

This Page is Inserted by IFW Indexing and Scanning Operations and is not part of the Official Record

BEST AVAILABLE IMAGES

Defective images within this document are accurate representations of the original documents submitted by the applicant.

Defects in the images include but are not limited to the items checked:

- ☐ BLACK BORDERS
- ☐ IMAGE CUT OFF AT TOP, BOTTOM OR SIDES
- ☐ FADED TEXT OR DRAWING
- ☐ BLURRED OR ILLEGIBLE TEXT OR DRAWING
- ☐ SKEWED/SLANTED IMAGES
- ☐ COLOR OR BLACK AND WHITE PHOTOGRAPHS
- ☐ GRAY SCALE DOCUMENTS
- ☐ LINES OR MARKS ON ORIGINAL DOCUMENT
- ☐ REFERENCE(S) OR EXHIBIT(S) SUBMITTED ARE POOR QUALITY
- ☐ OTHER: _____

IMAGES ARE BEST AVAILABLE COPY.

As rescanning these documents will not correct the image problems checked, please do not report these problems to the IFW Image Problem Mailbox.

34. L. Marufu, F. J. Dentener, J. Lelieveld, M. O. Andreae, G. Helas, *J. Geophys. Res.* 105, 14513 (2000).
35. We constructed an anthropogenic emission data set on a 1° by 1° grid resolution, based on the historical Emission Database for Global Atmospheric Research (EDGAR) inventory of Van Aardenne *et al.* (*36*), using recent updates of energy-, industry-, and agriculture-related data sets per country and economic sector. The trend in ship emissions over the Atlantic Ocean has been derived by scaling the EDGAR data with international bunker fuel data from Endresen *et al.* (*37*).
36. J. A. van Aardenne, F. J. Dentener, J. G. J. Olivier, C. G. M. Klein Goldewijk, J. Lelieveld, *Global Biogeochem. Cycles* 15, 909 (2001).
37. Ø. Endresen *et al.*, *J. Geophys. Res.* 108, 4560, 10.1029/2002JD002898 (2003).
38. J. Burkert *et al.*, *J. Geophys. Res.* 106, 5457, 10.1029/2000JD900613 (2001).
39. T. Brauers, M. Hausmann, A. Bister, A. Kraus, H.-P. Dorn, *J. Geophys. Res.* 106, 7399, 10.1029/2000JD900679 (2001).
40. A. M. Thompson *et al.*, *Geophys. Res. Lett.* 27, 3317, 10.1029/1999GL011273 (2000).
41. R. V. Martin *et al.*, *J. Geophys. Res.* 107, 4351, 10.1029/2001JD001480 (2002).
42. G. S. Jenkins, J.-H. Ryu, A. M. Thompson, J. C. Witte, *J. Geophys. Res.* 108, 4745, 10.1029/2002JD003297 (2003).
43. D. P. Edwards *et al.*, *J. Geophys. Res.* 108, 4237, 10.1029/2002JD002927 (2003).
44. We thank the crews and technicians on the vessels *Meteor*, *Polarstern*, *Walther Herwig*, *Anton Dohrn*, *Ymer*, *Academie Fedorov*, and *Berlin Express*, on which the ozone measurements were performed; A. Stickler for the trajectory analyses, completed as part of his thesis work; and the German Weather Service (DWD) and the Max Planck Society (MPG) for their support of the long-term O_3 measurements and their analysis.

Supporting Online Material
www.sciencemag.org/cgi/content/full/1096777/DC1
SOM Text
Fig. S1
References

13 February 2004; accepted 3 May 2004
Published online 13 May 2004;
10.1126/science.1096777
Include this information when citing this paper.

Atmospheric New Particle Formation Enhanced by Organic Acids

Renyi Zhang,[1]* Inseon Suh,[1] Jun Zhao,[1] Dan Zhang,[1]
Edward C. Fortner,[1] Xuexi Tie,[2]
Luisa T. Molina,[3] Mario J. Molina[3]

Atmospheric aerosols often contain a substantial fraction of organic matter, but the role of organic compounds in new nanometer-sized particle formation is highly uncertain. Laboratory experiments show that nucleation of sulfuric acid is considerably enhanced in the presence of aromatic acids. Theoretical calculations identify the formation of an unusually stable aromatic acid–sulfuric acid complex, which likely leads to a reduced nucleation barrier. The results imply that the interaction between organic and sulfuric acids promotes efficient formation of organic and sulfate aerosols in the polluted atmosphere because of emissions from burning of fossil fuels, which strongly affect human health and global climate.

Aerosols influence the Earth-atmosphere system in several distinct ways (*1*, *2*). Concerns over the human health effects of fine particulate matter constitute the most important element in formulating the national ambient air quality standard (*3*). Also, aerosols directly or indirectly affect the Earth's radiation budget (*4*, *5*), and light absorption by aerosols causes visibility degradation. Furthermore, modification of clouds and precipitation by aerosols may enhance lightning activity and thus influence tropospheric chemistry (*6*, *7*). The impacts of particulate matter on health, radiation, and cloud microphysics are strongly dependent on the particle sizes.

Several processes determine the aerosol size distribution, including new particle production (as a result of gas-to-particle conversion), growth due to condensation and coagulation, removal rates, and primary emissions. New particle formation or nucleation is the least understood of these steps (*8*). Much of the previous research has focused on nucleation of sulfuric acid, because sulfate represents an important component of the nucleation mode aerosol (*9*). It is commonly recognized that binary nucleation of H_2O-H_2SO_4 is not efficient enough to explain atmospheric new particle formation (*10*). Progress recently has been made in assessing the importance of ternary water–sulfuric acid–ammonia nucleation (*11*, *12*), ion-induced nucleation (*13*, *14*), and nucleation involving iodide species (*15*, *16*).

The role of organic compounds in new particle formation is another potentially important issue (*17*). Atmospheric measurements reveal that aerosols often contain a considerable amount of organic matter (*18*–*21*). During photooxidation of volatile organic compounds (VOCs), non- or semivolatile organic products are produced that contribute to secondary organic aerosol (SOA) formation. For example, in the urban atmosphere the aromatic component in gasoline (mainly toluene and xylenes) is responsible for SOA formation caused by oxidation of these compounds (*22*). Current theory of SOA formation assumes that condensation of low-volatility organic species such as carboxylic or dicarboxylic acids occurs on preexisting particles from primary emissions or formed by homogeneous nucleation, most probably involving sulfuric acid–ammonia–water or ions (*8*). Alternatively, it is suggested that SOA nucleation may occur through the formation of stable organic heterodimers (*23*). Currently, few experimental studies have investigated new particle formation from organic acids. Another process, which also influences the chemical composition of organic aerosols, involves absorption of gaseous species onto particulate matter. On the basis of consideration of the thermodynamic equilibrium distribution of a compound between the gas and condensed phases, a gas-particle partitioning model has been proposed (*24*) and invoked to explain the observed correlation between the SOA yield and the organic aerosol mass concentration (*22*, *25*). More recently, it has been suggested that sulfate aerosols catalyze heterogeneous reactions of carbonyl compounds, leading to a considerably enhanced SOA yield (*26*). The growth of SOA from both mechanisms depends on preexisting particles, which are linked to new particle formation or primary emissions.

To assess the role of low-volatility organic species in new particle formation, we performed laboratory studies of particle nucleation from aromatic acid vapors and their mixtures with H_2SO_4 (*27*). Aromatic acids, such as benzoic ($C_7H_6O_2$), *p*-toluic ($C_8H_8O_2$), and *m*-toluic ($C_8H_8O_2$) acids, are products from photochemical degradation of aromatic hydrocarbons emitted from automobiles in the urban atmosphere (*28*) and have been identified in the particle phase (*29*, *30*). Nanometer-sized particles were produced in an aerosol chamber, and the particle concentration and size distribution were monitored with an ultrafine particle counter (model 3025A, TSI Incorporated Particle Instruments, St. Paul, MN) and a nanodifferential mobility analyzer (model 3085, TSI Incorporated Particle Instruments) capable of measuring particle

[1]Department of Atmospheric Sciences, Texas A&M University, College Station, TX 77843, USA. [2]Atmospheric Chemistry Division, National Center for Atmospheric Research, Boulder, CO 80307, USA. [3]Department of Earth, Atmospheric, and Planetary Sciences and Department of Chemistry, Massachusetts Institute of Technology, Cambridge, MA 02139, USA.
*To whom correspondence should be addressed. E-mail: zhang@ariel.met.tamu.edu

UM00012554
NOVARTIS EXHIBIT 1017
Novartis v. Regents, IPR2023-01346
Page 1300 of 4460

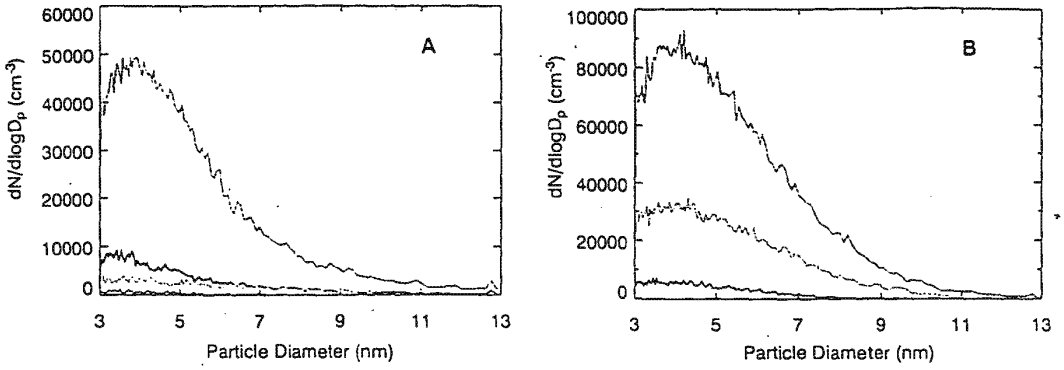


Fig. 1. Measured particle size distributions of the nucleating aerosols. In (A), the brown and black curves correspond to H_2SO_4 aerosol formation with a RH of 5% and gaseous H_2SO_4 concentrations of 6×10^9 and 8×10^9 molecule cm^{-3}, respectively. The green and orange curves are similar to the brown and black curves, respectively, except for addition of 0.04 ppb benzoic acid to the aerosol chamber. In (B), the brown curve corresponds to H_2SO_4 aerosol formation with a RH of 5% and a gaseous H_2SO_4 concentration of 7×10^9 molecule cm^{-3}. The green and orange curves are similar to the brown curve, except for the addition of 0.04 and 0.1 ppb benzoic acid (corresponding to 1×10^9 and 2.5×10^9 molecule cm^{-3}), respectively. The experiments were performed at 298 ± 2 K and a total pressure of 760 torr.

sizes as small as 3 nm (fig. S1). Gas-phase concentrations of the organic and sulfuric acids in the aerosol chamber were monitored with the use of proton-transfer reaction mass spectrometry and chemical ionization mass spectrometry, respectively (*31*, *32*). We initially generated H_2SO_4 aerosols by introducing gas-phase H_2SO_4 in a nitrogen carrier gas with a variable relative humidity (RH). For a gaseous H_2SO_4 concentration in the range of 10^9 to 10^{10} molecule cm^{-3}, the particle sizes formed ranged from 3 to 10 nm (Fig. 1), corresponding to the nucleation mode. The observed particle concentration increased when the gaseous H_2SO_4 concentration or RH was increased. A marked increase in the particle concentration occurred when benzoic acid vapor was added to the aerosol chamber (Fig. 1). With H_2SO_4 concentrations of 6×10^9 and 8×10^9 molecule cm^{-3}, addition of 0.04 ppb (parts per billion) benzoic acid increased the particle concentration by a factor of 5 (Fig. 1A). For a fixed H_2SO_4 concentration, higher amounts of benzoic acid resulted in more pronounced particle formation (Fig. 1B). Figure 1 shows that the measured peak diameter of the particle distribution shifted slightly to a larger size with addition of benzoic acid, implying that the presence of benzoic acid both enhanced nucleation and contributed to the growth of the newly nucleated particles. Substantially larger peak diameters (>10 nm) were detected when benzoic acid concentrations were increased by one to two orders of magnitude.

The aerosol nucleation rate, J, was estimated on the basis of the ratio of the measured particle concentration to the nucleation time (*33*). In the absence of organic acids, the nucleation rate is dependent on the gas-phase H_2SO_4 concentration and RH. Our measured nucleation rate of the H_2O-H_2SO_4 binary system is qualitatively in agreement with previous experimental

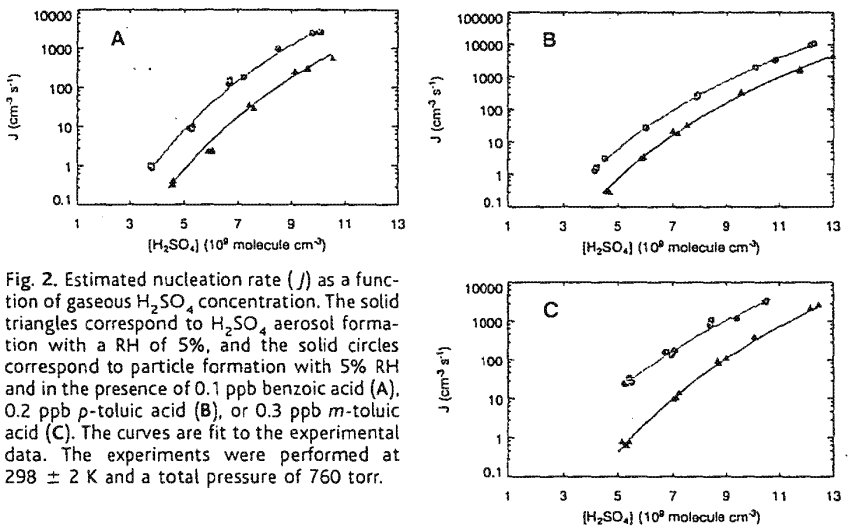


Fig. 2. Estimated nucleation rate (J) as a function of gaseous H_2SO_4 concentration. The solid triangles correspond to H_2SO_4 aerosol formation with a RH of 5%, and the solid circles correspond to particle formation with 5% RH and in the presence of 0.1 ppb benzoic acid (A), 0.2 ppb *p*-toluic acid (B), or 0.3 ppb *m*-toluic acid (C). The curves are fit to the experimental data. The experiments were performed at 298 ± 2 K and a total pressure of 760 torr.

studies (*12*). Figure 2 shows that the nucleation rate was considerably increased in the presence of the organic acids. The nucleation rate in the presence of 0.1 ppb benzoic acid is about a factor of 8 to 10 higher than that of the H_2O-H_2SO_4 binary system. Enhanced nucleation rates were also observed for *p*-toluic and *m*-toluic acids (Fig. 2, B and C). The nucleation rate was increased by a factor of 5 to 13 in the presence of 0.2 to 0.3 ppb of the two acids. For RH in the range of 4 to 15%, addition of sub-ppb levels of the aromatic acids consistently led to a larger nucleation rate by a factor of 5 or higher than that of the H_2O-H_2SO_4 binary system (fig. S2). The partial pressures of the aromatic acids in those experiments were several orders of magnitude smaller than their corresponding equilibrium vapor pressures; that is, the saturation ratio, S (*34*), was much smaller than unity. Interestingly, the high nucleation rate was also measured in the absence of water vapor for benzoic acid and *p*-toluic acid, indicating that binary nucleation of the organic acid–sulfuric acid system is responsible for the enhanced new particle formation (*35*). Hence, these results suggest a probable interaction between the aromatic acid and sulfuric acid that leads to a reduced (heteromolecular) nucleation barrier. The magnitude of the effect of aromatic acids on H_2SO_4 nucleation enhancement appears to be comparable to that previously reported for ammonia at similar H_2SO_4 and ammonia additive concentrations and RH (fig. S3).

We also examined (homomolecular) nucleation of the aromatic acids in the absence of sulfuric acid and water. New particle formation was only detected when a substantial saturation ratio was established in the aerosol chamber. The minimum S required to produce detectable new particles was about 45 for benzoic acid and even higher for *p*-toluic and *m*-toluic acids. Similarly, water was observed to have a negligible influence on the organic particle formation for benzoic and *p*-toluic acids,

UM00012555
NOVARTIS EXHIBIT 1017
Novartis v. Regents, IPR2023-01346
Page 1301 of 4460

Table 1. Bonding energies, D_0 (in kcal mol^{-1}), of the aromatic acid–sulfuric acid complexes. BA-SA denotes benzoic acid–sulfuric acid complex; PTA-SA, *p*-toluic acid–sulfuric acid complex; and MTA-SA, *m*-toluic acid–sulfuric acid complex. All energies are corrected with the zero-point energies (ZPE). The quantum chemical methods used in the present study are similar to those used by Suh *et al.* (*28*).

Complex	D_0
BA-SA	19.85*
	17.62†
	18.63‡
	17.84§
PTA-SA	19.99*
MTA-SA	23.72*

*Determined with B3LYP/6-31G(d,p)//B3LYP/6-31G(d,p). †Determined with CCSD(T)/6-31G(d) + CF//B3LYP/6-31G(d,p). ‡Determined with QCISD(T)/6-31G(d)//MP2(full)/6-31G(d). §Determined with G2(MP2, SVP).

because the two organic acids are insoluble in water and the organic aerosols formed are hydrophobic. In general, particle formation can be qualitatively predicted in terms of fundamental thermodynamic and kinetic principles (*36*). The spontaneous gas-to-particle conversion process corresponds to a decreased free energy and is thermodynamically favorable but kinetically hindered. During nucleation, a thermodynamically stable cluster or critical embryo is generated before condensation growth of the particle, and this embryo formation involves an energy barrier. Also, condensation growth of nucleated critical embryos will be retarded because of increased activity due to the Kelvin barrier. Hence, particle nucleation and subsequent growth in a single-component system occur only if the system is supersaturated ($S > 1$). It is conceivable that large barriers generally exist for other carboxylic or dicarboxylic acids, as shown in our experiments for the aromatic acids. The atmospheric concentrations of the low-volatility organic compounds are typically at the ppb level or less, even under polluted conditions (*1*, *2*). Although certain dicarboxylic acids do reach their saturation points in the atmosphere (*18*), the high supersaturation required for homomolecular nucleation likely renders new particle formation from those compounds implausible. Previous smog chamber studies reported homogeneous nucleation from low-volatility organic compounds, but those experiments were carried out with the use of hydrocarbon concentrations that were several orders of magnitude higher than those found under the ambient conditions (*25*).

To gain an insight into the nature of the interaction between aromatic and sulfuric acids at the molecular level, we performed quantum chemical calculations that show the formation of surprisingly stable aromatic acid–sulfuric acid complexes (fig. S4). The equilibrium aromatic acid–sulfuric acid structure exhibits a nearly planar eight-membered ring: There are two hydrogen bonds, with the organic acid molecule acting as both a hydrogen bond donor and acceptor. The strength of the hydrogen bonding is reflected by the calculated bond lengths. For the benzoic–sulfuric acid complex, for example, the hydrogen bond is 1.503 Å for C=O···HOS and 1.705 Å for COH···O=S, nearly comparable to weak covalent bonds. The energetics of the complexes was quantified with a series of quantum chemical calculations (Table 1). The bonding energies of the complexes are about 20 kcal mol^{-1} for benzoic and *p*-toluic acids and are about 4 kcal mol^{-1} higher for *m*-toluic acid. For comparison, the bonding energy is about 10 kcal mol^{-1} for the H_2O-H_2SO_4 complex (*37*) and 25 kcal mol^{-1} for the H_2O-H_2SO_4-NH_3 system (*38*). The large stability of the organic acid–sulfuric acid complex implies that the aromatic acid molecule bonds irreversibly to H_2SO_4 under atmospheric conditions. The complex formation between aromatic and sulfuric acids most likely reduces the barrier in heteromolecular nucleation and helps condensation growth of the nucleated critical embryo by overcoming the Kelvin effect, explaining the enhanced new particle formation observed in our experiments. Additional calculations were performed for glutaric acid, indicating that stable complex formation with sulfuric acid represents a general feature for organic compounds with the carboxylic or dicarboxylic functional group. It is likely, though, that for smaller organic acids the effect on H_2SO_4 nucleation may be less important than that observed for the aromatic acids (*39*).

Organic acids have been widely identified as common components in atmospheric particulate matter (*18*–*21*). Our experimental study shows that homomolecular nucleation of aromatic acids is unlikely to occur under atmospheric conditions, but that the interaction between aromatic acids and sulfuric acid promotes efficient heteromolecular nucleation. The gas-phase concentration of organic acids is substantially higher than that of gaseous H_2SO_4 in the atmosphere (*18*); thus, organic acids can also contribute considerably to the initial growth of the newly nucleated embryos, which is important for subsequent particle growth by adsorption or heterogeneous reactions of other organic vapors. The particle formation mechanism proposed in this study can have major implications for SOA and sulfate aerosol formation in polluted areas, because both organic and sulfuric acids are photochemical degradation products linked to the emissions from the burning of fossil fuels (*1*, *2*). In particular, new particle formation can occur efficiently over a large portion of northern America, eastern Asia, and some parts of central Europe because of the concurrent anthropogenic VOC and SO_2 emissions in those regions (fig. S5) (*40*). Our results suggest an alternative cause for efficient aerosol nucleation frequently observed in the polluted atmosphere, in addition to the available theories of water–sulfuric acid–ammonia ternary nucleation and ion-induced nucleation. For example, enhanced new particle formation (with a particle size of 3 to 4 nm) was observed in anthropogenic plumes advecting from Asia, which were identified by elevated CO and SO_2 concentrations (*41*). The high CO amount was indicative of the abundance of VOCs inside those plumes. It was speculated that a high SO_2 concentration, in conjunction with other unidentified, possibly co-emitted species, was responsible for nucleation. In contrast, the same study revealed that few 3- to 4-nm particles were detected in the clean background and even within a volcanic plume that had a high H_2SO_4 but low CO concentration. Also, measurements of aerosol hygroscopicity during the 1999 Houston Supersite Project indicated a dominance of the organic matter in the fine particle mode, which could not be explained by the formation of ammonium sulfate (*21*). Those measurements likely can be explained by the importance of organic acids in particle nucleation and growth in the presence of sulfuric acid, because of the large abundance of both types of acids in urban environments and in the tropospheric boundary layer influenced by anthropogenic pollution.

References and Notes

1. B. J. Finlayson-Pitts, J. N. Pitts Jr., *Chemistry of the Upper and Lower Atmosphere: Theory, Experiments, and Applications* (Academic Press, San Diego, CA, 2000).
2. J. H. Seinfeld, S. N. Pandis, *Atmospheric Chemistry and Physics: From Air Pollution to Climate Change* (Wiley, New York, 1998).
3. "Air quality criteria for particulate matter," EPA/600/P-95/001cF, Environmental Protection Agency (1996).
4. R. J. Charlson, J. E. Lovelock, M. O. Andreae, S. G. Warren, *Nature* 326, 655 (1987).
5. J. T. Houghton *et al.*, Eds., *Climate Change 2001: The Scientific Basis* (Cambridge Univ. Press, Cambridge, 2001).
6. R. E. Orville *et al.*, *Geophys. Res. Lett.* 28, 2597 (2001).
7. R. Zhang, X. Tie, D. W. Bond, *Proc. Natl. Acad. Sci. U.S.A.* 100, 1505 (2003).
8. M. Kulmala, *Science* 302, 1000 (2003).
9. A. Laskin *et al.*, *Science* 301, 340 (2003); published online 3 July 2003 (10.1126/science.1085374).
10. M. Boy *et al.*, *J. Geophys. Res.* 108, 10.1029/2003JD003838 (2003).
11. R. J. Weber *et al.*, *Geophys. Res. Lett.* 26, 307 (1999).
12. S. M. Ball, D. R. Hanson, F. L. Eisele, P. H. McMurry, *J. Geophys. Res.* 104, 23709 (1999).
13. F. Yu, R. P. Turco, *J. Geophys. Res.* 106, 4797 (2001).
14. S.-H. Lee *et al.*, *Science* 301, 1886 (2003).
15. C. D. O'Dowd *et al.*, *Nature* 417, 632 (2002).
16. C. E. Kolb, *Nature* 417, 597 (2002).
17. J. J. Martin *et al.*, *J. Geophys. Res.* 102, 6331 (1997).

UM00012556
NOVARTIS EXHIBIT 1017
Novartis v. Regents, IPR2023-01346
Page 1302 of 4460

18. A. Chebbi, P. Carlier, *Atmos. Environ.* **30**, 4233 (1996).
19. I. G. Kavouras, N. Mihalopoulos, E. G. Stephanou, *Nature* **395**, 683 (1998).
20. C. D. O'Down, P. Aalto, K. Hameri, M. Kulmala, T. Hoffmann, *Nature* **416**, 497 (2002).
21. R. Gasparini, R. Li, D. R. Collins, *Atmos. Environ.*, in press.
22. J. R. Odum, T. P. W. Jungkamp, R. J. Griffin, R. C. Flagan, J. H. Seinfeld, *Science* **276**, 96 (1997).
23. T. Hoffmann, R. Bandur, U. Marggraf, M. Linscheid, *J. Geophys. Res.* **103**, 25569 (1998).
24. J. F. Pankow, *Atmos. Environ.* **28**, 185 (1994).
25. J. R. Odum *et al.*, *Environ. Sci. Technol.* **30**, 2580 (1996).
26. M. Jang, N. M. Czoschke, S. Lee, R. M. Kamens, *Science* **298**, 814 (2002).
27. Information on the experimental apparatus and additional results are available as supporting material on *Science* Online.
28. I. Suh, R. Zhang, L. T. Molina, M. J. Molina, *J. Am. Chem. Soc.* **125**, 12655 (2003).
29. H. J. L. Forstner, R. C. Flagan, J. H. Seinfeld, *Environ. Sci. Technol.* **31**, 1345 (1997).
30. M. Jang, R. M. Kamens, *Environ. Sci. Technol.* **35**, 3626 (2001).
31. J. Zhao, R. Zhang, E. C. Fortner, S. W. North, *J. Am. Chem. Soc.* **126**, 2686 (2004).
32. R. Zhang, I. Suh, W. Lei, A. D. Clinkenbeard, S. W. North, *J. Geophys. Res.* **105**, 24627 (2000).
33. The nucleation rate is more precisely defined as the rate at which particles of critical size are produced. In this study, we detect only particles larger than 3 nm, and hence the value estimated from the rate of observed particle formation may be smaller than that of cluster formation.
34. S is defined as the ratio of the partial pressure of the organic acid to its equilibrium vapor pressure at a given temperature. For example, the equilibrium vapor pressures are 7.0×10^{-3} torr for benzoic acid and 1.9×10^{-3} torr for *p*-toluic acid at 298 K, corresponding to saturation mixing ratios of 9.2 and 2.5 ppm (parts per million) at 1 atm, respectively.
35. For benzoic and *p*-toluic acids and the experimental conditions similar to those in Fig. 2, the measured particle concentrations were slightly higher (by about 10 to 20%) when the water flow in the aerosol chamber was turned off.
36. S. M. Kathmann, G. K. Schenter, B. C. Garrett, *J. Chem. Phys.* **116**, 5046 (2002).
37. S. Re, Y. Osamura, K. Morokuma, *J. Phys. Chem. A* **103**, 3535 (1999).
38. L. J. Larson, A. Largent, F. M. Tao, *J. Phys. Chem. A* **103**, 6786 (1999).
39. The bonding energy of complexes represents one of the factors that determine particle nucleation. Other physicochemical parameters, such as the surface tension and equilibrium vapor pressures of the nucleated single or multicomponent system, also influence new particle formation. For example, our experimental results indicated a negligible effect of glutaric acid ($C_5H_8O_4$) on sulfuric acid nucleation, although the bonding energy of this organic acid with sulfuric acid is 19.2 kcal mol^{-1}, comparable to those of the aromatic acid–sulfuric acid complexes.
40. X. Tie *et al.*, *J. Geophys. Res.* **108**, 10.1029/2003JD003659 (2003).
41. R. J. Weber *et al.*, *J. Geophys. Res.* **108**, 10.1029/2002JD003112 (2003).

42. Supported by the U.S. Department of Energy's Atmospheric Chemistry Program (DOE-ACP), Robert A. Welch Foundation (A-1417), and Texas Air Research Center (TACR). The National Center for Atmospheric Research (NCAR) is sponsored by NSF. We acknowledge additional funding for the quantum chemical calculations from the Texas A&M University Supercomputing Facilities and the use of the Laboratory for Molecular Simulations at Texas A&M University. We thank D. Collins for assistance with the application of the differential mobility analyzer and helpful discussions.

Supporting Online Material
www.sciencemag.org/cgi/content/full/304/5676/1487/DC1
Figs. S1 to S5
References

29 December 2003; accepted 3 May 2004

The Acquisition of Exogenous Algal Symbionts by an Octocoral After Bleaching

Cynthia L. Lewis and Mary Alice Coffroth*

Episodes of coral bleaching (loss of the symbiotic dinoflagellates) and coral mortality have occurred with increasing frequency over the past two decades. Although some corals recover from bleaching events, the source of the repopulating symbionts is unknown. Here we show that after bleaching, the adult octocoral *Briareum* sp. acquire dinoflagellate symbionts (*Symbiodinium* sp.) from the environment. Uptake of exogenous symbionts provides a mechanism for response to changes in the environment and resilience in the symbiosis.

A diverse array of cnidarians form symbioses with photosynthetic dinoflagellates in the genus *Symbiodinium*. These are true mutualisms, in that the symbiont receives inorganic nutrients from the host and the host obtains translocated photosynthetic products from the symbionts (*1–3*). Symbiont species within the diverse genus *Symbiodinium* are classified into broad groups or clades (i.e., A, B, C, etc.) on the basis of sequence variation in the small-subunit ribosomal gene (*4–6*). Most cnidarians preferentially establish and maintain a stable symbiosis with either a specific clade of *Symbiodinium* (*7–10*) or a subset of the clades that vary with environmental gradients such as light intensity (*11–14*). Environmental perturbation (e.g., increased temperature, increased solar radiation) can result in the breakdown of the symbiosis (i.e., coral bleaching) that can lead to coral death and subsequent reef degradation. However, some corals recover, and bleaching has been posited as a mechanism whereby hosts acquire new, potentially better-adapted symbionts (*4*, *15*, *16*). The source of the symbionts that repopulate a host colony following bleaching is poorly understood (*11*, *16*, *17*). Are the symbionts derived from *Symbiodinium* populations remaining in the host at very low levels or from an exogenous pool of potential symbionts (*12*, *17–19*)?

To determine whether adult corals can acquire exogenous symbionts from the environment after a bleaching event, the Caribbean octocoral *Briareum* sp. was bleached and then exposed to exogenous *Symbiodinium* containing rare variants of the chloroplast 23*S* ribosomal DNA (rDNA) domain V region (cp23S-genotype) (*20*). The potential symbionts were derived from isoclonal lines of *Symbiodinium* clade B initially isolated from newly settled octocoral polyps (cp23S-genotypes B211 and B223) and an adult colony of *Plexaura flexuosa* (cp23S-genotype B224). Because these variants are not commonly found in adult *Briareum* sp., they served as markers for uptake of exogenous *Symbiodinium*. The markers B211 and B223 cp23S-genotypes were not detected in any of 255 *Briareum* sp. colonies collected from the field; one colony harbored *Symbiodinium* B224 (*21*); 254 colonies harbored either *Symbiodinium* B178 and/or B184, the cp23S-genotypes typically found in *Briareum* sp. (*21*). The cp23S-genotypes used as markers in the experiment were not found in *Symbiodinium* isolated from the experimental colonies before or immediately after bleaching (Fig. 1 and Fig. 2A, lanes P and B; table S1).

Cell counts of *Symbiodinium* within *Briareum* colonies immediately after bleaching confirmed a decrease in symbiont density to less than 1% of the original population density (Fig. 2B). Molecular analysis detected residual populations of B178 and/or B184 in 27 of the 39 colonies after bleaching (table S1). During the subsequent 6-week exposure to exogenous symbionts, cell densities within the hosts increased 9- to 31-fold, demonstrating that the symbiosis had begun to reestablish itself (Fig. 2B). Molecular analysis of the symbiont population within these hosts after 3 and 6 weeks of exposure to exogenous *Symbiodinium* cultures identified the marker cp23S-genotypes in 58% and 45% of the samples, respectively (Fig. 2A, lanes R). This demonstrates repopulation of adult *Briareum* by exogenous symbionts and thus establishes a potential exogenous source of symbionts following bleaching events (*22*). Furthermore, 37% of the colonies that initially harbored *Symbiodinium* B178 and/or B184 contained only *Symbiodinium* with the marker cp23S-genotypes when sampled after 3 weeks of exposure to the exogenous algal source ["switching" sensu (*11*)]. In contrast, six colonies, which initially contained *Symbiodinium* B178 and/or B184, did not acquire symbionts with the marker cp23S-genotype. This may be due to physiological differences between the different *Symbiodinium* strains

Department of Biological Sciences, State University of New York at Buffalo, Buffalo, NY 14260, USA.

*To whom correspondence should be addressed. E-mail: coffroth@buffalo.edu

UM00012557
NOVARTIS EXHIBIT 1017
Novartis v. Regents, IPR2023-01346
Page 1303 of 4460

This Page is Inserted by IFW Indexing and Scanning Operations and is not part of the Official Record

BEST AVAILABLE IMAGES

Defective images within this document are accurate representations of the original documents submitted by the applicant.

Defects in the images include but are not limited to the items checked:

- ☐ BLACK BORDERS
- ☐ IMAGE CUT OFF AT TOP, BOTTOM OR SIDES
- ☐ FADED TEXT OR DRAWING
- ☐ BLURRED OR ILLEGIBLE TEXT OR DRAWING
- ☐ SKEWED/SLANTED IMAGES
- ☐ COLOR OR BLACK AND WHITE PHOTOGRAPHS
- ☐ GRAY SCALE DOCUMENTS
- ☐ LINES OR MARKS ON ORIGINAL DOCUMENT
- ☐ REFERENCE(S) OR EXHIBIT(S) SUBMITTED ARE POOR QUALITY
- ☐ OTHER: _____

IMAGES ARE BEST AVAILABLE COPY.
As rescanning these documents will not correct the image problems checked, please do not report these problems to the IFW Image Problem Mailbox.

Science Supporting Online Material

Atmospheric New Particle Formation Enhanced by Organic Acids

Renyi Zhang,[1*] Inseon Suh,[1] Jun Zhao,[1] Dan Zhang,[1] Edward C. Fortner,[1]
Xuexi Tie,[2] Luisa T. Molina,[3] and Mario J. Molina[3]
[1]Department of Atmospheric Sciences
Texas A&M University, College Station, TX 77843
[2]Atmospheric Chemistry Division, National Center for Atmospheric Research
Boulder, CO 80307
[3]Departments of Earth, Atmospheric, and Planetary Sciences and Chemistry
Massachusetts Institute of Technology, Cambridge, MA 02139

* To whom correspondence should be addressed. E-mail: zhang@ariel.met.tamu.edu

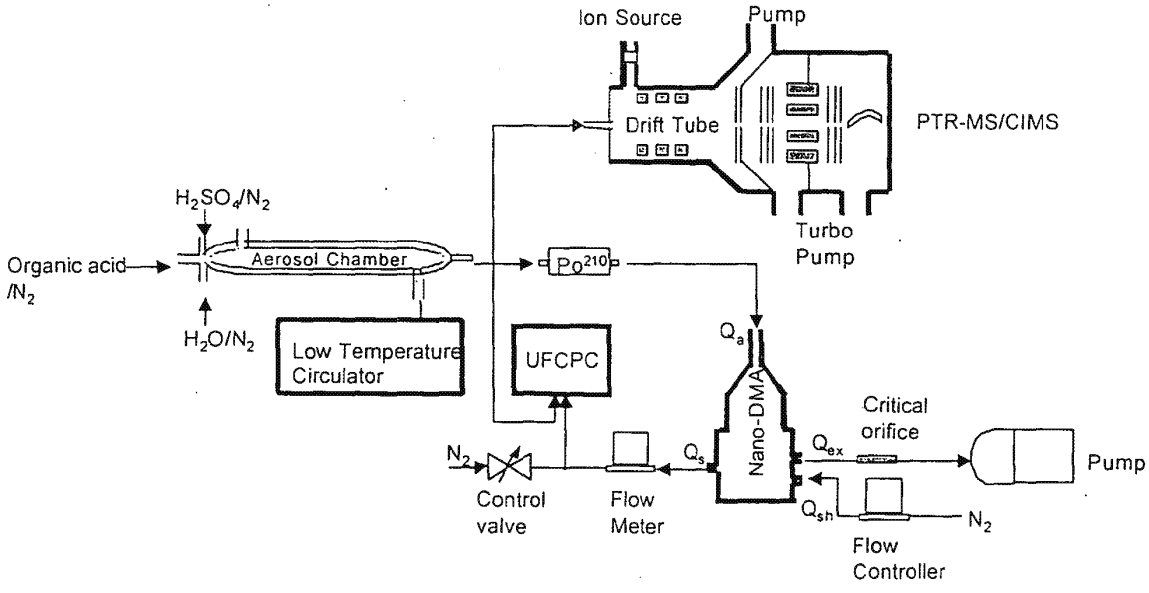


Fig. S1. Schematic representation of the experimental setup. The aerosol chamber is made of a jacketed glass tube of 2.45 cm i.d. and 60 cm in length. The nucleation time was estimated to be in the range of 7 to 12 s. For the nucleation experiments involving sulfuric acid and organic/sulfuric acid mixtures, the experiments were performed at 298 ± 2 K. For experiments involving homomolecular nucleation of organic acids, the emperature was regulated between 220 and 298 K. All experiments were performed at a pressure of one atm. The PTR-MS and CIMS methods have been discussed in our previous studies (*S1,S2*).

UM00012559

NOVARTIS EXHIBIT 1017
Novartis v. Regents, IPR2023-01346
Page 1305 of 4460

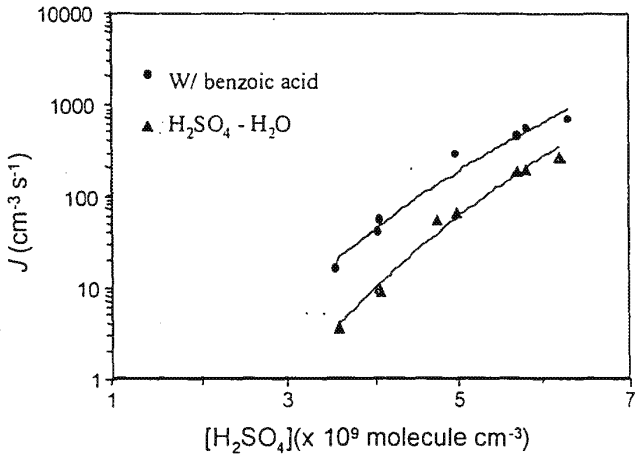


Fig. S2. Nucleation rates in the $H_2SO_4/H_2O/C_7H_6O_2$ system at 9.5% RH. The concentration of the benzoic acid is 0.04 ppb.

UM00012560

NOVARTIS EXHIBIT 1017
Novartis v. Regents, IPR2023-01346
Page 1306 of 4460

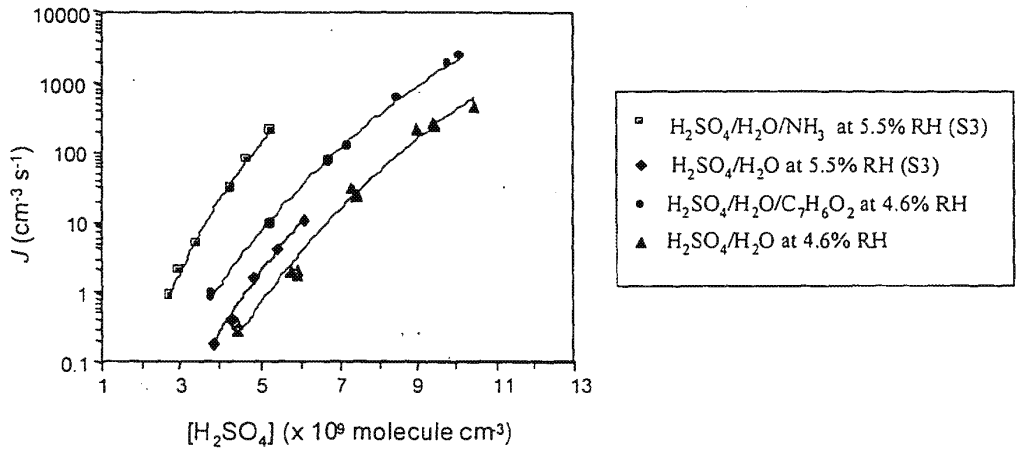


Fig. S3. Comparison of the nucleation rate in the $H_2SO_4/H_2O/C_7H_6O_2$ system at 4.6% RH with that in the $H_2SO_4/H_2O/NH_3$ system at 5.5% RH reported previously (*S3*). The amount of benzoic acid is 0.1 ppb in the present work, and the amount of NH_3 is 0.17 ppb (S3).

UM00012561

NOVARTIS EXHIBIT 1017
Novartis v. Regents, IPR2023-01346
Page 1307 of 4460

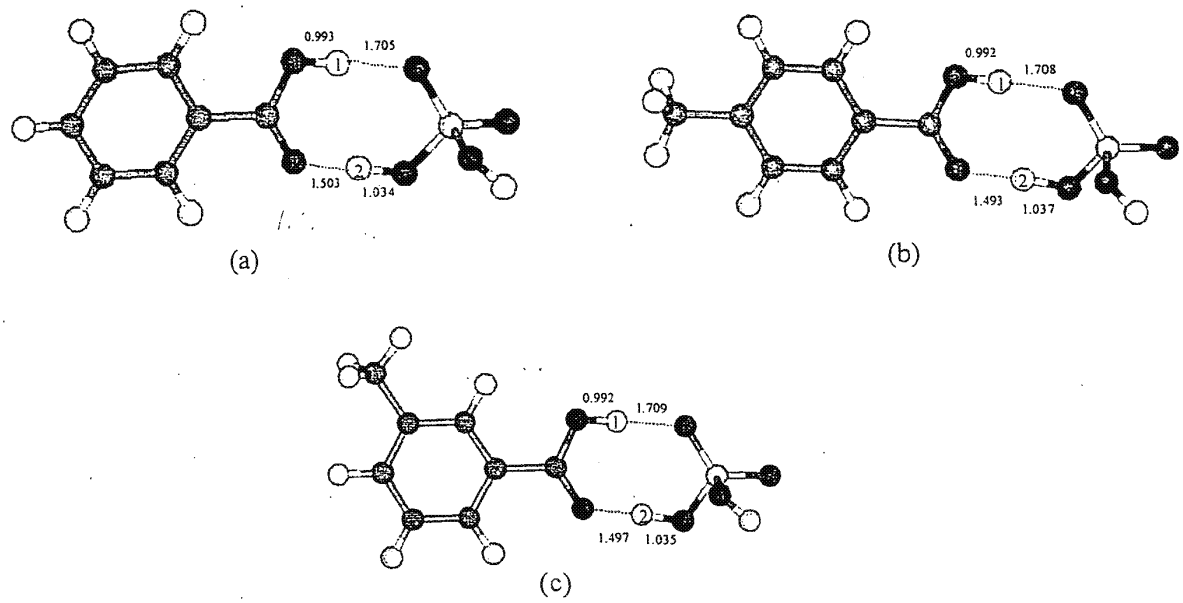


Fig. S4. Equilibrium geometries of the benzoic acid (a), *p*-toluic acid (b), and *m*-toluic acid (c) - sulfuric acid complexes obtained at the B3LYP/6-31G(d,p) level of theory.

UM00012562
NOVARTIS EXHIBIT 1017
Novartis v. Regents, IPR2023-01346
Page 1308 of 4460

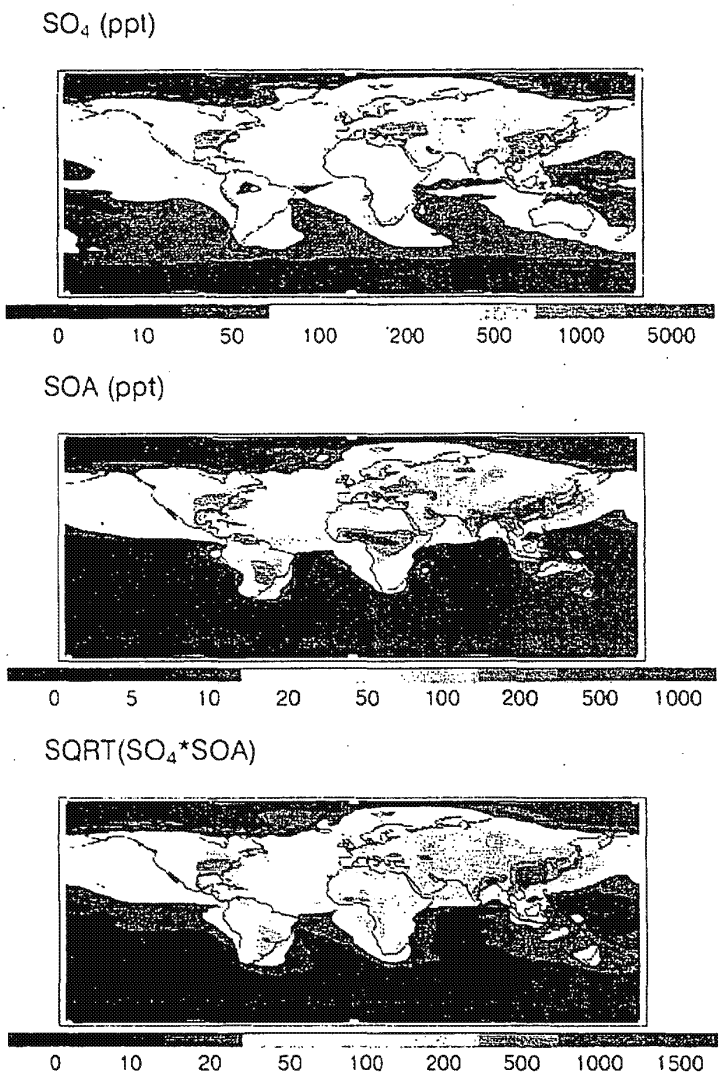


Fig. S5. Simulated global distributions of total concentrations of condensable species for sulfate aerosol (top) and SOA (middle) averaged for June, July, and August using a global chemical transport model (MOZAR – v2) (*S4*). The bottom panel corresponds to the square root of the product of the quantities shown in the top and middle panels. The amount of condensable organic species was computed according to the bulk aerosol yields from biogenic and anthropogenic VOCs on the basis of experimental studies of SOA formation (*S5*). A key feature of the figure is that the abundances of condensable SOA and sulfur compounds generally coincide because of the concurrent emissions from fossil-fuel burning, except for the regions in South Africa and South America where biogenic emissions contribute significantly to the condensable SOA species.

UM00012563
NOVARTIS EXHIBIT 1017
Novartis v. Regents, IPR2023-01346
Page 1309 of 4460

Supporting Online Material References

S1. J. Zhao, R. Zhang, E. C. Fortner, S. W. North, *J. Am. Chem. Soc.* **126**, 2686 (2004).

S2. R. Zhang, I. Suh, A. D. Clinkenbeard, W. Lei, S. W. North, *J. Geophys. Res.* **105**, 24627 (2000).

S3. S. M. Ball, D. R. Hanson, F. L. Eisele, P. H. McMurry, *J. Geophys. Res.* **104**, 23709 (1999).

S4. X. Tie, S. Modronich, S. Walters, P. Rasch, R. Zhang, W. Collins, *J. Geophys. Res.* **108(D20)**, 4642 (2003).

S5. J. R. Odum, T. Hoffmann, F. Bowman, D. Collins, R. C. Flagan, J. H. Seinfeld, *Env. Sci. Technol.* **30**, 2580, (1996).

NOVARTIS EXHIBIT 1017
Novartis v. Regents, IPR2023-01346
Page 1310 of 4460